

Modelling of Wear on a Cam Profile

Ilknur Keskin Oner¹, Adnan Parlak¹, Omer Savas¹, Huseyin Elcicek¹

Abstract

Life prediction for dynamic systems is an important concern for machine designers to consider for technical and economic reasons. Wear of components is often a critical factor influencing the product service life. Although wear is a commonplace phenomenon, it is by no means an uncomplicated one; on the contrary, the mechanisms and theory of wear are very complex functions of the system which include material properties, operating conditions (load, speed), contact geometry, surface roughness, and environment (lubrication, temperature). Therefore, predictions of wear based on the forces and slip velocities calculated using the unworn first cycle geometry will not accurately predict a mechanism's useful life. This is because there is a coupling between the contact conditions and the geometry of the components, which are changing as they wear.

The evolution of the geometry of different two-dimensional cams as a result of wear is studied using three complementary approaches: a closed form analytical expression, a computer simulation, and the development of an experimental apparatus. Using an Archard's wear constant, a closed form expression describing the coupled evolution of the contact loads and wear for a two-dimensional cam with a flat-faced follower is developed. This method has potential for predicting the shapes into which cams and followers will wear in service. The cam and follower profiles are modified according to the amount of wear estimated, and new cam and follower profiles are obtained.

Keywords: Cam, CMM, follower, wear, wear coefficient.

1. INTRODUCTION

Wear with a mathematical modeling studies to estimate the wear and consequently a deal that is been using for a years. In the literature there are many examples for it. However, most of models are based on the correlation and its seriously connected the system. So just set up a modeling, depends on a specific geometry, a couple of materials, operation conditions, environment conditions and lubricant. On this basis it is not possible to generalize it. The characteristic of wear modellings have many wear parameters and constants. It is also difficult to reach a consensus by the scientists, so everyone suggests its own modelling. Therefore wear prediction models seem far from being the solution to all the problems. The overall result is that all of them should be based on the mechanical system. It is not possible to make a general assessment for a modelling depends on the material, lubricant or wear mechanisms[1].

A special design of the cams give out a motion to the mechanical components by follower. These movements often have complex and perfect timing [2]. The contact between the cam and follower cause a destructive effects such as high temperature, less oil quantity, high contact stresses. This kind of the contact conditions highly effect the performance of the cam system. The wear on the surface of the cam and follower cause a deterioration of initially proposed performance (movement, timing or dynamic control). For this the wear is undesirable condition so should take certain precautions. The precautions can be taken depends on the where the wear can be happened and how much its. The wear is not depends on the material. The Surface working conditions (load, speed), contact geometry, surface roughness and the environment condition (lubrication, temperature) are a result of the complex interactions. There will be modeled according to the change of load components on the contact points of the surface and for it 'Archard's wear equation' will be used. The wear depth calculated analytically, the wear cam shall be compared with the value of the read coordinate measuring machine.

In the literature to simulate wear for finite element method (FEM) is used in many studies are available. Podre and Andersson studied the sliding abrasion using the finite element method in detail [3]. First Blanchette as an alternative approach [4] and Sawyer thrown out by [5] wear a simple line of simple mechanisms to continue the work supported by lifting term is assumed, closed-form analytical expressions have been developed. These statements, due to their limited depending on the types of problems are less common. However, this is limited to the consistent statements of the problem has proven to be highly effective in predicting the wear behavior. Dickrell III [6] and his friends in a two-dimensional circular cam profile wear analytical approach has been studied using computer simulation and experimental studies. He revealed that the mathematical model has been discussed in the context of force-time component wear. However, in order to simplify the audience expressed the acceleration due to inertial forces created conditions that limit the negligible size, it has just been included in the model the effect of the spring force. In this study the effect of inertial forces also be included in the system and limiting the system conditions were kept under

¹ Corresponding author: Yildiz Technical University, Department of Marine Engineering Operations, 34349, Beşiktaş/İstanbul, Turkey. keskin@yildiz.edu.tr

slightly wider. The wear depth calculated according to the mathematical model were compared with the values that have been read in the coordinate measuring machine cam worn. Coordinate measuring machine (CMM) has a three-axis 800 mm and can be used to measure freedom of movement per second.

2. TEST APPARATUS

The Cam and follower are developed to demonstrate the relationship between the load and the wear mechanism of the experimental setup consisting of a pair (Figure 1).

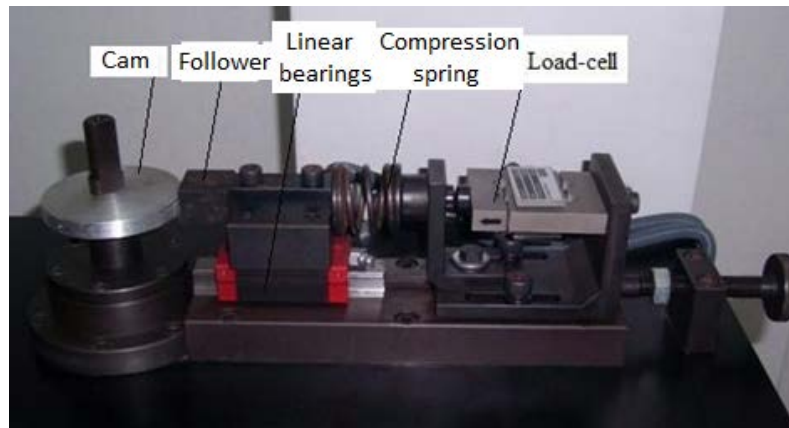


Figure 1-The experimental setup consists of a cam and follower pair

The material of the cycloidal cam profile is PTFE materials and 10 mm thick, and had a 6 mm eccentricity (Figure1). The follower counter-face wear surface was made of high speed steel, in order to ensure that the normal force behind 20 N / mm spring constant bass with spring is located. Approximate, a range of the 30N spring load shall be applied as a pre-load at the point where the cam radius is minimum. Thus, it is applied between 30 N to 270 N spring force to first round of the cam. an electric motor is used with inverter converting speed between 1365 rpm to 610 rpm, the speed transferred by the action of the cam shaft and belt transmission. The follower and linear bearings have mass of 1294 g.

The cam and followers materials toughness are tried to keep the maximum level so the followers are neglected to wear. The dimensions of the cam profile sizes are measured before test and after test with the coordinate measuring machine (CMM). Prior to specified cam angle, and then the difference between the results of the test results is formed which determines the depth of wear. The Experiments reveal that about 150000 cycles turning the wears appear on cam. The wear rate of the so-called K value is same for the cam and followers and also same for pin on disk apparatus '183.10⁻⁴ mm³ / (Nm)' was determined [7] for the High speed steel PTFE materials.

3. MATHEMATICS MODEL

The wear at the centered freak cycloidal cam profile is rotating against to flat surface followers, taken together with the geometry and touching load is required to be introduced as an analytical. Cam and follower mechanism also functions as the rolling of the flat surface corresponding to a follower two-dimensional disk. The cam geometric center radius 'R' and the center of rotation center 'e' size away from the geometric center and cam geometry width is defined as 'b'. Total wear of the system will be partitioned (for example, the follower wear will be ignored). touching conditions for all periods, so as to conform to the fixed coordinate system is expressed using the angular coordinates. The method of estimating the depth of wear at the contact point between cam and followers as it is expressed within 'equation1', 'Archard wear equation' will be used. The cam wear depth after the first cycle to be calculated by 'equation 1'



Figure 2.Cam Profile

$$h_1 = \frac{K \cdot F_n}{b} \tag{1}$$

Normal force components subject to said equation (F_n), the spring preload force, the sum of the spring force and the inertia force.

$$F_n = k \cdot d_0 + k \cdot s(\theta) + m \cdot a$$

If F_n replaces the equation 1,

$$h_1 = \frac{K(k \cdot d_0 + k \cdot s(\theta) + m \cdot a)}{b} \quad (2)$$

The second round of the erosion occurred in previous cycles in depth account of the depth of wear will occur as a result of the cam is also taken into account. In this case

$$h_2 = \frac{K}{b} (k \cdot (d_0 - h_1) + k \cdot (s(\theta) - h_1) + m \cdot \ddot{s}(\theta)) \quad (3)$$

The movement which was built with a center of rotation of the cam to the audience to distance from the geometric center is defined by simple harmonic motion. Displacement of cycloidal motion equation 4 is also the expression [8].

$$s(\theta) = \left(\frac{\theta}{180} - \frac{1}{2\pi} \sin 2\theta \right) H \quad (4)$$

Acceleration equations are expressed as equations 5.

$$\ddot{s} = \frac{2}{\pi} \sin 2\theta \cdot \omega^2 \cdot H \quad (5)$$

Displacement and acceleration we include express the equation 2,

$$h_1 = \frac{K}{b} (k \cdot d_0 + k \cdot \left(\frac{\theta}{180} - \frac{1}{2\pi} \sin 2\theta \right) \cdot H + \frac{2}{\pi} \sin 2\theta \cdot \omega^2 \cdot m \cdot H) \quad \text{it becomes.}$$

Cam must take into account the previous total wear depth from about transfer to the account at the end of each cycle wear depth. Therefore express some definitions will be made to convert more of them available.

$$K / b = C, \left(\frac{\theta}{180} - \frac{1}{2\pi} \sin 2\theta \right) = B, \frac{2}{\pi} \sin 2\theta \cdot \omega^2 \cdot m = A \quad \text{If defined as the following equation 3 becomes it.}$$

$$h_2 = C \cdot [k(d_0 - h_1) + k \cdot B \cdot (H - h_1) + A(H - h_1)]$$

Processing result

$$h_2 = h_1(1 - C(k + Bk + A))$$

Obtained wear depth in every period of this expression can be calculated with Equation 6 generalized door.

$$h_n = h_1 \left(1 - \frac{K}{b} (k + k \left(\frac{\theta}{180} - \frac{1}{2\pi} \sin 2\theta \right) + m \cdot \omega^2 \cdot \frac{2}{\pi} \sin 2\theta) \right)^{n-1} \quad (6)$$

The total depth of wear at the end of the desired speed of the cam can be calculated by Equation 7.

$$h_{top} = \sum_{N=1}^n h_N = h_1 \frac{1 - \left(1 - \frac{K}{b} (k + k \left(\frac{\theta}{180} - \frac{1}{2\pi} \sin 2\theta \right) + m \cdot \omega^2 \cdot \frac{2}{\pi} \sin 2\theta) \right)^n}{1 - \left(1 - \frac{K}{b} (k + k \left(\frac{\theta}{180} - \frac{1}{2\pi} \sin 2\theta \right) + m \cdot \omega^2 \cdot \frac{2}{\pi} \sin 2\theta) \right)} \quad (7)$$

The comparison is made with the measured results of the CMM consists of a total depth of wear in different angles like Table 1.

Table 1. Total depth of wear at different angles of rotation round after Cam 150000.

Cam angle (degree)	Total wear depth (mm) (theoric) h_{top}	Measured (experimental) total wear depth (mm)
30	1,465	1,670
60	2,196	2,503
90	2,776	3,164
120	3,281	3,740
150	3,830	4,366
180	4,458	5,082

210	3,830	4,366
240	3,281	3,740
270	2,776	3,164
300	2,196	2,503
330	1,465	1,670
360	0,626	0,714

As shown in Table 1, due to the maximum depth of wear laws take effect at the location where the force reaches the maximum value of about 180 degrees.

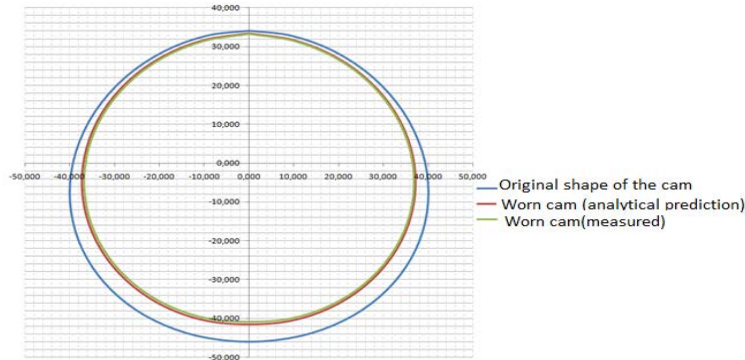


Figure 3. Comparisons between the measured analytical and for the cam shape

4. RESULTS AND DISCUSSION

Figure 3 plots the worn cam profile coordinates from the analytical model and the experimentally measured data from the CMM after 150 thousand cycles. Overall, the numerical model with the accelerated wear-rate, the analytical model with the assumed circular wear shape progression, and the experiment are in close agreement. The difference between the predicted shape and the measured shape is within 5 percent. Better agreement between the models and the experimental results could be obtained by fitting a wear-rate to the experimental results. However, the intention of this study was to investigate the suitability of making predictions of a wearing mechanism's performance without having to perform such curve fitting, using parameters gathered from other more simple laboratory measurements. Thus, no parameters were fit to the data, and the good agreement is encouraging. There are some differences between the shapes of the measured and predicted R and H curves; perhaps this suggests the need for cycle dependent wear rates in future modeling [6]. These results are acceptable in terms of gaining the ability to predict the wear depth feature that may occur. Therefore, it sets forth the mathematical model may be useful in different pairs of materials, or a different speed and number of turns. In the literature, in order to facilitate mathematical operations. In the literature, it is composed of only the spring force of the force components in order to simplify mathematical operations therefore valid model for conditions that limit the effect of inertial forces can be neglected in size available. However, these studies have been included to the model the impact of the inertia force and work has moved a step further by developing a model that can be used.

REFERENCES

- [1]. Özmen, Y., "Makine elemanlarının Tribolojik Hasarları ve Uygun Malzeme Seçimi", Makine Teknolojileri Elektronik Dergisi, 2004(1):31-37
- [2]. Fries, R.H. ve Rogers, C.A., "Predictions of Cam Wear Profiles", Proceedings of the 15 th Leeds-Lyon Symposium on Tribology, Leeds, Semp., 1988, 101-109.
- [3]. Podra, P. Ve Andersson, S., "Simulating Sliding Wear With Finite Element Method", Tribol. Int., 32, 71-81, 1999.
- [4]. Blanchet, T.A., "The Interaction of Wear and Dynamics of a Simple Mechanism", ASME, J. Tribol., 119, , 597-599, 1997.
- [5]. Sawyer, W.G., "Wear Predictions for a Simple-Cam Including the Coupled Evolution of Wear and Load", Lubr. Eng., 31-36, 2001.
- [6]. Dickrell III, D.J., Dooner, D. B. ve Sawyer, W. G., "The Evolution of Geometry for a Wearing Circular cam: Analytical and Computer Simulation With Comparison to "Experiment", Journal of Tribology, 125, 187-192, 2003.
- [7]. Engineering-abc.com, <http://www.tribology-abc.com/sub24.htm> [Erişim Tarihi; 10 Ocak 2008].

Biography

I was born in 1977 in Istanbul. I graduated from mechanical engineering from the Yildiz Technical University in 1999. I received the Ph.D. degree in mechanical engineering from the Yildiz Technical University in 2012. I am an Assistant Professor in the Department of Marine Engineering Operations at the Yildiz Technical University since 2014.

The Effect of Operating Parameters on Energy Consumption in the Treatment of Pistachio Processing Industry Wastewaters (PPIW) Using Electrocoagulation Process with Iron Plate Electrodes

Serkan Bayar^{1}, Recep Boncukcuoglu¹, Alper Erdem Yilmaz¹*

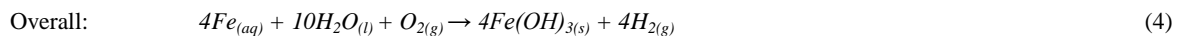
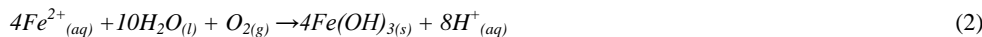
Abstract

The aim of study is to investigate the effect of operating parameters (such as stirring speed, initial pH, current density and supporting electrolyte concentrate) on energy consumption in the treatment of Pistachio Processing Industry Wastewaters (PPIW) using electrocoagulation process with iron plate electrodes. The energy consumption parameter is very important for electrochemical processes. The largest expense in electrochemical treatment processes is specific energy cost since no additional chemicals are needed. It is a requirement in electrochemical treatment and in the determination of optimum working conditions that the conditions where the best removal is performed as well as the lowest energy consumption is provided should be taken into consideration. We have examined the effect of stirring speed, initial wastewater pH value, current density and support electrolyte concentrations on the energy consumption. The obtained experimental results showed increasing current density and stirring speed energy consumption increased. But, increasing the supporting electrolyte concentration increased conductivity of wastewater and decreased energy consumption. In the pH experiment the highest energy consumption is experienced at initial pH of 5. In the experiments lowest energy consumption values have been obtained 16.20 kWhm⁻³ (for 200 rpm); 11.70 kWhm⁻³ (for pH 9); 2.40 kWhm⁻³ (for 1 mM-2) and 9.90 kWhm⁻³ (for 100 mmol NaCl) respectively.

Keywords: Electrocoagulation, energy consumption, pistachio processing industry

1. INTRODUCTION

Turkish Pistachio processing industry is a rapidly developing industry in Turkey. The harvest of pistachio was about 144,000 tons, in 2015 [1]. Pistachio processing industry produces approximately 6 m³ of wastewater per ton of pistachio. Wastewaters resulting from the processing of pistachio contain high levels of organics such as total phenol (TP), chemical oxygen demand (COD) and biochemical oxygen demand (BOD) [2]. One of the treatment methods, which can be used for the removal high organic pollutants is electrocoagulation (EC). Electrocoagulation is an alternative technology for wastewater treatment systems and most effective in removing inorganic and organic contaminants and pathogens. Electrocoagulation process has many advantages such as simple equipment, easy operation and compatibility with automation system, a short retention time, low sludge production and less chemical requirement. Electrocoagulation is most commonly used in the electrochemical treatment processes. Electrocoagulation is a process consisting of creating a floc of metallic hydroxides within the effluent to be cleaned, by electrodisolution of soluble anodes. The most commonly used electrodes in the electrocoagulation process are aluminum and iron [3]. When using iron electrodes the reactions take place as follows [4-5]



Aim of this investigation is to evaluate the effect of operating parameters on energy consumption in the treatment of (PPIW) using electrocoagulation process with iron plate.

2. MATERIAL AND METHOD

¹Atatürk University, Engineering Faculty, Department of Environmental Engineering 25240, Erzurum, Turkey
sbayar@atauni.edu.tr

The wastewater used in this work was collected from pistachio processing plant Gaziantep (Turkey). The chemical analysis of (PPIW) was given in Table 1. The pH of the wastewater was adjusted to at the desired value by adding 0.1 M nitric acid and 0.1 M sodium hydroxide. All chemicals were at analytical grade and supplied by Merck. The experiments carried out in a 1000 mL batch reactor made of plexiglass. Five anode plate electrodes and five cathode plate electrodes were constructed in the electrochemical reactor. The gap between electrodes was fixed at 0.5 cm. The effective surface area of the electrodes approximately 1000 cm² were arranged. The experimental setup is shown in Fig. 1. The current was maintained to be constant by means of a precision DC power supply (GW GPC-3060D) characterized by the ranges from 0 to 6 A for current and 0 to 30 V for voltage. The pH and conductivity were measured by a multimeter (WTW, Multiline 340i). The specific energy consumption was calculated by the following equation [6-7];

$$E(\text{kWhm}^{-3}) = \frac{V \cdot I \cdot t}{v} \quad (1)$$

where, E is electrical energy consumption (kWhm⁻³), V is average cell voltage (volt), I is current density (mAcm⁻²), t is electrolysis duration (min) and v is volume of the wastewater (m³).

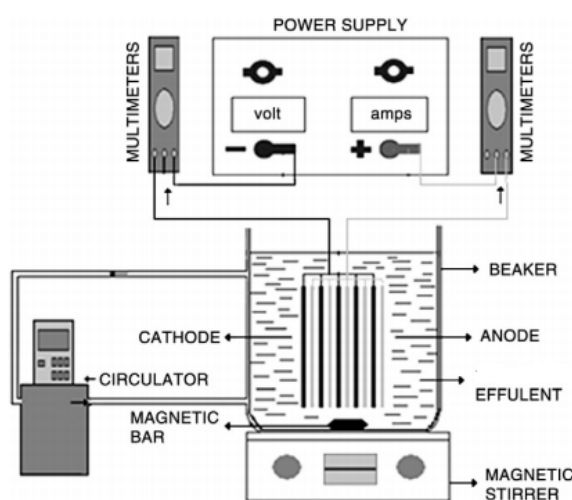


Figure 1. Schematic view of the experimental system

Table 1. The characterization of Pistachio Processing Industry Wastewaters

Parameters	Units	Values
Conductivity	(μs cm ⁻¹)	4.750 - 5.750
Turbidity	(NTU)	150 - 250
pH	-	5.0-5.50
COD	(mg L ⁻¹)	15.000-18.000
TOC	(mg L ⁻¹)	5.000 – 5.500
Total Phenol	(mg L ⁻¹)	3.800 - 4.500
Oil-Grease	(mg L ⁻¹)	50 - 59
Cl	(mg L ⁻¹)	600-650

3. RESULTS AND DISCUSSIONS

3.1. The Effect of Stirring Speed on the Energy Consumption

The mixing of the reactor contents provides uniform distribution of electrochemically generated the coagulant matter. Also, the mixing of the reactor contents cause the homogenization of system variables such as the temperature and the pH [2]. The effect of stirring speed (SS) on energy consumption in the experiments were examined in the range of 100-500 rpm and are presented in Fig. 2. In the experiments were kept at initial pH 5.20 (natural pH), current density 3 mAcm^{-2} and the temperature 293 K. When Fig. 2 is considered, the energy consumption values for 100, 200, 300, 400 and 500 rpm calculated to be 16.20; 18; 19.80; 21.60 and 23.40 kWhm^{-3} , respectively. Findings showed that it deposited between electrodes because of iron electrochemically solved in reactor could not mix homogeneously and this deposition caused increase of cell resistance at low stirring speed. As the cell resistance increased consumed energy amount per unit volume. The reason for high stirring speed to increase energy consumption is slow electron flow or additional resistance due in the reactor creating negative pressure on the flow of electrons [2].

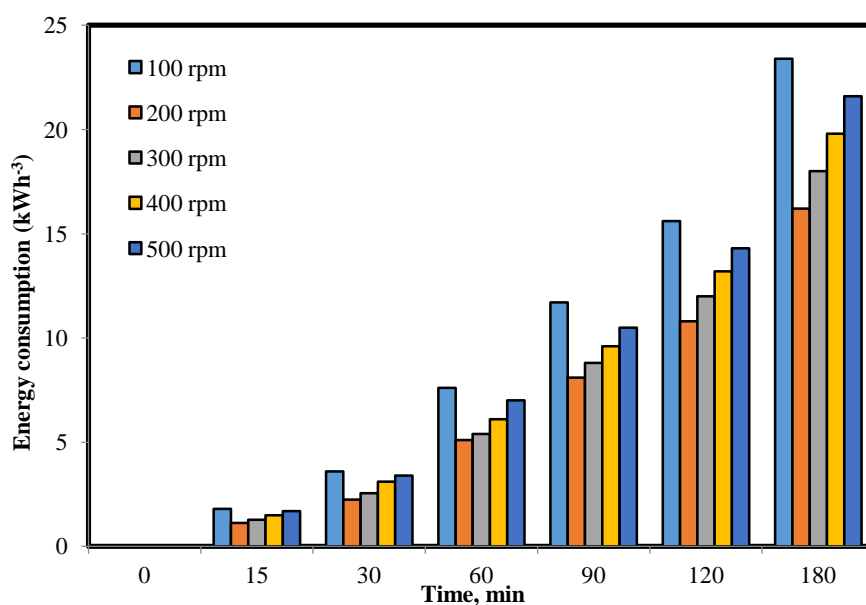


Figure 2. The effect of stirring speed on the energy consumption ($I=3 \text{ mAcm}^{-2}$; $\text{pH}=5.20$ ve $T= 293 \text{ K}$)

3.2. The Effect of initial pH on the Energy Consumption

In this study the effect of initial pH values on energy consumption were examined in the range of 2 - 9. In the experiments were kept at $I: 3 \text{ mAcm}^{-2}$, $SS: 200 \text{ rpm}$ and the $T: 293 \text{ K}$. The effect of current density on energy consumption is shown Fig 3. As seen in Fig. 3, system energy consumption has been affected from initial pH and the lowest energy consumption is experienced at initial pH of 9 followed by pH 2. For example, system energy consumptions are $11,70 \text{ kWhm}^{-3}$ for $\text{pHi} 9$ and 12.60 kWhm^{-3} for $\text{pHi} 2$. In order to adjusted pH of wastewater HNO_3 and NaOH were added in the solution. This situation caused to increase of electrical conductivity of wastewater and as a consequence low energy consumption values were obtained.

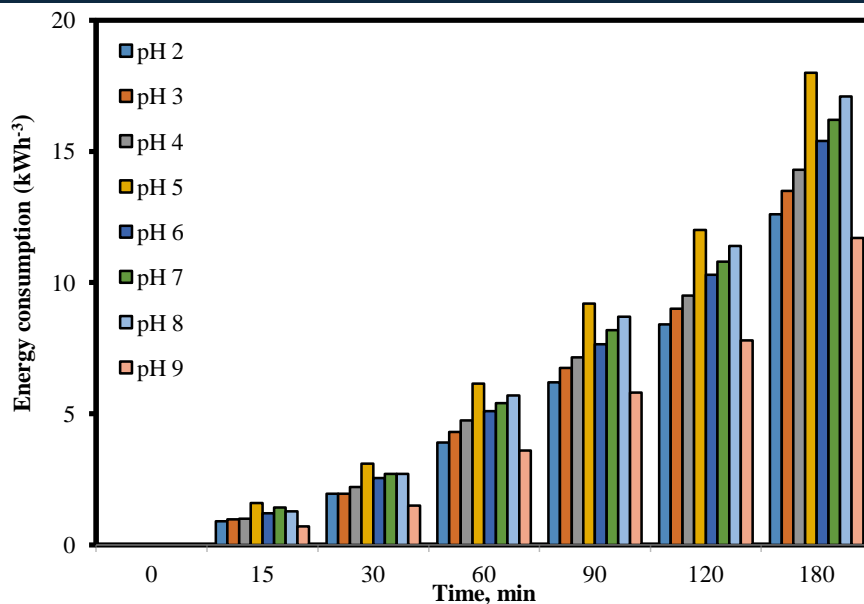


Figure 3. The effect of initial pH on the energy consumption ($I=3 \text{ mA cm}^{-2}$; $SS=200 \text{ rpm}$ ve $T= 293 \text{ K}$)

3.3. The Effect of Current Density on the Energy Consumption

Current density is one of the most important operating parameters (perhaps the most important one) for the electrochemical processes [8], which can determine the applicability of treatment technique is the operational cost of the system. The effect of current density on energy consumption in the experiments were examined in the range of 1-6 mAcm^{-2} . Throughout experiments initial pH was 5.20 (natural pH), stirring speed was 200 rpm and the temperature was 293 K. The effect of current density on energy consumption is shown Fig 4. As can be seen from Figure 4, of 2.4; 4.8; 9; 14.4; 22.5 and 34.2 kWhm^{-3} were obtained under a current density of 1, 2, 3, 4, 5 and 6 mAcm^{-2} respectively. The results indicated that the energy consumption values increased with the increase in the current density values. This situation was explained, as the current density increases the potential difference applied to the system also increases and the energy consumption rate also increases as seen in with Equation 1 [9].

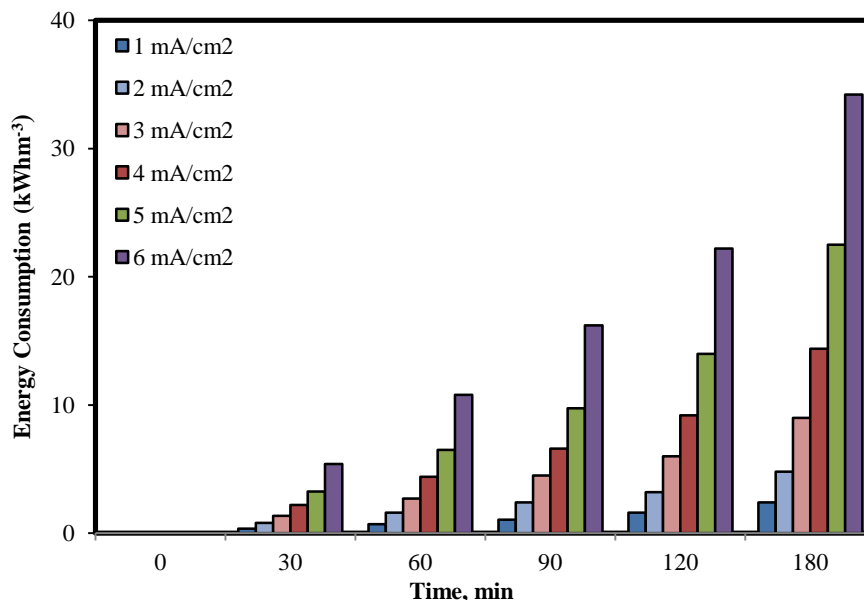


Figure 4. The effect of current density on the energy consumption ($pH= 7$; $SS: 200 \text{ rpm}$, $T: 293 \text{ K}$)

3.4. The Effect of Support Electrolyte Concentration on Energy Consumption

In the experiments, NaCl was used as support electrolyte. The effect of support electrolyte concentration on energy consumption in the experiments were examined in the range of 0-100 mM NaCl and the results are given Fig 5. Throughout experiments initial pH was 7, SS was 200 rpm, current density was 3 mA cm^{-2} and the temperature was 293 K. As can be seen from Figure 5, of 17.1; 15.9; 14.1; 12.8; 11.7; 10.8 and 9.9 kWh m^{-3} were obtained for NaCl concentration of 0; 10; 20; 30; 40; 50 and 100 mM respectively. The results indicated with the increase in supporting electrolyte concentration reduce the energy consumption values. This situation was explained increasing supporting electrolyte concentration applied potential decreased and the conductivity of solution increased under constant current density and so reduce energy consumption values.

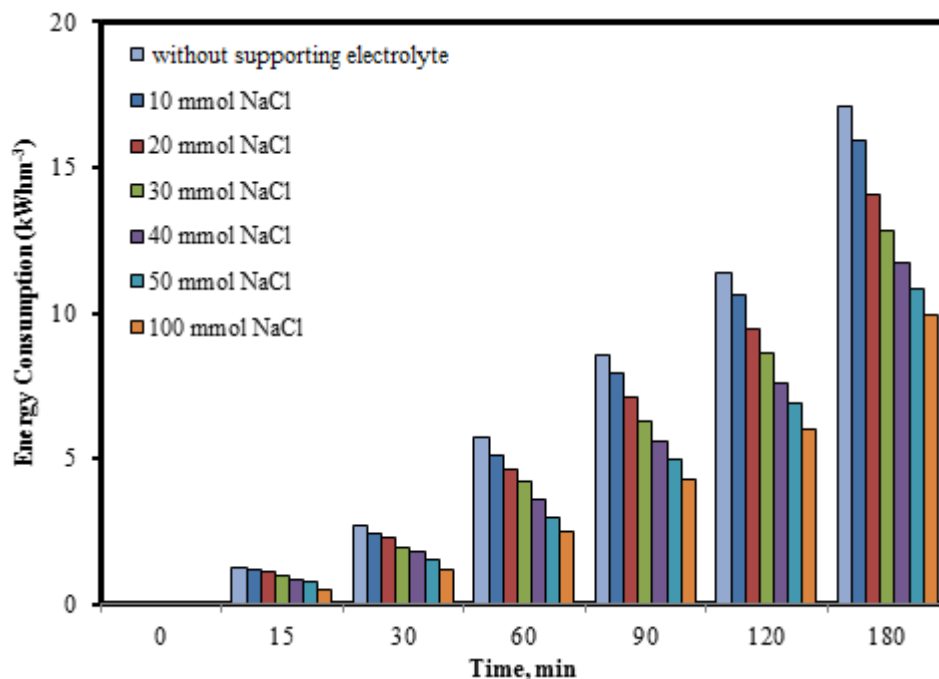


Figure 5. The Effect of Support Electrolyte Concentration on Energy Consumption ($I = 3 \text{ mA cm}^{-2}$, $\text{pH} = 7$, $\text{SS} = 200 \text{ rpm}$; $T = 293 \text{ K}$)

4. CONCLUSIONS

The most important operating costs for the electrochemical processes is the cost of electricity consumed by the system. Operating parameters were determined as initial pH of wastewater, current density, stirring speed and supporting electrolyte concentration. The following results were obtained:

- In the stirring speed experiments lowest energy consumption value was obtained at the 200 rpm stirring speed.
- An increase in current density from 1 to 6 mA cm^{-2} increased at energy consumption values clearly.
- In the initial wastewater pH experiments lowest energy consumption value was obtained at initial pH of 9 followed by pH 2.
- Increasing supporting electrolyte concentration decreased energy consumption values.

ACKNOWLEDGMENTS

This research was supported by the research project (BAP Code: 2011/147) by Atatürk University, Scientific Research Projects (BAP) Program, Erzurum, Turkey.

REFERENCES

- [1] (<http://www.tarimkredi.org.tr/index.php/tr/haber-arsivi/6942-2015-y-1-f-st-k-rekolte-tahmini-144-bin-112-ton.html>)
- [2] S. Bayar, R. Boncukcuoğlu, A. E. Yılmaz and B.A. Fil, "Pre-Treatment of Pistachio Processing Industry Wastewaters (PPIW) by Electrocoagulation using Al Plate Electrode," Separation Science and Technology Vol. 49, pp.1008-1018, Issue 7, 2014.
- [3] Y.S. Yıldız, A.S. Kopalal, S.İrdemez and B.Keskinler, "Electrocoagulation of synthetically prepared waters containing high concentration of NOM using iron cast electrodes," Journal of Hazardous Material. 139, pp.373-380, 2007.
- [4] M.Y.A Mollah, R.Schennach, J.R.Parga, D.L. Cocke, Electrocoagulation (EC): Science and applications. Journal of Hazardous Material. 84, pp.29-41. 2001.
- [5] I.B. Hariz, A. Halleb, N.Adhoum and L.Monser "Treatment of petroleum refinery sulfidic spent caustic wastes by electrocoagulation," Separation and Purification Technology 107, pp.150-157, 2013.
- [6] A.S. Kopalal, Y.S. Yıldız, B. Keskinler and N. Demircioğlu, "Effect of initial pH on the removal of humic substances from wastewater by electrocoagulation," Separation and Purification Technology, 59, pp.175-182. 2008.

- [7] F.Akbal and S.Camci, "Treatment of Metal Plating Wastewater by Electrocoagulation," Environmental Progress & Sustainable Energy, Vol.31, No.3, 2011.
- [8] A.E. M. Hisham Elnenay, E. Nassef, G. F. Malasha, M. H. Abdel Magid "Treatment of drilling fluids wastewater by electrocoagulation," Egyptian Journal of Petroleum doi:10.1016/j.ejpe.2016.03.005, 2016.
- [9] E. Yilmaz, S. Bayar, R. Boncukcuoğlu and B.A. Fil, "Removal of Cadmium by Electrocoagulation and a Cost Evaluation" Ekoloji 21, 85, 26-33, 2012.

The Thermal Stress Analysis of One- and Two-Dimensional Functionally Graded Circular Plates for In-Plane Sinusoidal Heat Flux

M. Didem Demirbas¹, M. Kemal Apalak²

Abstract

This study addresses thermal residual stress analysis of one- and two-dimensional functionally graded clamped hollow circular plates under in-plane sinusoidal heat flux for different compositional gradient exponents. The material properties of the functionally graded circular plates were assumed to vary with a power law along an in-plane direction. The transient heat condition and Navier's equations in polar coordinates which describe the two-dimensional thermo-elastic model were discretized using finite-difference method, also the set of linear equations were solved using the pseudo-singular-value method. In order to determine the effect of the plate material properties on the thermal strain and stress states, the plates were designed as one-dimensional functionally graded circular plates (1D-FGCP) and two-dimensional functionally graded circular plates (2D-FGCP). According to the result of the study, 1D-FGCP and 2D-FGCP exhibited similarities in temperature distributions, but differences in stress and strain distributions. In case of 2D-FGCP compared to in case of 1D-FGCP, the levels of temperature and stress had similar, however, levels of strain increased. When the compositional gradient exponent was changed from ceramic-rich to metal-rich compositions, the stress levels were not affected considerably, whereas the stress distributions changed. The strain levels increased and distributions were affected considerably with the increasing of the exponent of compositional gradient. The study showed that two-dimensional graded is necessary to calculate correctly the actual stress and strain levels and distributions were subjected to sinusoidal heat flux in the functionally graded circular plates.

Keywords: finite difference method, one- and two-dimensional functionally graded circular plate, thermal residual stress analysis

1. INTRODUCTION

The conventional composites show behavior discontinuous stress concentrations in the thermal and structural loads along bi-material interfaces owing to their discontinuous thermal and mechanical properties. The high technology materials capable of withstanding the high-temperature gradients have been studied in many investigations. The functionally gradient materials (FGMs) are one kind of the high technology materials that have been researched to decrease thermal stresses and to eliminate discontinuous stress concentrations [1]. FGMs overcome the disadvantage of the conventional composites plates that have been used as thermal barriers in the space planes, ultra-supersonic airplanes for the super-sonic transport, nuclear fusion reactors, and similar structures [2]-[3]. Reddy [4] presented the material distribution affected the through-thickness strain and stress states of functionally graded plates (FGPs). Reddy and Chin [5] studied a thermo-elastic boundary value problem for FGPs using plate theory and explained that the thermo-mechanical coupling played a significant role when the power law exponent changed. Reddy and Cheng [6] presented the result of FGPs of thermo-elastic deformations of simply supported by using an asymptotic method. They found that the assumption of a constant through-thickness deflection generally was made by 2-D plate theories which invalid for the thermal load, but this assumption is a good approximation for the mechanical load.

The composition variation and size of the through-thickness functionally gradient materials layer have an impact on the thermal stress distribution [7]. Besides, the averaging estimation methods and the finite element models reveal considerable differences in thermal stress distributions [8]-[9].

Apalak ve Bagci [10-13] analyzed the thermo-elastic response of functionally graded plates and adhesively bonded functionally graded rectangular and circular hollow plates with temperature-independent, in-plane, not through thickness, material composition variation subjected to an in-plane different heat flux. They expressed that type of in-plane heat flux affected heat transfer period and temperature levels, the residual thermal stresses were strongly dependent on the in-plane material composition gradient. They could be decreased by altering in-plane material composition. Nemat Alla [14] introduced a two-dimensionally functionally graded material (2D-FGM) to withstand the peak temperatures and to give more reduction in thermal stresses. He presented the suitable functions that can represent volume fractions of the introduced 2D-FGM and derived based on the volume fractions of the 2D-FGM and the rules of mixture of the conventional FGM. Besides, he compared between 2D-FGM and conventional

¹ Corresponding author: Erciyes University, Department of Mechanical Engineering, 38039, Melikgazi/Kayseri, Turkey.
mddemirbas@erciyes.edu.tr

² Erciyes University, Department of Mechanical Engineering, 38039, Melikgazi/Kayseri, Turkey.
apalakmk@erciyes.edu.tr

FGM and showed that 2D-FGM has high capability to reduce thermal stresses than the conventional FGM. Nemat-Alla et al. [15] also studied the elastic-plastic stress behaviors of the 2D-FGMs. They proposed a 3D finite element model of the 2D-FGM plates and found that heat conductivity of the constituents of FGM which has a major effect on the temperature distributions. The current studies have focused thermo-elastic or plastic stress analyses on the one- or two-dimensional functionally graded plates, and these structures are assumed as a functionally graded composition variations through the thickness. Nowadays, fuel cell technology applies successfully FGMs to solid oxide fuel cells in order to reduce thermal expansion coefficient mismatch between electrolyte and anode [16]. Wang et al. [17] examined inclusively five categories of fuel cells, and related studies. Fuel cells are popular examples that conductive and convective heat transfers, and mass transfer, multiple fluids flows moreover electrochemical reactions are experienced [18, 19]. Consequently, a tubular or planar design of a solid oxide fuel cell can experience in-plane or through-thickness heat transfer due to heat fluxes. Thus, an in-plane one- or two-dimensional functionally graded material distribution requires a theoretical investigation for the practical applications.

2. MATERIALS AND METHODS

In the current study, the FGPs have a material composition of two constituents, ceramic and metal, and the material composition is one- or two-directional in the plate plane. The material properties of the FGCPs at every point and thermal-stress analyses are explained as:

2.1. Material Properties

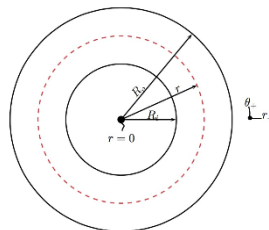


Figure 1. Functionally graded clamped circular plate

This study are assumed that the FGPs are designed as a homogeneous isotropic graded layer along the radial and tangential directions between ceramic and metal phases. The volume fraction of the ceramic (c) phase at every all position of the plate follows the power law as

$$V_c^r(\bar{r}) = \left(\frac{\bar{r}}{l}\right)^n \quad (1)$$

$$V_c^\theta(\theta) = (|\sin(p\theta)|)^m \quad (2)$$

$$V_c(\bar{r}, \theta) = V_c^r(\bar{r})V_c^\theta(\theta) \quad (3)$$

$$V_m(\bar{r}, \theta) = 1 - V_c(\bar{r}, \theta) \quad (4)$$

The ceramic volume fraction of the plate abide by the power law as, for the metal volume fraction of the plate, where r and θ are considered as distance along in-plane radial and tangential directions, respectively. n and m compositional gradient exponents along the r - and θ - directions, respectively. $\bar{r} = r - R_i$ is the radial distance from the inner edge of the circular plate, and $l = R_o - R_i$ is the circular plate length (Figure 1). R_i and R_o are the inner and outer radius of the circular plate, respectively. ' p ' is a period of periodic functions. The thermal, physical and mechanical properties of the constituents of $Ni-Al_2O_3$ composite material are explained in Table 1. The simple estimation method is the linear rule of the mixtures in which a material properties P at any point r and θ in the graded region are determined in terms of the linear combination of volume fractions of ceramic (c) and metal (m) as:

$$P(\bar{r}, \theta) = V_c(\bar{r}, \theta)P_c(\bar{r}, \theta) + V_m(\bar{r}, \theta)P_m(\bar{r}, \theta) \quad (5)$$

Tomota et al. [20] offered a mixtures rule for the elasticity modulus as

$$E(\bar{r}, \theta) = \left[\left(\frac{q + E_c}{q + E_m} \right) V_m E_m + V_c E_c \right] \left[\left(\frac{q + E_c}{q + E_m} \right) V_m + V_c \right]^{-1} \quad (6)$$

where E_c and E_m modulus of ceramic and metal phases, respectively, and a value $q=500$ GPa is recommended [7]. Wakashima-Tsukamoto [21] makes statement necessitate that the overall thermal expansion coefficient (α) for a diphase material is connected the averaged bulk modulus (K) using the Levin relation [22].

$$\alpha(r, \theta) = \alpha_m + \left(\frac{1}{\bar{K}} - \frac{1}{K_m} \right) \frac{(\alpha_c - \alpha_m)}{\frac{1}{K} - \frac{1}{K_m}} \quad (7)$$

$$\bar{K}(r, \theta) = K_m + \frac{\alpha V_c K_m (K_c - K_m)}{V_m K_c + \alpha V_c K_m} \quad (8)$$

and the overall shear modulus (μ) is

$$\bar{\mu}(r, \theta) = \mu_m + \frac{b V_c \mu_m (\mu_c - \mu_m)}{V_m \mu_c + b V_c \mu_m} \quad (9)$$

and where a and b are

$$a = \frac{K_c(3K_m + 4\mu_m)}{K_m(3K_c + 4\mu_c)} \quad b = \frac{(1 + e)\mu_c}{\mu_m + e\mu_c} \quad e = \frac{9K_m + 8\mu_m}{6K_c + 12\mu_m} \quad (10)$$

Table 1. The thermal, physical and mechanical properties of metal (Ni), ceramic (Al_2O_3) used [23].

Property	Unit	Ni	Al_2O_3
Density, ρ	kg/m ³	8880	3960
Thermal conductivity, k	W/m-K	60.5×10^{-3}	46×10^{-3}
Specific heat capacity, c_p	W-h/kg-K	0.11	0.21
Shear modulus, G	GPa	76	150
Bulk modulus, K	GPa	180	172
Coefficient of thermal expansion, α	1/C	6.6×10^{-6}	8.1×10^{-6}

The overall Poisson's ratio (ν) is

$$\nu(r, \theta) = \frac{3K - 2\mu}{2(3K + \mu)} \quad (11)$$

2.2. Heat Transfer

Transient three-dimensional heat transfer equation where $\lambda(r, \theta)$ is the heat conductivity coefficient, $\rho(r, \theta)$ is the density, $c_p(r, \theta)$ is the specific heat capacity,

$$\vec{\nabla}(\lambda \vec{\nabla} T) = \rho c_p \frac{\partial T}{\partial t} \quad (12)$$

$\vec{\nabla}$ del is operator in cylindrical coordinates

$$\vec{\nabla} = \frac{\partial}{\partial r} \vec{e}_r + \frac{1}{r} \frac{\partial}{\partial \theta} \vec{e}_\theta + \frac{\partial}{\partial z} \vec{e}_z \quad (13)$$

For the two-dimensional (plane) case,

$$\frac{\partial \lambda}{\partial r} \frac{\partial T}{\partial r} + \frac{1}{r^2} \frac{\partial \lambda}{\partial \theta} \frac{\partial T}{\partial \theta} + \frac{\lambda}{r} \frac{\partial T}{\partial r} + \lambda \frac{\partial^2 T}{\partial r^2} + \frac{\lambda}{r^2} \frac{\partial^2 T}{\partial \theta^2} = \rho c_p \frac{\partial T}{\partial t} \quad (14)$$

$T(r, \theta, t)$ at the nodal point (i, j) with the coordinate (r, θ) or with respect to time t and the space variables (r, θ) . Herewith, the heat transfer equation (14) can be written in terms of difference equations as

$$T_{i,j}^{k+1} = T_{i,j}^k + \frac{\lambda_{i,j}\Delta t}{(\rho c_p)_{i,j}(r_{i,j})\Delta r}(T_{i+1,j}^k - T_{i,j}^k) + \frac{\lambda_{i,j}\Delta t}{(\rho c_p)_{i,j}(\Delta r)^2}(T_{i+1,j}^k - 2T_{i,j}^k + T_{i-1,j}^k) + \frac{\lambda_{i,j}\Delta t}{(\rho c_p)_{i,j}(r_{i,j})^2(\Delta\theta)^2}(T_{i,j+1}^k - 2T_{i,j}^k + T_{i,j-1}^k) \quad (15)$$

Where $r_{i,j}$ is the radial distance at point (i, j) and Δr , $\Delta\theta$, and Δt , are space and time increments, respectively. The finite difference method requires that the plates be divided into a mesh of $n_r \times n_w$ divisions along the coordinates r and θ , respectively. The equation (15) we obtain for the internal grid points along $i = [2: n_r - 1]$ and $j = [2: n_w - 1]$, respectively. The equation (15) be inappropriate at the grid points along both the inner and outer edges $i = 1$ and $i = n_r$, $j = [1: n_w]$. Thus, the equation (15) can be arranged on thermal equilibrium of that cell as follows: for all grid points at $i = [2: n_r - 1]$ and $j = 1$ to $j - 1 \rightarrow n_w$, $j = n_w$ to $j + 1 \rightarrow 1$ are written.

$$T_{i,j}^{k+1} = T_{i,j}^k + \frac{\lambda_{i,j}\Delta t}{(\rho c_p)_{i,j}(r_{i,j})\Delta r}(T_{i+1,j}^k - T_{i,j}^k) + \frac{\lambda_{i,j}\Delta t}{(\rho c_p)_{i,j}(\Delta r)^2}(-T_{i+3,j}^k + 4T_{i+2,j}^k - 5T_{i+1,j}^k + 2T_{i,j}^k) + \frac{\lambda_{i,j}\Delta t}{(\rho c_p)_{i,j}(r_{i,j})^2(\Delta\theta)^2}(T_{i,j+1}^k - 2T_{i,j}^k + T_{i,j-1}^k) \quad (16)$$

for all grid points at $i = 1$ and $j = [1: n_w]$.

$$T_{i,j}^{k+1} = T_{i,j}^k + \frac{\lambda_{i,j}\Delta t}{(\rho c_p)_{i,j}(r_{i,j})\Delta r}(T_{i,j}^k - T_{i-1,j}^k) + \frac{\lambda_{i,j}\Delta t}{(\rho c_p)_{i,j}(\Delta r)^2}(-T_{i-3,j}^k + 4T_{i-2,j}^k - 5T_{i-1,j}^k + 2T_{i,j}^k) + \frac{\lambda_{i,j}\Delta t}{(\rho c_p)_{i,j}(r_{i,j})^2(\Delta\theta)^2}(T_{i,j+1}^k - 2T_{i,j}^k + T_{i,j-1}^k) \quad (17)$$

for all grid points at $i = n_r$ and $j = [1: n_w]$.

$$T_{i,j}^{k+1} = T_{i,j}^k + \frac{\lambda_{i,j}\Delta t}{(\rho c_p)_{i,j}(r_{i,j})\Delta r}(T_{i+1,j}^k - T_{i,j}^k) + \frac{\lambda_{i,j}\Delta t}{(\rho c_p)_{i,j}(\Delta r)^2}(T_{i+1,j}^k - 2T_{i,j}^k + T_{i-1,j}^k) + \frac{\lambda_{i,j}\Delta t}{(\rho c_p)_{i,j}(r_{i,j})^2(\Delta\theta)^2}(T_{i,j+1}^k - 2T_{i,j}^k + T_{i,j-1}^k) \quad (18)$$

2.3. Initial and Boundary Conditions

The initial temperature is given as $T(r, \theta) = 298 \text{ K}$ at $t = 0$, and the thermal boundary conditions are given as

$$q_o = q(R_o, \theta, t) = 200|\sin(0.5\theta)| \quad (19)$$

$$q_i = q(R_i, \theta, t) = 0 \quad (20)$$

The inner edge is subjected to adiabatic conditions. Where q_i and q_o are inner and outer heat fluxes along the radial direction r , respectively. The adaptation of the results of the boundary conditions (19-20) in Equation (14) to be written as, along the outer edge of the circular plate ($r_{n_r,j} = R_o$) with ($i = 1, j = [1: n_w]$) and

$$\frac{(\rho c_p)_{i,j}}{\lambda_{i,j}\Delta t}(T_{i,j}^{k+1} - T_{i,j}^k) = \frac{2q_o}{\lambda_{i,j}\Delta r} + \frac{2}{(\Delta r)^2}(T_{i-1,j}^k - T_{i,j}^k) + \frac{1}{(\Delta\theta)^2}(T_{i,j+1}^k - T_{i,j}^k) + \frac{1}{(\Delta\theta)^2}(T_{i,j-1}^k - T_{i,j}^k) \quad (21)$$

along the inner edge of the circular plate ($r_{1,j} = R_i$) with ($i = 1, j = [1: n_w]$) for adiabatic boundary conditions ($q_i = 0$).

$$\frac{(\rho c_p)_{i,j}}{\lambda_{i,j}\Delta t}(T_{i,j}^{k+1} - T_{i,j}^k) = \frac{2q_i}{\lambda_{i,j}\Delta r} + \frac{2}{(\Delta r)^2}(T_{i+1,j}^k - T_{i,j}^k) + \frac{1}{(\Delta\theta)^2}(T_{i,j+1}^k - T_{i,j}^k) + \frac{1}{(\Delta\theta)^2}(T_{i,j-1}^k - T_{i,j}^k) \quad (22)$$

2.4. Elasticity Equations in Terms of Displacement

Navier's equations of elasticity in the radial and tangential directions are written as ($\bar{T} = T(r, \theta, t) - T_0$ is the temperature difference)

$$(\lambda + 2\mu) \frac{\partial e}{\partial r} - 2\mu \left(\frac{1}{r} \frac{\partial w_z}{\partial \theta} - \frac{\partial w_\theta}{\partial z} \right) - (3\lambda + 2\mu) \alpha \frac{\partial \bar{T}}{\partial r} = 0 \quad (23)$$

$$(\lambda + 2\mu) \frac{1}{r} \frac{\partial e}{\partial \theta} - 2\mu \left(\frac{1}{r} \frac{\partial w_r}{\partial z} - \frac{\partial w_z}{\partial r} \right) - (3\lambda + 2\mu) \frac{\alpha}{r} \frac{\partial \bar{T}}{\partial \theta} = 0 \quad (24)$$

$$e = \frac{1}{r} \frac{\partial(ru)}{\partial r} + \frac{1}{r} \frac{\partial v}{\partial \theta} \quad w_r = \frac{1}{2} \left(\frac{1}{r} \frac{\partial w}{\partial \theta} - \frac{\partial v}{\partial z} \right) \quad w_\theta = \frac{1}{2} \left(\frac{\partial u}{\partial z} - \frac{\partial w}{\partial r} \right) \quad w_z = \frac{1}{2r} \left(\frac{\partial(rv)}{\partial r} - \frac{\partial u}{\partial \theta} \right) \quad (25)$$

and u, v, w are displacement components in the directions r, θ and z , respectively. For two-dimensional problem,

$$\frac{\partial w_r}{\partial z} = 0 \text{ and } \frac{\partial w_\theta}{\partial z} = 0 \quad (26)$$

Eventually, substituting equations (25) into equations (23) and (24) with the terms (26) yields

$$\left(r^2 \frac{\partial^2 u}{\partial r^2} + r \frac{\partial u}{\partial r} - u \right) - \frac{(\lambda + 3\mu)}{(\lambda + 2\mu)} \frac{\partial v}{\partial \theta} + \frac{(\lambda + \mu)}{(\lambda + 2\mu)} r \frac{\partial^2 v}{\partial r \partial \theta} + \frac{\mu}{(\lambda + 2\mu)} \frac{\partial^2 u}{\partial \theta^2} - \frac{(3\lambda + 2\mu)}{(\lambda + 2\mu)} r^2 \alpha \frac{\partial \bar{T}}{\partial r} = 0 \quad (27)$$

and

$$\frac{\partial^2 v}{\partial \theta^2} + \frac{(\lambda + 3\mu)}{(\lambda + 2\mu)} \frac{\partial u}{\partial \theta} + \frac{(\lambda + \mu)}{(\lambda + 2\mu)} r \frac{\partial^2 u}{\partial r \partial \theta} + \frac{\mu}{(\lambda + 2\mu)} \left(r^2 \frac{\partial^2 v}{\partial r^2} + r \frac{\partial v}{\partial r} - v \right) - \frac{(3\lambda + 2\mu)}{(\lambda + 2\mu)} \alpha r \frac{\partial \bar{T}}{\partial \theta} = 0 \quad (28)$$

and where $\lambda = \lambda(r, \theta)$, and $\mu = \mu(r, \theta)$, $\alpha = \alpha(r, \theta)$. Equations (27-28) can be written in terms of finite difference equations with the boundary conditions as

$$u(r, \theta) = 0 \text{ and } v(r, \theta) = 0 \text{ for } r = R_i \quad (29)$$

$$u(r, \theta) = 0 \text{ and } v(r, \theta) = 0 \text{ for } r = R_o \quad (30)$$

The finite-difference equations of the first- and second-order derivatives of a displacement component, temperature changes $\xi = \xi(r, \theta)$ with the respect to for the internal grid points along internal nodes, equations (27) and (28) we obtain for the internal grid points along $i = [2: nr-1]$ and $j = [2: nw-1]$, respectively.

$$\begin{aligned} & \left(r_{i,j}^2 \frac{u_{i+1,j} - 2u_{i,j} + u_{i-1,j}}{(\Delta r)^2} + r_{i,j} \frac{u_{i+1,j} - u_{i,j}}{\Delta r} - u_{i,j} \right) - \frac{(\lambda + 3\mu)}{(\lambda + 2\mu)} \frac{v_{i,j+1} - v_{i,j}}{\Delta \theta} \\ & + \frac{(\lambda + \mu)}{(\lambda + 2\mu)} r_{i,j} \frac{v_{i+1,j+1} - v_{i+1,j} - v_{i,j+1} - v_{i,j}}{\Delta r \Delta \theta} + \frac{\mu}{(\lambda + 2\mu)} \frac{u_{i,j+1} - 2u_{i,j} + u_{i,j-1}}{(\Delta \theta)^2} \\ & - \left(\frac{3\lambda + 2\mu}{\lambda + 2\mu} \alpha \right) r_{i,j}^2 \frac{\bar{T}_{i+1,j} - \bar{T}_{i,j}}{\Delta r} \end{aligned} \quad (31)$$

$$\begin{aligned} & \frac{v_{i,j+1} - 2v_{i,j} + v_{i,j-1}}{(\Delta \theta)^2} + \frac{(\lambda + 3\mu)}{(\lambda + 2\mu)} \frac{u_{i,j+1} - u_{i,j}}{\Delta \theta} + \frac{(\lambda + \mu)}{(\lambda + 2\mu)} r_{i,j} \frac{u_{i+1,j+1} - u_{i+1,j} - u_{i,j+1} - u_{i,j}}{\Delta r \Delta \theta} \\ & + \frac{\mu}{(\lambda + 2\mu)} \left(r_{i,j}^2 \frac{v_{i+1,j} - 2v_{i,j} + v_{i-1,j}}{(\Delta r)^2} + r_{i,j} \frac{v_{i+1,j} - v_{i,j}}{\Delta r} + -v_{i,j} \right) \\ & - \left(\frac{3\lambda + 2\mu}{\lambda + 2\mu} \alpha \right) r_{i,j} \frac{\bar{T}_{i,j+1} - \bar{T}_{i,j}}{\Delta \theta} \end{aligned} \quad (32)$$

for the internal nodes except for those along the inner and outer edges of the plate. In order to adaptation the boundary condition (29) the second order derivative of a displacement component 'r' in the equations (31) and (32) can be changed with the difference equations

$$\left. \frac{\partial^2 \xi}{\partial r^2} \right|_{i,j} = \frac{-\xi_{i+3,j} + 4\xi_{i+2,j} - 5\xi_{i+1,j} + 2\xi_{i,j}}{(\Delta r)^2} \quad (33)$$

Like wise, the boundary condition (30) the second order derivative of a displacement component r, θ , in the equations (31) and (32) can be changed with the difference equations

$$\left. \frac{\partial \xi}{\partial r} \right|_{i,j} = \frac{\xi_{i,j} - \xi_{i-1,j}}{\Delta r} \quad \left. \frac{\partial^2 \xi}{\partial r^2} \right|_{i,j} = \frac{-\xi_{i-3,j} + 4\xi_{i-2,j} - 5\xi_{i-1,j} + 2\xi_{i,j}}{(\Delta r)^2} \quad (34)$$

$$\left. \frac{\partial \bar{T}}{\partial r} \right|_{i,j} = \frac{\bar{T}_{i,j} - \bar{T}_{i-1,j}}{\Delta r} \quad \left. \frac{\partial^2 \xi}{\partial r \partial \theta} \right|_{i,j} = \frac{\xi_{i,j+1} - \xi_{i,j} - \xi_{i-1,j+1} + \xi_{i-1,j}}{\Delta r \Delta \theta} \quad (35)$$

Navier's equations (27) and (28) are evaluated at all internal and boundary points for the suitable difference equations, and are reduced to a system of linear equations in terms of unknown displacement components. The system of linear equations can be solved into the form $[C] \{u\} = \{B\}$, where $[C]$ is the coefficients matrix of unknown displacement components in the system of linear equations, $\{u\}$ is the vector of unknown displacement components and $\{B\}$ the vector of values in the right hand sides of linear equations. The sparse matrix of coefficients is singular; as a result of, the system of linear equations can be solved for the displacement components using the pseudo singular value methods. The explicit difference equations of the thermal analysis as well as the implicit difference equations of the stress analysis are coded and solved in MATLAB mathematical software [24].

3. RESULTS and DISCUSSION

In this study, the thermo-elastic stress analysis of one-dimensional and two-dimensional functionally graded circular plates was carried out based on two-dimensional heat transfer and elasticity equations. The property distribution of the ceramic to metal composition was designed in the plate plane rather than through the plate thickness. The material composition is considered as a ceramic-to-metal (CM) from pure ceramic outer edge to pure metal inner edge for the FGCPs. The inner and outer radius of plate are 100 mm and 200 mm, respectively. FGCPs have a radial length $l=100$ mm and thickness $t=1$ mm (Figure 1). Asinusoidal heat flux $q_o (R_o, \theta, t) = 200 \sin(0.5\theta)$ was applied in the radial direction along outer edge of the 1D-FGCP and 2D-FGCP, however an adiabatic condition is assumed for inner edge. The compositional gradient exponent n is related to the composition variations in the r -direction and considered as 0.1, 0.5 and 1.0 for 1D-FGCP. As for 2D-FGCP, the compositional gradient exponents n and m are related to the composition variations in the r and θ -directions, respectively, and considered as $n=0.1, 0.5$ and 1.0 that $m=1.0$ is constant. The initial temperature distributions are assumed to be uniform in the hollow circular plates at a temperature of 298 K. The inner and outer edges of the plate are clamped applying $u(r, \theta) = 0$ and $v(r, \theta) = 0$. The thermal analysis was ended when the temperature at a grid point in the plate having coordinates $T(R_o, \pi)$ reached a temperature of 900 K. After the thermal analysis was finished, the temperature distribution at the final time step was used in the thermal stress analysis. The distributions of ceramic volume fraction for $n=0.1, 0.5$, and 1.0 along the plate have been shown in Figure 2. (a). The ceramic phase of the plate decreases as it increases from $n=0.1$ to $n=1.0$. However, this decrease occurs beginning from the inner edge. As for 2D-FGCP, $m=1$ is constant (tangential direction); as it is increased from $n=0.1$ to $n=1.0$, at around $\theta=0^\circ$ of the area the effect of the ceramic rich composition falls in radial direction from the inner edge to outer edge (Figure 2. (c)). In Figure 2. (b) and (d) given the distribution of temperature along the plate for 1D-FGCP and 2D-FGCP. Since the sinusoidal heat flux at the ceramic rich area (at around $\theta=\pi$) is given symmetrically, the temperature distribution in this area occurs as symmetry. As the composition is increased from $n=0.1$ to $n=1.0$, the temperature levels remain unchanged. The temperature distribution, however, is enlarged up to the areas around $\theta=0^\circ$. When the transfer period in 2D-FGCP and 1D-FGCP were compared, the heat transfer period in 2D-FGCP increases by 4%-6% in relation to 1D-FGCP, and the areas affected by maximum temperature narrow toward the

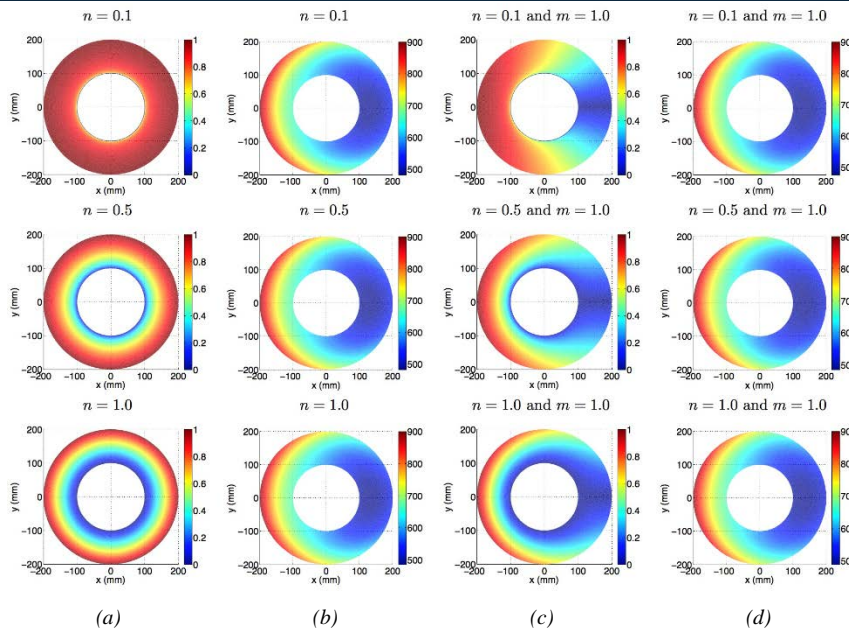


Figure 2. Distribution along the hollow circular plate for different composition gradient exponent in case of 1D-FGCP and 2D-FGCP, (a)-(c) ceramic volume fraction, (b)-(d) temperature (K)

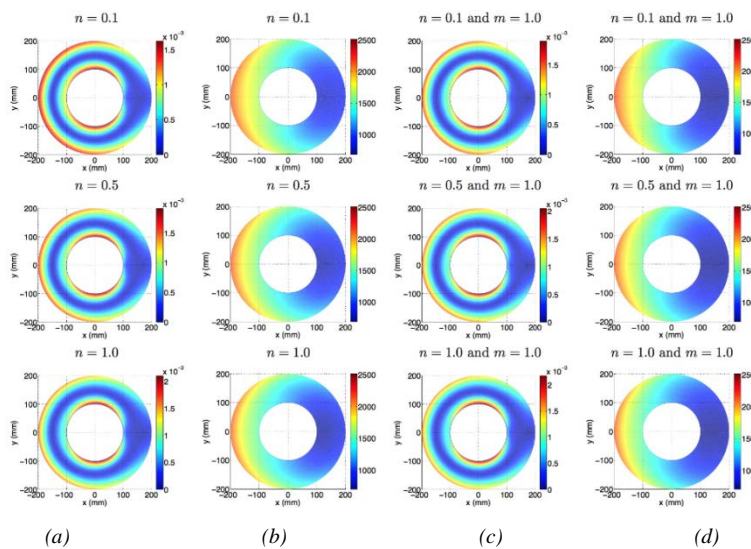


Figure 3. Distribution along the hollow circular plate for different composition gradient exponent in case of 1D-FGCP and 2D-FGCP, (a)-(c) equivalent strain, (b)-(d) equivalent stress (MPa)

right side of the plate. In the Figure 3.(a) and (c), is shown the distribution of equivalent strain for 1D-FGCP and 2D-FGCP. In Figure 3.(a) the levels of maximum equivalent strain for $n=0.1, 0.5,$ and $1.0,$ are $0.0016, 0.0019$ and $0.0021,$ respectively. The distribution, on the other hand, is maximum for ceramic rich composition along the area subjected to heat flux at the side of the outer edge. In addition, strain occurs at maximum levels of the inner edge of the plate depending on its constant edges. With the decrease in ceramic volume fraction, the areas of maximum strain occur in the inner edges of the plate. In Figure 3.(c), the levels of maximum equivalent strain for $n=0.1, 0.5,$ and 1.0 are $0.0019, 0.002$ and $0.0022,$ respectively provided that $m=0.1$ is constant in 2D-FGCP. The areas of maximum distribution occur along the inner and outer edges of the plate, and as the ceramic volume fraction falls the effect of these areas diminishes along the outer edge. In 2D-FGCP, the equivalent strain levels increase and the effect of the areas with maximum distribution decreases compared to 1D-FGCP. In Figure 3.(b) and (d) is given the distribution of equivalent stress along the plate for 1D-FGCP and 2D-FGCP. In 1D-FGCP, the levels of maximum equivalent stress at different compositional gradients are similar. Equivalent stress distributions are formed along the areas subjected to heat flux. The area affected by maximum stress occurs at around $\theta=\pi,$ and these areas narrow and the area of stress affecting the area of $\theta=0^\circ$ narrows as the compositional gradient exponent increases. In the 1D-FGCP and 2D-FGCP, the levels of stress and the distributions of stress present similarities. However, the area of stress distribution in 2D-FGCP narrows pronouncedly in relation to 1D-FGCP.

4. CONCLUSION

As a conclusion, 1D-FGCP and 2D-FGCP exhibited similarities in temperature distributions, but differences in stress and strain distributions. In case of 2D-FGCP compared to in case of 1D-FGCP, the levels of temperature and stress had similar, however, levels of strain increased. When the compositional gradient exponent was changed from ceramic-rich to metal-rich compositions, the stress levels were not affected considerably, whereas the stress distributions changed. The strain levels increased and distributions were affected considerably with the increasing of the exponent of compositional gradient.

REFERENCES

- [1] N. Noda, "Thermal stresses in functionally graded materials," *J. Therm. Stresses*, vol.20, pp. 477–512, 1999.
- [2] N. Noda, "Thermal stresses intensity factor for functionally gradient plate with an edge crack," *J. Therm. Stresses*, vol.20, pp. 373-387, 1997.
- [3] B. D. Choules, K. Kokini, "Architecture of functionally graded ceramic coating against surface thermal fracture," *ASME J. Eng. Mater. Technol.*, vol. 118, pp. 522–528, 1996.
- [4] J. N. Reddy, "Analysis of functionally graded plates", *International Journal for Numerical Methods in Engineering*, vol. 47 (1-3), pp. 63–684, 2000.
- [5] J. N. Reddy, C. D. Chin, "Thermo mechanical analysis of functionally graded cylinders and plates", *Journal of Thermal Stresses*, vol.21 (6), pp. 593–626, 1998.
- [6] J. N. Reddy, Z.-Q. Cheng, "Three-dimensional thermo mechanical deformations of functionally graded rectangular plates". *European Journal of Mechanics -A/Solids*, vol.20 (5), pp. 841 – 855, 2001.
- [7] J. Cho, J. Oden, "Functionally graded material: a parametric study on thermal-stress characteristics using the Crank- Nicolson-Galerkin scheme", *Computer Methods in Applied Mechanics and Engineering*, vol. 188(1-3), pp. 17-38, 2000.
- [8] J. Cho, D. Ha, "Averaging and finite-element discretization approaches in the numerical analysis of functionally graded materials", *Materials Science and Engineering: A*, vol.302 (2), pp.187-196, 2001.
- [9] J. Cho, D. Ha, "Volume fraction optimization for minimizing thermal stress in Ni-AIO3 functionally graded material". *Materials Science and Engineering: A*, vol.334 (1-2), pp.147-155, 2002.
- [10] M.K. Apalak, M.D. Bagci, "Thermal residual stresses in adhesively bonded in-plane functionally graded clamped plates subjected to an edge heat flux", *Journal of Adhesion Science and Technology*, vol. 25(15), pp.1861-1908, 2011.
- [11] M.D. Bagci, M.K. Apalak. "Thermal residual stresses in one-directional functionally graded plates subjected to in plane heat flux", *Numerical Heat Transfer, Part A: Applications*, vol.60 (1), pp.50-83, 2011.
- [12] M.K. Apalak, M.D. Demirbas, "Thermal residual stresses in adhesively bonded in-plane functionally graded clamped circular hollow plates", *Journal of Adhesion Science and Technology*, 27(14), pp. 1590-1623, 2013.
- [13] M.K. Apalak, M.D. Demirbas, "Thermal residual stresses in in-plane functionally graded clamped hollow circular plates subjected to an edge heat flux", *Proceedings of the Institution of Mechanical Engineering Part L- Journal of Materials-Design and Applications*, vol.229, pp.236-260, 2015.
- [14] M. Nemat-Alla, "Reduction of thermal stresses by developing two-dimensional functionally graded materials", *International Journal of Solids and Structures*, vol.40 (26), pp. 7339-7356, 2003.
- [15] M. Nemat-Alla, K.I.E. Ahmed, I. Hassab-Allah, "Elastic-plastic analysis of two-dimensional functionally graded materials under thermal loading", *International Journal of Solids and Structures*, vol. 46, pp.2774-2786, 2009.
- [16] C. Iwasawa, M. Nagata, Y. Seino, M. Ono, "A study on anode materials and structures for SOFC", *Proceedings of the Fifth International Symposium on Solid Oxide Fuel Cells (SOFC-V)*, Vol. 97(40), pp. 626–634, 1997.
- [17] Y. Wang, K.S. Chen, J. Mishler, S.C. Cho, and X.C. Adroher, "A review of polymer electrolyte membrane fuel cells: Technology, applications, and needs on fundamental research", *Applied Energy*, vol.88 (4), pp. 981-1007, 2011.
- [18] S. Kakac, A. Pramuanjaroenkij, X. Y. Zhou, "A review of numerical modeling of solid oxide fuel cells", *International Journal of Hydrogen Energy*, vol. 32(7), pp. 761-786, 2007.
- a. Ruys, E. Popov, D. Sun, J. Russell, C. Murray, C. "Functionally graded electrical/thermal ceramic systems" *Journal of the European Ceramic Society*, vol. 21(10-11), pp. 2025-2029, 2001.
- [19] Y. Tomota, K. Kuroki, T. Mori, T. Tamura T, "Tensile deformation of two-ductile-phase alloys: flow curves of $\alpha \rightarrow \gamma$ Fe-Cr-Ni alloys", *Mater. Sci. Eng.*, vol. 24, pp. 85–94, 1976.
- [20] K. Wakashima, H. Tsukamoto, "Mean-field micromechanics model and its application to the analysis of thermomechanical behavior of composite materials", *Mater. Sci. Eng. A*, vol.146, pp.291–316, 1991.
- [22] V.M. Levin, "On the coefficients of thermal expansion of heterogeneous material", *Mech. Solids.*, vol. 2, pp. 88–94, 1967.

Estimating UAV Route via Aerial Road Images

Mucahit Karaduman¹, Ahmet Cinar², Haluk Eren²

Abstract

Nowadays, unmanned aerial vehicles (UAV) are getting have important role in our life. These types of vehicles can accomplish several missions such as tracking, monitoring and security. The aim of this study is to give route suggestion for UAV to ease movement of the vehicle without remote control. Thus, the mission can be achieved in independent of an operator providing cost saving. This study is realized to get a path trajectory for UAV following detection process. Thus, it is desirable to provide security by monitoring and tracking along a specified road. Studies in the literature, generally using single method rather multiple ones for road detection, exemplified as classification, finding the right direction, color and tonal differences. In this study, two methods are exploited simultaneously to detect subject road, which are K Nearest Neighbor classification and Hough Transform. At the initial stage aerial image is taken by UAV mounted camera, and a noise filter is applied to current frame. Then, possible shadows accommodating in the image are detected and removed. Subsequently, the road portion are detected by KNN method. Simultaneously, HT is applied to the same image for detection of same road portion. Afterwards, both results are matched to get the final result indicating route suggestion. Employing the both methods simultaneously for the verification concern boost success rate. Consequently, the UAV is able to autonomously follow the desired path through instant route suggestion. Once the destination is reached, it can return to the starting point by following the route which is earlier estimated. This behavior of UAV stands for patrolling over the subject road without extra effort saving energy consumption and estimation cost.

Keywords: Road Detection, Unmanned Aerial Vehicles, Nearest Neighbor, Hough

1 INTRODUCTION

The state of the art technology enables to develop new devices which can help human being for security matters. Furthermore, remote sensing motivates users to take control these type of devices with the aim of tracking environment. Diverse usage type is to put them in to practice semi or full autonomous. Unmanned Aerial Vehicles (UAV) have been developed to do that. Especially, path planning plays important role in vehicle movement and keep its progress along the route. With this aim literature is full of researches and every single day one can meet to new studies [1,2,3,4]. Naturally, they comprise various methods for different aims. Such as image processing based detection, GPS data manipulation or other type of methods for manual control. Most of the UAV control and control mechanism need a pilot in a dedicated ground station. In the failure of connection case UAV can be lost and it cannot return to the control center. This type of control is widely preferred in actuality but in reality it is difficult to treat it as unmanned and it brings pilot and ground station cost. Another alternative is to follow GPS direction suggestions to reach targeted destination. The cost of this method is arguable due to its GPS data necessity. In this endeavor UAV may have trouble to get satellite data continuously because of unforeseen situations such as atmospheric alterations. Uncontrolled satellite data usage may cause the existing system to be more vulnerable which results in security weakness. Furthermore, intentional disturbing signals may prevent UAV to reach destination. All these matters are disadvantages for UAV management and security flaws are in question. Proposed approach in this study is to employ tracking by means of image processing methods. Which enable UAV to get independent movement capability without direction of satellite GPS or ground station management. For that reason, it is affordable and more secure rather than many of rivals.



¹ Corresponding author: Inonu University, Department of Computer Science, 44280, Malatya, Turkey. mucahit.karaduman@inonu.edu.tr

² Firat University, Department of Computer Engineering, 23119, Elazig, Turkey. acinar@firat.edu.tr

Figure 1. The UAV captured images of the road.

Many other studies have been made in this area. Such as Xinpeng et al., performed the road detection by means of circular areas. Initially, for detecting road, a template were created and then found similar places to this template [1]. Foedisch et al., utilized a neural network algorithm for road detection. Colors were extracted by histogram and then they were involved in the algorithm [2]. Fritsch et al. used KITTI-ROAD data set for detecting road area. They used pixel based detection on 2D world in Bird's Eye View spaces. [3]. [4]. Alvarez et al. detected road from RGB image. They introduced two approaches which are top down methods and bottom up technics. Top down method scene road traffic pattern on image level. Bottom up methods predict road area in each image superpixel [4]. Rathinam et al. interest with river detecting from image captured by UAV. They use both color and near infrared images. In infrared images the river appearance block color. They use likelihood classification to detect river area in image [5]. Frew et al. used vision based road detection and follow autonomously by small aircraft. They detect road used computer vision and aircraft controlled by hardware in the loop [6]. Maurya et al. used k-means classification and morphological operations on aerial image. They extracted non road area like building by morphological operation, and then detected road by k-means classification [7]. Hu et al. detected main road line from high resolution satellite image using hierarchical grouping strategy [8]. Liu et al., used hybrid genetic algorithms and classification from satellite images to extract roads [9]. Li et al., suggested a method using Random selective Hough transform for detecting road lines. They benefited from the difference between red and green channels, considering the white and yellow lines [10]. There is a lot more work done in this field which are used classification, hough transformation, road model and object feature [11,12,13,14]. In this approach, used Hough transformation and K-Nearest Neighbor segmentation for detecting road area, and then estimated route by that result. Both method runs simultaneously for detect their result. These results used with intersection detecting final road area. As a result, estimated route to follow by UAV.

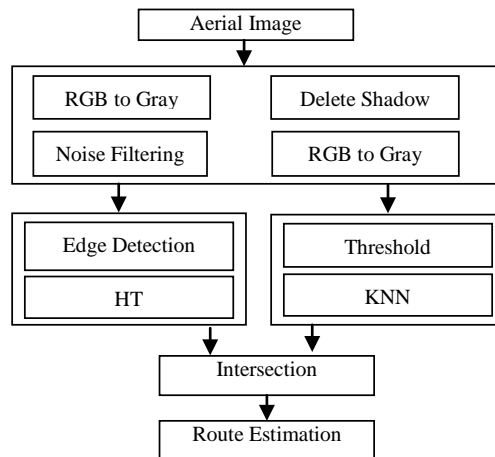


Figure 2. System Diagram.

2 PROPOSED METHOD

In this study, airborne camera images are dedicated for UAV guidance. The proposed scheme consists of several stages to detect subject road and to estimate UAV route. The system diagram revealing the overall approach is provided in Fig. 2.

All the components, including road detection, and route estimation, that are responsible for design stages in Fig. 2 can be briefly listed below:

- Step 1. Acquiring road frames by the UAV camera
- Step 2. Hough Transformation
 - RGB image conversion to gray level
 - Noise elimination
 - Edge detection from binary image (for HT).
 - Hough transformation for detecting road portion.
- Step 3. K-Nearest Neighbor segmentation.
 - Removing possible shadows from the image.
 - Conversion to binary image (for KNN).
 - K-Nearest Neighbor segmentation.
- Step 4. Road detection and Route estimation.
 - Combining KNN and HT results to find intersection.
 - Estimating route.

As the initial task, UAV captures road field images consecutively by its own mounted camera for detecting road and estimating route. Subsequently, steps 2 and 3 are run simultaneously. A couple of road field sample image captured by UAV is appeared in Fig. 3 which are converted to gray level equivalents ones.



Figure 3.a) RGB aerial image, b) Gray aerial image.

In the second stage Hough Transformation (HT) sub processes are executed to detect the targeted road. Initially captured image is converted gray level. Then Gaussian filter is applied to eliminate possible noise. Sobel edge mask is the subsequent process. Finally, HT is employed to find road border lines. This situation is sketched in Fig. 4.

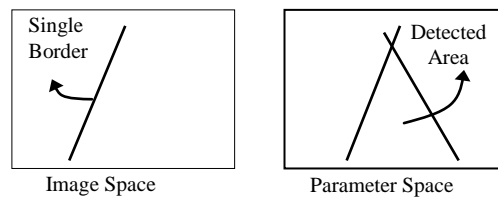


Figure 4. Road detection by Hough Transformation

In the third stage road detection is realized by K-Nearest Neighbor (KNN) segmentation. Possible shadows over the aerial image is primarily eliminated using minimum entropy method. Afterwards threshold is applied as converting the image into binary equivalent. The segments obtained by KNN are classified and the road is detected.

In the final stage of the proposed approach the result obtained by HT and KNN are matched and intersection area is extracted from overlapped image to get road portion. Subsequently resultant route can be estimated which motivates UAV to fly along the subject road.

In the intersection stage, the result obtained by KNN and that of HT are combined, by means of their intersection, as

$$\mathcal{R}_{est} = \{\mathcal{R}_{\mathcal{H}} \cap \mathcal{R}_{\mathcal{KNN}}, \quad \forall \mathcal{R}_{\mathcal{H}}, \mathcal{R}_{\mathcal{KNN}} \in I\} \quad (1)$$

where \mathcal{R}_{est} is the resultant road portion, $\mathcal{R}_{\mathcal{H}}$ is the detected road portion by HT, $\mathcal{R}_{\mathcal{KNN}}$ is the detected road portion by KNN, and I is binary image.

$$\begin{aligned} \mathcal{R}_{est} &\subseteq \mathcal{R}_{\mathcal{H}} \\ \mathcal{R}_{est} &\subseteq \mathcal{R}_{\mathcal{KNN}} \end{aligned}$$

$$I = \left\{ \mathcal{P}(nxm) \left| \begin{array}{l} m \in [1, 2, \dots, h] \\ n \in [1, 2, \dots, w] \end{array} \right. , \quad \mathcal{P} \in [0, 1] \right\}$$

where h is image height, w is image width, and \mathcal{P} refers to binary subject pixel.

The route to be suggested can be calculated by Equation 2 in which average x value is calculated and the next pixel forming UAV direction is obtained as

$$\mathcal{R}_{p_i} = \frac{1}{\max x - \min x} \sum_{i=\min x}^{\max x} x_i \quad (2)$$

where \mathcal{R}_{p_i} is the route pixel located in same row, $\min x$ and $\max x$ are minimum and maximum x values in the same row, and x_i is the road pixel at the same row.

3 EXPERIMENTAL RESULTS

In the proposed scheme, different aerial road images samples are dedicated to proceed the algorithm. Route estimation is conducted by the road intersection result of HT and KNN. The results of HT and KNN stages are respectively given in Fig. 5 and fig. 6.

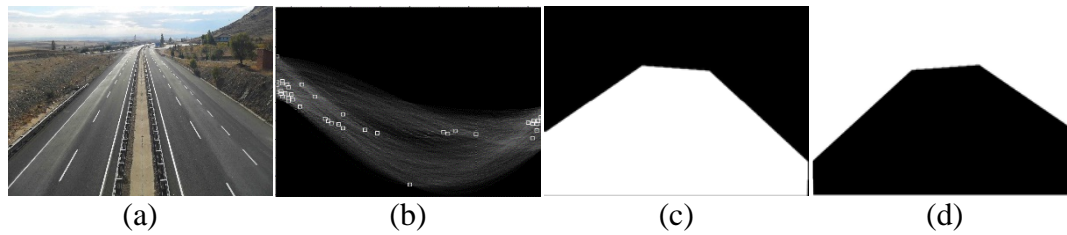


Figure 5. a) RGB aerial image, b) HT edge map graphic, c) HT result, d) HT detected road area.

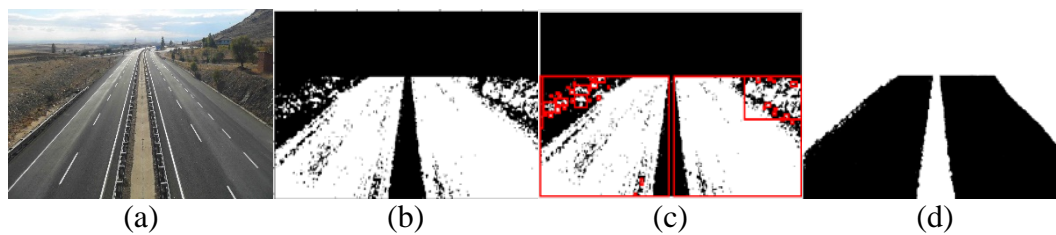


Figure 6. a) RGB aerial image, b) Thresholded image, c) KNN result, d) KNN detected road area.

The resultant image intersecting KNN and HT is revealed in Fig. 7(a), which is employed by calculation of UAV direction. Estimated route is provided in Fig. 7(b).

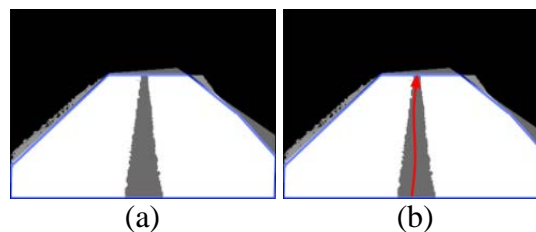


Figure 7. a) KNN and HT intersect result, b) Estimated route.

4 CONCLUSION AND FUTURE WORK

In this study, we have suggested a method combining KNN and HT for aerial road detection. KNN and HT algorithms are simultaneously executed. The intersection is taken by both results to get UAV direction. This approach enables UAV patrolling over a specified road. In the progress of this study we are planning a fusion scheme to get involve in proper stage of the proposed algorithm. In that way, the result will be improved to get more accurate route suggestion. As a complementary sub routine the altitude and perpendicular motion of the UAV will be included in the methods.

REFERENCES

- [1] T. Xinpeng, S. Shunlin, and Z. Yongzhao, "A novel road extraction algorithm for high resolution remote sensing images," *Appl. Math*, 8(3), 1435-1443, 2014.
- [2] M. Foedisch, and A. Takeuchi, "Adaptive real-time road detection using neural networks," In *Proceedings of the 7th international IEEE conference on intelligent transportation systems*, pp. 167-172, 2004.
- [3] J. Fritsch, T. Kuehl, and A. Geiger. "A new performance measure and evaluation benchmark for road detection algorithms," In *ITSC*, 2013.
- [4] J. M. Alvarez, M. Salzmann and N. Barnes, "Data driven road detection," *Applications of Computer Vision (WACV)*, IEEE, 2014.
- [5] S. Rathinam, P. Almeida, Z. Kim, S. Jackson, A. Tinka, W. Grossman, and R. Sengupta, "Autonomous searching and tracking of a river using an uav," in *American Control Conference, ACC '07*, pp. 359–364, 2007.
- [6] E. Frew, T. McGee, Z. Kim, X. Xiao, S. Jackson, M. Morimoto, S. Rathinam, J. Padial, and R. Sengupta, "Vision-based road following using a small autonomous aircraft," *Proc. IEEE Aerospace Conference, Big Sky, MT*, March 2004.
- [7] R. Maurya, P. R. Gupta, and A. S. Shukla, "Road Extraction Using K-Means Clustering and Morphological Operations," *International Journal Of Advanced Engineering Sciences And Technologies*, vol. 5, pp. 290 - 295, 2011.
- [8] X., Hu, and V., Tao, "Automatic Extraction of Main Road Centerlines from High Resolution Satellite Imagery Using Hierarchical Grouping," *Photogrammetric Engineering and Remote Sensing*, vol. 73, pp. 1049-1056, 2007.

- [9] H. Liu, J. Li, and M. A. Chapman, "Automated Road Extraction from Satellite Imagery using Hybrid Genetic Algorithms and Cluster Analysis," *Journal of Environmental Informatics*, vol. 1, pp. 40-47, 2003.
- [10] Q. Li N. Zheng and H. Cheng "Springrobot: A prototype autonomous vehicle and its algorithms for lane detection," *Intelligent Transportation Systems, IEEE Transactions on*, 5(4), 300-308, 2004.
- [11] Z. Kim, "Robust lane detection and tracking in challenging scenarios," *IEEE Trans. Intell. Transp. Syst.*, vol. 9, no. 1, pp. 16-26, Mar. 2008.
- [12] H. Dahlkamp, A. Kaehler, D. Stavens, S. Thrun, and G. R. Bradski, "Selfsupervised monocular road detection in desert terrain," in *Proc. Robot. Sci. Syst. Conf. (RSS)*, 2006.
- [13] J. McCall and M. Trivedi, "Video-based lane estimation and tracking for driver assistance: Survey, System, and Evaluation," *IEEE Trans. on Intelligent Transportation Systems*, vol. 7, pp. 20-37, Mar. 2006.
- [14] S. Yun, Z. Guo-ying, and Y. Yong, "A road detection algorithm by boosting using feature combination," In *Intelligent Vehicles Symposium, 2007 IEEE*, pp. 364-368, 2007.
- [15] R. Hartley, and A. Zisserman, "Multiple view geometry in computer vision," Cambridge University Press: Cambridge, UK, 2003.
- [16] G. D. Finlayson, M. S. Drew, and C. Lu, "Entropy minimization for shadow removal," *International Journal of Computer Vision*, 85(1), 35-57, 2009.

Generating Hydropower Map of Tigris River

Abdullah Muratoglu¹

Abstract

Hydropower is known as the most reliable, efficient and common type of renewable energy. The energy of a flowing river can be harnessed using large scale hydroelectric power plants, small scale dams or hydrokinetic turbines. The energy independency of developing countries can be provided by employing only natural resources. The aim of this study is to generate the hydropower map of Tigris River Basin to be used in hydropower production works in Turkey. The discharge rates of ungauged sites have been predicted by statistical regression analysis using long-term-averaged discharge data of 34 flow measuring stations. The channel cross sections were determined by making hydraulic geometry analysis using 10 different cross section measurements. Then, the discharge map of the basin have been generated. Consequently, the hydropower map is produced based on the discharge and cross section data of both gauged and ungauged sites considering basin's topology.

Keywords: Hydropower, potential, map, Tigris River

1 INTRODUCTION

Hydropower is the largest renewable resource to produce electricity and plays an important role in many regions of the world. More than 150 countries generate electricity using hydropower. It is also one of the cheapest source of energy. Predictability and regularity of the hydropower makes it to be one of the most favorite energy conversion methods.

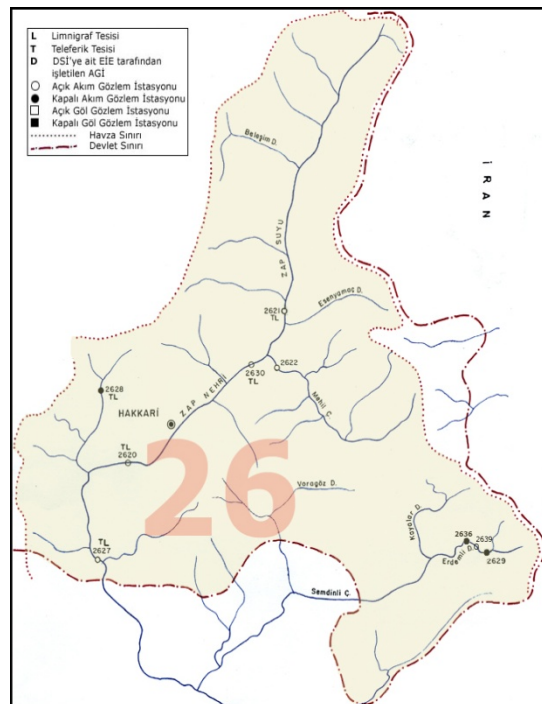


Figure 1. The map of West Tigris Basin [1]

This study is mainly concentrated on the part of Tigris Basin which lies within Turkey. Tigris Basin which is divided into East and West sub basins, is the second biggest basin amongst a total of 26 basins in Turkey. Tigris River reaches an average discharge of 1340 m³/s[2] with the addition of other tributaries in Iraq. The part of the Tigris Basin located within the borders of Turkey has an area of 41058 km² that is only 12% of the whole basin area, with

¹ Corresponding author: Batman University, Department of Civil Engineering, 72100 Batman, Turkey.
abdullah.muratoglu@gmail.com

an average annual discharge of $593.88 \text{ m}^3/\text{s}$ which makes roughly 51% of the total river discharge [3]. The maps of West Tigris Basins are given in Figures 1 and 2.

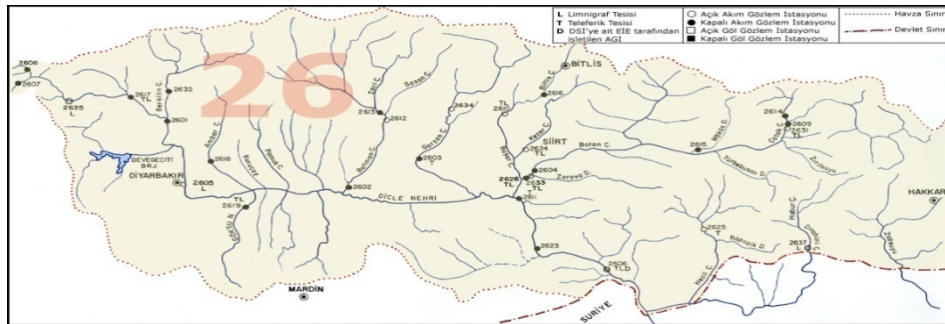


Figure 2. The map of West Tigris Basin [1]

The main scope of this study is to generate the hydropower map of the Tigris Basin in order to be used for both hydrostatic and hydrokinetic energy studies. Also this study will guide researchers to estimate the power and energy of any channel of the stream.

2 MATERIAL AND METHODS

2.1.Data

To calculate power in a system the discharge has to be defined. In Turkey, discharge measurements are made by mainly two government foundations. These are: State Power Works (DSI) and General Directorate of Electrical Power Resources Survey and Development Administration (EIE). Both foundations make the requiring flow observation, however; EIE has much more experience on the generation of discharge data and cross-sections. The flow measurement stations of EIE are very homogeneous, distributed large area and have reliable data, also they were located in much more suitable places. In the present study, the discharge data is mainly obtained from EIE's *Monthly Averages of Stream Flows for 1935-2005* book [4]. The long term average annual discharge values are used to assess the hydroelectric power potential. A sample data page is given in Table 1.

The average annual discharge data is generated for each flow measuring stations (FMS). FMS's are the channel flow observation stations that are placed by EIE at the suitable locations on rivers all around Turkey to perform the daily flow discharge, sediment load, etc. measurements.

Table 1. A sample of EIE discharge data page

EIE													
26 - TIGRIS BASIN													
2622 - NEHİL STREAM - KONAK													
Location: (44°04'14" E - 37°40'56" N) It is located under the suspension bridge that is													
4 km far from the Yuksekova division of Van-Hakkari highway													
Precipitation Area:	1136.0 km ²			Average Elevation:			1694 m						
Measurement Time:	19.08.1988			Long term average yearly discharge:			19.1 m ³ /s						
Measurement Tool	Staff Gage and Limnigraph												
Monthly average discharges (m ³ /s)													
Y/M	Oct	Nov	Dec	Jan	Feb	Mar	Apr	May	June	July	Aug	Sept	Y. Avg
1989	6.97	6.98	5.95	5.1	5.1	23.2	25.3	20.3	6.4	2.71	2.86	2.5	9.45
1990	-	-	-	-	-	-	-	-	-	-	-	-	-
1991	-	-	-	-	-	-	-	-	-	-	-	-	-
1992	-	-	-	-	-	-	-	-	-	-	-	-	-

1993	3.44	4.02	2.71	2.37	2.18	4.73	145	140	68	25.8	9.93	5.68	34.5
1994	4.57	8.29	7.33	7.35	6	18.9	116	71.2	29	10.8	5.36	5.18	24.2
1995	4.42	7.92	5.83	5.05	4.7	24.8	103	71.3	43	14.6	5.8	5.12	24.6
1996	4.59	5.96	3.66	2.88	3.52	9.32	69.7	44	15	6.77	3.13	3.35	14.3
1997	3.88	2.36	3.51	3.36	2.81	3.6	75.9	67.9	29	14.6	4.74	4.42	18
1998	3.69	3.42	2.81	2.91	3.21	14.1	51.9	34.8	11	5.29	3.66	3.61	11.7
1999	-	-	-	-	-	-	-	-	-	-	-	-	-
2000	-	-	-	-	-	-	-	-	-	-	-	-	-
2001	-	-	-	-	-	-	-	-	-	-	-	-	-
2002	-	-	-	-	-	-	-	-	-	-	-	-	-
2003	3.52	2.84	2.73	3.07	2.34	11.8	155	80.6	37	9.11	4.52	3.67	26.3
2004	4.75	11.1	6.18	4.19	6.48	66.2	36.4	42.1	23	10.4	4.27	3.47	18.2
2005	2.97	3.31	2.84	3.16	3.31	20.2	28.2	35.4	12	4.79	3.29	2.6	10.2
M. Avg	4.28	5.62	4.36	3.94	3.97	19.7	80.6	60.8	27	10.5	4.76	3.96	19.1
Eff.	3.77	4.95	3.83	3.47	3.49	17.3	71	53.5	24	9.2	4.19	3.49	16.9
R. off	10.1	12.8	10.3	9.3	8.44	46.4	184	143	62	24.7	11.2	9.04	532
Q	11.5	14.6	11.7	10.6	9.59	52.7	209	163	71	28.1	12.7	10.3	604

2.2. Hydropower

The hydropower systems run based on the potential power of water which is supplied by head difference. The power of a falling water is mainly calculated using the Equation 1 as follows;

$$P_{th} = \rho g Q H_N \quad (1)$$

where; P_{th} is the theoretical power potential (W), ρ is the density of water (kg/m^3), g is the ground acceleration coefficient, Q is the average discharge (m^3/s) and H_N is the net head difference of water (m).

According to the Equation 1; if the average discharge and net head difference of the stream is known, the theoretical power potential can be evaluated. However, the flow measuring stations are situated at central places and it is not possible to find the discharge data for majority of river branches. The locations where any flow measuring station is not situated are called as ungauged stations. In order to evaluate the hydropower potential at ungauged stations, a prediction method should be generated which details are given in Section 2.3.

2.3. Discharge prediction of ungauged stations

One of the oldest methods which puts a relationship between basin area and streamflow was introduced by [5] in which a relationship of the stream flow and drainage area has been provided. Similarly, in this study, the discharge estimations for ungauged sites are supplied from precipitation area in which the equation is generated using the linear regression approach on a log-log scale. The discharge data of 34 flow measuring stations are subjected to regression analysis and an exponential equation has been generated with the coefficient of determination (R^2) of around 0.85. The results has also been verified on real data with a good accuracy. The Equation for predicting the average annual flow rate which is a function of a precipitation area is shown at Equation 2. The regression analysis is also given in Figure 3.

$$Q_{avg,y} = 0.0414A_p^{0.8806} \quad (2)$$

where, $Q_{(avg,y)}$ is the long term averaged annual discharge (m^3/s) and A_p is precipitation area of the basin (m^2).

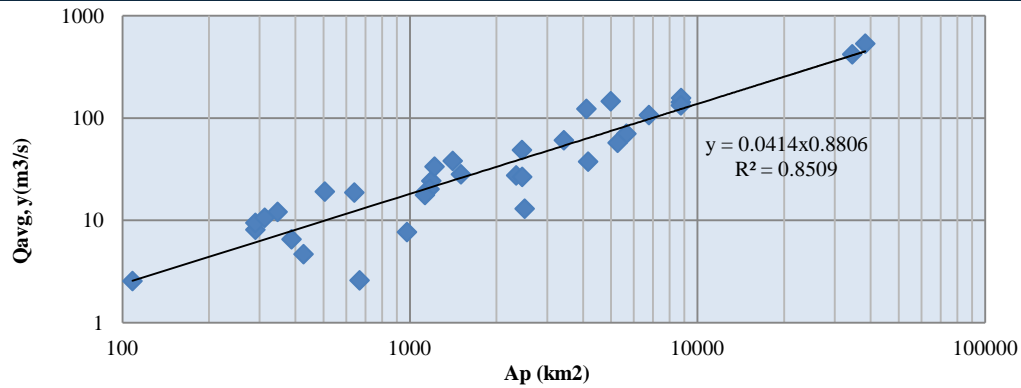


Figure 3. Regression analysis for precipitation area vs. discharge

3 RESULTS AND DISCUSSION

The detailed hydropower potential has been calculated by employing hydraulic discharge analysis. The basin is divided into 9 sub-basins and the precipitation area corresponding each branch or channel of the stream has been measured using a satellite based 3D software. The average annual discharge rates has been obtained using the Equation 2. Then, the hydropower of each channel is calculated by Equation 1. The channels having low value of discharge (below $5 \text{ m}^3/\text{s}$) are not considered. The total hydropower potential of the basin is calculated as 3055 MW. This value should be taken as the theoretical hydropower potential. The technical potential may vary according to used device and technology. The resulting hydropower potential of west and east Tigris Basins are illustrated in Figure 4 and 5.

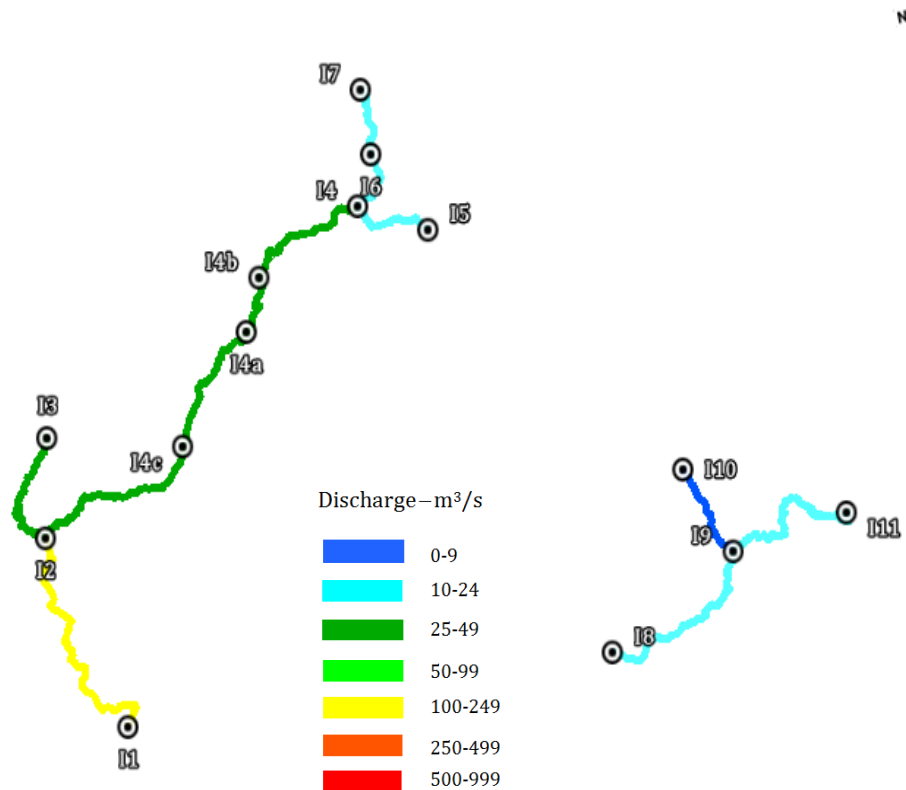


Figure 4. The hydropower map of East Tigris Basin

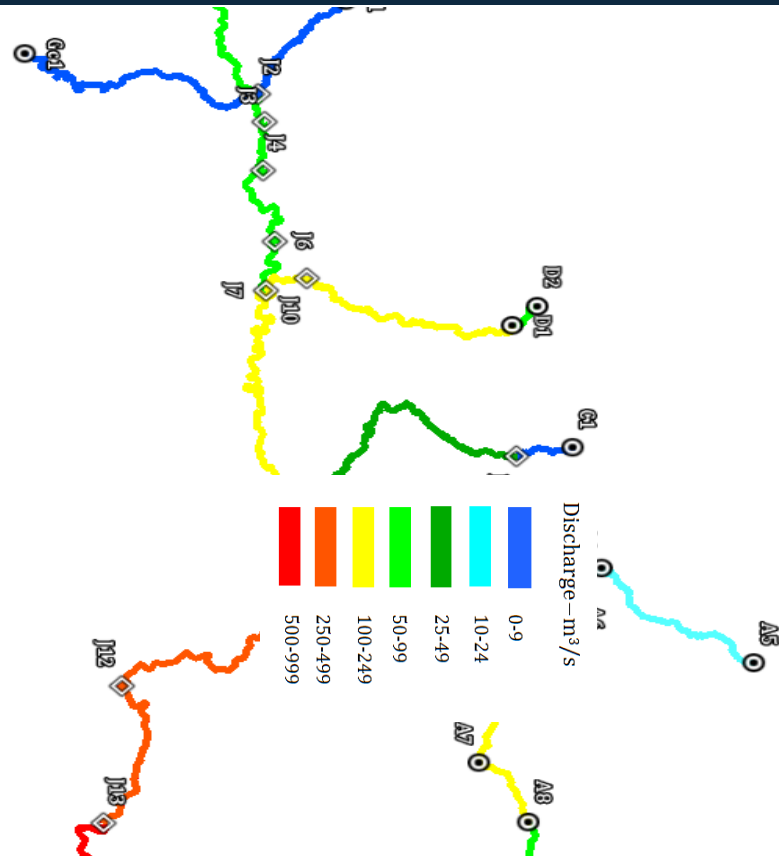


Figure 5. The hydropower map of East Tigris Basin

4 CONCLUSION

The gross hydropower potential is calculated to be 3055 MW for the whole part of Tigris Basin inside Turkey. The power of each channel has also been calculated. This available potential can be exploited by building dams, small hydroelectric power plants and river conversion systems or by utilizing hydrokinetic turbines.

REFERENCES

- [1] (2012) Elektrik Isleri Etut Idaresi website. [Online]. Available: www.eie.gov.tr
- [2] C. Zehir. *Ortadoğuda su medeniyetlerinden su savaşlarına*. İstanbul: Su Vakfı Yayınları, 2003.
- [3] L. Sehsuvaroğlu. *Su barışı-Türkiye ve Ortadoğu su politikaları*. İstanbul: Gümüş Motif Yayınları, 1997.
- [4] Elektrik Isleri Etut Idaresi. *Su akimlari aylık ortalamalari 1935-2005*. Ankara, 2008.
- [5] E. Kuichling, E. The relation between the rainfall and the discharge of sewers in populous areas. *ASCE*, 20, 1-56, 1889.

Landscape Planing Design in Bilecik Region

Hasan Bozkurt¹

Abstract

The negative affects of technology that grows rapidly is emerging that's irresponsible consumption of natural resources and in the form of pollution or degradation of nature. In this study we focussed landsce planning about highway design parameters in bilecik region. Bilecik has a mediterranean climate near the borderline of the continental climate with cold and often snowy winters and hot and dry summers. In developing countries, tourism, cultural and socio-economic structure in terms of highway is too important. Highways pass through without disturbing the landscape, in harmony with it, can respond to the needs of modern traffic and tourism must be in order.

After the highway opened to traffic, highway landscape, but with the route selection process should be addressed. In this reason construction of highways, the landscape is considered to be an important element of the visual and environmental values in terms of taking into account the driver must be provided. Moreover, highway and slope planting work (type selection and planting method) to the principles of landscape planning should be exercised.

In this paper, the features and models of highway landscapes are analyzed in detail, then a new concept of highway landscape design, which integrates highway planning, design, operation and landscapes into the highway's service life is presented.

Keywords: *Bilecik region; Highway design; Landscape Planning*

1. INTRODUCTION

Building a new transport infrastructure, or intervening on an existing one, is often considered an act of pure engineering. Therefore technicians usually disregard the effects that the project has on landscape, ecosystems and urban dynamics. Roads and railways tendentially settle on the ground in a self-referential way. Technical rules, functional and financial limitations are not, however, the only important factors in steering a project. Sustainability, environmental protection and the interest in the quality of the urban space are more and more weighty for the society. This should encourage infrastructure designers to be more conscious of the relation their projects have with places.

In a few cases roads, bridges or viaducts are made by famous designers with the intent to create a beautiful and meaningful symbol. But in most of the cases the choice made by the designer is to hide, camouflage and deny the presence of the artefact. This approach results from a romantic, outdated conception of landscape, intended as a scenery to maintain as intact as possible. Artefacts seems to renounce their responsibility, minimizing the impact they have on the environment. V.I.A procedure (Valutazione d'Impatto Ambientale: Environmental Impact Assessment) often lead to maquillage operations, unencumbered from the project: these solutions don't really mitigate the damage, acting just in a complementary way.

The discriminator in realizing an infrastructure is its usefulness (e.g.: to fulfil a traffic demand). We should be consistent with social needs: if there is an expressed need of more mobility, or to connect two places, we should exploit the opportunity to create a symbol, something that could enrich the land. A well designed infrastructure can have a dignity that allows it to become a significant element of identity in the context. Think about American streets and bridges: not only useful, but also symbols of lifestyle and culture. When artefacts are projected as positive expressions of the response to a social need through the designer's skill, they become positive symbol themselves.

Embankments become visual barriers. Cuttings and tunnels are "invisible", but constricting and alienating for the user; other assessments are therefore needed, in addition to the geological and geotechnical ones, already part of the common preliminary design. The choice of a cable-stayed or suspended bridge instead of an arch or frame one, is to be considered if there is a need of a landmark. A service station or rest area can become interesting elements, if they exalt the potential of the place.

2. STUDY AREA

Bilecik is the provincial capital of Turkey's Bilecik Province. The population of the town is 62,320 (as of 2010). The town is famous for its numerous restored Turkish houses. It is increasingly becoming more attractive to tourists. With its rich architectural heritage, Bilecik is a member of the European Association of Historic Towns and Regions. 30 kilometres (19 miles) southeast from Bilecik is Söğüt, a small town, where the Ottoman Empire was founded in 1299. Bilecik has a mediterranean climate near the borderline of the continental climate with cold and often snowy winters and hot and dry summers. Summers are hot and dry with temperatures usually exceeding 30 °C (86 °F) in the height

¹ Corresponding author: Bilecik Seyh Edebali University, Department of Civil Engineering, 11100, / Bilecik, Turkey.
hasan.bozkurt@bilecik.edu.tr

of summer, they are also the driest months. Winters are cold and it frequently snows a lot between the months of December and March. Figure (1-3) shows the Bilecik landscape beauty and historical monuments.

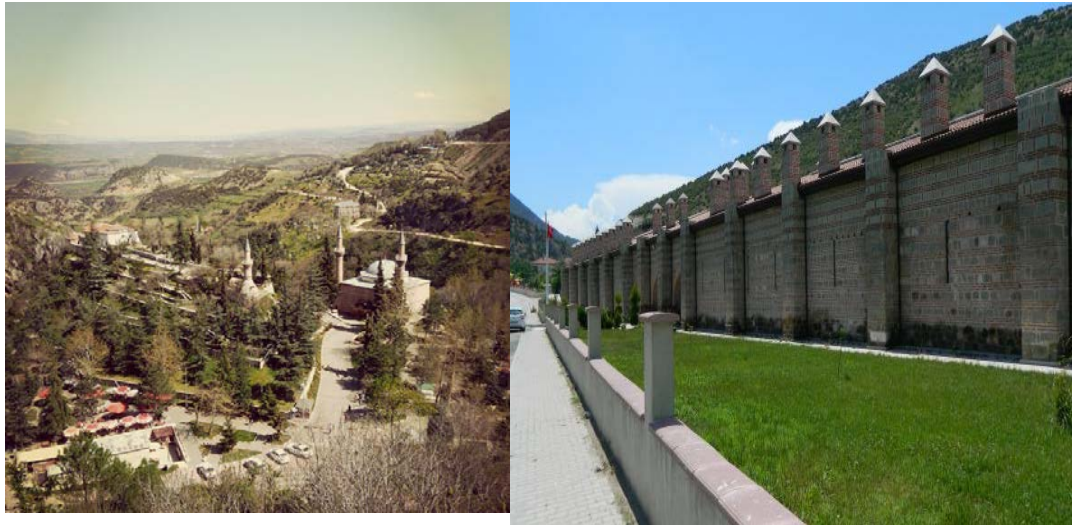


Figure 1. Bilecik Seyh Edebalı Tomb and Orhangazi Mosque (Seyh edebalı Founder of Ottoman Empire Osman Gazi Father in Law)

Figure 2. Koprulu Mehmet Pasa Kervan Saray near İstanbul-Antalya Highway Vezirhan-Bilecik



Figure 3). Ertugrul Gazi Tomb (Osman Gazi's Father) near Bilecik-söğüt Highway, Söğüt-Bilecik

3. MODELS OF HIGHWAY LANDSCAPES

While designing of roads and highways elements of landscape are altered to the highest degree. These roads are used for terrestrial communication. There are, of course, numerous benefits in having them although most of these benefits are social or economic rather than environmental. Here are few changes which occur during the construction.

3.1. Topography Changes.

Motorways are large-scale man-made projects. During their construction, the topography of the surrounding area will be subject to significant impact. As highways span over a large area including flat lands, mountains, valleys etc. topographical changes are bound to happen. Huge amount of cutting and leveling of land results into the elevation and geographical changes which are required for the better vehicular movement. As an effect, following are the major changes.

- Natural landscape is destroyed.
- Beautiful scenery and a lot of arable land is disturbed.
- Cultivable land is requisitioned.
- Serious degradation in natural land features.
- Untouched habitual spaces of different animal species are disturbed and it affects the wildlife.-

Area needed for construction of highways is larger than an ordinary road and thus, it is irreversible even if best known mitigation policies are referred. In flat and hilly areas, the land occupation ratio of a motorway is usually 8.0-10.7 hm²/km.

3.2. Soil Erosion.

Soil is one of the most important factors for the growth of vegetation along a motorway. During highway construction, quarrying, borrowing earth and spoil grounds will cause soil erosion. The fertility of soil is reduced, changing its physicochemical properties, which makes it more difficult for vegetation to grow and recover. If the soil structure of the land under construction changes due to compaction from machinery or the land being trampled on, the fertility of the soil may not recover for a long time. Soil erosion destroys the vegetation along the motorway. In turn, the loss of vegetation further exacerbates soil erosion. This vicious circle makes it very difficult for the vegetation to grow and recover. It also causes water and soil loss.

3.3. Climate.

Upon construction, motorways can generate a microclimate environment, which mainly depends on the properties of the underlying surface and the composition of the atmosphere. A motorway microclimate that is adverse to plant growth has the following features: fast air convection, hot pavement temperature in summer and drought in roadway.

3.4. Hydrology

In motorway construction the direction of surface water may often change its course. Due to the diversion of the river flow, water and soil loss worsens at areas where the flow of water is concentrated and erosion occurs where the structure of the water flow is adverse. In river or wetland areas, it is necessary to change the original direction of the river when a motorway is built. After the direction of the river has been changed, a very large flow is generated in areas where many waterways come together and the flow rate speeds up.

3.5. Vegetation

The impact of a motorway on vegetation mainly refers to the direct impact of land destruction, borrowing earth and spoil grounds during motorway construction, as well as the indirect impact of motorway traffic. The former is transient and irreversible; the latter is more long-term and reversible. During motorway construction, direct destruction of vegetation mainly stems from the following two aspects: permanent destruction from site clearing, and damage from the temporary spoil ground and construction road.



Figure 4 - Example for Vegetation and beautiful landscape in near the highway

3.6. Wildlife

Wild animals are the main victims of habitat fragmentation during motorway construction. As the forest decreases in size and is divided by residential areas and traffic networks, their habitat gradually shrinks. Increased traffic flow and expanding human activity also reduces their habitats, affecting their mating and reproduction, further aggravating the impact on them. In addition, newly built motorways directly cause a loss of habitat and terrain features, resulting in a change in climatic factors such as sunlight, wind speed, temperature and humidity.



Figure 5: Before and after photograph in construction site of roadway

Meanwhile, vibration, noise, atmospheric pollution and soil pollution from vehicles has a negative impact on the survival, reproduction and migration of local plants and animals.

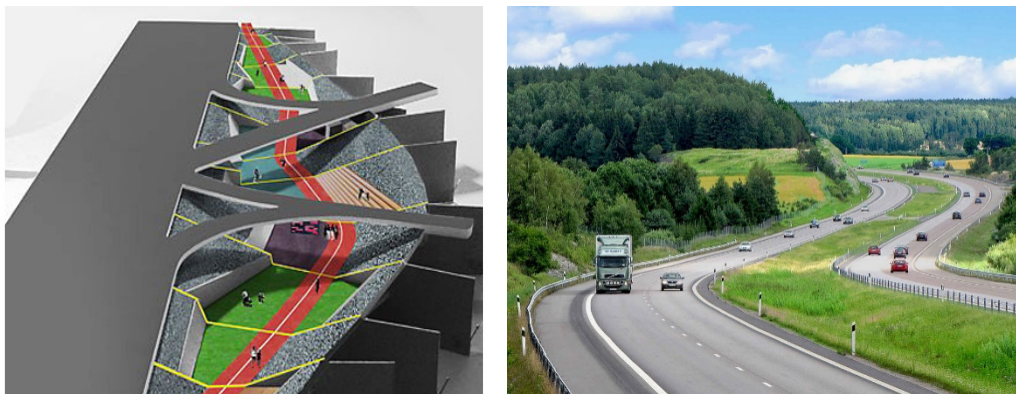


Figure 6: Landscape examples in highway design

4 CONCLUSIONS

The negative effects of technology that grows rapidly is emerging that's irresponsible consumption of natural resources and in the form of pollution or degradation of nature. In this study we focused landscape planning about highway design parameters in Bilecik region. In this reason construction of highways, the landscape is considered to be an important element of the visual and environmental values in terms of taking into account the driver must be provided. Moreover, highway and slope planting work (type selection and planting method) to the principles of landscape planning should be exercised.

In this paper, the features and models of highway landscapes are analyzed in detail, then a new concept of highway landscape design, which integrates highway planning, design, operation and landscapes into the highway's service life is presented.

REFERENCES

- [1] Highways, www.cambridgeshire.gov.uk/sub/eandt/env/landscape/pdf/3highways.pdf
- [2] Basic principles of landscape Design,
- [3] EIA and landscape assessment in Iceland, odin.dep.no/filarkiv/223398/Gunnarsson.pdf .
- [4] Greening and landscape enhancement, www.hyd.gov.hk/eng/public/publications/ER/doc/8.pdf
- [5] Integrating the Road with Historic Landscape Features,
- [6] <http://www.official-documents.co.uk/document/deps/ha/dmrb/vol10/section1/ha6092g.pdf> .

Effect of Self Compacting Concrete Compressive Stress Properties with Different Filler Materials

Hasan Bozkurt¹, Cenk Karakurt¹

Abstract

Self compacting concrete is the production of technological type of concrete. Different conditions effect the variable changeable values of self-compacting concrete. In this study it has been researched effect of strength with filler materials on self-compacting concrete.

Mainly, in this research has been worked on effects of different filler materials on compressive strength. Experiments studies have been prepared three type of concrete mixes which are contained marble powder, fly ash and stone dust. In addition the same concrete mixes have been prepared and in these mixes spreading in slump flow time in 50 cm diameter give significant values on fresh concrete.

Finally, we determined effect of self-compacting concrete compressive strength with different filler materials and is worked to research the highest strength mix for the mixes of self-compacting concrete

Keywords: *Marble powder, fly ash, Self compacting concrete, Pozzolan fillers and porosity*

1 INTRODUCTION

It was first developed in Japan in 1988 in order to achieve durable concrete structures by improving quality in the construction process. Self-compaction concrete is often described as the ability of the fresh concrete to flow under its own weight over a long distance without segregation and without the need to use vibrators to achieve proper compaction. This saves time, reduces overall cost, improves working environment and opens the way for the automation of the concrete construction [1–4].

Self compacting concrete (SCC) mixes always contain a powerful superplasticizer and often use a large quantity of powder materials and/or viscosity-modifying admixtures. The superplasticizer is necessary for producing a highly fluid concrete mix, while the powder materials or viscosity agents are required to maintain sufficient stability/cohesion of the mixture, hence reducing bleeding, segregation and settlement [4]. Benefits of using SCC also include: improving homogeneity of concrete production and the excellent surface quality without blowholes [5].

In Flow-able concrete, introduction of high volumes of mineral admixtures to concrete mixtures is limited due to their negative effects on water demand and strength of the hardened concrete. However, these mineral admixtures can be efficiently utilized as viscosity enhancers particularly in powder-type SCC. Thus, successful utilization of marble powder (Mp), fly ash (Fa) and stone dust (Sd) in SCC could turn these materials into a precious resource. Moreover, these mineral admixtures can significantly improve the workability of self-compacting [6,7]. When used in SCC, these mineral admixtures can reduce the amount of superplasticizer necessary to achieve a given property [8]. It should be noted that the effect of mineral admixtures on admixture requirements is significantly dependent on their particle size distribution as well as particle shape and surface characteristics. From this viewpoint, a cost effective SCC design can be obtained by incorporating reasonable

amounts of MP, FA and SD [9]. Incorporation of mineral admixtures reduced the cost per unit compressive strength of these SCC [9].

2. EXPERIMENTAL PROGRAMS

The present work aims to study the effect of filler types on fresh and hardened properties of SCC and Flow-able concrete. Fresh and hardened concrete properties such as slump, slump flow, sieve stability, bleeding, porosity, compressive strength and scanning of microstructure for Flow-able concrete (FAW) with slump of (220±20) mm and self compacting concrete were considered in this study.

¹ Corresponding author: Bilecik Seyh Edebali University, Department of Civil Engineering, 11100, Bilecik, Turkey.
hasan.bozkurt@bilecik.edu.tr

2.1. Materials

Three groups of filler were selected. The first group was pozzolanic filler fly ash (Fa) while the second one was non-pozzolanic fillers; Marble Powder (MP), stone dust (SD). These three types of fillers passing from sieve No. of 200 (125 μ m) were used. Portland cement classified as CEM I N 42.5 was considered in this study. The chemical compositions of these fillers and cement are presented in Table 1.

Natural siliceous sand with 2.66 fineness modulus and pink lime stone with nominal maximum size of 9.5 mm were used. Type G of high performance super plasticizer concrete admixture based on poly-carboxylic material was used.

Table 1 Chemical compositions of cement and filler materials.

Component %	Component % Cement	Component % SD	Component % FA	Component % GP
SiO ₂	21.92	95.32	79.02	3.30
Al ₂ O ₃	3.30	0.88	5.96	0.82
Fe ₂ O ₃	0.20	0.39	0.44	0.58
CaO	63.0	0.90	12.3	92.9
SO ₃	2.1	1.03	0.40	1.18
Loss of ignition	1.2	1.40	1.20	1.20

2.2. Concrete mix design

Mix proportions and test procedure The used water/binder ratio (w/b) for Flow-able and self compacting concrete was kept constant as 0.415, while the dose of used superplasticizer was changed to obtain the desired slump for Flow-able concrete and constant slump flow for self compacting concrete. For all the used concrete mixtures, the coarse/fine aggregate ratio was 1.0. Cement contents of 400 kg/m³ and 500 kg/m³ were considered in this study. For cement content of 400 kg/m³, the additional percentages of used filler materials were 7.5%, 10% and 15% while for cement content 500 kg/m³, only 10% was considered. By using different types of fillers, filler percentages and cement contents and Table 2 shows the mixture proportions of these mixes. Slump flow and T50 tests according to ACI 237R-07 were performed on fresh concrete, also sieve stability test was done.

Table 2. Fresh concrete mixture design and test results

Filler type	Cement	Filler content (%)	Water	Coarse aggregate	Fine aggregate	Admixture (lt)	Flow time (s)	Diameter flow (mm)
Fly ash	400	30	178.5	836	836	14.3	2.5	740
Fly ash	400	40	182.6	825	825	14.4	2.5	750
Fly ash	400	60	190.9	804	804	14.6	2.3	740
Marble Powder	400	30	178.5	835	835	15.9	3.5	720
Marble Powder	400	40	182.6	825	825	16.0	3.0	740
Marble Powder	400	60	190.9	805	805	16.1	2.7	750

Stone dust	400	30	178.5	835	835	15.9	3.0	720
Stone dust	400	40	182.6	825	825	16.0	3.0	730
Stone dust	400	60	190.9	805	805	16.1	2.5	750

2.3. Cube compressive strength

Fig. 1 shows the variation in concrete compressive strength of SCC at the different ages of curing for different types of fillers for concrete mixes with 400 kg/m³ cement content. From this figure, generally one can obviously observe that there is no significant variation between compressive strength of fly ash and marble powder and stone dust. This trend is the same at 7 days, 28 days and 56 days. The good performance of used Marble dust and stone dust filler is due to the micro-filling ability, improving the microstructure of the bulk paste matrix and transition zone. Further, it is clear that the increase in filler content from 30% to 60% has not any significant effect on concrete compressive strength for all types of fillers fly ash. There is a noticeable increase in concrete compressive strength

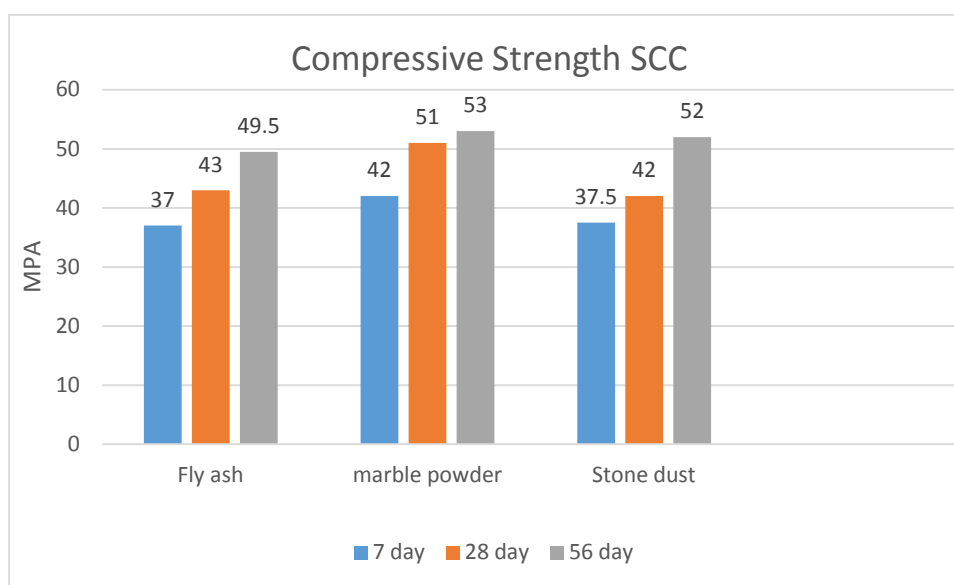


Figure 1. Compressive Strength different filler material results

3. CONCLUSIONS

Consider concrete as a matter containing different filler materials (aggregates of different sizes) joined together by binder material cement, fly ash etc. our priority is that voids in final concrete should be least aggregates help in filling those voids preference for aggregates is always such that one must be getting uniformly graded aggregates of various sizes and in good proportion. Also, aggregates also takes some load that's why we have impact, crushing test etc. but one need not worry about these with the strength as long as they are coming within the limit of 30% as specified by IS code but again beyond certain grades one would have to think about these values as the concrete will not be able to take loads if aggregates are not up to the mark because in these cases while taking load aggregates will start breaking first which will ultimately result in concrete failure.

Based on the findings of the current study, the following conclusions may be drawn:

Filler type has a significant effect on segregation resistance and bleeding resistance of SCC and Flow-able concrete. The use of non-pozzolonic fillers (Stone dust and marble dust) decreases the segregation and bleeding compared with pozzolonic fillers (Fly ash).

The increase in filler content improves bleeding resistance of SCC. The significant effect of filler type on bleeding resistance is obvious at high level of filler content, 60.0%, whereas there is no obvious effect of filler type on bleeding resistance at lower filler content. In addition, filler type has insignificant effect on water absorption. There is no negative effect of non-pozzolonic fillers on concrete compressive strength compared to that of pozzolonic fillers.

REFERENCES

- [1] H. Okamura, M. Ouchi, Self-compacting concrete. Development, present use and future, in: Proceedings of first international RILEM symposium on self-compacting concrete, RILEM Publications, S.A.R.L., Stockholm, 1999, pp. 3–14.
- [2] P.J.M. Bartos, M. Grauers, Self-compacting concrete, *Concrete* 33 (4) (1999) 9–13.
- [3] D.W.S. Ho, A.M.M. Sheinn, C.C. Ng, C.T. Tam, The use of quarry dust for SCC applications, *Cem. Concr. Res.* 32 (2002) 505–511.
- [4] Wenzhong Zhu, J.C. Gibbs, Use of different limestone and chalk powders in self-compacting concrete, *Cem. Concr. Res.* 35(2005) 1457–1462.
- [5] M. Ouchi, S. Nakamura, T. Osterson, S. Hellberg, M. Lwin, Applications of self compacting concrete in Japan, ISHPC, Europe and the United States, 2003, p. 1–20.
- [6] M. Sahmaran, H.A. Christianto, I.O. Yaman, The effect of chemical admixtures and mineral additives on the properties of self-compacting mortars, *Cem. Concr. Compos.* 28 (5) (2006) 432–440.
- [7] Mucteba Uysal, Kemalettin Yilmaz, Metin Ipek, The effect of mineral admixtures on mechanical properties, chloride ion permeability and permeability of self-compacting concrete, *Constr. Build. Mater.* 27 (2012) 263–270.
- [8] M. Sonebi, L. Svermova, P.J.M. Bartos, Factorial design of cement slurries containing limestone powder for selfconsolidatingslurry-infiltrated fiber concrete, *ACI Mater. J.*101 (2) (2004) 136–145.
- [9] Mucteba Uysal, Kemalettin Yilmaz, Effect of mineral admixtures on properties of self-compacting concrete, *Cement Concr. Compos.* 33 (2011) 771–776.

Assessment of Image Fusion Methods

Murat Uysal¹, Abdullah Varlik²

Abstract

Image fusion is the integration of high spatial resolution panchromatic images with low spatial resolution multispectral image to produce a high-resolution multispectral image. Image fusion, which is also called as pan-sharpening, merge resolution, and image integration. Nowadays, there are different image fusion methods used. According to the characteristics of satellite sensors, image fusion methods emphasize the color information or the spatial information. Therefore, visual and statistical evaluation of the image fusion process is needed. In this study, PCA, multiplicative, and Brovey transform methods were used to fusing multispectral and panchromatic images. Image fusion methods were compared by using visual and spectral analysis.

Keywords: *Image fusion, Pan-sharpening, IHS, Brovey, PCA*

1. INTRODUCTION

Remote sensing is using in different fields nowadays. The data can obtain in different resolutions with different sensors from satellites. The images that has different spatial and spectral resolution are using for different purposes depending on the characteristics of the sensor. Multiband and high-resolution spatial panchromatic images can be obtained from satellites such as IKONOS, Landsat, Spot and WorldView. Image fusion is performing to obtain data from both high spectral resolution and high spatial resolution images.

Image fusion is defining in different ways. "Data fusion is a formal framework in which are expressed means and tools for the alliance of data of the same scene originating from different sources. It aims at obtaining information of greater quality; the exact definition of greater quality will depend upon the application"[1]. Image fusion, also, called as pan-sharpening, merge resolution, and image integration. Pan-sharpening is the integration of high spatial resolution panchromatic images with low spatial resolution multispectral image to produce a high resolution multispectral image. Some of the image fusion methods damage the original multispectral image's color structure while transferring the spatial details [2].

Among the methods that are used for merging remote sensing images include principal component analysis (PCA), Brovey transform, IHS (Intensity Hue Saturation), the multiplicative transformation, HPF (high pass filters), neural networks and wavelet transform (WT)

Some image fusion techniques aim to emphasize the positional information while others aim to emphasize the color information. At the same time, each sensor has characteristic properties and not all pan-sharpening method may be available for each sensor. In this case, which pan-sharpening method gives best results for which image types needs to be analyzing.

In this study, Multiplicative, Brovey, PCA and Brovey image fusion methods had used to fuse Landsat 7 ETM+ multispectral and panchromatic bands. Results were compared by using visual interpretation and statistical methods. CC (correlation coefficient), RMSE (root mean square Error) and ERGAS (Erreur relative global dimensionnel de Synthèse) methods were used for assessment accuracy of color and position of the fused images.

2. MATERIAL AND METHODS

2.1 Image Fusion methods

¹Afyon Kocatepe University, Department of Geomatics Engineering, 42090, Afyonkarahisar, Turkey.

muysal@aku.edu.tr

²Corresponding author: Necmettin Erbakan University, Department of Geomatics Engineering, 42090, Meram/Konya, Turkey.

avarlik@konya.edu.tr

In the literature, there are many image fusion methods. In this study PCA, multiplecative and Brovey transformation methods were used.

2.1.1 Principle Component Analysis (PCA)

The PCA is useful for image encoding, image data compression, image enhancement, digital change detection, multitemporal dimensionality and image fusion. It is a statistical technique that transforms a multivariate data set of intercorrelated variables into a data set of new un-correlated linear combinations of the original variables (Pohl and Genderen, 1998). PCA method generates uncorrelated images (PC1, PC2, ..., PCn, where n is the number of input multispectral bands). The first principal component (PC1) is replaced with the panchromatic band, which has higher spatial resolution than the multispectral images. Afterwards, the inverse PCA transformation is applied to obtain the image in the RGB color model (Zheng, 2011)

2.1.2 Brovey Transformation

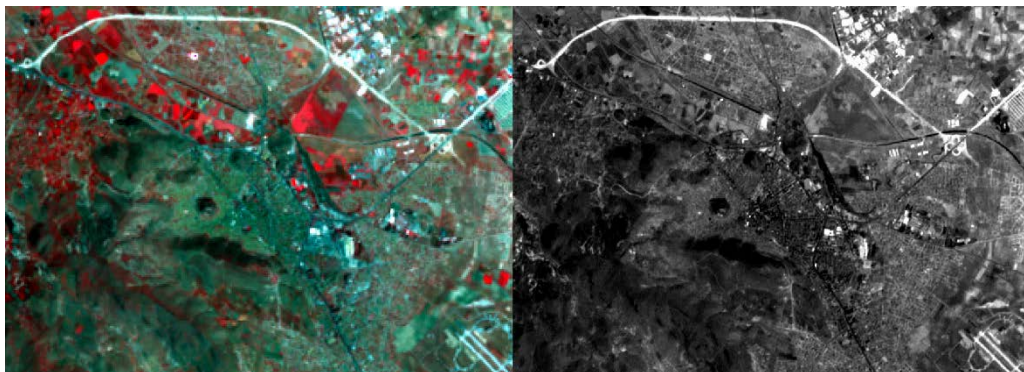
The Brovey transformation was developed to avoid the disadvantages of the multiplicative method [5]. The Brovey transformation, established and promoted by a Brovey, is also called the color normalization transform because it involves a red-green-blue (RGB) color transform method. It is a simple method for combining data from different sensors. It is a combination of arithmetic operations and normalizes the spectral bands before they are multiplied with the panchromatic image [6].

2.1.3 Multiplecative

The multiplicative method is derived from the four-component technique, as described by Crippen [7]. The four possible arithmetic methods that can be used to produce an intensity image into a chromatic image (addition, subtraction, division, and multiplication), only multiplication is unlikely to distort the color. This algorithm is a simple multiplication of panchromatic and multispectral bands with each band. The advantage of the algorithm is simple and easy. Therefore this algorithm is a simple multiplication of each multispectral band with the panchromatic image. The advantage of the algorithm is that it is straightforward and simple. By multiplying the same information into all bands, however, it creates spectral bands of a higher correlation which means that it does alter the spectral characteristics of the original image data. [5]

2.2. Datasets

In this study 04.14.2016 date of Landsat 7 ETM + multispectral bands of the satellite and the panchromatic band is used in Figure 1. Lansat 7 ETM + satellite of multispectral band 30 m, thermal tape 60 m and panchromatic band with 15 m resolution.



2.2. Quality Assessment

The evaluation procedures are based on the verification of the preservation of spectral characteristics and the improvement of the spatial resolution. First, the fused images are visually compared. The visual appearance may be subjective and depends on the human interpreter, but the power of the visual cognition as a final backdrop cannot be underestimated. Second, a number of statistical evaluation methods are used to measure the color preservation. These methods have to be objective, reproducible, and of quantitative nature. [5]. In this study, *CC (Corelation Coeficient)*, *RMSE (Root Mean Square Error)* and *ERGAS (Erreur Relative Globale Adimensionnelle de Synthèse)* methods were used quality assessment for each fused image.

The correlation coefficient (CC as shows equation 1) between the original multispectral and the fused bands. This value ranges from -1 to 1. The best correspondence between fused and original image data shows the highest correlation values [5].

$$CC = \frac{\sum \sum (MS_{ij} - MS_{ort})(F_{ij} - F_{ort})}{\sqrt{\sum \sum (MS_{ij} - MS_{ort})^2} \sqrt{\sum \sum (F_{ij} - F_{ort})^2}} \quad (1)$$

Root Mean Square Error (RMSE as shows equation 1) It is a measure of how different the two images [8].

$$RMSE = \frac{1}{ij} \sum \sum (MS_{ij} - F_{ij})^2 \quad (2)$$

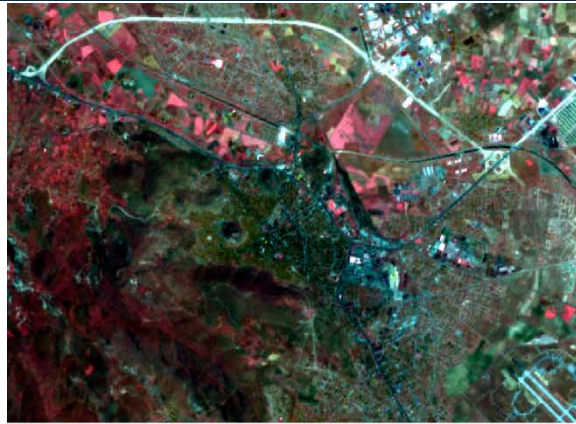
ERGAS (Erreur Relative Globale Adimensionnelle de Synthèse) This measure is related to the amount of distortion sharpened image, therefore, expected to be as small as possible [9].

$$ERGAS = 100 \frac{h}{l} \sqrt{\frac{1}{B} \sum_{b=1}^B \left(\frac{RMSE(b)}{\mu(b)} \right)^2} \quad (3)$$

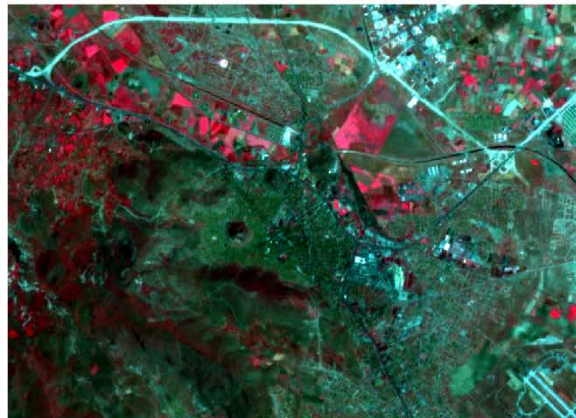
3. RESULTS

In this study, the quality of the results obtained has been demonstrated both visually and statistically and the produced images have been analyzed with comparing method. Visual comparison for the analysis of the produced image is an easy and effective method. It is very difficult that make this comparison objectively. Image quality depends on the observer and the person who does the analysis. Therefore, interpretation of the results are varies from person to person. This study explores the compare of produced merged images with original multi-band images. PCA, Brovey and Multiplicative methods were applied for merging images and merged images is shown in figure 2A, 2b and 2C, respectively.

The statistical comparison has been made with using CC, RMS and ERGAS criterias. These values have calculated for each merged image for this purpose and calculating the correlation coefficient was conducted with RMSE (root mean square error) criterias.



(a)



(b)



(c)

Figure 2. Phan-Sharpening image (a) PCA b) Brovey c) Multiplicative)

Table 1. CC method

Band	PCA	Brovey	Multiplicative
1	0,744795	0,743907	0,743572
2	0,744683	0,744089	0,743566
3	0,744257	0,743517	0,743476
4	0,747059	0,746514	0,746468
5	0,744263	0,744007	0,743827

6	0,743252	0,742919	0,743073
Average	0,744718	0,744159	0,743997

Table 2. RMSE method

Band	PCA	Brovoy	Multiplecative
1	59,52312	55,01631	45,81869
2	57,11029	52,86885	43,38253
3	72,17152	69,02441	52,32624
4	63,48086	50,81049	41,21304
5	89,68561	85,11074	60,98753
6	71,12887	65,732	52,60283
Average	68,85004	63,0938	49,38848

Table 3. ERGAS method

Band	PCA	Brovoy	Multiplecative
1	4,457346	4,176332	3,602832
2	4,499429	4,220663	3,597182
3	4,880045	4,699771	3,743263
4	5,00671	4,156279	3,512101
5	4,946914	4,73262	3,60265
6	5,438787	5,082716	4,216489
Average	4,904304	4,543656	3,734646

4 CONCLUSIONS

Positional clarity of the image, which is gained from fusing methods, can be evaluated visually and statistically. Color similarities, image distortions and distinguishable of the objects are taken into account in visual assessments [1]. Visual assessments cannot use alone for measure success of the method because it can be different from person to person. Statistical methods should use for making an objective assessment. The Visual results of study can be seen in Figure (3-6). The results of statistical assessment are presented in Table 1.

4.1 Visual Interpretation

Visual interpretation was performed in consideration of color similarity; image distortions and availability distinguish objects. It was observed that the color tones of the images are different with the various methods that using in the study. The spatial resolution increased while the spectral recovery has not taken place as expected in all studies. It has not been possible to extract detailed information with some methods.

PCA method show the best results in analyzing of color similarities. When comparing with original image, it was determined that PCA has darker colors. In the images obtained by PCA, buildings could not be detectable clearly.

Brovoy transformation increased spatial resolution also it caused to color changes. More different color tones have obtained by IHS method when it compared to other methods. We observed it is increasing spectral diversity of the image, which is obtain by high-permeability filter technique, but its colors has changed.

4.2 Statistical Methods

The mean and standard deviations of the original and merged images are shown in Figure 5. Produced image kept its spectral attributes when raw multi-band images' values comparing with produced images' values, which are obtained from various fusion algorithms. Reflection values of cross section have been extracted from each image for each band and correlation coefficients between these values were calculated. Correlation between each bands of the merged images (corresponding of original image band) and each bands that belongs to original image was calculated. The

degree of spectral diversity was determined in this study. Multi-band images have ideal spectral information in this research and it is possible to detect the images that have most ideal spectral information. The value of +1 shows that values are same (high correlation) and value of -1 indicates that the data are completely opposite of each other. Correlation coefficients between bands of original image and the merged images are shown in Figure 6.

In this study, Landsat 7 pan-sharpening performance was investigated. PCA, Brovey and IHS transformation methods were used to pan-sharpening process in Erdas imagine software. CC and RMSE criteria were used for statistical analysis of obtained images. Visual analysis of obtained images have been made for quality purpose. In generally, images, which obtained from Brovey transformation are seems have best quality but images that have produced with IHS methods are most quality than others.

REFERENCES

- [1] L. Wald, A European Proposal For Terms Of Reference In Data Fusion, In: International Archives of Photogrammetry and Remote Sensing, Vol. XXXII, Part 7, pp. 651-654, 1998
- [2] V. Yılmaz and O. Güngör, Performance Analysis On Image Fusion Methods, TUFUAB 2013, 23-25 Mayıs 2013, Trabzon
- [3] C., Pohl, and J. L. V. Genderen, Multisensor image fusion in remote sensing: concepts, methods and applications. International Journal of Remote Sensing, vol. 19, no. 5, 823-854, 1998
- [4] Y. Zheng., Image Fusion and Its Applications, Intech Publisher, ISBN 978-953-307-182-4, 252 pages, 2011
- [5] S. Klonus, and M. Ehlers, Performance of evaluation methods in image fusion. Proceedings of the 12th International Conference on Information Fusion, International Society of Information fusion 6-9 July, Seattle, Washington. 2009
- [6] R.A. Mandhare, S. Gupta, "Pixel Level Image Fusion Using Brovey Transform And Wavelet Transform," International Journal of Advanced Research in Electrical, Electronics and Instrumentation Engineering Vol. 2, Issue 6, June 2013
- [7] R.E., Crippen. A simple spatial filtering routine for the cosmetic removal of scan-line noise from Landsat TM P-tape imagery, Photogrammetric Engineering & Remote Sensing, 55(3):327-331. 1989
- [8] V., Vijayaraj, A Quantitative Analysis OF Pansharpened Images, Department of Electrical & Computer Engineering, Mississippi State University, 2004.
- [9] L., Alparone, B., Aiazzi, S., Baronti, A., Garzelli, F., Nencini, M., Selva, Multispectral and Panchromatic Data Fusion Assessment Without Reference. Photogrammetric Engineering & Remote Sensing 74, 193-200, 2008.

Prediction of the Dynamic Response of Repeated Low Velocity Impact on Adhesively Bonded Plates

Umut Caliskan*¹, Mustafa Yildirim¹, M. Kemal Apalak¹

Abstract

A three-dimensional (3-D) dynamic element analysis (FEA) was performed to study the repeated transverse low velocity impact behaviour of adhesively bonded plates. Adhesive bonding is an effective joining technique and has been widely applied in various industries. Compared to other joining methods such as welding, adhesive bonding is relatively easier to perform and does not require excessive enterprise costs. The adhesively bonding plate is subjected by a mass at one time in single impact, but sometimes multiple impact load can occur simultaneously and/or non-simultaneously. Single and multiple times impact loads were conducted for the different impact energy levels. Abaqus/Explicit (Version 6.14) finite element package programme was used for the numerical simulations. Plates and adhesive were used as aluminum 2024 and Araldite 2015 in numerical analysis, respectively. The variations of the contact force, kinetic energy histories and the deflection of the central impact region were investigated under single and multiple times low velocity impact loads.

Keywords: Repeated impact, adhesive, adhesively bonding joint, nonlinear finite element method

1. INTRODUCTION

Adhesive technology offers adhesives with high impact strength so that adhesively bonded joints can serve safely under an impact load for a short period. Impact mechanism develops strongly with surface conditions, and becomes more apparent on the metal surface whereas the damage may initiate inside the composite materials, such as along interfaces between the layers rather than on the surface of the composite material. Therefore, the prediction of the initiation and propagation of the damages in the composite materials needs various damage models to be considered. Low velocity impacts are considered as the most dangerous situations because of the difficulties to detect the damages. After an impact, a large reduction in the mechanical performance may occur. Thus, a good understanding of indentation, impact response and repeated impact response are necessary in order to predict and assess their residual strengths. Structures under repeated impacts are usually applied in engineering such as the landing gears of carrier-based aircrafts, excavator movable arms, rock crushers and firing system of artilleries. At these situations, high strain rate and accumulated plastic deformation are two significant features that increase the risk of failure. Hence, it is extremely essential to predict the residual life, i.e., the number of impacts to failure [1]. M. K. Sisi et al. [2] studied a theoretical method for low-velocity impact of composite laminated beams with arbitrary lay-ups and various boundary conditions subjected to repeated impacts of multiple masses. Their analyses was based on the higher-order partial differential equations of the motion were derived using the Lagrangian equations of the second kind. Numerical examples showed that the time of impact play an important role on contact forces, beam displacements, absorbed energies by the beam and normal and shear stresses by positive and negative superposition of induced waves. V. Arıkan and O. Sayman [3] investigated repeated impact response of E-glass fiber reinforced polypropylene and epoxy matrix composites and effect of resin type on the impact response of composites. They manufactured E-glass fiber reinforced composites with two types of resin, polypropylene and epoxy. They used impact energy levels of 20 J, 50 J, 80 J and 110 J for single impact tests while 50 J was chosen for repeated impact tests. They compared between the results of 110 J single and 50 J repeated impacted specimens. As a result of the study it was concluded that the resin type is a crucial parameter for the repeated impact response of the composites. C. Atas and A. Dogan [4] studied the effect of thermal ageing on low velocity impact response of E-glass/epoxy composites and also together with single impact case, repeated impact response of the composite samples. They chose impact energy levels of 20 J, 40 J, 60 J, 80 J and 100 J for single impact tests and 20 J for repeated impact tests. The conditioning humidity and temperature were chosen respectively as 70% and 95 °C, considering the glass-transition temperature (T_g) of the intact composites which was determined as 78 °C. The samples were exposed to ageing durations of 100, 400, 700, 1000 and 1300 h by using a climatic test cabin. As a result of the study it was

¹ Corresponding author: Erciyes University, Department of Mechanical Engineering, 38039, Melikgazi/Kayseri, Turkey. ucaliskan@erciyes.edu.tr

² Erciyes University, Department of Mechanical Engineering, 38039, Melikgazi/Kayseri, Turkey. my@erciyes.edu.tr

³ Erciyes University, Department of Mechanical Engineering, 38039, Melikgazi/Kayseri, Turkey. apalakmk@erciyes.edu.tr

found that in addition to the mechanical properties, damage resistance of the E-glass/epoxy composites was significantly affected by the thermal ageing. C. Atas et al. [5] studied the repeated impact response of woven E-glass/epoxy composites with various thicknesses. They showed energy profile diagrams of the samples, the variation of perforation thresholds with thickness and the variation of absorbed energy with repeat numbers. They found that the perforation threshold/energy for single impact varied linearly with thickness for the chosen composite plates. Considering different energy levels, the impact numbers corresponding complete perforation of the specimens with different thicknesses, i.e. layer numbers, were also provided. J. Aurrekoetxea et al. [6] investigated the repeated impact behaviour of self-reinforced polypropylene composite. Plastic deformation of the tape was the dominant mechanism, and the resulting penetration mode was a highly localised “star”-shaped hole. Damage and perforation thresholds are 5 J and 31.4 J respectively. Impact fatigue life exceeds 500 impact events up to 13 J, but drops sharply for 14 J. Strain-hardening was the origin of the trend of peak load increased and plastic deformation decreased with impact events. As a result of, the amount of energy absorbed by each impact was reduced.

2. MATERIAL AND METHODS

2.1. Finite Element Model

The low velocity impact behavior of adhesively bonded plates was studied using ABAQUS/Explicit (version 6.14) [7]. The impact behavior was investigated for single and multiple impact under four impact energy levels of 15, 30, 45 and 60 J. Aluminum plates were in dimension of 125x125x2 mm and were bonded using an epoxy based adhesive (Araldite 2015) in dimension of 125x125x0.2 mm. The Plates and adhesive layer were modeled as an elasto-plastic material. The stress and strain curves of plates and adhesive are shown in Figure 1 and the mechanical properties of materials are listed in Table 1.

Table 1. Mechanical properties of adhesively bonded plate

Material	Al 2024	Araldite 2015
Density (kg/m ³)	2700	1450
Poisson's ratio	0.3	0.36
Young's modulus (GPa)	70	1.16
Yield stress (Mpa)	240	24.7

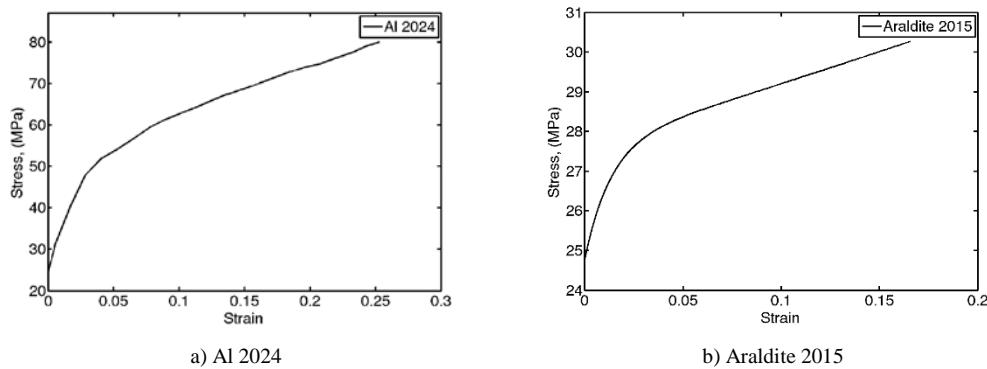


Figure 1. Stress-Strain curves of (a) Al 2024 and (b) Araldite 2015

The impactor was modeled as a rigid body behavior. The encastered boundary condition was applied to the adhesively bonded plates. Plates and adhesive layer were modelled using a three dimensional solid finite element with three degrees of freedom at each node (C3D8R). The hourglass control was also used for the finite elements of core material as another option to avoid excessive element distortions and calculate numerical integrations accurately. The mechanical contact between the impactor and adhesively bonded plates was simulated by the GENERAL CONTACT ALGORITHM in Abaqus/Explicit. The finite element model is shown in Figure 2.

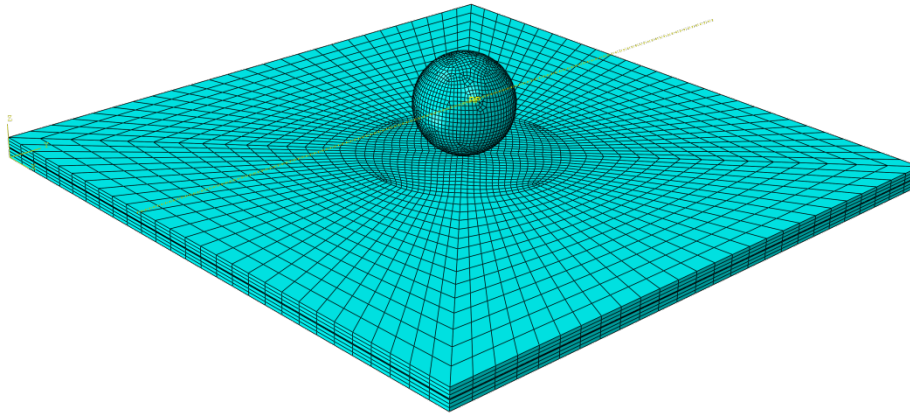
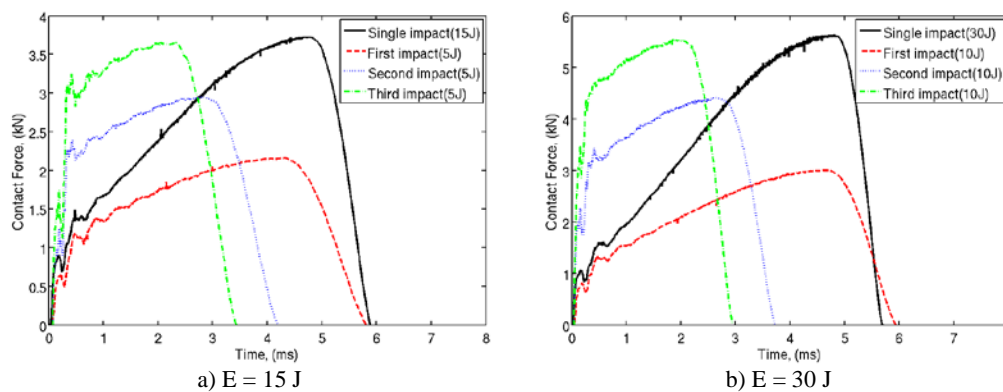


Figure 2. Finite Element Model

3 RESULTS AND DISCUSSION

Impact analyses were performed for impact energies of 15, 30, 45 and 60 J, respectively. The impactor was spherical tip geometry of 20 mm in diameter, and 5.045 kg of a mass. The effect of the single and multiple impact was investigated the adhesively bonded plates. The temporal variations of the contact force were determined for four impact energy levels of 15, 30, 45 and 60 J, respectively. The kinetic energies were evaluated to determine the energy absorption capability of adhesively bonded plates. The adhesively bonded plates thickness was 4.2 mm for the all specimens. Figure 3 shows the effect of the single and repeated impact on the temporal variations of the contact force under present impact energies, respectively. The peak contact forces are measured as 3.72, 5.63, 7.09 and 8.16 kN under the impact energy levels of 15, 30, 45 and 60 J for a single impact test, respectively, and the corresponding peak contact times are nearly same for all specimens as 4.8 ms. The impact analyses are completed in the total contact times of 5.9, 5.7, 5.6 and 5.5 ms.

As the repeated impacts analyses are considered, repeated impact energy is 5 J (three times) for the total impact energy of 15 J and for the total impact energy of 30 J, repeated impact energy is 10 J, for the total impact energy of 45 J, repeated impact energy is 15 J, for the total impact energy of 60 J, repeated impact energy is 20 J. As the first impact energy level 15 J is considered, peak contact forces are measured as 2.15, 2.94 and 3.65 kN for the first, second and third impact (5J), respectively. The repeated impact tests are completed in the total contact times of 5.8, 4.2 and 3.4 ms. As the impact energy level of 30 J is considered, the peak contact forces are measured as 3.01, 4.4 and 5.5 kN for the first, second and third impact (10 J), respectively. The repeated impact analyses are completed in the total contact times of 5.9, 3.7 and 2.9 ms. As the impact energy level of 45 J is considered, the peak contact forces are measured as 3.72, 5.56 and 6.98 kN for the first, second and third impact (15 J), respectively. The repeated impact analyses are completed in the total contact times of 5.9, 3.5 and 2.8 ms. As the impact energy level of 60 J is considered, the peak contact forces are measured as 4.42, 6.60 and 8.17 kN for the first, second and third impact (20 J), respectively. The repeated impact analyses are completed in the total contact times of 5.8, 3.3 and 2.7 ms. As the impact energy is increased, peak contact forces are increased and total contact durations are decreased for all specimens. Peak contact force levels for repeated and single impact are nearly same, but total contact durations of the repeated impact tests are longer than single impact analyses. Peak contact force levels are gradually increased caused by strain hardening effect for same energy levels in the repeated impact analyses.



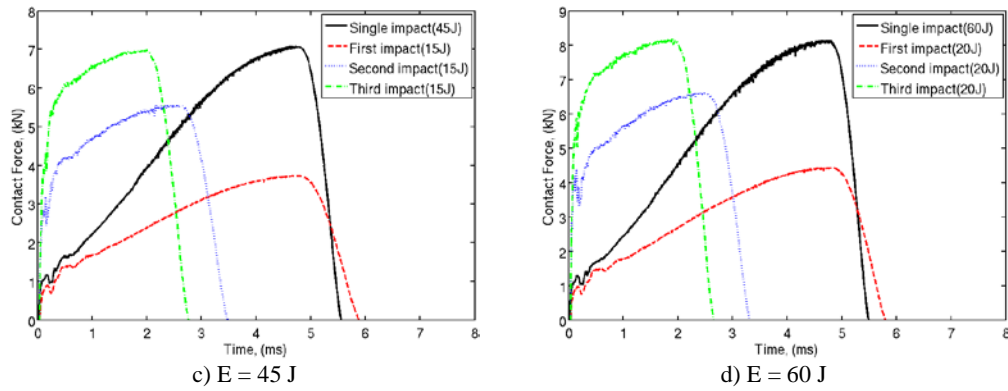


Figure 3. The effect of the single and repeated impact on the variation of contact force for the impact energy levels of 15, 30, 45 and 60J

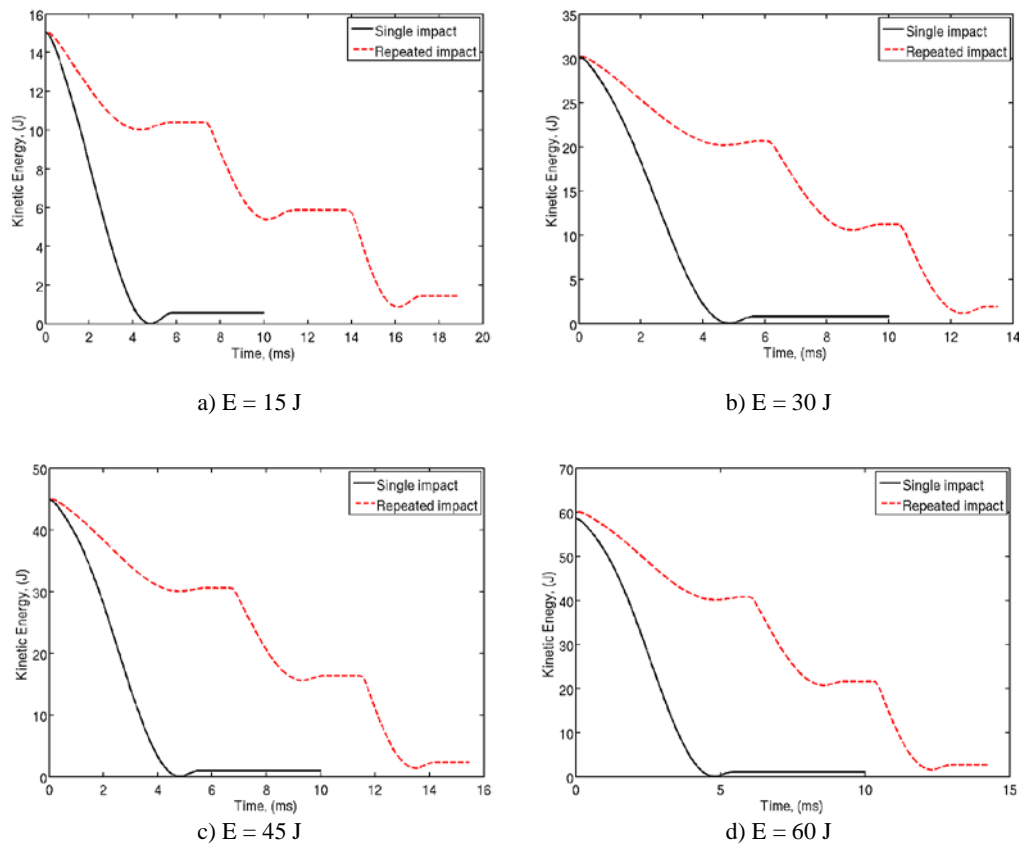
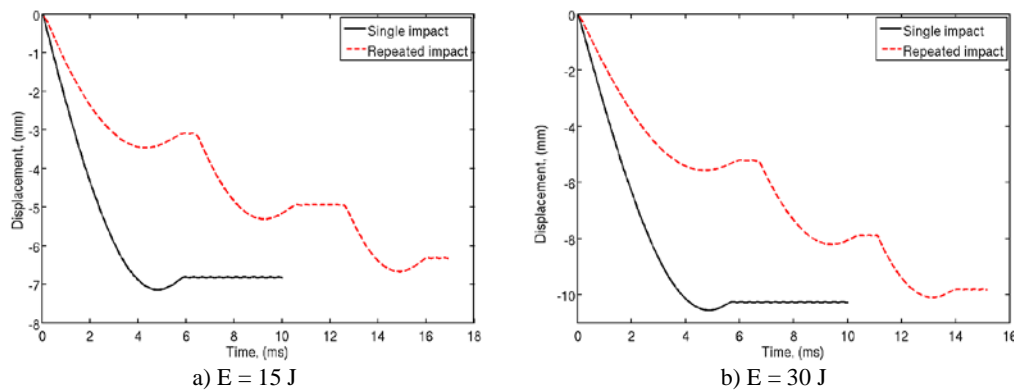


Figure 4. The effect of the single and repeated impact on the kinetic energy histories for the impact energy levels of 15, 30, 45 and 60J



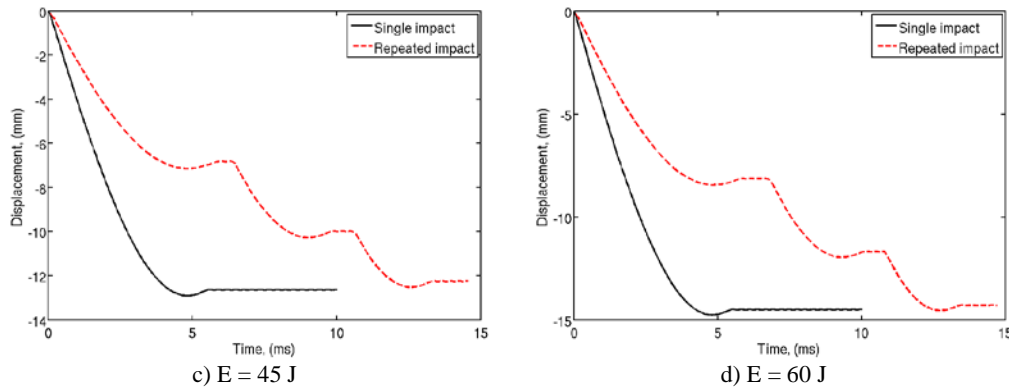


Figure 5. The effect of the single and repeated impact on the permanent deflection at the top plate of central impact region for the impact energy levels of 15, 30, 45 and 60J

Figure 4 shows the effect of the single and repeated impact on the kinetic energy histories under present impact energies, respectively. Impact energies of 15, 30, 45 and 60 J for the single impact are reduced to kinetic energy levels of 0.57, 0.79, 0.96 and 1.08 J, respectively; thus, the impact energies are dissipated by 96.2, 97.3, 97.8 and 98.2%, respectively. Impact energy of 15, 30, 45 and 60 J for the repeated impact analyses (5, 10, 15, 20 J) are reduced to kinetic energy levels of 1.43, 1.93, 2.3 and 2.63 J, respectively; thus, the impact energies are dissipated by 90.4, 93.5, 94.8 and 95.6%, respectively. As the impact energy is increased, the capability of the absorbing energy is increased. Impact energy absorption capability under single impact analyses is better than under repeated impact analyses. The capability of the energy absorbing are gradually decreased caused by strain hardening effect for same energy levels in the repeated impact analyses.

Figure 5 shows the effect of the single and repeated impact on the central permanent deflection at the impact region under present impact energies, respectively. Central permanent deflections under single impact analyses are 6.8, 10.3, 12.6 and 14.5 mm for the impact energies of 15, 30, 45 and 60 J. Central permanent deflections under repeated impact analyses (5, 10, 15, 20 J) are 6.3, 9.8, 12.2 and 14.3 mm for the impact energies of 15, 30, 45 and 60 J. As the impact energy is increased, the central permanent deflection at the impact region is increased. The specimens under repeated impact have less permanent deflection caused by strain hardening effect than under single impact for the same impact energy level.

4. CONCLUSION

This study presented the single and repeated impact response of adhesively bonded plates for various impact energies. The temporal variation of contact forces, kinetic energy histories and the permanent deflections at the top surface of plate assesses for the impact energies of 15, 30, 45 and 60 J. Strain hardening effect for the repeated impact analyses is appeared pretty much. Specimens have less permanent deflection in the repeated impact analyses than single impact analyses. Peak contact force levels are nearly same for the repeated and single impact but the contact durations for the repeated impact analyses are longer than single impact analyses. The capability of the impact energy absorption for the single impact analyses is better than in the repeated impact analyses due to strain hardening effect.

REFERENCES

- [1] L. Li, L. Sun, "Experimental and numerical investigations of crack behavior and life prediction of 18Cr2Ni4WA steel subjected to repeated impact loading", *Engineering Failure Analysis*, vol. 65, pp. 11-25 July 2016.
- [2] M. K. Sisi, M. Shakeri, M. Sadighi, "Dynamic response of composite laminated beams under asynchronous/repeated low-velocity impacts of multiple masses", *Composite Structures*, vol. 132, pp. 960-973, Nov 2015.
- [3] V. Arıkan, O. Sayman, "Comparative study on repeated impact response of E-glass fiber reinforced polypropylene & epoxy matrix composites", *Composites Part B: Engineering*, vol. 83, pp. 1-6, Dec 2015.
- [4] C. Atas, A. Dogan, "An experimental investigation on the repeated impact response of glass/epoxy composites subjected to thermal ageing", *Composites Part B: Engineering*, vol. 75, pp. 127-134, June 2015.
- [5] C. Atas, B. M. İcten, M. Küçük, "Thickness effect on repeated impact response of woven fabric composite plates", *Composites Part B: Engineering*, vol. 49, pp. 80-85, June 2013.
- [6] J. Aurrekoetxea, M. Sarrionandia, M. Mateos, L. Aretxabaleta, "Repeated low energy impact behaviour of self-reinforced polypropylene composites", *Polymer Testing*, vol. 30, pp. 216-221, April 2011.
- [7] ABAQUS/Explicit (Version 6.14), User's manual, Finite Element Software. Available from: <http://www.simulia.com>

Numerical simulations of composite sandwich panels under low velocity impact

Umut Caliskan¹, M. Kemal Apalak²

Abstract

This study addresses the low velocity impact behaviour of composite sandwich panels with glass fiber-reinforced polymer face-sheet and PVC foam core. Impact behaviour was investigated for various fiber angles and impact energy levels of composite sandwich panels. Material non-linearities were considered in the explicit analysis and cohesive zone model based on fracture mechanics was used to model adhesive layer and delaminations. Low velocity impact simulations were performed on a uni-directional laminate [0°]₄, [30°]₄ and [45°]₄ of E glass/epoxy composite sandwich panel of composite face-sheet thickness of 1 mm for impact energies of 10, 20 and 30 J. The dynamic response of foam core sandwich panels was studied using ABAQUS/Explicit. The variations of contact force, kinetic energy histories and damage areas were showed and also, the capability of energy absorbing of the panels was investigated.

Keywords: *Low velocity impact, composite, sandwich panel, PVC foam, finite element method*

1. INTRODUCTION

The sandwich structures are becoming increasingly popular in aerospace and marine industries and other areas where lightweight materials with high in-plane and flexural stiffness are needed. Impact mechanism develops strongly with surface conditions, and becomes more apparent on the metal surface whereas the damage may initiate inside the composite materials, such as along interfaces between the layers rather than on the surface of the composite material. Therefore, the prediction of the initiation and propagation of the damages in the composite materials needs various damage models to be considered. Composites and sandwich structures are used in aircraft, automobile, marine, defense, military, sports and structural applications where one of the major concerns is the strength to weight ratio. The advanced composite materials like Fiber Reinforced Polymer (FRP) composites are lighter than metal counter parts and many times stronger directionally. Sandwich structures are prone to impact threats from a wide range of projectile shapes, sizes and velocities during service and maintenance life. Low velocity impacts are considered as the most dangerous situations because of the difficulties to detect the damages. After an impact, a large reduction in the mechanical performance may occur. Thus, a good understanding of indentation and impact response is necessary in order to predict and assess their residual strengths. Flores-Johnson and Li [1] studied indentation of sandwich panels with carbon fibre-reinforced polymer face sheets and polymeric foam core. Both nose shape and foam core density have large influence on the indentation at failure and damage area and also C-scan images showed that these results. They observed a dependency of the indentation load on the supporting condition. They also found that the difference in indentation resistance between the sandwich panel and its corresponding core material depends on the core density. Singh et al. [2] investigated a damage evolution study of E-glass/epoxy composite under low velocity impact. Glass Fiber Reinforced Polymer composite is a popular material system that can be used in vehicles and is able to meet requirements in torsion, bending and crash. During the service of the components made of composite there is possible mass impact (stone and debris) which is considered as Low Velocity Impact (LVI). They compared two damage models and finally exponential model was used for low velocity impact simulations. They calculated material softening parameter m for different element sizes. Simulations were performed for low velocity impact of glass epoxy plate having two configurations i.e. unidirectional and crossply. They had good agreement between the predicted and measured strain was obtained. Namala et al. [3] investigated the low velocity impact behavior of a uni-directional laminate of E-glass-epoxy composite. The energy, contact forces, and displacement plots with respect to time are studied for a drop test. They observed the damage as a back face signature on the back face of both cross-ply and unidirectional laminate were plotted. The composite was speckled randomly and the impact phenomenon was recorded using a high-speed camera. The DIC data were analyzed to obtain displacement and strains on the surface of the plate. They observed that the visible damage is major on the back face of the laminate. This damage is a combined effect of top surface damage due to compressive stresses and crushing stresses, with bottom surface damage due to tensile stresses and delamination between plies. Schubel et al. [4] studied experimentally the low velocity impact behaviour of sandwich panels made of woven carbon/epoxy face-sheets and a PVC foam core by assuming a quasi-static load. Their straightforward method predicting the peak impact load estimation method exhibited a good agreement with experimental results. They also gave a contact force-indentation relationship under static load and studied some analytical models for applicability to the sandwich setup. Their first model did not model

¹ Corresponding author: Erciyes University, Department of Mechanical Engineering, 38039, Melikgazi/Kayseri, Turkey.
ucaliskan@erciyes.edu.tr

² Erciyes University, Department of Mechanical Engineering, 38039, Melikgazi/Kayseri, Turkey.
apalakmk@erciyes.edu.tr

the panel behavior beyond core yielding and their another model did account for core yielding. Their initial linear indentation behaviour until core yielding matched well. Lopes et al. [5] investigated low velocity impact damage resistance on dispersed stacking sequence laminates using the explicit finite element method. Their constitutive models which take into account the physical progressive failure behaviour of fibres, matrix, and interfaces between plies were implemented in an explicit finite element method and used in the simulation of low-velocity impact events on composite laminates. They compared experimental results with those of their numerical model with 24-ply laminate specimens. Their simulations showed that the energy dissipated through delaminations was higher for the their alternative configuration specimens than for the baseline within the 9-30 J impact energy range. Yu et al. [6] investigated the response and failure of dynamically loaded sandwich beams with an aluminum-foam core experimentally. They obtained the dynamic compressive stress-strain curves of the core material by a Split-Hopkinson pressure bar technique. They could not find strain-rate sensitivity. Quasi-static and dynamic bending tests are carried out for sandwich beams made of aluminum skins with an aluminum foam core. The deformation and failure mechanism were revealed by ‘frozen’ test using stop blocks. They found that large local indentation and damage the energy absorbing capacity of beams loaded dynamically was lower than that for quasi-static loading. Ivañez and Sanchez-Saez [7] investigated the response of composite sandwich beams with honeycomb core subjected to low-velocity impact by using a finite-element model implemented in Abaqus/Explicit code. They modelled face-sheet behavior through a VUMAT subroutine, in which a failure model based on Hou failure criteria was implemented and they modelled the aluminium honeycomb core behaviour as an elastic-plastic material. They had good agreement in terms of contact-force histories, energy histories, absorbed energy and failure of the sandwich beams between the experimental data and the numerical results. They found that the core controlled the energy absorption of the sandwich beams at the lowest impact velocities studied; however, at higher impact velocities the face-sheets were more involved. Atas and Sevim [8] presented an experimental investigation on impact response of sandwich composite panels with PVC foam core and balsa wood core. They analyzed damage process of the sandwich composites from cross-examining load-deflection curves, energy profile diagrams and the damage specimens. They observed the primary damage modes as fiber fractures at upper and lower skins, delaminations between adjacent glass-epoxy layers, core shear fracture, and face/core debonding. It was also seen from the load-deflection curves that the foam core sandwich is of lower bending stiffness. Zhou et al. [9] investigated the perforation resistance of foam-based sandwich panels with experimental and numerical techniques. The effect of oblique loading and an aqueous support on sandwich panels were studied. The perforation resistance of the plain foams and their sandwich panels was strongly dependent on the properties of the foam core. At intermediate and higher densities, the crosslinked PVC foams and their associated sandwich panels offered a superior perforation resistance to their linear PVC counterparts. It was shown that sandwich panels impacted in an aqueous environment exhibit a lower perforation resistance than tested in air.

2. MATERIAL AND METHODS

2.1. Finite Element Model

The low velocity impact behavior of sandwich panels was studied using ABAQUS/Explicit (version 6.14). The impact behavior was investigated for different fiber angles under three impact energy levels of 10, 20 and 30 J. Composite face-sheets and PVC foam were in dimension of 125x125 mm and were bonded using an epoxy based adhesive (Araldite 2015). The face-sheet thickness was taken as 1 mm, the core material was PVC (Airex C 70.75) foam in thickness of 10 mm and density of 80 kg/m³. Adhesive thickness was taken as 0.25 mm for the impact analyses of the foam core sandwich panels. The foam core was modeled as crushable foam material. The stress and strain curve of PVC foam material (C 70.75) is shown in Figure 1 and the mechanical properties of PVC foam is listed in Table 1.

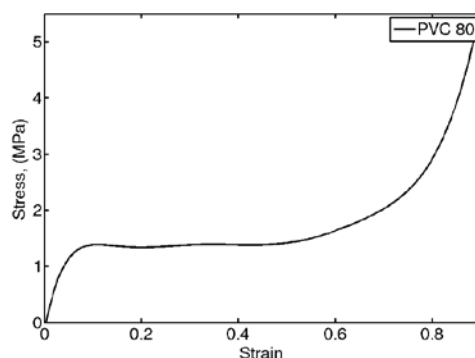


Figure 1. Stress-Strain curve of PVC C70.75 foam core

Table 1. Mechanical properties of core material (AIREX datasheet values)

Core Material	PVC Airex C70.75
Density (kg/m ³)	80

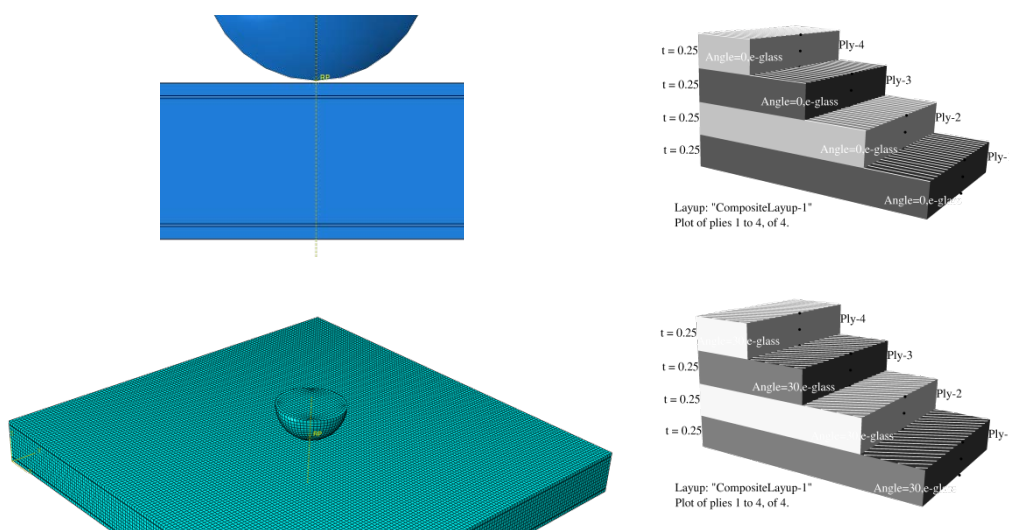
Compressive Modulus (MPa)	104
Compressive Strength (MPa)	1.45
Tensile Modulus (MPa)	66
Tensile Strength (MPa)	2.0
Shear Modulus (MPa)	30
Shear strength (MPa)	1.2

The impactor was modeled as a rigid body behavior. The encastered boundary condition was applied to the sandwich panel. Composite face-sheets were modelled using a continuum shell element with 8-node hexahedron (SC8R) and foam core were modeled using a three dimensional solid finite element with three degrees of freedom at each node (C3D8R). The hourglass control was also used for the finite elements of core material as another option to avoid excessive element distortions and calculate numerical integrations accurately. The mechanical contact between the impactor and sandwich panel was simulated by the GENERAL CONTACT ALGORITHM in Abaqus/Explicit. The adhesive layer between the face-sheets and foam core is simulated by means of the cohesive zone approach. The interfacial adhesive failure was modeled through this cohesive zone layer between the face-sheets and foam core. The cohesive parameters of the epoxy adhesive were given in Table 2 [10] and a three dimensional cohesive element (COH3D8) was used to model the cohesive response of the adhesive layer. The nominal traction stress vector t , with the components: t_n^0 , t_s^0 and t_t^0 , which represent the normal and the two shear tractions, respectively. G_n and G_s are the areas under the CZM laws in tension and shear. The cohesive thickness was taken as 0.25 mm for the adhesive layer. The finite element model of sandwich panel was shown in Figure 2.

Table 2: Cohesive parameters of adhesive Araldite 2015 used in CZM

Property	Araldite 2015
E (GPa)	1.85
G (GPa)	0.56
t_n^0 (MPa)	21.63
t_s^0 (MPa)	17.9
G_n^0 (N/mm)	0.43
G_s^0 (N/mm)	4.70

Composite face-sheets were modelled as four layer and unidirectional laminate fiber angle of 0°, 30° and 45°. The material damage initiation capability for fiber-reinforced materials requires that the behavior of the undamaged material is linearly elastic, is based on Hashin's theory and can be used in combination with the damage evolution model described in "Damage evolution and element removal for fiber-reinforced composites" in the Abaqus/Explicit code. Damage initiation refers to the onset of degradation at a material point. In Abaqus the damage initiation criteria for fiber-reinforced composites are based on Hashin's theory. These criteria consider four different damage initiation mechanisms: fiber tension, fiber compression, matrix tension, and matrix compression and mechanical properties for the composite plates E-glass/epoxy are given in Table 3.



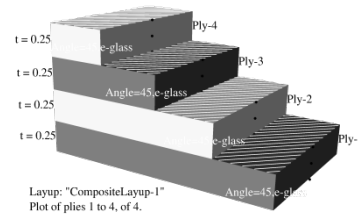


Figure 2. Finite element model and ply orientation

The initiation criteria have the following general forms:

Fiber tension ($\widehat{\sigma}_{11} \geq 0$)

$$F_f^t = \left(\frac{\widehat{\sigma}_{11}}{X^T}\right)^2 + \alpha \left(\frac{\widehat{\tau}_{12}}{S^L}\right)^2 \quad (1)$$

Fiber compression ($\widehat{\sigma}_{11} < 0$)

$$F_f^c = \left(\frac{\widehat{\sigma}_{11}}{X^C}\right)^2 \quad (2)$$

Matrix tension ($\widehat{\sigma}_{22} \geq 0$)

$$F_m^t = \left(\frac{\widehat{\sigma}_{22}}{Y^T}\right)^2 + \alpha \left(\frac{\widehat{\tau}_{12}}{S^L}\right)^2 \quad (3)$$

Matrix compression ($\widehat{\sigma}_{22} < 0$)

$$F_m^c = \left(\frac{\widehat{\sigma}_{22}}{2S^T}\right)^2 + \left[\left(\frac{Y^C}{2S^T}\right)^2 - 1\right] \frac{\widehat{\sigma}_{22}}{Y^C} + \left(\frac{\widehat{\tau}_{12}}{S^L}\right)^2 \quad (4)$$

$\widehat{\sigma}_{11}$, $\widehat{\sigma}_{22}$, $\widehat{\tau}_{12}$ are components of the effective stress tensor, $\widehat{\sigma}$, that is used to evaluate the initiation criteria and which is computed from:

$$\widehat{\sigma} = M\sigma \quad (5)$$

Where σ is the true stress and $\widehat{\sigma}$ is the damage operator:

$$M = \begin{bmatrix} \frac{1}{(1-d_f)} & 0 & 0 \\ 0 & \frac{1}{(1-d_m)} & 0 \\ 0 & 0 & \frac{1}{(1-d_s)} \end{bmatrix} \quad (6)$$

d_f , d_m , and d_s are internal (damage) variables that characterize fiber, matrix, and shear damage, which are derived from damage variables d_f^t , d_f^c , and d_m^c corresponding to the four modes previously discussed, as follows :

$$d_f = \begin{cases} d_f^t & \text{if } \widehat{\sigma}_{11} \geq 0 \\ d_f^c & \text{if } \widehat{\sigma}_{11} < 0 \end{cases} \quad (7)$$

$$d_m = \begin{cases} d_m^t & \text{if } \widehat{\sigma}_{22} \geq 0 \\ d_m^c & \text{if } \widehat{\sigma}_{22} < 0 \end{cases} \quad (8)$$

$$d_s = 1 - (1 - d_f^t)(1 - d_f^c)(1 - d_m^t) (1 - d_m^c) \quad (9)$$

Table 3. Elastic and strength properties for composite face-sheet [2]

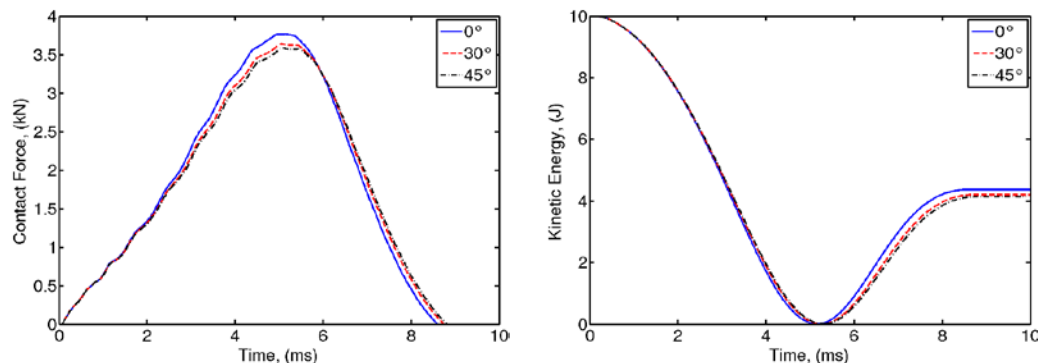
Longitudinal modulus, E_{11}	40 (GPa)
Transverse modulus, $E_{22} = E_{33}$	10 (GPa)
Shear modulus, $G_{22} = G_{33}$	3.15 (GPa)
Shear modulus, G_{23}	4.32 (GPa)
Volume fraction of fiber, V_f	0.54
Poisson's ratio, $\mu_{12} = \mu_{13}$	0.3
Poisson's ratio, μ_{23}	0.21
Density	1780 (kg/m ³)
Longitudinal tensile strength, X_T	988 (MPa)
Transverse tensile strength, $Y_T = Z_T$	44 (MPa)
Longitudinal compressive strength, X_C	1432 (MPa)
Transverse compressive strength, $Y_C = Z_C$	285 (MPa)
In-plane shear strength $S_{12} = S_{13}$	60.6 (MPa)
Interlaminar shear strength, S_{23}	22 (MPa)

3. RESULTS AND DISCUSSION

Impact analyses were performed for impact energies of 10, 20 and 30 J, respectively. The impactor was spherical tip geometry of 20 mm in diameter, and 5.045 kg of a mass. The mechanical design parameter of fiber angle orientation was investigated to improve the impact energy absorption capability of the structure. The temporal variations of the contact force were determined for three impact energy levels of 10, 20 and 30 J, respectively. The kinetic energies were evaluated to determine the energy absorption capability of structures. The composite sandwich panel thickness is 12.5 mm for the all specimens. Figure 3 shows the effect of the fiber angle on the temporal variations of the contact force and kinetic energy histories under present impact energies, respectively. The peak contact forces are measured as 3.76, 3.63 and 3.58 kN under the impact energy level of 10 J for a fiber angles of 0°, 30° and 45°, respectively, and the corresponding peak contact times are same for all specimens as 5.1 ms. The impact analyses are completed in the total contact times of 8, 8.7 and 8.8 ms.

The peak contact forces are measured as 6.56, 6.32 and 6.21 kN under the impact energy level of 20 J for a fiber angles of 0°, 30° and 45°, respectively, and the corresponding peak contact times are 4.5, 4.6 and 4.7 ms. The impact analyses are completed in the total contact times of 7.7, 7.8 and 7.9 ms, respectively. As the impact energy level of 30 J is considered, the peak contact forces become 9.06, 8.71 and 8.58 kN for a present fiber angles, respectively and the corresponding peak contact times are 4.2, 4.3 and 4.4 ms. The impact analyses are completed in the total times of 7.1, 7.3 and 7.4 ms, respectively. As the impact energy is increased, the peak contact force levels are increased and the total contact durations are decreased. The peak contact force levels are decreased with increasing the fiber angle. The total contact durations are increased with increasing the fiber angle. But these decrease and increase are quite small. Consequently, the changing fiber angle for this geometry does not effect preciously contact force histories.

The specimens with having fiber angles of 0°, 30° and 45° reduce impact energy of 10 J to kinetic energy levels of 4.36, 4.20 and 4.11 J, respectively; thus, the impact energies are dissipated by 56.4, 58 and 58.9%, respectively. For the impact energy levels of 20 J the specimens reduce to kinetic energy levels of 10.31, 9.91 and 9.77 J, respectively and the impact energies are dissipated by 48.45, 50.45 and 51.15%, respectively. The specimens with having fiber angles of 0°, 30° and 45° reduce impact energy of 30 J to kinetic energy levels of 16.9, 16.32 and 16.05 J, respectively; thus, the impact energies are dissipated by 43.6, 45.6 and 46.5%, respectively. As the impact energy is increased, the capability of the energy absorbing is decreased and as the fiber angle of composite face-sheets is increased, the capability of the energy absorbing is increased for the square specimen geometry. Because the fiber length is longer through the corner. So the structure is more stiff in the directions of 0° and 90°.



a) E= 10 J

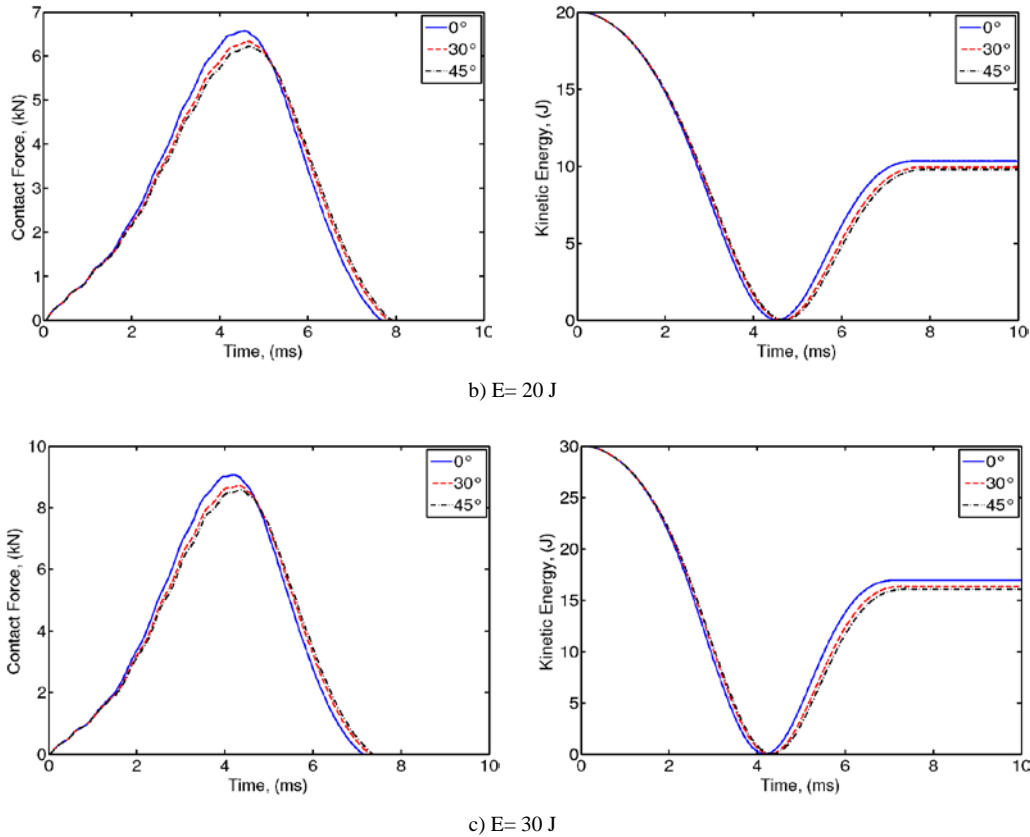
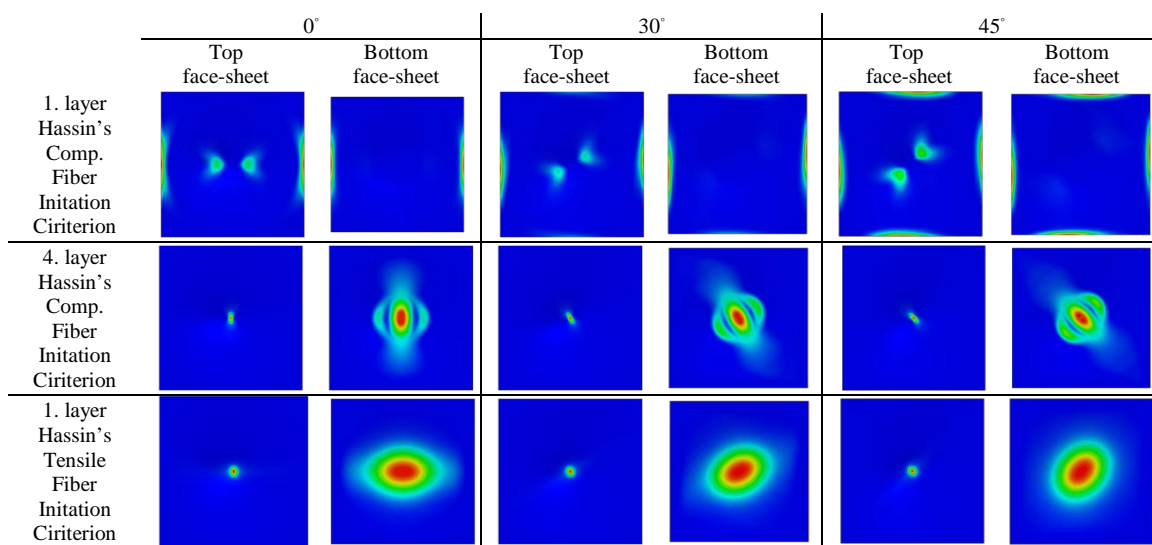


Figure 3. Effect of the fiber angle on the variations of contact force and kinetic energy for the impact energies of 10, 20 and 30 J.

Figure 4-6 shows the Hassin's fiber compression and tensile initiation criterion in the top and bottom face-sheets for the impact energies of 10, 20 and 30 J. The first layer of the top face-sheet is in contact with adhesive layer and fourth layer of the top face-sheet is in contact with impactor surface and the fourth layer of the bottom face-sheet is in contact with adhesive layer. Damage occurs in the fiber direction. Tensile fiber damage occurs in the first layer of the bottom face-sheet for all fiber angles and as the considering fourth layer of the bottom face-sheet, damage level is increased in the fiber angle of 45°. As the impact energies is increased, the damage area is increased, naturally.



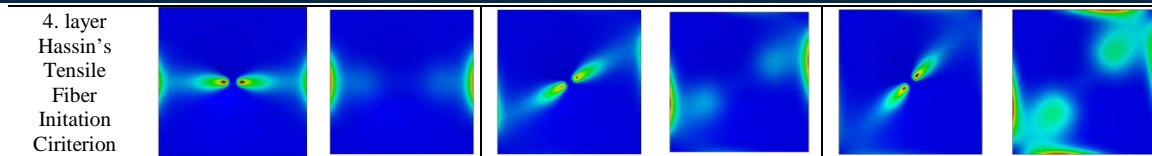


Figure 4. Effect of the fiber angel on the Hassin's fiber compressive and tensile initiation criterion in the top and bottom face-sheet for the impact energy of 10 J.

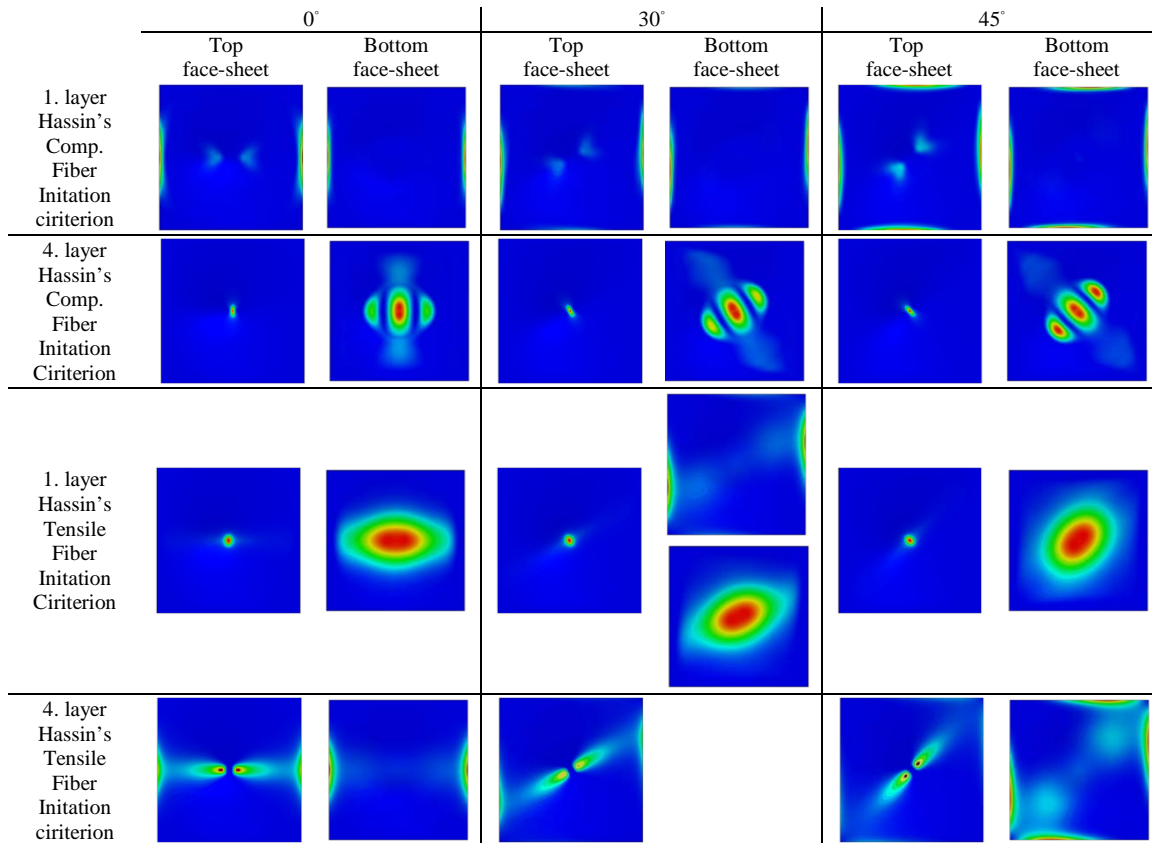
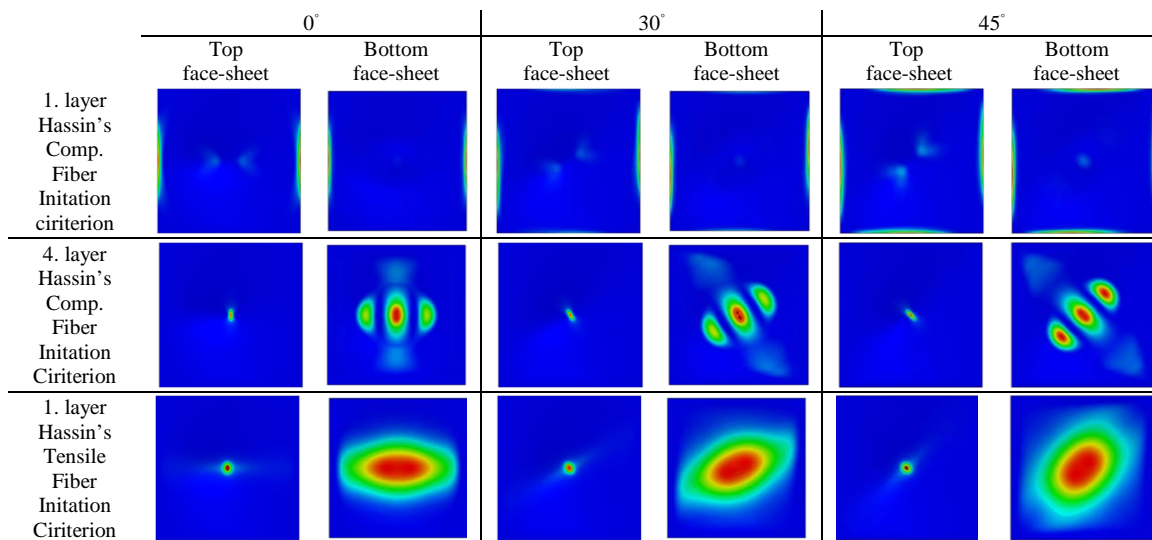


Figure 5. Effect of the fiber angel on the Hassin's fiber compressive and tensile initiation criterion in the top and bottom face-sheet for the impact energy of 20 J.



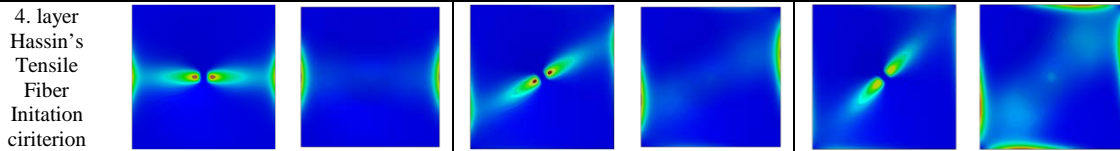


Figure 6. Effect of the fiber angel on the Hassin's fiber compressive and tensile initiation criterion in the top and bottom face-sheet for the impact energy of 30 J.

3. CONCLUSIONS

This study presented the impact response of PVC foam core composite sandwich panels for different fiber angles of various impact energies. The temporal variation of contact force, kinetic energy histories and Hassin's fiber damage of composite sandwich panels assessed for the impact energies of 10, 20 and 30 J. Cohesive zone model (CZM) implemented simulations to model adhesive layer. Panels with 45° fiber angle absorbed more much energy. Minimum contact force appeared for the panels with 45° fiber angle. As the impact energy is increased, the damage area is increased. Damage area of panel with 45° fiber angle is bigger than other panel with fiber angle. As the tensile forces were effective at the bottom face-sheet, compressive force were effective at the top face-sheet.

REFERENCES

- [1] E. A. Flores-Johnson and Q. M. Li, "Experimental study of the indentation of sandwich panels with carbonfibre-reinforced polymer face sheets and polymeric foam core", *Composite: Part B*, vol. 42, pp. 1212-1219, March 2011.
- [2] H. Singh, K. K. Namala, P. Mahajan, "A damage evolution study of E-glass/epoxy composite under lowvelocity impact", *Composites Part B*, vol. 76, pp. 235-248, Feb 2015.
- [3] K. K. Namala, P. Mahajan, and N.Bhatnagar, "Digital Image Correlation of Low-Velocity Impact on a Glass/Epoxy Composite", *International Journal for Computational Methods in Engineering Science and Mechanics*, vol. 15:3, pp. 203-217, Feb 2014.
- [4] P. M. Schubel, J. Luo and I. M. Daniel, "Low velocity impact behavior of composite sandwich panels", *Composites: Part A*, vol. 36, pp. 1389-1396, 2005.
- [5] C.S. Lopes, P.P. Camanho, Z. Gürdal, P. Maimí, and E.V. González, "Low-velocity impact damage on dispersed stacking sequence laminates. Part II: Numerical simulations", *Composites Science and Technology*, vol. 69, pp. 937-947, Feb 2009.
- [6] J.L. Yu, X. Wang, Z.G. Wei and E.H. Wang, "Deformation and failure mechanism of dynamically loaded sandwich beams with aluminum-foam core", *International Journal of Impact Engineering*, vol. 28, pp. 331-347, 2003.
- [7] I. Ivañez, and S. Sanchez-Saez, "Numerical modelling of the low-velocity impact response of composite sandwich beams with honeycomb core", *Composite Structures*, vol. 106, pp. 716-723, July 2013.
- [8] C. Atas and C. Sevim, "On the impact response of sandwich composites with cores of balsa wood and PVC foam", *Composite Structures*, vol. 93, pp. 40-48, June 2010.
- [9] J. Zhou, M. Z. Hassan, Z. Guan and W. J. Cantwell, "The low velocity impact response of foam-based sandwich panels", *Composites Science and Technology*, vol. 72, pp. 1781-1790, July 2012.
- [10] R.D.S.G. Campilho, M.D. Banea, J.A.B.P. Neto, and L.F.M. da Silva, "Modelling adhesive joints with cohesive zone models: effect of the cohesive law shape of the adhesive layer", *International Journal of Adhesion & Adhesives*, vol. 44, pp. 48-56, Feb 2013.

Determination of the casting cost using Fondweb ERP Software

Gurhan Deniz¹, Didem Guleryuz², Murat Colak²

Abstract

Nowadays, the enterprises need to optimize continuous growth, quality, efficiency, and cost elements in the best way, since they maintain their presence in the market. Because of this each company has its own specific critical success factors to grow and to improve. These factors may vary depending on sectors and a companies. The one constant is the necessity of keeping up with new technology, the expectation of high quality for the production and the providing efficient information management. The software industry has showed a growth for the providing knowledge management in recent years, as a result of this growth one of the greatest contributions to the industry is the Enterprise Resource Planning software.

ERP (Enterprise Resource Planning), covers all processes of the organizations that allows all business processes to be managed through an integrated information technology system from supplying to distribution. ERP is comprehensive software package due to its modular structure, it can be adapted to different sectors. Since all data is located in a single database, the departments which has different objectives and aims, work in harmony. In this study, after ERP software information is given, suitability of the Fondweb ERP software for foundry industry, and its necessity and benefits are evaluated. The casting cost is calculated using two different ways for a casting part which is manufacture in medium-sized cast enterprise in Turkey, to compare classical method results and results are obtained from ERP software.

Keywords: *Enterprise Resource Planning, Foundry Industry, Account of Cating Cost, Fondweb ERP*

1 INTRODUCTION

Nowadays, the presence of sustainable enterprises depend on optimizing the elements of growth, quality, efficiency and cost. It is only possible that if labors, raw materials, machinery and equipment resources use effectively, the functions of quality, productivity, cost and fast response can optimize. Production planning and control systems lead to effective and realistic using of resources. For this reason, the needing for an integrated information system has emerged. Enterprise Resource Planning-ERP is comprehensive software package which covers all the processes of company and it allows all business processes to be managed through an integrated information technology system from supply to delivery. Due to its modular structure it can be adapted to different sectors [1].

Enterprise resource planning eliminates manual systems used in the production, planning, finance, purchasing, human resources, marketing departments, it compounds that into a single computer system for all departments. All departments have own need and they work for different purposes, having a single database of all data provides to share information quickly and accurately and working in harmony. In addition, Enterprise resource planning systems increase the efficiency of the control function by regulating the flow of information for a company in the manufacturing sector [2].

1.1. Why Enterprise Resource Planning is a necessary?

The most important reason for the needs of enterprise resource planning to enable the activities of the organization, to make long-term planning which use of resources in the most effective manner by having reporting and analysis. In most companies, a simple request in a classical production system can be divided into even number of unnecessary parts this causes disconnection among departments. A process can unearth with the starting of demand. Enterprise resource planning eliminates the lack of communication, it provides a full integration with the developed modules by using integrated software among departments. Also, it provides a full integrity so that which is very important and necessary.

Also in today's globalized world, Enterprise Resource Planning, is becoming a key requirement for every business. Since ERP brings together too many solutions to ensure company's success in the market, the necessity of using in every corner of the company is advocated by researchers[3]. Companies using enterprise resource planning;

¹Corresponding author: Sakarya University, Department of Metal Education, 54187, Sakarya, Turkey. gdeniz@sakarya.edu.tr

²Bayburt University, Department of Industrial Engineering, 69000, Bayburt, Turkey. dguleryuz@bayburt.edu.tr

- Provides rapid response to unexpected events,
- minimizing costs through inventory management,
- the information can be viewed at any time with Central coordination
- Process times shorten and reduce the cost of waste
- Profits and losses can be clearly seen and its reports produce consistent results by using effective use of resources

1.2. Critical Success Criteria and Selection of Enterprise Resource Planning Software

Critical Success Factors, enabling enterprises to perform the activities required to identify strategies are the way to bring the goal-oriented management tools. Every business should identify their critical success factors, adopting and to be able to check and to manage by using the right strategies. They can adapt to rapidly changing conditions in this way. Difficulties in implementation of Enterprise Resource Planning lead to the significant failure rate factors. Therefore, the critical success factors should determine and be applied effectively [4].

Since there are lots of Enterprise Resource Planning softwares in the market, choosing the proper software is much more important for the company. Several feasibility studies should be done by company which needs ERP support and software firm. Businesses must use the appropriate enterprise resource planning software to achieve their goals. If they use a software, similarities of the old software can be taken basis to choose new software and selected software should be evaluated to see that it meets the expectations. It is very difficult to find proper software for each company. So that the appropriate software must be chosen utilizing the flexibility of company's processes and ERP software [5].

1.3. Importance of Enterprise Resource Planning in the institutionalization process for the foundry

When the structure of the companies in the foundry sector in our country examine, the majority of them are micro and medium-sized foundry company that managed the family-owned businesses of two generations [6]. Family-owned businesses; ownership and management of the company is owned by one or several families. Founder family is both the boss and manager in this business. Generally family businesses was established in the period of high profit margins and low expectations of the market. In business, founders are technically competent so 2nd generation usually makes some mistakes such as to continue using the methods without improvements, do not to question the habits and not optimizing business processes. In addition, family members can not be questioned in the areas they are responsible for their position, increasing costs and the operational inefficiencies, due to organizational dysfunction the refusal of the new team's by former staff as a result of this the high value-added professional staff may be lost. Besides as the nature of family-owned business profitability and competitiveness drops and brand image deteriorates. Institutionalizing plays a key role to develop and maintain, to continue its presence and the transfer to new generations [6,7].

Foundries need Enterprise Resource Planning software are more than any other sector due to its complex structure. However, this system is faced with many obstacles in the transition phase for instance management disbelief for institutionalization, not feel free to make critical moves in decision-making, lack of qualified staff, concerns about extra costs. Although in some firm believe in institutionalization, they do not recognize the difference between keeping data on Excell and an integrated structure of ERP software which is being part of the process. For this reason, software is seen the additional cost. However, Enterprise Resource Planning puts the main principles of the institutionalization for the company [6]. As it is shown in studies, firms using the software effectively have cost reduction of up to 20% and have 15% greater profitability in a short time [8, 9].

In this study, the molding parts cost is calculated and evaluated by using FondWeb Enterprise Resource Planning software. Example a piece of molding cost calculation stages are explained in a practical way. At the end of the study, software results and classic method results are compared.

2 CASTING COST CALCULATION WITH FONDWEB

FONDWEB is a special ERP software for foundry. In this study, whole processes of foundry are examined and cost calculation is made for an example.

2.1. Entering the New Client and New Supplier

'Client Management' is selected to enter 'New Client' in the menu. If customers have previously registered in the system, they find in the list and the selection is made. On the other hand, unless customer is registered from Customer Management menu, new customer is added. The new code is given to the new customer in Records Management window. Unless special situation, "next code" is chosen to give new code. So the code is given automatically to planned customers by the system (Figure 1).

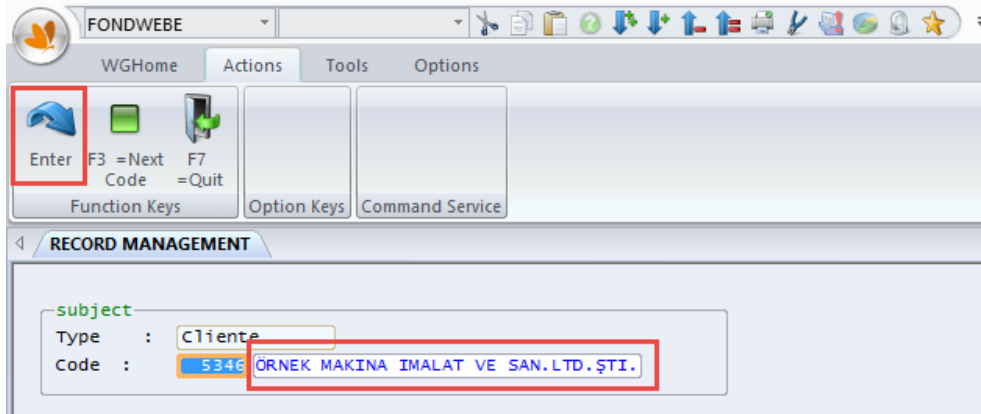


Figure 1. Client Recording Screen

After forming the new code automatically, customer and company name is written and to continue the recording by pressing the approval button. Company details, information about their accounts and payment processing, commercial data and contact information is entered and the company registration is completed. Since this information may vary depending on the commercial business requirements and the company request, Fondweb software allows its flexible structure. After filling the necessary information press the confirm button to complete the recording (Figure 2).

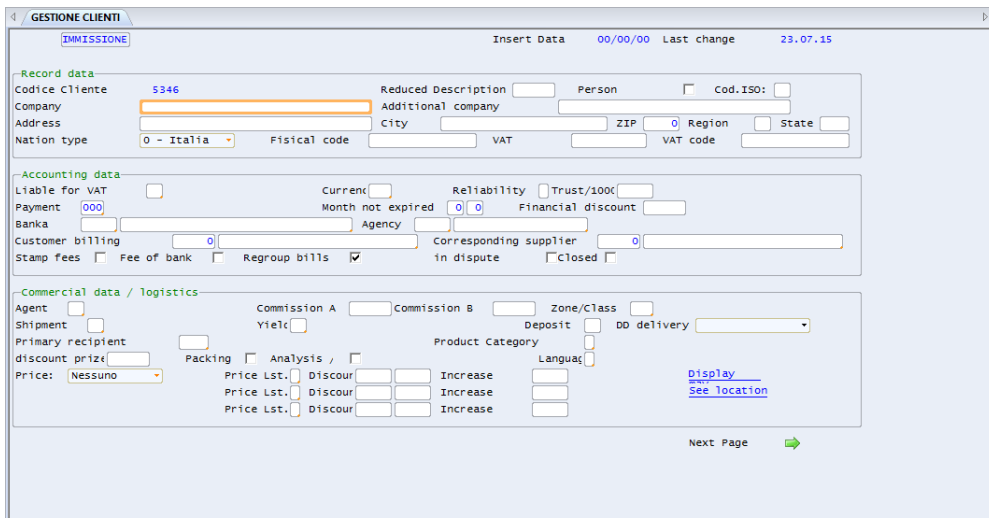


Figure 2. Customer and supplier database registration window.

In order to control the company's purchases and services, all suppliers must be recorded. So that all suppliers have to be recorded with firm information into the system in the same way.

2.2. Model Management

It is first necessary to define the model of the system, in order to give the required and order, cost accounting of the order from a customer and the material control. As the entering the model in the system Model Management is selected in the menu. In this window customer code is entered, unless customer code is known the customer searches via "??". After finding the customer, approval button is clicked. When the window open, prerecorded models which includes the information of model and casting can be seen. Unless the operation on a model previously saved, new model is saved via 'Enter' (Figure 3).

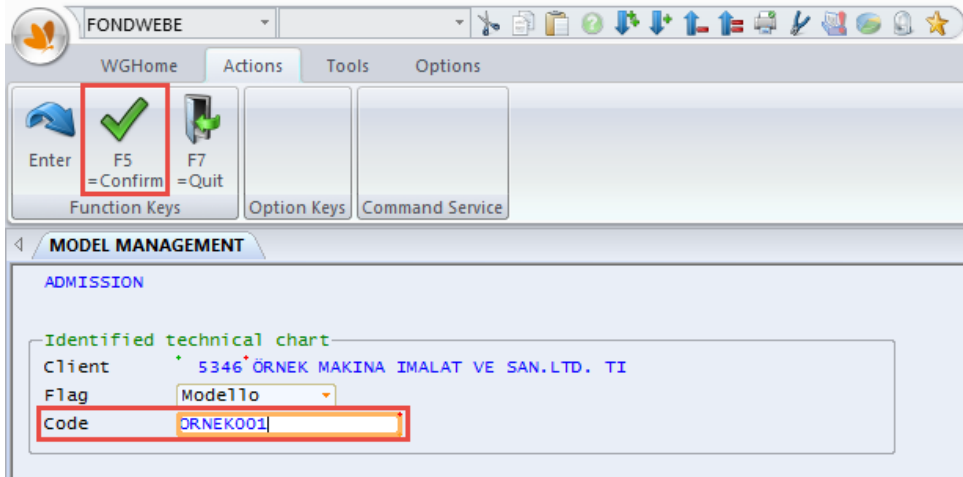


Figure 3. The registration of a new model order for customer firm.

A code should be defined for recording customer data for a new model. After adding the model code by pressing the approval, Technical Card Management page opens (Figure 4). On this page, some information about the model should be filled. This information is designed with an existing foundry process. It is possible to change the model, according to the needs of the foundry. Some information needs to be added in this section such as alloy, molding line information, degree measurements, the molding sand material are selected from the information we enter the system before. When the program installing, degrees and its dimensions, used alloy information, molding line information are recorded in the system.

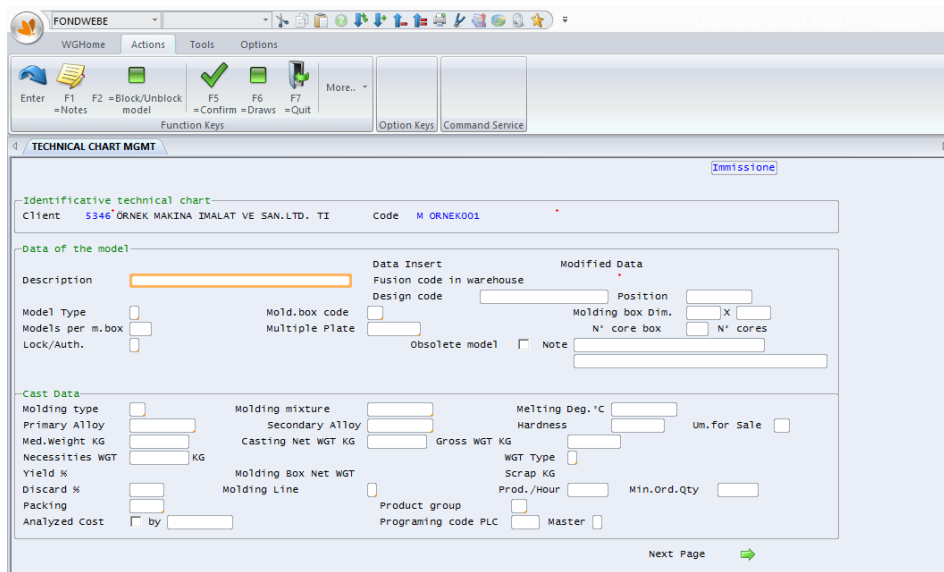


Figure 4. Technical card management registration page.

2.3. Defining Materials Used In Foundry In The System

In general, all materials used in foundry must be defined in the system with the necessary information. Some examples can be seen below,

2.4. Degree Type

OFFICE RECORDS menu is selected to define a new degree for foundry. Degree plate is written on the search button of the selected window and the related registration page is accessed by pressing the Confirm button. After degree plaque is written, arrangements can be made on a degree of information has already been registered or Plate Card Management page opens to record new degree by pressing 'Confirm'. By determining the degree code, 'Confirm' is clicked and go to the other page to add data degree information (Figure 5).

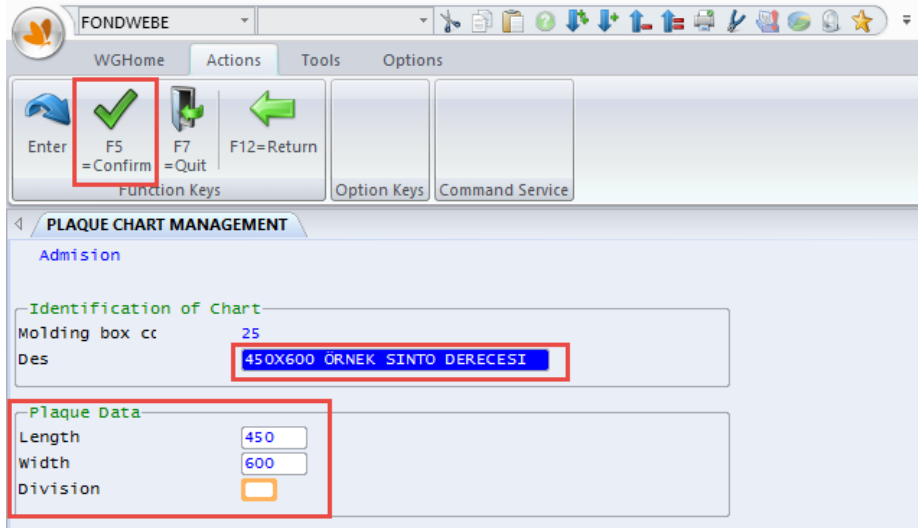


Figure 5. Degree type recording.

On this page, information of degree, length, width and division are written and the process is completed pressing 'Confirm'.

2.5.Molding Type

Casting type is written on the search button of the selected window and the related registration page is accessed by pressing the Confirm button. After degree plaque is written, arrangements can be made on a degree of information has already been registered or Plate Card Management page opens to record new degree by determining molding type (Figure 6). After the description is written, registration is completed via 'Confirm'.

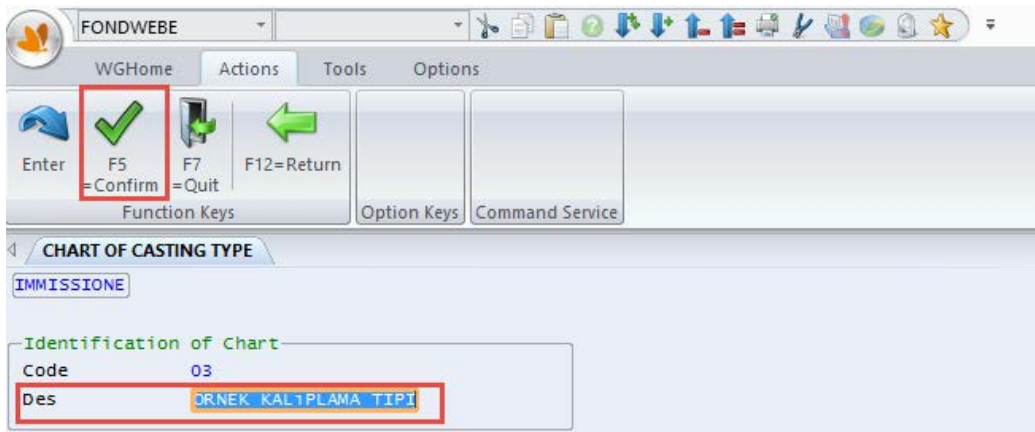


Figure 6. Defining the molding line .

2.6.Molding Mixture Alloy:

Alloy-Mixture Management is chosen to define a new molding mixture and a new alloy. The alloy and molding mixture load from same table in the menu. Alloy / Mixture is written on the search button of the selected window and the related registration page is accessed by pressing the Confirm button (Figure 7).

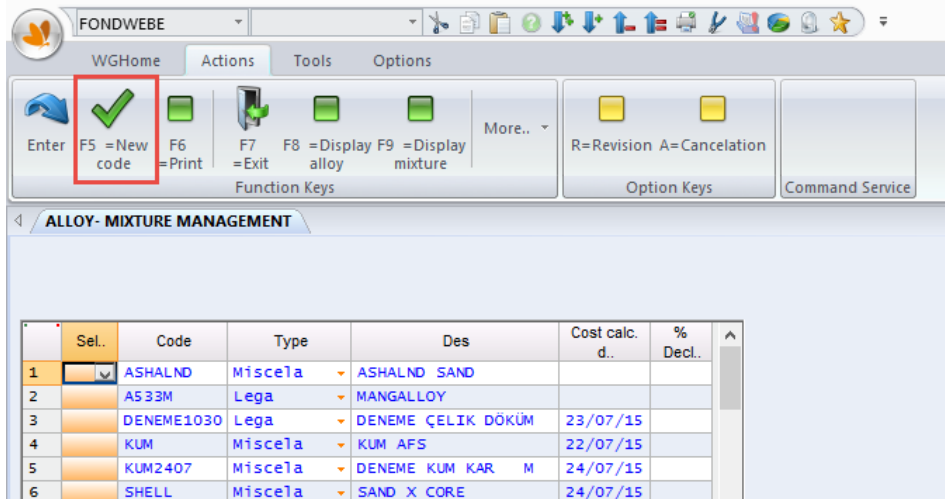


Figure 7. Alloy and molding mixture registration page.

After Alloy / mixture being selected stored materials are displayed in the system. Entering the new material and editing for alloy-mixture are done in this section. In order to modify existing materials, related materials are selected and editing is made. Since a new material entry, a new registration page is opened via New Code selecting. Required information is entered in the Alloy / Mixture Management page. The inserted material is indicated whether alloy or mixture. Material, cost and additional information is written and recording is completed. The indicated cost is only setup cost for this material. The cost of per material is calculated depending on the orders. When all data is entered into the system, the steps of process which is deadlines, the required materials list, material costs can be controlled and planned very easily.

3 COMPARISON OF CASTING COST

In a medium-sized foundries classical cost accounting is usually done in several phases. They are directly related to relevant staff experience. The main determining factors can be seen below,

- Casting material (alloy type)
- Casting weight
- Mandrel situation
- The number of Order
- Model situations.

As casting process is really complicated there are many factors to account in the production process so it is also quite difficult to account. For instance, even the degree used in sand mold casting do not take into account, but there is a cost significantly. After a certain period of time, a new degree is necessary. These and similar factors are ignored on costs calculation. Sometimes because of high profit expectations, bids become high this situation leads to loss of current customers. Consequently, in today's competitive world, a realistic cost analysis and knowledge management has significant importance. All available machinery, materials, tools, equipment are recorded with a special arrangement for each company using ERP. After that whole process is programmed.

ERP softwares are really substantial as providing information management and planning processes. Different pieces of production may have to walk simultaneously at the same time in foundries depending on the company. In this case, the casting line, the mold place, stove and charge accounts, warehouse inventory planning are extremely important.

4 CONCLUSIONS

When foundries do cost calculations in classical way they are able to ignore several costs. The whole process can be controlled with the using of ERP software.

When the structure of the companies in the foundry sector in our country examine, the majority of them are micro and medium-sized foundry company that managed the family-owned businesses of two generations. Institutionalization is important for the development of such enterprises, the first fundamental and important step towards institutionalizing the using of ERP.

Enterprise Resource Planning puts the main principles of institutionalization on the company without notice. Thus, companies that use ERP software effectively are reported to achieve cost reduction of up to 20% and greater profitability of up to 15% in a short time. Consequently, the institutionality is provided if functions such as sales,

inventory, purchasing, production, quality, maintenance, human resources, finance and cost management are managed in an integrated single database.

When the calculation is done with classical methods because of the shortage of planning emerges and extra costs, the real costs are found in difficulty. This is important to maintain the continuity of the company in today's competitive world.

As given in the summary below are some of the companies expected to benefit through the use of ERP;

- Timely delivery is done through coordination between departments
- The standardization of production processes, coordination, existing error and losses are analyzed and quality increases,
- Reduction of costs,
- Determining the actual cost of production,
- Improvement in operational decisions, accurate and fast and secure access to current technical documentation,
- Communication between clients and suppliers and interdepartmental coordination,
- Reducing the amount of idle stock,
- Procurement processes are complete timely,
- The financial information within the organization can be monitored and controlled in single database,

REFERENCES

- [1] Chung, S. H., Snyder, C. A., *ERP Adoption: a Technological Evolution Approach*, *International Journal of Agile Management Systems*, 2(1): 24-32, 2011.
- [2] Laudon, K.C., Laudon, J.P., *Management Information Systems: Organisation and technology in a networked enterprise*, 6th Ed. New Jersey:Prentice Hall,2010.
- [3] Tambovcevs, A., Merkurjev, Y., *Analysis of ERP Systems Implementation in the Construction Enterprises*. Scientific Journal of Riga Technical University. Computer Sciences, 39(1), 2009.
- [4] Umble, J., Haft, R., *Enterprise Resource Planning: Implementation Procedures and Critical Success Factors*, *European Journal of Operation Research*, 146(2): 241-257,2013.
- [5] Birdogan, B. and Kemal, C., *Determining the ERP package-selecting criteria – the case of Turkish manufacturing companies*, *Business Process Management Journal*, Vol. 11, No. 1, pp.75–86,2005.
- [6] Atmaca Çağlayık N., *Kurumsallaşma ve ERP*, 7.Uluslararası Ankiros Döküm Kongresi, 11-13 Eylül 2014.
- [7] Türk Döküm Sektörü Avrupa'nın 4. Büyüğü, <http://www.moment-expo.com/turk-dokum-sektoru-avrupa-nin-4-buyugu>, Erişim tarihi:10.10.2015.
- [8] Rcinformatica, <http://www.rcinformatica.it/en/>, Erişim Tarihi 10.04.2016.
- [9] Kollanus J., Nieminen M., and Orkas J., *Erp in foundries – Towards Optimized Cast Production with Order-Driven DES*, 68th WFC - World Foundry Congress, pp. 255-259, 7th - 10th February, 2008.

A Mobile Survey Application For Android Devices

Fatih Kayaalp¹

Abstract

Mobile communication is a world wide used communication method and has a large ratio over all alternative communication methods. At first stages of this technology, mobile phone models that have only calling function were used. Today, Internet access and smart mobile phones provides a great opportunity for public on different sectors like healthcare, electronic shopping, electronics banking, office applications and also education. A new survey system aimed to use on education for teacher and students to run on smart mobile phones with Android operating system is presented in this paper. This survey system can also be used in crowded participants group like civil meetings on different aims like discussion groups, members of an enterprise company or any other social meeting. This survey application is faster, safer, more easy to use, more useful and more technological than classical survey systems on paper.

Keywords: Mobile, Survey, Education

1 INTRODUCTION

Mobile communication is a world wide used communication method and has a large ratio over all alternative communication methods. At first stages of this technology, mobile phone models that have only calling function were used. But today's technology gives us the opportunity to use mobile phones with many functions like internet access, calling functions, video players and etc.

One of the properties of mobile phones is the operating system. By the operating systems of these phones, we are able to run many softwares that have been designed and coded for different purposes and these phones are called smart mobile phones. Mostly used operating systems on smart mobile phones are Android, IOS and Windows Phone. And Android is the most preferred operating system in this sector. It is an open source software coded with Java programming language announced by Google and many programmers all over the world contribute to the development of this operating system.

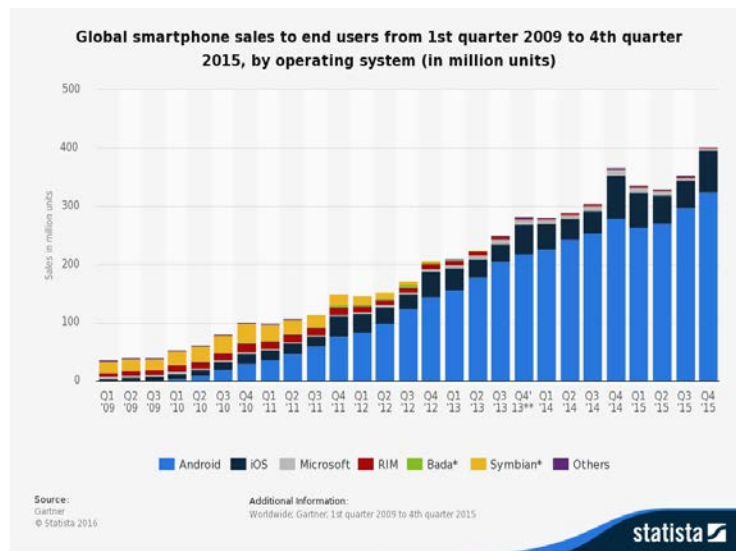


Figure 2 Global smartphone sales statistics 2009-2015 [1]

As seen in figure 1, global smartphone sales on the market and usage are increasing rapidly from 2009 to 2015 due to the ubiquity and popularity of smartphones among end-users[2]. And from children to adults, so many people prefer using smarhones for different aims. In this context, Android is the most preferred operating system and it is also the

¹Corresponding author: Duzce University, Department of Computer Engineering, 81620, Duzce, Turkey. fatihkayaalp@duzce.edu.tr

mostly targeted operating system on developing applications. Recent estimations indicate that by 2015 over 70% of all handset devices will be smartphones, capable of running mobile apps[3].

Today, internet access and smart mobile phones provide a great opportunity to public on different sectors like healthcare, electronic shopping, electronics banking, office applications and also education. There are many Android applications on Google Play (application loading center for Android devices) for different educational purposes for various age, subject and skills.

A new survey system aimed to use on education to run on smart mobile phones with Android operating system is presented in this paper. It provides the administrator and the attendees of the survey the ability to answer the questions. The presented application has the potential of double usage perspective. One of them is running as a conventional survey that the questions and answers can be used as a way to learn the opinions of the attendees about the questions. In this usage method, there is not a correct or false answer. Only the user opinions are gathered and classified according to the answers. The other usage type of the system is an online exam platform for a teacher and students. It allows both the teacher and the students meet on the same application.

The students or attendees are wanted to answer the questions on the survey which were inserted to the database before about a specified subject, by using their smart phones. Each student/attendee answers the questions one by one. No extra equipment for answering is needed. At the end of the answering stage, the teacher can analyze the answers on different views. For example how many students/attendees have chosen each answer for each question, the correct and wrong answers ratio to evaluate the results of the class in general, the answers of a specified student to evaluate the performance of that student. This survey system can also be used in crowded attendee group like civil meetings on different aims like discussion groups, members of an enterprise company or any other social meeting.

This smart phone based survey system is faster, safer, more easy to use, more useful and more technological than classical survey systems on paper. As the answers of the students and answering times are inserted into a database with the user name, it also provides the teacher to analyze the results in many ways that can be wanted.

2 RELATED WORKS

Joorabchi has given information to gain understanding of the challenges that mobile application developers face in practice through interviews and a survey of 188 respondents from different countries, genders, work experience years, and platforms[2]. In Voice of the Next-Generation Mobile Developer, topics on mobile application developers are discussed on different headings like HTML5 usage, Apple and Android platform dependent application development competition, cross platform development[4]. Mehdipour has given information about analysis of mobile learning, differences between E-Learning and mobile Learning, value and benefits of mobile learning and challenges and barriers of mobile learning. The results have shown that training when it is needed, training at any time, training at any place are the advantages of mobile learning[5]. Kinsella has remarked the communication problem with large classes of over 100 students like ones at universities. She tells that although several methods exist which allow students to communicate with lecturers in large groups, none of them combine ease of use, speed of transmission and student feedback in as cost-effective a manner as the one she has presented in her paper[6]. In lectures which use her application, students can send anonymous text messages to the phone number displayed in the application, and each student in the class can see the results of the communication, because the results of the text message output on the screen behind the lecturer when the lecturer chooses to release the messages on to the screen. This represents a new communication channel between the Many (students) and the One (lecturer). The application facilitates student interaction within the class and with the lecturer. And allows the lecturer to respond to student observations, questions and comments in a controlled manner within a large class.

3 BACKGROUND

3.1 Android Architecture

Android is a Linux-based open source operating system. And the Android architecture is formed by four layers from bottom to top as Linux Kernel, Libraries and Android Runtime, Applications Framework and Applications.

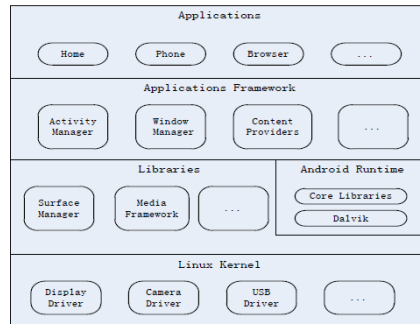


Figure 3- Android Architecture

Android applications are the programs that are used by the smart phones or mobile devices which are coded in Java programming language. Today there are many mobile applications in Play Store for different purposes like e-banking applications, instant messaging, dictionary and etc.

By the Application Framework, software developers are free to access the API functions and components of developing interface. This also provides the ability to reuse the components by many applications.

Libraries and Android Runtime work on the same level. Android Runtime includes Core Libraries for Java and Dalvik virtual machine which is used to execute applications for Android. Android system library is an important link between Application Framework and Linux Kernel which serves as a service for application developers.

Process Management, hardware management, storage management, internet and network management and all other core services in Android Operating System are based on Linux Kernel[7].

3.2 PHP

PHP is an open source, server-side scripting language designed for web development. It is also the most popular web programming technology used in many web sites for different web based interactions between web page and users. Originally created by Rasmus Lerdorf in 1994 but still many web developers contribute to the development of PHP[8].

3.3 MySQL

The most widely used open-source client-server model Relational Database Management System written in C and C++. It is now owned by Oracle. It is also the most popular database type chosen on PHP coded web sites. It is also used as the content database for many popular PHP based content management systems like Wordpress, Joomla, Drupal[9].

3.4 Android Studio

The official and widely used Integrated Development Environment (IDE) software used for Android applications development which was first announced on 2013[10]. It has been provided by Google to replace Eclipse ADT. It has packages to run on Windows, Linux and Max OS X operating systems[11].

4 ARCHITECTURE OF THE SURVEY APPLICATION

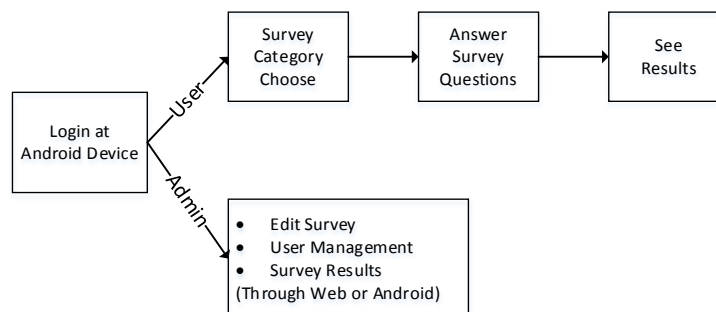


Figure 4 - Block Diagram of Mobile Survey Application

4.1 Database Architecture

The relational model of the designed database for the application is shown in figure 3 below. There are 6 tables to store the information about users, survey questions, answers, categories, subcategories, and surveys. The database is hosted on a web site with PHP support. The physical implementation of the relational model has been performed on MySQL as it is the mostly used dbms type on PHP coded web sites. The mobile application reads and writes from/to that database through a web service.

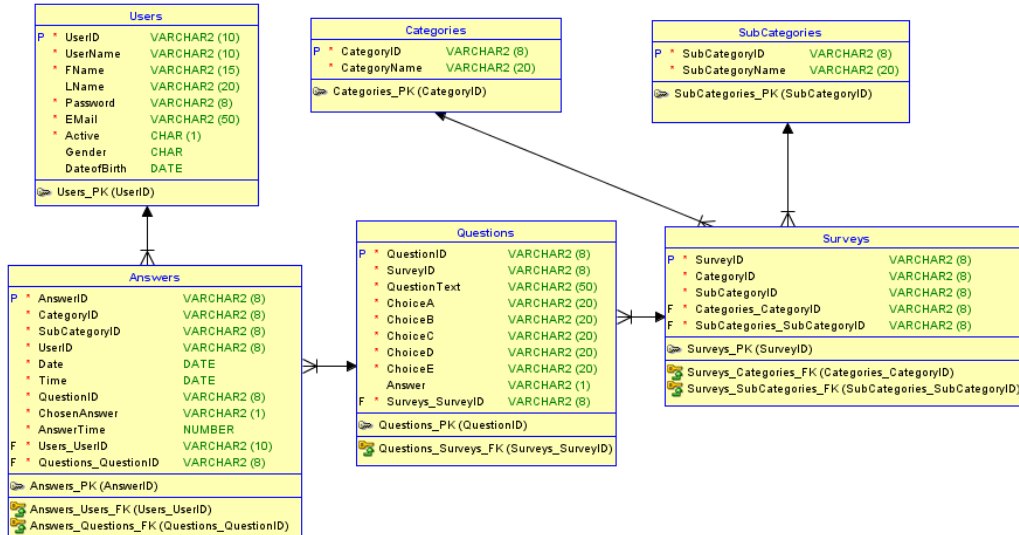


Figure 5 - Relational model of the implemented database

4.2 Login Page

Starting point of the application is the Login screen. After registering with the user name and passwords defined by the user, the user logs in. The admin of the application is able to enable or disable a user account by using “Active” field in “Users” table. By this way, any users which are not wanted to enter the system can be eliminated.

Survey App Login

User Name:

Password:

Figure 6 - Application Login screen

4.3 Tasks Page

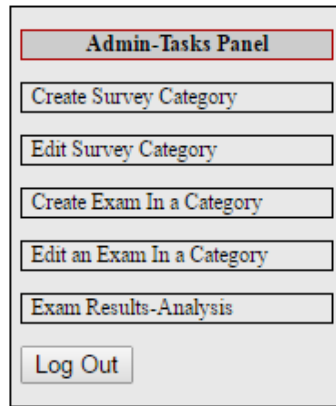


Figure 7- Admin Tasks panel

If the Admin user logs the application, Tasks panel shown in figure 6 is displayed. On tasks panel, the user can:

- Create a new survey category/lesson category
- Edit an existing survey/lesson category
- Create a survey/an exam in a survey/lesson category
- Edit a survey/an exam in a category
- Survey/Exam results of the selected category

Same tasks can be done also through web pages coded with PHP.

Inserting new questions screen is shown in figure 7 below as a sample screen for editing an exam. As shown on the figure, after choosing the survey/lesson category and exam name, question text and answers can be inserted through the text boxes.

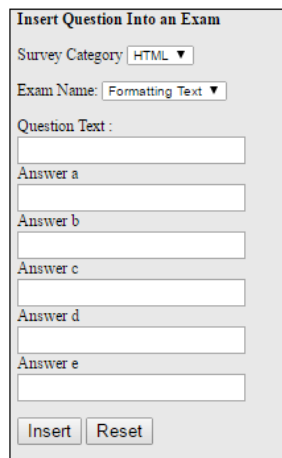


Figure 8- A new question insert screen

4.4 An Exam Page

After logging in as a standart user, the user selects category and survey/exam. When both of the selections are done in figure 8, the user is directed to the question-answer screens as seen in figure 9. The questions can be answered by touching screen on the correct answer. When an answer is chosen by touching, the next question and answers are selected from the database and shown on the screen again in the same screen order. The user can also skip the question without answering. By these steps, the exam is completed and the user is directed to the figure 8 again.

Figure 9 Category and Exam Selection screen

Figure 10 A sample Question-Answer screen

4.5 Exam Results Page

As the users login and answer the questions, many data are inserted to the system after a period of time. For analysis of this data, a results panel is designed for admin user which is shown in figure 10 below. The user is able to select category, exam, user name and question number. Any required data filtering alternatives can be added to this panel.

Figure 11 Results (Analysis) screen

According to the filtering selections of the admin user, some different views of data screens are designed and shown in figures 11, 12, and 13.

Question No	Answered Times	Correct Answer	Wrong Answer	Correct Ratio
1	8	6	2	75%
2	5	4	1	80%
3	3	1	2	33%
4	7	6	1	85%
5	9	9	0	100%
6	10	7	3	70%

Figure 11 Exam based results

UserName	Correct	False
Fatih	X	
Ahmet	X	
Hasan		X
Murat	X	
Fatma		X

Figure 12 Question based results

Question No	Correct	False
1	X	
2	X	
3		X
4	X	
5		X

Figure 13 UserName based results

5 RESULTS

According to the tests on mobile survey application, it is seen that:

- Making a survey through smart phones after a lesson or a presentation is so easier especially on large groups of attendees than classical on paper surveys.

- It takes a shorter time for a survey/exam than classical printed surveys/exams as the answers are inserted into the database when the user touches on the screen.
- The answers can be analyzed in different views according to the age, gender, subject, question, another attendee, class average...
- As all the answers are inserted to the database with date and time data, previous data for months or years can be stored without any additional cost. And if wanted, new data can be compared to the older data for any success comparison or opinion changes comparison.
- As the survey can be completed in a few minutes without spending any extra time about papers (filling the answers by hand, gathering the papers back, inserting the answers to a computer/software) and analyze; the results are listed faster than classical printed surveys either for a teacher/student or any general presentation groups.

ACKNOWLEDGMENTS

Thanks to my BS student Yakup Akdemir about his contributions on coding the application on Android. This project has been funded by Duzce University Research Fund Project Number: 2016.06.01.420.

REFERENCES

BIOGRAPHY

Received the BS Degree in Computer Science from Marmara University in 2000, the MS Degree in Computer Science from Sakarya University in 2005, and the PhD Degree in Computer Science from Sakarya University in 2014. Currently he is working as an Assistant Professor in Duzce University. His primary research interests include databases, web technologies, computer networks, wireless sensor networks and mobile computing.

MPPT for PV Arrays Based on Bat Algorithm with Partial Shading Capability

*Huseyin Demirel¹, M. Kadir Karagöz*², Bilgehan Erkal¹*

Abstract

The power–voltage (P-V) curve of photovoltaic (PV) arrays has several local peaks and one global peak under partially shaded conditions. Because the conventional maximum power point tracking algorithms are converge to the first peak of the P-V curve, they may not find global maximum power point. Soft computing methods such as bat algorithm (BA) may find GMPP of P-V curve. Therefore, this paper proposes a dual algorithm search method that consist of BA and perturb&observe algorithm (P&OA). Firstly, BA is used to determine the area of global peak, then P&OA is replaced to track the maximum power point in the area of global peak. As the sampling period of BA is very longer than P&OA's, the number of iteration of BA was limited. If the power greatly changes during the iteration process of P&OA, BA is reactivated. As a result of the simulations, performance of the proposed method is superior to either BA or P&OA.

Keywords: Bat algorithm, Perturb&Observe algorithm, Partial shading conditions

1. INTRODUCTION

Since solar energy has high potential and eco-friendliness, use of solar energy which is one of the renewable energy sources is increasing day by day. Photovoltaics (PV) is one of the methods of converting solar energy into electricity. Solar cells (or PVcells) are basic building blocks of PV systems. PV cells which are made of a semiconductor material directly convert sunlight into DC electricity at the atomic level. A PV module consists of PV cells which are connected electrically in series and/or parallel. Multiple PV modules can be wired together to form a PV array. PV modules output power depends on solar radiation and temperature. Because of the variation in the environmental condition, the power–voltage (P-V) curve of PV module exhibits a non-linear, time-varying maximum power point (MPP) problem. In order to continuously harvest maximum power from PV modules, the maximum power point tracking (MPPT) is employed in conjunction with the power converter.

To date, numerous conventional MPPT algorithms such as perturb and observe (P&O) [1]-[4], incremental conductance (IC) [5],[6] have been developed for PV systems. Besides, various soft computing methods such as fuzzy logic controller (FLC) [7],[8], artificial neural network (ANN) [9], particle swarm optimization (PSO) [10],[11] have been proposed for solar MPPT. The conventional MPPT methods have the advantages of simple structure, easy implementation, low equipment requirement and rapid convergence. However, they have the disadvantages of oscillation around the maximum power point (MPP). Also, they can not determine the global MPP under partially shaded condition (PSC). The soft computing methods can determine the global MPP under PSC despite the fact that they are generally harder, slower and more complex than conventional MPPT algorithms [12]. Due to the drawbacks of each MPPT method, superior MPPT method development works is still ongoing.

Ahmed and Salam [12] propose a MPPT method based Cuckoo Search (CS). They reported that CS outperforms both P&O and PSO with respect to tracking capability, transient behavior and convergence. Khanna et al. [13] propose an two-level adaptive control architecture (Ripple Correction Control and Model Reference Adaptive Control) with for solar MPPT. They reported that the proposed control algorithm enables the system to converge to the maximum power point in milliseconds.

Shi et al. [10] propose a dual-algorithm search method consist of dormant PSO and IC. They reported that the excellent performance of the proposed model is verified by simulations and experiments.

The purpose of this work is to develop a novel MPPT method that is better than conventional MPPT algorithms under PSC.

¹Karabuk University, Department of Electrical and Electronics Engineering, 78000, Karabuk, Turkey.

hdemirel@karabuk.edu.tr

²Corresponding author: Borusan Asım Kocabytık Mesleki ve Teknik Anadolu Lisesi, 34522, Esenyurt/İstanbul, Turkey.

karagozm@gmail.com

2. MATERIAL AND METHODS

2.1. Overview of Perturb and Observe Algorithm

The perturb and observe algorithm (P&OA) is one of the most used algorithm for MPPT. P&OA focuses on the perturbation of the operating voltage of PV module by modifying the duty cycle of power converter to find the MPP. It modifies the duty cycle of power converter periodically, and then it compares the PV output power with that of the previous cycle of perturbation. When PV power and PV voltage increase at the same time and vice versa, the duty cycle of power converter will be decreased. When PV power increases and PV voltage decreases and vice versa, the duty cycle of power converter will be increased. This process is repeated continuously [14].

P&OA has several drawbacks that reducing its tracking efficiency. P&OA is not able to determine the actual MPP. It oscillates around the MPP continuously. It fails to determine the direction of tracking under rapidly solar irradiance change [15]. P&OA has advantages as simplicity, ease of implementation and low cost.

Algorithm 1: Perturb and Observe MPPT Algorithm pseudo code

```

Initialize duty cycle,  $D=D(k-1)$ 
Initialize voltage and current,  $V(k-1)$  and  $I(k-1)$ 
Calculate initial power,  $P(k-1)$ 
while (true)
    if ( time  $\geq$  the sampling period of P&O )
        Measure voltage and current,  $V(k)$  and  $I(k)$ 
        Calculate power,  $P(k)$ 
        if ( $P(k) > P(k-1)$ )
            if ( $V(k) > V(k-1)$ )
                Increase module voltage (Decrease Duty)
            else
                Decrease module voltage (Increase Duty)
        end if
        else
            if ( $V(k) > V(k-1)$ )
                Decrease module voltage (Increase Duty)
            else
                Increase module voltage (Decrease Duty)
        end if
        end if
        Update the previous voltage and power,  $V(k-1) = V(k)$  and  $P(k-1) = P(k)$ 
        end if
    end while

```

2.2. Overview of Bat Algorithm

Bat algorithm (BA) is a bio-inspired meta-heuristic optimization algorithm, firstly proposed by Xin-SheYang (2010) in [16], has been developing rapidly then. BA was based on the echolocation features of micro-bats. Echolocation is the bio-sonar used to detect prey and avoid obstacles by bats. Micro-bats emit a loud sound pulse and listen for the echo that reflects from the objects. BA uses a frequency-tuning technique to increase the diversity of the solutions in the population. BA has a capability of automatically zooming into a region where promising solutions to reduce the convergence time [17]. BA, like Yang's previous algorithms, Cuckoo Search [18] and Firefly [19], combines the advantages of existing algorithms [20]. Moreover, Harmony Search and Particle Swarm Optimization algorithms can be considered the special cases of BA. Therefore, it is no surprise that BA is efficient. [21]

The standard BA has many advantages as very quick convergence, simplicity and flexibility. BA guarantees to converge to the true global optimality. BA have been applied area of optimization, classifications, image processing, feature selection, scheduling, data mining [17].

Algorithm 2: BAT algorithm pseudo code [16]

```

Initialize the bat population  $x_i$  and  $v_i$  ( $i=1,2,\dots,n$ )
Define pulse frequency ( $f_i$ ) at  $x_i$ 
Initialize loudness ( $A_i$ ) and pulse rates ( $r_i$ )
while (  $t <$  Max number of iteration )
    Generate new solutions by adjusting frequency,
    and updating velocities and locations/solutions [equations (1), (2) and (3)]
    if ( rand  $>$   $r_i$  )
        Select a solution among the best solutions
        Generate a local solution around the selected best solution

```

```

end if
    Generate a new solution by flying randomly
if( rand < Ai & f(xi) < f(x*))
    Accept the new solutions
    Increase ri and reduce Ai [equations (3) and (4)]
end if
    Rank the bats and find the current best x*
end while
Postprocess result and visualization
    
```

Initially, bats position x_i , rate of pulse r_i , loudness A_i , pulse frequency f_i , and velocity V_i are determined randomly. In the main loop the position x_i^t and the velocity V_i^t of the bats each time step t are updated as in (1) to (3).

Loudness A_i and rate of pulse r_i change during the iteration process. When a bat gets closer to prey its loudness decreases and the rate of pulses increases. In algorithm these changes are shown as in (4) and (5).

$$f_i = f_{min} + (f_{max} - f_{min}) \cdot \beta \tag{1}$$

$$v_i^t = v_i^{t-1} + (x_i^{t-1} - x_*) \cdot f_i \tag{2}$$

$$x_i^t = x_i^{t-1} + v_i^t \tag{3}$$

$$A_i^{t+1} = \alpha A_i^t \tag{4}$$

$$r_i^{t+1} = r_i^0 [1 - \exp(-\gamma t)] \tag{5}$$

where $\beta \in [0,1]$ is a random vector drawn from a uniform distribution, x_* is the current global best location among all bats, α and γ are constants.

For local search phase, once a solution is selected among the current best solutions, a new solution for each bat is generated locally using random walk.

$$x_{new} = x_{old} + \epsilon A^t \tag{6}$$

$$A^t = \langle A_i^t \rangle = \frac{1}{N} \sum_{i=1}^N A_i^t \tag{7}$$

where $\epsilon \in [-1,1]$ is random number, A^t is the average loudness of all the bats at this time step, and N is the number of bats.

2.3. Dual MPPT Algorithm Model

We propose a dual MPPT algorithm model with BA and P&OA for solar MPPT. Firstly, BA is executed for two iteration and then global MPP area is determined. P&OA is executed and the actual MPP is tracked in global MPP area.

Algorithm 3: BA-P&OA dual algorithm pseudo code

```

Initially the bat population xi and vi (i=1,2,...,n)
Define pulse frequency (fi) at xi
while(true)
    Initialize loudness (Ai) and pulse rates (ri)
    while ( t < Max number of BA iteration)
        Generate new solutions by adjusting frequency,
        and updating velocities and locations/solutions [equations (1), (2) and (3)]
    if ( rand > ri)
        Select a solution among the best solutions
        Generate a local solution around the selected best solution
    end if
        Generate a new solution by flying randomly
if( rand < Ai & f(xi) > f(x*))
    Accept the new solutions
    Increase ri and reduce Ai [equations (3) and (4)]
end if
    Rank the bats and find the current best x*
    
```

```

end while
do
Run P&O algorithm for MPPT in the global MPP area (Algorithm 1)
while(Power change < Limited power change parameter)
end while

```

To use BA as MPPT algorithm, appropriate parameters have to be selected for the search. The most important parameter is the number of bats. A large of bats can improve the optimization capability to find global MPP, but it will spend more time to converge all of bats. In this work, the number of bats is selected as 5. Other BA parameters are selected as follows: $A_i^0 = 0.9$ (initial loudness of each bat), $\alpha = 0.9$ (loudness update constant), $r_i^0 = 0.95$ (pulse rate upper limit) $\gamma = 0.8$ (pulse rate update constant), $f_{min}=0$, $f_{max} = 1/5$. Initially, pulse frequency constant β , pulse frequency f_i , and velocity V_i are determined randomly. But initial positions of bats are selected constant as [0.15 0.3 0.45 0.6 0.75]. The sampling period of BA is selected as 20 ms, and the sampling period of P&OA is selected as 1 ms.

2.4. Simulation

In this study, a modified buck-boost converter which was presented by Alnejaili and Drid [22] was used to implement MPPT control, as shown in Figure 1. Three PV modules (KC200GT) which is connected in series was used as PV array. Panel has the following specifications: $P_{MAX}=200W$, $V_{MPP}=26.3V$, $I_{MPP}=7.61A$, $V_{OC}=32.9V$, $I_{SC}=8.21A$. Simulations were carried out using Matlab/Simulink program.

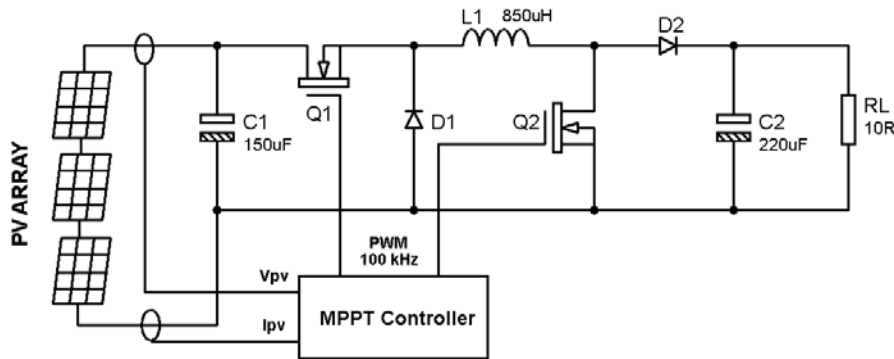


Figure 1. Simulation model of PV system

Simulations are implemented in Matlab/Simulink when PV arrays under partially shaded conditions (PSC1 and PSC2) and Standart Test Condition (STC). STC is irradiation of 1000 W/m^2 and temperature of 25°C . PSC1 is irradianations of 800W/m^2 - 200W/m^2 - 200W/m^2 and temperature of 15°C . PSC2 is irradianations of 400W/m^2 - 800W/m^2 - 1100W/m^2 and temperature of 35°C . The global MPPs are 600W , 160W and 330W , respectively. The simulation P-V curves of PV array are shown in Figure 2.

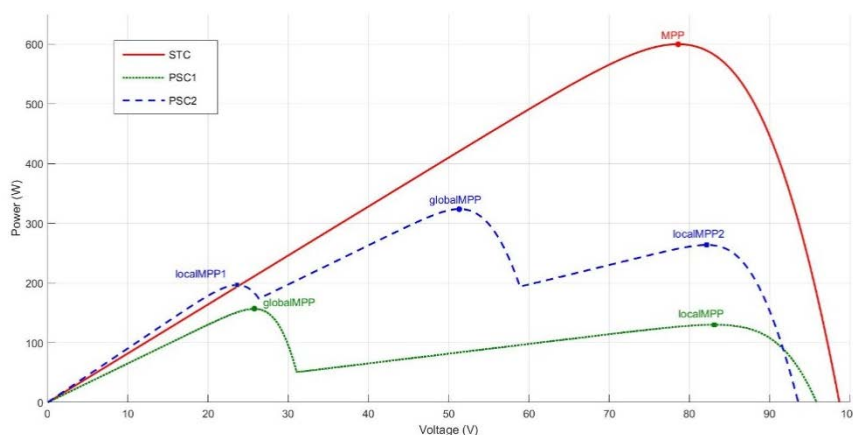


Figure 2. P-V curves under different simulation conditions (STC, PSC1 and PSC2)

3. RESULT AND DISCUSSION

Figure 3 shows the simulation results of BA-P&OA under STC and PSCs. BA is activated immediately at start under PSC1. The five bats iterate twice. The best solution which is determined within two iterations is transferred to POA. BA is replaced by P&OA at $t=0.21$ s. P&OA tracks the actual MPP in area of global MPP until the power changes greatly. At $t=0.3$ s, the irradiances and temperature are rapidly changed (PSC2). The algorithm is switched to BA again and the process is iterated. At $t=0.6$ s, environmental condition changes (STC), and the process is iterated again. Simulation results show that the proposed MPPT method could find the global MPP and maintain the operating point at the global MPP.

Figure 4 shows the simulation results of P&OA. P&OA converges a local MPP under PSC1 and PSC2. Due to convergence to a local MPP instead of the global MPP, the power loss is occurred.

When BA is used as single MPPT algorithm, it needs long time to converge all bats. Figure 5 shows simulation results of BA. Despite ten iterations, the actual MPP was not found in full. Each bat converges to the area of global MPP. Therefore, the number of iterations of BA should be reduced and BA should be used with the conventional MPPT algorithm.

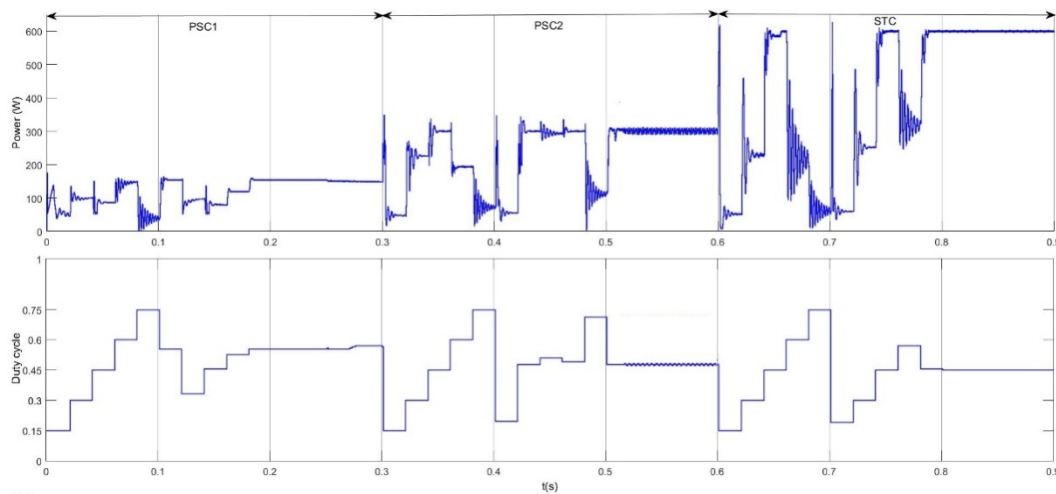


Figure 3. Simulation curves of BA-P&OA

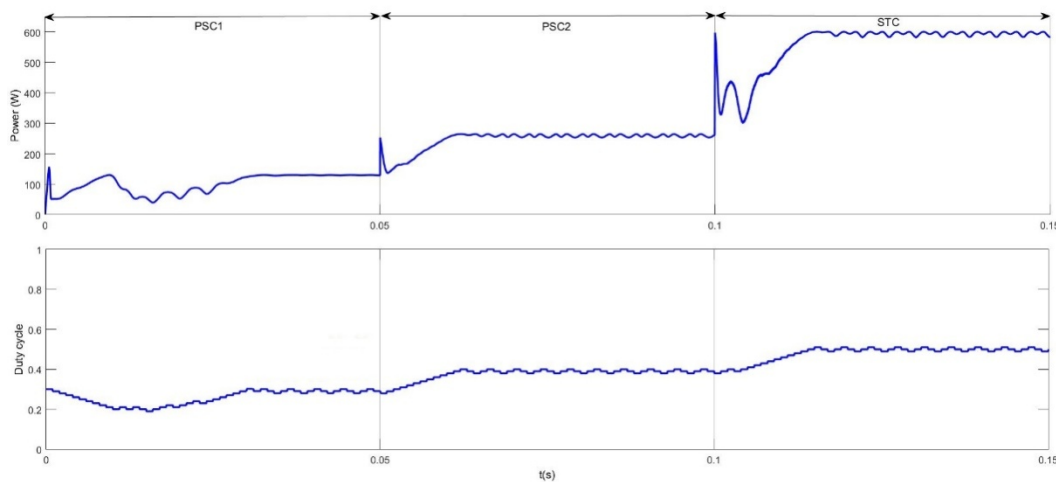


Figure 4. Simulation curves of P&O

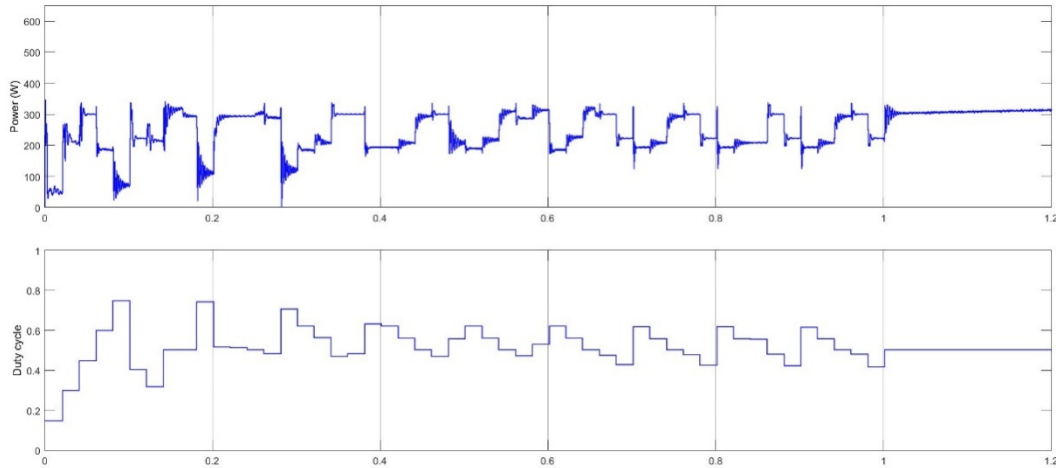


Figure 5. Simulation curves of BA

4. CONCLUSION

In this study, a dual algorithm MPPT method with BA and P&OA is proposed. Because the sampling period of BA is longer than P&O's, the proposed MPPT method is fast than BA. Whereas P&O algorithm can't find the global MPP, BA-P&OAMPPT method can find. Consequently, performance of the proposed method is superior to either BA or P&OA.

REFERENCES

- [1] L. Piegari, R. Rizzo, "Adaptive perturb and observe algorithm for photovoltaic maximum power point tracking", *IET Renewable Power Generation*, 2010, Vol. 4, Iss. 4, pp. 317–328.
- [2] N. Femia, D. Granzio, G. Petrone, G. Spanuolo, M. Vitelli, "Predictive & Adaptive MPPT Perturb and Observe Method", *IEEE Transactions on Aerospace and Electronic Systems*, vol. 43, NO. 3, July 2007.
- A. Murtaza, M. Chiaberge, M. De Giuseppe, D. Boero, "A duty cycle optimization based hybrid maximum power point tracking technique for photovoltaic systems", *Electrical Power and Energy Systems* 59, 2014, 141–154.
- [3] R. Ahmed, A. Namaane and N. K. M'Sirdi, "Improvement in Perturb and Observe Method Using State Flow Approach", *Energy Procedia* 42, 2013, 614 – 623.
- [4] F. Liu, S. Duan, F. Liu, B. Liu, and Y. Kang, "A Variable Step Size INC MPPT Method for PV Systems", *IEEE Transactions on Industrial Electronics*, vol. 55, NO. 7, July 2008.
- [5] P. Sivakumar, A. Abdul Kader, Y. Kaliavaradhan, M. Arutchelvi, "Analysis and enhancement of PV efficiency with incremental conductance MPPT technique under non-linear loading conditions", *Renewable Energy* 81, 2015, 543-550.
- [6] B. Bendiba, F. Krimb, H. Belmilia, M. F. Almia, S. Bouloumaa, "Advanced Fuzzy MPPT Controller for a stand-alone PV system", *Energy Procedia* 50, 2014, 383 – 392.
- [7] O. Guenounou, B. Dahhou, F. Chabour, "Adaptive fuzzy controller based MPPT for photovoltaic systems", *Energy Conversion and Management* 78, 2014, 843–850.
- [8] S. A. Rizzo, G. Scelba, "ANN based MPPT method for rapidly variable shading conditions", *Applied Energy* 145, 2015, 124–132.
- [9] J. SHI, W. ZHANG, Y. ZHANG, F. XUE, T. YANG, "MPPT FOR PV SYSTEMS BASED ON A DORMANT PSO ALGORITHM", *ELECTRIC POWER SYSTEMS RESEARCH* 123, 2015, 100–107.
- [10] M. Miyatake, M. Veerachary, F. Toriumi, N. Fujii, H. Ko, "Maximum power point tracking of multiple photovoltaic arrays: a PSO approach", *J. IEEE Transactions on Aerospace and Electronic System*, 2011, vol. 47, No. 1, 367–380.
- [11] J. Ahmed, Z. Salam, "A Maximum Power Point Tracking (MPPT) for PV system using Cuckoo Search with partial shading capability", *Applied Energy* 119, 2014, 118-130.
- [12] R. Khanna, Q. Zhang, W. E. Stanchina, G. F. Reed, Z. Mao, "Maximum Power Point Tracking Using Model Reference Adaptive Control", *IEEE Transactions on Power Electronics*, Vol. 29, No. 3, 1490-1499. 2014.
- [13] M. A. Eltawil, Z. Zhao, "MPPT techniques for photovoltaic applications", *Renewable and Sustainable Energy Reviews* 25, 2013, 793-813.

The Use of Color in Planting Design: The Preference of Landscape Architecture Students

Pelin Kececioglu Dagli¹, Gizem Cengiz Gokce¹, Ahmet Ergun¹

Abstract

Even if structural landscape elements come to the forefront in landscape design studies, plants are used as the essential materials of landscape architecture which is an ecological based discipline. Plants as being spatial design elements can be evaluated in terms of their ecological, aesthetical and functional characteristics. It is important to consider planting design principles in order to establish harmony between the structural and planting landscape elements in planting design projects. Plants are evaluated according to their size, shape, color, texture etc. characteristics, and offer many different usage possibilities in design projects within the aesthetical concept. Plants are introducing the impact of color into the landscape design projects through their characteristic parts such as leaves, flowers, seeds, stems and fruit. In the scope of this study, plants were assessed around the context of their color characteristics. Determination of the factors that influence the color choice for plant selection in the planting design projects which have been produced by landscape architecture undergraduate students in the project studio was aimed in this paper. Around this context, a survey was created to be applied to undergraduate students of the landscape architecture department. The composed survey was applied to 2nd, 3rd and 4th grade undergraduate students who had succeeded in the landscape design projects. The survey results were digitized and analyzed by using SPSS 22.0 statistical software. In conclusion, personal preferences were shown to be effective in the plant color selection in planting design projects of landscape architecture department students. Based on these survey results, proposals were developed in order to use the accurate color in the planting design.

Keywords: Landscape design, Planting design project, Color selection, Plant preference.

1 INTRODUCTION

The continuous increase of structural areas due to globalization increases the need of individuals for open and green areas. That is why, it has gained importance today for landscape architects to carry out ecology based sustainable landscape planning and design works at local and national scale that protects the natural and cultural values. Design criterias differ for each study in landscape design. Acar et.al.[1] attract attention to the determination of the aesthetic components of compositions consisting of plant material and different plant species as well as the lack of sufficient number of such studies. According to Uzun [2], taking into consideration the properties of lively and dynamic structured plants in external space organizations carried out for landscape design works will emphasize the structural and architectural arrangements inside the space thus according to Mason et.al. [3] they are increasing the value of the project and project application area.

Plants are the main material of landscape architecture. As spatial design elements, plants are used for different purposes with regard to ecology, aesthetic and function [4]. According to Waterman [5], the occupation of landscape architecture struggles with the delusion that its sole purpose is to planting. This perception will be eliminated with landscape designs which balance structural and plantal elements. According to Walker [4] and Korkut et.al.[6], plants are evaluated according to size, form, color and texture features, thus providing different usage possibilities with regard to aesthetics in different designs. Plants have positive or negative effects on landscape design projects with the color of their leaves, flowers, stems and fruits all of which perform a duty as a separate system [7].

1.1. Psychological and Perceptual Properties of Colors

Psychological and perceptual properties of color as an aesthetic element vary among individuals. According to Uzun (1998), using color as a design component in a system is interpreted as an expression of comprehensibility [8]. Among the main colors, red represents aggressiveness, uneasiness, vitality, struggle etc.; yellow represents joy, comfort, mind developing, sun, light etc.; blue represents calmness, happiness etc.; whereas among the intermediate colors, orange represents spaciousness, dynamism etc.; green represents relaxation, hope, satisfaction etc.; and purple represents sadness, fear, regret, coolness, creativity etc. Black which is among the neutral colors represents seriousness, pessimism, anxiety, mourning etc. whereas contrary to these white represents refreshment, purity,

¹ Corresponding author: Bartın University, Forestry Faculty, Department of Landscape Architecture, 74100, Merkez/Bartın, Turkey.
pkececioglu@bartin.edu.tr

cleanliness etc. Gray arouses feelings of maturity, trust etc. [2][9][10]. Red, yellow and orange are hot colors; they encourage excitement, motion, joy etc. and show spaces to be more closes, whereas cool colors which are blue, green and purple instill feelings of calmness, relaxation etc. thus creating an effect that makes the spaces seem farther away [2][6]. The effects of the colors of plants differ from season to season. Whereas green color of leaves creates a relaxation effect in spring, warm colors such as red, yellow and orange arouse positive feelings such as activity, liveliness and charm in autumn [11]. Expressions of colors lead to a psychological and perceptual variety on individuals due to various reasons such as ecologic conditions, traditions, fashion, living environment etc. However, common grounds were tried to be found and these generalizations were put forth as a result. Landscape architects use colors to strengthen design and give meaning to it.

1.2. Principles for Using Colors in Landscape Design Projects

It is important to take into consideration planting design principles for establishing the balance between structural and plant landscape elements in planting design works. The principles for using colors in landscape design can be summarized as below:

- Using a single color in areas that are integrated with nature will instill feelings of serenity, monotony and order. Whereas it will arouse feelings of liveliness and variety in children playgrounds [9].
- According to Akdoğan (1982), green leaf plants should be given priority in planting design. Dark green leaf plants provide effects of background and emphasis [9].
- According to Çubuk et.al. (1999), using neutral colors in transition areas will lead to feelings of protection, safety and harmony[9].
- Tones of a single color (monochrome) can be used in design, whereas more colors can also be used (polychrome). However, one of the colors should be the dominant one if polychrome is used [6][10]. In general, more than 5 colors should not be used in designs [6].
- According to Spulmann (1994), the use of contrast colors make the area more attractive [9].
- The use of red leaf plants should be limited in rural landscape since they are not natural species [9].
- Seasonal changes should be considered when selecting the plants. Color effect, leafing, flowering, fructification, defoliation time vary according to the various developmental periods of plants [11]. Plants that turn red or yellow in autumn should be used in a balanced manner with evergreen plants [6].

1.3. Objective of the Study

Plants were taken into consideration with regard to their color attributes within the scope of this study. The objective was to determine the reasons for the preference of colors when selecting plants for the planting design projects developed by landscape architecture department students in project studios. Suggestions for the proper use of colors in planting landscape design were put forth depending on the acquired results.

2. MATERIAL AND METHOD

A total 84 people who could be reached from among a group of 112 second, third and fourth year students who took the project class during the fall semester of the 2015-2016 academic year at the Bartın University Faculty of Forestry Landscape Architecture Department comprise the sample group and main material of the study. First year students were not included in the study since they do not take project class. Data acquired as a result of the relevant national and international literature as well as the survey carried out are the auxiliary material of the study. The objective of the study was to determine the reasons of color preference for the planting design projects carried out in the project studios by landscape architecture students. Within this framework, the study was carried out in four stages:

Relevant literature research was carried out at the national and international levels as the first stage of this study.

In the second stage, the surveys used in previous similar studies were examined and the survey form was developed by compiling the relevant questions from the references of Özer [12] and Seçgin [13]. The survey form was applied to undergraduate students via face to face interview method. The survey form consists of two sections one of which includes demographic data whereas the other includes general information related with the topic as headings. The first section consists of 3 questions which are about gender, age and what class they are. Whereas the questions in the second section have been prepared to determine the colors that the students prefer for their project on planting design and there are a total of 8 questions. The survey contains a total of 11 questions 2 of which are matrices consisting of 13 and 29 propositions and 9 multiple-choice questions. The choices for the questions were generated with basis on the main (red, yellow, blue), intermediate (orange, green, purple) and complementary/neutral (black, white, gray) colors according to Altınçekiç [9] and Yazgan et.al.[10].

The third stage consists of digitizing the surveys via SPSS 22.0 Statistical Package software and Frequency Analyse and Chi-square Tests were applied for the evaluation of these surveys. In addition, projects of the students prepared at the project studies which might set an example for the use of color in planting design were selected and evaluated within the scope of the study.

Whereas in the fourth and final stage the results were interpreted after which suggestions were developed for the use of the accurate color in planting landscape design.

3. FINDINGS

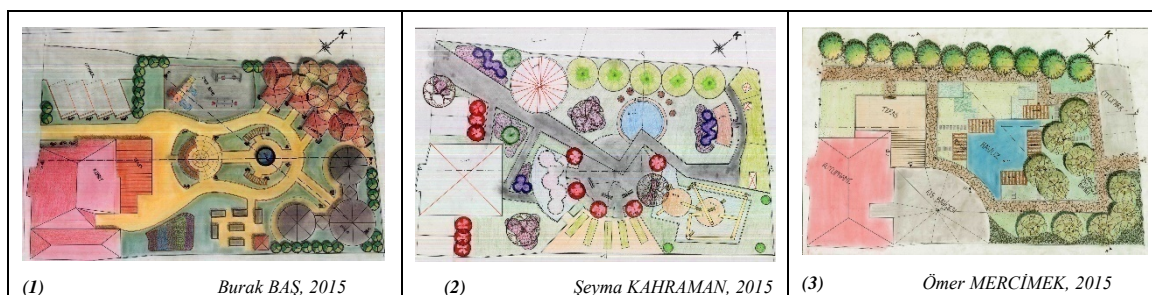
In this section, projects were given that might set an example for color preference in planting design and various evaluations were carried out. Frequency analyses were carried out for the data obtained as a result of the surveys applied to the second, third and fourth year students. Questions for which a statistically significant relationship was determined were crossed and evaluated via chi-square test.

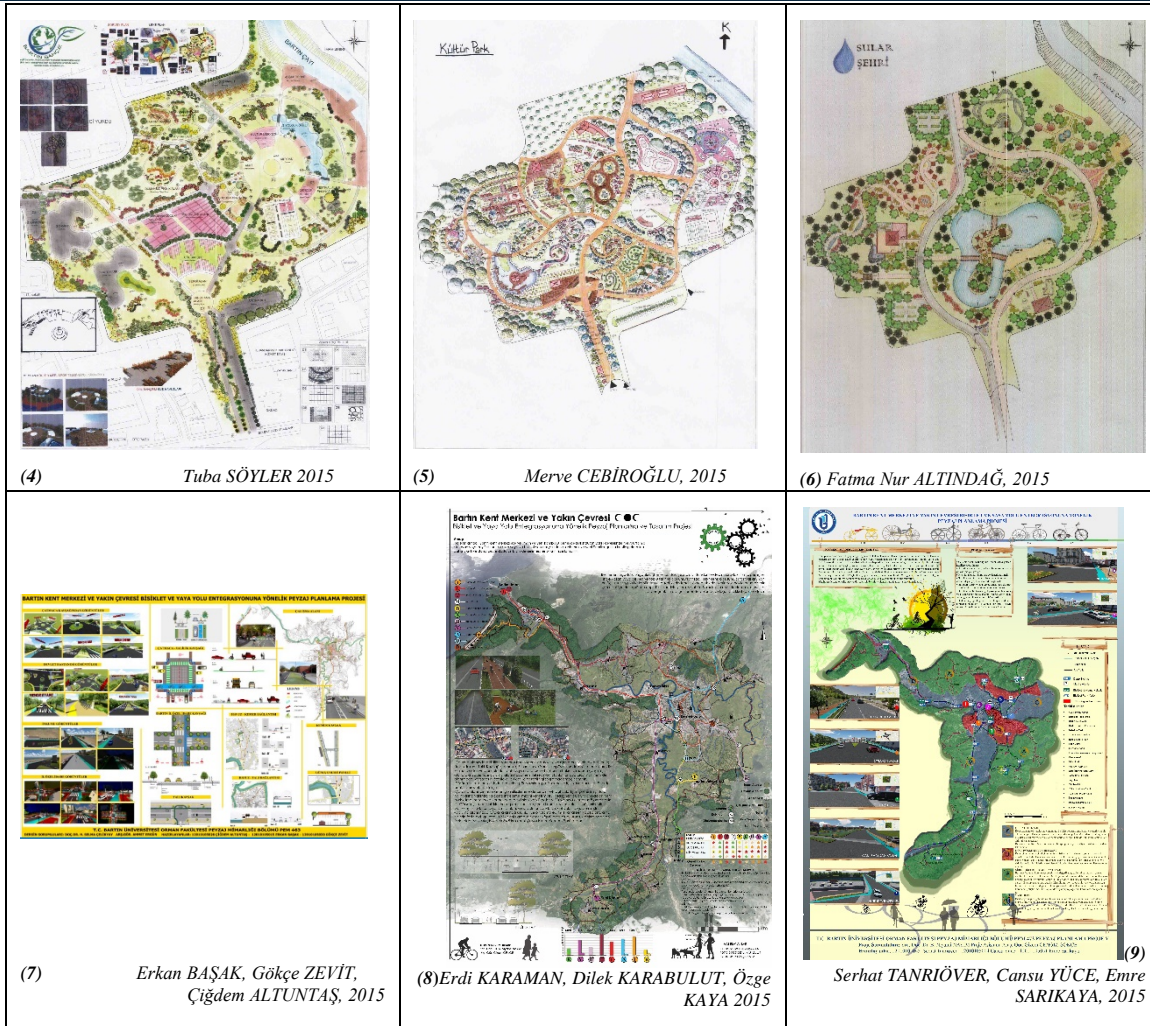
3.1. Selected Project Samples According to the Use of Color in Planting Design

As has been explained in the Method section, survey study was carried out with 84 people from among a group of 112 second, third and fourth year undergraduate students who have taken the project course in 2015-2016 fall term at the Bartın University Faculty of Forestry Landscape Architecture Department. Sample projects for the use of the most suitable color were selected from among the projects of these students with 3 projects from each class (Table 1). The project working area of each class is different. Whereas among the selected projects, the second year students work on residence garden landscape design, third year students have worked on recreation area and urban park design and fourth year students have worked on the planning and design for the integration of bicycle and pedestrian roads.

When the planting design of (1) (2) (3) sample plans were examined from second year projects, it is seen that aesthetical features are the most important criteria in plant preference for students. The second year students who are taking the plant design courses for the first time have weak information about plants. Therefore, it could be seen that the planting design studies are consists of non-functional and student's favorite color plants. Female prefer mostly colorful plants whereas male prefer mostly green. It is observed for the sample projects of third year students who have worked on recreation area and urban park design that planting design has been carried out more extensively and used more colorful plants at plans (4) and (5). Whereas mostly green colored plant species have been preferred for plan (6). Accordingly; it can be interpreted that a more active area was tried to be created in projects numbered (4) and (5), whereas a peaceful and serene area intended for a more passive use was tried to be created in the project numbered (6) due to the preference of green colored plants. Mostly green colored plants have been preferred in the sample projects of fourth year students who have worked on the planning and design for the integration of bicycle and pedestrian roads in order to include them in the open and green area system, to ensure traffic safety and to create a green corridor in the city in plans numbered (7), (8) and (9). The use of colored plants was avoided since they can cause distraction in traffic thus posing a danger.

Figure2. Sample Projects According to The Use of Color in Planting Design





3.2. Findings Related with Survey Data

3.2.1. Findings Related with the Demographic Structure of the Participants

70,2% (n:59) of the 84 people who were subject to the survey were female and 29,8% (n:25) were male. Whereas majority of the participants were students between the ages of 21-23 with a percentage of 65,5% (n:55), this was followed by the age group of 24-26 with a percentage of 23,8% (n:20). The remaining 6 % (n:5) consisted of students between the ages of 18-20 followed by students aged 27 and above with a percentage of 4,7% (n:4). 9,5 % (n:8) of the students reached for survey study were 2nd year students, whereas 34,5% (n:29) were 3rd year and 56% (n:47) were 4th year students (Table 2).

Table 3. Demographic Structure of The Participants

		Frequency	Percent (%)
Age	18-20	5	6
	21-23	55	65,5
	24-26	20	23,8
	27 ≤	4	4,7
Grade	2nd year	8	9,5
	3rd year	29	34,5
	4th year	47	56
Total		84	100

3.2.2. Findings Related with General Information About the Subject

More than half of the participants (65,4%, n:55) stated that they prefer to use the plants mostly according to their color features. It was determined that the aesthetic features of plants which are flower, branch and stem, leaf, fruit, evergreen and habitus features stand out with a ratio of 33,3% (n:28) followed by evergreen feature with a ratio of 26,2 (n:22) and flower feature with a ratio of 19% (n:16) (Table 3).

Table 4. Foreground Aesthetic Features On Plants in Planting Design

	Frequency	Percent(%)	
Aesthetical Features of Plants	Flower	16	19,0
	Branch and Stem	3	3,6
	Leaf	10	11,9
	Fruit	4	4,8
	Evergreen	22	26,2
	Habitus	1	1,2
	All	28	33,3
	Total	84	100,0

It was also approved with a ratio of 97,6% (n:82) by the participants via the matrix generated as a result of the survey study that the color of the plant material used is effective on user emotions. In this scope, it was determined that the red color arouses feelings of excitement (56%) in users; whereas blue results in peace (58,3%); green arouses feelings of peace (50%), comfort (51,2) and safety (51,2); black arouses feelings of pessimism (78,6%), introversion (61,4%) and aggressiveness (52,4%); whereas grey arouses feelings of introversion (54,8%). All of the participants (100%) stated that the red color does not arouse feelings of calmness; blue does not arouse feelings of introversion and pessimism; green does not arouse feelings of depressiveness; white does not arouse feelings of depressiveness and boredom; grey does not arouse feelings of happiness, peace and safety. It can be understood from these findings that colors have psychological effects on the designer.

It was questioned in another matrix via various choices what the main, intermediate and neutral colors remind the participants. Accordingly, it was observed that the colors yellow, orange, purple and grey do not remind anything to the participants. On the other hand, it was concluded that the color red reminds the participants of liveliness (58,3), attractiveness (69%), hot (71,4%), beauty (50%), energy (50%), self-confidence (51,2%), power (60,7%) and ambition (66,7%); that blue reminds the participants of hope (50%), depth (61,9%) and sea (85,7%); green reminds the participants of liveliness (53,6%), naturality (67,9%) and spring (71,4%); black reminds the participants of danger (59,5%) and formality (66,7%); whereas white reminds the participants of grace (60,7%), innocence (61,9%), light (65,5%) and purity (71,4%).

The choice 'colorful' is ranked the first with a percentage of 35,7% as the answer given to the question regarding which color is preferred to be seen in plants used in exterior spaces. This ratio supports the importance of color in plant preference. This value was followed by 19% for the color green and 8,3% for the colors white, yellow and red (Table 4).

Table 5. The Plant Color Preferred To Be Seen in Plants Used in Exterior Spaces

	Frequency	Percent(%)	
Colors	Yellow	7	8,3
	Red	7	8,3
	Blue	6	7,1
	Green	16	19,0
	Orange	3	3,6
	Purple	5	6,0

White	7	8,3
Grey	1	1,2
Colorful	30	35,7
Other	2	2,4
Total	84	100,0

When the plant color that the participants like the most as questioned, the first three were green (22,6%), red (21,4%) and colorful (20,2%). Orange and grey choices share the lowest ratio of 1,2% (Table 5).

Table 6. The Plant Color That The Participants Like The Most

	Frequency	Percent(%)
Colors		
Yellow	4	4,8
Red	18	21,4
Blue	3	3,6
Green	19	22,6
Orange	1	1,2
Purple	6	7,1
White	12	14,3
Grey	1	1,2
Colorful	17	20,2
Other	3	3,6
Total	84	100,0

When the seasonal activities of plants are considered, it was determined that the participants like the composition they create with the plants of their preference mostly in the spring season (53,6%) which was followed by fall with a ratio of 23,8% and summer with a ratio of 15,5% whereas winter was at the lowest spot with a ratio of 7,1%. (Table 6). The reasons why the students subject to the survey study selected spring were as follows: “Because the colors are livelier and more varied”, “Because flowering starts and it is the time of the year when the plants are the most beautiful and the most colorful”, “Because of the harmony of the green color with colorful plants”, “Because people tend to feel happy due to the coming of spring, liveliness of nature and the emergence of the colorful environment”, “Because plants flower to herald the coming of summer”.

Table 7. Favor Status Of The Plant Composition Related to Seasons

	Frequency	Percent(%)
Seasons		
Spring	45	53,6
Summer	13	15,5
Fall	20	23,8
Winter	6	7,1
Total	84	100,0

When the gender of the participants was crossed with their answers to the question regarding their favorite plant color, it was observed that there was a statistically significant relationship with a Pearson chi-square value of $< 0,05$. Accordingly, it was determined that 25,4 % (n:15) of the female participants prefer colorful planting designs, whereas

40% of the male participants (n:10) prefer the color red. In addition, when the favorite plant color of the participants was compared with their answer to the question, "In which season do you like the composition you created more when you consider the seasonal activities of plants?"; it was determined according to the spring coloring of plants that the red, green and colorful planting composition preferences had the same percentage of 22,2 % (n:10) (Table 7).

Table 8. The Comparison Of Favorite Plant Color With Gender and Seasons

		Favorite Plant Color										
		Yellow	Red	Blue	Green	Orange	Purple	White	Grey	Colorful	Other	Total
Gender	Female	2	8	3	11	1	6	10	0	15	3	59
	Male	2	10	0	8	0	0	2	1	2	0	25
19,384 ^a												
Seasons	Spring	3	10	2	10	0	1	6	0	10	3	45
	Summer	0	3	1	2	0	2	1	0	4	0	13
	Fall	1	4	0	7	0	3	3	0	2	0	20
	Winter	0	1	0	0	1	0	2	1	1	0	6
43,369 ^a												
Total		4	18	3	19	1	6	12	1	17	3	84

In addition to this information, the aesthetic features of plants that are forefront in the planting designs of the participants were compared with the question regarding their favorite plant color during the same analysis. When these questions were crossed, a statistically significant relationship was determined since the Pearson chi-square value was $< 0,05$. Accordingly, the flower, branch and stem, fruit, evergreen and habitus features had a ratio of 11,9% (n:10) for the color red and a ratio of 9,52% (n:8) for the colorful choice. The evergreen feature of various plants stood out and green color was preferred with a ratio of 7,14 (n:6) (Table 8).

Table 9. The Comparison of Favorite Plant Color with Aesthetical Features

		Favorite Plant Color										
		Yellow	Red	Blue	Green	Orange	Purple	White	Grey	Colorful	Other	Total
83,666 ^a												
Aesthetical Features	Flower	0	3	0	5	1	2	1	1	3	0	16
	Branch and Stem	1	1	0	0	0	0	0	0	0	1	3
	Leaf	0	1	1	4	0	1	2	0	1	0	10
	Fruit	0	0	0	1	0	0	0	0	3	0	4
	Evergreen	1	3	1	6	0	2	5	0	2	2	22
	Habitus	1	0	0	0	0	0	0	0	0	0	1
	All	1	10	1	3	0	1	4	0	8	0	28
	Total	4	18	3	19	1	6	12	1	17	3	84

4. CONCLUSION

Landscape architecture vocational discipline establishes the relationship between the other social and physical parameters of the landscape which is a whole with its natural and cultural elements, pays regard to the protection-usage balance for issues of ecological planning, natural protection, land use planning, landscape restoration and landscape management thus taking role in the design and planning works carried out in urban and rural areas. In addition, the accurate use of color which is one of the aesthetic features of the plants as the main material of living spaces is important for landscape design and planning works. Thus, importance given to people increases and an integrated relationship is established between nature and people.

The reasons for the preference of the plant colors by landscape architecture undergraduate students were questioned in this study. According to the results of the study, when the status of students taking plant related courses is considered, it was observed that students in their final years considered the aesthetic properties of the plants in addition to the functional properties. On the other hand, it was determined that the second year students who are

taking the project and plant design courses for the first time gave priority to the use of the color they prefer personally. In addition, color preference in planting design also differs in accordance with the variety of the project concept determined by the designer as well as the area where the project application will be carried out. For example, whereas second year students use less number of different plant species in residential garden landscape designs in order to be able to create wider spaces, third year students used a greater number of plant species with lots of colors when preparing a design project for recreation areas and urban park landscapes which require more liveliness. It was also observed as a result of the survey applied as part of this study that the color property from among the scent, texture, color and form properties of plants was preferred primarily by the participants. This emphasizes the importance of the concept of color for designers in planting design studies.

In conclusion; colors that are suited to the functions and forms of plant species should be selected by landscape architects in their landscape design and planning projects as is stated by Altınçekiç [9]. Color is one of the important aesthetic features of plants for planting design and it has direct effects on the users of the area due to its guiding property. In addition, it also has a function that can bring any desired element to the forefront or push it to the background. This factor that has significant importance visual importance should be used in a conscious, attentive and correct manner in planting design works.

REFERENCES

- [1] C. Acar, E. Demirbaş, P. Dinçer ve H. Acar, "Anlamsal Farklılaşım Tekniğinin Bitki Kompozisyonu Örneklerinde Değerlendirilmesi", *Süleyman Demirel Üniversitesi Orman Fakültesi Dergisi*, A, 1, pp. 15-28, 2003.
- [2] G. Uzun, *Temel Tasarım*, Çukurova Üniversitesi Ziraat Fakültesi Ofset Atölyesi, 3. Baskı, 2004.
- [3] S. C. Mason, T. W. Starman, R. D. Lineberger and B. K. Behe, "Consumer Preferences for Price, Color, Harmony, and Care Information of Container Gardens", *HortScience*, Vol. 43, 2, pp. 380-384, 2008.
- [4] T. D. Walker, "*Planting Design*", 2nd Edition, John Wiley & Sons, Inc., Canada, 1991.
- [5] T. Waterman, *Peyzaj Mimarlığının Temelleri*, Akademik Temeller Dizisi:7, 1. Basım, Literatür Yayınları, Eylül 2012.
- [6] A. B. Korkut, E. E. Şişman, ve M. Özyavuz, *Peyzaj Mimarlığı*, Verda Yayıncılık ve Danışmanlık, 1. Basım, Eylül 2010.
- [7] N. G. Mamikoğlu, *Türkiye'nin Ağaçları ve Çalıkları*, NTV yayınları, 2007.
- [8] H. Alper and S. Yılmaz, "Peyzaj Mimarlığında Işık ve Renk Kullanımının Erzurum Kenti Örneğinde İncelenmesi", *Atatürk Üniversitesi Ziraat Fakültesi Dergisi*, 35, 1-2, pp. 79-87, 2004.
- [9] H. Altınçekiç, *Peyzaj Mimarlığında Renk ve Önemi*, İstanbul Üniversitesi Orman Fakültesi Dergisi, 50, 2, pp. 79-83, 2001.
- [10] M. E. Yazgan, A. Uslu, ve E. Tanrıvermiş, *İç Mekan*, SASBÜD, Nisan 2003.
- [11] S. Kösa ve M. Atik, "Bitkisel Peyzaj Tasarımında Renk ve Form; Çınar (*Platanus orientalis*) ve Sığla (*Liquidambar orientalis*) Kullanımında Peyzaj Mimarlığı Öğrencilerinin Tercihleri", *Artvin Çoruh Üniversitesi Orman Fakültesi Dergisi*, Vol. 14, 1, pp. 13-24, Nisan 2013.
- [12] Özer, "İnsan Psikolojisi ve Peyzaj Tasarımı," Yüksek Lisans Tezi, Ankara Üniversitesi Fen Bilimleri Enstitüsü Peyzaj Mimarlığı A.B.D. Ankara, 2005.
- [13] Sezgin, "Çanakkale Kırsal Bölgesinde Ergenlik Dönemindeki Gençlerin (13-19 Yaş Grubu) Giysilerinde Renk Tercihi" Yüksek Lisans Tezi, Beykent Üniversitesi, Sosyal Bilimler Enstitüsü Tekstil Ve Moda Tasarımı A.B.D, Moda Tasarımı Sanat Dalı, İstanbul, 2013

The Color Removal Performance of CSTR Reactor Treating Real Textile Wastewater: Effect of Advanced Treatment by Application of Chemical Coagulation

Abdullah Kizilet¹, Dilda Gumuscu², Melis Ecem Kose², Seda Kundakci², Irem Sepet², Merve Yurdakul², Ozer Cinar^{2}*

Abstract

The aim of this study is to determine performance of treating real textile wastewater by biological and chemical treatment that combined continuous stirred tank reactor (CSTR) and chemical coagulation, respectively. The real textile wastewater was used for CSTR weekly provided from real scale treatment plant. Later on, advanced treatment was applied to the effluent of CSTR. In this context, type and dose of coagulant, pH adjustment and the stirring speed and time were examined as advanced treatment. Initially, the most commonly used coagulant $Al_2(SO_4)_3 \cdot 14(H_2O)$ was selected, later, $FeCl_3$ was added in sufficient quantities. Rapidly mixed each jar at 100 to 150 rpm for 1 minute with selected coagulants. The rapid mixing was helped to disperse the coagulant throughout each container. Then, the stirring speed reduced to 25 to 30 rpm and continued mixing for 15 to 20 minutes. To determine optimum pH for coagulation were tried various pH values (4 to 8) with jar testing and obtained results for selected two type coagulants were demonstrated in the results and discussion section. Consequently, in this study, the anaerobic biodegradability of the color-containing textile wastewater using a CSTR reactor and later on chemical coagulation were investigated. The obtained results demonstrated that chemical coagulation processes was inferred to be superior for the removal of both color and organic compounds from real textile wastewater. The highest color, COD, turbidity removal level was obtained by using $Al_2(SO_4)_3$ in conjunction with anionic polyelectrolyte, 73 PtCo, 25 mg/L COD, 2,37 NTU, respectively.

Keywords: Chemical treatment, Coagulants, Color removal, Textile wastewater

1. INTRODUCTION

The textile industry consists of many raw materials which fiber they use in their processes. These are non-synthetic fibers such as, cellulose, protein and also synthetic fibers which obtained in the laboratory. That's the main advantage of technology to obtain fibers from chemicals. But the majority of the fibers obtained from plant sources. The yield obtained from plant sources are more than the yield, obtained from animal or mineral sources [1]. Important pollutants are fundamentally persistent organics and some compounds such as, color, toxicants and inhibitory, surfactants, chlorinated compounds, salts, in the textile wastewater effluent. Textile wastewaters, contain color, are consist of very strong dye and also have wide range of pH from 2 to 14 [2]. The textile mills which are classified in two groups like spinning process (the dry process) mill and wet processing mills (involves usage of dyes [3,4]. The prevalent textile processing stages consists of desizing, scouring, bleaching, mercerizing and dyeing processes [5]. The constituents of these processes are generally; different chemicals used in each stages. It shows the textile wastewater contents the mixture of chemicals. Generally wet processes have high values of COD, BOD, TDS and high color. The most polluter processes that gives many hazardous chemicals such as bleachers, enzymes, starch, dyes, solvents, resins, oils, waxes, acids and bases etc. To wastewater are the most serious sources of wastewater pollutants. The largest source of the textile industry is desizing process, which removes chemicals from textile goods [6]. In this process significant amount of chemicals used in weaving process are thrown. In dyeing process, dye bath and washwater is the fundamental origin of wastewater. This wastewater typically involves by products, residual dyes

*Corresponding author: Yildiz Technical University, Department of Environmental Engineering, 34220, Esenler/Istanbul, Turkey.
ocinar@yildiz.edu.tr

¹Department of Bioengineering and Sciences, Kahramanmaraş Sutcu Imam University, 46100, Kahramanmaraş, Turkey,
abd.kizilet@gmail.com

²Yildiz Technical University, Department of Environmental Engineering, 34220, Esenler/Istanbul, Turkey.

and supporting chemicals also extra pollutants contain cleaning solvents like oxalic acid [7]. Also finishing process frequently contains natural and synthetic polymers and other toxic substances [8]. Generally COD, BOD, SS (Suspended Solids), DS (Dissolved Solids), Color, Turbidity and Heavy Metals etc. using for basic textile water characterization. Typically textile industry wastewater include low or high COD (COD from 131 to 17900) [9,10], pH and turbidity (pH from 2 to 14 [11,12]), turbidity from 15 to 5700 [13,14] and also strong color. The diversity of values arises from material variation.

1.1 Continuous Stirred Tank Reactor Color Removal Performance

Continuous Stirred Tank Reactor (CSTR); CSTR is the easiest probable continuous flow suspended growth bioreactor, which is formed of well mixed tank with rich polluted influent stream and a treated effluent including microorganisms. The wastewater volume in reactor is fixed and the mixing is adequate to make concentrations for all components uniform throughout the reactor and effluent is equal to interior volume concentration [15]. Therefore, these reactors also called as completely mixed reactors. Using SBR to color removal is fairly new approach compared to anaerobic-aerobic sequential treatment [16]. SBR used for many types of industrial wastewaters such as textile wastewaters. SBR modified as activated sludge process. Main advantages of this system are low build cost, high flexibility and low required spaces [17]. Significant disadvantages of SBR systems are extreme sludge production and high sludge volume index (SVI) values [18]. CSTR has many advantages that it operates in a steady state, it is well controllable, large heat transfer areas can be installed, although has disadvantage like necessary of high volume,

1.2 Advanced Treatment with Chemical Agents (Coagulation)

After pretreatment processes, the next unit process in a conventional water treatment system is a mixer, where the first chemicals are added in what is known as coagulation. There are special case occurs in small systems using underground water, when chlorine or other taste and odor control precautions are introduced at the intake and are the extent of treatment. Many researchers have worked the coagulation of synthetic and real textile wastewater using various inorganic chemicals (e.g., $FeCl_3$, $FeSO_4$, alum, lime, and $MgCl_2$) alongside components of biological origin [19]. Auxiliary poly-electrolytes are executed by the forced hydrolysis of a easy coagulant, like alum [20]. The process of coagulation is a series of chemical and mechanical operations by which coagulants are practical and made effective. There are two stages of this process: (1) fast mixing to disperse coagulant chemicals by violent mixing into the water being treated, and (2) flocculation to band together small particles into well-defined floc by attentive mixing for a much longer time. The coagulant must be added to raw water and completely disperse in the liquid; such stability of chemical treatment is achieved by the way of rapid mixing. Coagulation consequences from adding salts of iron or aluminum to the water and is a reaction between one of the following (coagulants) salts and water: Polymers, Sodium aluminate, Ferrous sulfate etc. [21].

1.3 Aim of the study

The aim of this study was to determine the removal of color natural organic and inorganic matter by enhanced coagulation after biological treatment with CSTR (continuous stirred tank reactor). Despite the fact that obtained satisfactory Chemical Oxygen Demand (COD) removal, the color removal results were unsatisfactory after CSTR. So, applied Advanced Treatment (with chemical agents) to effluent of CSTR, in this context; Jar tests were applied by using $Al_2(SO_4)_3$, $FeCl_3$ after enhanced coagulation conditions determined optimum dosage and optimum pH for each coagulant. Although obtained discharge standards by using $Al_2(SO_4)_3$, auxiliary polyelectrolytes were used for advance more stronger than wastewater.

2 MATERIAL AND METHODS

2.1. Design and operation of CSTR

Using of CSTR to color removal is fairly new approach. CSTR is the easiest probable continuous flow suspended growth bioreactor, which is formed of well mixed tank with rich polluted influent stream and a treated effluent including microorganisms. The wastewater volume in reactor is fixed and the mixing is adequate to make concentrations for all components uniform throughout the reactor and effluent is equal to interior volume concentration [15]. Therefore, these reactors also called as completely mixed reactors. In this study used CSTR was demonstrated as schematically in the Figure.1. The CSTR was operated with about constant 3000 ± 100 mg/L mixed liquid suspended solids (MLSS).

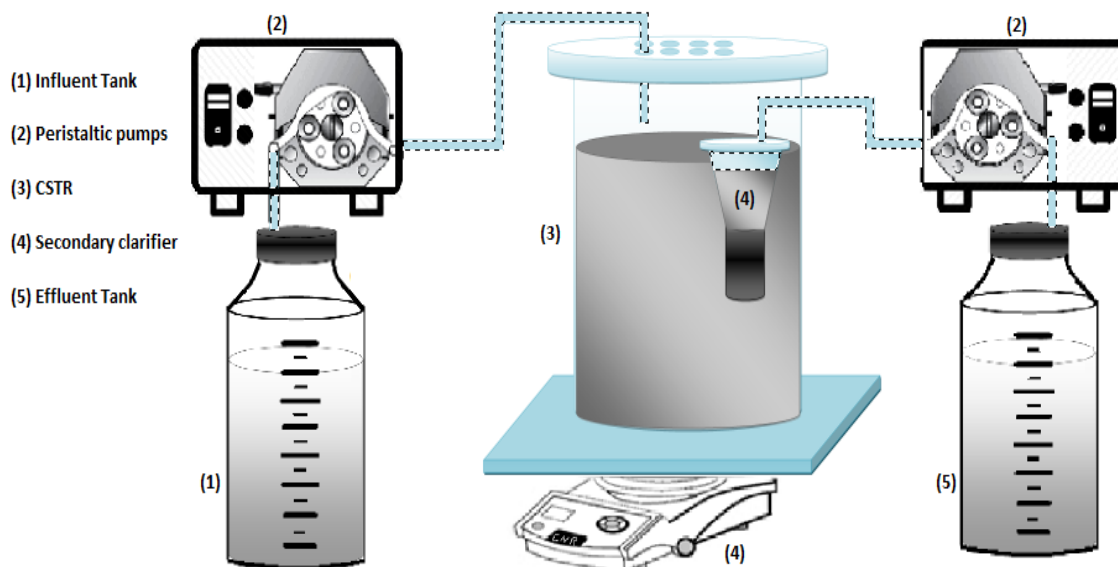


Figure 1. Schematic Representation of CSTR configuration: (1:Influent Tank, 2:Peristaltic pumps, 3:CSTR, 4:Secondary clarifier, 5:Effluent Tank)

2.2. Operation conditions

The CSTR was operated under the anaerobic conditions. Different hydraulic retention time (HRT) was examined to obtain optimum color and COD removal. In this context, CSTR was operated at HRT of 8 h, 16 h and 24 h, respectively. But, in this study, only HRT of 16 h results were chosen for applied advanced treatment (effect of different coagulants and dosage). The reactor was fed with real textile wastewater at $32 (\pm 1)^\circ\text{C}$ temperature. The reactor has 10 lt volume (7 lt active working volume). The influent pH value was daily adjusted to 7,2 for optimum media of living microorganisms. The CSTR was operated with hours of 8, 16, 24 hydraulic retention time as continuous flow with peristaltic pump (SHENCHEN V6-3L, China). But, only advanced treatment with coagulation was applied to 16 hours results (depend on color and COD removal, and cost of operation). The study gives wide coverage to effect of different coagulants such as $\text{Al}_2(\text{SO}_4)_3$ (Alum) and FeCl_3 . CSRT was used to treatment textile wastewater as simulated full-scale treatment plant conditions, and applied advanced chemical treatment.

2.3. Wastewater Characteristic

The real textile wastewater was obtained from full-scale treatment plant (TEKBOY Inc.). The used real textile wastewater wide range influent color (2000-3000 PtCo). Daily pH of the influent fed was adjusted to 7.2 (raw pH 9.2). The used real textile wastewater main characteristics average were tabulated in the Table.1.

Table.1. The used real textile wastewater main characteristics

Parameter	Unit	Raw Wastewater
Average COD	mg/L COD	800
PtCo	-	2500
Conductivity	mS/cm	5.6
436nm(abs)	CN (λ)	70.66
525nm(abs)	CN (λ)	52.16
620nm(abs)	CN (λ)	42.71
Turbidity	NTU	70
Suspended solids	mg/L	550 \pm 50
pH	-	9.2

The color unit of absorbance about the wave length was converted to Chrominance Number (CN) unit by using equation 1. Also daily wave length scanning was examined for influent water, the result of this scanning was 558 nm as shown also in the Table.1.

$$CN(\lambda) = \frac{A}{d} * f \quad (1)$$

Here;

CN (λ): λ wave length, number of chrominance value (m^{-1})

A= λ The absorbance value of the sample wave height (absorbance read) (cm^{-1})

d: Cell thickness (mm),

f: factor to obtain the spectral absorbance values of m^{-1} of unit, $f=1000$,

2.4. Analytical Methods

COD measurement

The COD measurement method determines the quantity of oxygen required to oxidize the organic matter in a waste sample, under specific conditions of oxidizing agent, temperature, and time. Since the test utilizes a specific chemical oxidation the result has no definite relationship to the Biochemical Oxygen Demand (BOD) of the waste or to the Total Organic Carbon (TOC) level. In this study, titrimetric method (Standard Method 5520) was used. The test result should be considered as an independent measurement of organic matter in the sample, rather than as a substitute for the TOC test. Organic and oxidizable inorganic substances in the sample are oxidized by potassium dichromate in 50% sulfuric acid solution at reflux temperature. Silver sulfate is used as a catalyst and mercuric sulfate is added to remove chloride interference. The excess dichromate is titrated with standard ferrous ammonium sulfate, using orthophenanthroline ferrous complex as an indicator. Samples are boiled with a strong oxidizing $K_2Cr_2O_7$ severe acid conditions in the thermoreactor (WTW-CR 3200, Wissenschaftlich-Technische Werkstätten, Weilheim, Germany). Two hours of boiling a standard amount of remaining oxidizing eventually consumed without allowing oxidation of reduced (ferrous ammonium sulphate) was assessed on the basis of substance solution with the volumetric determination of the road (APHA, 2005) [22].

Turbidity, pH, conductivity measurement

The turbidity analyses were measured by turbidimeter (WTW-Turb 550 IR, Wissenschaftlich-Technische Werkstätten, Weilheim, Germany) with NTU of unit. The measurement of free electrons released as a result of the biochemical reactions that occur in the CSTR. The conductivity is indicative of the free electrons. The pH of a solution indicates how acidic or basic it is in the reactor. The pH and conductivity of samples were measured using multimeter (HACH-HQ 40d Portable Multi-meter, Loveland, U.S.A). Standard methods used for the other series of analysis

Advanced Treatment (with chemical agents)

Jar tests were applied by using $Al_2(SO_4)_3$, $FeCl_3$ after enhanced coagulation conditions determined optimum dosage and optimum pH for each coagulant. Firstly tried determine optimum pH (2, 2.5, 4, 5, 7.5, 9) and optimum dosage mg/L; (5,10, 20, 50, 80,100,150, 200, 250) for both $Al_2(SO_4)_3$ and $FeCl_3$, Then, tried determine optimum stirring speeds, waiting periods for settlement. The best chosen results were shown in the Result and Discussion section.

3 RESULTS AND DISCUSSION

3.1 COD removal, pH and Conductivity Profiles of CSTR

At the end of 16 hours of HRT, 75% for Chemical Oxygen Demand (COD) (effluent average 282.85 mg/L COD), and average 65% for color (effluent average 799.2 PtCo), before advanced chemical treatment in the CSTR. Adjusted influent pH increased average from 7.2 to 8, also conductivity average from 5.6 to 5.99. The COD removal, pH and conductivity results were demonstrated in the Fig.2 (A) and (B), respectively.

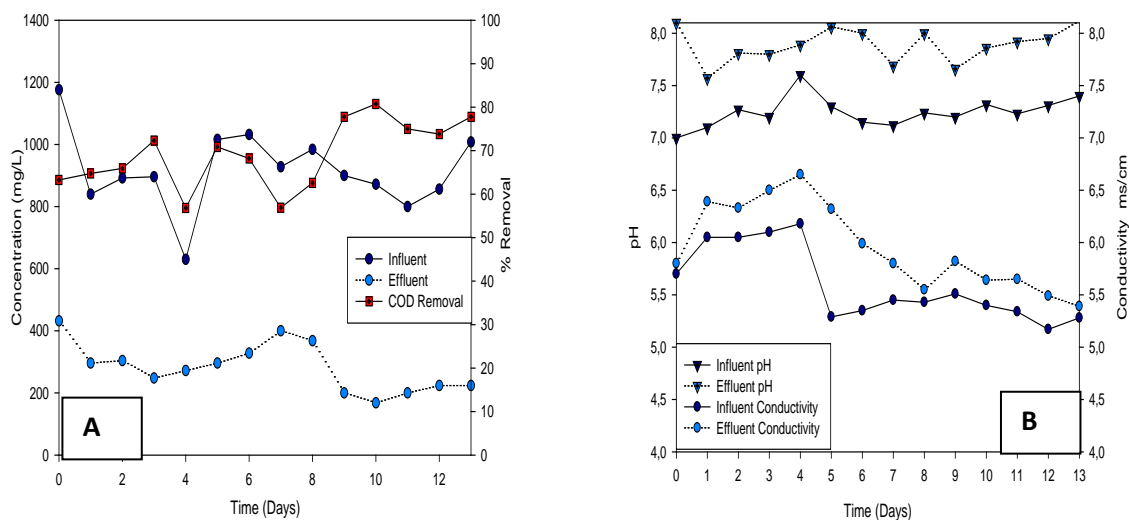


Figure 12. Schematically (A) COD removal, (B) pH and Conductivity profiles

In the previous studies, Smólka et al., demonstrated COD removal in the textile wastewater treatment with continuous system [23]. Their system was efficient in the COD reduction (> 88 %), the level forced by legislation for influents to surface water was exceeded. Furthermore, the outflow pH was around 9 irrespectively of the feed pH (about 7) similar to our study. Also, they showed that the effluent conductivity reached to 16 mS/ cm higher than our results.

3.2 Advanced treatment (chemical coagulation)

Determination of Optimum pH values for $Al_2(SO_4)_3$ and $FeCl_3$

Table 2. Determination of optimum pH values of $Al_2(SO_4)_3$ and $FeCl_3$

Parameters	Influent	$Al_2(SO_4)_3$, Alum pH 4		Alum pH 5.5		Alum pH 7		$FeCl_3$ pH 4		$FeCl_3$ pH 5.5		$FeCl_3$ pH 7	
		Effluent	Removal(%)	Effluent	Removal(%)	Effluent	Removal(%)	Effluent	Removal(%)	Effluent	Removal(%)	Effluent	Removal(%)
PtCo	920	263	71	110	88	440	52	210	77	754	18	820	11
Abs.	1,535	0,363	76	0,236	85	0,755	51	0,355	77	1,209	21	1,247	19
436nm(abs)	0,695	0,158	77	0,11	84	0,348	50	0,172	75	0,605	13	0,621	11
525nm(abs)	0,49	0,107	78	0,087	82	0,243	50	0,104	79	0,366	25	0,379	23
620nm(abs)	0,355	0,068	81	0,05	86	0,164	54	0,079	78	0,239	33	0,247	30
558nm(abs)	0,464	0,097	79	0,06	87	0,236	49	0,1	78	0,338	27	0,346	25
COD (mg/L)	368	172	53	106	71	236	36	140	62	260	29	285	23

To Determine optimum pH value of both $Al_2(SO_4)_3$ and $FeCl_3$, different dosages were tired range of dosage mg/L; (5,10, 20, 50, 80,100,150, 200, 250) for both $Al_2(SO_4)_3$ and $FeCl_3$. The optimum dosage of 100 mg/L and 250 mg/L for $Al_2(SO_4)_3$ and $FeCl_3$, respectively. To determine optimum pH values, jar tests were applied by using $Al_2(SO_4)_3$ and $FeCl_3$ after enhanced coagulation conditions determined optimum dosage and optium pH for each coagulant. Firstly tried to determine optimum pH (2, 2.5, 4, 5, 7.5, 9) for both $Al_2(SO_4)_3$ and $FeCl_3$.As a results of these tries the optimum pH values were obtained the optimum pH value of 5.5 for $Al_2(SO_4)_3$ based on both PtCo and COD removal, and the optimum pH value of 4 for $FeCl_3$ based on both PtCo and COD removal, respectively. The other parameters obtained with determine of optimum pH values tabulated in the Table 2.

Advanced Color, Turbidity and COD Treatment at different pH for chosen better coagulant (Alum)

In order to determine effect of different pH values on removal of color, turbidity and COD with different dose of Alum (10, 20, 40, 50,100 mg/L $Al_2(SO_4)_3$). In this context, four different pH values (5.5, 6, 6.6, 7) were examined. The

results were demonstrated in the Figure.3. The best color removals were obtained with about 100 mg/L Alum at pH values of 5.5. The best COD removal was obtained with about 150 mg/L Alum at pH values 5.5. Similarly, the optimum turbidity removal results were obtained at pH values of 5.5 also 6. But, the optimum turbidity removal results were obtained with 100 mg/L $Al_2(SO_4)_3$ and above.

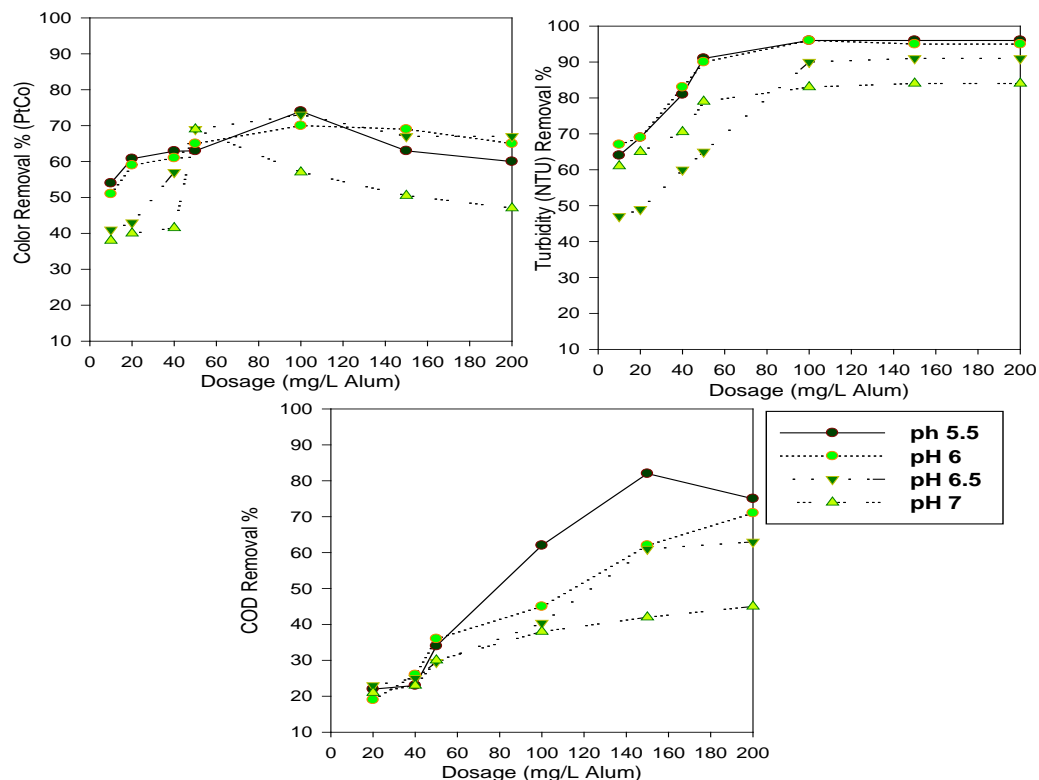


Figure 3. Efficiency of auxiliary polymers on the Color, Turbidity and COD removal at the best dosage of coagulants

Ersoy et al. turbidity removals with different dose of Alum were demonstrated in their study. They obtained optimum turbidity effluent (60 NTU) with 100 mg/L Alum. They increased the dosage of Alum of 500 mg/L and obtained highest effluent (50 NTU) [24]. In previous other studies many researchers were examined similar tests such as, Ching et al. Tried 1-3 mg/L Alum [25] and Pierre and Ma tried 100-3000 mg/L Alum [26].

Advanced Color, Turbidity and COD Treatment using Polyelectrolyte

Although obtained discharge standards by using $Al_2(SO_4)_3$, auxiliary polyelectrolytes were used for advance more stronger than wastewater. In this context, cationic and anionic polyelectrolytes were used in conjunction with these coagulants in order to further improve removal efficiency and for future studies about more stronger wastewater. The anionic polyelectrolytes did not effect to significantly removals of the color, COD and turbidity. We obtained the best results with using Alum in conjunction with cationic polyelectrolyte for color turbidity and COD removal. The PtCo, 558 nm wavelength scanning, turbidity and COD removals without polyelectrolyte were 69.5%, 71%, 59% and 70%, respectively. But polyelectrolyte we achieved to 81.1%, 85.19%, 84.6% and 90% with polyelectrolyte as shown in the Fig.4 (A). On the other hand, $FeCl_3$ used in conjunction with polyelectrolyte did not effect to significantly removals of the color, COD and turbidity as shown in the Fig.4 (B).

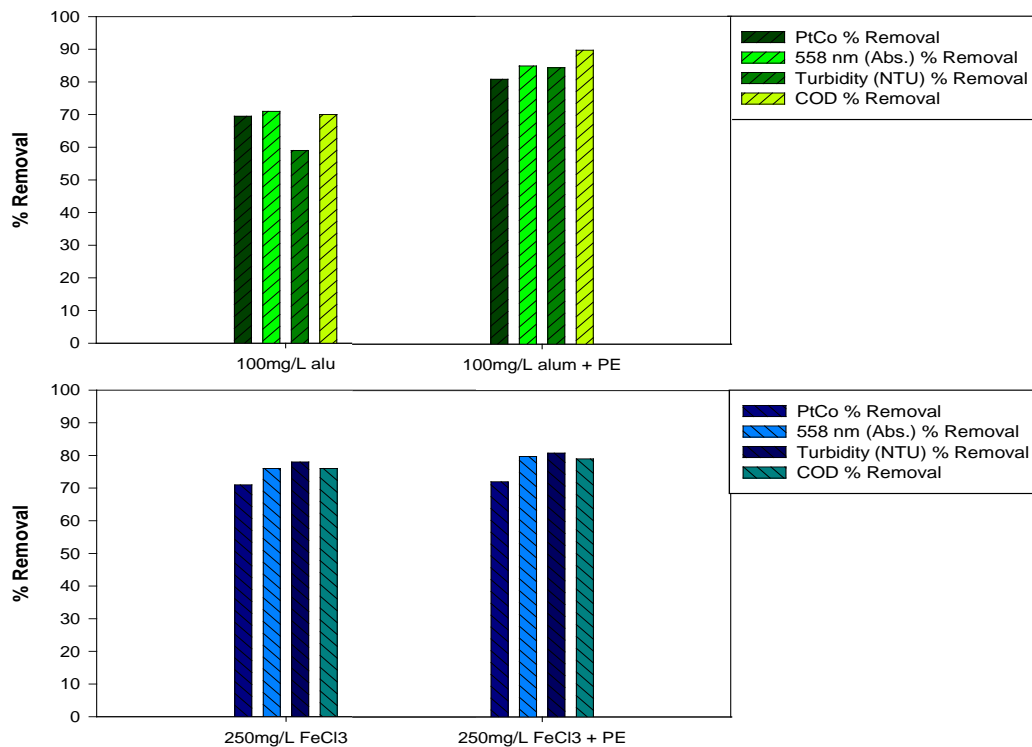


Figure 4. Removal Profiles of Color, Turbidity and COD in Conjunction with Polyelectrolyte (A) for Alum, (B) for FeCl₃

In the previous studies, Alkan et al. were demonstrated the turbidity removals with different polyelectrolyte in their study. They were obtained the total organic carbon (TOC) removal by 17% without polyelectrolyte. But they achieved 55% with the use of cationic polyelectrolyte [27]. In light of this findings, use of more than the optimum dose of polyelectrolytes cause to increasing the amount of sludge sourced polymer and cause to increasing cost of operation, although support have advantage using with optimum.

4 CONCLUSIONS

Findings of this study showed that natural organic and inorganic matter causing deterioration of water quality, also color was removed significantly by enhanced coagulation process, As a result of jar tests that removals were average above of 90% for COD, Turbidity and Color. Cationic and anionic polyelectrolytes were used in conjunction with these coagulants in order to further improve removal efficiency and for future studies about more stronger wastewater. The highest color, COD, turbidity removal level was obtained by using Al₂(SO₄)₃ in conjunction with anionic polyelectrolyte, 73 PtCo, 25 mg/L COD, 2.37 NTU, respectively, at the optimum (for both of them) contact time: 25 min, agitation speed: 25 rpm.

REFERENCES

- [1] T. Kuusisto, "Textile in Architecture" Ms.Thesis, Tampere University of Technology, Department of Architectural Design, Tampere, Finland, Apr. 2010.
- [2] E. Bazrafshan, M. R. Alipour and A. H. Mahvi "Textile wastewater treatment by application of combined chemical coagulation, electrocoagulation, and adsorption processes", *Desalination and Water Treatment*, 57, 9203–9215, 2016.
- [3] ISPCH., *Industrial Safety and Pollution Control Handbook*. 2nd ed., A joint publication of National Safety Council and Associate, Publishers Pvt. Ltd., Hyderabad, India, 1995
- [4] S. Sette, L. Boullart and L. Langenhive "Optimising A Production by A neural Network/Genetic Algorithm Approach", *Engng Applic ArtifIntell*, 9, 681-689, 1996.
- [5] A.B. Dos Santos, M.P. Madrid, F.A.M. De Bok, A.J.M. Stams, J.B. Van Lier, F.J. Cervantes, "The contribution of fermentative bacteria and methanogenic archaea to azo dye reduction by thermo-philic anaerobic consortium", *Enzyme Microbiol. Technol.* 39, 38–46, 2006.
- [6] I.A.E. Bisschops and H. Spanjers, "Literature review on textile wastewater characterisation", *Environmental Technology*, 24, 1399-1411, 2003.
- [7] USEPA, EPA Office of Compliance Sector Notebook Project. *Profile of the Textile Industry*, Washington, 1997.
- [8] Snowden-Swan, L.J., "Pollution prevention in the textile industries. In: Freeman, H.M. (Ed.)", *Industrial Pollution Prevention Handbook*. McGraw-Hill, Inc., New York, U.S.A, 1995.

- [9] G.E Ustun, S.K.A Solmaz and A. Birgul, "Regeneration of industrial district wastewater using a combination of Fenton process and ion exchange-A case study", *Resources Conservation and Recycling*, 52, 425-440, 2007.
- A. Rodriguez, G. Ovejero, M.D. Romero, C. Diaz, M. Barreiro and J. Garcia, "Catalytic wet air oxidation of textile industrial wastewater using metal supported on carbon nanofibers", *Journal of Supercritical Fluids* 46, 163-172.
- [10] W.J Lau, and A.F. Ismail. "Polymeric nanofiltration membranes for textile dye wastewater treatment: preparation, performance evaluation, transport modelling, and fouling control- a review" *Desalination* 245, 321-348, 2009.
- [11] D.J Joo, W.S Shin, J.H.; Choi, S.J.; Choi, M.C Kim, M.H. Han, T.W Ha, and Y.H.Kim, "Decolorization of reactive dyes using inorganic coagulants and synthetic polymer", *Dyes and Pigments*, 73, 59-64, 2007.
- [12] Ciabatti, I., Tognotti, F., Lombardi, L., 2010. Treatment and reuse of dyeing effluents by potassium ferrate. *Desalination* 250, 222e228.
- [13] Bayramoglu, M., Kobya, M., Can, O.T., Sozbir, M., 2004. Operating cost analysis of electrocoagulation of textile dye wastewater. *Separation and Purification Technology* 37, 117e125.
- [14] C. P. Leslie Grady, Jr., and Henry C. Lim "Biological Wastewater Treatment: Theory and Applications" 2nd ed. English, Book, Marcel Dekker, 1999.
- [15] K. Kapdan and R. Ozturk, "Effect of operating parameters on color and COD removal performance of SBR: Sludge age and initial dye stuff concentration", *J. Hazardous Materials*, 123, 217-222, 2005.
- [16] R. Ganjesh, G. Balaji, and R. A. Ramanujam, R. A., "Biodegradation of tannery wastewater using sequencing batch reactor Respirometric assessment", *J. Bioresource Tech.*, 97, 1815-1821, 2006.
- [17] D. P., Bernet, D., Nicolas, J., Philipe and R., Moletta, "Effects of oxygen supply methods on the performance of a sequencing batch reactor for high ammonia nitrification" *J. Water Env. Res.*, 72, 195-200, 2000.
- [18] B. H.; Tan, T. T.; Teng, A. K. M Omar, "Removal of dyes and industrial dye wastes by magnesium chloride", *Water Res*, 34, 597-601, 2000.
- [19] P, Moussas and A. Zouboulis, "A new inorganic-organic composite coagulant, consisting of Polyferric Sulphate (PFS) and Polyacrylamide (PAA)", *Water Res.*; 43, 3511-3524, 2009.
- [20] F. R. Spellman, "Mathematics manual for water and wastewater treatment plant operators", 2nd ed., English, Book, Taylor & Francis roup, 2014.
- [21] APHA, American Public Health Association (1995). *Standart Methods for the Examination of Water and Waste Water*, 19th ed., APHA-AWWA-WEF, Washington, DC. USA.
- A. K. Smólka, J. S. Ledakowicz, K. Pazdzior and S. Ledakowicz, "Application of anoxic fixed film and aerobic CSTR bioreactor in treatment of nanofiltration concentrate of real textile wastewater", *Chemical Papers*, 64 (2), 230-236, 2010.
- B. Ersoy, A.M. Alptekin, A. Sanisik, S. Gürcan, Z.E. Erkan and A. Yıldız, "Doğal Taş İşleme Tesisi Atık Sularından Bulanıklığın Giderilmesine Farklı Yöntemlerin ve Farklı Koagülantların Etkisi", *Symposium of Madencilik ve Çevre Sempozyumu*, 5-6 May 2005.
- [22] H. S. Ching, T. Tanaka, S. Theodore and E. Menachem, "Dynamics of coagulation of kaolin particles with ferric chloride", *Wat. Res.* 3: 559-569, 1994.
- [23] A., C. Pierre and K. Ma., "Sedimentation behaviour of kaolinite and montmorillonite mixed with iron additives, as a function of their zeta potential", *Journal Of Material Science*, 32, 2937-2947, 1997.
- [24] U. Alkan, A. Teksoy and H. S. Baskaya, "Yüzeysel Sulardaki Doğal Organik Maddelerin Gideriminde Uygun Koagülasyon Şartlarının Belirlenmesi", *Ekoloji*, 15, 59, 18-26, 2006.

A Review on Dynamic Membrane Bioreactors: Comparison of Membrane Bioreactors and Different Support Materials, Transmembrane Pressure

Ozer Cinar*¹, Abdullah Kizilet², Onur Isik³, Amar Ćemanović³, Mehmet Akif Veral¹, Selin Duman¹

Abstract

Over the past three decades, membrane bioreactors are being considered as a very useful alternative for biological wastewater treatment thanks to the important advantages over conventional biological treatment. Membrane bioreactors gain the upper hand in respect to high quality effluent water by solid-liquid separation. In current reviews, the focus is on the advantages of dynamic membrane bioreactors. Dynamic membrane bioreactors that used different support materials dramatically reduce the initial investment and operating costs in comparison to membrane bioreactors. Instead of ultrafiltration and microfiltration membranes, different support materials such as mesh, non-woven and woven fabric cloth can be used as the support materials. Also, transmembrane pressure and critical flow play a significant role to understand fouling of membrane bioreactors. In this context, different support materials performances are examined in respect to transmembrane pressure and critical flow. In addition, extracellular polymeric substances (EPS) and soluble microbial products (SMP) play an important role in the fouling phenomenon of both membrane bioreactors and dynamic membrane bioreactors. This review outlines advantages of dynamic membrane bioreactors with regard to different support materials, transmembrane pressure, SMP, EPS analogically membrane bioreactors.

Keywords: Different support materials, Dynamic membrane bioreactors, Transmembrane pressure

1 INTRODUCTION

Interest in membrane system in biological treatment of wastewater is increasing with each passing day. In conventional active sludge process (CAS), biochemical oxidation and water/biomass separation occurs in two different tank but MBRs make it convenient to proceed in one tank [1]. Although, effluent quality and low system footprint are mentioned as benefits of MBRs, it has some primary limitations like; low flux, energy demand, membrane cost and fouling control. All those problems can be solved by using dynamic membrane technology [2-5]. A dynamic membrane is a cake layer forms on a support material [6]. The cake layer consist of flocs, microbial cells, extracellular substances (EPS), and other organic and inorganic solid particles in wastewater. These matters accumulate on support material become denser overtime and formed a cake layer. This cake layer acts as a membrane [7]. The cake layer easily removed on support material or it can easily re-formed again, because of this situation the cake layer called as "dynamic membrane" (DM) [5]. Steel or plastic mesh and woven or non-woven cloth used as support material, besides of mikro-nanofilters [7]. Dynamic membrane bioreactors (D-MBRs) operation consist of three stages; DM layer formation, filtration and backwash [8]. At the initial stage, the cake layer has not consist on support material. D-MBR has poor effluent quality, and effluent contain high suspended solid (SS), because of the high pore size of support materials. In this stage effluent water containing high SS concentration is returned back to actthere or until it reaches high effluent quality. At this stage, dynamic membrane is formed, and effluent quality reach to Microfiltration/Nanofiltration membrane effluent quality. At lastest age, flux decreased because of fouling, therefore, backwashing is in progress [5, 8-10].

¹Corresponding author: Department of Environmental Engineering, Yildiz Technical University, 34220, Esenler/Istanbul, Turkey. ocinar@yildiz.edu.tr

²Department of Bioengineering and Sciences, Kahramanmaraş Sutcu Imam University, 46100, Kahramanmaraş, Turkey,

³Istanbul Technical University, Department of Environmental Engineering, Maslak/Istanbul, Turkey.

2 HISTORY and COMMERCIAL DEVELOPMENT OF MEMBRANE SYSTEMS

Membrane bioreactor technology was first presented in 1969 by Smith et al., [1] with a research program. In their study, ultrafiltration membranes were used for separating water and activated sludge without a clarifier. They operated a pilot plant for 6 months to get high-quality effluent from sewage generated by manufacturing plant in the U.S.A. The MBR technology was used for limited circumstances such as leachate and industrial wastewater treatment systems. High membrane capital costs, fouling problem and mixed liquor recirculation with high energy costs are restricted by the spread of the membrane technology to municipal wastewater treatment applications [2]. A new technology was developed [3] by using 0.1 μm size polyethylene hollow fiber (HF) membranes for separating water from the mixed liquor in an activated sludge aeration tank. There are two membrane type alternatives, the first option is submerged MBR configuration such as operating under a vacuum, instead of direct pressure. This configuration may be named immersed as the membrane is placed directly into the liquid. The second option is side-stream MBR configuration such as operating under pressure. In this approach, the membrane is separated from the bioreactor and a pump is required for pushing the bioreactor effluent into the membrane system and permeate through the membrane. This configuration may be named external cross-flow membrane. Flat sheet (FS) and hollow fiber (HF) membranes are generally used for submerged MBR configuration. Membrane was located in the aeration tank similarly with submerged MBR configurations, in this research. Submerged configuration was used to optimize the membrane module shape, the membrane pore size, operational principals to prevent membrane fouling, and the cleaning of membranes at the beginning the evolution of MBR technology. Since the middle of 1990s, the accumulation of operational knowledge via academic and field studies have rapidly increased the demand of MBR technology with the competition of MBR providers such as Zenon, Kubota, Mitsubishi Rayon, and US-Filter [2]. Additionally, microfiltration (MF) has been generally used in combination with activated sludge process to improve the purification in domestic wastewater treatment [4]. The membrane is not applicable for many circumstances because of its high cost and energy requirement. Fouling problem for membrane requires regular chemical cleaning, this makes its operation hard to control and costly [5]. Correspondingly, applying a non-woven fabric filter could be another alternative to using the membrane in an activated sludge process. At first, the non-woven fabric filter was applied for sludge thickening. Recently its application is expanded to wastewater treatment along with the activated sludge process since it has the following major characteristics: low-priced membrane filter material, high permeate flux and low filtration resistance and gravity filtration without energy requirement. Although uncommon researches have been conducted, it was proposed that the fabric filter has the potential to take the place of membrane (MF) in a combined membrane bioreactor for wastewater treatment [6]. In another research [7], that was also reported from the long time operation of the research system, that a water head of 1 cm was optimum to get a comparable flux of membrane bioreactor. Also, they found that the lower condensed part of the cake layer on the membrane filter surface was the basic reason for filtration resistance. There are some operational challenges for using the fabric filter system for wastewater treatment, because the fabric filtration has a dynamic system [5]. Dynamic membrane was also called secondary membrane or formed-in-place membrane. For generating dynamic membrane, the cheaper materials, such as mesh, non-woven fabric and filter-cloth were used as the filter stuff [8]. The dynamic membrane (DM) formed on large-pore support mesh is a new type of separation method, which displayed the advantages of high filtration flux, low cost of membrane module, and easy backwash. Compared with conventional membrane bioreactors, the dynamic membrane bioreactor could also be operated successfully incorporated with water treatment processes. The cake layer on the support mesh is the basic part in the dynamic membrane separation process. The dynamic membrane formed on the relatively large-pore mesh increases the intrinsic membrane retention capacity, and the fouling of dynamic membrane has a different meaning. Dynamic membrane fouling was interpreted as follows: the initial deposited materials on the underlying support mesh are actually DM-forming components (cake layer), which are essential and desired; the subsequent deposited materials are foulants, which induce additional increase of filtration resistance of DM. Although cake layer formation is a key factor of the DM process, the studies of cake layer to date are insufficient [7]. There is an absence of awareness relating to fouling of non-woven fabric filters. The pore size of the non-woven fabric is 10 or 100 times bigger than that of a microfilter, approximately. The parts of the membrane resistance due to cake layer or inner foulants have different appearances, since the general particle size of an activated sludge is likely to the pore size of the non-woven fabric. Severe fouling on the inside of large pores happens through the pore blockage by flocs in activated sludge. This fouling type may not be removed using simple aeration due to the complicated fiber structure and rough surface intercepting the flocs [9]. Fan and Huang [10], notified that the gel layer formed on the surface of mesh had a similar structure and function of a classic membrane. The cake layer was defined as a self-forming dynamic membrane which conduces to keeping pollutants or sludge flocs from being adsorbed immediately into pores. The generation and function of the dynamic membrane are dependent upon the cake density, structure and components [11].

3. ADVANTAGES and DISADVANTAGES of MBRS, D-MBRS OVER CAS

Biochemical reaction of the activated sludge is provided completely mixture with aeration and mixing in the bioreactor in the conventional activated sludge system (CAS). The reaction is eventually needed to secondary clarifier for separate microorganisms and processed wastewater. The membrane bioreactor (MBR) which used to micro filtration (MF) / ultra filtration (UF) membranes to separate solid and liquid in the bioreactor, and the reaction

is eventually do not needed to secondary clarifier. In this context, when compared with CAS, MBR and D-MBR, MBRs use membrane filtration for solid-liquid separation, supplying higher effluent quality for wastewater reclamation and reuse. The MBR and D-MBR systems have attracted increasing interest both academically and commercially in wastewater treatment as an alternative of CAS systems. MBR and D-MBR have many advantages such as, higher biomass concentration, smaller footprint, lower sludge production and rejection of SS (effluent SS is close to zero) [22]. Although many researchers now reconsider whether MBR has been the best choice for various treatment methods, choosing between MBR and CAS for wastewater treatment remains ambiguous [23]. MBR and D-MBR systems have been widely applied in full scale and laboratory scale wastewater treatment process thanks to supply higher MLSS concentration, better control of SRT, higher volumetric loading, production of high-quality effluent when compare with CAS[24]. However, the application of MBR is restricted by its high membrane module cost and membrane fouling [25]. So, many researchers attempted to use cheap covered material for replacing the expensive micro-/ultra-filtration membrane for decrease the high cost [26]. Despite it is claimed advantages of better treatment method performance and occupation of much less land, broader application of MBRs is still hindered by their relatively high construction cost and energy consumption [27]. For these reasons, in recent years done extensive research on D-MBR instead of MF and UF membrane is trying to eliminate the cost of the MBRs. Dynamic membrane is formed on the underlying a support materials when filtering the wastewater from the reactor, so is also called secondary membrane [28]. Mesh, woven and nonwoven fabrics are used instead of MF or UF [29] in the D-MBR, by this means operating costs of D-MBR are much lower than the CAS and MBR systems.

Table 1: The comparison of comparatively advantages and disadvantages of MBR, D-MBR and CAS

MBR		D-MBR		CAS	
Advantages	Disadvantages	Advantages	Disadvantages	Advantages	Disadvantages
High MLSS	-----	HighMLSS	-----	-----	LowerMLSS
Low footprint	-----	Low footprint	-----	-----	Large footprint
Higher volumetric loading	-----	Higher volumetric loading	-----	-----	Lower volumetric loading
Fine control of SRT	-----	Fine control of SRT	-----	-----	Workload for SRT control
Greater operational and process complexity	-----	Greater operational and process complexity	-----	-----	Easier operational and process complexity
Lower sludge production	-----	Lower sludge production	-----	-----	Higher sludge production
-----	Higher capital Low operational costs	Low capital Low operational costs	-----	-----	Higher capital High operational costs
-----	Greater foaming propensity.	-----	Greater foaming propensity	Lower foaming propensity	-----
Treated water that reusable	-----	Treated water that reusable	-----	-----	-----
Unlimited by settling due to gravity	-----	Unlimited by settling due to gravity	-----	-----	It is limited by settling due to gravity
-----	High Module Cost	Low module cost	-----	-----	-----
Sample TMP control based on constant flow	-----	-----	Complex TMP control based on constant flow	-----	Indifference
Sample fouling control	-----	-----	Complex fouling control	-----	Indifference
Chemical wash easier applied	-----	-----	Chemical wash not easily appliedby taking into account microorganisms	-----	Indifference
Very high physical disinfection performance	-----	Normal physical disinfection performance	-----	-----	Indifference
Affected indirectly by Bulking problem	-----	Affected indirectly by Bulking problem	-----	-----	Affected directly by Bulking problem

Membranes need physical and chemical washing due to frequent fouling by microorganisms. The main fouling reason was reported in the previous studies due to increased bacterial growth [30]. So, they do not frequently needed chemical and physical cleaning [31]. Despite physical operations such as water backwashing, air back washing, brushing, intermittent suction (relaxation) and cross flow are enough for MBR and D-MBR systems. Sometimes these operations temporarily cause to effluent quality (high MLSS). In the light of all these findings, although D-MBRs are

more advantageous compared to MBR and CAS, some disadvantages are associated with the cake layer developing on the membrane surface. This layer causes a considerable reduction of the permeate flow [32] and increase the transmembrane pressure (TMP). So, a well-defined and systematic comparison of D-MBR, MBR and CAS about wastewater treatment, must be of fundamental importance, thoroughly and meticulously [33]. The main advantage of MBR and D-MBR systems is sludge retention time (SRT) can be controlled easily as completely independent from hydraulic retention time (HRT). So, a very long SRT can be operated resulting in the complete retention of slow-growing microorganisms such as nitrifying or methanogenic bacteria and this results in greater flexibility of operation [34]. Based on the findings of several studies in the literature about the considering the relative advantages and disadvantages of MBR, D-MBR and CAS systems general information are tabulated in the Table. 1.

4. FUNDAMENTALS OF MBR AND D-MBR

As far as known that membrane bioreactors are used as an efficient and a convenient wastewater treatment method. The wastewater produced from factories and other industrial establishments will be treated by using MBRs and D-MBRs. In following years, it is estimated that most of the wastewater treatment plants will turn over to MBR and as a result of that the final settling tank will be eliminated. MBRs sustain convenient biological wastewater treatment and also provide physical separation of the water and biomass with the aid of membranes. The main advantage of the MBR systems is the whole process takes place in one tank, while two tanks have been used for biochemical oxidation and water/biomass separation processes in conventional active sludge process [2]. However MBRs also provide the conservation of the biomass by employment of the ultra/micro filtration. In that way, total biomass conservation and proceeding the process in high sludge accumulation have been permitted [2]. Membranes are also on the slope of fouling, due to the permeate flux through the membrane. The mixture (solid/sludge and liquid) inside of the reactor diminishes the filtration flux and it had required membrane area increased [35]. On the other hand MBRs needs different approached and developments for more global implementations. Fouling the membranes, that its physical structure is consisted of pores, and the high cost of implementation the membrane modules are the major obstacles that actually most of the MBRs systems come across. To reduce the cost and avoid the fouling and create a shear over the membrane, different kinds of materials have been tried to use. Dynamic membrane bioreactors (D-MBRs), as distinct from MBRs, are known as formed-in-place (FIP) membrane or with another name used in literature secondary membrane [36]. The formation of the D-MBRs is ensured during the diffusion of mixed liquor/solution through the surface of the membrane that filters one/more particular colloidal particles or materials already present in the mixture. Formation is sustained by different kind of materials like; mesh non-woven fabric and filter-cloth [37, 38, 39]. On the other side, D-MBRs come across with fouling intensively, even though aerosol shear is employed over the surface of the membrane. But the dynamic layer formed on the membrane can be changed by new deposited layer or the membrane itself can be changed with the new one. Major amount of studies center upon employment of the meshes as a membrane for the permeate flux of the mixed liquor [37].

4.1. Configurations of MBRs

Configuration of the membrane is one the most essential part in wastewater treatment process, due to the stream of water which can be directly affected from the geometrical shape of the membrane system and also the way it is mounted and oriented [Judd]. However, there are two types of membrane bioreactor patterns that are being performed with pressure and filtration for side-stream MBRs or vacuum-driven membranes submerged in the reactor. Required energy for the filtration of submerged MBRs is visibly lower than the side-stream MBR configuration. Conservation of the membranes is delicate matter for the fouling that causes serious blockage of the pores and hinders the flow of the liquid inside of the reactor but it should be known that, prevention from the fouling requires energy and this may be the reason why submerged MBR configuration is actually turns the scale. Likewise, fouling in side-stream MBR configurations is quite apparent, because of high liquid flow penetration. When the sludge inside of the reactor is pumped or stirred, it causes protection of the membrane to bacterial flocs which reduces the foulant material transition and also the amount of small particle drift autonomously [40]. Currently, there are six major membrane configurations used in practice and only the first three configurations suit to the MBR technologies [2]; Plate-and-frame/flat sheet (FS), Hollow fiber (HF), Multi Tubular (MT), Capillary Tube (CT), Plated Filter Cartridge (FC), Spiral-Wound (SW). In the hollow fiber (HF) configuration, major number of hollow fiber (HF) membranes create a sheaf and closely knocked together. Therefore, edges of the fibers are adhered to each other. Membranes, which can also work under pressure and vacuum, allows the flow of water from inside to outside and of course inside to outside and they are produced by the way of how actually manufacturers desire. They can be with support material, separator or both. Every single sheet piece is interlocked to the plate and process works by using vacuum. The water flows through the membrane and filtrated water is transported by pipes and gathered [41]. Side-stream MBR configuration is a convenient setup to use it. Hollow fiber (HF) and flat sheet (FS) configurations are submerged right inside of the reactor and processed flux is carried by vacuum pumps. Membranes can come across stringy substances during the process and it significantly increases the rate of cleaning surface of the membranes. Employment of 0.8 μm to 1.5 μm pore sized membranes provides better performance and it is also advised for the protection of the membrane dirtiness. Generally, 2-3 μm pore sized membranes are employed for the flat sheet (FS) membrane systems. Turbulence promotion, cleaning or both are indispensable parameters for a module. Because turbulence promotion enhances the

passing of feed, which is a synthetic preparation and water/air mixture from the membrane surface to help the flux of permeate [2].

4.2. Dynamic Layer Forming Materials

Self-forming and pre-coated dynamic membranes can consist of the main category of dynamic membranes (DMs). Self-forming dynamic membranes (SFDM) are formed by permeate flux through the membrane and constituents of mixed liquor create a layer during the process, i.e. suspended solids (SS) in wastewaters. However, pre-coated dynamic membranes (PDM) or also named formed-in-place (FIP) are consisted of the transition of the mixture or liquor, which includes one or more colloidal substances, through the porous material [42, 43]. During the process, while soluble substances inside of the mixture can pass through the pores, the other insoluble materials stay at the surface of the porous material. Due to the need of external material, SFDM has a kind of handicap. On the other hand, single additive and composite (bi-layer) membranes are the subgroup of the pre-coated membranes (PCM). In solitary stride, single additive membranes can be generated by using single material. In 2006, powdered activated carbon has been used to form single additive dynamic membrane [43]. Bi-layer membranes are formed more than one process [44]. Formed layer over the membrane turns into flocs in SFDM with the employment of aerobic membrane bioreactors and returned promotive outcomes [45, 37, 46,]. At the same time, pre-coated dynamic membrane configuration has been employed to form layer in aerobic D-MBRs. Some of the substances, which are PAC, kaolinite and bio-diatomite, have been used to create pre-coated membranes. Although self-forming dynamic membrane procedure has been used for anaerobic implementation [47], polytetrafluoroethylene has been used for the surface change-over. It is also known that in physical dynamic filtration, zirconium oxide (ZrO_2) is thriving widespread chemical to create dynamic membrane layers [48, 49,].

4.3. Support materials used in the D-MBR

As a dynamic membrane, different kinds of membrane materials have been chosen through the researches; particularly selection process has been carefully and sizably made but the support material of interest has been mostly mesh, woven and non-woven fabrics. Different kinds of mesh fragments can be found because the main material inside of the mesh can be fiber, metal or other nonrigid/tensile substances. The physical structure of the mesh may be disadvantageous for the MBRs, in terms of inadequate amount of sludge accumulation [37]. However, a woven fabric can be generated from single type of string called monofilament, which has glabrous surface, and it can also be generated from multiple strings called multifilament which are consisted of several monofilament strings spun together and exist as one individual yarn. A non-woven fabric can be human-made or natural and also it can be in sheet form or in web form. Paper is omitted because it cannot be produced as a spun or string [36]. It is known that non-woven strings are quite slim, and affiliation of the sludge can be seen at the pores and also in the midst of string matrix. Due to its matrix structure, the sludge cannot be easily fended off, which is a kind of difficulty, in long run processes [37]. Different kinds of materials such as; ceramic membranes [50], woven fabrics [45], meshes [37, 47] and non-woven fabrics [46] have been stated for an/aerobic D-MBRs and liquid-solid dispersion.

5. FACTORS AFFECTING THE REMOVAL PERFORMANCE

5.1. Transmembrane Pressure and Flux

Transmembrane Pressure (TMP) is directly related to membrane fouling. In MBR systems, TMP increased in the case of pore blocking. In D-MBR systems, TMP increased in the situation of decrease of dynamic membrane (cake layer) porosity at a constant flux [51,52]. In the mesh filter D-MBR systems, compaction and thickness of dynamic membrane layer have great importance on TMP and filtration characteristic [Poostchi, Zhang]. Poostchi et al. [53] studied the long-term filtration of mesh filter D-MBR, and monitored effects of thickness, and compactness of dynamic membrane layer on TMP. They reported that TMP profile closely related with thickness and compactness of dynamic cake layer. In this context, TMP is main operational parameter to monitoring filtration behaviour of the mesh filter and the characteristics of dynamic membrane layer. It also observed that in the long-term filtration tests, after the initial stages of the dynamic membrane layer formation TPM had no effect on the effluent water quality. So, in the case of specific threshold of dynamic membrane formation exceeded, only TMP rises without any permeate quality improving. At the pressure controlled region; significant membrane fouling is not observed, because of low flux which is under the critical flux level. At transitional region; operating flux exceeds the critical flux. So, solid materials in the sludge start to deposit on membrane surface in vast amount and consists dynamic membrane layer. Linearity between TMP and flux is break down. If the TMP increase continuously, the dynamic membrane layer (cake layer which formed on support material) starts become more compact due to higher pressure. Because of this compaction, porosity of dynamic membrane layer is decrease, and correspondingly flux is decrease [Seong]. At mass transfer controlled region; in this region flux is almost fixed regardless of TMP increase. Cross flow velocity, liquid viscosity and temperature has important affect on maximum flux condition [15].

6. MECHANISMS OF MEMBRANE FOULING OF MBRS AND DMRS

The fouling of bioreactor membranes involves accumulation of foulants, such as sludge flocs, colloidal particles and solutes, on the membrane surface [12]. Since fouling is directly affecting the filtration capacity, proper conditions have to be maintained to prevent such an outcome. The parameters affecting proper membrane filtration are demonstrated in Figure 1.

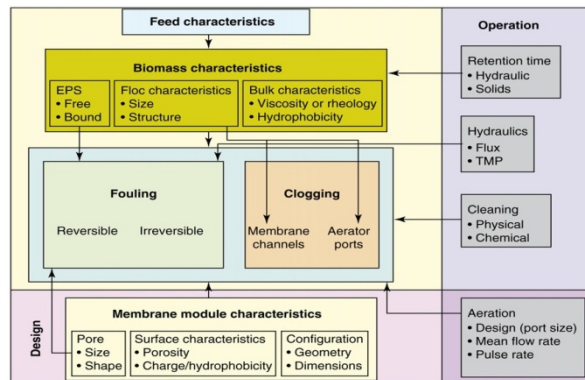


Figure 13. Interrelationship between MBR parameters and fouling [54]

The mechanisms of membrane fouling are presented in Figure 2, based on the way in which the foulant interacts with the membrane.

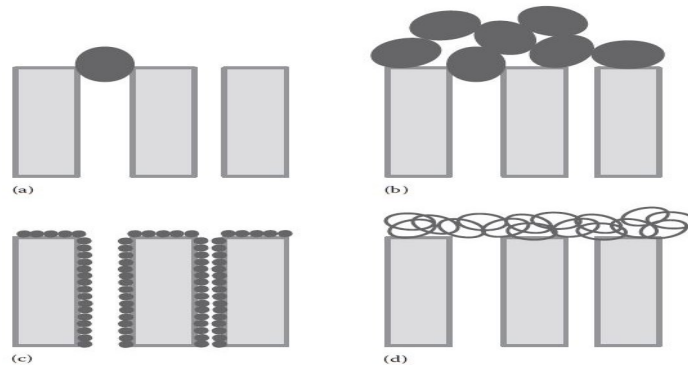


Figure 14. Mechanisms of membrane fouling according to Hermia: a) complete blocking, b) internal pore blocking, c) intermediate blocking, and d) cake formation [12].

6.1 The Function of EPS, SMP, SRF and CST

Compounds identified as the primary causal factor of membrane fouling are EPS (extracellular polymeric substances) and SMP (soluble microbial product). Both are secreted by microorganisms - the former are bound to their cell walls, forming a network, whereas the latter are unbound, free in solution [54]. EPS and SMP may lead to membrane fouling in one of the ways described in the previous section.

SRF (specific resistance to filtration) and CST (capillary suction time) are the most common parameters measured to determine the efficiency of sludge dewatering, i.e. filtration. SRF is defined as the resistance of the membrane to the transport of filtrate [55], whereas CST describes the time water needs to travel from one electrode to another at a set capillary suction. The latter is independent of the amount of sludge, provided there is enough for the measurement to be made [56].

6.2 Cleaning methods for membrane applications

Al-Malack and Anderson [57] examined that cleaning is not feasible for a dynamic membrane in their study due to chemical washing not easily applied by taking into account microorganisms. Rather, it should be removed completely (e.g. by brushing), before engaging into a cleaning process for the primary membrane. The primary membrane can be cleaned in various ways: physically, chemically, physico-chemically and biologically. Physical cleaning includes methods such as periodic back flushing, vibration, air sparging, ultrasonication and automatic sponge ball cleaning. Chemical cleaning is based on the use of various cleaning agents, physico-chemical on a combination of the former two, and biological on the use of cleaning mixtures based on microbial cultures or enzymes [58]. Out of the mentioned methods, physical cleaning in the form of flushing (both forward and reverse) stands out as an economical solution. A deeper understanding of the interactions between the foulant and the membrane is needed to pave the way for the development of more economical and optimized cleaning methods. Together with the prevention of membrane fouling, this is the major challenge in the struggle to design highly efficient and optimized membrane bioreactor systems.

7. PROBLEMS ENCOUNTERED and FUTURE PERSPECTIVES

The relative advantages of D-MBR and MBR over the CAS process were tabulated in the section 3 Table.1. As shown in the table, although fouling control and operation process are more complex and D-MBR systems have many advantage in terms of cost. MBR and D-MBR technologies have the potential to contribute to water supplies through their use in treating degraded waters in reuse or recycling applications since membrane technology can remove microorganisms and many organic contaminants from feed water. When comparing the three systems, D-MBR has several advantages as shown in the previous sections. However, the product sludge tends to fouling problems for D-MBRs. So, should be chosen appropriate support materials, and operation conditions. Optimization the operating parameters includes the selection of the best operating conditions in terms of scouring aeration, sludge retention time SRT, HRT, MLSS concentration and TMP control in the bioreactor to minimize the fouling on the membrane [12]. The Membrane fouling, main problem of membranes systems, is closely related to energy consumption; hence, reducing membrane fouling in MBR while keeping energy consumption as low as possible is the main focus of D-MBR and MBR. The future directions in the MBR are mostly in the fields of membrane/module and operation/maintenance as should be take into consideration. In this context, different support materials (eg. woven or non-woven, mesh) can be used instead of more expensive membrane, although fouling control is more complex.

8.CONCLUSIONS

The study demonstrated comparison of D-MBR, MBR and CAS systems, examined in detail mainly in terms of advantages and disadvantages. There are two principal advantages of MBR and D-MBR systems. The first advantage is that, compared to CAS, D-MBR and MBR membrane technologies generally have low capital costs, low operational costs and require less energy. The second advantage of MBR and D-MBR systems is that the SRT can be controlled completely independently from HRT. Therefore, a very long SRT can be maintained resulting in the complete retention of slowly growing microorganisms. The other advantages can be summarized as following; high-quality effluent, space savings (low footprint), enabling upgrading of plants without land expansion; shorter start-up time compared to conventional treatment systems; low operating and maintenance labor force requirement. Stable performance in the activated sludge process could be achieved independently of bulking problem and shock loadings by D-MBR and MBR systems as they have perfect solid-liquid separation ability. Finally, when taken into consideration, D-MBR and MBR can be used both for drinking water and wastewater, with many advantages compared to CAS. However, the product sludge tends to suffer from fouling problems in the case of D-MBRs. To combat this, appropriate support materials and operational conditions should be chosen.

ACKNOWLEDGEMENTS

Author Amar Ćemanović is supported by the Scientific and Technological Research Council of Turkey (Tübitak) through the 2215 Graduate Scholarship Programme.

REFERENCES

- [1] Judd, S., 2011. The Mbr Book: principles and applications of membrane bioreactors for water and wastewater treatment, Order A Journal On The Theory Of Ordered Sets And Its Applicatios.
- [2] Judd, S., 2006. The MBR Book Principles and Applications of Membrane Bioreactors in Water and Wastewater Treatment. Elsevier, Oxford, UK.
- [3] Fan, B., Huang, X., "Characteristics of a self-forming dynamic membrane coupled with a bioreactor for municipal wastewater treatment". *Environ. Sci. Technol.* 36, 5245–5251, 2002.
- [4] Wu, Y., Huang, X., Wen, X., Chen, F., 2005. Function of dynamic membrane in self-forming dynamic membrane coupled bioreactor. *Water Sci. Technol.* 51 (6–7), 107–114.
- [5] Ersahin, M.E., Özgün, H., Dereli, R.K., Öztürk, I., Roest, K., ve Van Lier, J.B. (2012). Malzemelerin, uygulamalar ve gelecek perspektifleri: Dinamik membran filtrasyon üzerine bir inceleme. *Bioresource Teknolojisi*, 122, 196-206.
- [6] Ersahin, M.E., Özgün, H., van Lier, J.B. (2013). Dinamik Membran Filtrasyon Performans Destek Materyalleri Özelliklerinin Etkisi. *Ayrırma Bilimi ve Teknolojisi*, 48 (15), 2263-2269.
- [7] Mustafa Evren Erşahin, Hale Ozguna Yu Taoa, J. B. van Lier, "Anaerobik membran Biyoreaktörlerde dinamik membran teknolojisinin uygulanabilirliği", *Water Research*, 48 (1), 420-429, 2014.
- [8] H.Q. Chu, D. Cao, W. Jin, B.Z. Dong. Characteristics of bio-diatomite dynamic membrane process for municipal wastewater treatment. *J. Membr. Sci.*, 325 (2008), pp. 271–276.
- [9] W. Wang, Y.J. Jung, Y. Kiso, T. Yamada, K.S. Min. Excess sludge reduction performance of an aerobic SBR process equipped with a submerged mesh filter unit *Process Biochem.*, 41, 745–751, 2006.
- [10] Y. Kiso, Y.J. Jung, K.S. Min, W. Wang, M. Simase, T. Yamada, K.S. Min. Coupling of sequencing batch reactor and mesh filtration: operational parameters and wastewater treatment performance.
- [11] C.V. Smith, D.D. Gregorio and R.M. Talcott, "The use of ultrafiltration membranes for activated sludge separation", 24th Annual Purdue Industrial Waste Conference, Lafayette, IN pp. 130-1310, 1969.
- [12] H.-D. Park, I.-S. Chang and K.-J. Lee, *Principles of Membrane Bioreactors for Wastewater Treatment*, Boca Raton, FL, USA: CRC Press, Taylor and Francis Group, 2015.
- [13] K. Yamamoto, M. Hiasa, T. Mahmood and T. Matsuo, "Direct solid-liquid separation using hollow fiber membrane in an activated sludge aeration tank", *Water Science and Technology*, 21: 43-54, 1989.
- [14] G.T. Seo, T.S. Lee, B.H. Moon, J.H. Lim and K.S. Lee, "Two stage intermittent aeration membrane bioreactor for simultaneous organic nitrogen and phosphorus removal", *Wat. Sci. Tech.*, 41, 217-225, 2000.
- [15] G.T. Seo, B.H. Moon, T.S. Lee, T.J. Lim and I.S. Kim, "Non-woven fabric filter separation activated sludge reactor for domestic wastewater reclamation", *Water Science and Technology*, 47, 1, 133-138, 2002. (4_MBR)

- [16] T. Kitao, B. Kim, Y. Kiso and K. Yamamoto, "Treatment of domestic wastewater with filtration bio-reactor and anaerobic contact sedimentation method", *J of Japan Sewage Works Association, Japanese*, 28 (334), 21-31, 1991.
- [17] T. Kitao, K. Nishida, T. Ide and Y. Kiso, "Performance of long-term operation of a filtration bioreactor with nonwoven fabric filter", *J of Japan Sewage Works Association, Japanese*, 35 (425), 12-21, 1998.
- [18] H. Chu, Y. Zhang, X. Zhou, Y. Zhao, B. Dong and H. Zhang, "Dynamic membrane bioreactor for wastewater treatment: Operation, critical flux, and dynamic membrane structure", *Journal of Membrane Science*, 450, 265-271, 2014. (8_D-MBR)
- [19] M.R.A. Moghaddam, Y. Guan, H. Satoh and T. Mino, "Filter clogging in coarse pore filtration activated sludge process under high MLSS concentration", *Water Sci. Tech.*, 54, 55-66, 2006.
- [20] B. Fan and X. Huang, "Characteristics of a self-forming dynamic membrane coupled with a bioreactor for municipal wastewater treatment", *Environ Sci. Tech.*, 36, 5245-5251, 2002.
- [21] F. Meng, S.R. Chae, A. Drews, M. Kraume, H.S. Shine and F. Yang, "Recent advances in membrane bioreactors (MBRs): membrane fouling and membrane material", *Water Res.*, 43: 1489-1512, 2009.
- [22] Defrance, L. and Jaffrin, M.Y. "Comparison between filtrations at fixed transmembrane pressure and fixed permeate flux: application to a membrane bioreactor used for wastewater treatment", *J. Membr. Sci.*, 152, 203-210, 1999.
- [23] B. Lesjean, A. Tazi-Pain, D. Thauere, H. Moeslang, H. Buisson. Ten persistent myths and the realities of membrane bioreactor technology for municipal applications, *Water Sci. Technol.* 63 32-39, 2011.
- [24] Seo, G.T., Moon, B.H., Lee, T.S., Lim, T.J. and Kim, I.S. (2002). Non-woven fabric filter separation activated sludge reactor for domestic wastewater reclamation. *Wat. Sci. Tech.*, 47(1), 133-138.
- [25] H. van der Roest, A. van Bentem, P. Schyns, C. Uijterlinde,. "Ten years of MBR development: lessons learned from the Netherlands," *Water* 2117-23, 2012.
- [26] Fan, B., Huang, X., 2002. Characteristics of a self-forming dynamic membrane coupled with a bioreactor for municipal wastewater treatment. *Environ. Sci. Technol.* 36, 5245-51.
- [27] J. Sun , K. Xiao, X. Yan, P. Liang, Y. Shen, X. Huang and N. Zhu," Membrane bioreactor vs. oxidation ditch: full-scale long-term performance related with mixed liquor seasonal characteristics", *Process Biochemistry*, 50, 2224-2233, 2015.
- [28] V.T. Kuberkar, R.H. Davis, Modeling of fouling reduction by secondary membrane, *J. Membr. Sci.* 168 (2000) 243-25
- [29] Lee, J., Ahn, W.Y., Lee, C.H., 2001. Comparison of the filtration characteristics between attached and suspended growth microorganisms in submerged membrane bioreactor. *Water Res.* 35 (10), 435-2445.
- [30] Erkan Sahinkaya Nesrin Dursun Use of elemental sulfur and thiosulfate as electron sources for water denitrification *Bioprocess Biosyst Eng.* 38, 531-541, 2015
- [31] Chu, H.Q., Cao, D., Jin, W., Dong, B.Z., 2008. Characteristics of bio-diatomite dynamic membrane process for municipal wastewater treatment. *J. Membr. Sci.* 325, 271-276.
- [32] Chang In-S., Judd S.J. Air sparging of a submerged MBR for municipal wastewater treatment. *Process Biochemistry*, 37, 915-920, 2002.
- [33] K. Xiao, Y. Xu, S. Liang, T. Lei, J.Y. Sun, X.H. Wen, H.X. Zhang, C.S. Chen and X. Huang, "Engineering application of membrane bioreactor for wastewater Treatment in China: current state and future prospect", *Front. Env. Sci. Eng.* 8, 805-819, 2014.
- [34] C. Visvanathan, R. Ben Aim, and K. Parameshwaran, "Membrane Separation Bioreactors for Wastewater Treatment", *Critical Reviews in Environmental Science and Technology*, 30(1),1-48, 2000.
- [35] E.H. Bouhabila, R. Ben Aim, H. Buisson, "Microfiltration of activated sludge using submerged membrane with air bubbling (application to wastewater treatment)." *Desalination* 118, 315-322, 1998.
- [36] V.T. Kuberkar, R.H. Davis, "Modeling of fouling reduction by secondary membranes." *J. Membr. Sci.* 168. 158-243, 2000.
- [37] Xxx Y. Kiso, Y.J. Jung, K.S. Min, W. Wang, M. Simase, T. Yamada, K.S. Min, "Coupling of sequencing batch reactor and mesh filtration: operational parameters and wastewater treatment performance." *Water Res.* 39, 4887-4898, 2005.
- [38] M.R. Alavi Moghaddam, H. Satoh, T. Mino, "Effect of important operational parameters on performance of coarse pore filtration activated sludge process", *Water Sci. Technol.* 46, 229-236, 2002.
- [39] G.T. Seo, B.H. Moon, Y.M. Park, S.H. Kim, "Filtration characteristics of immersed coarse pore filters in an activated sludge system for domestic wastewater reclamation." *Water Sci. Technol.* 55 (1-2), 51-58, 2007.
- [40] Wisniewski C, Grasmick A *Coll Surf A: Physicochem Eng Aspects* 138:403, 1998.
- [41] J. Radjenović, M. Matošić, I. Mijatović, M. Petrović, D. Barceló, "Membrane bioreactor (MBR) as an advanced wastewater treatment technology." In *Emerging Contaminants from Industrial and Municipal Waste* (pp. 37-101). Springer Berlin Heidelberg, 2008.
- [42] Al-Malack, M.H., Anderson, G.K., 1996. Formation of dynamic membranes with crossflow microfiltration. *J. Membr. Sci.* 112, 287-296.
- [43] M. Ye, H. Zhang, Q. Wei, H. Lei, F. Yang, X. Zhang, "Study on the suitable thickness of a pac-pre-coated dynamic membrane coupled with a bioreactor for municipal wastewater treatment." *Desalination* 194, 108-120, 2006.
- [44] A.W.C. Ip. "Dynamic membranes formation and characterisation studies", Ph.D. Thesis, UNESCO Centre for Membrane Science and Technology, The University of New South Wales, 2005.
- [45] W. Fuchs, C. Resch, M. Kernstock, M. Mayer, P. Scoeberl, R. Braun, "Influence of operational conditions on the performance of a mesh filter activated sludge process", *Water Res.* 39 (4), 803-810, 2005.
- [46] Y. Wu, X. Huang, X. Wen, and F. Chen, "Function of dynamic membrane in self-forming dynamic membrane coupled bioreactor" *Water Sci. Technol.* 51 (6-7), 107-114, 2005.
- [47] D. Jeison, I. Diaz, J.B. van Lier, "Anaerobic membrane bioreactors: are membranes really necessary?" *Electron. J. Biotech.* 11 (4), 1-7, 2008.
- [48] A.E. Marcinkowsky, K.A. Kraus, H.O. Phillips, J.S. Johnson, A.J. Shor, "Hyperfiltration studies IV. Salt rejection by dynamically formed hydrous oxide membranes." *J. Am. Chem. Soc.* 88 (24), 5744-5750, 1966.
- [49] D. Freilich, G.B. Tanny, "The formation mechanism of dynamic hydrous Zr(IV) oxide membrane on microporous supports." *J. Colloid Int. Sci.* 64, 362-370, 1978.
- [50] F. Li, J. Chen, C. Deng, "The kinetics of crossflow dynamic membrane bioreactor." *Water SA* 32 (2), 199-203, 2006.
- [51] B. Hwanga, C. Leec, I. Chang, A. Drewse and F. Fielda, "Membrane bioreactor: TMP rise and characterization of bio-cake structure using CLSM-image analysis", *J. Membr. Sci.*, 419-420 33-41, 2012.
- [52] H. Yu, Z. Wang, Z. Wu, C. Zhu "Dynamic Membrane Formation in Anaerobic Dynamic Membrane Bioreactors: Role of Extracellular Polymeric Substances" 2015
- [53] Poostchi, A.A., Mehrina, M.R., Rezvani, F. Dynamic membrane behaviours during constant flux filtration in membrane bioreactor coupled with mesh filter. 36, 1751-1758, 2015.
- [54] S. Judd, "The status of membrane bioreactor technology", *Trends in Biotechnology*, 26, 2, 109 - 116., 2008.

- [55] H.Y. Ng, and S.W. Hermanowicz, "Specific resistance to filtration of biomass from Membrane Bioreactor Reactor and Activated Sludge: Effects of Exocellular Polymeric Substances and Dispersed Microorganisms," *Water Environment Research*, 77(2), 187-192, 2005.
- [56] M. Scholz, "Review of Recent Trends in Capillary Suction Time (CST) Dewaterability Testing Research," *Ind. Eng. Chem. Res.* 44, 8157-8163, 2005.
- [57] M.H. Al-Malack, and G.K. Anderson, "Cleaning techniques of dynamic membranes", *Separation and Purification Technology*, Volume 12, Issue 1, pp. 25-33, Sep. 1997.
- [58] Z. Yan-jun, W. Kai-fen, W. Zheng-jun, Z. Liang, and L. Shu-shen, "Fouling and cleaning of membrane – a literature review," *Journal of Environmental Sciences*, 12, 2, 241-251, 2000.

Cost Comparison of Thermal and Chemical Defoliation Applications in Cotton Production*

Erkan Simsek¹, Mustafa Bulent Coskun²

Abstract

The leaves should be removed from plant before harvesting to save cotton fiber quality. To carry out this process, chemicals are widely used. Harvest is possible at the end of 15th-20th days after chemical treatments are done. In defoliation, another method, which has been tried during recent years, is to use defoliation machines that utilize thermal energy. In applications carried out by thermal defoliation machine, almost all leaves are dried/killed, and leaf dropping starts as soon as following treatment day. In thermal treatment plots, it is possible to take the harvest time to an early date in comparison with chemical defoliation. By having early harvest, it is able to prevent negative effects of environmental conditions on cotton quality. With this study, it is aimed to compare the cost of chemical and thermal defoliation treatments. In conclusion, the two-years average defoliation cost of three different cotton varieties was realized as around 20.89\$/da in thermal treatment plots, 3.39 \$/da in chemical treatment plots. In case, harvest date is taken early in thermal treatment plot, average income of three different cotton varieties for two-years, is more about 28.04 \$/da per year because of cotton quality. As it is compared in regardless of process cost of thermal and chemical defoliation method, these two methods were found to be competitive.

Keywords: Thermal defoliation, defoliants, cotton production

1 INTRODUCTION

When the machine harvesting comes into cotton, it is required that the 60-65% of bolls on the plant should be opened and the leaves should be removed from the plant [13], [18]. To avoid any damages that may occur as a result of the late harvest, the implementation time of defoliant is critical in terms of cotton quality and yield values [12]. After 10-14 days later from the chemical implementation of defoliant, the leaves of plant come down [16]. However, because of negative effect of chemical implementations on environment, it is not possible to use in organic cotton agriculture [8], [17]. In addition, the success of chemical implementation depends on the environmental conditions [10]. For successful implementation, quite a few parameters should be chosen correctly [19], [2], [18], [11].

The operation of thermal defoliation on cotton was described firstly by Nisbet and Nisbet [14]. The first implementations were carried out by Kent and Porterfield in 1967 and by Batchelder et al. in 1971, [7]. Porterfield and Batchelder succeeded to defoliate the 80% of leaves with heated air application [15]. The cotton is subjected to the heated air without any damages to the cotton fibers in implementations carried out nowadays and the defoliation at a sitting can be achieved removing of the leaves suddenly with the effect of heated air. It is possible to reduce the critical amount of time required for harvest with thermal implementation. With this implementation, the negative effects of defoliant chemicals on soil and plant that is used in defoliation process can also be eliminated [7], [9], [17]. Thermal implementation can also be used as alternative of chemical implementations on organic cotton cultivation [17], [6].

Within the scope of this study, it was aimed to compare the cost elements of thermal and chemical implementation as defoliant in different cotton types that was grown in conditions of Turkey.

2 MATERIALS AND METHODS

A single row prototype thermal defoliant machine that ground clearance of it can be adjustable and it has 3500 mm tunnel length, and 75 cm row space was used in the study. A burner on a strength of 300000 kcal/h and a ventilator with 20000 m³/h @1500 min⁻¹ flow were located on the machine. The picture of Machine was presented in the Figure 1. [20].

*This study is a part of PhD thesis.

¹Corresponding author: Adnan Menderes University, Aydn Vocational School, Department of Machinery and Metal Technologies, Aydn, Turkey,

erkansimsek@adu.edu.tr

²Adnan Menderes University, Faculty of Agriculture, Department of Biosystem Engineering, Aydn, Turkey, mbulentco@yahoo.com



Figure 1. Photo considering the field implementation carried out with thermal effect defoliant prototype machine [20]

Carmen, Beyazaltin 119, Nazilli 84S cotton varieties were used in the study. The experiments were carried out by creating 9 piece of incident parcel for the study that had three different implementations as control, chemical and thermal. As a test material, planting was done as 75 cm row space and 16.7 cm intrarow. Tests were repeated two years in a row.

Any implementation was not carried out in the control parcels. Plants were exposed to heated air as approx. 11.8 m/s speed at 145°C temperature in the parcels performed with thermal implementation. The defoliant chemical implementation (including 119.75 g/l thidiazuron, 59.88 g/l diuron) was done in the chemical implementation parcels as 60 ml/da suitably to the suggested norm.

The time of defoliant was decided according to the cottonseed color and opened boll rate. During the chemical and thermal effective defoliant machine implementation, the 5ml sensitive measuring cylinder (graduated cylinder) was used in the determination of fuel amount used by tractor [22]. The values of the fiber fineness, maturity rate, fiber length, uniformity, percentage of short fiber, fiber elasticity, fiber endurance, brightness, chlorosis, foreign material field, foreign material percentage were studied [5], [4].

The thermal effective defoliant machine to be used in thermal implementation and the field crop sprayer to be used in chemical implementation was used with the tractor. The value of the tractor fuel consumption was determined with the following equality.

$$B_{avr} = \frac{B_f}{t} \quad (1)$$

Where,

B_{avr} : The average fuel consumption per unit of time (l/h)

B_f : In the result of implementation, the amount of fuel reduced from the fuel store (l)

t : Duration (h)

The amount of Liquid Petroleum Gas (LPG) consumed by the thermal effective defoliant prototype machine was calculated with the following formula.

$$B_{LPGavr} = \frac{m_{LPG1} - m_{LPG2}}{t_{th}} \quad (2)$$

Where,

B_{LPGavr} : The average LPG consumption per unit of time (kg/h)

m_{LPG1} : Before the implementation, LPG cylinder weight (kg)

m_{LPG2} : After the implementation, LPG cylinder weight (kg)

t_{th} : Thermal application time (h)

The time keeper was used in the study for determining the idled time during the implementation, preparation time for work, tractor pace [22],[23]. The effective work successes of field pulverizator used in the defoliant implementation and thermal effective defoliant machine were calculated with following equality [21].

$$E_f = \frac{v_i \cdot b_m \cdot K}{1000} \quad (3)$$

Where,

E_f : Effective working success (da/h)

v_i : Machine velocity (km/h)

b_m : Machine working width (m)

K : Time utilization coefficient

The thermal effective defoliant machine is a single row machinery. Therefore, the distance was named as the distance between working width and plant row. The working width of field pulverizator was calculated with following formula [3].

$$b_p = m_{nd} \cdot m_{nn} \quad (4)$$

Where,

b_p : Working width of field pulverizator (m)

m_{nd} : The distance between two spraying nozzle (m)

m_{nn} : The number of spraying nozzle

Time utilization coefficient was calculated with following formula.

$$K = \frac{K_{work}}{K_{total}} \quad (5)$$

$$K_{total} = K_{work} + K_{free} \quad (6)$$

Where,

K : Time utilization coefficient

K_{work} : Elapse time in work (h)

K_{total} : Total application time (s)

K_{free} : The idled time (h) of the machine (turnings on the parcel ends and unanticipated failures)

In the costs calculation of chemical (defoliant) implementation with thermal effective defoliant implementation, cultivation costs were ignored because the cultivation costs done until the defoliant implementation time were the same. The thermal implementation cost was calculated in the following,

$$TA_m = \frac{B_{TAfavr} \cdot F_p + B_{LPGavr} \cdot LPG_p}{E_{fi}} \quad (7)$$

Where,

TA_m : Thermal application cost (\$/da)

B_{LPGavr} : Average LPG consumption (kg/h)

LPG_p : LPG price (\$/kg)

E_{fi} : Effective working success of thermal effective defoliant machine (da/h)

B_{TAfavr} : The average fuel consumption of tractor during the thermal implementation (l/h)

F_p : Fuel price (\$/l)

The chemical implementation cost was calculated in the following.

$$DA_m = \left(\frac{B_{DAfavr} \cdot F_p}{E_{fp}} \right) + B_{Davr} \cdot D_p \quad (8)$$

Where,

DA_m : Defoliant implementation costs (\$/da)

B_{DAfavr} : The average fuel consumption of tractor during defoliant implementation (l/h)

F_p : Fuel price (\$/l)

B_{Davr} : Average chemical (defoliant) consumption (l/da)

D_p : Defoliant price (\$/l)

E_{fp} : Effective work success of field pulverizator (da/h)

3 RESULTS AND DISCUSSION

The implementation costs for first and second year are presented as a comparative in the Table 1.

Table 1. Data for operating costs of implementations

Year*	Control		Chemical Treatments		Thermal Treatments	
	I	II	I	II	I	II
Duration of preparation work, min	-	-	15	15	5	5
Operating temperature, °C	-	-	-	-	~ 145	~ 145
Working speed, km/h	-	-	~ 3.8	~ 4	~1.5	~1.6
Time utilization coefficient	-	-	0.70	0.68	0.88	0.89
Working width, m	-	-	8	8	0.75	0.75
Business success, da/h	-	-	21.4	21.8	1	1.1
Chemical consumption, ml/da	-	-	60	60	-	-
Chemical cost, \$/da	-	-	2.88	3.19	-	-
LPG consumption, kg/h	-	-	-	-	4.8	4.6
LPG consumption, kg/da	-	-	-	-	4.8	4.2
LPG cost, \$/da	-	-	-	-	12.4	13.82
LNG cost, \$/da	-	-	-	-	2.76	2.50
Tractor fuel consumption, l/h	-	-	3.90	4.05	4.20	4.30
Gas price, \$/l	-	-	1.74	2.11	1.74	2.11
Activity of Defoliation	~ 10%	~ 3%	~ 47%	~ 44%	~ 89%	~ 83%
Total cost of chemical application, \$/da	-	-	3.19	3.58	-	-

Total Thermal Implementation (LPG) Cost, \$/da	-	-	-	-	19.71	22.06
Total Thermal Implementation (LNG) Cost, \$/da**	-	-	-	-	10.07	10.74
* I. Year implementation has been carried out in 9 October 2009 and II. Year implementation has been carried out in 3 November 2010.						
** When assuming the same quantity of LNG consumption, the resulting total cost.						

While the cost was 19.71 \$/da of the 1 da/h success with 4.8 kg/da fuel consumption by first year thermal implementation, the cost was observed as 22.06 \$/da with reducing the fuel consumption to 4.2 kg/da and increasing the work success 1.1 da/h in the second year thermal implementation. In the use of liquefied natural gas (LNG) instead of 45 kg LPG tank, it is possible to reduce of 1/4 of fuel costs per hectare. While the cost was 3.19 \$/da of the 21.4 da/h success in the 60 ml/da defoliant dose by first year thermal implementation, the cost was observed as 3.58 \$/da with increasing the work success 21.8 da/h in the second year chemical implementation.

Funk et al. [8],[9] were found in their studies that the thermal implementation costs were respectively 2.1 \$/da, 3.7 \$/da, 5.4 \$/da and the chemical cost was 10.2 \$/da with the use of 9.35 l/da (~4.9 kg/da), 9.35-14.0 l/da (~4.9-7.3 kg/da), 14.0 l/da (~7.3 kg/da) propane gas Funk et. al have been used the ~4,9 kg/da fuel amount used in the low density implementations, and this amount (4.2-4.8 kg/da) was considerably same of the thermal implementation in our study. Furthermore, while the LPG cost was average ~13.1 \$/da, the fuel cost of Funk et all was 2.1 \$/da. When the LNG was used as an alternative fuel in the turkey conditions, it was possible to reduce the fuel cost as 2.5 \$/da. The chemical cost (2.88 \$/da – 3.19 \$/da) implemented in the Turkey was considerably low according to the chemical cost of Funk et al. (10.2 \$/da).

While Funk was reaching the 0.9 da/h working success with the thermal effective defoliant single row prototype machines, Showler et al. reached 4 da/h field working success with double row self-propelled prototypes [7],[17]. Beside the single row prototype machines of Funk et al., they had a separate trailer pulling a propane tank, so it caused the decrease the maneuverability [8]. In the prototype machine that was used in our scope of study, the burner fuel was stored on the machine and was reached 1.1 da/h field work success with the single row thermal effective defoliant machine.

There were considerably difference between the thermal and chemical defoliant implementation costs. This difference made also essential comparisons of returns to be provided by resulting product. It was possible to predate the harvest time with thermal implementation. With the early harvest, the loss of quality in the product and hence the loss of value was prevented. It was possible to balance the cost occurred by this way.

There was difference respectively between with highest quality “Standard Guarantee” and “White Standard1” as I and II year 0.069\$/kg-0.071 \$/kg and “White Standard2” 0.171 \$/kg – 0.177\$/kg and “Spotted Standard1” 0.137\$/kg-0.142 \$/kg [1]. In the loss of quality that might arise due to the delay of harvest, it was observed to loss of as approx. average 0.103 \$/kg – 0.106 \$/kg for the I. and II. year. It was possible to prevent the losses of quality with early harvest by thermal defoliant implementation. The net gains that could be provided with early harvest, were presented in the Table 2 by taking into consideration of type yields.

Table 2. The values of thermal implementation costs for returns with early harvest on the basis of varieties

Treatme nt Year	Varieties	Yield (kg/da)	Incoming gain with early harvest (\$ /da)	Net return after the thermal implementation cost (\$ /da)
I	Beyaz Altın 119	506	52.12	32.41
	Nazilli 84S	398	40.99	21.28
	Carmen	463	47.69	27.98
II	Beyaz Altın 119	493	52.26	30.20
	Nazilli 84S	470	49.82	27.76
	Carmen	476	50.46	28.40

The parcels in which thermal defoliant implementation carried out and in the case of the implementation carried out after a few days later from the implementation and the same yield obtained, net feedbacks were observed maximum in the Beyazaltın 119 type as 32.41 \$/da and minimum in the Nazilli 84S type as 21.28 \$/da in the I. year implementations. With the earlier harvest, it was possible to reach average 28 \$/da net return by thermal implementation.

4 CONCLUSIONS

The thermal defoliant implementation is not affected by atmospheric conditions such as rainfall, wind speed, differences of air temperature that affect the chemical implementations as negatively. The effect of thermal implementation moves to the time of removing the leaves from plant to an earlier time compared to chemical implementation. Thus, it is possible to take the date of harvest in an earlier time. It is possible to prevent the cotton fiber quality loss caused by rainfall in the harvest season. The statistically difference is not observed in the parcels that thermal and chemical implementation are carried out for cotton fiber quality and yield. In addition, thermal implementation is unobjectionable implementation for machine harvest in organic cotton production.

Reducing the operating costs of thermal defoliant machine can be provided by increasing the work success of thermal effective defoliant. Instead of using 45 kg cylinder for supplying liquid petroleum gas used in the heating of air, the alternative models used fuels such as liquid natural gas (LNG) can be reduced the implementation costs. When either defoliation or implementation costs, analyzing the implementation with thermal defoliant machine is seen as competitive with the chemical implementation.

ACKNOWLEDGMENTS

A research and development project related to the subject presented in this paper was submitted to The Ministry of Science, Industry and Technology, by Department of Agricultural Machinery, Faculty of Agriculture, Adnan Menderes University and Uzel Makine A.S., and was supported by The Ministry of Science, Industry and Technology with titled 'Designing and Developing Thermal Defoliator Which Will Be Used in Cotton Cultivation' and No:141.STZ.2007-2 SAN-TEZ Project. This study is a part of PhD dissertation and project.

REFERENCES

- [1] (2012)Web Site. [Online]. Available: <http://www.itb.org.tr/TR/Default.asp>
- [2] Burmester C., Patterson M.G., Monks, C.D. 2001. Cotton Defoliation Time. Alabama Cooperative Extension System , ANR-715, USA.
- [3] Çilingir, İ., Dursun, E. 2002. Bitki Koruma Makinaları. Ankara Üniversitesi Ziraat Fakültesi, Yayın No:1531, Ders Kitabı:484, Ankara.
- [4] Dong, H., Li, W., Tang, W., Li, Z., Zhang, D., Niu, Y. 2006. Yield, quality and leaf senescence of cotton grown at varying planting dates and plant densities in the Yellow River Valley of China. *Field Crops Research* 98:106–115.
- [5] Faircloth, J.C., Hutchinson, R., Barnett, J., Paxson, K., Coco, A., Price III, P. 2004. An Evaluation of Alternative Cotton Harvesting Methods in Northeast Louisiana –A Comparison of the Brush Stripper and Spindle Harvester. *The Journal of Cotton Science* 8:55–61 (2004) 55, Available: <http://journal.cotton.org>
- [6] Fletcher, R.S., Showler, A.T., Funk, P.A. 2007. Surveying Thermally-defoliated Cotton Plots with Color-infrared Aerial Photography. Available: <http://www.plantmanagementnetwork.org/pub/cm/research/2007/thermal/>
- [7] Funk, P.A., Armijo, C.B., Lewis, B.E., Steiner, R.L., McAlister III, D.D. 2002. Thermal Defoliation of Cotton. ASAE Meeting Paper No: 021149.
- [8] Funk, P.A., Armijo, C.B., McAlister III, D.D., Brashears, A.D., McGuire, M.R., Lewis, B.E., Hutmacher, R.B., Roberts. B.A. 2004a. 2003 Thermal Defoliation Trials. Proceedings of the Beltwide Cotton Conferences, January 5-9, San Antonio, TX, USA, S:755-759.
- [9] Funk, P. A., Armijo, C. B., McAlister, III, D. D., Lewis, B.E. 2004b. Experimental thermal defoliator trials. *The Journal of Cotton Science*, 8:230–242.
- [10] Gwathmey, C.O., Hayes, R.M. 1997. Harvest-Aid Interactions under Different Temperature Regimes in Field-Grown Cotton. *The Journal of Cotton Science*, 1:1-28.
- [11] Gwathmey, C.O., Bednarz, C.W., Fromme, D.D., Holman, E.M. Miller, D.K. 2004. Response to Defoliation Timing Based on Heat-Unit Accumulation In Diverse Field Environments. *The Journal of Cotton Science*, 8:142–153.
- [12] Larson, J.A., Gwathmey, C.O., Hayes, R.M. 2002. Cotton Defoliation and Harvest Timing Effects on Yields, Quality, and Net Revenues. *Journal of Cotton Science*, 6:13-27.
- [13] Mart, C. 2005. Pamukta Entegre Üretim. Kahramanmaraş Sütçü İmam Üniversitesi, Yayın No: 119, Kahramanmaraş.
- [14] Nisbet, C., Nisbet, C.S.Jr. 1954. Apparatus for Subjecting Cotton Plants and The Like to Hot Gases. U.S. Patent Office, Patent No: 2682728.
- [15] Porterfield, J.G., Batchelder, D.G. 1969. Thermal Defoliator. U.S. Patent Office, Patent No:3442262.
- [16] Sağlam, R., Akyol, B. 2002. Ceylanpınar Tarım İşletmesi'nde Makinalı Pamuk Hasadında Ürün Kayıplarının Belirlenmesi Üzerine Bir Araştırma. Türkiye V. Pamuk, Tekstil ve Konfeksiyon Sempozyumu Bildirileri, Polat Matbaası, Ankara.
- [17] Showler, A., Funk, P., Armijo, C. 2006. Effect of Thermal Defoliation on Cotton Leaf Desiccation, Senescence, Post-harvest Regrowth, and Lint Quality. *The Journal of Cotton Science*, 10: 39–45.
- [18] Siebert, J.D., Stewart, A.M. 2006. Correlation of Defoliation Timing Methods to Optimize Cotton Yield, Quality, and Revenue. *The Journal of Cotton Science*, 10: 146–154
- [19] Stewart, A.M., Edmisten K.L., Wells, R. 2000. Boll openers in cotton: effectiveness and environmental influences. *Field Crops Research*, 67:83-90.
- [20] Şimşek, E., 2012. Designing and Developing Thermal Defoliator which will be used in Cotton Cultivation, Fen Bilimleri Enstitüsü, Adnan Menderes Üniversitesi, Aydın.
- [21] Ülger, P., Güzel, E., Kayışoğlu, B., Eker, B., Akdemir, B., Pınar, Y., Bayhan, Y., Sağlam, C. 2002. Tarım Makinaları İlkeleri. Fakülteler Matbaası, İstanbul.

- [22] Yalçın, 1999. Değişik Toprak İşleme ve Pamuk Ekim Tekniklerini Aydın Yöresi Koşullarına Uygulama Olanakları. Ege Üniversitesi Fen Bilimleri Enstitüsü (PhD Thesis), İzmir.
- [23] Yalçın, H., Çakır, E., Gülsoylu, E., Keçecioglu, G. 2001. Tohum Yatağı Hazırlamada Uygulanan Farklı Toprak İşleme Yöntemleri Üzerine Bir Araştırma. Ege Üniversitesi Ziraat Fakültesi Dergisi, 38(1):71-78.

The Examination of the Level of Resident Perception towards Environmental Problems: Bartin City (Turkey)

Canan Cengiz¹, Pelin Kececioglu Dagli²

Abstract

Humanity forms the environment they live in in time accordance with the requirements of the age. Within the context of landscape planning and design applications, the enhancement of meeting the social needs and quality of life as well as ensuring the sustainability of all natural, cultural, ecological, economical and aesthetical values of the living environment are among the important targets. Therefore, different professional disciplines is working on environmental issues on the agenda at national and international level. In terms of increasing the livability and sustainability of cities for individuals, the attitude towards the problems of the people's living environment at the local level is important. In this context, because of having the importance of natural and cultural characteristics, Bartin City is selected as the research area. To determine and examine the level of perception of Bartin City residents towards environmental problems, a questionnaire was carried out. Ultimately, the level of perception regarding the environmental problems of Bartin City residents were determined, and evaluations and recommendations were made for the development of modern environmental awareness.

Keywords: Environmental problems, level of perception, sustainability, modern environmental awareness, Bartin.

1 INTRODUCTION

Equilibrium between man and environment began to degrade due to extreme human intervention with nature as of late 20th century, whereupon environmental problems emerged [1]. According to Çabuk & Karacaoğlu [2], environmental issues, which complicate meeting the requirements about life, originate from the rise in artificial environment due to destruction of natural environment. In the course of time, these problems became global and common problems of the world [3]. Environmental problems, pollution of air, water and soil above all, began threatening human health together with insensible technological developments [2].

According to Aydın & Kaya [4], the essential reason behind environmental problems is rapid industrialization and urbanisation due to global population growth. Accordingly, environmental awareness and conscience consist of how the society perceives relevant factors such as pollution of air, water and soil, rise in waste amount, rapid consumption of natural resources, decline in species etc. In this regard, the first ever environmental awareness and conscience institution in Turkey was established in 1955 under title of Association for Natural Protection in Turkey (Türkiye Tabiatını Koruma Derneği); it was followed by organisations such as ÇEKÜL (Foundation for Protection of Environmental and Cultural Assets), TEMA (Turkish Foundation for Combating Soil Erosion, for Reforestation and the Protection of Natural Habitats) etc. [4]. According to Ertürk (2009), environmental problems are maintain their actuality in various manners such as climate change, ozone depletion, decline in biodiversity, radioactive contaminations, acid rains, desertification, toxic wastes etc. [5]. Environmental problems came to agenda of the society back in 1952, when 4000 died of air pollution in London. Accordingly, United Nations Conference on the Human Environment summoned in Stockholm in 1972, whereupon United Nations Environment Programme (UNEP) was established. In 1992, United Nations Conference on Environment and Development was held in Rio de Janeiro and Agenda 21 was accepted [5][6]. Current international organisations include International Union for Conservation of Nature (IUCN), World Wide Fund for Nature (WWF) etc.. In this respect, it is a significant objective to meet social requirements, enhance life quality and maintain sustainability of all natural, cultural, ecologic, economic and aesthetic values of the environment by means of landscape planning and design applications. Therefore, various occupational disciplines conduct studies on current environmental problems at national and international level.

For elimination of ecological problems, it is important how society perceives environment [7]. For this reason, individuals should be provided with appropriate education on environment and thus have environmental awareness; besides, such environmental awareness and attitudes should be sustainable in order to annihilate factors that pave way for environmental problems [3]. Moreover, it is necessary to ensure active participation of individuals at organisations and institutions for studies about environment so as to improve perception about their environment [2]. The youth should be the primary target [7]. Pursuant to study by Cohen in 1984, negative attitude and behaviour among children against environment is very likely to become unavoidable and to continue in upcoming periods of

¹ Corresponding author: Bartin University, Forestry Faculty, Department of Landscape Architecture, 74100, Merkez/Bartın, Turkey. canancengiz@bartin.edu.tr

² Bartın University, Forestry Faculty, Department of Landscape Architecture, 74100, Merkez/Bartın, Turkey. pkececioglu@bartin.edu.tr

their lives [8]. Therefore, environmental education should be employed in order to provide the youth with permanent behavioural change for sustainability among posterities [7].

The attitude of residents in face of problems in their environment is very crucial for enhancing the livability and sustainability of cities for individuals. In this respect, Bartın Province was selected as research area, and pursuant to Report on Environmental Problems and Primary Inventory Assessment in Turkey [9], the essential environmental problems in Bartın in 2009-2010 were listed as air pollution, water pollution, wastes, noise pollution, soil pollution, erosion and destruction on natural environment, whereas, according to Report on Environmental Problems and Assessment of Priorities in Turkey (2014), the problems, in order of importance, changed as follows: water pollution, air pollution, wastes and noise pollution [10]. The environmental problems in Bartın were manifested through a public environmental report; hereby article, on the other hand, treats the issue through participation of locals.

In this respect, a survey was carried out in order to determine and analyse the perception level of Bartın people with regard to environmental problems in Bartın Province, which possesses a significant amount of natural and cultural assets. Consequently, the awareness of residents about environmental problems was determined; accordingly, certain assessments and suggestions for improvement of modern environmental conscience were developed.

2 MATERIAL AND METHOD

2.1 Material

The essential material of study consists of Bartın, a province in Black Sea Region known for its significant natural and cultural characteristics (Figure 1). National and international literature and survey data from field works constitute other materials of hereby study.

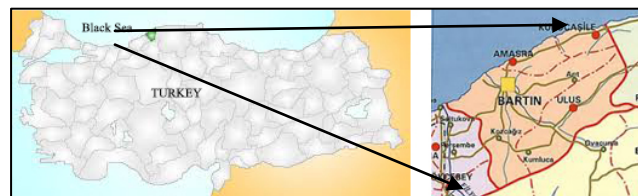


Figure 15. Location of Bartın Province in Turkey

2.2 Method

The study consists of four main stages:

- I. Literature review on relevant researches in Turkey and abroad relating to environmental problems and relevant topics,
- II. A survey was applied on residents of Bartın Province through field work,
- III. Survey data were entered in statistics software SPSS 22.0 in order to generate analyses for determination of awareness level among residents about environmental problems,
- IV. Assessments and suggestions for development of modern environmental awareness.

Questions in the survey on residents were influenced by or derived from the following references Demirekin (2001), Çabuk & Karacaoğlu [2], Güven ve Aydoğdu [3], Aydın ve Kaya [4], Sam et.al. [5], Özbebek Tunç et.al. [8] and Demirekin [11]

Survey study consists of two parts. First part comprises a total of five questions about socio-demographic structure. The second part includes 34 questions in total about the research area. Questions in second part include those for determining views about current situation (7 questions), about environmental awareness and education (9 questions), about individual habits (10 questions) and about relevant suggestions (8 questions). The questionnaire, as a whole, consists of 39 questions.

Survey was applied by face-to-face interview with residents in Bartın Province. In total, 103 people participated in the survey. In the part on views about current situation, the participants were presented several options and asked to sort their first three options pursuant to order of importance. Questions in parts on environmental awareness and education, individual habits and relevant suggestions included inquiries such as “Yes/I have no idea/No”. The software SPSS Statistics 22 is employed in evaluation of surveys. Frequency Analysis and Chi-square Tests are applied.

3 FINDINGS

Demographic structure and views of participants were evaluated pursuant to Frequency Analysis and Chi-Square Test.

3.1 Survey Results with regard to Demographic Structure of Participants

According to Frequency Analysis on 103 participants of the survey, 53.4% (n:55) are female and 46.6% (n:48) are male. A significant amount of participants are in the age group between 31-40 (25.2%; n:26), followed by age groups 21-23 with 21.4% (n:22) and 24-26 with 17.5% (n:18).

As for educational background, participants with undergraduates are the most common with 55.3% (n:57). The rest consists of graduates from high schools with 17.5% (n:18), postgraduates with 17.5% (n:18), secondary school with 6.8% (n:7) and finally, primary school with 2.9% (n:3).

An analysis on occupations reveal that university students are the most crowded group (35%), followed by workers (12.6%) and academicians (11.7%) (Table 1).

As for monthly income, 27.2% of participants earn more than 2501 TL per month. They are followed by the income range 1501-2500 TL (18.4%), 751-1000 TL (16.5%), less than 500 TL (14.6%), 501-750 TL (12.6%) and 1001-1500 TL (10.7%).

Table 10. Occupations of participants

	Frequency	Percent
Housewife	11	10,7
Retired	8	7,8
Undergraduate	36	35,0
Academicians	12	11,7
Civil Servant	9	8,7
Worker	13	12,6
Self-Employed	8	7,8
Postgraduate Student	6	5,8
Total	103	100,0

3.2 Survey Results with regard to Research Area

Hereby chapter is examined under four main titles. Under the first title, participants were asked about the current situation with regard to environmental problems in Bartın. Under second title, environmental conscience and environmental education among participants were analysed. Then comes inquiries about individual habits; finally there are suggestions about elimination of present environmental problems in Bartın.

3.2.1 Survey Findings about Current Situation in Bartın

Participants were asked to list first three options. Under frequency analysis, according to their responses, the most important environmental problems in Bartın were expressed as follows: air pollution (62.1%), water pollution (37.9%) and waste (31.1%) (Table 2). Asked about main factors behind air pollution in the province, 72.8% of participants told about the effects of domestic heating. The second factor was production/industrial enterprises (9.7%). Mining businesses and insufficient supervision came last with an equal proportion of 4.9%. Main factors for water pollution are considered to be domestic wastes (35.9%), industrial wastewater (20.4%) and irresponsibility of public institutions (18.4%). According to residents of Bartın, main factors for soil pollution are wastes (22.3%), unplanned urbanisation (15.5%) and water pollution (14.6%); whereas the problem about wastes was expressed as disorganised waste storage area (23.3%), insufficient action by local administration (18.4%) and indifference of people (17.5%). For participants, the main factors behind noise pollution in Bartın are announcements with loudspeakers (43.7%), traffic-highway (32%), and construction works (23.3%). The main reasons of destruction of natural environment and erosion are listed as follows: land clearing (32%), provision of firing (30.1%) and unconscious soil cultivation (16.5%).

Table 2. The First Three Environmental Problems in Bartın

Environmental Problems	Percent (%)
Air pollution	62,1
Water pollution	37,9
Wastes	31,1

3.2.2. Survey Findings about Environmental Awareness and Education among Residents

According to Frequency Analysis, most participants indicated they had environmental education; they believe they are educated enough for awareness about air, water, soil pollution and ecological balance, and educational institutions improve environmental conscience. On the other hand, according to participants, the efforts about environment in Bartın Province are insufficient; besides, they do not participate in efforts by voluntary institutions and do not know about non-governmental organisations on environment in the province (Table 3).

Table 3. Survey Findings about Environmental Awareness and Education among Residents

	Yes (%)	I have no idea/Neutral(%)	No (%)
Did you get any education about environment?	55,3	3,9	40,8
Do you think you are educated enough to have awareness about air, water, soil pollution and ecological balance?	54,4	8,7	36,9
Do educational institutions enhance environmental awareness?	45,6	24,3	30,1
Do you follow publications about environment?	44,7	16,5	38,8
Do you attend/participate in scientific studies about environment such as seminars, panels or conferences?	33	17,5	49,5
Do you know the non-governmental organisations about environment in Bartın?	28,2	13,6	58,3
Do you participate in the efforts by voluntary institutions about environment?	15,5	13,6	70,9
Are efforts about environment sufficient?	4,9	21,4	73,8
Do you think mass media contributes to environmental awareness?	25,9	33	31,1

Nevertheless, Chi-Square Analysis reveals that the participants, who say they follow publications about environment, do not participate or attend scientific organisations about environment such as seminars, panels and conferences (Table 4).

Table 4. Result of Chi-Square Test between Following of Publications on Environment and Participation in Scientific Organisations about Environment

		Do you attend/participate in scientific studies about environment such as seminars, panels or conferences?			
		Yes	I have no idea	No	Total
Do you follow publications about environment?	Yes	24	11	11	46
	I have no idea	3	7	7	17
	No	7	0	33	40
Total		34	18	51	103

3.2.3. Survey Findings about Individual Habits of Residents

Pursuant to frequency analysis, the residents in survey indicate they care for reaching of wastes to dustbin, they can prefer, instead of coal etc., natural gas that can dramatically reduce air pollution in Bartın, they warn the people around them about problems such as pollution of air, water, soil and noise, destruction of natural environment and erosion; they also state people should not blow the horn unnecessarily, they do not classify their domestic wastes, and they will not opt for public transport just to avoid air pollution if they already have a private vehicle (Table 5).

Table 5. Survey Findings about Individual Habits of Residents

	Yes (%)	I have no idea/Neutral(%)	No (%)
Do you classify your domestic wastes?	37,9	12,6	49,5
Do you care for reaching of wastes to dustbin?	93,2	1	5,8
Do you put your wastes in the most suitable recycling bins for reuse?	64,1	14,6	21,4
Are you an economiser about water consumption in all conditions?	74,8	17,5	7,8
Do you mind about the contamination of harmful substance such as frying oil, paint etc. with sewage system?	71,8	13,6	14,6
Do you avoid using consumer goods that are harmful for ozone layer (such as deodorant and other sprays)?	47,6	20,4	32
Do you prefer public transport just to avoid air pollution even if you have a private vehicle?	31,1	22,3	46,6
Would you prefer natural gas that will significantly reduce air pollution in Bartın to coal and similar firing?	86,4	4,9	8,7
Do you blow the horn repeatedly?	11,7	7,8	80,6
Do you warn people around you for awareness about air, water, soil and noise pollution, wastes, destruction of natural environmental and erosion?	81,6	12,6	5,8

Nevertheless, according to Chi-Square Test results, the participants, who believe in contribution of educational institutions to environmental awareness in the part about environmental awareness and education, do not classify their domestic wastes as is seen under the part on individual habits (Table 6).

Table 6. Results of Chi-square test between Contribution of Educational Institutions to Environmental Awareness and Classification of Domestic Wastes

		Do you classify your domestic wastes?				
		Yes	I have no idea	No	Total	
17,307 ^a p<0,05	Do educational institutions enhance environmental awareness?	Yes	22	11	14	47
		I have no idea	9	1	15	25
		No	8	1	22	31
Total		39	13	51	103	

3.2.4. Survey Findings About Suggestions by Residents for Solution of Environmental Problems in Bartın

According to Frequency Analysis, suggestions by participants about solution of environmental problems in Bartın often touch upon recycling of wastes; accordingly, the residents think that the local administrations in Bartın should

have higher power and people should change their consumption habits that pave way for environmental problems (Table 7).

Table 7. Survey Findings about Suggestions by Residents for Solution of Environmental Problems in Bartın

	Yes (%)	I have no idea/Neutral(%)	No (%)
If you were sure about an absolute solution for environmental problems in Bartın, would you provide financial aid for the institution with such an objective?	62,1	22,3	15,5
Do you think that environmental problems in Bartın and solution suggestions should be taught at schools?	84,5	6,8	8,7
Do you think some heavy punishments should apply for those who pollute the environment and degrade ecological balance?	84,5	13,6	1,9
Do you think the local administrations in Bartın should have higher power in this respect?	93,2	4,9	1,9
Do you think obligatory environmental programmes should be given coverage in local and national press?	87,4	9,7	2,9
Do you think environmental impact assessment should be conducted for prevention of environmental problems?	88,3	8,7	2,9
Do you think the wastes should be sent to recycling?	96,1	1,9	1,9
Do you think the people should change their consumption habits that lead to environmental problems?	92,2	2,9	4,9

According to results of Chi-Square Test Analysis, it is revealed that the participants, who warn people around them about air, water, soil and noise pollution, wastes, destruction of natural environment and erosion in the part about individual habits, suggest change of consumption habits which lead to environmental problems in the present chapter (Table 8).

Table 8. Results of Chi-Square Test between Warning about Awareness on Environmental Problems and Necessity for Change of Consumption Habits that lead to Environmental Problems

		Do you think the people should change their consumption habits that lead to environmental problems?			Total		
		Yes	I have no idea	No			
10,662a	p<0,05	Do you warn people around you for awareness about air, water, soil and noise pollution, wastes, destruction of natural environmental and erosion?	Yes	80	1	3	84
		I have no idea	10	2	1	13	
		No	5	0	1	6	
Total			95	3	5	103	

4 CONCLUSION

Today, the ever-increasing environmental problems necessitate environmental education and detection of environmental awareness among locals for elimination of these problems. The attitude of people about the problems in their environment is crucial for enhancing livability and sustainability of cities for individuals at local level; accordingly, hereby study evaluates the perceptions of awareness and sensibility among Bartın locals with regard to air pollution, water pollution, soil pollution, wastes, noise pollution, destruction of environment and erosion; it also examines the views of participants about environmental awareness and education, individual habits and suggestions.

Pursuant to certain findings, hereby research puts forth a difference between environmental awareness of residents about environmental problems in Bartın, depending on some characteristics:

According to survey results, the essential environmental problems in Bartın are air pollution, water pollution and wastes, respectively.

Pursuant to survey data, the residents consider domestic wastewater, industrial wastewater and indifference of people as main factors behind water pollution.

In the eyes of participants, main factors behind air pollution are domestic heating, production/industrial enterprises, mining business and insufficient supervision by public institutions, respectively.

Wastes are considered to bring along disorganised storage. Pursuant to survey data, locals see disorganised storage, irresponsible attitude of local administration and people as main factors behind waste accumulation.

Local inhabitants believe that educational institutions contribute to environmental awareness; they, however, do not participate or attend scientific studies or efforts by voluntary organisations about environment in Bartın, do not know about relevant nongovernmental organisations and do not find sufficient the efforts about environment in their city. Therefore, there is a need for incentive application in order to ensure participation of locals to mentioned efforts. Public institutions should be in direct contact with voluntary and official environmentalist bodies and organise relevant activities in order to ensure participation of inhabitants. Integration can be established with students through invitations by authorised bodies to educational institutions. Once awareness among youth is increased at local level, this will contribute to formation of a more habitable environment in a larger scale in the future.

As for individual habits, the locals tend to refrain from behaviours that may lead to environmental problems. However, they do not abandon private vehicles that provide comfort in daily life or classify domestic wastes for recycling. Therefore, there is a need for encouraging publications through local communication means, recycling bins should be placed in public spaces and adjustments should be made for encouraging use of public transport in order to ensure awareness.

For a higher perception level through awareness and conscience about environmental problems, the first task is determination of strong objectives at local scale. It is necessary and important that local administrations assume appropriate responsibility and sensibility in order to conduct efforts to enhance the perception level among locals. In this respect, disincentive punishments should apply for those who pollute the environment or harm ecological balance; besides, local press should treat upon environmental problems and publications.

Higher perception level among individuals about environment will bring along caring for environmental problems at personal and local level. In parallel with the rise in level of sensibility and awareness, it will be possible to develop permanent measures for solving environmental problems. Consequently, strong perception will be established for conscious utilisation of environment.

Finally, the analyses reveal that residents of Bartın do have awareness about primary and actual environmental problems in the province.

REFERENCES

- [1] N. B. Grimm, S. H. Faeth, N. E. Golubiewski, C. L. Redman, J. Wu, X. Bai and J. M. Briggs, "Global Change and The Ecology of Cities", *Science*, Vol. 319, 5864, pp. 756-760, DOI: 10.1126/science.1150195, 2008
- [2] B. Çabuk ve C. Karacaoğlu, "Üniversite Öğrencilerinin Çevre Duyarlılıklarının İncelenmesi", *Ankara Üniversitesi Eğitim Bilimleri Fakültesi Dergisi*, Vol. 36, 1-2, pp. 189-198, 2003.
- [3] E. Güven ve M. Aydoğdu, "Çevre Sorunlarına Yönelik Farkındalık Ölçeğinin Geliştirilmesi ve Öğretmen Adaylarının Farkındalık Düzeylerinin Belirlenmesi", *Öğretmen Eğitimi ve Eğitimcileri Dergisi*, Vol. 1, 2, pp. 185-202, 2012.
- [4] F. Aydın ve H. Kaya, "Sosyal Bilimler Lisesi Öğrencilerinin Çevre Duyarlılıklarının Değerlendirilmesi", *Marmara Coğrafya Dergisi*, 24, pp. 229-257, Temmuz 2011.
- [5] N. Sam, S. Gürsakal ve R. Sam, "Üniversite Öğrencilerinin Çevresel Risk Algısı ve Çevresel Tutumlarının Belirlenmesi", *Akademik Bakış Dergisi*, 20, pp. 1-16, Nisan-Mayıs-Haziran, 2010. [Online]. Available: <http://www.akademikbakis.org/eskisite/20/13.pdf>.
- [6] "Uluslararası Çevre Konuları", T.C. Dışişleri Bakanlığı, [Online]. Available: <http://www.mfa.gov.tr/uluslararasi-cevre-konulari.tr.mfa>
- [7] N. Tokat ve A. Mutlu, "Çevre Bilinci ve Duyarlılığı Bakımından Çorum'daki Orta Öğretim Öğrencileri Üzerine Bir Araştırma", *G.Ü. Çorum İktisadi ve İdari Bilimler Fakültesi Dergisi*, 1, pp. 207-220, 2004.
- [8] A. Özbebek Tunç, G. Akdemir Ömür ve A. Z. Düren, "Çevresel Farkındalık", *İstanbul Üniversitesi Siyasal Bilgiler Fakültesi Dergisi*, 47, pp. 227-246, Ekim 2012.
- [9] *Türkiye Çevre Sorunları ve Öncelikleri Envanteri Değerlendirme Raporu 2012*, Çevre ve Şehircilik Bakanlığı, Ankara, [Online]. Available: http://www.csb.gov.tr/db/ced/editordosya/cevre_sorun_2012.pdf
- [10] *Türkiye Çevre Sorunları ve Öncelikleri Değerlendirme Raporu 2014*, Çevre ve Şehircilik Bakanlığı, Ankara, [Online]. Available: https://www.csb.gov.tr/db/ced/editordosya/cevre_sorun_2014.pdf
- [8] H. Demirekin, "Isparta İlinde Çevre Sorunlarına Duyarlılık Analizi", Basılmamış Yüksek Lisans Tezi, Süleyman Demirel Üniversitesi Sosyal Bilimler Enstitüsü İşletme Anabilim Dalı, Isparta, Türkiye, 2001.

Maximizing and Sustaining the Values through Project Management Office

Aynur Kazaz¹, Cenk Ocal², Murat Cevikbas³,

Abstract

Projects become more complicated day by day and organizations prefer to implement the projects concurrently in order to improve total value. These complications are resulted from tight schedules and short budget due to competition among firms. Not only time and cost but also quality come into prominence and require know-how, lessons learned and proper procedures in line with the company organization and perception of value. Therefore, all these requirements are to be developed by means of Project Management Office (PMO) and trigger to improve the project standards, procedures and methods. Establishing PMOs by the organizations has been evolving in time. Mainly two factors enhance the motivation of PMOs, namely improving the effectiveness of project management tasks and achieving the common project management approach. Additionally, all these project documents can be used as lessons learned for the future projects and improve the total quality management in projects. Studies show that these improvements correlate with project performance and success accordingly (Dai C.X. et al., 2004). In this improved standard of process and proper lessons learned contribute to sustainability of organization. Moreover, studies depict that PMO competency and function are also vital for the project success (Hobbs B. et al., 2007). Furthermore, efficiency of process can be increased by means of software such as Enterprise Resource Planning (ERP), Building Information Modeling (BIM) supporting the 4D to 6D. Therefore, Project Manager (PM) should take the advantage of the all aforementioned requirements above in order to achieve planned project value. This study contributes to highlighting the importance of project standards, using integrated project software and their positive effects on the project management success respectively. However, new researches have to be made to improve the process of PMO.

***Keywords:** Project Management Office (PMO), process improvement of projects, PMO software*

1 INTRODUCTION

Projects become more sophisticated day by day in order to satisfy the demand. For instance, companies require their investments to be completed in line with expected quality in less time and budget. It results in complexity of management of disciplines such as procurement, design, cost control, planning, quality management, accounting, warehouse etc. Coordination of these multi discipline is very difficult concerning the big project. Today this coordination is performed by Project Management Office in a Project. Mostly, disciplines of PMO can be working directly under a Project Manager or working under a Programme and Portfolio and coordinate the dependent projects. But any means, PMO provides biggest supports to PM in terms of the area related to project management. Therefore, PMOs' scope is very wide from the initiation stage to closing stage in a project. So It requires proper multi-disciplinary team work with a proper leadership which can be achieved by PMO. Since PMO is vital for a project because of project success, establishing of PMO structure in a project should be closely paid the attention.

¹Corresponding Author: Süleyman DemirelUniversity, Faculty of Technology, Department of Civil Engineering, Isparta, Turkey, Cenk Öcal

² Süleyman DemirelUniversity, Faculty of Technology, Department of Civil Engineering, Isparta, Turkey, Murat Çevikbaş

2 MATERIALS AND METHODS

Academic papers have been reviewed against field experience of Silkar Golf Hotel Project which is located in between Side and Belek regions in Antalya. One of the most relevant academic study derived from Project Management Institute (PMI) is a "Project Triangle/Triple Constraints" as depicted below. Each member of this constraint is dependent on others. Any deviation effect the others. For instance, if we consider fixed quality in a project with a fixed scope, any increase or decrease in time results in increase or decrease in cost respectively. Silkar Golf Hotel Project had deviation in time and scope and reasons of these changes are compared with the Project Triangle/ Triple Constraints. Thus, this project is elaborated in this study in order to figure out weakness of the project concerning delays and emphasis on the areas in which PMO competency can be improved.

Project Triangle/Triple Constraints



3 RESULTS AND DISCUSSION

3.1 Project Information

Planned Facts & Figures of Golf Hotel project are tabulated against actual figures below.

Table 1 - Silkar Golf Hotel Project's Facts & Figures

Project Facts & Figures		
	Planned	Actual
Project Start	November 2005	November 2005
Project Completion	March 2007	January 2009
Project Budget	45million Euro + VAT	85 million Euro + VAT
Total Project Area	1.000.000 m ²	1.000.000 m ²
Closed Area	400.000 m ²	400.000 m ²
Golf and Other Areas	600.000 m ²	600.000 m ²
Number of Room	499	499

As seen in the table, there is 22 months delay, although there is no change in the other figures except project budget which is almost doubled. According to Triple Constraint, the reasons beyond the increase in time can result from the increase in the factors of cost and scope. Actually, during the execution stage, as depicted in the Triple Constraint, scope was increased as requested by client. Consequently, cost was increased as well depending on increase in

scope. During these excessive changes, PMO faced with many problems in terms of coordination. Additionally, they didn't have enough procedures collected from their experiences to resolve these problems. Because Silkar Holding is a tourism company and has many hotels in Turkey. They needed another Hotel. Therefore, they established their construction firms. Thus, this new organization encountered many problems in terms of competency. According to Hill [2], PMO competency requires five stages which are project oversight, process control, process support, business maturity and center of excellence respectively. All these stages are in line with the PMI standards and will maximize the business value in terms of both tangible and intangible elements such as profit, recognition and reputation of organization etc.

Additionally, Hurts M. and Thomas J. L [4] examined the three companies and compared according to their PMO effecting the project management. The study came to conclusion that these three organizations had increased their effectiveness of PMO, organization capacity and structure according to PMO needs in time by means of improving PMO competency.

Moreover, PMO in project encountered problems with relates to monitoring the project. Therefore, PMO struggled the controlling the project according to project disciplines. With respect to the study made by Hobbs, B., & Aubry, M. [3], twenty seven PMO functions are grouped under six headlines which are vital for the project success, namely monitoring and controlling project performance, development of project management competencies and methodologies, multi project management, strategic management, organization learning and other functions (not in any group).

Table 2 - Twenty seven PMO functions are grouped under six headlines

<p>1. Monitoring and Controlling Project Performance</p> <ul style="list-style-type: none"> • Report project status to upper management • Monitor and control of project performance • Implement and operate a project information system • Develop and maintain a project scoreboard 	<p>2. Development of Project Management Competencies and Methodologies</p> <ul style="list-style-type: none"> • Develop and implement a standard methodology • Promote project management within organization • Develop competency of personnel, including training • Provide mentoring for project managers • Provide a set of tools without an effort to standardize 	<p>3. Multiproject Management</p> <ul style="list-style-type: none"> • Coordinate between projects • Identify, select, and prioritize new projects • Manage one or more portfolios • Manage one or more programs • Allocate resources between projects
<p>4. Strategic Management</p> <ul style="list-style-type: none"> • Provide advice to upper management • Participate in strategic planning • Benefits management • Network and environmental scanning 	<p>5. Organization Learning</p> <ul style="list-style-type: none"> • Monitor and control performance of PMO • Manage archives of project documentation • Conduct postproject reviews • Conduct project audits • Implement and manage database of lessons learned • Implement and manage risk database 	<p>Other Functions (Not in Any Group):</p> <ul style="list-style-type: none"> • Execute specialized tasks for project managers • Manage customer interfaces • Recruit, select, evaluate, and determine salaries for project managers

All these are closely related to and correlated with the project success and lessons learned. Hence, contribution, roles and effectiveness of PMO in the projects should be reinforced in the project in order to maximize project values in terms of cost, time, lessons learned, reputation, recognition, community benefits etc.

Furthermore, software related to PMO tasks is vital. In the project, there was no integrated software between disciplines. Each project department used their own software such as MS Project for Planning, AutoCAD for design, Access for warehouse, Outlook for communication between disciplines. Most of the delay resulted from miscommunication. However, if the project used Integrated software such as Enterprise Resource Planning (ERP), Project could have been completed early. In addition to this, in the design, many superimposed problems between

architecture, electrical and mechanical works were observed and caused some delay in project. Building Information Modeling (BIM) is an alternative solution to tackle with the design coordination problem and increase the maturity of PMO. BMI supports the 4D to 6D. 4D contains 3D Modeling and Schedule, 5 D consists of 3D Modeling, Schedule and Budget. As understood, using the BIM allows to control design, scheduling, budgeting.

4 CONCLUSION

With respect to academic review supporting the main problems arise by Silkar Holding Golf Hotel Project, following finding can be summarized;

- PMO Competency should be improved through project management standards and procedures with relates to planning, cost, procurement, design and construction. Therefore, organizational learning is vital for PMO.
- PMO has to have enough skilled staff to monitor and control project disciplines.
- Efficiency of process can be increased by means of software such as Enterprise Resource Planning (ERP), Building Information Modeling (BIM) supporting the 4D to 6D. Therefore, Project Manager (PM) should take the advantage of the all aforementioned requirements above in order to achieve planned project value.
- Project standards and using integrated project software have positive effects on the project management success.

REFERENCES

- [1] Dai, C.X. and Wells, W.G (2004) '*An exploration of project management office features and their relationship to project performance*' International Journal of Project Management, 22(7), pp. 523-532
- [2] Hill, G.M. (2004), '*Evolving the Project Management Office: A Competency Continuum*', 21(4), pp.45-51
- [3] Hobbs, B., & Aubry, M. (2007) '*A multiphase research program investigating project management offices (PMOs): The results of phase 1*' Project Management Journal, 38(1), pp.74–86.
- [4] Hurt, M. & Thomas, J.L. (2009) '*Building value through sustainable project management offices*', Project Management Journal, 40 (1), pp.55-72.
- [5] Kerzner, H. (2003) '*Strategic planning for a project office*.' Project Management Journal, 34(2), 13–25.
- [6] Ward, J. & Daniel, E.M. (2013) '*The role of Project Management Offices (PMOs) in IS project success and management satisfaction*', Journal of Enterprise Information Management, 26 (3), pp.316-336.

Determination of Priority Contamination Factors in Lake of Manyas (Bird Paradise)

Elif Ozmetin¹, Cengiz Ozmetin¹, Yeliz Suzen, Mustafa Korkmaz¹

Abstract

Wetlands of which importance has been begun to understand better day by day, are rapidly contaminated as results of population growth, irregular urbanization, industrialization and agricultural activities. The Lake of (Bird) Manyas of Balıkesir, which is one of the most important wetlands protected with Ramsar Convention and hosts Bird Paradise National Park in is under the high pollution risks because of increasing industrial activities in its surrounding. Furthermore, in consequence of the lack of knowledge on the current pollution levels of the lake and the impact of industries on the lake, the management plans prepared to lake protection cannot be got in the act and not be executed in a seriously. For this reason, by determining the general state of the lake, taking of measures to minimize pollution and ensuring of sustainability of the ecosystem is of great importance. In this study, to determine pollution level of the Manyas Lake and sectoral effects on, in addition to conventional parameters, other pollution parameters determined by considering of the lake stress elements were examined. In the monitoring stage, from the previously determined sampling points of the lake and streams, water and sediment samples were taken by manual sampling method and analysed to determine the type, amount and change of contaminants. Results obtained from the monitoring studies carried out in last four years compared with Water Pollution Control Regulations (WPCR) of Turkey. It was concluded that the main pollution parameters of the lake were determined as DO, COD, NO₃, PO₄, B, Al, Zn. According to the specified pollutants, wastes from agricultural activities, mining activities, poultry farms and slaughterhouses mostly reach to the lake. It is concluded that these sectors are the major stress factors for the lake.

Keywords: Wetlands, Manyas Lake, Bird Paradise, Contaminants, Monitoring

1 INTRODUCTION

The wetlands can be describe as; "Natural or artificial, continuous or seasonal, drinkable, bitter or salty, calm or flowing water masses, marshes, peat bogs and sea water that not passing to six meter after tide of sea". The wetlands in the Mediterranean and its around are inlet, river delta, shore lagoon, lake, marshes and oasis, natural or artificial salty waters and dams [1]. The wetlands are ecosystems that have the highest biological variety after tropical forests. The wetlands that provide appropriate nourishment, reproduction, and accommodation media for the living creatures with rich variety, is not only rich museums of owner countries but also rich museums of the entire World [2].

The main reasons of the wetlands losses or damage in environmental quality level are that environmental property and services of wetlands do not take part in economical system. Therefore, to realize the sustainable usage of the natural sources like wetlands, it is necessary to evaluate the positive or negative directions of every operation to be applied to this type sources in respect to community comfort [3]. The wetlands are under threat due to humane usage. The some of factors causing species loss and ecosystem destruction are; spoil of water quality due to pollution causing from agricultural, municipal and industrial wastes, construction of dams on wetlands, changing of direction and extreme water supply, extreme fish hunting, pulling water plants and burning the reed beds [4]. Turkey is assumed as the most important country in Europe and Middle East in respect to wetlands due to geographical and climate conditions. Turkey has about 300 wetlands that have totally two million hectare area. Of them, it is established that 135 piece has international importance [5].

The lake of Manyas comprise 20.400 hectare field that formed around the lake and its surroundings. The most important and rich region of the lake is the delta forming by Sığircı Delta and Manyas Stream. The 64 hectare delta that is formed by Sığircı Stream is declared as the National Park at 1959, 25.000 hectare field containing the lake and near surroundings is declared as Wild Life Protection Field at 1977 and the National Park and its surroundings are declared as first degree natural protection field at 1981. According to 2873 counted National Park law, the Bird Paradise is the unique natural sources that has simultaneously "Natural Protection Field" and "Wild Life Protection Field" properties. Together with becoming side of Turkey to Ramsar Agreement, firstly 10.200 hectare field and then the whole of the lake were included to Ramsar Agreement at 1998 [6]. The reed bed field where the Sığircı Stream comes together with the lake was taken to protection at 1959 as "Bird Paradise National Park". As Manyas is known as the first Bird Paradise field in Turkey has pioneered to known of wetlands, nature and birds. The lake of Manyas is rich in respect to water products and it has 23 different fish types. In addition, at the lake and its

¹Corresponding author: Balıkesir University, Department of Environmental Engineering, 10145, Çağış/Balıkesir, Turkey.
eozen@balikesir.edu.tr

surrounding, there are 266 different bird types have been determined and some are birds that their generation has come to an end [7].

The lake of Manyas is located in the border of Balıkesir City and Manyas District, at south of Marmara Sea and in a graben going over between Biga Peninsula and Ulu mountain. The average surface area of the lake of Manyas is 200 km² and at summer seasons this value decreases. The length and width of the lake are 20 km and 14 km, respectively and the lake has inclined shape. The lake has 14 km height from sea level and exhibits shallow property. The lake is nourished by Kocaçay and Sığırcı Streams. In addition, Dutludere, Köydere and other small several streams nourish the lake of Manyas. The extra water of the lake is transferred to Susurluk Stream by Karadere Stream [8].

In this study, the parameters causing stress on the Lake of Manyas that is important for Turkey were determined. In the samples taken from streams and the lake, DO, COD, NO₃, PO₄, B, Al, Zn analysis were done. The contaminating levels and seasonal changes of the parameters were examined. The pollutant sources and solution suggestions for decreasing of pollutants were taken hand



Figure 1. (a) Lake of Manyas on Turkey Map

(b) Lake Of Manyas (Bird Paradise)

2 MATERIALS AND METHODS

2.1 Sampling Points

Geographical location of the Lake of Manyas has 40° 11' 36" the North and 27° 58' 0" the East coordinates. Sea height changes between 14.5-17.5 meter based on water level. To determine the water quality in the Lake of Manyas, the water samples from the predetermined points was taken and their analysis were done. To determine the seasonal change of pollutants, samples were taken at rainless and rainy periods. While selecting the sampling points, the points that well represent the whole water sources were selected.

The volume of the Lake of Manyas is 800 million m³. The water sources feeding the lake is Kocaçay (74%) and other streams and rainfall. The big portion of water reaches from Karadere to Susurluk Stream and spills to Marmara Sea [8]. Therefore, samples were taken from Sığircı Stream, Kocaçay, Mürvetler Stream that feed the lake and from Karadere that is onique water exiting points from the lake. The sampling points are shown in Figure 2.

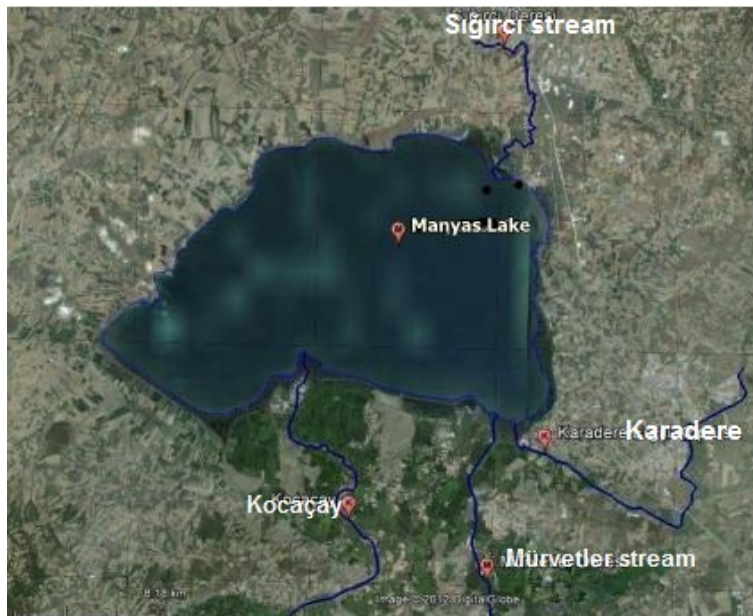


Figure 2. Sampling Points

While the water is being sampled, these criterions are taken into consideration; sampling points were determined at enough number so that they represent the water quality in sampling regions and characterize the water quality change. The waters entering the lake and exiting from the lake were taken into consideration, in addition, at least one sampling from interior of the lake was done. While samplings were being done interior of the lake, the points at which water flows and complete mixing occurs, were selected. At streams, after last discharge point, the samplings were done at points at which the water is fluid water and is near to the lake.

2.2 Analysis

The taken samples were protected by appropriate chemicals and stored at $t \leq +4^{\circ}\text{C}$ and the chemical using for protecting water is used according to parameter that would be analyzed. pH and dissolved oxygen measurements were done timely. In our laboratory, COD, NO₃, PO₄, B, Al, Zn analysis were done. On the other hand, the analysis results belonging to past years were taken evaluation. All analysis were conducted based on Standard Methods [9].

3 RESULTS AND DISCUSSION

3.1 Analysis Results and Quality Classification

Description of water quality is made by Continent Interior Surface Waters Classification of Surface Water Quality Control Regulation. Four main water quality classes (I- IV) that take part here, have been described with 45 parameters. The waters belonging to class I is the waters which can be used for drinking and daily usage without any treatment and only should be disinfected. The waters belonging to class II is the waters which can be used as drinking and daily usage after treatment. The waters belonging to class (III) is the waters which can be used in the industries (except food, textile industries) for industrial water supply and cannot be used as drinking and use water. The waters belonging to class (IV) is low quality waters from class (III) and by a treatment they are usable surface waters [10].

The classification of the studied water sources according to Continent Interior Surface Waters Classification is given in the below Tables. In these tables, the I, II, III, and IV quality waters are indicated as green yellow, orange and red colours, respectively.

Table 11. Analysis Results for Lake of Manyas

LAKE OF MANYAS						
PARAMETER	UNIT	2012	2013	2014	2015	2016
TEMPERATURE	(°C)	15,3	10,5	8,7	8,6	17
pH		9,45	9,26	8,52	8,08	8,75
DO	mg/L	7,23	7,28	-	-	12,66
BOD	mg/L	5	0	-	-	5
COD	mg/L	19	58	56	34	48,03
NITRATE	mg/L	1,7	4,52	25,37	1,3	-
PHOSPHATE	mg/L	-	0,1293	0,16	0,03	0,017
COPPER	(µg/L)	1,55	0,282	0,003	0	<5,9
LEAD	(µg/L)	0,24	0,014	0,006	0	<6,5
MANGANESE	(µg/L)	-	0,041	0,08	-	-
IRON	(µg/L)	1,86	0,167	1,147	0,03	<4,1
ZINC	(µg/L)	1,59	0,17	-	0,48	<3,9

Table 2. Analysis Results for Kocaçay

KOCAÇAY						
PARAMETER	UNIT	2012	2013	2014	2015	2016
TEMPERATURE	(°C)	16	12,2	8,7	12,1	18
pH		8,3	7,77	7,58	7,82	8,73
DO	mg/L	5,79	6,46	-	-	12,44
BOD	mg/L	2,5	0,2	-	-	5
COD	mg/L	4,77	16	10	17,82	49,755
NITRATE	mg/L	2,3	10,54	10,32	6,6	-
PHOSPHATE	mg/L	-	0,298	0,1	0,13	0,07
COPPER	(µg/L)	1,36	0,020	0,001	158,8	<5,9
LEAD	(µg/L)	0,96	0	0,005	23,76	<6,5
MANGANESE	(µg/L)	-	0,144	0,167	-	-
IRON	(µg/L)	1,71	0,230	0,288	153,4	<4,1
ZINC	(µg/L)	<0,43	0	-	23,7	<3,9

Table 3. Analysis Results for Mürvetler Stream

MÜRVELLER STREAM						
PARAMETER	UNIT	2012	2013	2014	2015	2016

TEMPERATURE	(°C)	16,6	11,7	8,4	9,8	12,7
pH		8,45	8,29	7,5	8,06	7,51
DO	mg/L	8,75	6,8	-	-	8,62
BOD	mg/L	3,1	0,4	-	-	3
COD	mg/L	5,57	4	8	31,16	45,39
NITRATE	mg/L	3,2	2,9	12,64	2,9	-
PHOSPHATE	mg/L	-	0,496	0,2	0,24	0,135
COPPER	(µg/L)	1,09	0,017	0,003	495,2	<5,9
LEAD	(µg/L)	0,35	0,004	0,001	2,3	<6,5
MANGANESE	(µg/L)	-	0,051	0,022	-	-
IRON	(µg/L)	1,71	0,256	0,201	86,9	<4,1
ZINC	(µg/L)	<0,43	0	-	1	<3,9

Table 4. Analysis Results for Karadere

KARADERE						
PARAMETER	UNIT	2012	2013	2014	2015	2016
TEMPERATURE	(°C)	20,5	11	8,2	9,37	16
pH		8,19	8,5	7,15	7,7	9,2
DO	mg/L	9,38	7,46	-	-	6,55
BOD	mg/L	7,6	0,3	-	-	5
COD	mg/L	11,95	18	22	10,72	28,82
NITRATE	mg/L	11,3	2,12	9,78	1,2	-
PHOSPHATE	mg/L	-	0,193	0,15	0,05	0,041
COPPER	(µg/L)	1,62	-	0,001	432,6	<5,9
LEAD	(µg/L)	0,78	-	0,003	7,1	<6,5
MANGANESE	(µg/L)	-	-	0,217	-	-
IRON	(µg/L)	1,71	-	0,455	232,4	<4,1
ZINC	(µg/L)	<0,43	-	-	8,1	<3,9

Table 5. Analysis Results for Siđirci Stream

SIĐIRCI STREAM						
PARAMETER	UNIT	2012	2013	2014	2015	2016
TEMPERATURE	(°C)	24	11,3	8,3	8,9	17,8
pH		7,66	7,93	7,42	8,6	8,72

DO	mg/L	5,63	4,45	-	-	12,52
BOD	mg/L	25,8	0	-	-	6
COD	mg/L	39,2	12	46	23,16	50,915
NITRATE	mg/L	5,3	6,44	56,73	7,7	-
PHOSPHATE	mg/L	-	0,885	1,03	0,76	0,022
COPPER	(µg/L)	2,15	0,094	0,002	194,8	<5,9
LEAD	(µg/L)	1,4	0,006	0,002	0,3	<6,5
MANGANESE	(µg/L)	-	0,314	0,316	-	-
IRON	(µg/L)	1,71	0,288	0,267	341,6	<4,1
ZİNC	(µg/L)	<0,43	0,593	-	11,6	<3,9

When compared the Sığircı Stream with other streams, it is seen that the organic load of the Sığircı Stream is higher than other streams. Especially, the reason of high COD and BOD levels at 2007 and 2008 years is related with the rainless years.

The agricultural industries and hen slaughters located at the north regions of Bandırma District are the main reason of organic pollution in the Sığircı Stream. In addition, the municipal wastewaters of the vicinity villages are the other reason of the organic pollution in the Sığircı Stream.

The lake waters is belonging to (II) and (III) classification according to BOD parameter and belonging to (I) and (II) classification according to COD parameter. If it is thought that the Sığircı Stream is responsible for 3% of water feeding the lake, it is seen that Sığircı Stream is important for the lake.

It is clear from the analysis results of Mürvetler Stream that its water quality is not of problematic contaminants for the Lake of Manyas. The reason of this is that there is not any industrial activity and discharge of municipal wastewater to Mürvetler Stream. This has provided that the Mürvetler Streams remains over as clean when compared the other streams. The other water supplier of the lake, Kocaçay Stream, is the clean water source for the lake like Mürvetler Stream except heavy metal pollution.

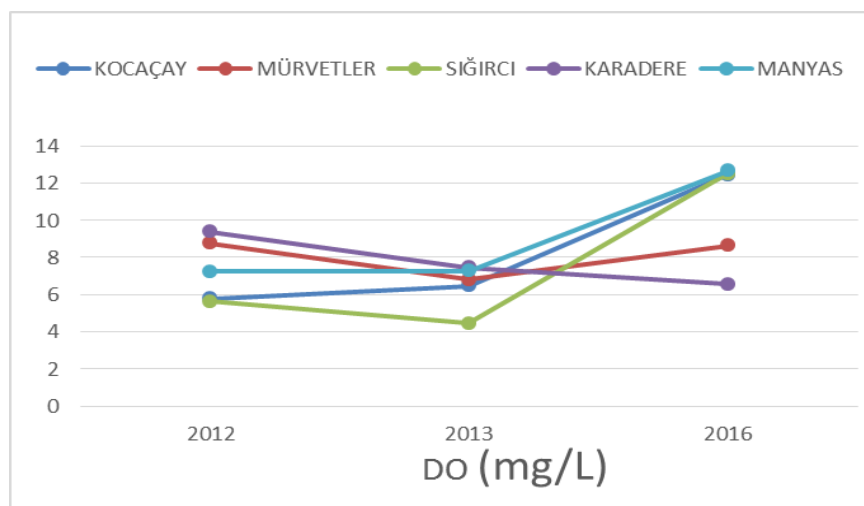


Figure 3. DO concentration changes based on years

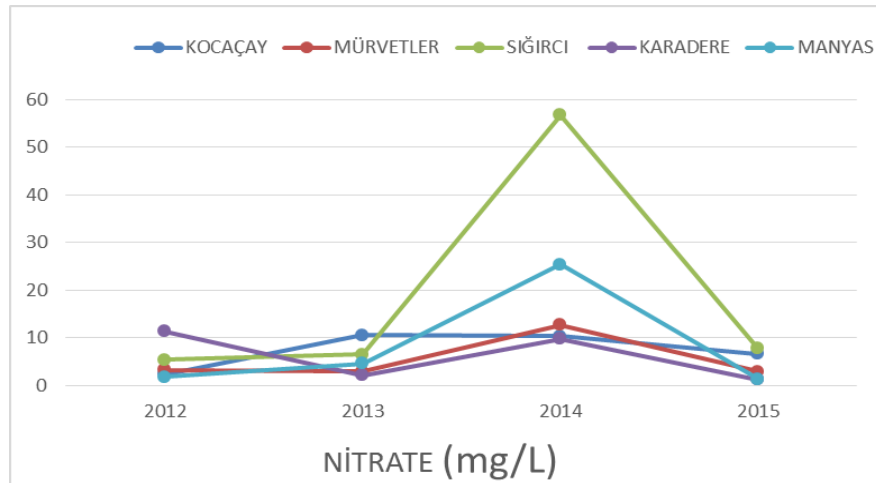


Figure 4. Nitrate concentration changes based on years

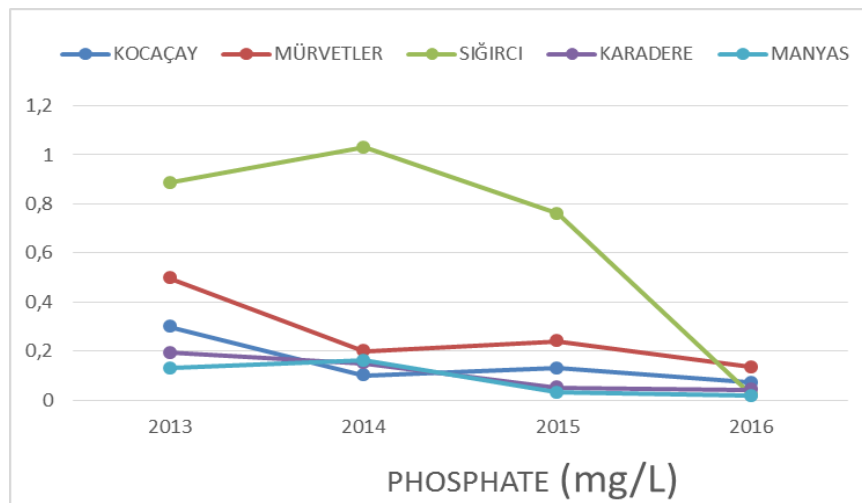


Figure 5. Phosphate concentration changes based on years

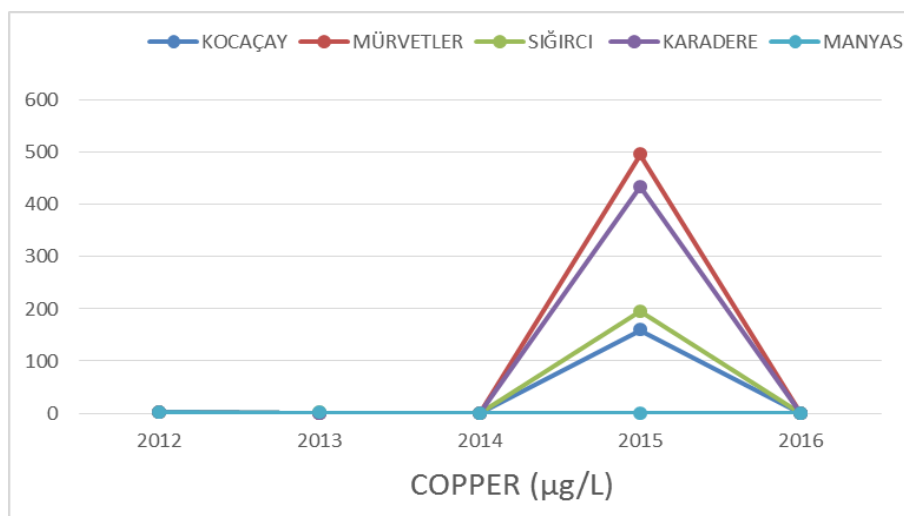


Figure 6. Copper concentration changes based on years

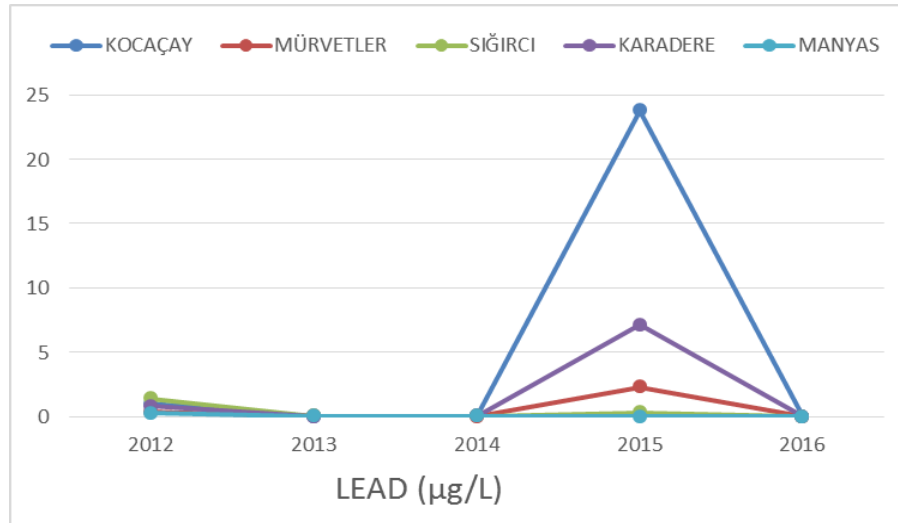


Figure 7. Lead concentration changes based on years

4 CONCLUSIONS

For the aim of prevention of pollution of the Lake of Manyas that is important natural source of Turkey, some precautions should be taken. These precautions can be summarized as follows:

- The industries in the lake regions must build the treatment systems and their operations should be controlled in respect to whether they are properly operated or not. When the treatment systems are not operated, strict sanction should be applied.
- The municipal wastewaters from houses around the lake should be treated.
- The water quality should be monitored by continuous monitoring devices at appropriated points and thus the controls will become continual.
- The flotation wastes which exist in the flood beds of Kocaçay and the stream connected to it should be collected from that region. Thus, the heavy metal transmigration to the lake is prevented. At the same time, these wastes are economically valuable wastes as they are rich in zinc and lead.
- The alternatives that reduce the artificial fertilizer use and enable to use of mechanical agricultural struggle methods should be investigated and applied.

ACKNOWLEDGMENT

The authors are grateful for the financial support of the Balıkesir University Scientific Research Project Department (Project No: 2012/105)

REFERENCES

- [1] (2016) Doğa Koruma Derneği website. [Online]. Available: <http://dogakorumaderneği.org/index.php/component/content/article/47-biocesitlilik/102-sulak-alanlar>
- [2] Su Dünyası Dergisi,91.Sayı DSİ, 2011
- [3] S. Gürlük, "Manyas Gölü ve Kuş Cenneti'nin çevresel değerlemesi üzerine bir araştırma," Phd. thesis, Uludağ Üniversitesi, Bursa, Türkiye, 2006.
- [4] (2016)Orman Su İşleri Bakanlığı website. [Online]. Available: <http://bolge9.ormansu.gov.tr/9bolge/AnaSayfa/faliyetlerimiz/sulakalanlar.aspx?sflang=tr>
- [5] "Kuş (Manyas) Gölü Sulak alan Yönetim Planı 2011-2015," Orman ve Su İşleri Bakanlığı, 2012.
- [6] N. Dalkılıç, "Manyas (Kuş) Gölü Doğal Çevre Sorunları," M. Eng. Thesis, Ankara Üniversitesi, Ankara, Türkiye, 2000.
- [7] Sulak Alanlar Kitabı, Orman ve Su İşleri Bakanlığı, Doğa Koruma ve Milli Parklar Genel Müdürlüğü, Ankara, 2013.
- [8] B. Hoşcan, "Tarımsal Kullanımlar Yönünden Kuş (Manyas) Gölü Su Kalitesi," M. Eng. Thesis, Ankara Üniversitesi, Ankara, Türkiye, 1990.
- [9] *Standart Methods for Examination of Water and Wastewater*, American Public Health Association (APHA), 17th ed, Washington, DC, 1992.
- [10] *Yüzeysel Su Kalitesi Yönetimi Yönetmeliği*, Orman ve Su İşleri Bakanlığı, Sayı : 28483, Ankara, 2012.

Computational Investigation of A Gas Cooled, Full Vacuum and Magnetic Beared Flywheel Energy Storage System in Respect of Energy Storage Capability and Efficiency

Metin Varan¹

Abstract

Much of the increase in the developing world's energy use sources from growing population and emerging technological advances. That increases interests for importance of electricity generation and storage technologies. In this context, using the Flywheel Energy Storage Systems to meet energy storage needs and support power systems become familiar and their usage in energy management practices have been spreading day by day. FESS has been used in many areas such as integration of renewable generation, traction systems, industrial applications, energy management systems. Like other energy storage systems, FESS also has fundamental dynamics that affect on energy storage capability and efficiency. In this study, a computational investigation has been held on gas cooled, full vacuum and magnetic beared flywheel energy storage system in respect of storage capability and efficiency. Computational investigation argues that losses about increased thermal stress, rotor loss, self-discharge of FESS in regard of vacuum rate cooling-heat transfer rate, effects of magnetic bearing. To reduce these losses, and to get high power density and energy efficiency, optimal conditions (vacuum ratio, thermal management, etc.) of FESS have been revealed by computational comparisons. Results highlight those critical considerations about design principles of highly efficient FESS technologies.

Keywords: FESS, Computational investigation, Magnetic Beared Flywheel, Gas Cooling, Full Vacuum

1 INTRODUCTION

Flywheel is a device that stores kinetic energy with accelerating a heavy cylindrical mass (flywheel) using an electric motor. For electricity generation flywheel uses kinetical energy stored in electric motor for driving a generator. Motor/generator sets, DC machines and induction machines are used for energy conversion. The amount of energy stored in a flywheel is proportional to the square of angular velocity and to its inertia for a given design stress.

FES systems and electrochemical batteries can be designed to have comparable energy storage capacities. But, FES systems offer bulky-volume of energy discharge rates which are considerably higher than in comparable electrochemical battery systems. This characteristic makes FES systems attractive for certain applications. Table-1 shows energy storage characteristic and benefits of FES systems.

Table 1. Flywheel Energy Storage Characteristics and Benefits

Energy Storage Characteristic	Benefits
5 to 10+ times greater specific energy	Lower mass
Long life (15 yr.)	Reduced logistics, maintenance, life cycle costs and enhanced vehicle integration
85-95% round-trip efficiency compared with < 70-80% for battery sys.	More usable power, lower thermal loads,
High charge/discharge rates & no taper charge required	Peak load capability, 5-10% smaller solar array
Deterministic state-of-charge	Improved operability
Inh. bus regulation and power shunt cap.	Fewer regulators needed

The energy storage technologies have their own advantages and disadvantages but the following advantages make flywheels a viable alternative to other energy storage systems[1]:

- Low cost
- High power density

¹ Corresponding author: Asst. Prof. Dr., Sakarya Univ. Faculty of Technology - Department of Electrical and Electronics Engineering.,
mvaran@sakarya.edu.tr

- Ruggedness
- Greater number of charge discharge cycles
- Longer life
- Less maintenance
- Environmental friendly
- Fast response during energy release

FESS are especially well-suited to several applications including electric service power quality and reliability[2], ride-through while gen-sets start-up for longer term backup, area regulation, fast area regulation and frequency response[3]. FESS may also be valuable as a subsystem in hybrid vehicles that stop and start frequently as a component of track-side or on-board regenerative braking systems.

An example of a commercial flywheel energy storage system is shown in Figure 1. The installation of clusters of FES units provides for power capacity in the megawatt-level, which enables electrical utilities to perform fast-response regulation of the grid frequency. FES technology lends itself to a range of similar applications, such as peak power support in off-grid industrial systems and energy supply management infrastructure involving renewable energy sources (wind and solar power)[4].

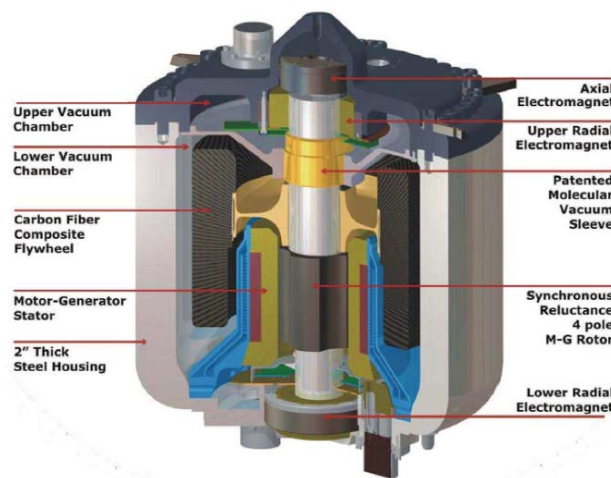


Figure 1. Illustration of a commercial flywheel energy storage system (courtesy of POWERTHRU, Livonia, MI, USA - www.power-thru.com)

Flywheels are traditionally made of steel and rotate on conventional bearings; these are generally limited to a revolution rate of a few thousand rpms. This is because of friction and material integrity. Most of energy is lost in overcoming frictional losses. By development of technological advances on the use of high-strength composite materials, the new generation flywheels have been designed. These flywheels can store more energy at higher speeds for a given mass than a metallic flywheel. It was after this breakthrough that engineers thought of using a composite flywheel energy storage system for electric vehicles and stationary power backup [5].

Modern commercial flywheel energy storage systems are supported by a bearing system for rotation inside an evacuated container. Modern flywheels are made of carbon fiber materials, stored in vacuums to reduce drag, and employ magnetic bearings, enabling them to revolve at speeds up to 60,000 rpms [6].

At studied flywheel system, a brushless motor and generator are coupled to the flywheel for accelerating and decelerating the flywheel for storing and retrieving energy. The system includes a heat energy transfer system that passively cools the stator by heat transfer from the stator to a gas coolant- full vacuum surrounding the coils and in intimate contact with the conductors in the coils. The full vacuum coolant limits the maximum temperature of the coils during discharging of the flywheel power source.

2 MODELLING OF FLYWHEEL ENERGY STORAGE SYSTEM (MOFESS)

The wheel is energy storage component of a FESS. The energy stored in a basic cylindrical wheel is determined as follows;

$$E = \frac{1}{2} I \cdot \omega^2 \quad [1]$$

where, I is inertia

$I = m \cdot r^2$ is inertia for thin walled cylindrical shape and $I = \frac{1}{2} m (r_1^2 + r_2^2)$ is for thick walled cylindrical shape respectively. Here m is mass, r is radius of thin walled cylinder, ω is rotation speed and r_0 and r_i are outer and inner radius of thick walled cylinder. The moment of inertia is a physical quantity, which depends on the mass and shape of the flywheel. It is defined as the integral of the square of the distance 'x' from the axis of rotation to the differential mass dm_x .

$$I = \int X^2 dm_x \quad [2]$$

Hence, it can be written as below;

$$E = \frac{1}{2} m (r_1^2 + r_2^2) \cdot \omega^2 \quad [3]$$

Because of the energy stored is proportional to the square of angular velocity, increasing the angular speed increases stored energy more effectively than increasing mass. On the other hand, increasing angular speeds result in increased frictional losses and hence thermal problems. With the help of magnetic bearing technology, the frictional losses due to bearings can be overcome, but at the expense of reliability.

The stored energy can also be expressed in terms of peripheral velocity 'v' that is expressed as the times of perpendicular distance from the axis of rotation and angular speed:

$$v = r \cdot \omega^2 \quad [4]$$

The tensile strength, ' σ ' of the material limits the peripheral velocity, and hence the amount of energy stored. For a mass density ' ρ ', the tensile strength is defined as:

$$\sigma = \rho \cdot v^2 \quad [5]$$

The volume energy density, 'Ev', is obtained by substituting 'm' in the stored energy equation, as the product of volume and the mass density:

$$Ev = \frac{1}{2} \rho (r_1^2 + r_2^2) \cdot \omega^2 \quad [6]$$

Therefore, if the dimensions are fixed, the maximum energy stored per volume 'Evmax' depends on the tensile strength of the material as:

$$Ev_{max} = \frac{1}{2} \sigma_{max} \quad [7]$$

where ' σ_{max} ' is the maximum tensile strength of the flywheel material. Similarly the maximum energy stored per mass 'E' is

$$Em_{max} = \frac{1}{2} \frac{\sigma_{max}}{\rho} \quad [8]$$

Therefore, the maximum energy storage capacity can be achieved by using a material with a low density and high tensile strength.

The energy density expressions above apply for a simple rim type flywheel. There are many designs for flywheels, and the general expression of maximum energy stored per mass is:

$$Em_{max} = K \frac{\sigma_{max}}{\rho} \quad [9]$$

where 'K' is defined as the flywheel shape factor, which depends on the geometry of the flywheel. The flywheel shape factors for several different types of flywheels are given in Table 2.

Table 2. Flywheel Shape Description and Shape Factors

Flywheel Shape Description	Shape Factor (K)
Constant stress disc	0.931
Constant thickness disc	0.606
Thin rim	0.500
Constant stress bar	0.500
Rod or circular brush	0.333
Flat pierced disc	0.305

The value of 'K' is obtained from the Equation-2 for the moment of inertia . The stress distribution in a flywheel due to centrifugal loading becomes complex for shape factors greater than 0.5, and a detailed analysis needs to be done to safely achieve it. For low speed flywheels, the best way to maximize stored energy is by increasing moment of inertia. A massive rim or disc made of high density material such as cast iron or steel is sufficient in these cases. The main advantages of low speed flywheels are that they use a well-established technology and they are cheaper to build[2].

3 PERFORMANCES OF ENERGY STORAGE CAPABILITY AND EFFICIENCY FOR PROPOSED FLYWHEEL ENERGY STORAGE SYSTEM

Proposed FESS has been analyzed in respect of gas cooled, full vacuum and magnetic bearing properties. Proposed system is supported by a bearing system for rotation inside an evacuated container. The system includes a heat energy transfer system that passively cools the stator by heat transfer from the stator to a gas coolant- full vacuum surrounding the coils and in intimate contact with the conductors in the coils. The coolant- full vacuum coolant limits the maximum temperature of the coils during discharging of the flywheel power source.

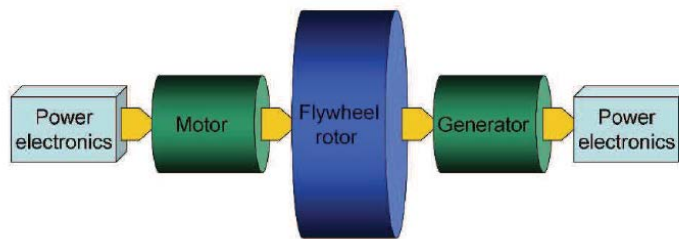


Figure-2 Sketch for power flow in a FES system

Figure-2 shows power flow in mentioned FES system. During working process, switching losses occur in the power electronics controller, iron and copper losses occur in the motor and friction and windage losses occur in the rotating parts. As the power and speed terms are not constant, these losses are variable and are function of the speed and the power.

3.1 Temperature Rise

The heat generated in the rotor of motor/generator will dissipate only through radiation in vacuum. Energy radiated per second is given by Stefan-Boltzmann of radiation as;

$$H = \epsilon \cdot s \cdot A \cdot T^4 \quad [10]$$

Where

ϵ is emissivity (0-1),

s is Stefan-Boltzmann constant ($5.67 \times 10^{-8} \text{ J/s.m}^2.\text{K}^4$)

A is surface area of object

T is temperature in Kelvin.

The relation of the established heat and temperature-rise can be given as;

Rate of Heat Developed = Rate of Temperature Rise of Rotor Body + Heat Dissipated through Radiation

$$P_{\text{rotor-loss}} = \frac{mc\Delta t}{dt} + \epsilon \cdot s \cdot A \cdot (T_f^4 - T_0^4) \quad [11]$$

m is mass of rotor body

c is specific heat coefficient of the rotor material

$\Delta t/dt$ is rate of temperature rise

T_f is final steady-state temperature of rotor in Kelvin.

T_0 is ambient temperature in Kelvin.

The steady state flywheel temperature is determined by the windage losses and the heat transfer in the vacuum environment. The primary components of heat transfer from the wheel to the surroundings are convection and radiation[7].

The windage loss and flywheel temperature can be controlled by the vacuum level in the containment. Both will be unacceptably high if the vacuum level is not deep enough. This can be illustrated by a parametric study to this subject.

In this study “*EMAFER: Electro Mechanical Accumulator For Energy Reuse*” calculation model has been assembled to predict the power dissipated in fluid friction and the steady state temperature of a circle cylindrical flywheel [8]. By varying the parameters which describe the flywheel system (energy density, diameter/height ratio, storage capacity and vacuum pressure), important trends in the scaling of the windage loss and the flywheel temperature were discerned:

- Windage loss and flywheel temperature increase substantially with pressure.
- Windage loss and flywheel temperature increase with energy density, but decrease with mass density. This behaviour strongly penalizes high energy density, composite flywheels in comparison to steel flywheels. Composite flywheels are the more critical so as their high temperature behaviour is poor.
- For equal energy per mass, the temperature of aramid and steel flywheels are about equal; the losses with aramid flywheels are approximately twice those with steel flywheels.
- If the temperature of a composite flywheel is within acceptable limits, the windage loss is also acceptable.
- The windage loss shows a modest dependance on flywheel diameter/height ratio,for which reasons flywheels may be designed for bearing and packaging constraints without incurring a large penalty loss.

Active magnetic bearings are not considered because of their complexity, costs and low force density. As a passive bearing, magnet bearings are attractive in combination with rolling element bearings for load reduction of the last ones. The recent development of autostable magnetic bearings with superconducting materials may be interesting for the future as these bearings are self centering without requiring an active control system [9]. The bearing system of studied FESS is based on *EMAFER* high precision angular contact ball bearings[8]. At *EMAFER* design, the bearings are directly mounted on the stator journals. The lower bearing is fixed on the stator journal whereas the upper bearing is mounted on a sliding sleeve which is supported via O-rings on the stator journal. This sliding sleeve is hydraulically pressed for preloading the bearings and provides compensation of elongation differences due to thermal expansion and centrifugal load. Machine can be loaded both axially and radially and are in general the most common approach for high speed machinery.

High speed and full-vacuum rotating machinery, such as a flywheel system, is always a potential source of danger. Therefore, a safety factor which limits the amount of stored energy available for discharge should be considered [3]. When this is considered, the useful energy stored per mass is given by:

$$E_m = (1 - S^2)K \frac{\sigma}{\rho} [12]$$

where ‘S’ is the ratio of minimum to maximum operating speed, it is set at 0.35 with full vacuum and magnetic beared model. At that situation the maximum amount of energy stored doesn’t depend directly on inertia or on the angular velocity, since either of these can be chosen independently to obtain the required design stress.

Table 3. Comparison of Useful Energies with Different Rotor Materials

Material	Density(10^3 kg/m ³)	Useful Energy(10^3 J/kg)	Flywheel Mass(10^3 kg)
Wood birch	0.55	27.16	1720
Mild steel	7.80	38.15	1220
S-Glass	1.90	90.73	509
Maraging steel	8.00	111.74	417
Carbon 60% fibre	1.55	239.78	194
Kevlar 60% fibre	1.40	354.76	131

For high-speed applications, small discs with a constant stress profile, built with a low density and high strength materials, are better for maximizing useful energy density. The most commonly used composite material is Kevlar, a plastic material reinforced with glass, carbon or aramid fibers.

4 CONCLUSION

Modern commercial flywheel energy storage systems are supported by a bearing system for rotation inside an evacuated container. Modern flywheels are made of carbon fiber materials, stored in vacuums to reduce drag, and employ magnetic bearings, enabling them to revolve at speeds up to 60.000 rpms. The windage loss and flywheel temperature can be controlled by the vacuum level in the containment. Both will be unacceptably high if the vacuum level is not deep enough.

At studied flywheel system, a brushless motor and generator are coupled to the flywheel for accelerating and decelerating the flywheel for storing and retrieving energy. The system includes a heat energy transfer system that passively cools the stator by heat transfer from the stator to a gas coolant- full vacuum surrounding the coils and in intimate contact with the conductors in the coils. The coolant- full vacuum coolant limits the maximum temperature of the coils during discharging of the flywheel power source.

Depending on the application, either volume energy density or mass energy density takes precedence during the design stage. Composite materials such as carbon fiber have desired properties and result in a lightweight wheel that

operate at high rotation speed or have a large radius. High speed flywheels offer distinct advantages, such as high power density, compact design, very high energy efficiency, very low heat output, extremely high uptime availability and exceptionally infrequent low-cost maintenance.

Due to the dependence of energy storage both mass and speed, it is inevitable that high bearing loss will occur. If materials with high strength to weight ratios are used this loss can be reduced. To increase the rotational speed of a compact flywheel energy storage system superconducting magnetic bearings (SMB) and permanent magnet bearings (PMB) have been used.

ACKNOWLEDGMENT

This work is supported in part by the Scientific Research Support Program Fund in Sakarya University with grant-number: 2014-50-01-041 (http://www.eee.sakarya.edu.tr/tr/arastirma_projeleri.)

REFERENCES

- [1] Brown, D. R. & Chvala, W. D. (2005). Flywheel energy storage: An alternative to batteries for UPS systems, *Energy Engineering: Journal of the Association of Energy Engineering* 102(5): 7–26.
- [2] Bornemann, H. J. & Sander, M. (1997). Conceptual system design of a 5 mwh/100 m w superconducting flywheel energy storage plant for power utility applications, *IEEE Transactions on Applied Superconductivity* 7(2 PART 1): 398–401.
- [3] Tarrant, C. (1999). Revolutionary flywheel energy storage system for quality power, *Power Engineering Journal* 13(3): 159–163.
- [4] Malte Krack, Marc Secanell and Pierre Mertiny (2011). Rotor Design for High-Speed Flywheel Energy Storage Systems, *Energy Storage in the Emerging Era of Smart Grids*, Prof. Rosario Carbone (Ed.) Genta, Kinetic Energy Storage-Theory and practice of advanced flywheel systems, chapter 3, Butterworths, 1985, London.
- [5] A., Coppa, Design and fabrication of containment rings for use in tests of six prototype flywheel rotors, General Electric Company, Energy systems program department, Report prepared for Lawrence Livermore Laboratory, subcontract 6624409, February 1981.
- [6] L., Lawson, Design and Testing of High Energy Density Flywheels for Application to Flywheel/Heat Engine Hybrid Vehicle Drive, IECEC 1971, paper 719150, pp 1142-1150.
- [7] F.J.M. Thoolen, Development of An Advanced High Speed Flywheel Energy Storage System, 1993, pp.78-82, Netherlands.
- [8] Me Michael, C. et al, Practical adaptation in bulk superconducting magnetic bearing applications., *Appl. Phys. Lett.* 60 (15), 13 April 1992.

Analysis of the Relationship between the Aircraft Performance Parameters and the EGT Parameter by Using Multiple Regression Analysis

Mustagime Tulin Yildirim¹, Bulent Kurt²

Abstract

In literature, there are lots of methods for using aircraft engine performance analysis. In all of these methods, observing the Exhaust Gas Temperature-EGT parameter has very important situation. In this study by using multiple regression analysis, data of aircraft is analyzed and the relationship between the flight performance parameters and EGT parameters are evaluated. The results of the analysis show that the flight parameters of aircraft (like N1, N2, altitude, air speed, ground speed, pitch, AOA (angle of attack), roll, heading, vertical acceleration, latitude acceleration, longitude acceleration, speed break, TAT (true air temperature), air/ground flight performance parameters) and EGT parameters have meaningful relationship. The results of this study are used as a pre-study for the aircraft online failure estimation model.

Keywords: Flight performance parameters, EGT parameters, multiple regression analysis.

1 INTRODUCTION

Maintenance has great importance in aviation sector. To maintain “Airworthiness Directives”, airway companies obey the aviation authorities’ regulations and make periodic maintenance for their aircrafts. During the maintenance all aircraft components are removed and checked by aircraft technician; airframe materials are tested for material fatigue test, engines and its components are checked and tested, aircraft flight data are evaluated offline, recording data during the engine tests are evaluated for engine life usage and health management, etc. Exhaust gas temperature -EGT- parameter is an engine parameter and it shows engine exhaust gas temperature. If EGT value is high, it causes more deterioration and erosion in engine. Exceeding the EGT limit can cause reducing the life usage of engine components. Because of this, it is important to make EGT value low. It is very useful parameter to decide engine health, life usage and maintenance type. In literature there are lots of studies about engine health monitoring that studies observe the EGT value with different methods. Some of them uses artificial neural network, some of them uses fuzzy logic, some of them uses genetic algorithm and sometimes they use hybrid of this methods [1-7].

In this study we investigate the relationship between aircraft performance parameters and EGT parameter, by using multiple regression analysis. Specifying this relationship is very important. By using results of the analysis of the relationship between the aircraft performance parameters (like N1, N2, altitude, air speed, ground speed, pitch, AOA (angle of attack), roll, heading, vertical acceleration, latitude acceleration, longitude acceleration, speed break, TAT (true air temperature), air/ground flight performance parameters) and EGT parameters, as pre-study, engine failure can be estimated without any expert knowledge by pilots. Now, we have one conference paper which used this study’s result and it is under evaluation process [8]. By using the result of this study, we can estimate engine failure with aircraft performance parameters.

2 METHOD

2.1 Purpose of the Study

In this study, we want to specify the relationship between some aircraft performance parameters and EGT parameter. For this purpose, we investigate the N1 speed, N2 speed, altitude, air speed, ground speed, pitch, AOA (Angle of Attack), roll, heading, vertical acceleration, latitude acceleration, longitude acceleration, speed break, TAT (True Air Temperature), air/ground parameters effect on the EGT parameter. Schematic illustration of this study is given in Figure 1.

¹Corresponding author: Erciyes University, Faculty of Aeronautics and Astronautics, Department of Aircraft Electrical and Electronics, 38039, Melikgazi/Kayseri, Turkey tulin@erciyes.edu.tr

²Erzincan University, Aircraft Technology Program, 24100, Erzincan, Turkey bkurt@erzincan.edu.tr

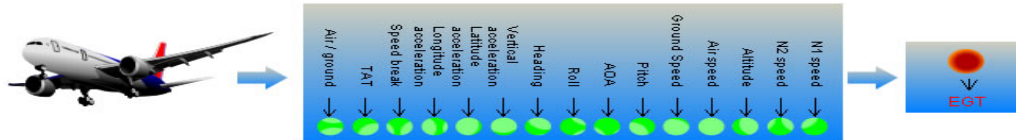


Figure1.Schematic illustration of this study

2.2 Hypothesis

H0: There is no N1 speed, N2 speed, altitude, air speed, ground speed, pitch, AOA (Angle of Attack), roll, heading, vertical acceleration, latitude acceleration, longitude acceleration, speed break, TAT (True Air Temperature), air/ground parameters effect on the EGT parameter.

H1: N1 speed, N2 speed, altitude, air speed, ground speed, pitch, AOA (Angle of Attack), roll, heading, vertical acceleration, latitude acceleration, longitude acceleration, speed break, TAT (True Air Temperature), air/ground parameters have meaningful effect on the EGT parameter.

2.3 Analysis of Data

For this study we have 19230 data which are N1 speed, N2 speed, altitude, air speed, ground speed, pitch, AOA (Angle of Attack), roll, heading, vertical acceleration, latitude acceleration, longitude acceleration, speed break, TAT (True Air Temperature), air/ground parameters and EGT parameter. 1282 of this data are used in SPSS 15 Program for analysis. In data analysis, multiple regression analysis method is used.

3 FINDINGS

For investigating the parameters effect the EGT parameter, multiple regression analysis method is used and the results of that analysis are given in Figure 2, Figure 3 and Figure 4. The results of the analysis between dependent variables and independent variables are given in Figure 2. Here, “Adjusted R Square” value shows the equation’s estimation power. Estimation power of this model is 94.2%.

Model	R	R Square	Adjusted R Square	Std. Error of the Estimate
1	,971 ^a	,943	,942	,0638133

a. Predictors: (Constant), GroundAir, Vertical_acceleration, Longitude_acceleration, Roll, Speed_break, Latitude_acceleration, AOA, Heading, TAT, Pitch, Airspeed, N2, altitude, N1, Groundspeed
b. Dependent Variable: EGT

Figure2.Spss programscreenshot

In Figure 3, it is seen that “Sig.” value is 0.000<0.05. This “Sig.” value shows, our model is meaningful model.

Model		Sum of Squares	df	Mean Square	F	Sig.
1	Regression	94,784	15	6,319	1551,745	,000 ^a
	Residual	5,774	1418	,004		
	Total	100,558	1433			

a. Predictors: (Constant), GroundAir, Vertical_acceleration, Longitude_acceleration, Roll, Speed_break, Latitude_acceleration, AOA, Heading, TAT, Pitch, Airspeed, N2, altitude, N1, Groundspeed
b. Dependent Variable: EGT

Figure3.Spss programscreenshot

In Figure 4, it is seen that “Airspeed” variable’s “Sig.” value is 0.148>0.05, “Ground_speed” variable’s “Sig.” value is 0.48>0.05 and “Heading” variable’s “Sig.” value is 0.983>0.05. These three values show these variables have no meaningful effect on the dependent variable EGT. From that table it is seen that other variables have meaningful effect on the dependent variable EGT. By using these results we obtained regression equation (mathematical equation of model) which is given in Equation (1).

$$EGT = -0,134 + 1,254 * N1_{speed} - 0,569 * N2_{speed} - 0,173 * Altitude + 0,454 * Pitch + 0,140 * AOA + 0,192 * Roll - 0,087 * Vertical_{acceleration} + 0,073 * Latitude_{acceleration} - 0,124 * Longitude_{acceleration} - 0,130 * Speed_{break} + 0,499 * TAT - 0,209 * GrounAir \quad (1)$$

Coefficients ^a						
Model		Unstandardized Coefficients		Standardized Coefficients	t	Sig.
		B	Std. Error	Beta		
1	(Constant)	-.134	.036		-3,746	.000
	N1	1,254	.050	1,593	25,020	.000
	N2	-.569	.056	-.597	-10,085	.000
	altitude	-.173	.055	-.258	-3,132	.002
	Airspeed	.104	.072	.127	1,447	.148
	Groundspeed	.085	.120	.104	.707	.480
	Pitch	.454	.029	.292	15,830	.000
	AOA	.140	.024	.091	5,924	.000
	Roll	.192	.023	.057	8,171	.000
	Heading	.000	.021	.000	-.021	.983
	Vertical_acceleration	-.087	.023	-.027	-3,838	.000
	Latitude_acceleration	.073	.028	.019	2,589	.010
	Longitude_acceleration	-.124	.053	-.064	-2,343	.019
	Speed_break	-.130	.038	-.048	-3,378	.001
	TAT	.499	.051	.392	9,722	.000
	GroundAir	-.209	.025	-.265	-8,374	.000

a. Dependent Variable: EGT

Figure4.Spss program screenprint

In Figure 5, comparison of Real EGT value (it is obtained from sensors) and the regression analysis model's EGT value are shown. In Figure 5, it is easily seen that two EGT values have similar react.

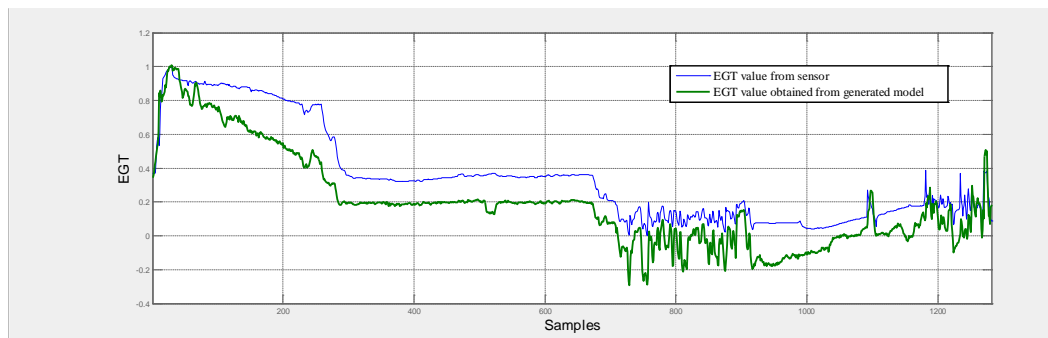


Figure5. Comparison of Real EGT value and the regression analysis model's EGT value

4 RESULTS

In this study it is specified that N1 speed, N2 speed, altitude, AOA (Angle of Attack), roll, vertical acceleration, latitude acceleration, longitude acceleration, speed break, TAT (True Air Temperature), air/ground parameters have meaningful effects on the EGT parameter.

Results of this study are used in another study which estimates the engine failure by using EGT parameter value.

BIOGRAPHY

Mustagime Tülin YILDIRIM was born in Adana. She graduated high school in Gaziantep Science College. She had BS, Ms and PhD degree from Erciyes University and PostDoc from TAMU (Texas A&M University). Her interesting areas are signal processing, artificial intelligence techniques and optimization methods. She is married and has 3 daughters.

REFERENCES

- [1] G.S.Anastassios, Engine condition monitoring and diagnostics, progress in gas turbine performance, Dr. Ernesto Benini, ISBN 978-953-51-1166-5, June 19, 2013.
- [2] C.Kong, "Review on advanced health monitoring methods for aero gas turbines using model based methods and artificial intelligent methods", Int'l J. of Aeronautical & Space Sci. 15(2), pp 123-137, 2014.
- [3] R.B.Joly, S.O.Togaji, R.Singh, and S.D.Probert, "Gas-turbine diagnostics using artificial neural-networks for a high bypass ratio military turbofan engine", Applied Energy, Volume 78, Issue 4, pp. 397-418, August 2004.

- [4] A.Pashayev, D.Askerov, C.Ardil, R.Sadiqov, and P.Abdullayev, "Identification of aircraft gas turbine engine's temperature condition", World Academy of Science, Engineering and Technology 2, pp. 356-364, 2007.
- [5] A.Babbar, V.L.Syrmos, E.M.Ortiz, M.M.Arita, "Advanced diagnostics and prognostics for engine health monitoring", 2009 IEEE Aerospace conference, 7-14 March 2009, pp. 1-10, Big Sky, MT.
- [6] A.R.Yukitomo, V.L.Syrmos, "Forecasting gas turbine exhaust gas temperatures using support vector machine experts and genetic algorithm", Control & Automation (MED), 2010 18th Mediterranean Conference on, June 23-25 2010, pp. 345-350, Marrakech.
- [7] S.Ackert, "Engine maintenance management, Managing technical aspects of leased assets", 12 May 2015, pp. 1-31, Madrid.
- [8] M.T. Yildirim, B. Kurt, "Engine Health Monitoring in Aircraft by Using Levenberg-Marquardt Feedforward Neural Network and Radial Basis Function Network", INISTA 2016, Romania (under evaluation process).

A Comparative Study of Isotropic and Anisotropic Sky Models to Determine the Optimum Orientation Angles Of PV Arrays

Huseyin Akdemir¹, Ali Ajder¹, Hakan Akca¹, Mugdesem Tanrioven¹

Abstract

The importance of solar energy has been increasing gradually by the years. The energy obtained from photovoltaics (PV) is directly proportional to incident solar radiation on photovoltaic (PV) panels. To obtain the maximum energy from the sun, PV arrays are positioned according to optimum tilt and azimuth angle. In order to optimize orientation angles, the solar radiation on tilted surface needs to be analyzed taking into account its components direct, diffuse and reflected. There are two approaches for analyzing of the solar radiation which are named isotropic and anisotropic models. In this study, three isotropic (Liu Jordan, Koronakis, Badescu) and three anisotropic models (Hay and Davies, Reindl et. al, Hay and Davies-Reindl- Klutcher) are employed by using hourly solar radiation of Istanbul, Turkey. Then, results of sky models are compared with the real solar radiation and statistical test methods are used for validation of model performances. Finally, results showed that under 400 W/m² radiation level Koronakis model and over 400 W/m² Reindl et.al. model has the best performance for Istanbul radiation data

Keywords: *Photovoltaics, Istanbul radiation*

1 INTRODUCTION

The popularity of PV systems have been increasing day by day. Solar energy production is important for a multitude of reasons including reduced carbon emissions; renewable, domestic and distributed. In order to obtain maximum energy from PV arrays, they must be positioned at optimum tilt and azimuth angles. The azimuth angle, which shows north-south direction of PV panel. These positioning angles are connected with solar irradiance calculation on tilted surface.

Many empirical models have been developed to calculate the solar radiation on tilted surfaces [1]. There are three components of solar radiation on a surface, direct beam, diffuse from the sky and the reflected from the ground [2]. Many models use the same methods for calculating the direct, beam (or diffuse) and reflected, but differ on methods of calculating incident diffuse from the sky. Models are named as isotropic (e.g., Liu and Jordan [3], Koronakis[4],Badescu[5]) and anisotropic models (e.g. Hay and Davies (HD) [6], Reindl et.al. [7], Hay and Davies, Klucher and Reindl (HDKR) [1]) according to calculation of diffused radiation. According to isotropic models, the intensity of diffuse sky radiation is uniform and incident diffuse from the sky has just isotropic component. On the other hand, anisotropic models claim that diffuse radiation from the sky has two more components as circumsolar and horizon brightening [9]. All of these models are obtained with empirical equations.

Also isotropic and anisotropic models can be affected by many climatic conditions such as, temperature, latitude, longitude, humidity and wind speed [10]. So, several studies have been proposed for estimating global radiation on sloped surfaces. Reference [11] compared results of its model with the actual values of diffuse and global radiation. Artificial neural network is proposed to obtain direct and diffuse radiation on horizontal surfaces for different locations in Turkey [12]. Different sky models are evaluated to estimate the global solar surfaces on sloped surfaces for Belgium climatic conditions in [13]. Reference [13] shows that sky models have different results for different conditions and proposed a new model for different sky conditions in Belgium based on this situation. Another study compared isotropic and anisotropic models using monthly average daily solar radiation to calculate solar radiation incident on tilted surface on Bhopal City, India [9]. For Bhopal City, found out BA model gives the best results. Generally, studies use monthly radiation data. In this paper, three isotropic and three anisotropic models are evaluated using hourly global radiation data. Using of hourly data is more reliable than monthly data. The effect of radiation level on model performance investigated, too. Additionally, statistical test methods are used for validation of model performance and consequently according to radiation level best models are preferred for Istanbul.

2 METHODOLOGY

In this study, firstly beam and diffuse components of global radiation on horizontal surface were obtained. Secondly, four different radiation intervals are determined and for each interval the solar radiation incident on inclined surface was calculated using six sky models. As a next step, results of isotropic and anisotropic models are presented with

¹ Corresponding author: Yildiz Technical University, Department of Electrical Engineering, 34220, Esenler/Istanbul, Turkey.
hakdemir@yildiz.edu.tr

charts. Additionally, some statistical tests are used to evaluate the accuracy of the results of models. Finally, the best models are determined according to the real radiation level.

2.1 Calculation of Solar Radiation for Horizontal Surface

Most radiation data is based on measurement of global radiation on many meteorological station. In the literature, monthly average daily total radiation on a horizontal surface \bar{H} and hourly total radiation on a horizontal surface I are defined as global radiation. To obtain radiation values for tilted surfaces, beam and diffuse components of solar radiation are used. Solar radiation is affected by many environmental factors until it reaches the earth's surface. Therefore, global radiation is defined as the total solar radiation reaching earth's surface and also empirical formulas are used when calculation of beam and diffuse radiation on horizontal surface. Here, as a radiation permeability value of atmosphere clearness index is defined by;

$$\bar{K}_T = \frac{\bar{H}}{\bar{H}_0} \quad (1)$$

\bar{K}_T is the ratio of monthly average daily radiation on a horizontal surface to the monthly average daily radiation to the extraterrestrial radiation. The value of \bar{K}_T is between 0 and 1.

There is also can be defined a daily clearness index and an hourly clearness index following equations respectively;

$$K_T = \frac{H}{H_0} \quad (2)$$

$$k_T = \frac{I}{I_0} \quad (3)$$

In Eq. (1),(2) and (3), \bar{H} , H and I are measured global solar radiation data by a pyranometer. \bar{H}_0 , H_0 and I_0 are calculated mathematical equations. In this work, real data are based on hourly global radiation and because of this reason I_0 hourly extraterrestrial radiation calculated by;

$$I_0 = \frac{24 \times 3600}{\pi} G_{sc} \left(1 + 0,033 \cos \frac{360n}{365} \right) \times \left[\cos \Phi \cos \delta (\sin \omega_2 - \sin \omega_1) + \frac{\pi(\omega_2 - \omega_1)}{180} \sin \Phi \sin \delta \right] \quad (4)$$

where G_{sc} is the solar constant and its value is 1367 W/m^2 . Also, n is the day of the year, Φ is latitude, δ is declination and ω is hour angle. All angles are taken into account as degree. After the value of I_0 is calculated, hourly clearness index k_T can be determined according to Eq. 3. In addition, global radiation I is known that is measured data. In this way, diffuse component of global radiation I_d can be calculated from following equations;

$$\frac{I_d}{I} = \begin{cases} 1.0 - 0.09k_T & k_T \leq 0.22 \\ 0.9511 - 0.1604k_T + 4.388k_T^2 - 16.638k_T^3 + 12.336k_T^4 & 0.22 \leq k_T \leq 0.80 \\ 0.165 & k_T > 0.80 \end{cases} \quad (5)$$

As previously said that, global radiation is sum of beam and diffuse components. Therefore, beam radiation is obtained from below equation,

$$I_b = I - I_d \quad (6)$$

It is note that all radiation values (I , I_b and I_d) are hourly radiation value.

2.2 Calculation of Solar Radiation for Inclined Surface

The incident solar radiation on tilted surfaces, has 3 components as direct, beam (or diffuse) and reflected also can be seen in Figure 1.

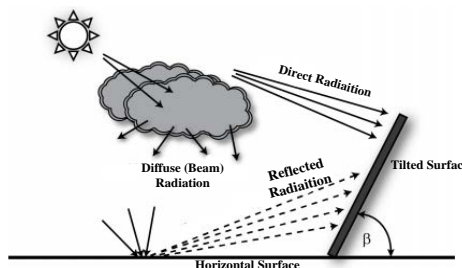


Figure 16. Components of incident solar radiation on a tilted surface.

Also, the diffuse component is composed by isotropic, circumsolar and horizon brightening factor terms. Hence, the hourly total incident solar radiation on tilted surfaces I_T can be written below equation;

$$I_T = I_{T,b} + I_{T,d,iso} + I_{T,d,cs} + I_{T,d,hz} + I_{T,refl} \quad (7)$$

In Equation (7), first term $I_{T,b}$ is beam radiation, second term $I_{T,d,iso}$ is isotropic part of diffuse radiation, third term $I_{T,d,cs}$ is circumsolar part of diffuse radiation, fourth term $I_{T,d,hz}$ horizon brightening factor of diffuse radiation and last term $I_{T,refl}$ is ground reflected radiation.

2.2.1 Calculation of Beam Radiation

Many models have been developed to calculate I_T in the literature. Beam radiation and reflected radiation are defined on the same way for all models.

Beam radiation on a tilted surface is can be written;

$$I_{T,b} = I_b R_b \quad (8)$$

where I_b is the hourly beam radiation on horizontal surface and R_b is the function of transmittance of atmosphere estimated by $I_{T,b}/I_b$ ratio. The ratio of beam radiation on the tilted plane to on a horizontal surface given by Equation (9)-(11);

$$R_b = \frac{\cos(\theta)}{\cos(\theta_z)} \quad (9)$$

$$\cos\theta = \sin\delta \cdot \sin\phi \cdot \sin\beta - \sin\delta \cdot \cos\phi \cdot \sin\beta \cdot \cos\gamma + \cos\delta \cdot \cos\phi \cdot \cos\beta \cdot \cos\omega + \cos\delta \cdot \sin\phi \cdot \sin\beta \cdot \cos\gamma \cdot \cos\omega + \cos\delta \cdot \sin\beta \cdot \sin\gamma \cdot \sin\omega \quad (10)$$

$$\cos\theta_z = \cos\phi \cdot \cos\delta \cdot \cos\omega + \sin\phi \cdot \sin\delta \quad (11)$$

where δ is the declination, ϕ is the local latitude, β is the tilt of the surface, γ is the surface azimuth angle and ω is the hour angle. All angles are considered as degree.

2.2.2 Calculation of Reflected Radiation

Another component of the hourly total incident solar radiation on a tilted surface is reflected radiation $I_{T,refl}$. As can be seen in Figure (1), $I_{T,refl}$ is reflected by ground and by other objects on the earth's surface. Reflected radiation is given by Equation (12):

$$I_{T,refl} = I \cdot \rho_g \cdot \frac{(1 - \cos\beta)}{2} \quad (12)$$

In Equation (12), β is the slope of tilted surface, ρ is called the ground reflectance or albedo and its value can be changed between 0.2 and 0.9. Generally, the value of albedo is set to $\rho=0.2$, so in this study the value is taken into account as 0.2.

2.2.3 Calculation of Diffused Radiation

The incident solar radiation on inclined surface, is diffused through the atmosphere due to many environmental and physical factors. Therefore, calculation of the diffused component of solar radiation on a inclined surface is difficult. In addition, it is function of condition of cloudiness and clearness which are extremely predictable. Thus, many models are improved to obtain the diffused radiation in the literature. According to the [] isotropic models are simplest, conservative and anisotropic models estimate more radiation on tilted surface because of taking into account circumsolar diffuse and/or horizon brightening components. Isotropic models assume that propagation of the diffuse radiation is homogenous along the sky dome and express this condition using isotropic term. Anisotropic models, use an anisotropy index in order to demonstrate circumsolar and horizon brightening factor. All of isotropic and anisotropic models are based on empirical equations. In Section 2.3.3 three isotropic models Liu Jordan(LJ), Koronakis(KO) and Badescu(BA), also three anisotropic sky models Hay and Davies (HD), Reindl et.al.(RE) and HDKR will be explained respectively.

2.3 Isotropic and Anisotropic Models for Calculation of Diffuse Radiation on Inclined Surface

2.3.1 Liu and Jordan Model(LJ)

As previously said that, diffused radiation on tilted surfaces the combination of three elements namely isotropic, circumsolar and horizon brightening. Liu and Jordan (LJ) model is assumed that the diffuse radiation is composed only isotropic term. According to this model, values of circumsolar and horizon brightening are zero. Hence, if circumsolar and horizon brightening value are 0 in Equation (7); total incident solar radiation on tilted surfaces I_T can be written as;

$$I_T = I_b R_b + I_d \frac{(1 + \cos\beta)}{2} + I \rho_g \frac{(1 - \cos\beta)}{2} \quad (13)$$

In Equation (13), second term is diffused radiation which is composed by just isotropic component. The first and third term are beam and reflected components as the explained before section.

2.3.2 Koronakis Model (KO)

The isotropic sky assumption was questioned in Hamilton and Jackson [] where it was found that the sky's southern part is responsible for 63% of the total intensity of diffuse radiation. Koronakis improved LJ model according to this approach and updated Equation (13) as:

$$I_T = I_b R_b + I_d \frac{(2+\cos\beta)}{3} + I\rho_g \frac{(1-\cos\beta)}{2} \quad (14)$$

where diffused radiation is composed by just isotropic component again.

2.3.3 Badescu Model (BA)

According to the Badescu Model, total incident solar radiation on tilted surfaces as follows:

$$I_T = I_b R_b + I_d \frac{(3+\cos 2\beta)}{4} + I\rho_g \frac{(1-\cos\beta)}{2} \quad (15)$$

2.3.4 Hay and Davies Model (HD):

Isotropic models consider the atmosphere as isotropic, but developed models are found out that there are also circumsolar diffuse and horizon brightening components of diffused radiation. Hay and Davies model claimed that diffuse radiation has isotropic and circumsolar components. Accordingly, I_T can be written as:

$$I_T = (I_b + I_d A_i) R_b + I_d \frac{(1+\cos\beta)}{2} (1 - A_i) + A_i R_b + I\rho_g \frac{(1-\cos\beta)}{2} \quad (16)$$

where A_i is called as anisotropy index. A_i is directly proportional with clear conditions and its defined as

$$A_i = \frac{I_b}{I_0} \quad (17)$$

If the value of A_i is equal to zero, its means that diffuse radiation is composed by just isotropic components as in isotropic model. The key difference between isotropic and anisotropic model is the anisotropy index A_i .

2.3.5 Reindl et. al. Model (RE):

Reindl et. al. developed the Equation (16) adding horizon brightening factor as follows;

$$I_T = (I_b + I_d A_i) R_b + I_d \left\{ \frac{(1+\cos\beta)}{2} (1 - A_i) [1 + f \sin^3 \left(\frac{\beta}{2} \right)] \right\} + A_i R_b + I\rho_g \frac{(1-\cos\beta)}{2} \quad (18)$$

Where f is a modulating factor and is can be determined as;

$$f = \sqrt{\frac{I_b}{I_0}} \quad (19)$$

2.3.6 Hay and Davies, Klucher, Reindl Model (HDKR):

In literature HDKR model is given as:

$$I_T = (I_b + I_d A_i) R_b + I_d \frac{(1+\cos\beta)}{2} (1 - A_i) [1 + f \sin^3 \left(\frac{\beta}{2} \right)] + I\rho_g \frac{(1-\cos\beta)}{2} \quad (20)$$

HDKR model is composed by HD, Klucher and RE models which has beam, ground reflected and all terms of diffused radiation (isotropic, circumsolar and horizon brightening).

2.4 Comparing Sky Models

2.4.1 Evaluation of Sky Models for Istanbul Data

As it is said that on previous section, real solar data of Istanbul are measured hourly global solar data. Because of this reason, hourly global parameters are used when solving of equation of models. In Figure 2, hourly global radiation on Istanbul for 1 year (8760 hours) is illustrated.

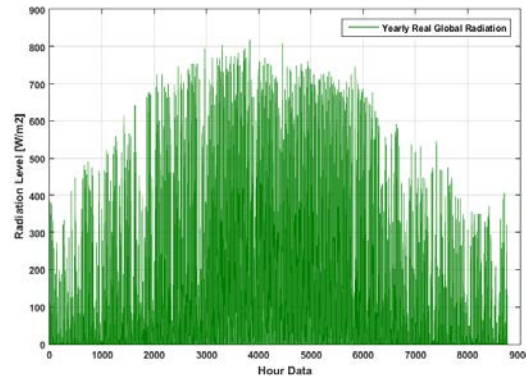


Figure 2. Measured hourly global solar data (real data) on Istanbul for 1 year (8760 hours)

As can be seen on Figure 2, different radiation levels can be observed all the year round. The average solar radiation level of Istanbul is more than 400 W/m^2 and the highest radiation level is 816.43 W/m^2 . Klucher [14] found that the isotropic model gave good results for overcasts skies but underestimates irradiance under clear and partly overcast sky condition. Thus, the comparison of sky models can be made based on radiation level. In this study, 4 radiation intervals are decided to compare sky models as $0\text{-}200 \text{ W/m}^2$, $200\text{-}400 \text{ W/m}^2$, $400\text{-}600 \text{ W/m}^2$ and $600\text{-}800 \text{ W/m}^2$ by taking into consideration the real data. In this chapter, all sky models evaluated for each radiation interval. According to each model, total radiation on sloped surface is calculated. Then, results of the sky models are presented on charts together real radiation data. Figure 3 (a) and (b) shows variation of irradiance for isotropic and anisotropic models on one day, respectively. The radiation level is under 200 W/m^2 and the measured mean radiation is 102.09 W/m^2 for the day.

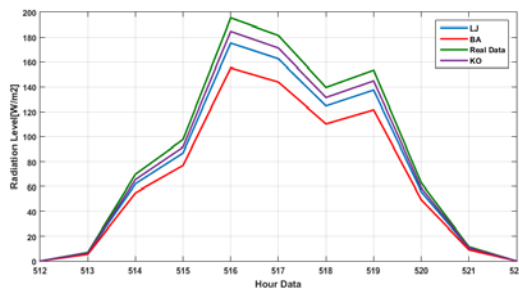
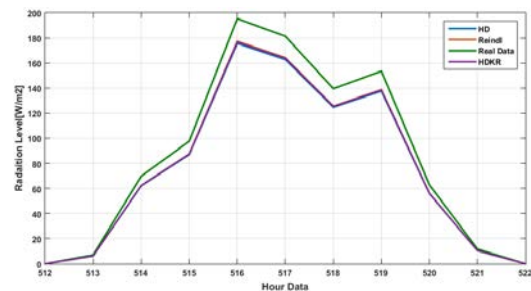


Figure 3. (a) For $0\text{-}200 \text{ W/m}^2$ the variation of isotropic models



(b) For $0\text{-}200 \text{ W/m}^2$ the variation of anisotropic models

As seen in Figure 3 (a), for $0\text{-}200 \text{ W/m}^2$ radiation level, estimated radiations by 3 isotropic models (LJ, KO, BA) are lower than real data. KO model has the closest result to the real data and BA model estimated the lowest radiation level. Results of anisotropic models are illustrated in Figure 3 (b). 3 anisotropic models (HD, Reindl, HDKR) almost have same results. Their radiation values are 175.7 , 177.3 and 176.7 W/m^2 respectively for 516^{th} hour data while real radiation level is 195.4 W/m^2 .

On Figure 4 (a) and (b), there are variation of estimated radiation with using isotropic and anisotropic models respectively for $200\text{-}400 \text{ W/m}^2$ radiation interval. The mean value of real radiation data is 163 W/m^2 . All isotropic and anisotropic models are lower than real data. All anisotropic models again almost have the same value. Estimated values are 362.5 , 366.2 372.7 W/m^2 of HD, HDKR and Reindl respectively for 1766^{th} hour data. On 1766^{th} hour data, real radiation level is 397.7 W/m^2 .

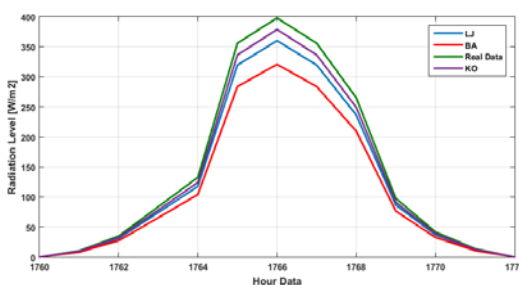
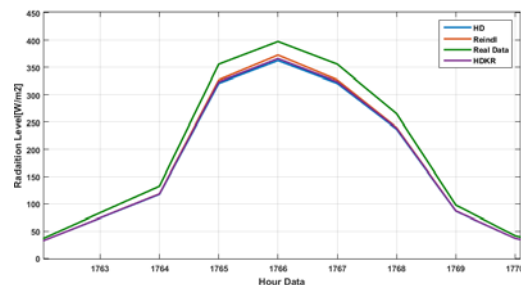


Figure 4. (a) For $200\text{-}400 \text{ W/m}^2$ the variation of isotropic models



(b) For $200\text{-}400 \text{ W/m}^2$ the variation of anisotropic models

Hourly variation of sky models for $400\text{-}600 \text{ W/m}^2$, is given in Figure 5 (a) and (b). The mean radiation level is 357.3 W/m^2 on this interval. Isotropic models have the same variation as before radiation level intervals. However, as can be seen in Figure 5 (b), Reindl model estimate more radiation level than real data for 4669^{th} hour data. While real radiation level is 605.8 W/m^2 , Reindl model estimated the radiation as 617.9 W/m^2 .

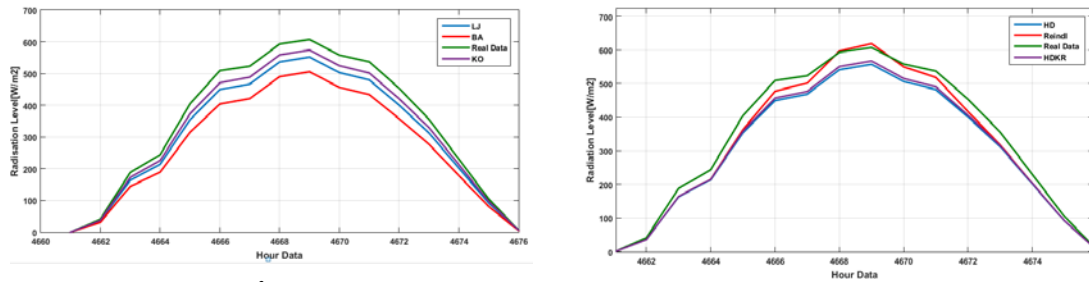


Figure 5. (a) For 400-600 W/m² the variation of isotropic models (b) For 400-600 W/m² the variation of anisotropic models

As seen in Figure 2, the highest radiation level for Istanbul is 816.43 W/m². Hence, the fourth radiation interval was determined as 600-800 W/m² on before sections. Figure 6 (a) and (b) can be explainable about model performance for clear days. On the Figure 6 (a), KO model has the closest results to real data as isotropic model. Also, as is shown in Figure 6 (b), Reindl model estimates more radiation level over the 700 W/m². HD and HDKR model have the same results again like before radiation levels and under the real data radiation level.

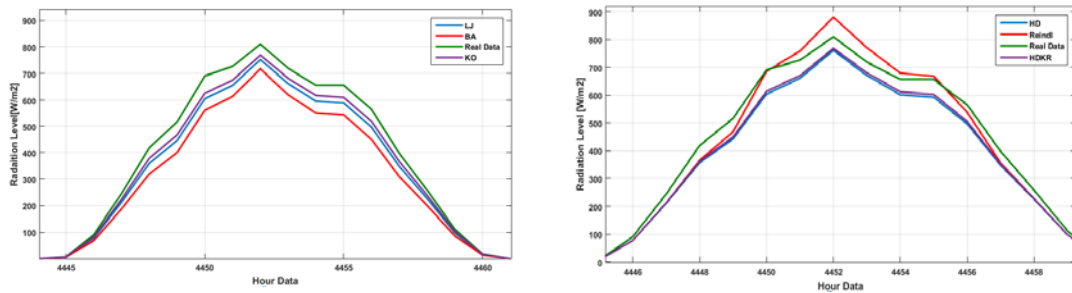


Figure 6. (a) For 600-800 W/m² the variation of isotropic models (b) For 600-800 W/m² the variation of anisotropic models

2.4.2 Statistical Validation of Sky Models

In this paper, the real solar radiation data for Istanbul is compared with estimated radiation results. In previous section, real and calculated hourly solar radiation values are illustrated for different radiation intervals. These illustrations can suggest about model results. However, to make a reliable comparison some statistical methods are used considering all data values.

In this section, mean bias error (MBE) and root mean square error (RMSE) method are used to evaluate the sky models. The Mean Bias Error (MBE) is a guide for the average deviation between estimated and measured values term by term. MBE is calculated by:

$$MBE = \frac{1}{n} \sum_{i=1}^n (I_{ei} - I_{mi}) \quad (21)$$

where n is the data number, I_{ei} is the estimated value and I_{mi} is the measured value. On the other hand, the use of RMSE is very common and it makes an excellent general purpose error metric for numerical predictions. RMSE is a frequently used measure of the differences between values (sample and population values) predicted by a model or an estimator and the values actually observed. RMSE can be computed as;

$$RMSE = \sqrt{\frac{1}{n} \sum_{i=1}^n (I_{ei} - I_{mi})^2} \quad (22)$$

where n is data number, I_{ei} the estimated value and I_{mi} is the measured value.

Ideally, MBE and RMSE are equal to zero. If MBE has negative value, its means that estimated data is lower then real data.

Also it is possible that MBE and RMSE can be express as percentage to significant comparing with real and estimated data as following equations:

$$MBE\% = \frac{MBE}{M_M} \quad (23)$$

$$RMSE\% = \frac{RMSE}{M_M} \quad (24)$$

where M_M is the mean of measured data for related interval.

In Table1, for each radiation interval MBE, MBE%, RMSE and RMSE% values of sky models are presented in W/m².

Table 1. Statistical Validation of Sky Models

Radiation Level[W/m ²]	Sky Model	MBE	MBE %	RMSE	RMSE %
0-200 W/m ²	LJ	8.8653	10.61	11.5543	13.84
	BA	17.4349	20.87	22.8097	27.38
	KO	4.8256	5.78	6.2499	7.48
	HD	8.7647	10.49	11.4014	13.65
	Reindl	8.2167	9.84	10.6192	12.71
	HDKR	8.3919	10.04	10.8832	13.03
200-400 W/m ²	LJ	16.9453	12.31	20.3212	14.76
	BA	28.2373	20.51	40.3824	29.33
	KO	7.7862	5.66	10.8761	7.90
	HD	13.9024	10.10	19.5550	14.20
	Reindl	11.7902	8.56	16.0680	11.67
	HDKR	12.9463	9.40	18.0238	13.09
400-600 W/m ²	LJ	36.7357	10.97	42.4998	12.67
	BA	66.648	19.89	77.0860	23.01
	KO	22.6349	6.76	26.2046	7.82
	HD	35.7897	10.69	41.2410	12.31
	Reindl	17.5241	5.23	23.5924	7.04
	HDKR	31.5083	9.40	35.9877	10.74
600-800 W/m ²	LJ	41.0593	10.74	49.9456	13.00
	BA	68.7512	18.00	82.7926	21.00
	KO	28.0053	7.32	34.5785	9.04
	HD	39.917	10.43	48.6981	12.73
	Reindl	4.2910	1.12	32.8332	8.5
	HDKR	35.1077	9.17	42.6653	11.15

As shown in Table 1, for days with low radiation level KO model gives best performance. MBE% and RMSE% values of KO model are 5.78% and 7.48% while hourly solar radiance is changing 0-200 W/m². For 200-400 W/m² radiation level, KO has 5.66% MBE% and 7.90% RMSE% values. Furthermore, BA model has the highest statistical value for all irradiance level. It means that, BA has the worst model performance for Istanbul conditions. This situation have been already shown in Figure 3 (a), (b), and Figure 4 (a), (b).

Under 400 W/m², anisotropic models HD, Reindl and HDKR have almost same statistical values as illustrated in Figure 3 (a), (b) and Figure 4 (a), (b). Table 1 shows that, as long as the radiation increases, MBE, MBE%, RMSE and RMSE% values of anisotropic models become better than low irradiance level. Reindl model has the lowest statistical results over 400W/m². MBE% value of Reindl is 5.23%, RMSE% value is 7.04% on between 400 W/m² and 600 W/m². For 600-800 W/m² radiation level, Reindl model has 1.12% MBE% and 8.5 RMSE% value. Besides, KO model performance is better than HD and HDKR models.

3 CONCLUSION

In this study, three isotropic (LJ, KO and BA) and 3 anisotropic (HD, Reindl and HDKR) model performances are examined comparing real radiation data for Istanbul. The real data composed hourly measured global radiation from meteorological station for one year (8760 hours) and so all estimates are based on hourly parameters. The tilt angle was fixed at 45°. 4 different radiation levels are determined as 0-200 W/m², 200-400 W/m², 400-600 W/m² and 600-800 W/m². For each radiation levels, all models are evaluated and compared with real data of Istanbul. Results of

these models are presented with graphics. Moreover, MBE and RMSE statistical assessments are used to verify this illustration.

It shows that, the performance of BA model is worse than other isotropic and anisotropic models. KO model gives the best results for low irradiance level (under 400 W/m^2). All anisotropic models (HD, Reindl and HDKR model) almost give same results under 400 W/m^2 . While radiation level increase, the performance of anisotropic models also increases. Over the 400 W/m^2 radiation level Reindl model has the best performance. The performance of KO model is decreasing based on increasing of radiation level. Nevertheless, as a isotropic model, KO model gives better performance than HD and HDKR model.

Consequently, all sky models are obtained by empirical formulas. Therefore, sky models can give different results for calculation of radiation on tilted surface. Under 400 W/m^2 KO model and over 400 W/m^2 Reindl model gives best performance for Istanbul global radiation. When sizing of PV arrays on Istanbul, to determine of optimum orientation angles for Istanbul these results should be considered. Its mean that, when optimum orientation angles are being calculated, KO model can be used for the seasons/months of the low irradiance and Reindl model can be used for the seasons/months of the high irradiance.

REFERENCES

- [1] J. Duffie and W. Beckman, *Solar engineering of thermal processes*, Second Edi. New York: John Wiley and Sons, 1991
- [2] J.E. Hay and D. C. McKay, *Intl. Solar Energy*, 3,203 "Estimating Solar Irradiance on Inclined Surfaces: A Review and Assesment of Methodologies, 1985.
- [3] Liu B, Jordan R., "Daily Insolation on Surfaces Tilted Towards the Equator". *ASHRAE*,53,526-41,1962.
- [4] Korokanis P. "On the choice of the angle of tilt for south facing solar collectors in the Athens basin area". *Solar Energy*,36,217-25, 1986
- [5] Badescu V. "3d isotropic approximation for solar diffuse irradiance on tilted surfaces", *Renewable Energy*,26,221-3, 2002
- [6] J.E. Hay and J.A. Davies, "Calculations of the Solar Radiation Incident on an Inclined Surface". In: *Proceedings of First Canadian Solar Radiation Data Workshop*, Canadian Atmospheric Environment Service, Canada, pp. 59-72, 1980.
- [7] D. Reindl, W. Beckman, J.Duffie, "Evaluation of hourly tilted surface radiation models", *Renewable Energy*,45.9-17,1990.
- [8] K.N. Shukla, Saroj Rangnekar, K.Sudhakar, "Comparative Study of isotropic and anisotropic sky models to estimate solar radiation on tilted surface: A case study for Bhopal, India", *Energy Reports*, 1.96-103,2015.
- [9] *Energy*, vol. 84, no. 12, pp. 2068–2084, 2010
- [10] S. Ozan, K. Tuncay, "Estimation of solar radiation over Turkey using artificial neural network and satellite data", *Appl. Energy* 86, 1222-1228, 2009.
- [11] Colienne Demain, Michael Journee, Cedric Bertrand, "Evaluation of different models to estimate the global solar radiation on inclined surfaces, *Renewable Energy*, 50, 710-721, 2013.
- [12] A.A. El-Sebaei, A.A. Trabea, "Estimation of horizontal diffuse solar radiation in Egypt", *Energy Convers. Manage.*,44.2471-2482, 2003
- [13] Padovan and D. Del Col, "Measurement and modeling of solar irradiance components on horizontal and tilted planes," *Sol.*
- [14] T. Klutcher, "Evaluation of models to predict insolation tilted surface", *Solar Energy*, 23.111-4, 1979.

Impact of Renewable Energy Systems on Spinning Reserves

Ali Ajder¹, Huseyin Akdemir¹, Mugdesem Tanrioven¹

Abstract

Generation and consumption of electrical energy must be balanced all the time to ensure frequency, voltage and stability standards. In order to manage supply and demand imbalances, system operators use ancillary services which include various generation capacities and demand managements. In addition to this, the term spinning reserve is used to refer the capability of power system to cope with contingencies with the already synchronized generation. Spinning reserve is required to meet sudden increase in demand or to cover generation and transmission losses. In recent years, percentage of renewable energy systems (RES), especially wind farms, has been increasing significantly in power systems all around the world. As a result of this, increasing of intermittent generation units disable system operators to decide the amount of reserves and this fact reveal some problems. In this study impacts of RES to electric network are evaluated in economic and technical aspects.

Keywords: *Renewable energy systems, spinning reserves, supply and demand imbalances*

1 INTRODUCTION

In recent years, electricity power networks have been changing greatly all around the world. There are many reasons to this change like anxieties with climate change, liberalization of electricity markets, technological developments... etc. Climate change is a global phenomenon, so the international political response has been going forward with fighting global warming at the Rio since 1992. In November 2015, Conference of Parties (COP21) took place in Paris, for the first time in over 20 years of UN negotiations, aim to keep global warming below 2°C [1].

Global warming and climate change from the energy generation point of view have led to consider alternative energy sources, particularly wind and solar energy, instead of fossil fuels. However, these Renewable Energy Sources (RES) differ from conventional generation in terms of the variability and uncertainty [2]. Variability expresses the maximum available generation limit which changes with time (like wind and solar plants) and also this limit is not known precisely means uncertainty [3].

System Operator (SO) have to manage supply and demand imbalances in power system. If the SO cannot cope with sudden increase in demand or generation- transmission losses, this might cause to load shedding, instability, machine damages and blackouts [4]. Electric power systems which have high scale RES penetration need larger amounts of flexibility, in order to balance generation and consumption. Flexibility means maintaining to balance generation and load by adjusting of generating units outputs or managing load consumption [5].

Before the penetration of highly variable generation units in power system, the term 'reliability' refers to serving resource to manage rare events in long term planning, and the ability to operate the system. However, in present systems it is considered in a time frame from a few minutes to a few days ahead. This means short term or operational reliability which is closely related with variability and uncertainty [6]. In order to support system reliability, the SO uses ancillary services which typically contain spinning, non-spinning and regulation reserves [7].

Although spinning reserve decreases the considerable social and economic cost of supply and demand imbalances, the provision of spinning reserve is costly. If the amount of spinning reserve increases (it comes at a cost), the system risk reduces. On the other hand, under- scheduling spinning reserve results in the increasing expected cost of outages (this increases the system risks). As a result, the SO have to determine the optimal level of spinning reserve [8].

This study can be divided two main parts. The first part of work summarizes energy outlook of Europe and Turkey. Especially, it emphasize the change of sharing energy sources in Europe and explain the reasons why RES is essential for us. The second part of study is about problems and solutions when integrating large- scale RES to power network.

2 ENERGY OUTLOOK OF EUROPE AND TURKEY

2.1 Europe

The Europe total installed electricity power capacity reached 908 GW at the end of 2015. Figure 1 shows a comparison of EU total installed power capacity in 2000 and 2015 [9].

¹ Corresponding author: Yildiz Technical University, Department of Electrical Engineering, 34220, Esenler/Istanbul, Turkey.
aliajder@yildiz.edu.tr

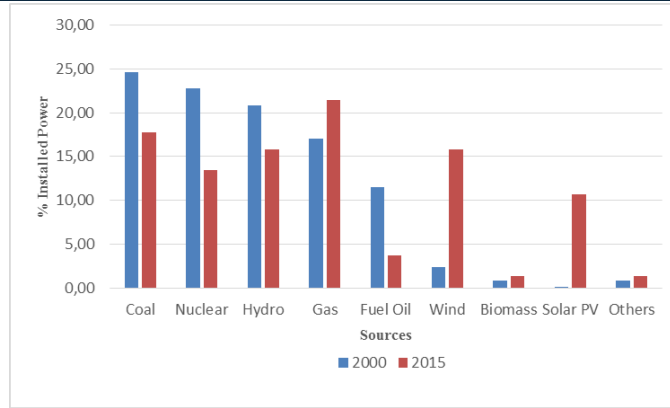


Figure 1. The comparison of installed electricity power capacity in Europe, 2000 and 2015

While fossil-fuel based thermal plants share (except Gas turbines) of total installed power capacity has been notably decreasing since 2000, the renewable energy technologies, especially wind and solar power, remarkably increased. Net electricity generating installation in the Europe in 1995- 2015 is shown in Figure 2 (Note: The change under 5 GW of other sources is not shown in Figure) [9].

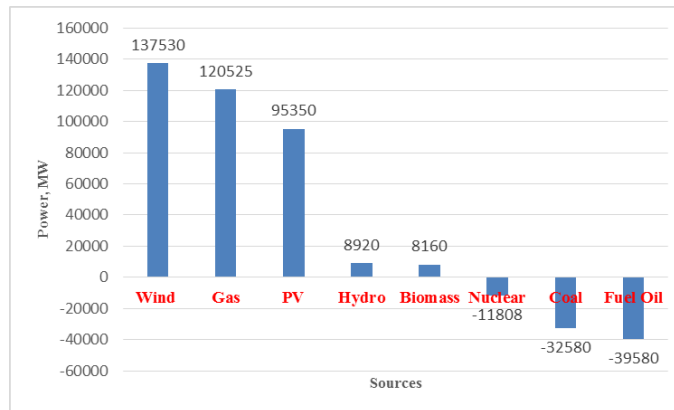


Figure 2. Net electricity generating installations in the Europe, 1995-2015

The renewable energy sources, especially wind and solar, increased their share in total power capacity.

In European countries, Germany has the largest installed wind capacity (45 GW), Spain (23 GW), the UK (14 GW), France (10 GW) and 16 European countries have over 1 GW, nine of these have more than 5 GW. More than €25 billion to finance wind energy development was invested in Europe in 2015 [9].

In installed solar power, Germany has also the largest capacity (38 GW), Italy (18 GW), France, Spain, the UK (5 GW), and 7 European countries have over 1 GW [10].

2.2 Turkey

Turkey total installed electricity power capacity is about 70 GW in 2014, its share and electricity generation based on sources are shown in Figure 3 [11].

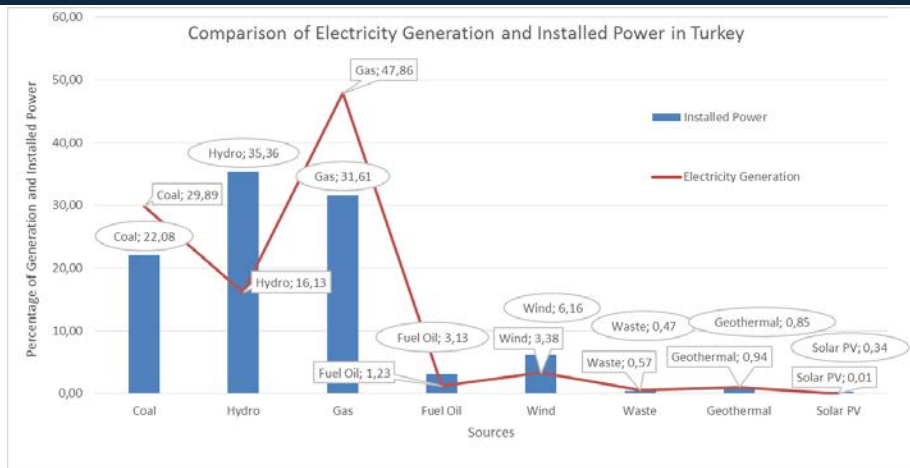


Figure 3. Installed power and electricity generation of Turkey in 2014

Turkey total electricity consumption was about 258 TWh in 2014; approximately 252 TWh was generated from power plants of Turkey and remainder was supplied with energy trade.

Turkey has comparatively small fossil fuel reserves, therefore it should change its energy policy in order to increase sources diversity. When we take a look at the energy outlook of Europe, it is easy to see the change of sharing energy sources. We should accommodate to this evolution, if we take care to protect our environment.

3 EFFECTS OF LARGE SCALE VARIABLE GENERATION

The main problems to penetrate RES into the power systems are variability and uncertainty. System operator has already been used to cope with load uncertainty. In addition to this, increasing variability with high scale RES integration, balancing will consequently be more difficult. Power system operators will need more flexible systems to manage imbalances between generation and consumption. This flexibility can be provided by flexible generation technologies or from alternative sources of flexibility such as flexible demand and storage [12].

In recent years, increasing RES (inverter-coupled generation) and the planned retirements of conventional plants cause to decline amount of inertia and spinning reserve. This issue must be studied how this will affect the system reliability at different RES levels. There is a simulation study which shows wind power plants can provide frequency response and analyses high level RES penetration effects on frequency [4].

There are no detailed requirements managing the performance of conventional plants, if large scale variable output power plants penetrate to electric network. Engineers and policy makers must take a close interest in some issues like frequency and voltage regulation, real and reactive power modeling, ancillary services and market design according to RES [13].

The following three subsections of this paper will summarize both the technical, economic effects and the impacts on spinning reserve of high- scale RES to electricity network.

3.1 Technical Effects

High-scale RES penetration causes technical effects on the operation of the power system because of the variable behavior and uncertainty of wind and solar power. In order to manage this variability and uncertainty in the renewable energy generation, other units have to be operated more flexibly to balance of supply and demand.

Renewable energy sources, i.e. wind and solar power, generate electricity depend upon wind speed or solar radiation. Wind and solar power are the displacement of conventional plants which maintain system balance and reliability, so until some level of RES penetration, new conventional generation is not required as 'reserve capacity' [14]. Allocation of a generating unit's capacity and reserves are shown in Figure 4 [36].

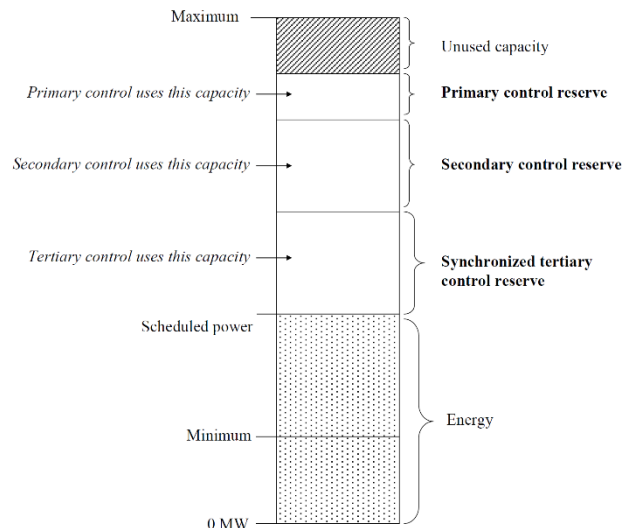


Figure 4. Allocation of the capacity of a generating unit

There are lots of studies to examine the technical issues related with the high scale RES penetration in the U.S. [15]–[20], Europe [6], [21], [22] and Germany electricity system [23]–[25]. Europe has some of the highest large scale RES penetration levels in the world and even higher targets. European experience and approaches to balance supply and demand, frequency control and related high scale RES penetration technical issues are of general interest [14]. In addition to this, there are lots of international studies which explore the possibility of achieving high levels of renewable electricity penetration will primarily effect greenhouse gas (GHG) mitigation [23], [24], [26].

Electric transmission infrastructure is very essential to penetrate large scale RES into the power network. For example, in windy areas, human activity is generally restricted, therefore the electrical grids are weak. A number of new approaches and solutions related with this topic are being explored [27], [28].

The dynamic behavior of power system and ancillary services to manage system imbalances are needed to study under large scale RES conditions and also monitoring and control of RES plants is crucial for power system reliability.

3.1 Economic Effects

To manage consumption and production imbalances, the reserves are kept in power system. In order to keep the supply and demand in balance, the spinning and non-spinning reserves are used. Up and down regulation are utilized to manage the total balance in a control or balancing area. These effects in system operation have certainly cost and so price implications. Besides this, the feed-in of the wind generation will impact the spot market price.

When we consider about wind energy, it is likely to substitute peak load generators, i.e., combined cycles with natural gas and oil burning units. The contribution of imported primary energy is also expected to be reduced in the EU thus increasing the diversity of supply. This experience includes market-based approaches (i.e., design of balancing markets, optimization of the resources, and a fair sharing of the cost) should be evaluated to balancing and frequency control services to ensure system security by developing countries' electricity markets regulatory [29].

The variability of wind and solar power will impact to electricity markets, as they can be forecasted some hours or a day ahead. In the power system, the uncertain part of the variability is left for reserves. The imbalance of wind is added to all other imbalances during the operating hour. The wind power imbalances are treated in balance settlement after the operating hour in many EU countries, like all other generation and consumption. Through the imbalance costs, wind power producers see the cost which incurred by the reason of the increased use of reserves. The system operator covers the imbalance costs in these countries. However, if a fixed feed-in tariff is provided to wind and solar power plants, the average electricity cost is likely to be increased. It should be declared that according to researches, faster markets (e.g., 10 min rather than 1 h) can reduce wind and solar integration cost.

The greenhouse gases emissions are expected to drop with high scale RES penetration. For example, with wind generation replaces mainly peak and load-following units, this must be quantified taking into account estimations about the share of each fuel to the future energy mix. The external cost of energy should be considered in design of the future emission market structure and it is crucial for wind and solar development [14].

3.2 Effects on Spinning Reserve

Large scale RES integration to electric grid makes it more difficult to maintain the balance of supply and demand at all times. Electricity market participant submit their offers on a day-ahead basis in Europe and they have chance to adjust their their day-ahead schedules through intraday markets.

There are lots of studies on the effects of RES on reserve planning were conducted from which a variety of reserve sizing methods, like deterministic or probabilistic as well as static or dynamic approaches [8], [30], [31], [31]–[34].

In many power systems, basic methods based on statistical indicators (e.g. standard deviation of imbalances) or deterministic approaches linearly summing up reserve requirements are generally used. However, these methods do not consider the stochastic nature of the determinants and ignore less severe events' probability and as a result tend to overestimate the actual reserve requirements. Therefore, probabilistic reserve sizing techniques can be a solution for large scale RES penetration [33].

In order to determine optimum reserve requirement, most approaches are based on power system reliability analysis methods which are on the basis of reliability indices (such as loss of load expectation, loss of load probability, or loss of energy expectation calculations, etc.) [35].

When planning power system design by taking into consideration large scale RES, it is essential to consider the existing thermal generators' limits. Their technical characteristics limit to RES penetration and they are related to the load-following capability. For example: the technical minimum of thermal generators, the start-up and shut-down times (especially for coal-fired units), the ramp-up and ramp-down rates of thermal generators may be also limiting factors that should be considered [33].

4 CONCLUSION

Although high scale RES penetration in power system raises a number of technical challenges for the system operator, it is expected to contribute essentially the environmental targets. Apart from the technical issues, high scale RES integration will have some impacts on power system economics and will also affect the electric market participants. As a result, special solution should be found to the design of electricity market regulations in order to ensure the reliability of supply.

First of all, the detailed planning studies and dynamic behavior of RES should be studied. A major technical problem with significant RES power in electricity grid is frequency control/ load following. Special case with high scale RES, that requires flexibility to power system— system operator can manage to expected and unexpected changes in generation and consumption. For Turkey, it is important to strengthen electricity network with Europe in order to system flexibility.

Advanced forecasting techniques can improve system operation and reduce the amount of system flexibility needed to integrate large scale RES.

Expanded transmission capacity is crucial to penetrate high scale RES in power system. In Turkey case, extra-high voltage transmission projects may be given priority to that reduce east/west congestion. Besides, new transmission lines may be designed to serve of new capacity at remote and varied RES sites were key to integration.

Finally, power system economics will be essentially influenced; the effects on energy balances, sharing of sources, inter- transmission system operator trading, electricity cost, emissions reduction, etc., should be studied and suitable market regulations must be adopted.

REFERENCES

- [1] "COP21 | United nations conference on climate change." [Online]. Available: <http://www.cop21.gouv.fr/>.
- [2] M. Milligan, H. Holttinen, J. Kiviluoma, A. Orths, M. A. Lynch, and L. Soder, "Market designs for high levels of variable generation," *2014 IEEE PES Gen. Meet. / Conf. Expo.*, pp. 1–5, 2014.
- [3] E. Ela, S. Member, and M. O. Malley, "Scheduling and Pricing for Expected Ramp Capability in Real-Time Power Markets," *IEEE Trans. Power Syst.*, vol. 31, no. 3, pp. 1–11, 2015.
- [4] V. Gevorgian, Y. Zhang, and E. Ela, "Investigating the Impacts of Wind Generation Participation in Interconnection Frequency Response," *IEEE Trans. Sustain. Energy*, vol. 6, no. 3, pp. 1004–1012, 2015.
- [5] Y. Dvorkin, D. S. Kirschen, and M. a. Ortega-Vazquez, "Assessing flexibility requirements in power systems," *IET Gener. Transm. Distrib.*, vol. 8, no. 11, pp. 1820–1830, 2014.
- [6] H. Holttinen, M. Milligan, E. Ela, N. Menemenlis, J. Dobschinski, B. Rawn, R. J. Bessa, D. Flynn, E. Gomez-Lazaro, and N. K. Detlefsen, "Methodologies to determine operating reserves due to increased wind power," *IEEE Trans. Sustain. Energy*, vol. 3, no. 4, pp. 713–723, 2012.
- [7] E. Ela, V. Gevorgian, A. Tuohy, B. Kirby, S. Member, M. Milligan, and M. O. Malley, "Market Designs for the Primary Frequency Response Ancillary Service — Part I: Motivation and Design," *Power Syst. IEEE Trans.*, vol. 29, no. 1, pp. 421–431, 2014.
- [8] M. Vazquez, "Optimizing the spinning reserve requirements," 2006.
- [9] Ewea, "Wind in power," 2016.
- [10] SolarPower Europe, "Global Market Outlook for Solar Power 2015-2019," *Glob. Mark. Outlook*, p. 32, 2014.
- [11] (2016) TEİAS website. [Online]. Available: www.teias.gov.tr
- [12] H. Holttinen, A. Tuohy, M. Milligan, V. Silva, S. Müller, and L. Soder, "The Flexibility Workout," *IEEE Power Energy Mag.*, vol. 11, no. 6, pp. 53–62, 2013.
- [13] J. C. Smith, R. Piwko, W. Grant, M. Patel, S. Beuning, and M. Ahlstrom, "NERC Integrating Variable Generation Task Force (IVGTF) interconnection and operating tasks," *IEEE PES Gen. Meet. PES 2010*, pp. 2010–2012, 2010.
- [14] J. Kabouris and F. D. Kanellos, "Impacts of large-scale wind penetration on designing and operation of electric power systems," *IEEE Trans. Sustain. Energy*, vol. 1, no. 2, pp. 107–114, 2010.

- [15] T. Mai, M. M. Hand, S. F. Baldwin, R. H. Wiser, G. L. Brinkman, P. Denholm, D. J. Arent, G. Porro, D. Sandor, D. J. Hostick, M. Milligan, E. A. Demeo, and M. Bazilian, "Renewable electricity futures for the United States," *IEEE Trans. Sustain. Energy*, vol. 5, no. 2, pp. 372–378, 2014.
- [16] E. Ela and M. O'Malley, "Studying the variability and uncertainty impacts of variable generation at multiple timescales," *IEEE Trans. Power Syst.*, vol. 27, no. 3, pp. 1324–1333, 2012.
- [17] E. Ela, M. Milligan, B. Parsons, D. Lew, and D. Corbus, "The evolution of wind power integration studies: Past, present, and future," *2009 IEEE Power Energy Soc. Gen. Meet.*, pp. 1–8, 2009.
- [18] J. C. Smith, M. O'Malley, D. Osborn, R. Piwko, and R. J. Thomas, "R&D requirements for integration of wind generation," *Proc. Annu. Hawaii Int. Conf. Syst. Sci.*, pp. 1987–1996, 2011.
- [19] N. W. Miller, M. Shao, S. Pajic, and R. D. Aquila, "Western Wind and Solar Integration Study Phase 3 – Frequency Response and Transient Stability : Executive Summary Western Wind and Solar Integration Study Phase 3 – Frequency Response and Transient Stability : Executive Summary," no. December, 2014.
- [20] B. Practices, J. Cochran, L. Bird, J. Heeter, and D. J. Arent, "Integrating Variable Renewable Energy in Electric Power Markets : Summary for Policymakers," no. April 2012.
- [21] L. Söder, H. Abildgaard, A. Estanqueiro, C. Hamon, H. Holttinen, E. Lannoye, E. Gomez-Lazaro, M. O'Malley, and U. Zimmermann, "Experience and challenges with short-term balancing in European systems with large share of wind power," *IEEE Trans. Sustain. Energy*, vol. 3, no. 4, pp. 853–861, 2012.
- [22] A. Tuohy and H. Chandler, "Flexibility assessment tool: IEA grid integration of variable renewables project," *IEEE Power Energy Soc. Gen. Meet.*, pp. 1–4, 2011.
- [23] K. Trepper, M. Bucksteeg, and C. Weber, "Impacts of renewables generation and demand patterns on net transfer capacity: implications for effectiveness of market splitting in Germany," *IET Gener. Transm. Distrib.*, vol. 9, no. 12, pp. 1510–1518, 2015.
- [24] H. Holttinen, A. G. Orths, P. B. Eriksen, J. Hidalgo, A. Estanqueiro, F. Groome, Y. Coughlan, H. Neumann, B. Lange, F. Van Hulle, and I. Dudurych, "Currents of change," *IEEE Power Energy Mag.*, vol. 9, no. 6, pp. 47–59, 2011.
- [25] S. Spiecker and C. Weber, "Integration of fluctuating renewable energy - A German case study," *IEEE Power Energy Soc. Gen. Meet.*, pp. 1–10, 2011.
- [26] H. Holttinen, J. Kiviluoma, J. Mccann, M. Clancy, M. Milligan, P. B. Eriksen, A. Orths, and O. Wolfgang, "Reduction of CO2 Emissions due to Wind Energy – methods and issues in estimating operational emission reductions," *Power Energy Soc. Gen. Meet. 2015 IEEE*, 2015.
- [27] A. Helander, H. Holttinen, and J. Paatero, "Impact of wind power on the power system imbalances in Finland," *IET Renew. Power Gener.*, vol. 4, no. 1, p. 75, 2010.
- [28] M. Bartels, C. Gatzel, M. Peek, W. Schulz, R. Wissen, A. Jansen, J. P. Molly, B. Neddermann, H.-P. Gerch, E. Grebe, Y. Saßnick, and W. Winter, "Planning of the grid integration of wind energy in Germany onshore and offshore up to the year 2020," *Int. J. Glob. Energy Issues*, vol. 25, no. 3, pp. 257–275, 2006.
- [29] R. Barth, H. Brand, P. Meibom, and C. Weber, "A stochastic unit-commitment model for the evaluation of the impacts of integration of large amounts of intermittent wind power," *2006 9th Int. Conf. Probabilistic Methods Appl. to Power Syst. PMAPS*, 2006.
- [30] T. Yong, C. R. Philbrick, R. Entriken, and A. Tuohy, "Multi-settlement simulation of reserve procurement using stochastic optimal power flow," *IEEE Power Energy Soc. Gen. Meet.*, pp. 1–7, 2012.
- [31] M. Ghofrani, A. Arabali, M. Etezadi-Amoli, and Y. Baghzouz, "Operating reserve requirements in a power system with dispersed wind generation," *2012 IEEE PES Innov. Smart Grid Technol. ISGT 2012*, pp. 1–8, 2012.
- [32] E. N. Dialynas, L. G. Daoutis, C. Toufexis, and I. Charalambous, "Reliability and reserve capacity assessment of isolated power systems with increased penetration of renewable energy sources," *7th Mediterr. Conf. Exhib. Power Gener. Transm. Distrib. Energy Convers. (MedPower 2010)*, no. November, pp. 242–242, 2010.
- [33] M. Bucksteeg, L. Niesen, and C. Weber, "Impacts of Dynamic Probabilistic Reserve Sizing Techniques on Reserve Requirements and System Costs," vol. 3029, no. April 2015, pp. 1–12, 2016.
- [34] J. Kiviluoma, M. O. Malley, A. Tuohy, P. Meibom, M. Milligan, B. Lange, H. Holttinen, M. Gibescu, and M. O'Malley, "Impact of wind power on the unit commitment, operating reserves, and market design," *2011 IEEE Power Energy Soc. Gen. Meet.*, pp. 1–8, 2011.
- [35] William W. Cooper, "Integrating Renewables in Electricity Markets," *International Series in Operations Research & Management Science*. 2011.
- [36] Y. Rebours, D. Kirschen "What is spinning Reserve?," *The University of Manchester*. 2005.

Connected Revisit Path Planning For Flying Ad Hoc Networks in Dynamic Environment

Ilker Bekmezci¹

Abstract

Flying ad hoc networks (FANET) is one of the most important communication designs for multi-UAV systems. It can relay real time data from the UAVs to the ground station even if the UAV is outside of the UAV-to-ground station communication range. By the help of infrastructureless structure of FANET, it can be ideal especially for disaster or military scenarios. As in all kinds of ad hoc networks, in FANET based multi-UAV systems, connectivity is a hard constraint to be able to function properly, so FANET path plans must satisfy the connectivity requirement. In most of the connected path plan studies, the objective is to visit a predefined set of waypoints in a connected manner. However, only one visit of a waypoint is not adequate in highly dynamic environments, as in disaster or military applications. The waypoints must be revisited as frequent as possible so that the information gathered from the waypoints can be up-to-date. In this paper, connected revisit path plan problem (cRPP) is proposed and formulated. Because of the NP-complete structure of the problem, a distributed polynomial time heuristic algorithm is also proposed. Simulation studies show that the proposed algorithm is effective for FANET based multi-UAV system operates on highly dynamic environment.

Keywords: flying ad hoc networks, multi UAV, path plan, revisit

1 INTRODUCTION

FANET can be defined as an ad hoc network between UAVs, so FANET can be basically considered as a new type of mobile ad hoc networks (MANET) [1]. The main difference of the FANET from a MANET depends on high mobility capacity of the UAVs. Because of high mobility of the UAVs, the network topology of multi UAV systems changes very frequently. In addition, FANET data traffic is not based on peer-to-peer connections as in MANET. FANET mostly collects data from the environment and relays to the command control center. FANET has several advantages over the existing multi-UAV communication designs. It is especially effective when there is no available infrastructure and if real-time data communication is needed without the communication range restriction between the central station to the UAVs. FANET can be applied for extending the scalability of multi-UAV operations, reliable multi-UAV communication, complex missions with the swarm behavior of multiple small UAVs and decreasing payload and cost in communication of a multi-UAV system. However, in order to have an effective performance for the FANET, it should be ensured that all nodes are connected for all time. Thus, the multi UAV path planning algorithms should consider the connectivity requirement.

Although there are several studies about multi-UAV path planning strategies [2], there is a few number of connected path planning algorithms in the literature. In [3], connectivity to a sink is ensured only within a time window that each target must be visited rather than connectivity for all time. Consequently, information gathered at a target point is able to be transferred to a base station without any delay within a desired time window. To the best of our knowledge, the first algorithm ensuring all time connectivity for multi UAV networks is proposed in [4]. In that work, the objective is to minimize the required number of vehicles to complete the tasks within predefined time windows.

In the most of the planning algorithms for multi UAV systems, minimization of total route length or total elapsed time to visit all targets once by an UAV are used as an objective function [5]. Single visit problem formulation is adequate for many applications like aerial mapping. However, single visit at each task may not be enough for an effective mission execution under a dynamic environment in which conditions of the resources and tasks change frequently. For example, in the military operations, conditions changes rapidly. Consequently, revisits at the tasks are needed to assess the current status accurately. In this paper, Connected Revisit Multi UAV Path Plan (cRPP) is defined and formulated. A polynomial time heuristic is also proposed to this NP-complete problem.

In Section 2, the cRPP is defined formally and a heuristic solution method for the cRPP is proposed in Section 3. In Section 4, performance of the proposed method is presented and Section 5 concludes the paper.

¹Corresponding author: Turkish Air Force Academy, Department of Computer Engineering, Yesilyurt/Istanbul, Turkey.
i.bekmezci@hho.edu.tr

2 BASIC NOTATIONS AND THE PROBLEM DEFINITION

The objective of the Connected Revisit Multi UAV Path Plan is to collect the most updated information from the goal points on the terrain and relay the collected data to a command center. In order to collect the most updated information, the goal points must be revisited as frequent as possible.

Multi UAV system is modeled as a set of UAV, U , and all UAVs are organized to compose a FANET, which can be defined as a mobile ad hoc network (MANET) between UAVs. Even if there is no direct link between two UAVs, they can communicate with each other by the help of the ad hoc network. It is assumed that only one of the UAVs contains heavy and expensive satellite communication hardware. So only the UAV with satellite communication circuit can communicate with the command center directly. Fortunately, by the help of the FANET structure, all other UAVs also can communicate with each other and the command center.

Connectivity assumption for this FANET system is based on the Euclidean distance between UAVs, denoted as $d(i,j)$. If the Euclidean distance between UAV _{i} and UAV _{j} is shorter than the communication range, c_{thr} , UAV _{i} and UAV _{j} are assumed to be connected.

The goal points, G , are a set of predefined coordinates, $G=\{g_1, g_2, \dots\}$, and $|G|$ is the number of goals. The number of UAVs in U is denoted as $|U|$. Operation of the system starts at time 0, and ends at time T . For each $a \in U$, a has its own take off location, $init_a$.

Definition 2.1. A valid multi UAV path plan, P , is a set of function, $P=\{f_1(t), f_2(t), \dots, f_{|U|}(t)\}$, so that there is a corresponding function for each UAV in U . Each function in P gives the location of its corresponding UAV at time t with the following conditions: For any UAV tuple (a,b) , $(a,b \in U)$; and for any moment t , distance between $f_a(t)$ and $f_b(t)$ is not closer than a certain threshold and in this way UAVs can fly safely. Each UAV can track its path with its kinematic capabilities. For each UAV $a \in U$, $f_a(0)=init_a$ and $f_a(T)=init_a$.

The above definition considers the path plan as a set of continuous functions. Alternatively, it can be defined as a set of discrete time functions.

Definition 2.2. For a given UAV set U , a goal set G and a path plan P , assume that n^{th} visit time of goal g is denoted as t_g^n , and goal g is visited N_g times. Revisit time intervals of g is $T_g=\{t_g^2-t_g^1, \dots, t_{N_g}^2-t_{N_g-1}^1\}$, and maximum revisit time interval, t_{max} , is the maximum revisit time interval among all T_g .

Maximum revisit time interval represents the worst case of a given path plan. The user of the system has to wait at most t_{max} time to get the updated information from any goal coordinate.

Definition 2.3. For a given UAV set U , a goal set G and a path plan P , $G_t(V,E)$ is the FANET communication graph at time t . $V = U$, and E is the set of edges between nodes so that for $a, b \in V$, $(a, b) \in E$ and $(b,a) \in E$ iff $d(f_a(t),f_b(t)) \leq c_{thr}$, where $d(f_a(t),f_b(t))$ is the Euclidean distance between UAV a and b at time t .

FANET communication graph definition is needed to represent the all time connectivity requirement of FANET.

Definition 2.4. For a given UAV set U , a goal set G , Connected Revisit Multi UAV Path Plan Problem, denoted as cRPP, is to search for a valid path plan, P , to minimize t_{max} , while all $G_t(V,E)$ are connected, for $t, 0 \leq t \leq T$.

Connected Revisit Multi UAV Path Plan Problem (cRPP) is defined as a minimization of the maximum revisit time interval. The most important constraint is the FANET connectivity. Path plan must be produced so that its underlying FANET structure must form a connected network during the operation of the system.

cRPP is similar to multiple Traveling Salesman Problem (mTSP). However, while only one visit of each goal is satisfactory in most of the TSPs, cRPP must revisit goals to minimize the maximum revisit time interval. It is believed that cRPP is harder than classic mTSP. It is proved that mTSP is NP-complete. It concludes that cRPP is also at least an NP-complete problem.

3 BASIC ASSUMPTIONS AND THE PROPOSED HEURISTIC APPROACH FOR CRPP

Because of the NP-complete nature of cRPP, it is not feasible to construct exact model. So, instead of finding the optimal cRPP solution with exact model, we propose a polynomial time heuristic algorithm. Before introducing the details of the heuristic algorithm, the basic assumptions are presented as follows. UAVs are homogeneous. Each UAV knows its own location during the operation by the help of its GPS. Each UAV also knows the exact location of the other UAVs. The height of the UAVs are slightly different so that no UAVs collides with each other. Terrain is modeled as a 2D area, and there is no occlusion. All goals are predefined and UAVs know the exact coordinates of the goals. If the Euclidean distance between two UAVs is less than a predefined communication threshold, c_{thr} , two UAVs are connected to each other directly.

In this paper, we proposed a CRPP heuristic which is presented in Figure 1, while the network includes an immobile ground station. The first step of the algorithm is to assign a specific UAV to a specific task. without any network connectivity constraint. In order to perform the assignment, we need a utility function that measure the value of assigning a UAV to a task. One of the main inputs of the function is the time elapsed since the last visit of a given task has taken place (t). Another parameter that must be considered is the distance between the UAV and the task (d). Utility function takes these two parameters and calculates the value of assigning a specific UAV to a specific task. By

the help of the utility function, all the values are calculated for each UAV to each task, and a UAV is assigned to a task that maximizes the utility function.

```

Input:  $U, GS, G, c_{thr}$ 
Output: Multi UAV path plan
for all ( $g \in G$ ),  $g \leftarrow$  unvisited,  $t_g \leftarrow 0$ 
while the mission is not completed do
     $t \leftarrow t + \Delta t$ , and update all  $t_g$ 
     $L \leftarrow$  the links that risks the network connectivity for comm. threshold  $c_{thr}$ 
    while all the UAVs are not assigned do
        Assign UAV a to Goal g if  $U(a,g)$  is maximized and a is unassigned.
        for all neighbors n of UAV a with critic link do
             $L_a = \text{Pull}(a,n)$ ,  $L_a$  is the set of UAVs pulled by leader UAV a.
        end for
        if  $GS \in L_a$  and  $L_a$  has less UAVs than needed to visit Goal g then
            Assign the needed number of unassigned UAVs which are closest to  $L_a$ 
        end if
    end while
    For all UAV  $u \in L_a$  and  $GS \in L_a$ , Move u for line formation
    Otherwise move UAVs to the assigned Goal g.
    Label the visited goals g, and  $t_g \leftarrow 0$ 
end while

```

Figure 1. The proposed heuristic for CRPP with an immobile ground station (GS).

The utility function used in this paper is $U(A,s) = t^2/d(A,s)$. In this function, t (revisit time) is again the most important part of the utility function. However, it can be maximized even if t is not maximized for some exceptional cases. If t is high enough and a UAV is very close to s, it can be higher than a task with maximum t.

If all the assignments are performed according to the utility function and the assigned UAVs move towards to its assigned task, connectivity of the network may not be preserved. In order to preserve the connectivity, a leader-follower schema is developed. According to this strategy, firstly, the critical links must be identified. A link between two UAVs is critical if the network cannot be connected without that link. If a is assigned to a specific task g_a and there is a critical link between a and b, a becomes the leader of b, and the leader pulls its followers. In this way, all critical links and the network connectivity can be preserved. It should be noticed that this leader-follower pull algorithm is recursive. If b becomes the follower of a, and if it has other critical links, b becomes the leader of its critical link neighbors.

The algorithm described above works without any problem if all the nodes can move. However, if immobile ground station is also a part of the network, there can be some problems. When a UAV has a critical link with ground station, and if it is assigned to a task, it has to pull its neighbors with critical links, including the ground station. Because of the immobile structure of the ground station, its leader has to stop and cannot visit its task.

Because of the recursive structure of the pull function, this problem can be realized in a chain reaction, as in Figure 2(a). Let us assume that a-b, b-c and c-GS links are critical and a is assigned to Task1. UAV a wants to move towards Task1, and in order to preserve the connectivity, it pulls b. In the same way, b also pulls c and c pulls GS. However, GS cannot move, and a, b, and c have to stop, and cannot visit Task1.

One of the solutions is line formation movement. In Figure 2(a), because of the ground station, UAVs cannot move. However, if the UAVs move into closest point in the line segment between GS and Task1, eventually these UAVs are on the line between GS and Task1. This formation decreases the distance between UAVs and some critical links disappears. Finally a can move to Task1 and Task1 can be visited as in Figure 2(b).

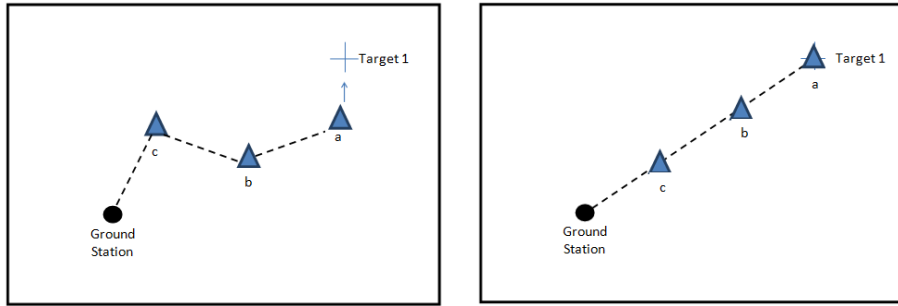


Figure 2. (a) All the UAVs have to stop

(b) Line formation solution

Although line formation is necessary for our heuristic, it is not sufficient. Let us assume that there are n UAVs that have to stop as in Figure 3(a). Even if they form a line between GS and the task, maximum distance they can reach is $c_{thr} \times n$. If the distance between GS and the task is greater than this value, the task cannot be visited. This situation may result in a deadlock state which is illustrated in Figure 3(a). Let us assume that some UAVs are in line formation to visit Task1, and the other UAV is in line formation to visit Task2. However, they cannot visit the assigned task, because they have to stop. It must be noted that deadlock situation occurs only if one of the leaded UAVs has a critical link with the ground station.

The solution of the deadlock problem is to be sure to assign enough number of UAVs for a leader. If a UAV leads the other UAVs to visit a certain task, and if the number of leaded UAVs is not enough to visit, and if one of the followers has a critic link with ground station, it is a potential deadlock position. If a leader is in a potential deadlock state, enough number of UAVs should be assigned for the leader UAV's task. Let us assume that the leader and its followers is a subset of UAVs, L . This strategy finds the needed number of unassigned UAVs which are closest to L . Line formation movement forces the UAVs to move within the line between the ground station and the assigned task. In this way, the leader can visit the task properly. In figure 3(b), UAV c is also assigned to Target 1, and according to line formation strategy, it move to the line segment between Target 1 and the ground station.

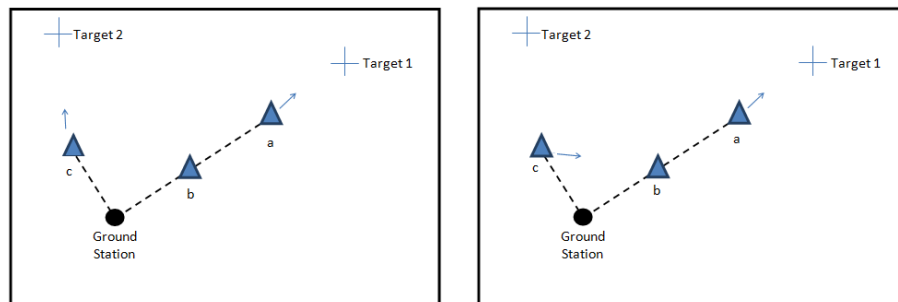


Figure 3. (a) Deadlock state

(b) Deadlock solution

4 PERFORMANCE RESULTS

In this section, we present the results of computational experiments in order to evaluate the effectiveness of the algorithms used for the connected multi UAV task planning problem for FANET. The cRPP algorithm and simulation environment are coded in MATLAB, and the computational experiments have been conducted on a machine, which has an Intel Xeon 2.33 GHz processor running the Linux operating system. The default settings are presented in Table 1.

Table 12. Default Settings Of The Selected Parameters

Parameter	Value
Terrain dimensions	2500m × 1500m
UAV speed	4.5 m/s
Communication range	[200m, ..., 800m]
Number of UAVs	[5, ..., 20]
Number of Goals	# of UAVs × 2

Mission completion time	600 s
Ground Station Location	Center

Figure 4 shows the maximum revisit time performance of the proposed heuristic. It shows that maximum revisit time decreases, when the communication threshold increases. It is valid almost for all number of UAVs. When the threshold is lower, UAVs have to pull each other to preserve the connectivity. Especially when the number of UAVs is relatively less, the network becomes more sparse. In this case, UAVs have to pull each other more frequently.

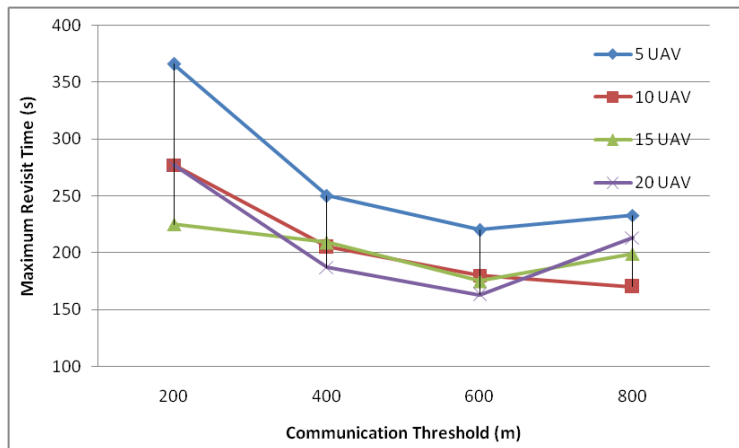


Figure 4. Maximum revisit time performance.

In addition to maximum revisit time performance, average revisit time is also investigated. Figure 5 shows the performance results for average revisit time. For lower number of UAVs, communication threshold is more important. However, when there are higher number of UAVs, this effect becomes limited. For example, when there are 20 UAVs, the average revisit time performance is almost the same for all threshold levels. It shows that when the network is highly connected, communication threshold is less important for the proposed heuristic.

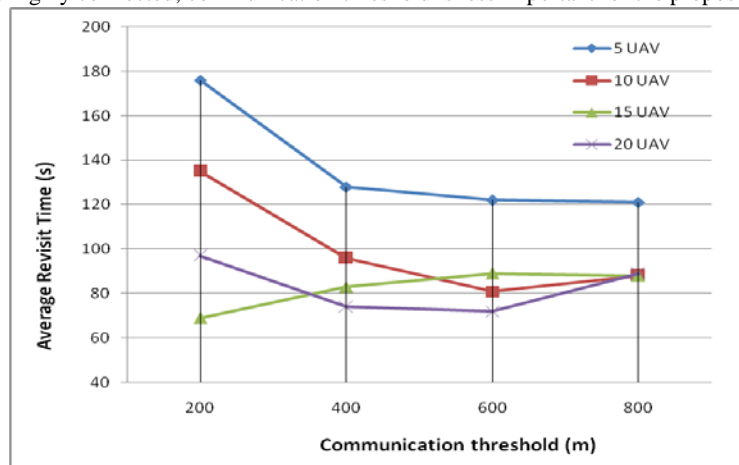


Figure 5. Average revisit time performance.

5 CONCLUSION

FANET is a new type of ad hoc network, so that the nodes are UAVs. It can be used when real time data is needed from infrastructureless environments. One of the most important constraint of FANETs is connectivity. UAVs must be navigate so that the connectivity of the network can be preserved. In most of the existing papers about connected multi UAV path planning, the objective is to produce an optimal path to visit a set of predefined waypoints. In many application scenario, this waypoint visit model is valid. However, in some applications, especially when the environment changes rapidly, as in military operations, visiting waypoints may not be enough. In these applications, waypoints must be revisited as frequent as possible to get the most updated information. In this paper, connected

revisit path plan problem (cRPP) is proposed and formulated. In addition, a polynomial time heuristic is also proposed to solve cRPP which is an NP-complete problem.

ACKNOWLEDGMENT

This research was supported by The Scientific and Technological Research Council of Turkey (TUBITAK) under Grant 113E565.

REFERENCES

1. Bekmezci, O.K.Sahingoz and S.Temel, "Flying Ad-Hoc Networks (FANETs): A survey", *Ad Hoc Networks* 11(3):1254-1270, 2013.
- [2]. L. Luo, N. Chakraborty, and K. P. Sycara, "Multi-robot assignment algorithm for tasks with set precedence constraints.," in *ICRA*, pp. 2526–2533, IEEE, 2011.
- [3]. S. S. Ponda, L. B. Johnson, A. N. Kopeikin, H.-L. Choi, and J. P. How, "Distributed Planning Strategies to Ensure Network Connectivity for Dynamic Heterogeneous Teams.," *IEEE Journal on Selected Areas in Communications*, vol. 30, no. 5, pp. 861–869, 2012.
- [4]. S. Chopra and M. B. Egerstedt, "Multi-robot routing under connectivity constraints," *3rd IFAC Workshop on Distributed Estimation and Control in Networked Systems*, 2012.
- [5]. G. A. Korsah, A. Stentz, and M. B. Dias, "A Comprehensive Taxonomy for Multi-robot Task Allocation," *Int. J. Rob. Res.*, vol. 32, pp. 1495–1512, Oct. 2013.

Study On the Effect of The Mechanical Vibration on Solidification in Process of A356 Aluminum Alloy Casting

Murat Colak¹, Murat Balci¹

Abstract

Metal and almost all of its alloys are liquid in a phase. Materials can be applied in cases of solidified, heat treatment or mechanical processing. Therefore, the materials working performance and the solidification process in physically relevant time are very important. The design resulting of the Cast aluminum-based alloy solidification process affects all of the mechanical properties and also needs other process to obtain the desired properties. In particular, the design in any particle size and shape can be controlled by solidification. Once reactant liquid aluminum alloys generally melting pot the grain refining thinners make heterogeneous nucleation centers and play a role in creating the design in a more fine-grained one. It has been long known that grain refining process increase the fluidity of the aluminum alloy, provides better nutrition, provides a more porous formation of a structure, improve the mechanical properties, provides a better fatigue resistance, which increases the leakage resistance and also has a better nutrition. Additionally to Grain refining under casting aluminum alloys many other methods are available to such as; mechanical vibration casting, electromagnetic interference during solidification and curved cooling plate casting.

In this study, it is going to be aimed to make available the A356 aluminum casting alloy solidification under varying intensities of vibrations. So without vibration and changing intensities vibration A356 alloy is going to be characterized and all the features will be determined both microstructures and mechanical aspects after the casting. This study includes sand mold casting, microstructure analysis, density measurement and analysis. At the end of this research it is expected that with the increasing rate of the vibration and with also the breaking of the dendrites structure inside the aluminum alloy, a more fine - grained structure will be occur.

Keywords: *Alüminyum Döküm, A356, Katılma, Mekanik Titreşim, Tane İnceltme*

1 INTRODUCTION

The rapid growth in the aluminum industry is due to the combination of these unique properties of metal and these features make aluminum is one of the most versatile building and engineering materials. The best known properties of aluminium is being lightweight and even has a more strength values than structure steels when being alloyed. On the other hand A356 alloy is a kind of material that has a high elongation values, good machinability, high stress values and a ductile material. The A 356 alloys are widely used in heavy duty structural parts so that requiring high tensile values, in the automotive industry and in the aircraft industry[1].

In the automotive industry to reduce the negative impact of fuel savings on the environment, many light alloys are also required like aluminum. In the automotive industry and as an option for manufacturing many parts of the materials the interest in aluminum gets increase and with these interests the cost is expected to fall. In accordance with the demands of the automotive industrialists the microstructure and mechanical properties of aluminum alloys needs to be developed [2-4].

To improve the properties of aluminium alloy among the foundry practices there are many methods which are commonly known as Grain refinement, mechanical mixing, ectromagnetic stirring method, casting in the inclined cooling solidification and casting under vibration plate. In aluminum the grain refining practices, provide considerable reduction in the grain structure and improves the alloy 's castability [1].

¹Corresponding author: Bayburt University, Department of Material and Nanotechnology Engineering, 69000, Bayburt, Turkey. mucolak@bayburt.edu.tr

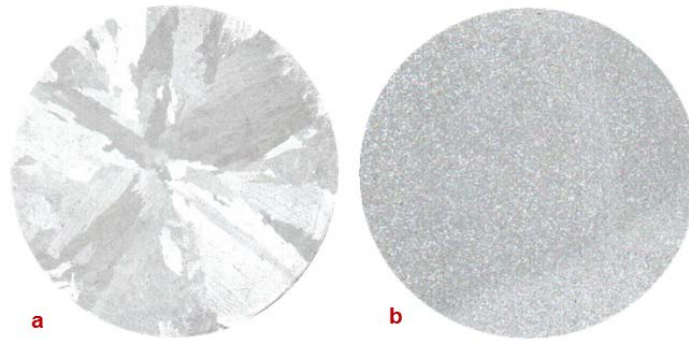


Figure 1. (a) Grain with no refining, (b) the grain structures efficiency of Al-5Ti-1B addition [1]

In liquid metal even into small quantities, such as 0.01% amount with the addition of titanium (Ti) and boron (B) elements, a quick and significant grain refining effect are observed in the structure. In Liquid metal into even in small quantities, the addition of structure elements such as 0.01 % titanium (Ti) and boron (B) to quickly and significantly effect in the structure element are observed. It can be seen from the histogram of Figures 1(a) and 1(b) effect of the addition of Ti and B elements on a aluminum alloy grain structure.

It is observed In Figure 1.a unrefined grain structures in the form of long wings aluminum grains and also a small , regular and coaxial grain structure into a grain refining structure in Figure 1b. With the thanks of a transformation of the grain structure into a small and coaxial formats ,the mechanical properties become more isotropic and the alloy becomes more resistant. Grain refining process reduces the porosity and size ,thereby it increase the supply ability of alloy [5-7]. In a grain refining process within A356 alloy which is also a eutectic Al - Si alloy by Li, Wang and Kung [8] with three different grain refinement master alloys such as Al-%5Ti, Al-%5Ti-%1B and Al-%4B, It is observed that boron as a grain refining is more effective than titanium. In a similar study Sigworth and Guzows [9] reported that Al -B master alloys containing AlB₂ showed much more excellent grain refining effect. In a grain refining addition for the reasons of additional cost and practising problems many alternative modification process are required.

In casting of Aluminum alloy mechanical mixing method, the liquid mixing process is generally provided with mounting of the drill, wheel or multi- wheel on a shaft which is rotating in the center [10,11].. For the reason of being the non- dendritic structure, multiplication is applied during the solidification. In Figure 2 it can be seen an example of a simple mechanical mixing unit. However, in mechanical mixing process there have been many problems faced with application and process.

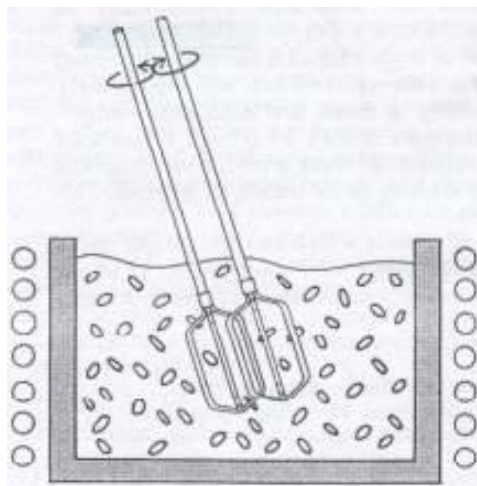


Figure 2. Mechanical mixing unit [12].

In order to eliminate the problems in a mechanical mixing process, electromagnetic mixing method has been developed. In this technique the electromagnetic stirring with a continuous caster creating and the non- dendritic microstructure rods were produced. In Figure 3 it can be seen the electromagnetic stirring as schematically. In many products produced by this method, the grains size such as the particle size of between 330 μ m-100 μ m are specified [13,14]. The main problem in the magnetic stirring method is the high cost of production. It is also big problems for a structure if it has no homogeneity and a shape of badge instead of an orbicular one [15].

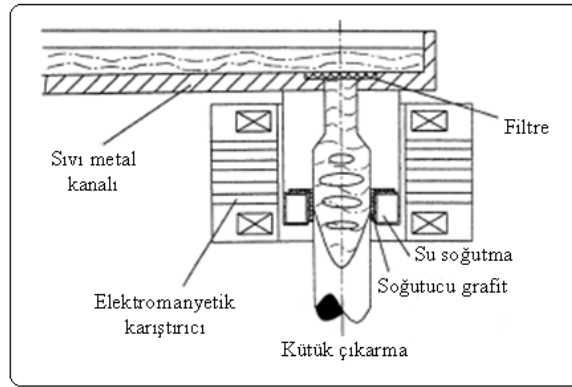


Figure 3. Schematic representation of the electromagnetic stirrer [15]

In the curved cooling plate casting process ; it is achieved by pouring the mixing , in a melted state , through an inclined surface which is of the water –cooled by the water. In this process the metal which is melted in a appropriate temperature is being poured into the mold along a curved plate which is made from plain carbon steel. The surface of the Curved cooling plate is usually coated with boron nitride so as to prevent the solidified metal sticking on the surface. The solid cores take form due to the rapid heat transferring in the point of the contact between the melted and curved plate. These cores are removed from the surface as a result of the applied shear stress and metal flow. As a result of this process, solidification begins at the surface of the cooled plate , the cored grains are grown, and with the liquid movement the plate separates from the plate surface and creates a structure that the dentirit disrupted. In this method a decrease in the temperature of the liquid alloy which is expected to be pored through the cooling surface which will also provide the solidification once flowing from surface. [16-21] .

Eğimli soğutma plakasında döküm yönteminde; ergiyik haldeki alaşımın su ile soğutulan eğimli bir yüzey üzerinden dökülmesi suretiyle gerçekleştirilir. Bu proseste, uygun sıcaklıktaki ergimiş metal sade karbonlu çelikten yapılmış eğimli plaka boyunca akıtılarak kalıp içine dökülmektedir. Eğimli soğutma plakasının yüzeyi, katılaşılan metalin yüzeye yapışmasını engellemek için çoğunlukla bor nitrid ile kaplanmaktadır. Katı çekirdekler ergiyik ve eğimli plaka arasındaki temasta hızlı ısı transferinden dolayı şekillenmektedir. Bu çekirdekler uygulanan kayma gerilmesi ve metal akışının bir sonucu olarak yüzeyden ayrılır. Sonuç olarak, soğutulan plakanın yüzeyinde katılaşma başlar, çekirdeklenen taneler büyür ve sıvı hareketi ile plaka yüzeyinden ayrılarak kalıbı doldururken dentiritleri bozunmuş bir yapı oluşturur. Bu yöntemde soğutulmuş yüzey üzerinden dökülecek sıvı alaşımın sıcaklığı da, yüzeyden akarken katılaşmanın başlamasına sağlayacak şekilde düşük olmalıdır [16-21]. Şekil 4.de eğimli soğutma plakasında döküm yöntemi şematik olarak verilmiştir.

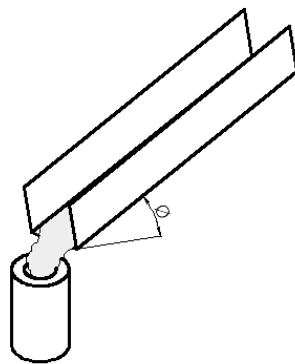


Figure 4. Schematic representation of the Curved cast cooling plate [17].

Once we examine all these we notice that in these techniques, the dendritic structure is also degradation and in parallel with this situation the properties of materials developed positively, but many advantages and disadvantages of all these methods are available. It has been observed on the other hand the mechanical properties of these alloys hand has been also found to be dependent on the morphology of the eutectic Si particles. [22-24] .

In this study, it is aimed to use the solidification technique(which is also an alternative one) for improving the properties of aluminum alloys under the mechanical vibration. The solidification of the A356 aluminum casting alloy

will be provided under the varying vibration intensity. In the present study, the A356 alloy has been used here, because it has a wide range of solidification based on Al-Si alloy and has high fluidity rate. Thus, without vibration the structure of the A356 alloy will be characterized in terms of microstructure, and the properties will be determined. In this study there are many analysis methods such as; sand casting, microstructure analysis and measurement of density.

2 EXPERIMENTAL STUDY

In this study, the solidification technique under mechanical vibrations has been used at the time of filling the liquid metal in the mold and this technique is also a time when the dendrite arms break and provide many particles in straight shape that is like half orbicular shaped. For mechanical vibration a machine has been designed as shown schematically in Figure 5.

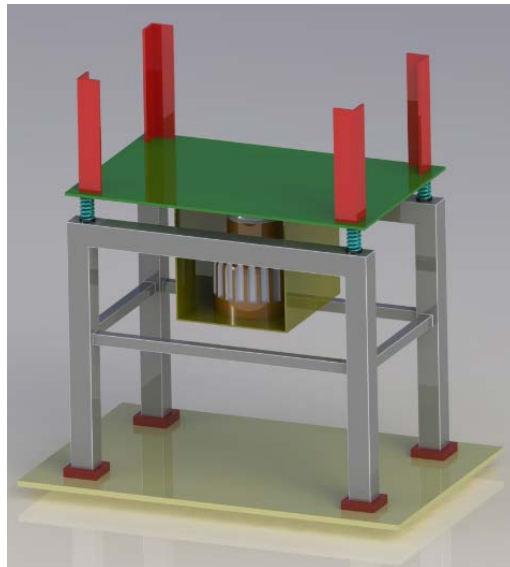
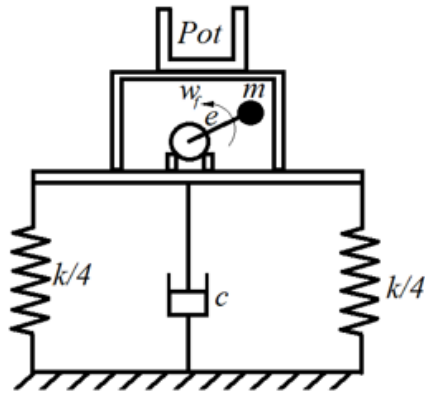


Figure 5. Schematic image of solidification machinery setup under mechanical vibration image

A sand mold in the shape of rectangular prism bases dimensions 10 cm x 10 cm x 5 cm has been prepared for aluminum block casting. The degreed plate in the sand mold has been fixed on steel plates with L-shaped profiles. The plate springs are connected to a plate which is connected with the electric motor. This plate is connected to a plate in which the electric motor is also connected with the springs. In the experiments, an alternating current electric motor is used with properties of rev / min bases 11 kW / 3 phase / Δ 380 V / 50 Hz / $\omega_f = 1450$. In order for the motor to do the vibration, many substances bases 20g, 50g and 100g weight have been added in the rotor of the motor. Thus, depending on the change of the weight a solidification has also been created under different violent vibration. Calculations related to vibrations induced to the weight of the loaded rotor is as shown below.

Table 1. Properties of vibration system.

The total mass (M)	Spring Costant (k)	Extinction Costant (c)	Distance to rotor shaft center (e)	Angular velocity (w)
10 kg	9350 N/m	50 N.s/m	0.03 meter	1450 rev/min



$$x = \frac{r^2 * m * e}{M \sqrt{(1 - r^2)^2 + (2 * \xi * r)^2}}, \quad r = \frac{w_n}{w_f}, \quad w_n = \sqrt{\frac{k}{M}}$$

Figure 6. Schematic view of test system and formulas.

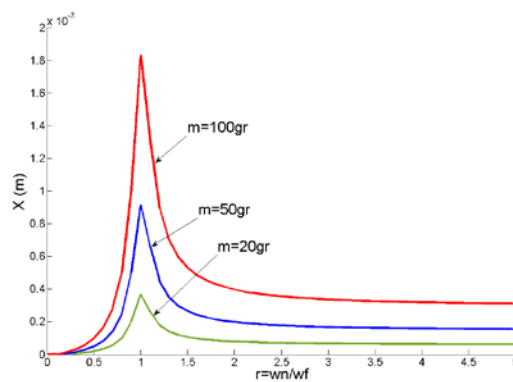


Figure 7. Diagram of amplitude changes graph depending on the added mass on the vibration system

The castings conducted within the study are made under the same conditions to determine the variation and the change of vibration. In present study a normal non-vibrating casting experiment has been performed to determine the effects of casting and vibration intensity in three different vibrations. The reliability of the results and in terms of the control each of experiment has been repeated in three times. In experiments the A356 casting alloy has been used which is having a high viscosity and a wide solidification range. Table 2 shows the chemical analysis of A356 alloy performed using the spectrometer.

Table 2. Chemical analysis of A356 alloy (wt.%)

Al	Si	Mg	Cu	Fe	Mn	Ti
Balance	7.28	0.412	0.027	0.122	0.03	0.056

A356 alloy has been melted in a pot based on silicon carbide and type electric furnace. When the temperature of the liquid metal comes to 750 °C in order to clean gas in the liquid metal the alloy was washed with nitrogen.

After the liquid metal casted into the mold, the temperature has been controlled by the thermocouple connections and then the vibration has started when the temperature reaches to 620 °C solidification temperature and it has been continued until solidification completed. The temperature of liquid metal in the sand mold falls to 540 °C after about 120 seconds. Because of liquid metal has no effect to solidification under solidus temperature, the motor setting has been shut down when the temperature fell under 540 °C and mold continued to cooling under normal conditions.

After mold cooling, the casting samples have been removed from the mold and then in order to determine the sample internal structures in changed casting conditions many microstructure photos have been taken by Nikon Eclipse L150 optical microscope but before it has been prepared as metallographic in advance. Furthermore, for detecting the casting feeding ability the density measures have been made according to Archimedes principle.

According to Archimedes principle, each samples have been weighted before in water, then in the air. The determined sample weights are as below ;

$$d_n = \frac{m_h}{m_h - m_s} \times d_s \quad (1)$$

(m_h), is for weight of sample In the air

(m_s), is for weight of sample In the the water

(d_n), is for the intensit of water in the room temperature

3 CONCLUSION AND RESULTS

The microstructure photos of A356 alloy have been obtained from experiments as shown in Figure 7. Normal casting structure with no – vibration is given in Figure 7. The microstructure images are given in (a), (b), (c) and (d), are the examples of different vibration intensities applied to A356 alloy after solidification. As it can be seen from the microstructure image the solidification under vibration has provided the dendritic structure greatly degenerate in A356 alloy, lead to breakage in dendrite arms and aslo it provided a solidification in these arms so as in α -Al grains, which are more coaxial relatively close to orbicular in morphology.

As the intensity of the vibration increased, the α -Al grains gradually gained a coaxial morphology and with this increasing intensity it has been observed that not only the dendritic arms has been broken but it has also spent all the grains prodigally with the effect of mixing.

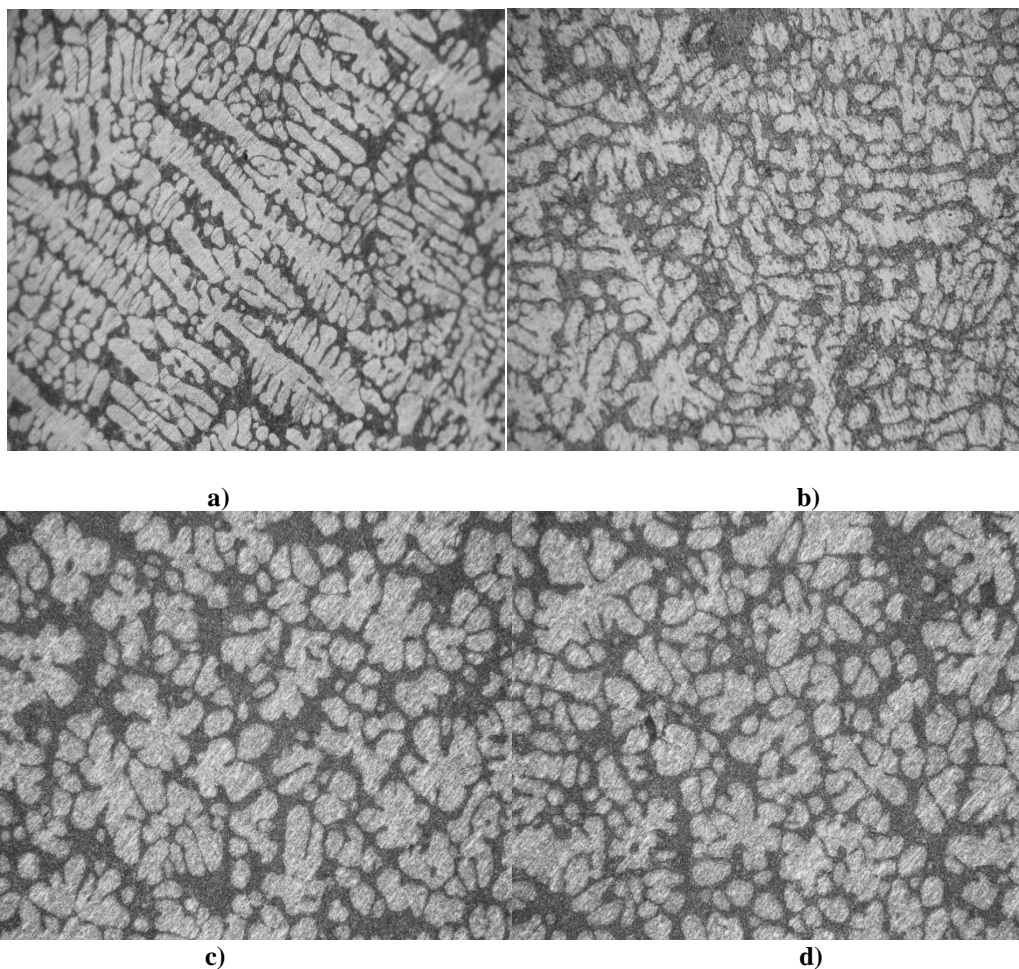


Figure7. The casting structure in different vibration, a) Non - vibrating b) $m=20gr$, c) $m=50 gr$ d) $m=100$

Intensity measurements have been conducted according to the Archimed principles. The calculated intensity and pore results of the samples obtained by sand mold casting have been given in Table 3. The Intensity measurements have been made from casting samples obtained after the gating and supply have been cut down.

Table 3. Measurements of intensity and porosity of the casting sample.

Sample name	Weight in air (Gram)	Weight in water (Gram)	Experiemental Density (gr / cm ³)	Reference Density (gr / cm ³)	Measured porosity %
Non vibrating	1316,84	812,22	2,60	2,67	2,44
m=20 gr	1322,46	821,18	2,63	2,67	1,37
m=50 gr	1320,14	823,36	2,65	2,67	0,65
m=100 gr	1326,62	829,14	2,66	2,67	0,30

When the samples of intensity and porosity in sand mold casting as shown above analyzed, the first attracted result has been the intensity increasing of casting samples with the effect of vibration. The same conditions as in the flicker intensity values of pouring pouring samples in the sample 2.6 g / cm³, while these values increased due to vibration. While the value of intensity has shown about 2,6 gr/cm³ In the same casting samples, these values onces have been increased in the situation of vibration. The intensity value has been obtained as about 2.66 g / cm³ in experiments of the Maximum vibration. When the values of porosity (obtained from the experimented samples) examined and proportioned to intensity alloy reference depended on intensity rate a porosity in amount of 2.44 % has been measured. On the other hand this value has decreased about %0,30 depending on the paralel of vibtation intensity during the solidification. The amount of intensity increasing and porosity change are on attractive levels than non-vibrating casting even at the lowest intensity of the vibration applied in the experiements. But the change of vibration and porosity have'tt been changed in a proportional way. The reference intensity value used in the pore standard values even at very low levels in the alloy can vary widely in of the same standard. The value of reference intensity used in porosity calculating are the standard values and even at lower levels alloy of same standard it may show many varieties in chemical changes. However, the aim in here is to make a comparison depends on the the changes of the vibration intensity. The reason of the change in the castings depending on the amount of porosity vibration is the degradation of dendrite in solidification and with this issue a new grained structure has been formed. This situation is also in a confirmable quality by micro-structure pictures given in Figure 8.

4 CONCLUSIONS

In investigating the effects of different vibration intensities which are applied during the solidification of A356 alloy and in the study which is aimed to show the comparisons with the casting piece.

At the end of the experiements, as can be seen on the photographs taken from the microstructure, the grains in casting are smaller by the vibration applied during the solidification and dendrites arms have been broken. I has also been seen that with the more intensity of vibration, the more dendrite arms have been broken and not only that it has distributed the broken dendrites arms. It has also been thought that the broken small dendrites arms create a new center for nucleation of liquid metal. Thus, as created in a more amount, grains becomes a more homogeneous coaxial structure than dentritic structure. It can be possible to see similar results once look at the other studies related to the this subject.

During solidification under the vibration, because it causes a large amount of breakages and prevents the increasing in the dendrite arms we can see a less drawings than a normal casting. While the value of intensity is about 2.6 g / cm³ in a normal casting, it increases to 2.66 g / cm³ in a casting with vibration. In the Sand mold casting samples, the intensity values have been conducted by Archimed principle and the porosity values have been estimated by using the standart reference intensity.

While the value of porosity is 2.5 % in a normal casting, the smaller porosities has been determined in the solidification process under vibration. The lowest amount of porosity has been determined as 0.3% in the experiement includes much more vibration. The decrease in the amount of porosity has been associated with the dendrite arms breakage during solidification under vibration effect and in paralel with this more fine-grained structure has been formed. Because of increasing in vibration also increase the property and this is not in a

proportional way of materials in intensity, we try to find how the relationship changes between the property of materials and vibration intensity and for this reason we also think it will be useful to conduct many experiments on other stages in the study.

REFERENCES

- [1] Sigworth, G. K., Kuhn, T. A., "Refinement of Aluminium casting Alloys", AFS Transactions, Vol.115, Page (s): 1-12, 2007.
- [2] Chiarmetta, G., "Thixoforming of Automobile Components", in: Proceedings of the Fourth International Conference on Semi-Solid Processing of Alloys and Composites, Page(s): 204-207, 1996.
- [3] Birol, Y., Çakır, O., Alageyik, F., "Elektromanyetik Karıştırma İle Tiksotropik Alüminyum Biyet Üretimi", 13. Uluslararası Metalurji ve Malzeme Kongresi Bildiriler Kitabı, İstanbul, s. 1704-1712, 2006.
- [4] Birol, Y. "AA6061 Alaşımında Tiksotropik Yapı Elde Edilmesi", 13. Uluslararası Metalurji ve Malzeme Kongresi Bildiriler Kitabı, İstanbul, s. 1752-1759, 2006.
- [5] Metals Handbook, Vol.15. Casting, Ed. ASM International Handbook Committee, 743-770, Metals Park, OH, ASM International, 1989.
- [6] Kayıkcı, R., Çolak, M., Kuma Dökülen Etial160 Alüminyum Alaşımında Tane İnceltmenin Beslenebilirlik Üzerine Etkisinin İncelenmesi, 5. Uluslararası İleri Teknolojiler Sempozyumu (IATS'09), 13-15 Mayıs 2009.
- [7] Giocai, C., *Dendrite Coherency During Equiaxed Solidification in Aluminum Alloys*, Chemical Communications, Stockholm University, 83 pages, 1994.
- [8] Lu, H. T., Wang, L. C., Kung, S. K., *Grain Refining in A356 Alloys*, J. Chinese Foundrymen's Association, Vol. 29, pp. 10-18, 1981.
- [9] Sigworth, G.K., Guzowski, M. M., *Grain refining of Hypo-eutectic Al-Si Alloys*, AFS Transactions, Vol 93, pp. 907-12, 1985.
- [10] Fan, Z., "Semisolid Metal Processing" International Materials Reviews, 47(2): 49-85(2002).
- [11] Figueredo, A., "Science and technology of semi-solid metal processing", North America Die Casting Association, USA, 2.1-2.17, (2001).
- [12] Flemings, M., "Behavior of Metal Alloys in the semi solid state", Metall Trans. A, 22A:957-981(1991).
- [13] Flemings, M., Riek, R., Young K., "Rheocasting", Mater sci. Eng. 25:103-117(1976).
- [14] Sukumaran, K., Pai, B.C., Chakraborty, M., "The effect of isothermal mechanical stirring on an Al-Si alloy in the semisolid condition", Materials Science and Engineering, A369: 275-283 (2004).
- [15] Atkinson, H.V., Kapranos, P., Liu, D., Chayong, S.A., Kirkwood, D., "Thixoforming of normally wrought aluminium alloys", Materials Science Forum, 396-402:131-136(2002).
- [16] Salarfar, S., Akhlaghi F. and M. Nili-Ahmadabadi, "Influence of Pouring Conditions in the Inclined Plate Process and Reheating on the Microstructure of the Semi-solid A356 Aluminum Alloy", Proceedings of the 8th International Conference on the Processing of Semi-solid Alloys and Composites, 2004.
- [17] Kasman S., S. Gencalp, N.Saklakoğlu, S.Ucar, "Dokum Yonteminin ETIAL 160 Alaşımının Mekanik Özelliklerine Etkisinin İncelenmesi", 5.Uluslararası İleri Teknolojiler Sempozyumu (IATS'09), 2009.
- [18] Haga, T., "Semi-solid roll casting of aluminum alloy strip by melt drag twin roll caster", Journal of Materials Processing Technology, 111:64-68, 2001.
- [19] Haga, T. and P. Kapranos, "Billetless Simple Thixoforming Process", Journal of Materials Processing Technology, Vol.130-131, pp. 581-586, 2002.
- [20] Haga, T., Suzuki, S., "Casting of aluminium alloy ingots for thixoforming using a cooling slope", Journal of Materials Processing Technology, 118 (1-3): 169-172, 2001.
- [21] Taghavi, F., Ghassemi, A., "Study on the effects of the length and angle of inclined plate on the thixotropic microstructure of A356 aluminum alloy", Materials and Design, 30:1762-1767, 2009.
- [22] Hafız, M.F., Kobayashi, T., "The Contribution of microstructure to the fracture toughness of hypoeutectic Al-Si casting alloy", in: Proceedings of the Fourth International Conference on Aluminium Alloys, Page(s): 107-114, 1994.
- [23] Jung, B.I., Jung, C.H., Han, T.K., Kim, Y.H. "Electromagnetic Stirring and Sr modification in A356 Alloy", J.Mater. Process. Technol. Vol.111 Page(s): 69-73, 2001.
- [24] Tahamtan, S., Fadavi Boostani A., Nazemi, H. "Mechanical Properties and Fracture Behavior of Thixoformed, Rheocast and Gravity-Cast A356 Alloy", Journal of Alloys and Compounds 468 Page(s): 107-114, 2009.
- [25] Taylor, R.P., McClain S.T., Berry J.T., *Uncertainty analysis of metal-casting porosity measurements using Archimedes' principle*. Int J Cast Met, 11:247-57, 1999.

Improving the Isolation between Two Port Microstrip Dipole Antennas

Oguzhan Akgol¹

Abstract

2-Port microstrip dipole antennas with operation frequencies of 2.4 GHz and 6 GHz are designed. In order not to prevent the antennas to affect each other, the isolation should be improved or the separation distance between these two antennas must be chosen large enough. However, in most applications, the latter solution is not possible due to the physical space requirements so more efficient solutions should be used. In this study, a Metamaterials (MTM) based structure is used to improve the transmission parameter, known as the isolation between two antennas without sacrificing any board space is designed. The geometry has simple shape and not requires a lot of installing area. In addition the isolation with and without the MTM structure is compared by using CST Microwave studio and the results are shown. Isolation behavior improved significantly proving that the structure can be used in many existing antennas offering much better performances and it can also be seen as another method for antenna minimization.

Keywords: MTM, CST

1 INTRODUCTION

Metamaterials are defined as the materials showing unusual and extraordinary features comparing to the ones from nature. MTMs consist of periodically arranged resonators and the combinations of wires or strips depending on the design. With MTMs, it is possible to have various features like negative refractive index. The idea of having negative permittivity and negative permeability values at the same time goes back to Veselago's theoretical work [1]. However, his work had not been received so much attention from the scientific community until Pendry's and Smith's works where they achieved to realize MTMs [2-4]. After that many application areas are found for MTMs including, super lenses, perfect absorbers, source imaging, polarization rotators, sensors, electromagnetic harvesting and etc.

There are various techniques in the antenna industry to improve isolation from adding resonators on the top the antennas to adding metallic bridges on the structures. In this study, one of the most commonly used MTM type, Split Ring Resonators in circular shapes are used to achieve better isolation between two microstrip dipole antennas designed for two different frequencies. The dimensions of the structures and their placements are optimized by using genetic algorithm and found the best solution for two particular frequency bands.

2 CONFIGURATION AND DESIGN OF THE DIPOLE ANTENNAS AND MTMS

In this study, two individual antennas are optimized and designed for lowband ($f=2.4\text{GHz}$) and highband ($f=6\text{GHz}$). The antennas consist of two copper layers and a dielectric layer between them. As a dielectric I have used FR4 for its good performance and efficient cost. Since the geometry is similar for the antennas, I have only shown the low-band microstrip dipole antenna for reference (Fig. 1). Dimensions of the antenna are chosen to comply with a traditional half-wave dipole. Microstrip antenna is used because it is more consistent and cost friendly comparing to the other antennas for dipoles.

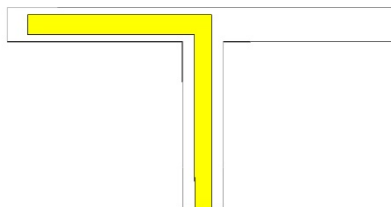


Figure 17. Geometrical Structure of the microstrip dipole antenna (for 2.4GHz)

As it is known, working frequency of a dipole can be adjusted by simply optimizing the dipole branches. For the low band dipole, the dimensions are chosen so that it can give a resonance in 2.4GHz which is the lowband target in this

¹Iskenderun Technical University, oguzhan.akgol@iste.edu.tr

study. Return loss characteristic of the proposed antenna can be seen in Fig. 2. As seen from the figure, return loss goes down to -12.5dB levels which is more than enough for working efficiently.

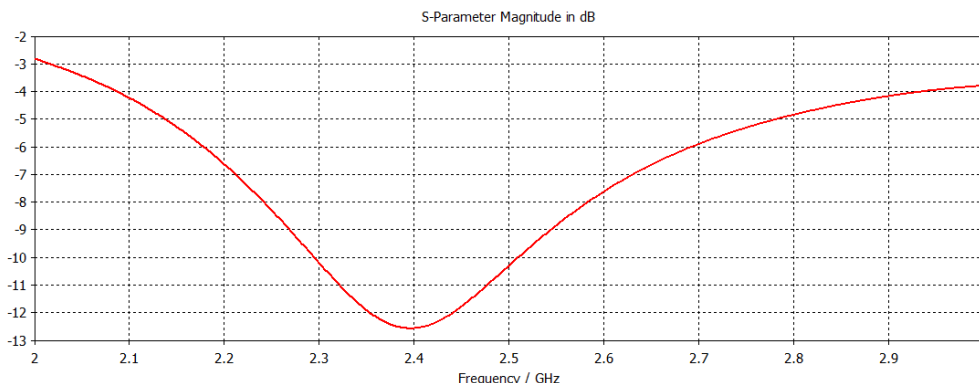


Figure 2. Return loss graph of the dipole antenna (f=2.4GHz) in dB

Radiation pattern needs to be investigated in order to find the directivity, efficiency and thus the gain of the antenna. Two principle cuts of the farfield radiation pattern of the antenna can be seen in the following figure. Left side of Fig. 3 shows the elevation cut of the pattern while the right side illustrates the azimuth cut of it. In order to clarify the radiation pattern, 3D farfield pattern are also captured and shown in Fig. 4. The gain of the antenna is about 2.3 dBi and the antenna has a donut shape radiation pattern which is also expected for a traditional dipole antenna.



Figure 3. Principal Cuts Of the Polar Plot of The Farfield Patterns For The Microstrip Dipole Antenna (for 2.4GHz)

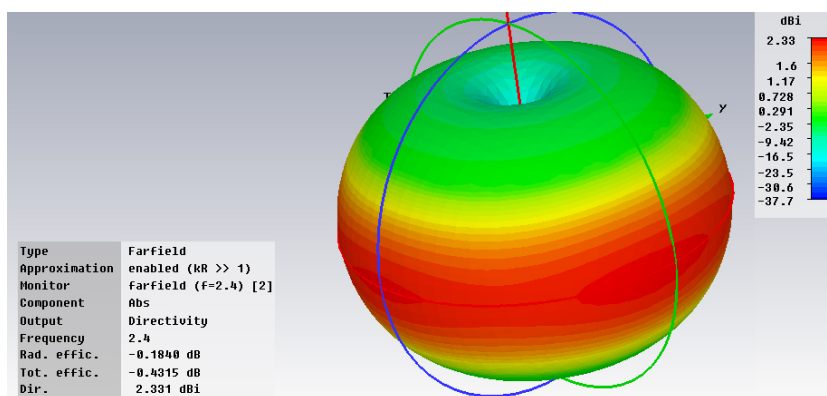


Figure 4. 3D Farfield Radiation Pattern for the dipole antenna (f=2.4GHz)

The high band section of the system consists of an antenna designed for f=6GHz. S11 parameters of the high band antenna can be seen in Fig. 5. In addition, 3D farfield radiation plot is also given in Fig. 6 which is similar to the lowband as expected. Gain of this antenna is about 2.6 dB which is reasonable for this type of antenna. Return loss curve may not seem quite perfect but the focus of this research is on improving the isolation for two port systems having these low and high band antennas together in a single structure. That is why, no extra tuning is performed for

improving the return loss parameters in the given frequency band other than obtaining the resonances at those particular points.

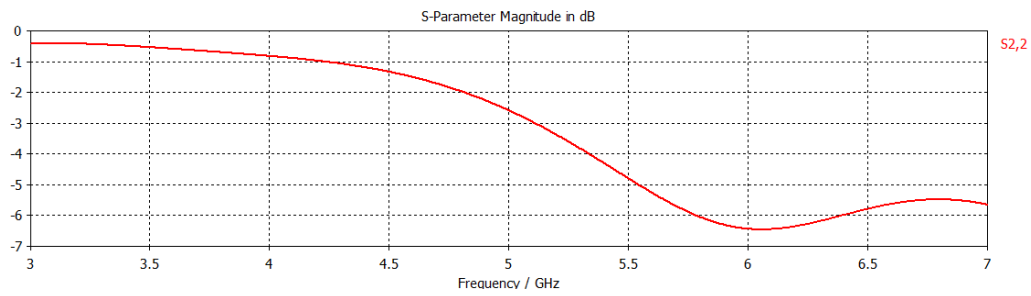


Figure 5. Return loss graph of the highband dipole antenna ($f=6\text{GHz}$) in dB

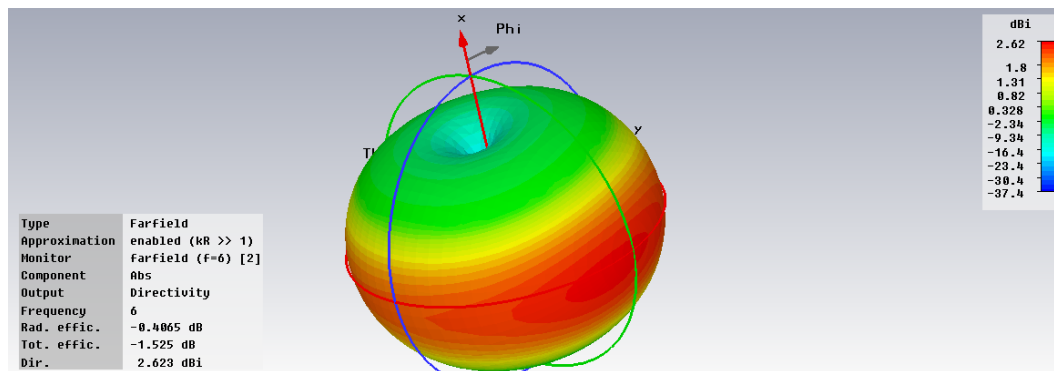


Figure 6. 3D Farfield Radiation Pattern for the highband dipole antenna ($f=6\text{GHz}$)

Even though various techniques are used to improve the isolation of multiport antennas in antenna industry, using metamaterials (MTMs) is relatively new technique and there is only a limited number of studies performed in this particular problem.

I have used split ring resonators (SRRs) as the MTMs for improving the isolation. Geometrical structure of the model can be seen in Fig. 7 below. As seen from the figure, the structure consists of two confocal rings having openings in opposite sites located on a FR4 substrate.

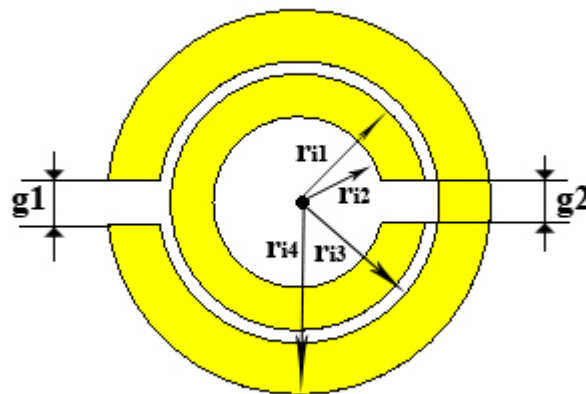


Figure 7. MTM unit cell structure 2D view

Five SRRs are placed in a row and five of these rows are placed between the lowband and high band antennas. Separation distance of the plates, gaps on the rings, separation of SRRs, and radius of SRRs are optimized by using genetic algorithm that came with CST Microwave Studio. Geometrical presentation of the system can be seen in Fig. 7.

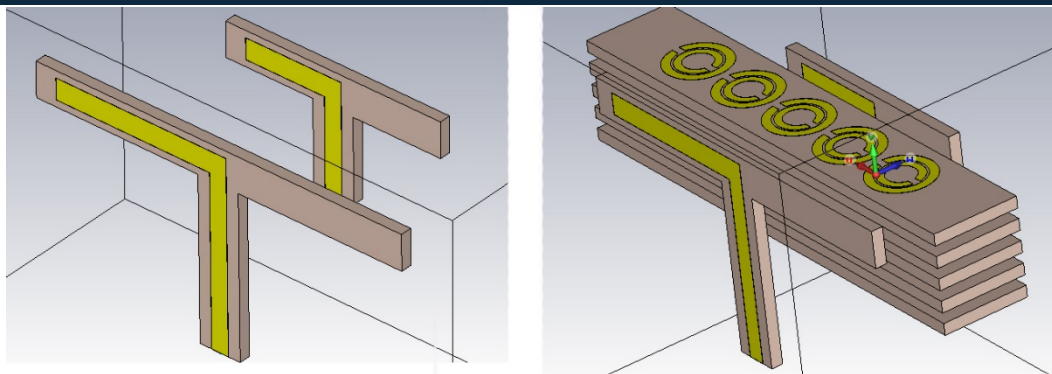


Figure 7. Antenna system with (right side) and without MTMs (left side.)

3 RESULTS AND DISCUSSION

As a result of the genetic algorithm, the geometry that work quite well for the isolation of this two port antenna system is designed. In order to illustrate the working mechanism for the isolation, scattering parameter (S_{21}) which is an indicator showing the energy transmitted from one port to the other is selected. The results for both low band and the high band are drawn in Fig. 8 and Fig. 9.

As seen from Fig. 8, the antenna system with MTMs structure placed in shows better isolation than the antennas themselves. The lowest level is reached to almost -25dB which can be considered a good isolation for this type of closely placed antenna system.

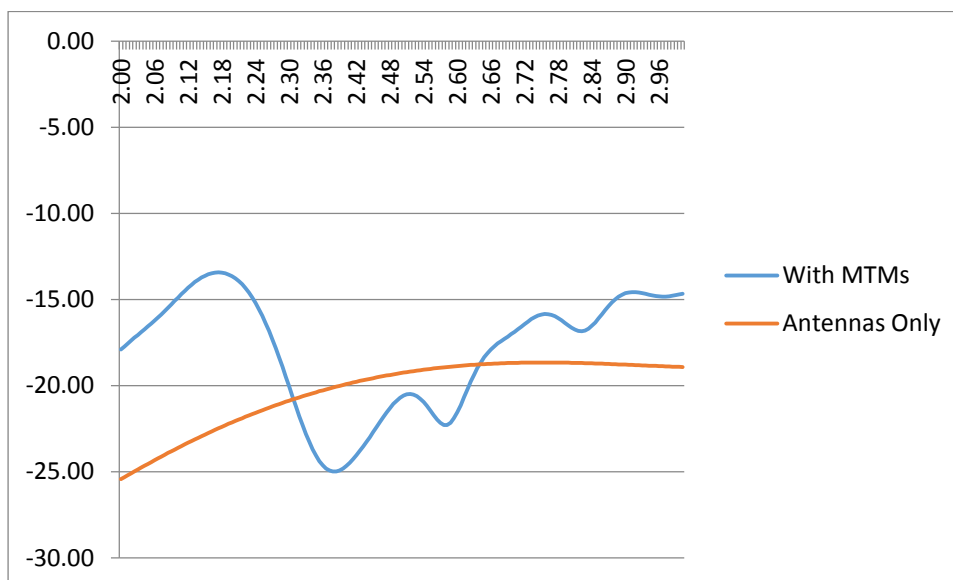


Figure 8. Transmission Graph (S_{21}) for low band ($f=2.4\text{GHz}$) for the system with and without MTMs in dB.

A better result is obtained for the high band section. As in the figure, the transmission values goes down to -50-60dB levels at around 6GHz. If the system is compared with and without MTM structures, the improvement can be easily seen.

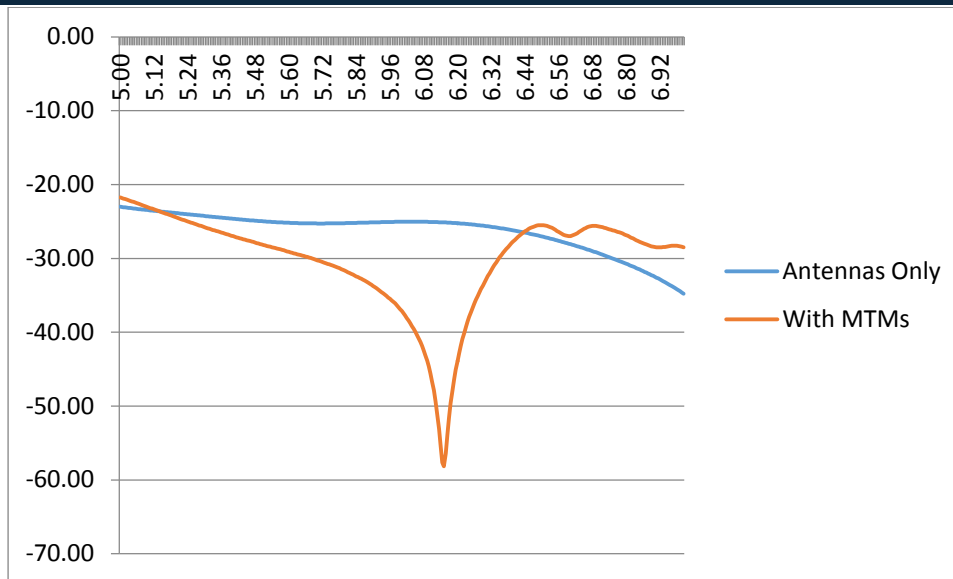


Figure 9. Transmission Graph (S_{21}) for high band ($f=6\text{GHz}$) for the system with and without MTMs

4 CONCLUSION

Even though there are some studies using MTMs for improving the isolation, most of them focus on using MTM antennas rather than using the MTMs directly existing antenna system currently used in the daily life. In this study, the isolation between two microstrip dipole antenna is improved dramatically by using SRR type MTMs. The antenna system works in two separate bands, low band ($f=2.4\text{GHz}$) and high band ($f=6\text{GHz}$). These frequency intervals have quite large application areas namely, Wi-Fi systems, Bluetooth, communication, satellite communication, radiolocation, amateur satellite services and etc. In both band, the structure helps to improve the isolation significantly, particularly in high band. The structure has simple and cost friendly structure that can be manufactured easily and cheaply. It can also be adjusted to any desired frequency ranges by adjusting the geometrical parameters.

REFERENCES

- [1] Veselago, V. G., The electrodynamics of substances with simultaneously negative values of ϵ and μ , " Sov. Phys. Usp., Vol. 10, No. 4, 509{514, 1968.
- [2] Pendry, J. B., Holden, A. J., Stewart, W. J., Youngs, I., \Extremely low frequency plasmons in metallic mesostructures," Physical Review Letters, Vol. 76, 4773{4776, 1996.
- [3] Pendry, J. B., Holden, A. J., Robbins, D. J., Stewart, W. J., \Magnetism from conductors and enhanced nonlinear phenomena," IEEE Transactions on Microwave Theory and Techniques, Vol. 47, 2075{2084, 1999.
- [4] Smith, D. R., Padilla, W. J., Vier, D. C., Nemat-Nasser, S. C., Schultz, S., \Composite medium with simultaneously negative permeability and permittivity," Physical Review Letters, Vol. 84, 4184{4187, 2000.
- [5] Karaaslan M, Bakir M., Chiral metamaterial based multifunctional sensor applications. Progress in Electromagnetics Research. 2014; 149: 55-67.
- [6] Sabah C, Dincer F, Karaaslan M, Unal E, Akgol O, Demirel E. Perfect metamaterial absorber with polarization and incident angle independencies based on ring and cross-wire resonators for shielding and a sensor application. Opt. Comm. 2014; 322: 137-142.
- [7] F. Dincer, M. Karaaslan, O. Akgol, E. Unal, C. Sabah, "Polarization-Insensitive FSS based Perfect Metamaterial Absorbers in GHz and THz Frequencies", Radio Science, 49, 2014, pp. 306-314.
- [8] F. Dincer, O. Akgol, M. Karaaslan, E. Unal, C. Sabah, "Perfect Metamaterial Absorbers for Solar Cell Applications in the Microwave, Infrared, and Visible Regime" Progress In Electromagnetics Research, Vol. 144, 93-101, 2014 Polarization Angle Independent
- [9] F. Dincer, M. Karaaslan, E. Unal, K. Delihacioglu, C. Sabah (2014) "Design of polarization and incident angle insensitive dual-band metamaterial absorber based on isotropic resonator". Prog Electromagn Res 144:123
- [10] F. Dincer, M. Karaaslan, E. Unal, and C. Sabah, "Dual-band polarization independent metamaterial absorber based on omega resonator and octa-star strip configuration," Prog. Electromagn. Res, vol. 141, pp. 219, 2013

Application of Deep Eutectic Solvents on Wood Chemistry

Esra Guner¹, Ayben Kilic Pekgozlu²

Abstract

Wood is one of the renewable and natural industrial raw materials and wood cell wall is a complex entity with cellulose, lignin, hemicelluloses and minor low molecular-weight components in its structure. There are different chemicals used as solvent (i.e. sulfuric acid, sodium hydroxide, nitric acid, diethyl ether, petroleum benzene, acetone, methanol, dichloromethane) in conventional methods for the extraction of these components from cell wall to analyse wood. However with increasing demand for analytical methods, whether the chemicals used in these methods should be less harmful or should have less toxic effect has become an issue of discussion. The harmful effects of chemical solvents on human health and environment is now seen as a problem. Research on alternative environmentally-friendly solvents has been made and deep eutectic solvents (DES) emerged as alternatives to organic solvents. Green technology aims to reduce the negative effects to human and environment in the field of chemistry. Moving from the benign Solvents & Auxiliaries principle of green chemistry, DES saves time and energy and because it could be recycled, it does not leave waste behind. By changing such physical characteristics as temperature and pressure and by using new green solvents, green technology enables to develop new and environmentally-friendly solvent extraction techniques. In this study, the area of use for des and the advantages it may provide for wood chemistry were investigated. For this purpose, national and international literature review was conducted and presented as a review paper to propose that des can suggest a novel and environmentally-friendly alternative to other solvents which would add a green approach to chemistry of wood.

Keywords: *Wood chemistry, Deep eutectic solvents, green chemistry.*

1 INTRODUCTION

Being a renewable and organic material, wood is material which has served in various areas of use since the beginning of the existence of mankind. Used from cradle to grave, in each aspect of life, wood's areas of use were increased even further by being decomposed to its compounds in time, owing to the opportunities, provided by the developing technology. Various chemicals such as sulfuric acid, sodium hydroxide, nitric acid, diethyl ether, petroleum benzene, acetone, methanol, dichloromethane etc. are used to separate wood in order to analyze. With the developing technology and the increasing awareness, the harms of these chemicals to nature and humans were begun to be discussed.

The damage of environmental pollution, seen as a serious problem today, is increasing with each passing day. By realizing the seriousness of this damage, scientists began to seek for new solutions which can be remedies for environmental pollution, by taking the advantage of the developing technology. And green chemistry technology has also appeared in this way. The principles of the green chemistry can be listed as; the prevention of waste production, atom economy, less syntheses, designing harmless chemicals, harmless solvents and equipment, designing with the purpose of energy efficiency, use of renewable raw materials, reduction of derivatives, catalysis (against stoichiometry), designing with the purpose of degradation, real-time analyses to prevent pollution. The purpose of green chemistry is to provide an alternative way, with the chemicals which are safer, more effective, and more economic and prevent pollution, and can also be recycled or reused, along with the developed new methods which also does not harm nature or less harm [1].

Deep eutectic solvents were also environment-friendly solvents, which were invented to serve this purpose.

1.1 Chemical Structure of Wood

Wood is an organic material with a complex structure. Woody tissue is consisted of numerous chemical compounds, which display irregular distribution, and found in the form of basic and physical mixtures, as a result of the anatomic structure. Wood, a large part of which has a high molecular weight, can be defined as a system of high polymers that pervade into one another. The main compounds of wood are cellulose, hemicellulose and lignin [2]. As Fengel and Wegener [3] also remarked woods are, as a chemical composition, consisted of three natural polymers which are cellulose, lignin and hemicelluloses, at the rate of almost 90-99 %. Besides, as it is in a lesser ratio (1-10 %), it contains inorganic material (ash) and some organic extractive materials such as color, smell. Composed by monomeric sugars, by getting together in a specific form of arrangement, cellulose and hemicelluloses' (polysaccharide) ratio is about 70-75 % as it changes in respect to the species. The rate of the 3rd main component of wood, namely lignin, changes between 20-40 % [4].

Wood contains carbohydrates, phenolic materials, terpenes, aliphatic compounds, alcohols, aldehydes, hydrocarbons, alkaloids, proteins, polyhydric alcohols, acids with double bond and inorganic compounds [2]. Various chemicals (sulphuric acid, sodium hydroxide, nitric acid, diethyl ether, petroleum benzene, acetone, methanol, dichloromethane,

hexane, ethanol etc.) are used in extracting these compounds from wood. Most of the used chemicals are toxic and harmful to nature.

1.2 Deep Eutectic Solvents

The word “eutectic” is derived from Greek word “Eutectos” which means “easily solvable”. They provide a solvent which has a much lower melting point than the materials from which it is prepared, by creating two times more solid materials. Hydrogen bonds cause that the melting point of the prepared solvent is low. Since its polarities are very high, they are capable of solving many materials like cellulose which cannot be solved in classical solvents [5]. That DES can be obtained in an easy and cheap way by mixing two or three compounds is one of its most interesting advantages. DES mixtures can be prepared by mixing quaternary ammonium salts (generally choline chloride) in natural amino acids (alanine or glycine) or in carboxylic acids which are contained in fruit and vegetables [6][7]-[8].

It was invented in 2003 by mixing choline chloride and urea at the ratio of 1:2. With the mixture of choline chloride, which has a melting point of 302 °C, and urea, melting point 133 °C, a solvent is prepared with the melting point of 12 °C. Choline chloride is a cheap and easily accessible material which is used as an additive in chicken food. And urea is a material which is consisted in the metabolisms of mammals and used as an azote source in fertilizers. Choline chloride-urea mixture is one of the most commonly used DESs. In the combinations, which can be prepared instead of this mixture, glycerol, ethylene glycol, tri-ethylene glycol, 2,2,2-trifluoroacetamide can be used instead of urea; and methyltriphenylphosphonium bromide, N,N diethylene ethanol ammonium chloride can be used instead of choline chloride [9]-[10].

DESs have an important role as a solvent, which can solve, deposit and carry metabolites in live cell and organisms. Primer metabolites that exist in many plants create DESs by transmuting from solid to liquid form by being mixed in convenient ratios. There are more than 100 compounds in nature to be used in a DES mixture. DESs, with different features, can be obtained by preparing mixtures with different compositions with more than 100 compounds [11].

As Capello et al. also stated the general features of deep eutectic solvents (DES) are having high melting points, being able to get biologically solved easily in environmental conditions, having low toxicity, being able to be reused again [12]. They are in liquid form below 150 °C, in general. DES is composed of natural products (amides, sugars, alcohols and monoacids). Its steam pressure is low; is not volatile; and has low inflammability [13]. As well as this, some DESs’ being expensive, having toxic features on human and environment and being in liquid form in the room temperature limit their use in the chemical industry [11]. Abbott et al. presented these new solvents, which are created by being mixed from renewable sources – choline chloride and urea – at the ratio of 1:2, in their study, in 2003. However, the term of DES (Deep eutectic solvents) was occurred by their displaying these solvents as an alternative to ionic solvents because of their being environment-friendly, in one of their studies, dated 2004 [8].

1.3 Areas of Use of Deep Eutectic Solvents

There have been many researches, made about DESs since when they were discovered. There are researches, being made on the density of DESs’ usage in the areas of pharmacology, chemistry, food technology, biology, biofuel production, paper industry and similar ones. These researches can be used as guides in terms of used DESs instead of conventional solvents, by examining.

In a research, conducted on Bunge plant, named *Salvia miltiorrhiza*, a fast and environment-friendly extraction method, ball mill-assisted deep eutectic solvent-based extraction were used as an alternative to the methods like methanol based ultrasound-assisted extraction and heat reflux extraction and to evaluate the efficiency of the developed extraction method, tanshinones were used as target compounds. As the result of this study, it was stated that ball mill-assisted deep eutectic solvent-based extraction method has a wide usage potential as it is effective in obtaining (e.g. flavonoids, phenanthraquinones) and environment-friendly [14].

In a conducted research, the extraction results that were made with DESs, acquired by using malic acid, lactic acid, proline, glucose, fructose, sucrose, 1,2-propanediol and choline chloride, were compared with anthocyanins which were obtained as the result of extraction of the petals – in two different colors – of *Charanthus reouseus* species with methanol and ethanol. When the results are analyzed under proper conditions, it was stated that some DESs had a similar efficiency with the conventional solvents (acidic methanol) and cyanide is more stable with some DESs than acidic ethanol [15].

In a study, aiming at the developing the pretreatment of corn stover with DESs for biobutanol fermentation, DESs – which were prepared with choline chloride: formic acid – were used. As the result of the pretreatment, it was stated that DESs, which performed perfectly in the removal of hemicellulose from lignin, can be used for the lignocellulosic biomass into biofuel as a promising and biocompatible pretreatment method [16].

In a research on the potential implementations of DESs in nanotechnology, it was remarked that DESs can be used as exfoliating agents, diluent and templates for nanomaterials. Besides displaying similarities with ionic liquids in terms of chemical, physical, physiochemical or electrochemical synthesis of nanoparticles, DESs’ being solvents which can be prepared easily and are environment-friendly gives them an advantage compared to ionic liquids [17].

In a study, in which DESs’ effect on the stability of natural colorants that are acquired from Safflowers (*Carthamus tinctorius*), it was claimed that the natural pigments – which are obtained from Safflower – are more stable than water

or 40 % ethanol solution in sugar-based DES. It was remarked that by reducing water content with increasing viscosity, the stabilization capacity of DES can be adjusted and the strong stabilization capacity is based on the reactions of H binding, occurring between the solute and DES molecules. It was put forth that DESs' stabilizing feature can have promising implementation areas for phenolic compounds in food, cosmetic and medicine industries [18].

To decompose a phenolic material, which is a very important group of materials for organic chemistry industry, from fats, it has to be processed with strong acids and bases. And this is a process which is harmful to environment. In a study, intending to terminate this damage, it was aimed at obtaining 26 different phenolic materials from toluene by using DESs, instead of acids or bases. As the result of the performed analyses, 16 different phenolic materials could be removed from toluene in a single session. It was stated the formation of hydrogen bonds between phenolic compounds and choline derivative salts – which causes reducing the removal efficiency of the phenolic compounds – weakens due to phenolic compounds' self-association by intramolecular or intermolecular interaction. The typical examples, having stronger intramolecular hydrogen bonds, were 2,4-dichlorophenol, 2, 6-dichlorophenol, 2-nitrophenol and 4-methyl-2-nitrophenol. Choline derivative salts and phenolic compounds' strong solvation in oil, on the other hand, did not cause the formation of immiscible DESs like 4-ethylphenol, 4-phenoxyphenol, 2-tert-butylphenol, 4-isopropylphenol and [N1, 1, 8 C2IH]C1. They cannot be used for the separation of phenols from oil. Hence, it was expected that the findings given above can be a useful guide for DES-based separation technology of phenols from oil designs [19].

In a research, making a microwave-assisted (MAE) extraction from *Cajanus cajan* plant by using DES, and examining the determination of the most convenient method and DES mixture for phenolic material analysis in ultra-performance liquid chromatography (ULPC), it was found that the best DES for the extraction of phenolics from *C. cajan* leaves was 20 % of water in choline chloride/maltose (1/2). The following is the optimized conditions for microwave-assisted extraction: extraction temperature 60 °C, liquid/solid ratio 30:1 ml/g and irradiation time 12 min. As the result of this study, it was stated that the method – developed on the basis of microwave-assisted extraction with DES and UPLC – could be an alternative for the extraction and quantitative assessment of active components in plant materials [20].

In the study about ultrasound-assisted extraction of antioxidant polyphenols from common native Greek medicinal plants with lactic acid-based natural deep eutectic solvents, dittany, fennel, marjoram, mint and sage were used to test the efficiency of some novel lactic acid-based natural DES to extract polyphenolic compounds. As an eutectic mixture, lactic acid: choline chloride, lactic acid: sodium acetate, lactic acid: ammonium acetate and lactic acid: glycine: water, with corresponding molar ratios of 3:1, 3:1, 3:1 and 3:1:3 were used. In the acquisition of the control samples, water and 60 % (v/v) aqueous ethanol was used and as the result lactic acid: glycine: water exhibited high efficiency, yet in some examples, it was stated that lactic acid: sodium acetate and lactic acid: ammonium acetate were equally efficient. It was also suggested by the data that extracts, having high polyphenol concentration, might also have higher antiradical activity and reduce power. Consequently, they remarked that DESs are non-toxic, renewable and exceptionally efficient solvents for polyphenol recovery from medical plants [21].

In the study of Bruinhorst and Kroon, they made some experiments on an alternative biomass treatment with the extraction of lignin with specifically designed solvents (Low transition temperature mixtures and deep eutectic solvents). Despite the efficient and high solution of the researches that they performed in mild reaction conditions, they stated that not being able to separate lignin from biofuels restricted the extraction performance. However, they claimed that the effective extraction efficiency could be improved by changing the extraction conditions and solvent features [22].

In their study, Xia et al. displays results for Avicel cellulose pretreatment by neat and aqueous solutions of 20 different ionic liquids and tree DES, correlating enzymatic hydrolysis rates of pretreated cellulose with various ionic liquids properties like hydrogen bond basicity, polarity, Hofmeister ranking and hydrophobicity. Treated by neat ILs, cellulose's hydrolysis rate can be correlated with the H-bond basicity of the constituent anions and the empirical IL polarity, but the cellulose's hydrolysis rates by aqueous ILs cannot be simply associated with any single property of ILs (for example, H-bond basicity, polarity, Hofmeister ranking, hydrophobicity). As the result, they put forth that promising and inexpensive alternative solvent systems were represented by aqueous ILs and aqueous DESs for pretreating lignocellulose to obtain rapid saccharification rates of both cellulose and hemi cellulose [23].

1.3.1 Use of Deep Eutectic Solvents in Wood Chemistry

Carbohydrates, phenolics, terpenes, aliphatic compounds, alcohols, aldehydes, hydrocarbons, alkaloids, proteins, polyhydric alcohols, divalent acids and inorganic compounds are contained in wood. Sulfuric acid, sodium hydroxide, nitric acid, diethyl ether, petroleum benzene, acetone, methanol, dichloromethane, hexane, ethanol can be used to obtain these compounds. However, these chemicals are toxic and harmful for nature. With the discovery of DESs, it was possible to develop alternative methods for these harmful chemicals.

As it is not common to use DESs in the wood chemistry, the researches about wood have just begun to be conducted. In the literature, there was not a study, made on woods in relation with DESs. There are many conducted researches on the production of cellulose, but generally the non-wood products were used in these studies.

2. CONCLUSIONS

Because they are environment-friendly, it was seen that the interest in DESs increased and in parallel with this, there was an increase in the number of studies for designing new DES methods as an alternative for the previously methods. That they have not been used in the industrial areas yet was caused because there was not enough research on DESs. By trying the different combinations of DESs in different environment conditions and with different methods, it is required to design the most convenient methods. However, it is a fact that this process is going to take a long time.

DES applications are only restricted to paper industry with non-wood products. Its expansion is a virgin area for new researches. New and detailed experiments can be doable by using different DESs, with different extraction conditions on wood. In this manner, it can be an alternative to pre-existing methods. Studies in this field can be increased by extending DES usage for decomposing wood into its main components (cellulose, lignin, hemicelluloses). By using DES, many new researches, that have not been done yet, could be conducted on wood and non-wood forest products with modeling recently studies about alkaloids, biodiesel production pretreatments, polyphenols, aromatic hydrocarbons.

REFERENCES

- [1] J. C. Anastas, P. T.; Warner, *Green Chemistry: Theory and Practice*. Oxford University Press: New York, 1998.
- [2] . Hafizoğlu and İ. DENİZ, *Odun Kimyası Ders Notları*, KTÜ Orman Fakültesi, Trabzon.
- [3] D. Fengel and G. Wegener, 1984. "Wood Chemistry, Ultrastructure, Reactions", Walter De Gruyter Verlag, Berlin.
- [4] B. Yollu, "MYRTUS COMMUNIS (Yabani Mersin) TÜRÜNÜN FARKLI KISIMLARINDA (YAPRAK, MEYVE VE ODUN) KİMYASAL BİLEŞENLERİN BELİRLENMESİ," İstanbul Üniversitesi, 2009.
- [5] A. P. Abbott, D. Boothby, G. Capper, D. L. Davies, and R. R. K., "No Title," *J. Am. Chem. Soc.*, p. 126/9142, 2004.
- [6] A C. Ruß, B. König. *Green Chem.* 14 (2012) 2969.
- [7] M. Francisco, A. van den Bruinhorstand, and C. Kroon, "Green Chemistry," *Green Chem.*, p. 14/2153, 2012.
- [8] S. L. García, "PHASE EQUILIBRIA FOR EXTRACTION PROCESSES WITH DESIGNER SOLVENT," University of Santiago de Compostela, 2013.
- [9] A. P. Abbott, G. Capper, D. L. Davies, R. K. Rasheed, V. Tambyrajah. *Chemistry Community*. (2003) 70.
- [10] Y. Dai, J. van Spronsen, G. J. Witkamp, R. Verpoorte, and Y. H. Choi, "Natural deep eutectic solvents as new potential media for green technology," *Anal. Chim. Acta*, vol. 766, pp. 61–68, 2013.
- [11] C. Capello, U. Fischer, K. Hungerbühler. *Green Chemistry*. 9 (2007), 927.
- [12] <http://www.cepi.org/system/files/public/epw-presentations/2013/8%20Westenbroek%20DES.pdf>
- [13] M. Wang, J. Wang, Y. Zhang, Q. Xia, W. Bi, X. Yang, D. Da, and Y. Chen, "Fast environment-friendly ball mill-assisted deep eutectic solvent-based extraction of natural products," *J. Chromatogr. A*, vol. 1443, pp. 262–266, 2016.
- [14] Y. Dai, E. Rozema, R. Verpoorte, and Y. H. Choi, "Application of natural deep eutectic solvents to the extraction of anthocyanins from *Catharanthus roseus* with high extractability and stability replacing conventional organic solvents," *J. Chromatogr. A*, vol. 1434, pp. 50–56, 2016.
- [15] G. C. Xu, J. C. Ding, R. Z. Han, J. J. Dong, and Y. Ni, "Enhancing cellulose accessibility of corn stover by deep eutectic solvent pretreatment for butanol fermentation," *Bioresour. Technol.*, vol. 203, pp. 364–369, 2016.
- [16] A. Abo-hamad, M. Hayyan, M. Abdulhakim, and M. Ali, "Potential applications of deep eutectic solvents in nanotechnology," *Chem. Eng. J.*, vol. 273, pp. 551–567, 2015.
- [17] Y. Dai, R. Verpoorte, and Y. H. Choi, "Natural deep eutectic solvents providing enhanced stability of natural colorants from safflower (*Carthamus tinctorius*)," *FOOD Chem.*, vol. 159, pp. 116–121, 2014.
- [18] Y. Zhang, Z. Li, H. Wang, X. Xuan, and J. Wang, "Efficient separation of phenolic compounds from model oil by the formation of choline derivative-based deep eutectic solvents," *Sep. Purif. Technol.*, vol. 163, pp. 310–318, 2016.
- [19] Z. Wei, X. Qi, T. Li, M. Luo, W. Wang, Y. Zu, and Y. Fu, "Application of natural deep eutectic solvents for extraction and determination of phenolics in *Cajanus cajan* leaves by ultra performance liquid chromatography," *Sep. Purif. Technol.*, vol. 149, pp. 237–244, 2015.
- [20] C. Bakirtzi, K. Triantafyllidou, and D. P. Makris, "common native Greek medicinal plants," *J. Dermatol. Sci.*, 2016.
- [21] A. Van Den Bruinhorst and M. C. Kroon, "Applying novel natural solvents to the delignification of lignocellulosic biomass chemicals and fuels . [1] , [2] Lignin , one of the three main biopolymers present in lignocellulosic designed for that task . Ionic Liquids (ILs) have proven to selectively extract lignin from biomass [6 – 8] . Encouraged by these developments , Low Transition Temperature Mixtures (LTTMs) and Deep Eutectic Solvents (DESs) were examined for the selective extraction of lignin from biomass at mild conditions . LTTMs do not require complicated synthesis routes , but can be easily prepared by mixing," vol. 13, no. 11, p. 5612, 2014.
- [22] S. Xia, G. A. Baker, H. Li, S. Ravula, and H. Zhao, "Aqueous Ionic Liquids and Deep Eutectic Solvents for Cellulosic Biomass Pretreatment and Saccharification," vol. 4, no. 21, pp. 10586–10596, 2015.

Production and Export of Laurel (*Laurusnobilis L.*) in Turkey

Elif Catikkas¹

Abstract

Laurel (Laurusnobilis L.) has belonged to Lauraceae family. It is always green and could grow as far as from 2 m to 15 m. It is a plant with two protective cases and in the form of atree. The parts of it which are benefitted economically are its leaf and seed. Laurel (Laurusnobilis L.) is an aromatic herb which has animportant chemical composition and potential therapeutic effects. It is spread naturally in Turkey in the regions of Aegean, Mediterrian, and the Black Seacoasts. Based on 2015 data, there has been \$35,873,957 exchange income for 12,739,957 kg laurel in Turkey. Turkey provides 90% of the world requirement of quality laurel leaf according to those values. The average number of countries to which laurel is exported each year is 72. In this study, the export of quality laurel leaf will be evaluated for the last five years on the basis of countries.

Keywords: Laurel (*Laurusnobilis L.*), export, medicinal and aromatic plants

1 INTRODUCTION

Laurel (*Laurus nobilis L.*) is a tree species, reaching a height of 2 to 15 meter, belongs to Lauraceae family. Laurus able to keep its green coloured texture all around a year. Laurus is one of the specially characterized species of Mediterranean flora called Tarsius spectrum [1]. Although the Flowers period varying from region to region, that period occurs generally between March and April. Laurel is a Dioic type plant. Laurel also has a strong shoot forth capability both for its root and body [2-3-4].

Laurel habitation spreading along the coastline of Turkey from Hatay region at southern to Eastern Black Sea region at northern, and also seen up to 600 - 800 meters altitude above sea level [5].

There are many different areas of Laurel; in a form of powder as spice, leaves of laurel are used in meat and fish meals, for landscape point of view as a hedge plant and in industries such as medicine, soap, cosmetics, chemicals [6].

2. RESULTS AND DISCUSSION

In this paper, Turkey's last 10 years Laurel production since the year 2014, but also the Last 5- year Laurel export quantities and amounts have been evaluated.

In addition to above depicted evaluation, Examination of the Turkey's top Laurel exporters regarding the Last 5-year export quantity data, is in the scope of this paper.

As seen from the figure 1, from the General Directorate of Forests (OGM) data; for the year 2014, total 15.581 tonnes of raw laurel production has been achieved by Turkey. 12.255 tonnes of that 15.581 tonnes production has been exported, earning the country around \$35.762.159 (figure 2) by the year 2014 [7].

¹Corresponding author: Karamanoğlu Mehmetbey University, Ermenek Vocational School, Department of Medicinal and Aromatic Plants, 70400, Ermenek/Karaman, Turkey. ecatikkas@kmu.edu.tr

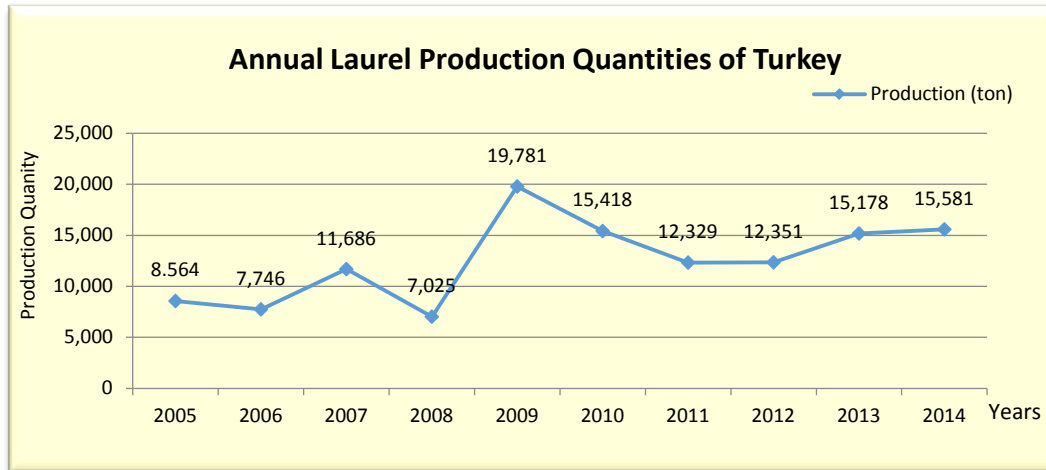


Figure 1. Annual Laurel Production Quantities of Turkey

As seen from the table figure 2, from the Turkish Statistical Institute (TUIK) data; Turkey's average quantity of Laurel exports have been around 11.096.800 kg, that gives the average income to country around \$30.766.227 for the last 5 years.

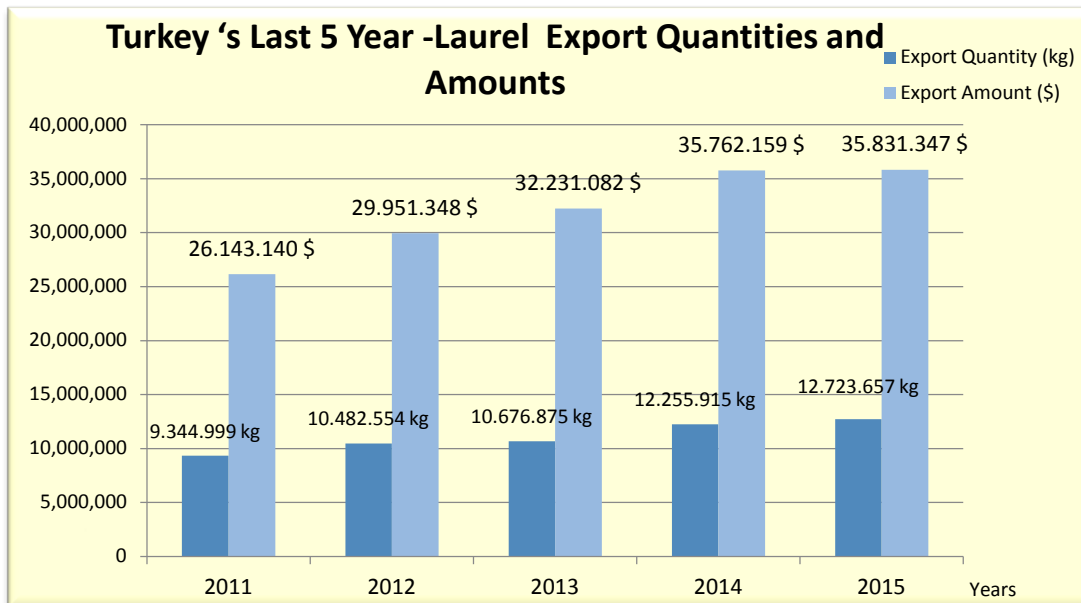


Figure 2. Turkey's Last 5 Year- Laurel Export Quantities and Amounts

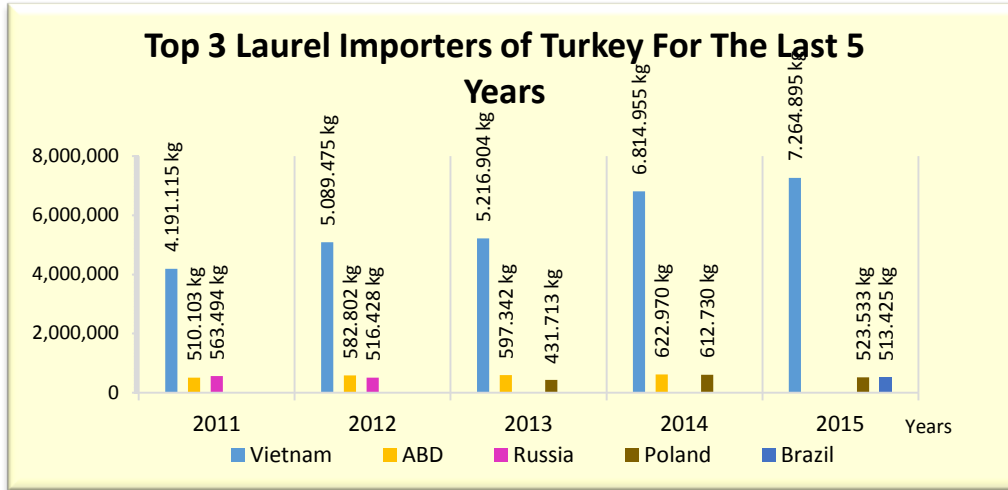


Figure 3. Top 3 Laurel Importers of Turkey For The Last 5 Years

Turkey not only keeps the %90 market share of the world's Laurel trade market alone but also has a significant position in the world market by means of the price quality and production [6].

According to the figure 2 mentioned data for the year 2015; Turkey's 12.723.657 kg of export, earning the country around \$35.831.347. According to figure 3 Vietnam (7.264.895 kg), Poland (523.533 kg), Brazil (513.425), become the top 3 Laurel importers by the year 2015 [7].

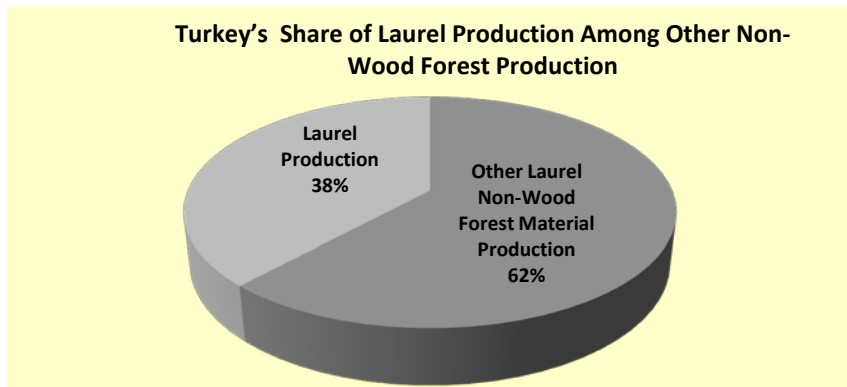


Figure 4. Turkey's Share of Laurel Production Among Other Non-Wood Forest Productions

As seen from the Figure 4, Turkey's Share of Laurel Production is 38%, among Other Non-Wood Forest Products, according to OGM 2014 data [8].

3. CONCLUSION

Turkey is one of the world's significant producers of high-quality Laurel. As a result of this situation; the statement "Turkey is theirsource of the top quality Laurel", become the well-remembered statement all around the world. Turkey, nowadays becomes the top Laurel exporter of the world, according to registered export quantities.

REFERENCES

- [1]. Ege arastirma.ogm website.[Online], Available: http://www.efri.gov.tr/yayinlar/Son_defne_elkitabi.pdf, 2016.
- [2]. İ. Baktır, *Ağaçlar ve Çalılar*, Akdeniz Üniversitesi Yayın No:39 Akdeniz Üniversitesi Basımevi, Antalya, 1991.
- [3]. H. Kayacık, *Orman ve Park Ağaçlarının Özel Sistematiği*, İstanbul Üniversitesi Orman Fakültesi Yayınları, İ.Ü Yayın No: 986, O.F. Yayın No: 93, 152s, İstanbul, 1963.
- [4]. Y.S. Lewis, *Spices and Herbs for The Food Industry*, Food Trade Press, Orpington, ISBN: 900379, England, 1984.
- [5]. M. İ. Acar, *Defne Yaprağı ve Yaprak Eterik Yağının Üretilmesi ve Değerlendirilmesi*, Ormançılık Araştırma Enstitüsü Yayınları, Teknik Bülten Serisi, No:186, Ankara, 1987.
- [6]. F. Bilgin, İ. Şafak, Ö. Kiracioğlu, *Ege Bölgesinde Defne (Laurus Nobilis L.) Üreticiliğinin Sosyo-Ekonomik Önemi ve Üretici Profiline Belirlenmesi* T.C. Çevre ve Ormanlık Bakanlığı Ege Ormanlık Araştırma Müdürlüğü, Teknik Bülten No: 28, Yayın No:260, İzmir, 2005.
- [7]. TÜİK website. [Online], Available: <https://biruni.tuik.gov.tr/disticaretapp/menu.zul>(2016).
- [8]. OGM website. [Online], Available: <http://www.ogm.gov.tr/ekutuphane/Sayfalar/Istatistikler.aspx> (2016).

Behavioral Modeling of 2.4GHz RF Power Amplifier Using Data Mining

Bilge Senel¹, Mehmet Fatih Caglar², Fatih Ahmet Senel³

Abstract

Behavioral modeling of ISM band 2.4GHz RF power amplifier has been carried out in this study using data mining. Some models available in data mining as ANFIS, ANN, KNN, KStar and M5Rules have been used to estimate G_T , PAE, IIP_3 , OIP_3 and THD performance parameters of 2.4GHz RF power amplifier as a function of DC biasing conditions and input power. Results have been compared and the best model is obtained for each performance parameter of 2.4 GHz RF power amplifier has been obtained. ANFIS model for all performance parameters has given preferred results.

Keywords: RF power amplifier, data mining, behavioral modeling, ANFIS, ANN

1 INTRODUCTION

The RF power amplifier (PA), a critical element in transmitter units of communication systems, is expected to provide a suitable output power at a very good gain with high efficiency and linearity. The output power from a PA must be sufficient for reliable transmission [1]. RF PA in wireless communication system is of one of the most important block of transmitters. In particular, high power consumption, linearity, distortion and efficient are the most important performance parameters in power amplifier design [2]. Transducer gain (G_T), power added efficiency (PAE(%)) input third order intercept point (IIP_3), output third order intercept point (OIP_3) and total harmonic distortion (THD) are important performance parameters of a PA while examining the behavior of PA. These performance parameters vary depending on the input signals applied to input power of the amplifier and the DC bias conditions. Power value which is applied to the input of the power amplifier affects its performance. Input power of a PA could be divided into three groups that are; low, medium and high power levels. Low power levels are the linear regions that PAs behave linearly in this region and distortions resulting from the non-linear behavior of the amplifier can be ignored in this region. For low input power levels although linearity performance of amplifier is optimum, efficiency is very poor. In this linear region efficiency is not sufficient to meet the standard transmitter system efficiency. In contrast to high linearity performance efficiency value obtained is not sufficient to meet the requirement of the transmitter. Efficiency of PA which is used in transmitter in mobile devices plays an important role in battery life affects whole system. Therefore, it is needed to be a PA has high linearity for quality of data communication as well as it has high efficiency performance for battery life and power consumption. Linearity behavior of PA goes bad in medium signal region although its efficiency performance increases. In large signal region linearity behavior of PA deteriorates in contrast to PA has its maximum efficiency performance. It is clear that there is a tradeoff between linearity and efficiency for RF PAs. In addition to input power, DC biasing conditions significantly affect and change linearity and efficiency performance of PA. To examine performance parameters of PA like G_T , PAE(%), IIP_3 , OIP_3 and THD for determining optimum input power level and DC bias conditions it is required to change sensitively DC bias conditions together with input power levels. These performance parameters of PA are obtained by means of simulation programs by changing the input power and DC bias conditions and parametrically analyzing of these data (obtained performance parameters of PA by simulation program) is performed with programming languages. Both simulation and parametric analyzing of these data take a long time. Estimation of the performance parameters of PA like G_T , PAE(%), IIP_3 , OIP_3 and THD by models using data mining would be a more practical solution for this process.

Hayati et al., have created an artificial neural network (ANN) model for Class-F PA. The proposed ANN model is used to predict the output power of designed class-F PA as a function of input and DC power [3]. Yuan and Feng aimed to estimate output value of the IIP_3 using multilayer neural network model in their study [4]. Al-Hilali has developed a model with feedforward neural network to predict output spectrum values of PA. In addition, dynamic nonlinear AM/AM and AM/PM graphics of PA, real PA output and ANN prediction have been showed graphically in their study [5]. Nunez-Perez et al., have run their artificial neural network models on faster and more accurate FPGA and DSP hardware. Thus, they have achieved the desired results very fast and precisely. They have modeled AM/AM and AM/PM conversions of 2W-3GHz, 5W-1840MHZ, 5W-2.7GHz of three different PAs[6]. Grinbergs et al., have showed a method to improve MESFET large signal models for multiport GaAs and compact multi-FET which is used for 2GHz hybrid PA. FET model parameters have been extracted from small signal S-parameters and DC

¹ Süleyman Demirel University, Department of Electronics and Communication Engineering, 32260, Isparta, Turkey. bilgeturkel@sdu.edu.tr

² Corresponding Author: Süleyman Demirel University, Department of Electronics and Communication Engineering, 32260, Isparta, Turkey. fatihcaglar@sdu.edu.tr

³ Süleyman Demirel University, Department of Computer Engineering, 32260, Isparta, Turkey. fatihsenel@sdu.edu.tr

measurement results. Linear transformation and regression algorithms that exists in IC-CAP software program have been used for parameter extraction [7]. Cedano et al., have showed application of NARX neural network algorithm using FPGA. AM/AM and AM/PM inverse characteristic of designed PA has been modeled. Modeling has been carried out 2GHz GaN Class-F LTE signal PA [8]. Nonlinear dynamic input and output characteristics and memory characteristics of PA have been modeled using ANN and memory polynomial (MP) models in the study and their performances have been compared. ANN model is based TDNN. Dynamic AM-AM and AM-PM conversions of PA have been modeled with TDNN and MP. Comparison results shows that both models are suitable for modeling PA, but TDNN model has better results according to MP model[9]. Cárdenas-Valdez et al., have been designed in a study simulation tool capable of modeling the degree of nonlinearity and memory effect for the conversion curve of PA. The developed system predict behavior and analyzes with data obtained from measurements AM-AM and AM-PM distortion curves [10]. Turkel and Caglar have been investigated linearity performance of 2.4GHz PA by changing DC bias conditions. In addition to amplifiers linearity performance efficiency and gain of amplifier have been investigated [1]. Aguilar-Lobo et al., have been modeled output spectrum and AM/AM, AM/PM characteristics of a commercial PA with WCDMA and GSM multi-standard signals by using 5MHz LTE signal by using RVNARXNN ANN [11]. Zhai et al., have been modeled output spectrum and AM/AM, AM/PM characteristics of 3.5GHz LDMOS RF power amplifier with WCDMA signals with MANFIS. The results obtained with MANFIS have been compared with ANFIS, RVTDDNN and RBFNN models [12]. Zhai et al., have been modeled power spectral density and AM/AM, AM/PM characteristics of 10W 3.5GHz LDMOS RF PA with WCDMA signals with adaptive neuro-fuzzy inference system (ANFIS). It has been showed that ANFIS based Hammerstein model gave better results than static ANFIS for memory effect modeling of PA[13].

In this study, some data mining models have been used to estimate G_T , $PAE(\%)$, IIP_3 , OIP_3 and THD performance parameters of 2.4GHz ISM band RF PA as a function of DC biasing conditions and input power. Obtained results have been compared and the best model has been obtained for each performance parameter. When the literature is reviewed, it has been seen that ANN is used while creating behavioral models the behavioral modeling of PAs. However it has been meet rarely that the behavioral modeling of PA is created different data mining methods. Therefore in this study, selected performance parameters have been modeled with K-Nearest Neighbor (KNN), ANN, KStar, M5Rules and ANFIS. The output spectrum of PA and AM/AM and AM/PM characteristics has been also modeled. Instead of modeling the amplifier output spectrum and AM/AM and AM/PM characteristics, modeling of G_T , $PAE(\%)$, IIP_3 , OIP_3 and THD performance parameters of PA which gives more detailed information about the performance of PAs as aimed.

2 DATA MINING

Data mining can be defined as the data analysis process which is presenting relationships from large data using computer programming for estimates about the future. Data mining is basically divided into three groups; classification-regression (CR), clustering and association rules. In this study, we have studied some CR methods. Used CR methods are ANFIS, ANN, KNN, KStar and M5Rules. These models were established by Weka 3.7 and MATLAB. Determination coefficient (R^2) (Eq.1), root mean square error (RMSE) (Eq.2) and mean absolute error (MAE) (Eq.3) have been computed to determine the success for generated models. These equations are given by

$$R^2 = 1 - \frac{\sum_{i=1}^N (A_i - P_i)^2}{\sum_{i=1}^N (A_i - A_{mean})^2} \quad (1)$$

$$RMSE = \sqrt{\frac{\sum_{i=1}^N (P_i - A_i)^2}{N}} \quad (2)$$

$$MAE = \frac{\sum_{i=1}^N |P_i - A_i|}{N} \quad (3)$$

where N denotes the number of total sample, A_i is real (original) value, P_i is estimation value and A_{mean} is the average of the real values.

2.1 Adaptive Neuro-Fuzzy Inference System (ANFIS)

ANFIS is an artificial intelligence method which is a combination of learning characteristics of neural networks and fuzzy logic. ANFIS determines the learning rules to reach zero error and it works with Mamdani or Sugeno-type fuzzy inference system. ANFIS can work with different membership functions such as triangular, trapezoidal and Gaussian etc. In this study, 64 rules are taken for ANFIS model with Gaussian membership function.

2.2 Artificial Neural Network (ANN)

ANN is an improved artificial computation which is inspired by the learning mechanism of the human brain neurons. ANN realizes the learning process with training data and online testing with cross validation data. After the learning process, network is tested with test data to good agreement. In this study, ANN has been trained with cross validation

technique. The ANN model has three inputs, two hidden layers and an output as in Figure 1. The first hidden layer has five neurons and second has ten neurons.

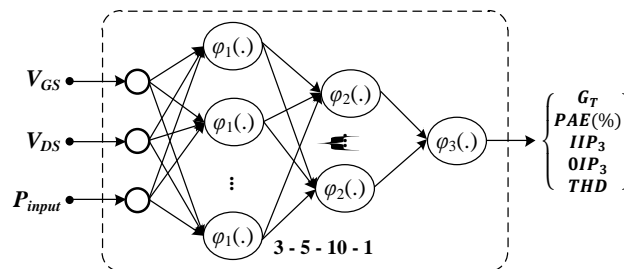


Figure 1. ANN model structure

2.3 K-Nearest Neighbors (KNN)

KNN algorithm is a classification and regression method used in data mining. A sample which belongs to a class is decided its class by looking K pieces nearest neighbors. Euclidean distance is used to measure closeness. The K number is determined by the user and it represents the number of neighbors. In this study, best results have been obtained when the K value is three.

2.4 KStar Algorithm

KStar algorithm is a method that decides the class of new examples based on the entropic distance. In this method, the class similarity is measured for each sample with sets with similar functions. The assignment is carried out to most similar class.

2.5 M5Rules

M5Rules is a decision-making like decision tree and it is created with if-else sentences. Each new sample is evaluated in decision point. The sample proceeds by divided into different leafs.

3 EXPERIMENTAL STUDIES

3.1 Simulation Results and Parametric Analysis of 2.4 GHz PA

As mentioned earlier, 2.4GHz ISM band RF PA is modeled with KNN, ANN, KStar, M5Rules and ANFIS individually with data obtained by changing DC biasing conditions (V_{GS} and V_{DS}) at different certain input power (P_{input}) levels. Parametrically analyzed PA has been designed for 2.4 GHz ISM band with Agilent ADS and G_T , $PAE(\%)$, IIP_3 , OIP_3 and THD performance parameters of PA have been obtained. Avago technology produced ATF501P8 pHEMT transistor has been used. V_{GS} and V_{DS} which represent DC bias conditions of PA have been changed with certain intervals for different input powers. Performance parameters of PA have been investigated considering the upper limits of the DC operating conditions of selected RF transistor of $PAV_{GSmax} = 0.8V$, $V_{DSmax} = 7V$, $I_{DSmax} = 1A$, by changing gate source voltage V_{GS} intervals and drain source voltage V_{DS} intervals. Input power of PA has been changed in selected values from 0dBm to 25dBm. For different amplifier input powers according to different DC biasing conditions (V_{GS} and V_{DS}) G_T , $PAE(\%)$, IIP_3 , OIP_3 and THD performance parameters of PA have been obtained. With these obtained results of 2.4GHz RF PA, it has been modeled with data mining methods to compare results and to find best model among these models. All analyzed models used in this study have been performed with independent variables of (P_{input} , V_{GS} and V_{DS}) which has total 208 data line. G_T , $PAE(\%)$, IIP_3 , OIP_3 and THD parameters of PA have been modeled individually with ANFIS, ANN, KNN, KStar and M5Rules by using these data sets.

3.2 Data Set

Eight data sets have been used which each data set consisting of 26 data, totally 208, by changing V_{GS} which has intervals of $0.42V \leq V_{GS} \leq 0.67V$ with selectivity of 0.01V and V_{DS} which has intervals of $1V \leq V_{DS} \leq 6V$ with selectivity of 0.2V for P_{input} values of 0dBm, 10dBm, 15dBm, 16dBm, 17dBm, 18dBm, 20dBm and 25dBm.

3.3 Creating Models

In this study, five different performance parameters (G_T , $PAE(\%)$, IIP_3 , OIP_3 and THD) have been modeled with ANFIS, ANN, KNN, KStar and M5Rules. Model which has the best estimation for each performance parameter has been determined and estimated models performance results have been represented in tables.

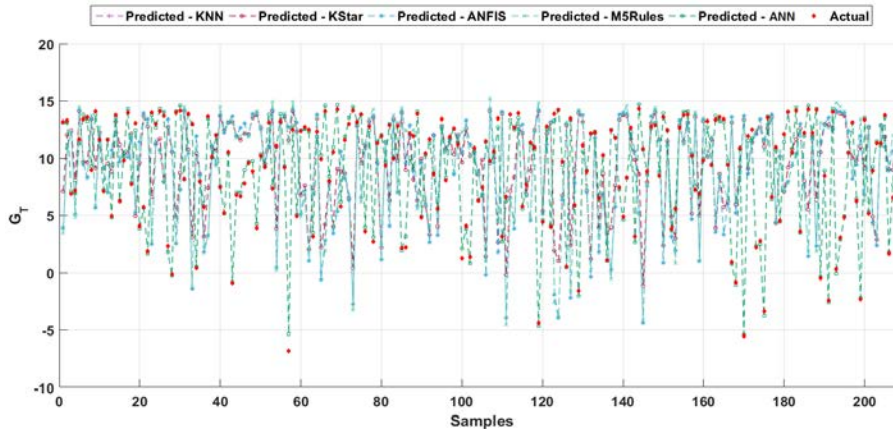


Figure 2. Estimated models results of G_T

Figure 2 shows estimated results which is created by models for G_T graphically. Model results have been compared by plotting estimated model values corresponding to the real values. As it is seen from Table 1 the best result has been obtained with ANFIS model for performance parameters of G_T . It is also seen that ANN model for G_T performance parameter yielded great closed results.

Table 13. Comparison of Models with R^2 , RMSE and MAE for G_T

Model Name	R^2	RMSE	MAE
KNN	0.9799	0.6707	0.3665
KStar	0.9287	1.6652	1.0561
ANFIS	0.9929	0.3848	0.2233
M5Rules	0.9797	0.7154	0.4685
ANN	0.9922	0.4152	0.2738

Figure 3 shows the results of IIP_3 performance parameter estimated by models. It has been seen that ANFIS is the best model for IIP_3 . Numerical results of models for IIP_3 have been demonstrated in Table 2.

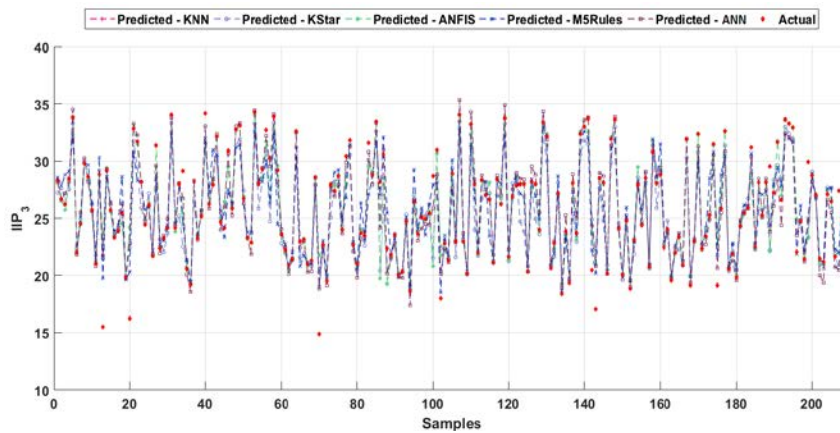


Figure 3. Estimated models results of IIP_3

Table 2. Comparison of Models with R^2 , RMSE and MAE for IIP_3

Model Name	R^2	RMSE	MAE
KNN	0.8615	1.6619	0.6493
KStar	0.8140	1.9880	1.2509
ANFIS	0.9749	0.6573	0.4341
M5Rules	0.8777	1.5942	1.0965

ANN 0.9085 1.3531 0.7917

When OIP_3 performance parameter is analyzed it is seen that the best model for OIP_3 is ANFIS. Model results of OIP_3 shown in Figure 4 and the numerical data of model results have been demonstrated in Table 3.

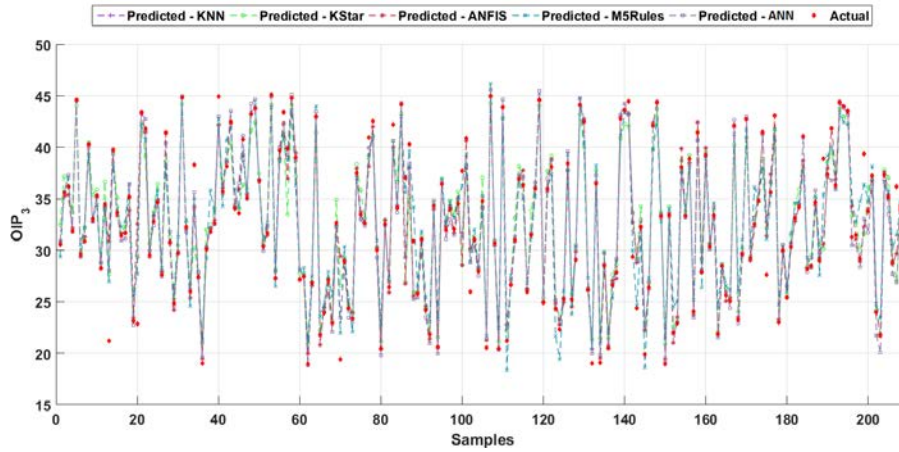


Figure 4. Estimated models results of OIP_3

Table 3. Comparison of Models with R^2 , RMSE and MAE for OIP_3

Model Name	R^2	RMSE	MAE
KNN	0.9215	2.0189	0.8628
KStar	0.9029	2.2907	1.4408
ANFIS	0.9856	0.8240	0.5503
M5Rules	0.9555	1.6366	1.2759
ANN	0.9403	1.7624	0.9557

THD performance parameter is estimated the best with ANFIS model like OIP_3 parameter. Model results of THD corresponds to the real value are shown in Figure 5. Model results have been compared in Table 4.

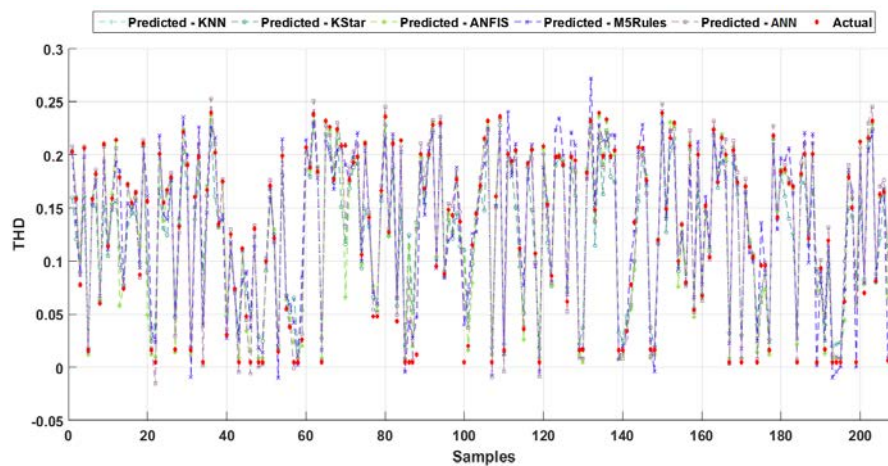


Figure 5. Estimated models results of THD

Table 4. Comparison of Models with R^2 , RMSE and MAE for THD

Model Name	R^2	RMSE	MAE
KNN	0.9140	0.0228	0.0095
KStar	0.8734	0.0305	0.0208

ANFIS	0.9767	0.0114	0.0073
M5Rules	0.9553	0.0166	0.0128
ANN	0.9439	0.0186	0.0097

Finally $PAE(\%)$ parameter is analyzed. Models applied to other parameters have been applied to $PAE(\%)$ and the best result has been obtained with ANFIS as in all other parameters. Estimated model results for $PAE(\%)$ performance parameter shown in Figure 6. Numerical results of applied models for $PAE(\%)$ parameter are listed in Table 5.

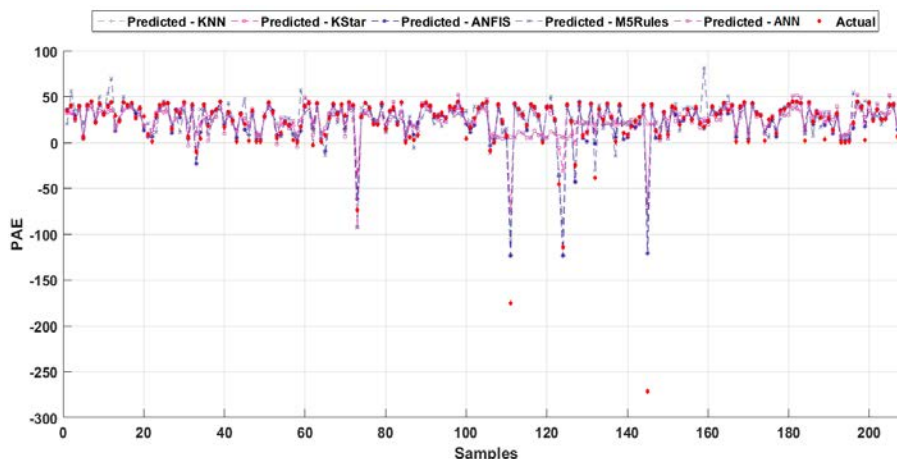


Figure 6. Estimated models results of $PAE(\%)$

Table 5. Comparison of Models with R^2 , RMSE and MAE for $PAE(\%)$

Model Name	R^2	RMSE	MAE
KNN	0.8839	12.3275	4.0541
KStar	0.8610	18.6639	6.8798
ANFIS	0.9934	1.9844	1.4404
M5Rules	0.7112	17.7723	9.1745
ANN	0.2220	28.2446	11.4423

4 RESULTS AND CONCLUSION

In this study DC biasing conditions (V_{GS} and V_{DS}) of RF PA have been changed for different values of input power. Outcomes of G_T , $PAE(\%)$, IIP_3 , OIP_3 and THD have been modeled individually with KNN, ANN, KStar, M5Rules and ANFIS by using obtained data set and estimated results have been compared. When comparison results have been analyzed, it has been seen that all models have similar results with ANFIS. ANFIS model for all performance parameters has given smallest RMSE and MSE and best R^2 . As a result, it has been seen that data mining models should be used for modeling of performance parameters of RF PAs. Especially, as an example work, ANFIS model demonstrates best behavior for 2.4GHz ISM band RF PA.

REFERENCES

- [1] P. Saad, "Design a Highly Linear Power Amplifier Based on HBT (MSc thesis)," University of Gävle Department of Technology, 2006.
- [2] B. Senel, M. F. Caglar, and A. Genc, "Effects of DC bias conditions to performance of 2.4GHz power amplifier," in *2014 22nd Signal Processing and Communications Applications Conference (SIU)*, 2014, pp. 353–356.
- [3] M. Hayati, F. Shama, S. Roshani, and A. Abdipour, "Linearization design method in class-F power amplifier using artificial neural network," *J. Comput. Electron.*, vol. 13, no. 4, pp. 943–949, Dec. 2014.
- [4] X.-H. Yuan and Q. Feng, "Behavioral Modeling of RF Power Amplifiers With Memory Effects Using Orthonormal Hermite Polynomial Basis Neural Network," *Prog. Electromagn. Res. C*, vol. 34, pp. 239–251, 2013.
- [5] A. W. A. A.- HILALI, "Nonlinear Modeling of Radio Frequency Power Amplifier by Using Artificial Neural Network (MSc thesis)," Atilim University, 2015.
- [6] J. C. Nunez-Perez, J. R. Cardenas-Valdez, J. A. Galaviz Aguilar, C. Gontrand, B. Goral, and J. Verdier, "Measure-based

- modeling and FPGA implementation of RF Power Amplifier using a multi-layer perceptron neural network,” in *2014 International Conference on Electronics, Communications and Computers (CONIELECOMP)*, 2014, pp. 237–242.
- [7] O. Grinbergs, L. Dunleavy, S. Gross, B. Schmitz, and T. Winslow, “Non-linear Modeling of a Multi-FET Multi-Port IC,” in *55th ARFTG Conference Digest*, 2000, vol. 37, pp. 1–7.
- [8] J. A. Renteria-Cedano, L. M. Aguilar-Lobo, J. R. Loo-Yau, and S. Ortega-Cisneros, “Implementation of a NARX neural network in a FPGA for modeling the inverse characteristics of power amplifiers,” in *2014 IEEE 57th International Midwest Symposium on Circuits and Systems (MWSCAS)*, 2014, pp. 209–212.
- [9] E. R. Srinidhi, A. Ahmed, and G. Kompa, “Power Amplifier Behavioral Modeling Strategies Using Neural Network and Memory Polynomial Models,” *Microw. Rev.*, vol. 12, no. 1, pp. 15–20, 2006.
- [10] J. Ricardo Cárdenas-Valdez, J. Cruz Núñez-Pérez, J. Alejandro Galaviz-Aguilar, A. Calvillo-Téllez, C. Gontrand, J. Apolinar Reynoso-Hernández, and E. Tlelo-Cuautle, “Modeling memory effects in RF power amplifiers applied to a digital pre-distortion algorithm and emulated on a DSP-FPGA board,” *Integr. VLSI J.*, vol. 49, pp. 49–64, 2015.
- [11] L. M. Aguilar-Lobo, J. R. Loo-Yau, S. Ortega-Cisneros, P. Moreno, and J. A. Reynoso-Hernandez, “Experimental study of the capabilities of the Real-Valued NARX neural network for behavioral modeling of multi-standard RF power amplifier,” in *2015 IEEE MTT-S International Microwave Symposium*, 2015, pp. 1–4.
- [12] J. Zhai, J. Zhou, L. Zhang, J. Zhao, and W. Hong, “The dynamic behavioral model of RF power amplifiers with the modified ANFIS,” *IEEE Trans. Microw. Theory Tech.*, vol. 57, no. 1, pp. 27–35, 2009.
- [13] J. Zhai, J. Zhou, L. Zhang, J. Zhao, and W. Hong, “Dynamic Behavioral Modeling of Power Amplifiers Using ANFIS-Based Hammerstein,” *IEEE Microw. Wirel. Components Lett.*, vol. 18, no. 10, pp. 704–706, Oct. 2008.

Biography

Mehmet Fatih ÇAĞLAR got B.S. degree from Electronics and Communication Engineering from Istanbul Technical University, M.S. degree from Suleyman Demirel University and PhD degree from Yıldız Technical University. He is an assistant professor in Suleyman Demirel University.

Performance Analysis of Time Series Forecasting Models for Short Term Wind Speed Prediction

Alper Kerem¹, Ismail Kirbas², Ali Saygin³

Abstract

Being uncontrollable and variability of wind power can lead to problems in terms of power quality, production-consumption balance and power system reliability in the networks with high wind power. Wind speed forecasting methods with high accuracy are an effective tool that can be used to minimize these problems. In this study, 63m wind measurement station has been assembled with corresponding wind sensors in Mehmet Akif Ersoy University campus and the system has been engaged. From the recorded data total 4464 wind data of March 2014 have been studied and 8 different models (random walk, linear trend, quadratic trend, simple moving average, ARIMA (1,0,2), ARIMA (2,0,1), ARIMA(2,0,2), NARX) have been developed by using time series forecasting methods. Performance analyses have been carried out by using Root Mean Square Error (RMSE) method and comparison of model performances of developed models have also been carried out. The developed models make wind speed estimations when two consecutive wind speed data is entered. According to the results it has been seen that the most successful model is Nonlinear Autoregressive with External Input (NARX) obtained with the use of artificial neural network and as a result of running of this model regression coefficient has been found as 97.82%, RMSE value has been found as 0.80. Consequently, the results show that the developed NARX model is quite effective for short term wind speed prediction.

Keywords: ARIMA, NARX, time series analysis, wind speed forecasting, wind speed prediction

1 INTRODUCTION

The wind energy is fast growing among all the renewable energy sources because of its high efficiency and low pollution. The power created by the wind energy transformation systems directly depends on wind speed and atmosphere meteorology. However, the untidy behaviour of wind is a great challenge to the steadiness and consistency of power system. The fluctuations of the power generation can cause operating expenses for the electricity, and places potential risks to the reliability of electricity supply. For this reason, wind speed forecasting is helpful for unit assurance, economic dispatch and power system operations [1].

The wind power system workers have to forecast variations of the wind power production to accomplish the grid processes, and to plan the spinning backup capacity. In order to increase the wind power penetration and shrink the reserve capacity, more precise predicting of wind speed is an essential need [2].

Moreover, wind speed forecasting is important because it has a significant role in the allocation of balancing power. In addition, wind speed estimating is used for transaction of electricity and the day-ahead scheduling of conventional power plants [3].

2 DATA ACQUISITION

First of all, in order to obtain real-life data about the potential of wind power generation in the Istiklal campus of Mehmet Akif Ersoy University, a wind measurement station was settled [4]. Before the settlement, coordinate determination works have carefully been performed in the campus for the construction of wind measurement station in the campus. For this purpose, different points in the field have been visited at different times and wind speeds were observed. Based on the criteria in the literature, the most appropriate point at the field has been identified as UTM E 263254 and N 4173479 coordinates at 1313m altitude. Wind measurement station has been constructed to detect coordinates, wind speed sensor, wind direction sensor, temperature and humidity sensor, pressure sensor and data

¹Osmaniye Korkut Ata University, Department of Electricity and Energy, Osmaniye, Turkey,
alperkerem@osmaniye.edu.tr

²Mehmet Akif Ersoy University, Department of Computer Engineering, Burdur, Turkey,
ismailkirbas@mehmetakif.edu.tr

³Gazi University, Department of Electrical and Electronics Engineering, Ankara, Turkey,
asaygin@gazi.edu.tr

logger has been assembled. System has been engaged and data has been tracked. Schematic illustration of the measuring stations is given in Figure 1.

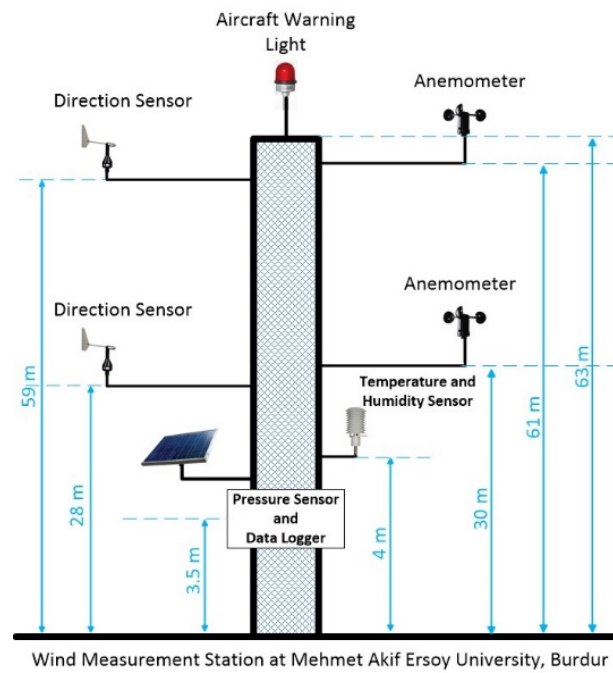


Figure 1. Schematic illustration of the wind measuring station

For this study, wind speed measurement was carried out in 10 minute intervals at the wind measurement station during the month of March 2014. A total of 4464 pieces of data are obtained and converted into a time series for further analysis of this data. Figure 2 depicts daily based average wind speed measurements.

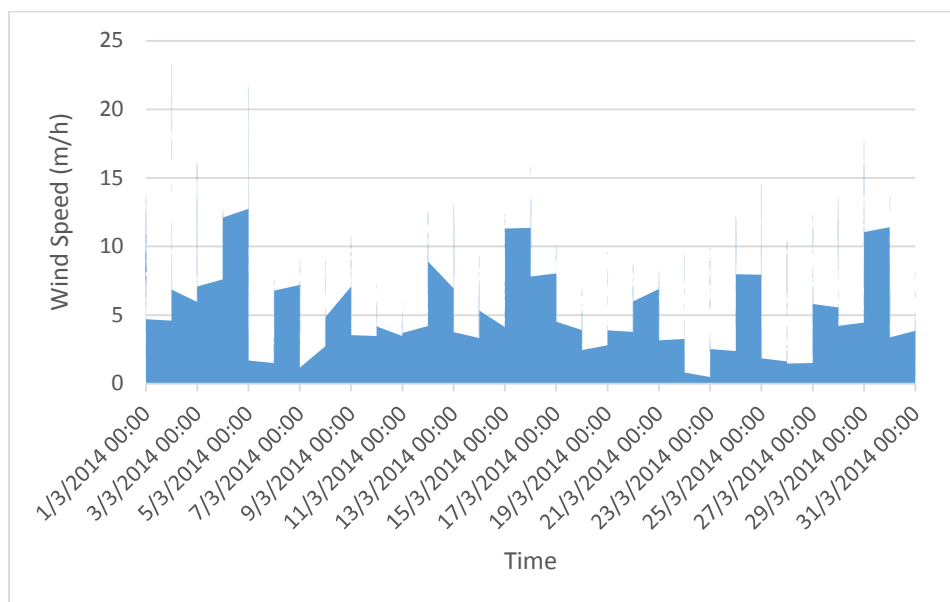


Figure 2. Daily based average wind speed measurements in March 2014

Table 1 also gives some fundamental statistical information about collected data.

Table 2. Statistical results for wind speed measurement.

Statistical Calculation	Value
Average	6.424

Standard Error	0.055
Standard Deviation	3.740
Median	5.926
Variance	13.989
Skewness	0.340
Kurtosis	0.701
Range	23.310
Maximum	23.310
Minimum	0
Total	28677.409
Quantity	4464

Measurements were made has a volatile results as shown in Figure 2 and table 1 respectively. For short term wind speed prediction, eight different methods are investigated and compared in the rest of the paper.

3 TIME SERIES FORECASTING MODELS

Statistical methods purpose discovering the relationship of the gathered data. The historical data of the wind speed can be used for a statistical model easily. Statistical models are low-cost to develop compared to other models and useful to model. Principally, statistical approach is reliable especially for short time periods. The main disadvantage of the approach is that the forecast error rises as the estimation time rises [1].

Statistical methods mainly contain the auto regressive (AR), auto regressive moving average (ARMA), auto regressive integrated moving average (ARIMA), grey predictions and Bayesian approach. These techniques can be used to answer the questions in finance, natural sciences and engineering that have countless data where the observations are inter-reliant [1].

Firat et al. [5] suggested a new statistical process using independent component analysis and AR model. According to acquired results, the projected technique noticeably provides higher precision compared with direct forecasting.

Erdem and Shi [6] projected 4 methods based on ARMA method for the forecasting of the wind direction and speed. The outcomes revealed that the component model is much better at forecasting the wind direction than the traditional-linked ARMA model, although the contradictory is detected for wind speed predicting.

Palomares-Salas et al. [7] used an ARIMA model for time-series forecast including wind speed measurements. Their work grants the method of model validation with a regression analysis. The obtained results confirm that ARIMA model is superior to back propagation neural network for short time-intervals.

In recent times, various new techniques for wind speed and power forecast have been developed with the advance of artificial intelligence. The new developed methods embrace fuzzy logic methods, neuro-fuzzy network, artificial neural network (ANN), support vector machine (SVM), and evolutionary optimization algorithms and adaptive neuro-fuzzy inference system (ANFIS).

ANN could handle complex and non-linear problems in terms of forecasting or classification. ANN based method is a suitable way to apply into the problem to predict the wind speed.

Chang [8] offered a technique using RBF neural network to forecast wind speed. Zeng and Qiao [9] projected a SVM-based technique to predict wind power. Guo et al. [10] studied a modified empirical mode decomposition based on feed-forward neural network. Sfetsos [11] introduced an ANN technique for the predicting of mean hourly wind speed data by means of time series analysis. Yang et al. [12] proposed an ANFIS method to interpolate the invalid and missing data. Chang [13] suggested a wind speed predicting approach based on back propagation neural network.

In this study, we have used 7 different statistical time series forecasting models. Table 2 shows model abbreviations from A to G and their model names respectively.

Table 2. Model abbreviations and model names.

Model Abbreviations	Model Name
A	Random walk
B	Linear trend = $7.24416 + -0.000367306 t$
C	Quadratic trend = $9.31918 + -0.00315506 t + 6.24356E-7 t^2$
D	Simple moving average
E	ARIMA(1,0,2)
F	ARIMA(2,0,1)
G	ARIMA(2,0,2)

Statistical methods can be modelled effortlessly and it is inexpensive compared to other techniques. They process the former wind data to estimate the present over the next few hours. This approach are successful especially for short time periods. The main weakness of the statistical method is error value growths with the forecast time. These approaches are mainly used to forecast up to six hours in advance.

The auto regressive moving average (ARMA) is a recognised model which is based on time series analysis. The main purpose of the ARIMA method is to predict the future value of time series, benefiting from its past values and the past forecast errors. It is popular because it can handle any series, with or without seasonal elements. ARIMA model has three parts as auto regressive, integrated, and moving average. At the same time, the model is also known as Box-Jenkins approach and can give the reliable predicting outcomes within 1 to 2 hours. Equation (1-4) define 4 different ARIMA models as following.

$$ARIMA(1,0,0)y_t = a_1y_{t-1} + \varepsilon_t \quad (1)$$

$$ARIMA(2,0,0)y_t = a_1y_{t-1} + a_2y_{t-2} + \varepsilon_t \quad (2)$$

$$ARIMA(2,0,1)y_t = a_1y_{t-1} + a_2y_{t-2} + b_1\varepsilon_{t-1} \quad (3)$$

$$ARIMA(2,1,0) \Delta y_t = a_1\Delta y_{t-1} + a_2\Delta y_{t-2} + \varepsilon_t, \text{ where } \Delta y_t = y_t - y_{t-1} \quad (4)$$

In literature, there are many statistical evaluation method to evaluate the developed models. In this study we choose mean error (ME), mean absolute error (MAE), mean squared error (MSE), root mean squared error (RMSE), Akaike information criterion (AIC), Hannan–Quinn information criterion (HQC) and Schwarz-Bayesian information criterion (SBIC). As the root mean squared error method is preferred as the main evaluation criteria, each model has been evaluated using the model evaluation methods given in Table 3.

Table 3. Model evaluation methods.

The mean error (ME)	$ME = \frac{1}{n} \sum_{i=1}^n (y_i - \hat{y}_i)$
The mean absolute error (MAE)	$MAE = \frac{1}{n} \sum_{i=1}^n y_i - \hat{y}_i $
The mean squared error (MSE)	$MSE = \frac{1}{n} \sum_{i=1}^n (y_i - \hat{y}_i)^2$
The root mean squared error (RMSE)	$RMSE = \sqrt{\frac{1}{n} \sum_{i=1}^n (y_i - \hat{y}_i)^2}$
Akaike information criterion (AIC)	$AIC = 2k - 2\ln(L)$
Hannan–Quinn information criterion (HQC)	$HQC = -2 \cdot L_{max} + 2k \cdot \log \log n$
Schwarz-Bayesian information criterion (SBIC)	$SBIC = -2 \cdot \ln \hat{L} + k \cdot \ln(n)$

The results obtained from the statistical model evaluation criteria are shown in Table 4.

Table 4. Statistical model evaluation results.

<i>Model</i>	<i>RMSE</i>	<i>MAE</i>	<i>ME</i>	<i>AIC</i>	<i>HQC</i>	<i>SBIC</i>
A	0.834294	0.579629	-0.00118642	-0.362339	-0.362339	-0.362339
B	3.71065	3.04828	9.58115E-16	2.62331	2.62432	2.62618
C	3.59325	2.9544	1.41705E-13	2.55946	2.56098	2.56376
D	0.940994	0.658987	-0.00171022	-0.12119	-0.120684	-0.119755
E	0.831831	0.577612	0.0385374	-0.366909	-0.365392	-0.362605
F	0.832543	0.577968	0.0404928	-0.365198	-0.36368	-0.360894
G	0.832559	0.57791	0.0402586	-0.364711	-0.362688	-0.358973

Artificial neural networks (ANN) are known as the best solution for predicting the time series. Artificial neural networks modelling motivation was specified by human intelligence. So there is a solid relation between organic neurons and artificial neural networks.

The Nonlinear Autoregressive with External Input (NARX) neural network model, which is developed in MATLAB software, is shown in figure 3.

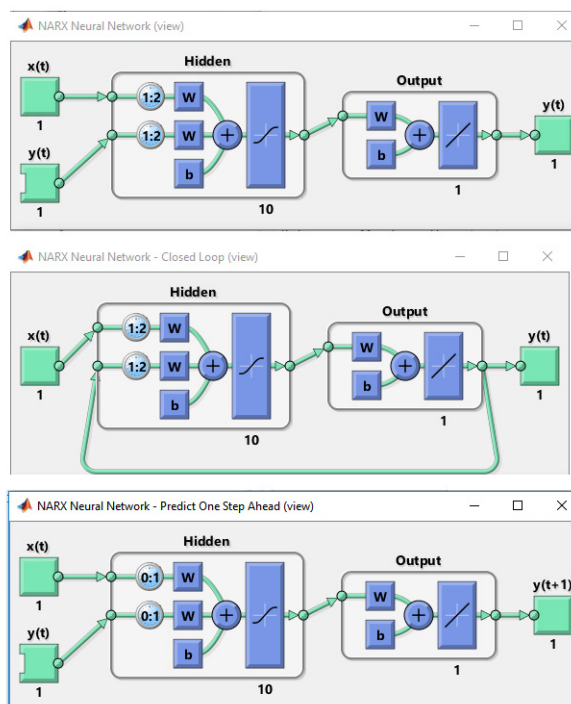


Figure 3. The Nonlinear Autoregressive with External Input (NARX) neural network model developed in MATLAB software.

NARX networks can learn to forecast one time series given past values of the same time series. These networks can be expressed as Equation 5 wherein given d past values of $y(t)$ and another series $x(t)$.

$$y(t) = f(x(t-1), \dots, x(t-d), y(t-1), \dots, y(t-d)) \quad (5)$$

The developed network model has 10 neurons in hidden layer and 1 neuron for output layer. For network training, 3124 pieces of data were selected randomly, then the network model was validated with 670 measurement values. Finally, the trained network was tested with 670 different data. Obtained results and error values can be seen in Table 5.

Table 5. The evaluation results for NARX neural network model.

	Target Values	MSE	RMSE	R
Training	3124	0.6696	0.8182	0.9757
Validation	670	0.7169	0.8466	0.9740
Testing	670	0.6392	0.7994	0.9782

Figure 4 shows output response of the developed network including the error graph.

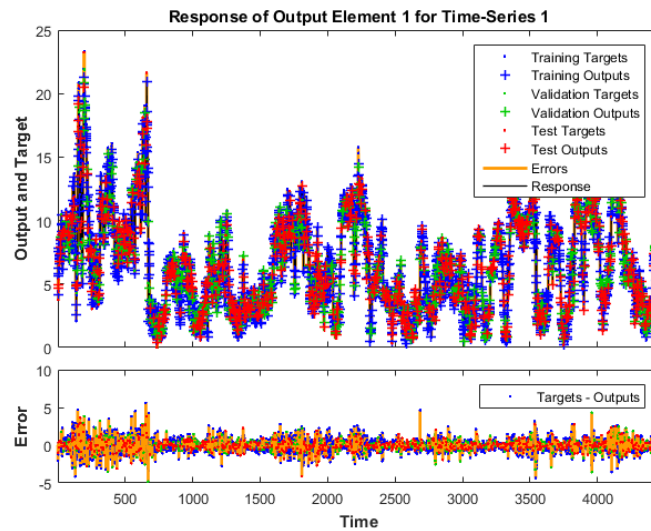


Figure 4. The model evaluation results for NARX model.

Figure 5 also gives a detailed picture and information obtained from training, validation and test phases. Calculated R values are converging to 1 means that the created network model almost exactly fits the problem.

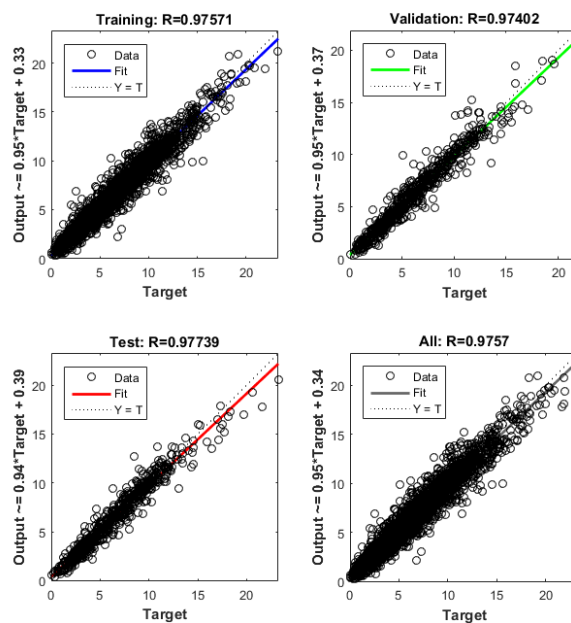


Figure 5. Graphical results for NARX model evaluation.

4 CONCLUSION

In this study, we have established a wind measurement station in the Istiklal campus of Mehmet Akif Ersoy University to reveal the potential of wind power generation. Well-directed forecasting of wind speed is essential to predict generated electric energy. Thus, we tried to estimate next wind speed values according to past ones accurately as possible. For this reason, eight different methods are investigated and compared according to evaluation criteria such as mean error, mean absolute error, mean squared error, root mean squared error, Akaike information criterion, Hannan–Quinn information criterion and Schwarz-Bayesian information criterion.

In accordance with the results obtained, ARIMA models and NARX neural network model appear more successful than others. If we consider root mean square error values as the main criteria, NARX neural network model has the best RMSE and R values. Three ARIMA models (ARIMA(1,0,2), ARIMA(2,0,1) and ARIMA(2,0,2)) are following it.

This study finds out that NARX neural network model and ARIMA models can be used for short time wind speed prediction in reliable fashion.

ACKNOWLEDGMENT

This research was supported by West Mediterranean Development Agency (BAKA, Project Number: TR61/13/DFD/036) and Mehmet Akif Ersoy University Scientific Research Projects Commission (Project Number: 0212-Gudumlu-13). We thank project coordinator Prof. Dr. Serdar SALMAN who provided insight and expertise that greatly assisted the research.

REFERENCES

- [1] W.-Y. Chang, "A Literature Review of Wind Forecasting Methods," *J. Power Energy Eng.*, vol. 2, no. 4, pp. 161–168, 2014.
- [2] D. R. Chandra, M. S. Kumari, and M. Sydulu, "A detailed literature review on wind forecasting," in *Power, Energy and Control (ICPEC), 2013 International Conference on*, 2013, pp. 630–634.
- [3] M. Lange and U. Focken, "New developments in wind energy forecasting," in *Power and Energy Society General Meeting - Conversion and Delivery of Electrical Energy in the 21st Century, 2008 IEEE*, 2008, pp. 1–8.
- [4] A. Kerem, Y. Atayer, S. Gorgulu, and S. Salman, "Preparation and Implementation of Wind Energy Feasibility Infrastructure of Mehmet Akif Ersoy University," *J. Grad. Sch. Nat. Appl. Sci. Mehmet Akif Ersoy Univ.*, vol. 5, no. 1, pp. 18–24, 2014.
- [5] U. Firat, S. N. Engin, M. Saraclar, and A. B. Ertuzun, "Wind Speed Forecasting Based on Second Order Blind Identification and Autoregressive Model," in *Machine Learning and Applications (ICMLA), 2010 Ninth International Conference on*, 2010, pp. 686–691.
- [6] E. Erdem and J. Shi, "ARMA based approaches for forecasting the tuple of wind speed and direction," *Appl. Energy*, vol. 88, no. 4, pp. 1405 – 1414, 2011.
- [7] J. C. Palomares-Salas, J. J. G. de la Rosa, J. G. Ramiro, J. Melgar, A. Aguera, and A. Moreno, "ARIMA vs. Neural networks for wind speed forecasting," in *2009 IEEE International Conference on Computational Intelligence for Measurement Systems and Applications*, 2009, pp. 129–133.
- [8] W. Y. Chang, "Wind Energy Conversion System Power Forecasting Using Radial Basis Function Neural Network," *Appl. Mech. Mater.*, vol. 284–287, pp. 1067–1071, 2013.
- [9] J. Zeng and W. Qiao, "Support vector machine-based short-term wind power forecasting," in *Power Systems Conference and Exposition (PSCE), 2011 IEEE/PES*, 2011, pp. 1–8.
- [10] Z. Guo, W. Zhao, H. Lu, and J. Wang, "Multi-step forecasting for wind speed using a modified EMD-based artificial neural network model," *Renew. Energy*, vol. 37, no. 1, pp. 241 – 249, 2012.
- [11] A. Sfetsos, "A novel approach for the forecasting of mean hourly wind speed time series," *Renew. Energy*, vol. 27, no. 2, pp. 163 – 174, 2002.
- [12] Z. Yang, Y. Liu, and C. Li, "Interpolation of missing wind data based on {ANFIS}," *Renew. Energy*, vol. 36, no. 3, pp. 993 – 998, 2011.
- [13] W.-Y. Chang, "Application of Back Propagation Neural Network for Wind Power Generation Forecasting," *Int. J. Digit. Content Technol. Its Appl.*, vol. 7, pp. 502–509, 2013.

Biography

Alper KEREM, He was born in 1983, Kahramanmaraş, Turkey. He received the BS degree in 2006, the MSc degree in 2012 from Gazi University, Ankara, Turkey. He is studying PhD in Department of Electrical- Electronic Engineering at Gazi University. He is a Lecturer at Department of Electricity and Energy, Osmaniye Korkut Ata University. His research interests comprise power electronics, multi level inverter technologies, Space Vector PWM and wind energy.

İsmail KIRBAŞ, He got his bachelors' degree in the Computer Education Department in Technical Education Faculty at Kocaeli University, Kocaeli/Turkey in 2000, his master degree in the Electronics and Computer Education at Kocaeli University in 2008, PhD degree in Electronics and Computer Education Department at Sakarya University in 2013. He is still an academic member of the Computer Engineering Department at Burdur Mehmet Akif Ersoy University. His major areas of interests are: Wireless Sensor Networks, Embedded Systems, Design of Experiments and Mobile Programming.

Ali SAYGIN, He was born in 1974, Sivas, Turkey. He received the BS degree in 1995, the MSc degree in 1998, and the PhD degree 2004 from Gazi University, Ankara, Turkey. He is currently an Asst.Prof.Dr. Department of Electrical and Electronics Engineering at Gazi University. His research interests include, PLC, Automation, Power Electronics, DSPACE and DSP.

Ultraviolet Radiation (UV) Applications In Milk Industry

Ayhan Duran¹, Halil Ibrahim Kahve²

Abstract

During the production of dairy products, some thermal processes such as pasteurization and sterilization are used commonly to inactivate microorganisms. But as a result of thermal processes, loss of nutrient and aroma, non-enzymatic browning and organoleptic differentiation especially in dairy products are seen. Because of this, alternative methods are needed to provide microbial inactivation and as major problems are caused by high temperatures, non-thermal processes are focused on. For this purpose, some methods such as ultraviolet radiation (UV), high pressure (HP), pulsed light (PL), supercritical carbon dioxide (SC-CO₂) or pulsed electric field (PEF) are used in food. Ultraviolet (UV) light occupies a wide band of wavelengths in the non-ionizing region of the electromagnetic spectrum between X-rays (200 nm) and visible light (400nm). UV radiation affects the DNA of bacteria, viruses, fungi and other microorganisms exposed to it in such a way that prevents them from reproducing. UV radiation is one of the new processing technology, thermal processing applications shorter duration of activity and dairy products because of the high can be used as alternatives.

Keywords: *Ultraviolet, radiation, milk, dairy.*

1 INTRODUCTION

Treatments on food products are carried out to extend its shelf life, but above all to ensure its safety for consumers. Thermal technologies are the most widely applied to achieve these purposes, but these treatments have a negative effect on certain components of the food itself, reducing its vitamin content and other nutrients, as well as sensory features that make them less attractive in terms of color and textural properties. Non-thermal technologies are an alternative to thermal treatment that are being studied and developed in order to obtain a better final product sensory quality, but without neglecting microbial safety. In this way, these alternatives to thermal technologies can produce food products without enzymes and harmful microorganisms, while maintaining nutritional characteristics and minimizing the loss of quality in terms of flavor, color and nutritional value. One of these innovative technologies is ultraviolet irradiation [1].

Ultraviolet light can be used to inactivate many types of organisms, including viruses, but it is currently known that UV light only works on surfaces or clear liquids such as water. UV light radiation has been used for many years in pharmaceutical, electronic, and aquaculture industries as a disinfection medium. A monochromatic UV light (254 nm) is obtained by using low-pressure mercury (LPM) vapour germicidal lamps. The UV light acts as a physical method for microbial disinfection [2].

UV light is generally produced by mercury lamps at low or medium pressure as a continuous beam in a mono or polychromatic mode, respectively. When applied under controlled conditions, UV light can lead to non-thermal processes, which have been shown to inactivate microorganisms in edible liquids, such as in apple, grape, cranberry and grapefruit juices, milk, sugar solutions, citron, water and other liquid foods and liquid eggs [3].

Many nonthermal technologies, such as the germicidal portion of ultraviolet light (UV-C) ranging from 200 to 280 nm, are now being investigated as an alternative to thermal treatment of milk to inactivate pathogens and improve shelf life [4].

2 THE CHARACTERISTIC OF UV

Ultraviolet (UV) light occupies a wide band of wavelengths in the non-ionising region of the electromagnetic spectrum between X-rays (200nm) and visible light (400nm). For practical purposes the UV spectrum can be subdivided into three regions:

- short-wave UV (UV-C) with wavelengths from 200 to 280nm;
- medium-wave UV (UV-B) with wavelengths from 280 to 320nm;

¹Corresponding author: Aksaray University, Department of Food Engineering, 68000, Aksaray Turkey. aduran@aksaray.edu.tr

²Aksaray University, Department of Food Engineering, 68000, Aksaray Turkey hibrahimkahve@gmail.com

- long-wave UV (UV-A) with wavelengths from 320 to 400nm.

The intensity of UV radiation is expressed as irradiance or intensity flux (Wm^{-2}), while the dose, which is a function of the intensity and time of exposure, is expressed as radiant exposure (Jm^{-2}) [5].

3 IMPACT ON LIVING CELLS UV APPLICATIONS IN THE DAIRY INDUSTRY

UV radiation in the range of 250-260nm is lethal to most micro-organisms, including bacteria, viruses, protozoa, mycelial fungi, yeasts and algae. The relationship between germicidal effect and wavelength is which shows the maximum effect at 254nm. The damage inflicted by UV-C probably involves specific target molecules and a dose in the range from 0.5 to 20 Jm^{-2} leads to lethality by directly altering microbial DNA through dimer formation [6]. The main types of photoproduct in UV-irradiated DNA are cyclobutyl-type dimers (pyrimidine dimers), pyrimidine adducts and DNA-protein cross-links [7]. Purines are approximately 10-fold more resistant to photochemical alteration than are the pyrimidines, and because of this difference in sensitivity it has been implied that the photochemistry of the purines is not important biologically; by the time a significant amount of purine damage has occurred, the cells would have been inactivated by pyrimidine damage anyway [8].

Once the DNA has been damaged, the microorganisms can no longer reproduce and the risk of disease arising from them is eliminated. Temperatures between 5 and 37°C have little, if any, influence on the microbiocidal action of radiation, but moisture exerts a very marked effect. Where bacteria are suspended in air, an increase in relative humidity results in a greatly reduced death rate, especially at humidities greater than about 50%. Similarly, bacteria suspended in a liquid medium are much more resistant than those suspended in air, even after making allowance for the absorption of the medium [5].

4 UV APPLICATIONS IN THE DAIRY INDUSTRY CONCLUSION

In his study Matak and friends, sensory and chemical consequences of treating goat milk using an UV fluid processor were assessed. Milk was exposed to UV for a cumulative exposure time of 18 s and targeted UV dose of $15.8 \pm 1.6 \text{ mJ/cm}^2$. A triangle test revealed differences between the odor of raw milk and UV irradiated milk. Ultraviolet irradiation at the wavelength 254 nm produced changes in the sensory and chemical properties of fluid goat milk [9].

In another study, fresh goat's milk was inoculated with *Listeria monocytogenes* (L-2289) at 10^7 CFU/ml and exposed to UV light. A greater than 5-log reduction was achieved ($P < 0.0001$) when the milk received a cumulative UV dose of $15.8 \pm 1.6 \text{ mJ/cm}^2$. The results of this study indicate that UV irradiation could be used for the reduction of *L. monocytogenes* in goat's milk [10].

Reinemann et al. in this study, Ultraviolet (UV) system was shown to be capable of reliably achieving in excess of a 3 log₁₀ reduction in bacteria measured as standard plate, psychrotrophic, coliform and thermotolerant counts. Sensory analysis indicated that excessive or improper treatment may affect milk flavor so that care must be taken in the way that UV treatment is applied [11].

UV light inactivation of *Mycobacterium avium* subsp. *paratuberculosis* in Middlebrook 7H9 broth and whole and semiskim milk was investigated using a laboratory-scale UV machine that incorporated static mixers within UV-penetrable pipes. UV treatment proved to be less effective in killing *M. avium* subsp. *paratuberculosis* suspended in milk (0.5- to 1.0-log₁₀ reduction per 1,000 mJ/ml) than that suspended in Middlebrook 7H9 broth (2.5- to 3.3-log₁₀ reduction per 1,000 mJ/ml) [12].

5 CONCLUSION

UV technology is an emerging non-thermal process technology for disinfection of foods in the food industry. Ultraviolet processing can potentially provide more ideal food products with fresh-like characteristics. Short wave UV-C radiation is lethal to most microorganisms and can be applied to render safe food products. At present, the application of UV light for disinfection of food products is no longer used, but it could easily be applied to liquid and solid food products. Each food processing method is indeed different, and the performance of UV lamps for treatment of liquids or solids should be studied to obtain basic information regarding microbial disinfection (Guerrero-Beltrán and Barbosa-Cánovas, 2004).

Currently, this technology is not widely used in food processing, but it could potentially be applied in dairy industry, although in each process the correct type of lamp to use should be taken into account in order to optimize its effects on pathogens and spoilage. It is also very important to conduct studies on the effect that this type of radiation has on food, regarding nutritional and sensory evaluation.

REFERENCES

- [1] Butz, P., & Tauscher, B. (2002). Emerging technologies: Chemicals aspects. *Food Research International*, 35, 279–284.
- [2] J.A. Guerrero-Beltrán and G.V. Barbosa-Cánovas. (2004). Review: Advantages and Limitations on Processing Foods by UV Light. *Food Sci Tech Int* 2004; 10(3):0137–11.
- [3] Ismael Kasahara, Valentina Carrasco, Luis Aguilar. (2015). Inactivation of *Escherichia coli* in goat milk using pulsed ultraviolet light. *Journal of Food Engineering* 152 (2015) 43–49.
- [4] Jennifer A. Crook, Paul V. Rossitto, Jared Parko, Tatiana Koutchma, and James S. Cullor (2015). Efficacy of Ultraviolet (UV-C) Light in a Thin-Film Turbulent Flow for the Reduction of Milkborne Pathogens. *FOODBORNE PATHOGENS AND DISEASE* Volume 12, Number 6.
- [5] Thomas Bintsis, Evanthia Litopoulou-Tzanetaki and Richard K Robinson. (2000). Existing and potential applications of ultraviolet light in the food industry – a critical review. *Journal of the Science of Food and Agriculture*. 80:637-645.
- [6] Ferron WL, Eisenstark A and Mackay D. (1972). Distinction between far- and near-ultraviolet light killing of recombinationless (recA) *Salmonella typhimurium*. *Biochim Biophys Acta* 277:651-658.
- [7] Harm W. (1980). *Biological Effects of Ultraviolet Radiation*. Cambridge University Press, Cambridge.
- [8] Smith KC and Hanawalt PC. (1969). *Molecular Photobiology Inactivation and Recovery*. Academic Press, London.
- [9] Matak K. E., S. S. Sumner, S. E. Duncan, E. Hovingh, R. W. Worobo, C. R. Hackney and M. D. Pierson. (2007). Effects of Ultraviolet Irradiation on Chemical and Sensory Properties of Goat Milk. *Journal Dairy Science*. 90:3178-3186.
- [10] Matak K.E., Churey J.J, Worobo R.W., Sumner S.S., Hovingh E., Havkney C.R., Pierson M.D. (2005). Efficacy of UV light for the reduction of *Listeria monocytogenes* in goat's milk. *J Food Prot*, 68 (10): 2212-2216.
- [11] Reinemann DJ, Gouws P, Cilliers T, Houck K, Bishop JR. (2006). New methods for UV treatment of milk for improved food safety and product quality. *ASABE Annual International Meeting*. 9-12 July 2006, Oregon, Portland, Paper number 066088.
- [12] Altic L.C, Rowe T.M, Grani R. (2007). UV Light inactivation of *Mycobacterium avium* subsp. *paratuberculosis* in milk as assessed by FAST Plaque TB phage assay and culture. *Appl Environ Microbiol*, 73: 3728-3733.

Energy Management And Sustainability Of Agricultural Perspective: Case From Çankırı, Turkey

Bekir Cengil¹, Gokhan Ipek², Mehmet Ali Biberçi²

Abstract

Growing population and the developments of the people's living standards continuously increasing that it demands for energy in worldwide. Today, using a large portion of the energy, which will be known run out in the near future from fossil-based sources, it reveals the environmental problems of global dimension. That case, instead of fossil fuel reserves are rapidly diminishing, and that cause environmental pollution, reveals the need for utilization of renewable and clean energy sources. Nowadays, intensive agricultural production system is dependent on fossil fuels, it is carried out with limited water and intensive use of natural resources. At the same time, to meet the needs of a growing world population, climate change as well, especially on land and water resources is reduced by the effect of energy sources as well as in natural resources makes it efficient and sustainable use forced.

In this study; Central Anatolia Region and the provinces of Çankırı, with an average annual production of alternative energy sources that can be utilized in the agricultural field, aimed to determine the highest and lowest solar radiation exergy value. For this purpose; State Meteorology Affairs General Directorate, which is measured by months and regions based on solar radiation intensity and mean temperature data were utilized.

Keywords: Çankırı, energy, intensive, radiation exergy

1 INTRODUCTION

It is a known fact that energy in one of the most important components of the agricultural production process. Energy diversity can be used in this process has increased tend to different energy sources. The renewable major sources are solar energy, wind energy, geothermal energy and biomass energy.

Renewable energy as it is defined "the nature of their evolution, the next day to produce the same energy source may be present. Although fossil fuels are exhausted and non-renewable, those are the clean and sustainable natural resources like hydraulics, sun, biomass, and geothermal.

Sustainable energy is "today's energy needs, without damaging the ability of future generations to meet their own needs". In this context, "the sustainable agriculture is to protect the environment in the long term productivity and agricultural activities, to ensure economic growth, it is directed to improving the quality of rural life.

It's an essential requirement taking advantage of alternative energy resources instead of fossil energy sources economically profitable for producers on the purpose of preserving energy asset and avoiding from environmental pollution on agricultural production. Therefore, efficient and sustainable use of alternative energy sources such as natural resources became crucial in the agricultural production process. In this study, the Central Anatolia Region and Çankırı annual basis average of solar energy from alternative energy sources in the province, to determine the highest and lowest solar radiation exergy value is assessed on the basis of agricultural aspects of energy management and sustainability principles.

2 MATERIALS AND METHODS

2.1 Material

Exergy of a form of energy or substance, its potency in the environment can change is a measure of quality or usefulness. [5]. Exergy, as a result of interaction with the surroundings, the heat transfer is the maximum theoretical useful work that can be obtained only in case of the environment. [6]. Exergy is the portion of the entire energy can be converted into other forms of energy. [7].

Exergy of solar radiation, thermal radiation is important for the process to transform the work and different events, such as heat. Radiation in the transformation process, Exergy efficiency must be defined taking into account the

¹Corresponding author: ÇankırıKaratekin University, Kızılırmak Vocational School, Çankırı, Turkey, bcengil@karatekin.edu.tr

²ÇankırıKaratekin University, Yapraklı Vocational School, Çankırı, Turkey

specific features of the processing. Exergy efficiency of conversion of thermal radiation work, radiation benefiting from the work done, defined as the ratio of the radiation exergy. [6, 8].

The average solar radiation exergyvalue by region in Turkey have been calculated based on the average solar radiation intensity values given in Table 1. According to the average temperature for the duration of the sun, it is taken into account, which was published by to the State Meteorology Affairs General Directorate (DMI). [9].An easy way to comply with the symposium paper formatting requirements is to use this document as a template and simply type your text into it.

Table 1. Solar radiationvaluesbyregion in Turkey. [10]

REGIONS	Average Solar Radiation Intensity (W/m ²)		
	YEARLY	JULY	DECEMBER
Southeastern Anatolia	477	767	283
Mediterranean	463	723	183
Central Anatolia	457	720	160
Aegean	450	723	167
EastAnatolia	447	667	163
Marmara	363	593	133
Black Sea	343	510	157

2.2 Method

Exergy values of solar radiation is calculated by the following equation

$$\hat{E}_r = \hat{I} \cdot \psi \quad (1)$$

Equation (2) in ψ value indicates the relative amount of energy present in the highest amount of radiation and is calculated as follows.

$$\psi = 1 + \frac{1}{3} \left(\frac{T_o}{T} \right)^4 - \frac{4}{3} \left(\frac{T_o}{T} \right) \quad (2)$$

In this equation; \hat{E}_r ; exergy of solar radiation (W/m²); solar radiation (W/m²), T_o ; ambient temperature (K) and T_s ; surface temperature of the Sun (6000K).

3 RESULTS AND DISCUSSION

The annual average calculated for Turkey in general, the changes in the highest and lowest solar radiation exergy value is given in Figure 1.

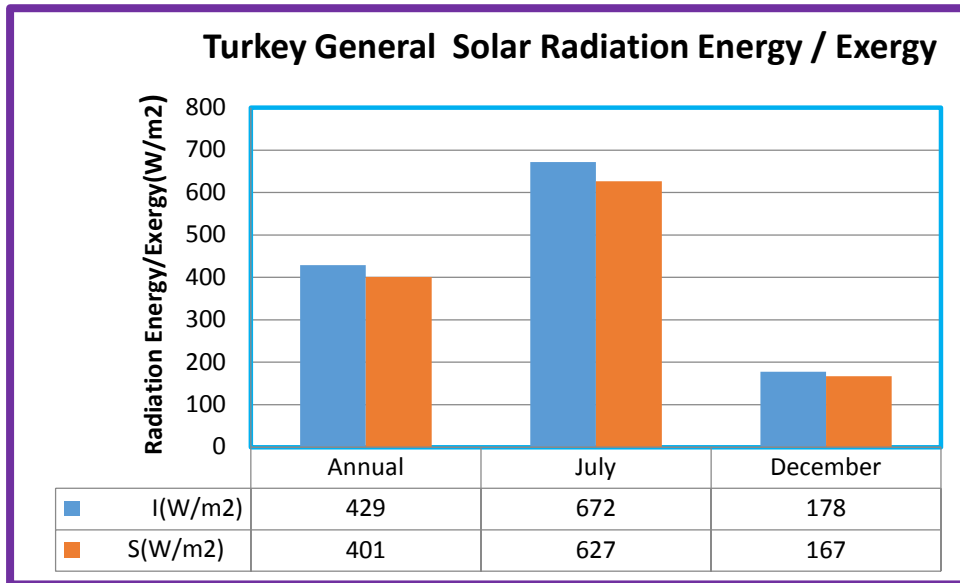


Figure 1. Turkey General of Solar Radiation Energy / Exergy

Turkey in the average annual solar radiation energy of 428.6 W/m^2 , while the average annual solar radiation exergy is designated as 401.1 W/m^2 . The average annual solar radiation energy of 671.9 W/m^2 for July to be in with the highest levels of solar radiation exergy of 626.8 W/m^2 is calculated. The annual average solar radiation energy of 178 W/m^2 of solar radiation exergy for December, which is the lowest level of 166.8 W/m^2 , respectively.

The average annual solar radiation exergy by region in Turkey, a parallel shift of the average annual solar radiation is shown in Table 1, as expected. In Turkey, the average annual solar radiation exergy of the richest regions in terms, as well as in terms of solar radiation energy of 446 W / m^2 with the Southeastern Anatolia. Respectively, the Southeastern Anatolia Mediterranean (433 W / m^2), Central Anatolia (428 W / m^2), Aegean (421 W / m^2), East (419 W / m^2), Marmara (340 W / m^2) regions eyeing the each other, the lowest value of 321 W / m^2 is seen in the Black Sea region.

Turkey and Solar Radiation Exergy Change in Çankırı Province



Figure 2. Turkey's total solar radiation values map

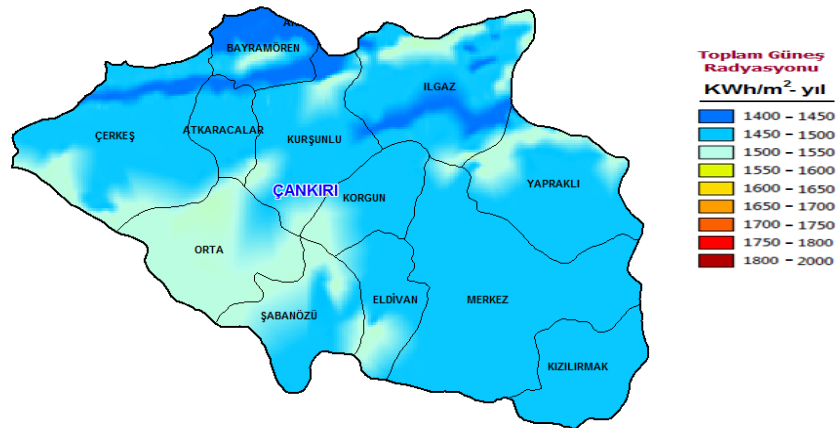


Figure 3. Çankırı total solar radiation values map

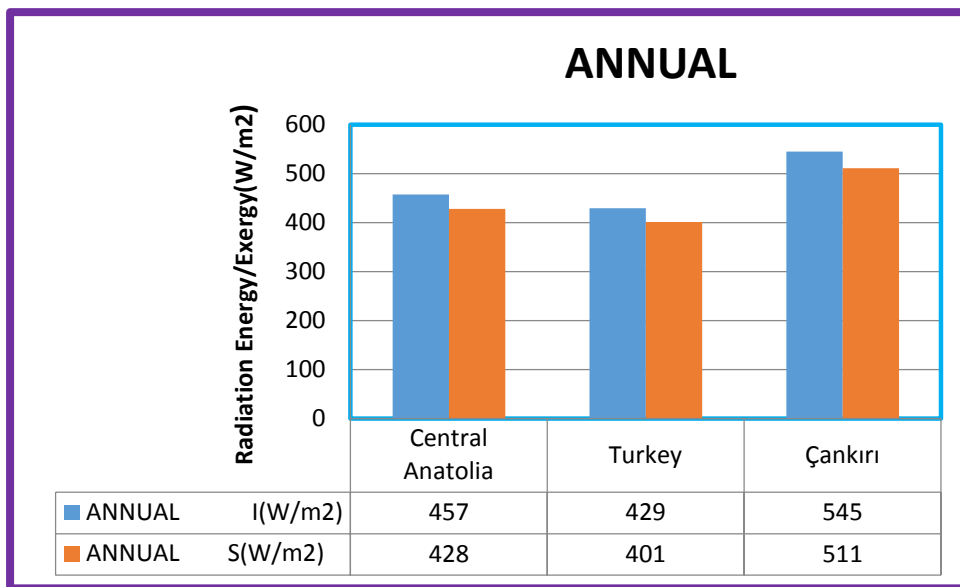


Figure 4-Turkey, Central Anatolia and Çankırı the annual energy/exergy radiation values

Turkey in the average annual solar radiation energy of 429 W/m^2 while the average annual solar radiation exergy is designated as 401.1 W/m^2 . The average annual solar radiation energy of 545 W/m^2 with the highest level because it is in Çankırı province, exergy of solar radiation 511 W/m^2 is calculated. The average annual solar radiation energy / exergy when value as in Fig 4 during the year of Çankırı Province by the general of Turkey and Central Anatolia to have more solar energy potential and these values are observed to exceed the average value considering.

Çankırı months of radiation energy and exergy values for the provinces when examined, solar energy best month in terms of potential, 719 W / m^2 radiation power of 673 W / m^2 , while May and Exergy value and the lowest month 424 W / m^2 radiation power and 398 W / m^2 with exergy value is calculated as of December.

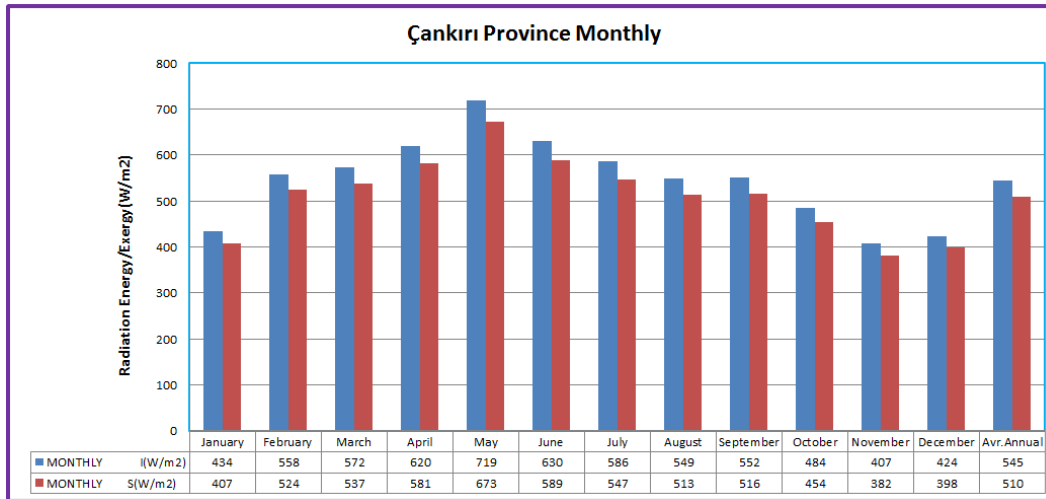


Figure 5- Monthly energy / exergy radiation value for Çankırı.

4 CONCLUSIONS AND RECOMMENDATIONS

Maintain energy efficiency and in order to prevent environment pollution is a priority requirement instead of fossil energy sources that in win-win situation as economic using of alternative energy sources for producers. In agricultural production therefore, efficient and sustainable use of alternative energy sources as in all natural resources has also important in the agricultural production process. In this study, In the Central Anatolia Region and city of Çankırı from alternative energy sources as solar energy determining of the average annual the highest and lowest solar exergy value was evaluated on the basis of agricultural aspects of energy management and sustainability principles.

Central Anatolia Region of Turkey and the average annual for the province of Çankırı is determined by the highest and lowest solar radiation exergy value. Turkey in general, Çankırı Central Anatolia Region and the result set for the province can be summarized as follows:

1. As the average annual solar radiation energy in Turkey, 428.6 W/m^2 , the average annual solar radiation exergy 401.1 W/m^2 is defined,
2. As the average annual solar radiation energy in the Central Anatolian Region of Turkey 457 W/m^2 , the average annual solar radiation exergy of 428 W/m^2 is designated.
3. As the average annual solar radiation energy of Çankırı province 545 W/m^2 , the average annual solar radiation exergy of 510 W/m^2 is designated.

As a result; province of Çankırı; because of geographical, ecological conditions and in terms of alternative energy sources that can be used in agricultural production has more potential of solar energy than the general of Turkey and Central Anatolia Region of Turkey. Therefore, it will be found within the framework of the principles of sustainable agriculture and renewable resources more efficient energy management in an important position in terms of agricultural production potential with the use.

REFERENCES

- [1] Gönüllü, M.T.2009.Yenilenebilir Enerji Kaynaklarının Kullanımının Çevreye Olumlu Etkileri.
- [2] Standard Dergisi, 560 (48): 31-35.
- [3] Ediger, V. Ş., 2008. "National Energy Report of Turkey: Energy Situation, Challenges, and Policies for Sustainable Development", AASA Beijing Workshop on Sustainable Energy Development in Asia 2008, November 17-18 in Beijing, China, InterAcademy Council, p. 77-93.
- [4] Anonim, 1987. WCED, Our Common Future (World Commission on Environment and Development), Oxford University.
- [5] Francis, C.A., Flora, C.B., King, L.d., 1990. Sustainable Agriculture in Temperate Zones, USA.
- [6] I. Dinçer, M. Hussain, I. Al-Zaharah, "Energy and Exergy Use in Agricultural Sector of Saudi Arabia". Energy Policy, vol 33, pp 1461-1467, 2004.
- [7] P. Petela, 2003. "Exergy of undiluted thermal radiation", Solar Energy, vol. 74, pp. 469-488.
- [8] D.C. Spanner, 1964. Introduction to Thermodynamics. Academic Press, London,
- [9] S.M. Jeter, 1981. "Maximum conversion efficiency for the utilization of direct solar radiation", Solar Energy, vol. 26(3), pp. 231-236.
- [10] Anonim, 2016. <http://www.mgm.gov.tr/veridegerlendirme/il-ve-ilceler-istatistik.aspx?m=CANKIRI>
- [11] Ültaır, 1998. M.Ö. 21. Yüzyıla girerken Türkiye'nin enerji stratejisinin değerlendirilmesi, Yayın No: TÜSİADT/98-12/239, ISBN: 975-7249-59-9, Lebib Yalkım Yayınları ve Basım İşleri A.Ş., İstanbul,

Spectra of the [MLCl₂] (M= Mn(II), Fe(II), Co(II); L= 2,2'-Bipyridine) Complex from Theoretical Calculations

Berna Catikkas^{1,2}, Ziya Kantarci²

Abstract

The structural, electronic and vibrational spectral parameters of the [MLCl₂] (M= Mn(II), Fe(II), Co(II); L= 2,2'-Bipyridine) complexes have been calculated by using HF/gen and DFT/mPW1PW91+iop(3/76=0572004280)/gen levels. Firstly, geometric parameters (bond length, bond angle, torsion angle) of the most stable form of the complexes were determined. Their binding, reorganization, atomization, HOMO-LUMO (FMOs) and ionization potential energies have been obtained. Secondly, anharmonic infrared and Raman frequencies were calculated. Lastly, SQM analysis has been performed.

Keywords: Density Functional Theory, Raman Spectra, Infrared Spectra, 2,2'-bipyridine

1 INTRODUCTION

2,2'-bipyridine (bpy) is a bidentate chelating ligand, and an important isomer of the bipyridine family. These kinds of ligands have been playing an important role in the development of coordination chemistry [1,2]. 2,2'-bipyridine transition metal complexes show antifungal, antibacterial and antiviral activity. The aim of this study is to predict the structural, electronic and vibrational spectral parameters of the [MLCl₂] (M= Mn(II), Fe(II), Co(II); L= 2,2'-Bipyridine) donor-acceptor complexes. Their structures were characterized using HF / gen and DFT / mPW1PW91 + iop (3/76=0572004280) / gen levels. Some physical properties such as, molecular electrostatic potential surface, frontier molecular orbital properties, dipole moment (μ) were calculated with Gaussian 03W software package [3].

2 CALCULATION

Quantum chemical calculations were carried out with Gaussian 03W software package [3], with GaussView 3.0 molecular graphic visualizing program [4]. Optimized ground state geometry of ligand and their complexes were computed using HF / gen and DFT / mPW1PW91 + iop (3/76=0572004280) / gen levels. Used basis sets were 6-311+G for atom no: 1, 2, 6, 7, 19, 20; SV for atom no: 3, 4, 5, 8, 9, 10, 11, 12, 13, 14, 15, 16, 17, 18; Cl: 6-31G(2df), M: sddall and M: sdd. All calculations were carried out by using this DFT hybrid scheme. Harmonic, anharmonic infrared and Raman frequencies of the complexes were calculated at the same level. The Total Energy Distribution (TED) of the all fundamental modes was calculated by Scaled Quantum Mechanics Solutions (SQM). Eight scaling groups have been used in SQM calculation [5 – 14].

Gas-phase binding energy (ΔE) was calculated using the following equation (1):

$$\Delta E = E_{[LMCl_2]} - E_{MCl_2} - E_L \text{ for } MCl_2 + :L \rightarrow [LMCl_2] \quad (1)$$

Reorganization energy (ΔE_{RE}) was calculated using equation (2),

$$\Delta E_{RE} = E(\text{reorganized compound energy}) - E(\text{free compound energy}) \quad (2)$$

Where, reorganized energy E is calculated by using freeze coordinate of the complexes.

The number of electrons transferred (ΔN) was calculated according to Pearson [15,16],

$$\Delta N = \frac{(\chi_L^0 - \chi_{MCl_2}^0)}{2(\eta_L + \eta_{MCl_2})} \quad (3)$$

¹ Corresponding author: Mustafa Kemal University, Department of Physics, 31034, Hatay, Turkey. berna@mku.edu.tr, agberna@yahoo.com

² Gazi University, Department of Physics, 06500, Ankara, Turkey.

hereionization potential $I = -E_{\text{HOMO}}$, electron affinity $A = -E_{\text{LUMO}}$, $\eta = (I-A)/2$, $\chi = (I+A)/2$ global electrophilicity index ($\omega = \mu^2/2\eta$) were calculated according to Koopmans theory [16].

The molecular electrostatic potential $V(r)$, is defined following equation (4)

$$V(r) = \sum_A \frac{Z_A}{(R_A - r)} - \int \frac{\rho(r')}{(r' - r)} d(r') \quad (4)$$

where, Z_A is the charge of nucleus A, located R_A , $\rho(r')$ is the electronic density function [18,19].

3 RESULTS AND DISCUSSION

a. Structural parameters

Structural parameters of 2,2'-bipyridine (bpy) were determined for trans conformation (as shown in Fig. 1a) taken from X-ray diffraction data [20]. This form has a C_{2h} symmetry. However, bpy exists in a cis conformation in the metal complexes (as shown in Fig. 1b) and has C_{2v} symmetry.

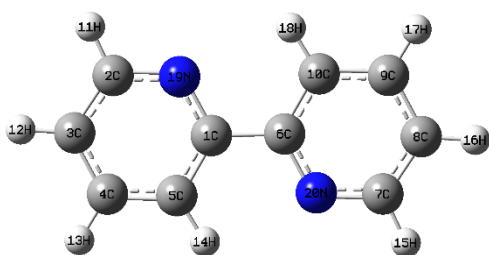


Figure 1. (a) trans-bpy structure

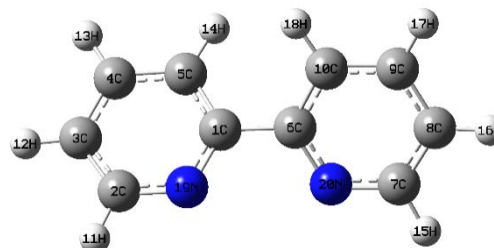


Figure 1. (b) cis-bpy structure

Table 14. The calculated and the experimental geometrical parameters for trans-2,2'-bipyridine

Left side				Right side				Left side			Right side		
Bond length (Å)	HF	DFT	Exp.*	Bond length	HF	DFT	Exp.*	Dihedral angle	HF	DFT	Dihedral angle	HF	DFT
C ₁ ,C ₅	1.395	1.395	1.410	C ₆ ,C ₁₀	1.395	1.395		C ₆ ,C ₁ ,C ₅ ,C ₄	180.0	180.0	C ₁ ,C ₆ ,C ₁₀ ,C ₉	180.0	180.0
C ₁ ,N ₁₉	1.336	1.342	1.350	C ₆ ,N ₂₀	1.336	1.342		C ₆ ,C ₁ ,C ₅ ,H ₁₄	0.0	0.0	C ₁ ,C ₆ ,C ₁₀ ,C ₁₈	0.0	0.0
C ₂ ,C ₃	1.389	1.390	1.370	C ₇ ,C ₈	1.389	1.390	1.370	N ₁₉ ,C ₁ ,C ₅ ,C ₄	0.0	0.0	N ₂₀ ,C ₆ ,C ₁₀ ,C ₉	0.0	0.0
C ₂ ,H ₁₁	1.077	1.084	1.080	C ₇ ,H ₁₅	1.077	1.084		N ₁₉ ,C ₁ ,C ₅ ,H ₁₄	180.0	180.0	N ₂₀ ,C ₆ ,C ₁₀ ,H ₁₈	180.0	180.0
C ₂ ,N ₁₉	1.330	1.334	1.370	C ₇ ,N ₂₀	1.330	1.334	1.370	C ₅ ,C ₁ ,N ₁₉ ,C ₂	0.0	0.0	C ₁₀ ,C ₆ ,N ₂₀ ,C ₇	0.0	0.0
C ₃ ,C ₄	1.394	1.394	1.370	C ₈ ,C ₉	1.394	1.394	1.370	C ₆ ,C ₁ ,N ₁₉ ,C ₂	180.0	180.0	C ₁ ,C ₆ ,N ₂₀ ,C ₇	180.0	180.0
C ₃ ,H ₁₂	1.081	1.086	1.080	C ₈ ,H ₁₆	1.081	1.086		H ₁₁ ,C ₂ ,C ₃ ,C ₄	180.0	180.0	H ₁₅ ,C ₇ ,C ₈ ,C ₉	180.0	180.0
C ₄ ,C ₅	1.392	1.391	1.400	C ₉ ,C ₁₀	1.392	1.391	1.400	H ₁₁ ,C ₂ ,C ₃ ,H ₁₂	0.0	0.0	H ₁₅ ,C ₇ ,C ₈ ,H ₁₆	0.0	0.0
C ₅ ,H ₁₄	1.077	1.084	1.080	C ₁₀ ,H ₁₈	1.077	1.084		N ₁₉ ,C ₂ ,C ₃ ,H ₁₂	180.0	180.0	N ₂₀ ,C ₇ ,C ₈ ,H ₁₆	180.0	180.0
C ₁ ,C ₆	1.481	1.470	1.500					C ₃ ,C ₂ ,N ₁₉ ,C ₁	0.0	0.0	C ₈ ,C ₇ ,N ₂₀ ,C ₆	0.0	0.0
Bond angles (°)				Bond angles (°)				H ₁₁ ,C ₂ ,N ₁₉ ,C ₁	180.0	180.0	H ₁₅ ,C ₇ ,N ₂₀ ,C ₆	180.0	180.0
C ₅ ,C ₁ ,C ₆	121.6	121.3		C ₁ ,C ₆ ,C ₁₀	121.6	121.3		C ₂ ,C ₃ ,C ₄ ,C ₅	0.0	0.0	C ₇ ,C ₈ ,C ₉ ,C ₁₀	0.0	0.0
C ₅ ,C ₁ ,N ₁₉	121.5	121.9		C ₈ ,C ₇ ,N ₂₀	122.6	122.9	124.3	C ₂ ,C ₃ ,C ₄ ,H ₁₃	180.0	180.0	C ₇ ,C ₈ ,C ₉ ,H ₁₇	180.0	180.0
C ₆ ,C ₁ ,N ₁₉	116.9	116.8		C ₁ ,C ₆ ,N ₂₀	116.9	116.8	116.1	H ₁₂ ,C ₃ ,C ₄ ,C ₅	180.0	180.0	H ₁₆ ,C ₈ ,C ₉ ,C ₁₀	180.0	180.0
C ₃ ,C ₂ ,H ₁₁	121.3	121.1		C ₈ ,C ₇ ,H ₁₅	121.3	121.1		H ₁₂ ,C ₃ ,C ₄ ,H ₁₃	0.0	0.0	H ₁₆ ,C ₈ ,C ₉ ,H ₁₇	0.0	0.0
C ₃ ,C ₂ ,N ₁₉	122.6	122.9	124.2	C ₁₀ ,C ₆ ,N ₂₀	121.5	121.9	122.5	C ₃ ,C ₄ ,C ₅ ,C ₁	0.0	0.0	C ₈ ,C ₉ ,C ₁₀ ,C ₆	0.0	0.0
H ₁₁ ,C ₂ ,N ₁₉	116.2	116.0		H ₁₅ ,C ₇ ,N ₂₀	116.2	116.0		C ₃ ,C ₄ ,C ₅ ,H ₁₄	180.0	180.0	C ₈ ,C ₉ ,C ₁₀ ,H ₁₈	180.0	180.0
C ₂ ,C ₃ ,C ₄	118.0	118.2	118.3	C ₇ ,C ₈ ,C ₉	118.0	118.2	118.5	H ₁₃ ,C ₄ ,C ₅ ,C ₁	180.0	180.0	H ₁₇ ,C ₉ ,C ₁₀ ,C ₆	180.0	180.0
C ₄ ,C ₃ ,H ₁₂	121.5	121.4		C ₉ ,C ₈ ,H ₁₆	121.5	121.4		C ₅ ,C ₁ ,C ₆ ,C ₁₀	180.0	180.0	N ₁₉ ,C ₁ ,C ₆ ,N ₂₀	180.0	180.0
C ₃ ,C ₄ ,C ₅	119.3	119.1	119.4	C ₈ ,C ₉ ,C ₁₀	119.3	119.1	119.7	C ₅ ,C ₁ ,C ₆ ,N ₂₀	0.0	0.0	N ₁₉ ,C ₁ ,C ₆ ,C ₁₀	0.0	0.0
C ₁ ,C ₅ ,C ₄	118.7	118.8		C ₆ ,C ₁₀ ,C ₉	118.7	118.8	118.3						
C ₄ ,C ₅ ,H ₁₄	121.9	122.4		C ₉ ,C ₁₀ ,H ₁₈	121.9	122.4							
C ₁ ,N ₁₉ ,C ₂	119.9	119.1	116.4	C ₆ ,N ₂₀ ,C ₇	119.9	119.1	116.7						

* Xray diffraction values [15]

The found structural conformation of 2,2'-bipyridine molecule in the gas phase differs from the conformation in the crystalline structure. This difference is likely due to the molecular packing effects in the crystal form. The most stable form (shown in Figure 1) has been optimized at the selected methods and basis sets. The structural parameters of this form are given in Table 1, together with the x-ray structural data for comparison. The reliability of the calculated structural parameters was appraised by the criterion stated by Foresman and Frisch [4]. For accurate geometries, we generally refer to bond lengths that are within about 0.01-0.02 of the experiment; bond and dihedral angles that are within about 1-20 of the experimental values. Based on this criterion, as seen from Table 1, our optimized bond lengths and angles are in good agreement with the x-ray structural results [20]. This structural agreement indicates that the intermolecular forces in the crystal form are very mild. As seen in Table 1, structural DFT values are better than HF approach. A similar conclusion also be reached from the vibrational results.

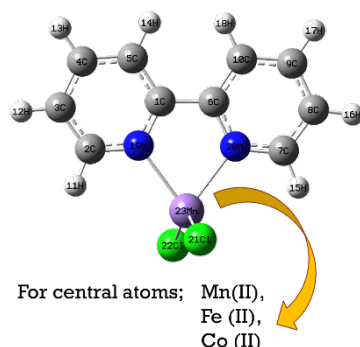


Figure 2. $[M(bpy)Cl_2]$ $M=Mn(II), Fe(II), Co(II)$ structure

Table 2. Selected optimized geometrical parameters for 2,2'-bipyridine (bpy-cis and complexes), in angstroms for bond lengths and degrees for angles

Bond length (Å)	bpy-cis		[Mn(bpy)Cl ₂]		[Fe(bpy)Cl ₂]		[Co(bpy)Cl ₂]	
	HF	DFT	HF	DFT	HF	DFT	HF	DFT
C ₁ ,C ₅	1.395	1.396	1.391	1.392	1.391	1.391	1.390	1.391
C ₁ ,C ₆	1.484	1.474	1.489	1.475	1.488	1.474	1.490	1.476
C ₁ ,N ₁₉	1.334	1.341	1.340	1.345	1.340	1.345	1.341	1.346
C ₂ ,C ₃	1.391	1.391	1.388	1.388	1.389	1.388	1.389	1.388
C ₂ ,H ₁₁	1.077	1.084	1.077	1.083	1.076	1.082	1.076	1.082
C ₂ ,N ₁₉	1.331	1.334	1.331	1.334	1.330	1.334	1.330	1.333
C ₃ ,C ₄	1.392	1.392	1.390	1.392	1.390	1.392	1.390	1.392
C ₃ ,H ₁₂	1.081	1.086	1.079	1.085	1.079	1.085	1.079	1.085
C ₄ ,C ₅	1.393	1.392	1.394	1.392	1.394	1.393	1.395	1.393
C ₄ ,H ₁₃	1.082	1.087	1.081	1.086	1.081	1.086	1.081	1.086
N ₁₉ ,M ₂₃			2.272	2.209	2.208	2.139	2.146	2.073
N ₂₀ ,M ₂₃			2.272	2.209	2.208	2.139	2.146	2.073
Cl ₂₁ ,M ₂₃			2.357	2.282	2.307	2.231	2.289	2.216
Cl ₂₂ ,M ₂₃			2.357	2.282	2.307	2.231	2.289	2.216
Bond angles (°)								
C ₅ ,C ₁ ,C ₆	121.2	121.0	123.0	123.3	123.4	123.7	123.3	123.7
C ₅ ,C ₁ ,N ₁₉	121.6	121.8	120.4	120.5	120.5	120.7	120.3	120.4
C ₆ ,C ₁ ,N ₁₉	117.2	117.1	116.6	116.2	116.1	115.7	116.3	115.9
C ₃ ,C ₂ ,H ₁₁	121.2	121.0	121.3	121.6	121.5	121.9	121.7	122.1

C ₃ ,C ₂ ,N ₁₉	122.9	123.2	122.1	122.0	122.0	121.9	121.8	121.7
H ₁₁ ,C ₂ ,N ₁₉	116.0	115.8	116.6	116.3	116.5	116.2	116.5	116.2
C ₂ ,C ₃ ,C ₄	118.1	118.2	118.0	118.2	118.0	118.3	118.0	118.4
C ₈ ,C ₇ ,N ₂₀	122.9	123.2	122.1	122.0	122.0	121.9	121.8	121.7
C ₆ ,C ₁₀ ,C ₉	119.0	119.1	119.2	119.2	119.0	119.1	119.1	119.1
C ₆ ,C ₁₀ ,H ₁₈	120.2	120.2	121.2	121.0	121.2	121.0	121.2	121.0
C ₁ ,N ₁₉ ,M ₂₃			117.1	116.7	116.8	116.3	115.0	114.4
C ₂ ,N ₁₉ ,M ₂₃			122.0	122.7	122.3	123.1	123.8	124.7
C ₆ ,N ₂₀ ,C ₇	119.5	118.9	120.9	120.6	120.9	120.6	121.1	120.9
C ₆ ,N ₂₀ ,M ₂₃			117.1	116.7	116.8	116.3	115.0	114.4
C ₇ ,N ₂₀ ,M ₂₃			122.0	122.7	122.3	123.1	123.8	124.7
N ₁₉ ,M ₂₃ ,N ₂₀			72.6	74.2	74.3	76.1	77.3	79.5
N ₁₉ ,M ₂₃ ,Cl ₂₁			108.1	107.5	108.0	107.5	109.8	109.6
N ₁₉ ,M ₂₃ ,Cl ₂₂			108.1	107.5	108.0	107.5	109.8	109.6

b. Vibrational Spectra

Calculation of 2,2'-bipyridine (bpy) was carried out in normal mode analysis and the SQM vibrational study [21, 22]. While *trans*-bpy has 19A_g, 8B_g, 9A_u, 18B_u symmetry mode for C_{2h} point group, *cis*-bpy has 19A₁, 9A₂, 8B₁, 18B₂ symmetry mode for C_{2v} point group. The correlation between the calculation DFT (anharmonic) and SQM frequencies with observed frequencies are given in Figure 3 and 4, respectively. As seen in Figure 3 and 4, the calculated and the observed values exhibit a good correlation, R²=0.9995. The calculated observed frequencies [23, 24] are shown in Table 3.

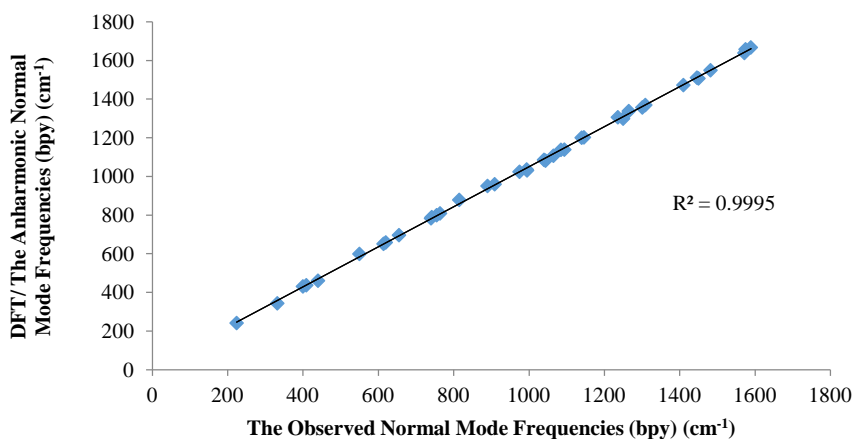
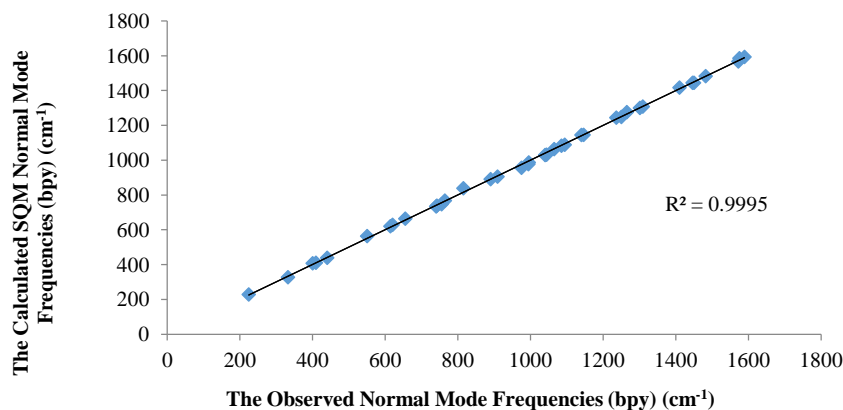


Figure 3. The calculated DFT and the observed normal mode frequencies (bpy) (cm⁻¹)



c. Electronic Properties

According to the frontier molecular orbital (FMO) theory, the E_{HOMO} is directly related to the ionization potential and characterizes the susceptibility of the molecule toward attack by electrophiles [16,26]. The E_{LUMO} measures the ability of a molecule to accept electrons in intermolecular interactions [27]. Theoretically, calculated frontier molecular orbitals of the title compounds are shown in Figure 5.

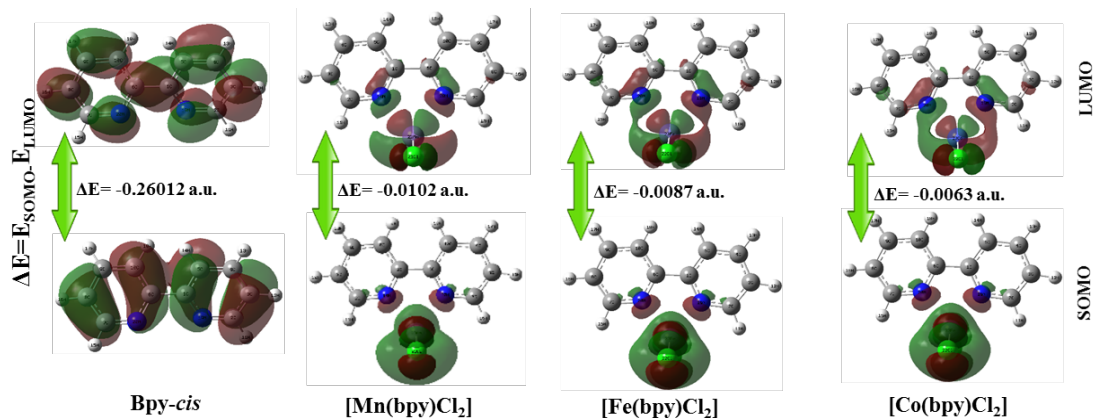


Figure 5. Frontier molecular orbitals of the compounds.

Chemical reactivity parameters of the title compounds are listed in Table 4. Reorganization energy and $\Delta E[(\text{MCl}_2)_{\text{LUMO}}-\text{L}_{\text{(HOMO)}}]$ energy increase towards to $[\text{Co}(\text{bpy})\text{Cl}_2]$ complex while the bonding energy, $\Delta E_{\text{SOMO-LUMO}}$, chemical hardness (η) and the number of electrons transferred (ΔN) from ligand to MCl_2 decrease because the M-N bond length are decreasing (Table 4).

Table 4. Calculated quantum chemical parameters of the studied complexes.

	[Mn(bpy)Cl ₂]	[Fe(bpy)Cl ₂]	[Co(bpy)Cl ₂]
M-N Bond Length (Å)	2.2089	2.1391	2.0733
Binding Energy (eV)	2.9171	1.9375	1.7579
Number of Transfer Electron (ΔN)	0.6590	0.6190	0.5240
Reorganization Energy (eV)	0.0327	0.0381	0.0435
E_{LUMO} (eV)	-4.6926	-4.4687	-4.9098
E_{SOMO} (eV)	-4.9707	-4.7059	-5.0804
$\Delta E_{\text{SOMO-LUMO}}$ (eV)	0.2781	0.2373	0.1706
$\Delta E[(\text{MCl}_2)_{\text{LUMO}}-\text{L}_{\text{(HOMO)}}]$ (eV)	1.9592	2.2041	2.4218
Chemical Hardness (η)	0.1391	0.1186	0.0853

Map of molecular electrostatic potential (MEP) plots charges distribution in the ground state geometry. As seen in Figure 6, negative region of the free *bpy-cis* ligand is found around N atom, however the negative charges around the ring on the complexes.

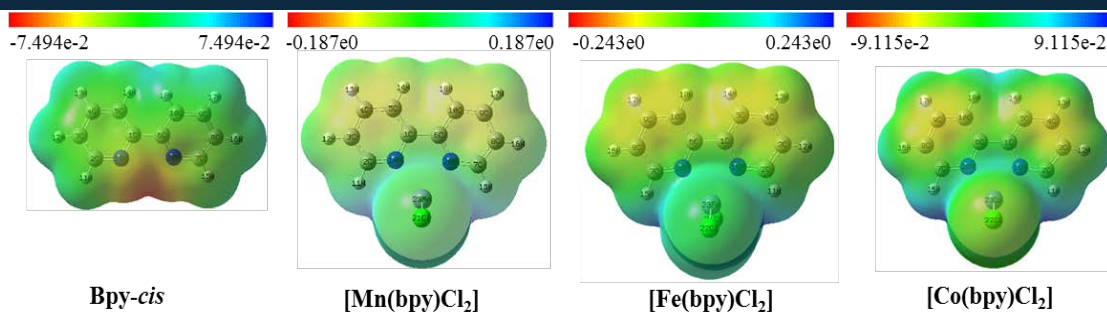


Figure 6. Map of the molecular electrostatic potential of the compounds.

4 CONCLUSION

[MLCl₂] (M= Mn(II), Fe(II), Co(II); L= 2,2'-Bipyridine) donor-acceptor complexes have been studied by using HF/gen and DFT/mPW1PW91+iop(3/76=0572004280)/gen levels. All observed vibrational bands have been examined and assigned with the help of TED values on the basis of our calculations. The results from the experimental and the hybrid DFT theoretical method and gen basis set indicate that the density functional methods provide valuable information for understanding the vibrational spectra and electronic properties of the ligand and complex molecules.

ACKNOWLEDGMENT

The numerical calculations reported in this paper were performed at TUBITAK ULAKBIM, High Performance and Grid Computing Center (TRUBA Resources).

REFERENCES

- [1] M. Hashemi, DFT Study of Nucleophilicity of Organometallic (2,2-bipyridine)platinum(II) Complexes. *Journal of Organometallic Chemistry*, 776, 77–82, 2015.
- [2] M. J. Frisch, G. W. Trucks, H. B. Schlegel, G. E. Scuseria, M. A. Robb, J. R. Cheeseman, J. A. Montgomery, Jr., T. Vreven, K. N. Kudin, J. C. Burant, J. M. Millam, S. S. Iyengar, J. Tomasi, V. Barone, B. Mennucci, M. Cossi, G. Scalmani, N. Rega, G. A. Petersson, H. Nakatsuji, M. Hada, M. Ehara, K. Toyota, R. Fukuda, J. Hasegawa, M. Ishida, T. Nakajima, Y. Honda, O. Kitao, H. Nakai, M. Klene, X. Li, J. E. Knox, H. P. Hratchian, J. B. Cross, V. Bakken, C. Adamo, J. Jaramillo, R. Gomperts, R. E. Stratmann, O. Yazyev, A. J. Austin, R. Cammi, C. Pomelli, J. W. Ochterski, P. Y. Ayala, K. Morokuma, G. A. Voth, P. Salvador, J. J. Dannenberg, V. G. Zakrzewski, S. Dapprich, A. D. Daniels, M. C. Strain, O. Farkas, D. K. Malick, A. D. Rabuck, K. Raghavachari, J. B. Foresman, J. V. Ortiz, Q. Cui, A. G. Baboul, S. Clifford, J. Cioslowski, B. B. Stefanov, G. Liu, A. Liashenko, P. Piskorz, I. Komaromi, R. L. Martin, D. J. Fox, T. Keith, M. A. Al-Laham, C. Y. Peng, A. Nanayakkara, M. Challacombe, P. M. W. Gill, B. Johnson, W. Chen, M. W. Wong, C. Gonzalez, and J. A. Pople, *Gaussian 03, Revision E.01, Gaussian, Inc.*, Wallingford CT, 2004.
- [3] L.A. Summers, A.R. Katritzky (Ed.), *Advances in Hetero-cyclic Chemistry*, vol. 35, Academic Press, Orlando, p. 281, 1984.
- [4] J.B. Foresman, E. Frisch, *Exploring Chemistry with Electronic Structure Methods*, Gaussian, Inc., Pittsburgh, PA, 118, 1996.
- [5] P. Pulay, G. Fogarasi, G. Pongor, J. E. Boggs, A. Vargha, *J. Am. Chem. Soc.* 105, 7037. 1983.
- [6] G. Rauhut, P. Pulay, *J. Phys. Chem.* 99, 3096. 1995.
- [7] J. Baker, A. A. Jarzecki, P. Pulay, *J. Phys. Chem. A*, 102, 1412, 1998.
- [8] K. Koch, Holthausen, M. C. *A Chemist's Wiley-VCH*: Weinheim, York, 2001.
- [9] N. C. Hardy, P. E. Maslen, R. D. Amos, J. S. Andrews, C. W. Murray, G. Laming, *J. Chem. Phys. Lett.* 197, 506. 1992.
- [10] P. J. Stephens, F. J. Devlin, C. F. Chabalowski, M. J. Frisch, *J. Phys. Chem.* 98, 11623, 1994.
- [11] A. A. El-Azhary, H. U. Suter, *J. Phys. Chem.*, 99, 12751, 1995.
- [12] S. Y. Lee, B. H. Boo, *Bull. Korean Chem. Soc.* 17, 760, 1996.
- [13] S. Y. Lee, *Bull. Korean Chem. Soc.* 22, 605, 2001.
- [14] T. Sundius, *Vib. Spectrosc.*; 29, 89, 2002.
- [15] R.G. Pearson, Absolute electronegativity and hardness: application to inorganic chemistry, *Inorg. Chem.* 27, 734–740, 1988. doi:10.1021/ic00277a030.
- [16] T. Koopmans, Über die Zuordnung von Wellenfunktionen und Eigenwerten zu den Einzelnen Elektronen Eines Atoms, *Physica*. 1, 104–113. 1934. doi:10.1016/S0031-8914(34)90011-2.
- [17] P. Politzer, J.S. Murray, The fundamental nature and role of the electrostatic potential in atoms and molecules, *Theor. Chem. Acc.* 108, 134–142. 2002. doi:10.1007/s00214-002-0363-9.
- [18] P. Politzer, P.R. Laurence, K. Jayasuriya, Molecular electrostatic potentials: an effective tool for the elucidation of biochemical phenomena, *Environ. Health Perspect.* 61, 191–202. doi:10.1289/ehp.8561191.
- [19] Koch, E. C., "Acid-Base Interactions in Energetic Materials: I. The Hard and Soft Acids and Bases (HSAB) Principle-Insights to Reactivity and Sensitivity of Energetic Materials", *Propellants, Explosives, Pyrotechnics*, 30 (1): 5, 2005.
- [20] L. L. Merritt, and E. D., Schroeder, The Crystal Structure of 2,2'-Bipyridine, *Acta Cryst.*, 9: 801-804. 1956.
- [21] N. Neto, M. Muniz-Miranda, L. Angeloni, E. Castellucci, Normal mode analysis of 2,2'-bipyridine—I. Internal modes, *Spectrochimica Acta Part A: Molecular Spectroscopy*. doi:10.1016/0584-8539(83)80063-4, Volume 39, Issue 2, p. 97-106. 1983.
- [22] F. Márquez, I. López Tocón, J.C. Otero, J.I. Marcos, A priori SQM vibrational spectrum of 2,2'-bipyridine, *J. Mol. Struct.* . doi:10.1016/S0022-2860(96)09700-1. 410-411, 447–450. 1997.

- [23] L. Ould-Moussa, M. Castell-Ventura, E. Kassab, O. Poizat, D.P. Strommen, J.R. Kincaid, Ab initio and density functional study of the geometrical, electronic and vibrational properties of 2,2'-bipyridine, *J. Raman Spectrosc.* doi:10.1002/1097-4555(200005)31:5, 31, 377-390, 2000.
- [24] P. Pulay, J. Baker, K. Wolinski, SQM version 1.0, *Parallel Quantum Solutions*, 2013 Green Acres Road, Suite A, Fayetteville, 2007.
- [25] A. E. Ozel, S. Kecel, S. Akyüz., Vibrational analysis and quantum chemical calculations of 2,2'-bipyridine Zinc(II) halide complexes, *J. Mol. Struct.*, 834: 548-554, 2007.
- [26] M. Karelson, V. S. Lobanov, A.R. Katritzky Quantum-chemical descriptors in QSAR/QSPR studies. *Chemical Reviews.*;96:1027-1043, 1996.
- [27] J.W. Chen X. Xue K.W. Schramm X. Quan F. Yang A. Kettrup Quantitative structure-property relationships for octanol-air partition coefficients of polychlorinated biphenyls. *Chemosphere*, 48:535-544, 2002.

BIOGRAPHY

Berna ÇATIKKAŞ

Education:

Bachelor of Science: Department of Physics, Selçuk University, 2000

Master of Science: Department of Physics, Gazi University, 2003

Doctor of Philosophy: Department of Physics, Gazi University, 2010

Research Areas:

Vibrational Spectroscopy, Raman Spectroscopy, Infrared Spectroscopy, Molecular Modelling

Academic Experience:

Research Assistant: 2004, Department of Physics, Faculty of Art and Science, Mustafa Kemal University, Hatay, Turkey

Research Assistant: 2004-2010, Department of Physics, Faculty of Art and Science, Gazi University, Ankara, Turkey

Research Assistant: 2010, Department of Physics, Faculty of Art and Science, Mustafa Kemal University, Hatay, Turkey

Assistant Professor: 2011, Department of Physics, Faculty of Art and Science, Mustafa Kemal University, Hatay, Turkey

A New Numerical Mapping Approach for Identification Protein Coding Regions in DNA Sequences by using SVD Method

Bihter Das¹, Ibrahim Turkoglu²

Abstract

DNA sequences are symbolic signals and they must be converted to digital sequences to use these signals in Digital Signal Processing applications. This conversion case is called mapping. There are some digital mapping techniques in literature. They are classified into two categories according to the structure of the base. These categories are called Fixed Mapping and Physico Chemical Property Based Mapping. Combinations of double or triplebases, correspond to a gene in the DNA sequence and RNAs are synthesized from these genes. Each amino acid in protein synthesis is encoded by three nucleotides. These trinucleotide in the DNA are called "Code", that are encoded amino acids. If they in the RNA are called "Codon". There are 64 types of codons in the RNA.

In this paper, a new numerical mapping technique has been proposed for converting string to numerical values and this proposed technique is applied in Singular Value Decomposition method in the first time. This new technique can be briefly described follows: Each codon is mapped by improved fractional derivative of Shannon equation. The proposal novel technique has showed significant improvement in identification protein coding regions as compared with the current techniques.

Keywords: Codon, Exons, Introns, DNA sequence, Numerical Mapping, Shannon Entropy.

1 INTRODUCTION

Deoxyribonucleic acid (DNA) is a molecule that carries most of the genetic information. Each nucleotide consists of three subcomponents: a phosphate, a sugar and nucleobases-either cytosine (C), guanine (G), adenine (A), or thymine (T). The sequence as ACCTTGACAGTT is read left to right in the 5' to 3' direction. [1-6] Figure 1 illustrates the structure of the DNA molecule.

Proteins are large biomolecules, consisting of one or more long chains of amino acid residues. Each amino acid in protein synthesis is encoded by three nucleotides. These trinucleotides in the DNA are called "Code", that are encoded amino acids. If they in the RNA are called "Codon". Each code and codon consist of three bases, it corresponds to an amino acid. The code is converted to the codons during mRNA synthesis in DNA. Code and codon are complementary. There are 64 types of codons in the RNA. All of codons are assigned to an amino acid. For example the codon "CUU" represents the amino acid Lösin, and "UAU" and "UAC" represent Tirozin[7]. The START codon is AUG. This codon represents the amino acid Methionine. There isn't another codon encoding methionine. The UAA, UAG and UGA codons indicating the end of protein synthesis. They are called STOP codons.

During the production of proteins and enzymes, RNA copy sequences that corresponding to genes in DNA are extracted. During the removal of the RNA copied, the base sequence of gene is not read from the beginning to the end completely. After the reading of a part of the sequence and the extraction of RNA copies, long section is skipped before reading and it is passed to another section, it is then continued where it left off. This encoded and unreadable section of the gene is called 'intron' and the coded section of the gene is called 'exon'. Where is a protein coded? How much is encoded? Where are growth and development regulated? Where are stem cells converted to other cells? In which cases are cells replicating? The answer to all of these questions and the investigation of genetic diseases, such as cancer, are possible by DNA sequences that can be classified as the exon and intron [8].

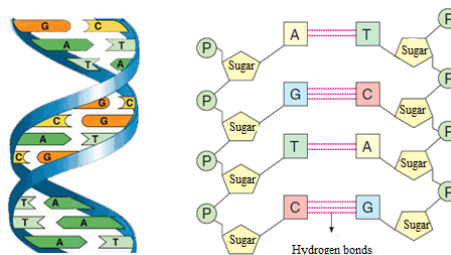


Figure 1: The structure of DNA

¹ Corresponding author: Department of Software Engineering, Technology Faculty, Firat University, Elazığ, Turkey, bihterdas@gmail.com

2 A NEW PROPOSED APPROACH FOR MAPPING TECHNIQUE

In this section a novel numerical mapping technique for DNA sequence is described. It is used a new Shannon entropy method for the first time to convert string to numerical values. The Shannon entropy is a standard measure to measure disorder of symbolic sequences such as DNA sequences. For incorporating correlations between the symbols, the entropy of n-mers (n - subsequence) has to be identified [9]. The Shannon entropy can be computed by Equation 1. [10]

$$S = -\sum_i p(x_i) \log(p(x_i)) \quad (1)$$

Where a random variable is distributed on the values (x_i) with probabilities . For a given number of possible states this function has a maximum when the probabilities of all states are equal. The applications of entropy and information theory principles proved to be useful in providing the fundamental insights on genetic sequence evolution [11]. One of the interpretations of entropy is the information content of the message. However the first interpretation is subjectively for genomic sequences where we assume that entropy reflects the degree of functionality. The functionality of a sequence means interaction specificity, thus the higher sequences variability (entropy) is, the large number of specific interactions such sequences may perform. Hence the assumption is that sequence entropy may serve as the averaged measure of functionality, aiding the localization of non-coding functional regions. Shannon entropy is inadequate or identification protein coding regions in DNA sequence. It is known that three-five percent of the DNA sequence is exon (protein coding regions and more than ninety percent of DNA is intron (non-coding regions).

The Shannon entropy is applied for entropy calculations in nucleotide sequence analysis, identify and predict binding sites the literature [12-14]. Moreover topological entropy has been implemented to conclude that entropy of exons is higher than of introns [15]. It is accepted that the entropy as a measure of information taking into account the different length of DNA sequences [16]. The large volume of genomic information is integrated by averaging the lengths and entropy quantities of different species in other study [17].

Shannon entropy is seen insufficient for numerical representation of DNA sequences in our application. Therefore it is used a new entropy method for the first time to convert string to numerical values in this paper. This method is a fractional derivative of Shannon equation that is proposed by Ali Karci [18]. When applying equation of fractional entropy to the DNA sequences as a new numerical representation technique, important some changes are required. This proposed mapping approach can be applied in many applications not only identification exon and intron regions. In this method the entropy is computed for the distributions of a codon. For one codon, the entropy reflects the balance between 64 possible states- AAA, ATT, TGC, GCC, etc. The method is defined by equation 2.

$$S = -\sum_i \left[(-p(x_i))^\alpha p(x_i) \log(p(x_i)) \right] \quad (2)$$

“ $P(x_i)$ ” is a repetition frequency of codon in the DNA sequence.

It has defined a new formula for “ α ” in equation 3.

$$\alpha = \frac{1}{\log(p(x_i))} \quad (3)$$

3 PROTEIN CODING REGIONS PREDICTION AND SINGULAR VALUE DECOMPOSITION

Singular Value Decomposition (SVD) is important issue that is used in Linear Algebra with the real and complex matrices. The SVD method is defined by equation 4 [19].

$$A_{n \times p} = U_{n \times n} S_{n \times p} V_{p \times p}^T \quad (4)$$

where $U^T U = I_{n \times n}$ $V^T V = I_{p \times p}$

U is the left singular vector, S is diagonal and V^T has the right singular vector rows. The SVD method places the original data in the coordinate plane. There is a need to find two variable. These are the eigenvalues and eigenvectors. It is represented as AAT and ATA. The eigenvector ATA variable composes the columns of V, on the other hand AAT compose the columns of U. Square roots of eigenvalues are the singular values in S. Diagonal matrix of S matrix that holds singular values. These singular values are real. If the matrix A is a real matrix, in the same way U and V are real [20-22]. In application k has been taken 3 and frame size has been 81 to detect protein coding regions DNA signal.

The implementation of exon prediction with the proposed mapping approach in SVD technique is expressed in the block diagram. It is shown in Figure 2:

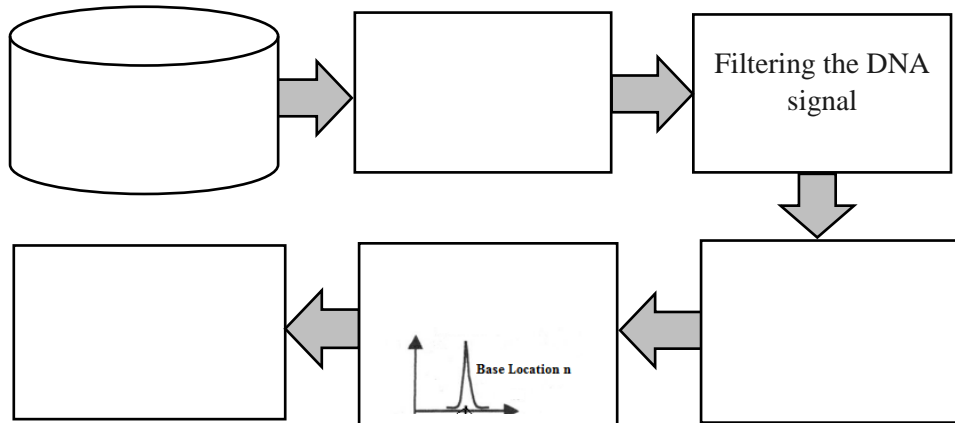


Figure 2: Exon prediction with the proposed mapping technique by using SVD

It has been used AJ229040 gene in the range of 3500 and 10500 bases. This 7000-length DNA sequence, which obtained from NCBI Database [23].

4 COMPARISON OF THE NUMERICAL MAPPING METHODS

Figure 4 shows comparison of different mapping technique for identification protein coding regions. It can be observed that our proposed mapping technique performs with high accuracy compared with the current other techniques in six exon region of specified range of DNA sequence. These objective six exon regions are 3770-3826, 4584-4601, 4671-4730, 4999-5277, 5730-5823, 6719-6898 in AJ229040 gene. For comparing efficacy of these digital mapping techniques, it has been used receiver operating characteristic (ROC) curves [24]. In the representation of the protein-coding region TPF, TNF, FPF, FNF are used.

TPF: Protein coding region is estimated correctly

FPF: Protein coding region is estimated wrongly

FNF: Non-coding region is estimated wrongly

TNF: Non-coding region is estimated correctly

For coding region points $TPF + FNF = 1$ and for non-coding region points $TNF + FPF = 1$. It has been selected 0.6 for decision threshold in graphs of Figure 4. When you look to figure 4 (f) carefully, we can see that the estimates of the true exon. The exon regions drawn with points. The proposed mapping method has guessed correctly in six regions. But when we look at other charts (Figure 4 (a), (b), (c), (d), (e)), the other mapping techniques don't found all of six exon regions. The integer technique performs the second highest accuracy after the proposed technique to detect exon regions.

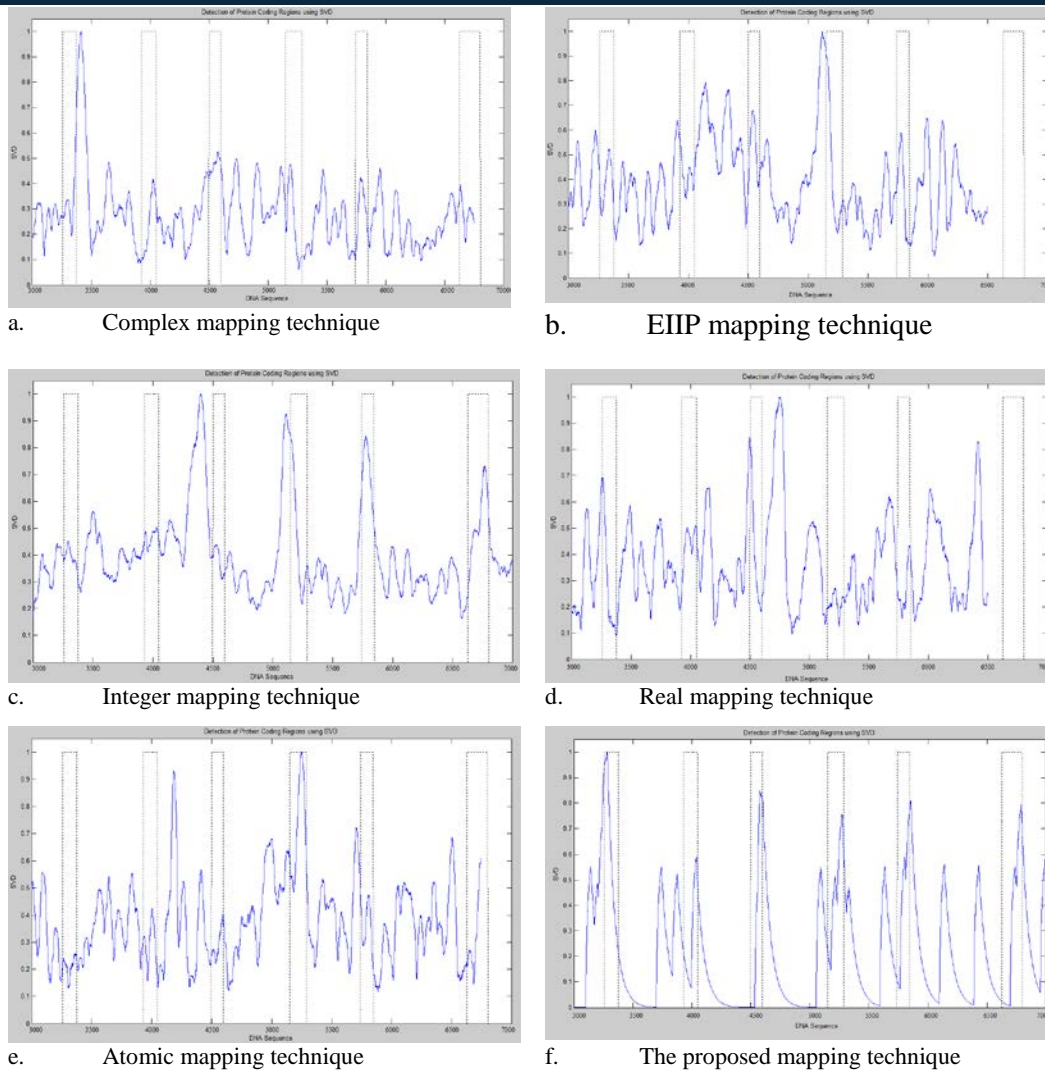


Figure 4: Comparison of different mapping technique for identification protein coding regions

5.CONCLUSION

In this paper, a novel mapping approach for identification protein coding regions(exon) is introduced. It is a numerical representation of DNA sequence that maps each codon by improved fractional derivative of Shannon equation. The proposed technique showed a significant achievement for finding six exon regions. The other techniques have not been identified six exon regions in desired range of DNA sequence. Future work will include digitizing performance for greater lengths of DNA sequences. It will be use a method from different SVD. The performance of the proposed mapping technique will be checked on the other signal processing application.

REFERENCES

- [1] Zahhad, M. A., A novel circular mapping technique for spectral classification of exons and introns in human DNA sequences. IJ. Information Technology and Computer Science. 2014.
- [2] Zahhad, M. A., Ahmed, S. M., Elrahman, S. A. A., Genomic analysis and classification of exon and intron sequences using dna numerical mapping techniques. IJ. Information Technology and Computer Science. 2012.
- [3] Wang, S. Y., Tian F. C., Liu X., Wang, J., A novel representation approach to DNA sequence and its application. IEEE Signal Processing Letters. 16(4): 275 – 278, 2009.
- [4] Zahhad, M. A., Ahmed, S. M., Elrahman, S. A. A., A new numerical mapping technique for recognition of exons and introns in DNA sequences. National Radio Science Conference. 2013.
- [5] Cosic, L, Macromolecular bioactivity: is it resonant interaction between macromolecules? Theory and applications. IEEE Transactions on Biomedical Eng. 1101-1114, 1994.
- [6] Fickett, J. W., Tung, C. S., Recognition of protein coding regions in DNA sequence. Nucleid Acids Research. 10(17): 5303-5318, 1982.
- [7] Fickett, J. W., Tung, C. S., Assessment of protein coding measures. Nucleic Acid Research. 20(24): 6441-6450, 1992.

- [8] Tugan, J., Rushdi, A., A DSP based approach for finding the codon bias in DNA sequences. *IEEE Journal on Signal Processing*. 2(3), 2008.
- [9] Schmitt, A. O., Herzel H., Estimating the entropy of DNA sequences. *Journal of Theoretical Biology*. 188(3): 369-377, 1997.
- [10] Shannon C. E., A mathematical theory of communication June 27,379-423.
- [11] Schneider T. D., Evolution of biological information. *Nucleic Acids Res*. 28(14):2794-9, 2000.
- [12] Schneider, T. D., A brief review of molecular information theory. *Nano Commun Netw*. 1(3): 173–180, 2010.
- [13] Kozarzewski, B., A method for nucleotide sequence analysis. *Computational Methods In Science And Technology*. 18(1):5-10, 2012.
- [14] Machado, J. A. T., Shannon entropy analysis of the genome code. *Mathematical Problems in Engineering*. 2012.
- [15] Koslicki, D., Topological entropy of DNA sequences. *Bioinformatics*. 27(8):1061-7, 2011.
- [16] Riyazuddin, M., "Information Analysis of DNA Sequences" A Thesis, Master of Science in The Department of Electrical and Computer Engineering By Bachelor of Engineering, Osmania University, December 2003.
- [17] Vinga, S., Almeida, J. S., Local Renyi entropic profiles of DNA sequences. *BMC Bioinformatics*. 8:393, 2007.
- [18] Karci, A., New kinds of entropy: fractional entropy. *International Conference on Natural Science and Engineering (ICNASE'16)*. March 19-20, Kilis, 2016.
- [19] Massachusetts Institute of Technology, Biological Engineering, [Online] http://web.mit.edu/be.400/www/SVD/Singular_Value_Decomposition.htm (accessed on 03-Jan-2016)
- [20] Alter, O., Brown P. O., Botstein, D., Singular value decomposition for genome-wide expression data processing and modeling. *Proc Natl Acad Sci U S A*, 97, 10101-6. 2000.
- [21] Golub, G. H., Van Loan, C. F., *Matrix Computations*, 2nd ed. (Baltimore: Johns Hopkins University Press). 1989.
- [22] Greenberg, M., *Differential equations & Linear algebra* (Upper Saddle River, N.J.: Prentice Hall). 2001.
- [23] NCBI GenBank database, online access: <http://www.ncbi.nlm.nih.gov/Genbank/> Accessed January 2016.
- [24] Akhtar, M., Ambikairajah, E., Epps, J., Detection of period-3 behavior in genomic sequences using singular value decomposition. *International Conference on Emerging Technologies*. 2005.

A New Mapping Technique for Separation of Exons and Introns by using DFT Method

Bihter Das¹, Ibrahim Turkoglu²

Abstract

Recognition exons and introns is very difficult in genomic research. The most important stage to solve this problem is map the DNA sequences into numerical values. This paper introduces a new mapping approach for converting string to numerical values. Each codon is mapped by improved fractional derivative of Shannon equation in this approach and then the approach has been used in Fourier Method for estimation position of exon in the DNA sequence for the first time. The obtained numerical DNA signal is filtered by the Antinotch filter. Exon regions are separated successfully in the filtered DNA signal according to the specified percentile threshold. Our proposed technique has been compared with the other current mapping techniques. It shows a very high classification success.

Keywords: DNA sequence, Exon, Intron, Antinotch filter, Fourier transform, Entropy, Biostatistics

1. INTRODUCTION

Digital Signal Processing (DSP) examines digital signals and processing method of these signals. The aim of DSP is usually measuring analog signals or filtering. It uses primarily uses an analog-digital converter to perform this operation. So it makes it can process signals. In Genome Analysis DNA symbolic signals cannot be used with DSP techniques. DNA sequences must be converted from symbolic to numeric. Hence some digital mapping techniques have been developed in literature to digitize DNA sequences. DNA and proteins sequences have been represented by character strings. In case of DNA sequence, the alphabet is of size 4 letters. These letters are A, G, C, T. In case of protein the alphabet is 20. [1] In a DNA gene the order of these 4 bases determines the genetic diseases and variation, the gene prediction, nature of species habits and living [2]. The structure of a gene shown in Figure 1.

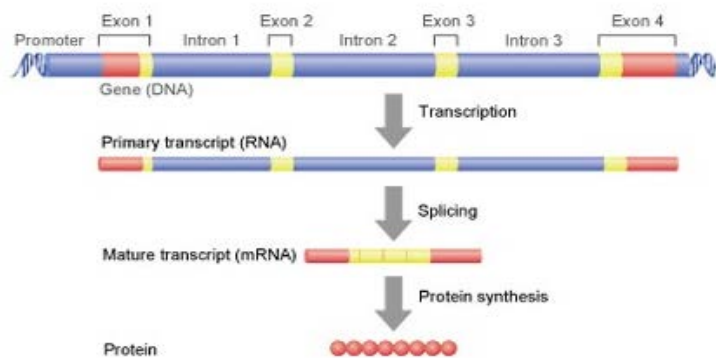


Figure 1: The structure of a gene [3]

The gene is consist of exon and intron regions. The genes are divided protein coding regions (exons) and non-coding protein regions (introns) [3]. There is the intron in the between two exons. The discovering exon and intron regions is very important in genomic applications. For this discovering DSP is more useful tool [2].

2. EXISTING MAPPING TECHNIQUES OF DNA SEQUENCE

It must be converted to digital signals to work on the DNA sequences in signal processing. The used methods in this transformation are referred as digital mapping techniques. These techniques are classified into two groups: Fixed Mapping and Physico-Chemical Property Based Mapping according to structural features of DNA.

2.1 Fixed Mapping Techniques

The most known FM techniques are Voss representation technique, Tetrahedron representation technique, Complex representation technique, Integer representation technique, Real number technique. The Voss technique maps the nucleotides A, C, T, and G into the four binary indicator sequences $X_A(n)$, $X_T(n)$, $X_G(n)$, $X_C(n)$. Each base in the DNA sequence is represented with '0' or '1' [5]. In Tetrahedron technique number of the indicator sequences is three.

¹Corresponding author: Department of Software Engineering, Technology Faculty, Firat University, Elazığ, Turkey, bihterdas@gmail.com

Four indicator sequences $X_A(n)$, $X_T(n)$, $X_G(n)$ and $X_C(n)$ are mapped to the 3 dimensional vectors [6]. Position of sequences are from the center to the vertices [7]. In the complex technique the dimensionality of the tetrahedral mapping technique is two. It is obtained complex representations of A, G, C, T bases. It is shown below complex representation of the $X(n)$ sequence. $x(n) = axA(n) + cxC(n) + txT(n) + gxG(n)$ $a = 1 + j, t = 1 - j, c = -1 - j$ and $g = -1 + j$ [8]. The Integer technique is a one dimensional mapping technique. Values of the bases are $T = 0, C = 1, A = 2, G = 3$ [9]. In the real number technique value of the bases are $A = -1.5, T = 1.5, C = 0.5, G = -0.5$ [6-11].

2.2 Physico Chemical Property Based Mapping Techniques

It was taken into account biochemical properties of DNA in this category of mapping techniques. The general PCPBM techniques are EIIP mapping technique, Single Atomic Number mapping technique, Paired Numeric mapping technique, DNA Walk mapping technique, Z-Curve Mapping technique. In the EIIP technique values of the bases are $C = 0.1340, A = 0.1260, T = 0.1335, G = 0.0806$ [6,11]. In the Single Atomic Number technique the bases are mapped by $C = 58, A = 70, G = 78, T = 66$ [6,12]. In the Paired technique, bases paired with A-T and C-G bases take +1 and -1 values. This digital conversion combine DNA structural features by reducing the complexity of the DNA [13]. In DNA Walk technique values of bases are $C = 1$ or $T = 1$ and $A = -1$ or $G = -1$ [14]. The Z-Curve technique is a three-dimensional curve [15-16].

3. THE PROPOSED APPROACH FOR MAPPING TECHNIQUE

In this section a novel numerical mapping technique for symbolic DNA sequence is described. It is used a new Shannon entropy method for the first time to convert string to numerical values. The Shannon entropy is a standard measure to measure disorder of symbolic sequences such as DNA sequences. For incorporating correlations between the symbols, the entropy of n -mers (n - subsequence) has to be identified [17]. The Shannon entropy can be computed by Equation 1. [18]

$$S = -\sum_i p(x_i) \log(p(x_i)) \quad (1)$$

Where a random variable is distributed on the values (x_i) with probabilities . For a given number of possible states this function has a maximum when the probabilities of all states are equal. The applications of entropy and information theory principles proved to be useful in providing the fundamental insights on genetic sequence evolution [19]. One of the interpretations of entropy is the information content of the message. However the first interpretation is subjectively for genomic sequences where we assume that entropy reflects the degree of functionality. The functionality of a sequence means interaction specificity, thus the higher sequences variability (entropy) is, the large number of specific interactions such sequences may perform. Hence the assumption is that sequence entropy may serve as the averaged measure of functionality, aiding the localization of non-coding functional regions. Shannon entropy is inadequate or identification protein coding regions in DNA sequence. It is known that three-five percent of the DNA sequence is exon (protein coding regions and more than ninety percent of DNA is intron (non-coding regions).

The Shannon entropy is applied for entropy calculations in nucleotide sequence analysis, identify and predict binding sites the literature [20-22]. The entropy has been implemented to conclude that entropy of exons and introns [23]. It is accepted that the entropy as a measure of information. But different length of DNA sequences may affect this measure [24]. The large volume of genomic information is integrated by averaging the lengths and entropy quantities of different species in other study [25].

Shannon entropy is seen insufficient for numerical representation of DNA sequences in our application. Therefore it is used a new entropy method for the first time to convert string to numerical values in this paper. This method is a fractional derivative of Shannon equation that is proposed by Ali Karci [26]. When applying equation of fractional entropy to the DNA sequences as a new numerical representation technique, important some changes are required. This proposed mapping approach can be applied in many applications not only identification exon and intron regions. In this method the entropy is computed for the distributions of a codon. For one codon, the entropy reflects the balance between 64 possible states- AAA, ATT, TGC, GCC, etc. The method is defined by equation 2.

$$S = -\sum_i [(-p(x_i))^\alpha p(x_i) \log(p(x_i))] \quad (2)$$

“ $P(x_i)$ ” is a repetition frequency of codon in the DNA sequence. It has defined a new formula for “ α ” in equation 3.

$$\alpha = \frac{1}{\log(p(x_i))} \quad (3)$$

3.1 Prediction of Protein Coding Regions using Discrete Fourier Transform

It has been used F56F11.4 gene the range of 7080 – 15080 bases. This 8000-length DNA sequence, which obtained from NCBI database [27]. The 8000-length DNA base sequence was taken as input data for the application. This relative positions of base sequences in the protein-coding regions are 867-1065, 2505-2915, 4038-4365, 5404-5690, 7376-7638 value intervals.

Discrete-time Fourier transform (DFT) plays an important role in DSP applications such as correlation analysis and spectrum analysis, discrete-time signal processing analysis of algorithms and system, linear filtering. The signals are evaluated for a limited number of points. In this paper DFT is used to extract the period-3 value of DNA sequences. The reason of the period-3 value is that the amino acid codon is producing 3 bases length. DFT is identical with evenly spaced frequency examples of Fourier transformation [28-38].

The calculation of a DFT -n points [34] is shown in equation 4.

$$X[k] = \frac{1}{\sqrt{N}} \sum_{n=1}^N x[n] W_N^{(k-1)(n-1)} \quad 1 \leq k \leq N \quad W_N = e^{-\frac{j2\pi}{N}} \quad (4)$$

x [n] is an DNA sequence that has been converted into a digital format.

N is the length of DNA sequence (The total number of the bases)

It is used the rectangular window length of L bases

$$X_T[k] = \frac{1}{N_w} \sum_{m=1}^{N_w} X_m[k] \quad (5)$$

$X_m[k]$ is each of the windowed sequences in equation 5.

$X_T[k]$ is the normalized sum

N_w is the number of shifted windows.

The power spectrum of the sequence is calculated with equation 6.

$$S[k] = |X_T[k]|^2 \quad (6)$$

P_3 is the 3-period spectral component is shown in equation 7.

$$P_3 = S[N/3+1] \quad (7)$$

3.2 The Used Filtering Approach

The Fourier-based spectral estimation methods were used determining the protein-coding regions (exons) in this paper. Exons 3-periods behavior were removed by filtering DNA sequences. Antinotch filter has been used by filtering approach. Antinotch filter magnitude response is composed from sharp hill. It is $2\pi/3$. If binary indicator sequences ($U_A(n)$, $U_T(n)$, $U_C(n)$, $U_G(n)$) are given as input to anti notch filter, outputs are $y_A(n)$, $y_T(n)$, $y_C(n)$, $y_G(n)$ corresponding to them in the protein coding region. The passband value of this filter is $2\pi/3$. The formula used in the calculation feature is shown in equation 8.

$$Y(n) = \sum_{i \in F} |y_i(n)|^2 \quad F = \{A, T, C, G\} \quad (8)$$

The hills show exons and weak outputs shows non-coding regions (introns) in Y(n) graph. It has been utilized from this feature to determine protein coding regions (exon) [39]. The IRR antinotch filter which is recommended by Yoon and Vaidyanathan is narrow band pass filter Vaidyanathan and recommended by Yoon and used to determine the exons antinotch IR filter is narrow band pass filter [40-41]. The antinotch filter is shown in equation 9.

$$H(z) = \frac{1}{2} \frac{(1-R^2)(1-z^{-2})}{(1-2R\cos\theta z^{-1}+R^2z^{-2})} \quad (9)$$

3.3 Application Results

It is difficult to determine the exons in genomic applications because of 3-period basis (codon) of exon. In this exon detection application it has been estimated exons in which the base position using Fourier transform based filtering approach [37-38]. Firstly the symbolic DNA signal was transformed to digital signal with the proposed mapping technique. Then the estimated position has been compared with the actual position of exon in DNA sequence from the gene bank and accuracy rates were determined. Figure 2 shows power spectrums which express the position of exon in the result of application. The threshold value that is 99th percentile of filtered sequence of Y. The base positions in the range 2505-2915, 4038-4365, 5404-5690, 7376-7638 has exceeded the threshold energy 0.0275 according to Figure 2. But base position in the range 867-1065 is weak.

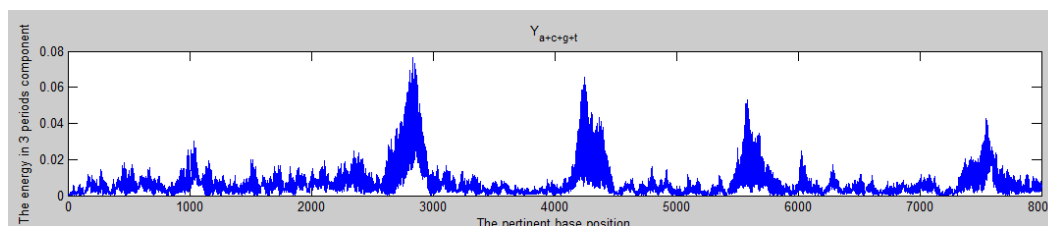


Figure 2: The exons that expressing power spectrum according to the base position

It was compared exon position that is received DNA sequences from in the gene bank with the exon positions that is found by the method in Table 1. It has been extracted the accuracy of the method each exon position and the average success of the method at each position is approximately 96 %.

Table 15: The comparison the exon position in gene bank with the exon position in the method

Base position in Gene Bank(NCBI)	Fourier Based Antinotch Filter Approach	Protein Coding Regions Accuracy Rate (%)
867-1065 (198 bp)	867-1065 (164)	82,85
2505-2915 (410 bp)	2505-2915 (410)	100
4038-4365 (328 bp)	4038-4365 (328)	100
5404-5690 (287 bp)	5404-5690 (287)	100
7376-7638 (262 bp)	7376-7638 (256)	97,72

It has been compared the proposed mapping technique with the exiting techniques according to accuracy rate in table 2.

Table 2: The comparison of existing mapping techniques

Mapping Technique	Threshold Value	Protein Coding Regions Accuracy Rate (%)
Integer Technique	0.0463	86,125
EIIP Technique	0.000142	77,53
DNA Walk Technique	0.0305	90,82
Paired Numeric Technique	0.0290	87,79
The Proposed Technique	0.0275	96,114

CONCLUSION

The main purpose of genetic research is to determine specific functions that are encoded by genes and understand the information carries these genes. Genes are located as the exon and intron DNA sequences. In this paper the symbolic DNA sequence has been converted to digital DNA sequence with the proposed new mapping technique. Then it been used in Fourier- based filtering approach firstly for finding exon regions in DNA sequences. According to this approach it has been estimated positions of exon in 8000 length DNA sequence and it has been compared with the actual position. It was observed this method which is used to predict the position of the exon is effective and successful. It shows that the proposed mapping technique is more convenient in DFT application. The proposed technique gave accurate results in finding exon regions. The average success of DFT methods using the proposed mapping technique is 96%.

REFERENCES

- [1] Zahhad, M. A., Ahmed, S. M., Elrahman, S. A. A., Genomic analysis and classification of exon and intron sequences using DNA numerical mapping techniques. *I.J. Information Technology and Computer Science*. 2012.
- [2] Zahhad, M. A., Ahmed, S. M., Elrahman, S. A. A., A new numerical mapping technique for recognition of exons and introns in DNA sequences. *National Radio Science Conference*. 2013.
- [3] <http://schoolworkhelper.net/dna-mrna-introns-and-exons/>
- [4] Kwan, H. K., Arniker, S. B., Numerical representation of DNA sequences. *IEEE Inter. Conf. on Electro/Information Technology, EIT '09, Windsor*, 307-310, 2009.
- [5] Voss, R. F., Evolution of long-range fractal correlations and 1/f noise in DNA base sequences. *Physical Review Letters*, 68(25):3805–3808, 1992.
- [6] Zahhad, M., A., Ahmed, S., M., Abd-Elrahman S., A., Integrated Model of DNA Sequence Numerical Representation and Artificial Neural Network for Human Donor and Acceptor Sites Prediction, *International Journal of Information Technology and Computer Science(IJITCS)*, Vol. 6, No. 8, July 2014.
- [7] Silverman, B. D., Linker, R., A measure of DNA periodicity [J]. *Theor. Biol.* 118:295-300, 1986.
- [8] Cristea, P. D., Conversion of nucleotides sequences into genomic signals [J]. *J. Cell. Mol. Med.* 6:279-303, 2002.
- [9] Cristea, P. D., Genetic signal representation and analysis. *SPIE Inf. Conf. Biomedical Optics*. 77–84, 2002.
- [10] Chakravarthy, N., Spanias, A., Lasemidis, L. D. Tsakalis, K., Autoregressive modeling and feature analysis of DNA sequences. *EURASIP Journal of Genomic Signal Processing*. 1: 13-28, 2004.
- [11] Zahhad, M. A., Ahmed, S. M., Elrahman, S. A. A., A new numerical mapping technique for recognition of exons and introns in DNA sequences. *National Radio Science Conference*. 2013.
- [12] Holden, T., Subramaniam, R., Sullivan, R., Cheng, E., Sneider, C., Tremberger, G., Flamholz, J. A., Leiberman, D. H., Cheung, T. D., ATCG nucleotide fluctuation of deinococcus radiodurans radiation genes. In *Proc. of Society of Photo-Optical Instrumentation Engineers (SPIE)*, 2007.
- [13] Buldyrev, S. V., Goilberger, A. L., Havlin, S., Mantegna, R. N., Masta, M. E., Peng, C. K., Simons, M., Stanley, H. E., Long-range correlation properties of coding and noncoding DNA sequences: GenBank analysis. *Phy. Rev. E*, 51(5): 5084-5091, 1995.
- [14] Peng, C.-K., Buldyrev, S.V., Goldberger, A.L., Havlin, S., Sciortino, F., Simons, M., Stanley, H. E., Goldberger, A.L., Havlin, S., Peng, C. K., Stanley, H. E., Viswanathan, G. M., Analysis of DNA sequences using methods of statistical physics. *Physica A, Elsevier Science B.V.* 249: 430-438, 1998.
- [15] Zhang, R., Zhang, C. T., Z curves: an intuitive tool, for visualizing and analyzing the DNA sequences [J]. *J. BioMol. Struct. Dyn.* 11: 767-782, 1994.
- [16] Zhang, R., Zhang, C. T., Identification of replication origins in archaeal genomes based on the Z-curve method. 2005 Heron Publishing-Victoria, Canada, *Archaea*. 2004.
- [17] Schmitt, A. O., Herzel H., Estimating the entropy of DNA sequences. *Journal of Theoretical Biology*. 188(3): 369-377, 1997.
- [18] Shannon C. E., A mathematical theory of communication June 27,379-423.
- [19] Schneider T. D., Evolution of biological information. *Nucleic Acids Res.* 28(14):2794-9, 2000.
- [20] Schneider, T. D., A brief review of molecular information theory. *Nano Commun Netw.* 1(3): 173–180, 2010.
- [21] Kozarzewski, B., A method for nucleotide sequence analysis. *Computational Methods in Science and Technology*. 18(1):5-10, 2012.
- [22] Machado, J. A. T., Shannon entropy analysis of the genome code. *Mathematical Problems in Engineering*. 2012.
- [23] Koslicki, D., Topological entropy of DNA sequences. *Bioinformatics*. 27(8):1061-7, 2011.
- [24] Riyazuddin, M., "Information Analysis of DNA Sequences" A Thesis, Master of Science in The Department of Electrical and Computer Engineering By Bachelor of Engineering, Osmania University, December 2003.
- [25] Vinga, S., Almeida, J. S., Local Renyi entropic profiles of DNA sequences. *BMC Bioinformatics*. 8:393, 2007.
- [26] Karci, A., New kinds of entropy: fractional entropy. *International Conference on Natural Science and Engineering (ICNASE'16)*. March 19-20, Kilis, 2016.
- [27] NCBI GenBank database, online access: <http://www.ncbi.nlm.nih.gov/Genbank/> Accessed January 2016.
- [28] Kotlar, D., Levner, Y., Gene prediction by spectral rotation measure: A new method for identifying protein-coding regions. *Genome Res.* 13, 1930–1937, 2003.
- [29] Ramachandran, P., Lu, W.-S., Antoniou, A., Location of exons in DNA sequences using digital filters. *Proceedings of IEEE ISCAS*, pp. 2337–2340, 2009.

- [30] Akhtar, M., Epps, J., Ambikairajah, E., Time and frequency domain methods for gene and exon prediction in eukaryotes. In Proc. IEEE ICASSP, pp. 573–576, 2007.
- [31] Kwan, H. K., Arniker, S. B., Numerical representation of DNA sequences. IEEE Inter. Conf. on Electro/Information Technology, EIT '09, Windsor, 307-310, 2009.
- [32] Cristea, P. D., Representation and analysis of DNA sequences. In Genomic signal processing and statistics: EURASIP Book Series in Signal Processing and Communications, (Eds) Edward R. Dougherty et al Hindawi Pub. Corp, 2:15-66, 2005.
- [33] Kwan, J. Y. Y., Kwan, B. Y. M., Kwan, H. K., Novel methodologies for spectral classification of exon and intron sequences. [J]. EURASIP Journal on Advances in Signal Processing, 2012.
- [34] Kwan, J. Y. Y., Kwan, B. Y. M., Kwan, H. K., Spectral analysis of numerical exon and intron sequences , Proceedings of IEEE Inter. Conf. on Bioinformatics and Biomedicine Workshops, Hong Kong, 876-877, 2010.
- [35] Law, N. F., Cheng, K., Siu, W., on relationship of Z-curve and Fourier approaches for DNA coding sequence classification, Bioinformation, 242-246, 2006.
- [36] Akhtar, M., Epps J., Ambikairajah, E., On DNA numerical representations for period-3 based exon prediction, IEEE Workshop on Genomic Signal Processing and Statistics (GENSIPS), Tuusula, 1-4, June 2007.
- [37] Mena-Chalco, J. , Carrer, H., Zana, Y., Cesar, R. M. Identification of protein coding regions using the modified Gabor-wavelet transform, IEEE/ACM Trans. Comput. Biol. Bioinform. 5 (2008) 198–207
- [38] Kotlar, D., Levner, Y. Gene prediction by spectral rotation measure: A new method for identifying protein-coding regions, Genome Res. 13 (2003) 1930–1937.
- [39] Türkoğlu, İ., Das, B., DNA Dizilimlerindeki Protein Kod Bölgelerinin Tanımlanması İçin Fourier Tabanlı Filtreleme Yaklaşımı, Sinyal İşleme ve İletişim Uygulamaları (SİU) Kurultayı-2015.
- [40] Vaidyanathan, P. P. ve Yoon, B.-J. The role of signal-processing concepts in genomics and proteomics, J. Franklin Inst. 341, Special Issue on Genomics, 111–135, 2004.
- [41] Vaidyanathan, P.P. ve Yoon, B.-J. Gene and exon prediction using allpass-based filters, in: Workshop on Genomic Signal Process. Stat., Raleigh, NC, 2002.

Trend Analysis in Resources of Water Intended for Human Consumption in Balıkesir

Elif Ozmetin¹¹, Cengiz Ozmetin¹, Yilmaz Yilirim², Elif Tekin¹

Abstract

While demands of water resources for different usage purposes have been increased, world public have been started to be sensitive for water related problems, one of the main element. The aim of the management of water resources are to determine the amount and quality of the surface and ground water reservoir in currently or in the future; to evaluate the possibilities of the supply; to determine water demand of the public; to plan water resources; to regulate water consumptions; to balance water resources and to develop long term strategy for rational usage of the water resources. The water for human consumption and irrigation for agricultural activities in the City of Balıkesir have been supplied from İkizcetepeler dam. Sustainable usage of the water resources in the dam is gaining more attention due to increase of urban and agricultural water utilization. In order to put out a long term water policy, domestic, agricultural and other water usage demands should be evaluated in respect to possible future developments. The aim of this study is to whether water reservoir of the İkizcetepeler dam is to supply water for human consumption or not in the City of Balıkesir, in future. Therefore, the volumes of the dam, precipitation, inflow and outflow have been investigated in trend analysis of Seasonal Kendall Method between 2010-2014. In trend analysis, while a decrease have been found in volume of the dam (reservoir) and precipitation, an increase or a decrease have been not found in inflow and outflow. An increase in draught conditions has been observed from beginning of the 2013. According to trend analysis in respect to the last five year data, water reservoir in the İkizcetepeler dam have enough water for drinking, agricultural and industrial activities except abnormal increase in these sectors.

Keywords: *Trend Analysis, Seasonal Kendall Method, Water Management*

1. INTRODUCTION

As in the world, demands for water also increased steadily in Turkey, the earth has a limited amount of water resources and water resources show an irregular distribution. The increase in water use has remained at high levels than the general population growth. While the world population in the 1990-1995 periods has been doubled, at the same period the water usage has been increased in six-fold. In addition to population growth, the progress in living standards has led to the increase of the demand for water [1].

As the needs to drinking waters, irrigation waters and energy have increased day by day, the number of storage facilities increases in parallel to these needs. Therefore the use of water in dams as programmed and planned has gained importance due to limited water sources. The programmed usage of water sources is possible with true application of operation hydrology to water source and possible with share of water with partner after storage of water in dams at maximum level [2].

65% of Turkey water need is supplied from falls in first four months of the year. These falls originates from melting snows. The waters flowing from high mountains enable to construction of dams. Accurate and reliable estimates of the flow from snowmelt is important for economical operation of the dams, and for protection of water beds in the regions from flood [2,3]. In Turkey, in respect to usage of water resources, the total amount of water originating from surface and underground is 110 billion m³ per year. Of this amount, it is accepted that approximately 95 billion m³ water comes from inlands of Turkey, 3 billion m³ water from outside of Turkey by rivers and 12 billion m³ of water from underground resources [4].

In this study, water budget of Balıkesir-İkizcetepeler dam, the increase in the volume of the lake due to decrease in the coming years and the results were trying to achieve. It is predicted that in coming years whether the volume of water that is sufficient for the population of Balıkesir. Further development and sustainable use of water resources in the lake is important due to increase in water demand for industrial, urban and agricultural activities. Different sectors of water supply, for the evaluation of sustainable development and the long-term effects of water policy in the basin, domestic, industrial, agricultural and environmental water needs should be evaluated for current and possible future trends. Analyzing the Lake according to the socio- economic factors, in respect to the continuation of the current situation, the current situation of the river system and its future performance have been evaluated using trend analysis

¹Balıkesir University, Department of Environmental Engineering, 10145, Balıkesir, Turkey.
eozyetin@balikesir.edu.tr

²Bülent Ecevit University, Department of Environmental Engineering, 67100, Zonguldak, Turkey

of annual water budget simulation model depending on the available amount of water [4]. In determining the trend of any series and there are a lot of test to quantify. The first step in the analysis of data sets will usually draw the graph of data as a function of time or place. Graphical representation of data is not sufficient to comply with terms of making the general trend or cycle. The methods used in the detection of trends and analysis are summarized in Table 1. Although having the advantages and disadvantages of each technique, appropriate methods should be used according to available data types and quantities [5].

Table 1: The methods used in Trend Analysis [5]

Graphical Methods	It just shows that whether the trend exists. It does not result in quantity
Linear Regrasyon	Slope the forecasting, it gives the confidence interval and define the degree of matching. Multiple used in arguments. It is not used with missing data. It is highly affected from cyclical and data which is out of the data set.
Mann-Kendall	For existing slope, it could be detected by yes / no test. It is a non-parametric test. It allows the data with missing values and is not affected by external data sets.
Sen Method	It estimates the value of the slope and confidence intervals. It allows missing data

a. Mann-Kendall Analysis

Using statistical test trends "it is not a trend in the observed value" by checking the hypothesis "accept " or "reject" decision is given. The decision depends on the level of significance in the chosen hypothesis. Mann-Kendall trend analysis is a useful method that can tolerate the presence of missing data and does not search for the obligation to comply with a certain distribution of the data [6].

X_i as observed values by time,

$$S = \sum_{k=1}^{n-1} \sum_{j=k+1}^n \text{Sgn}(X_j - X_k) \quad (1)$$

Here, X_j and X_k are values following one another. n is the data set length.

$$\begin{aligned} \text{Sgn}(X_j - X_k) &= +1; \text{ if } (X_j - X_k) > 0 \\ \text{Sgn}(X_j - X_k) &= 0; \text{ if } (X_j - X_k) = 0 \\ \text{Sgn}(X_j - X_k) &= -1; \text{ if } (X_j - X_k) < 0 \end{aligned} \quad (2 \text{ and } 3)$$

$$\text{Var}(S) = n(n-1) * (2n+5) / 18; \quad (\text{variance of test statistics})$$

If the data contain similar values, $\sum t(t-1) * (2t+5) / 18$ is subtracted from its numerator. Wherein, t represent similar x numbers in the any link and $\sum t$ shows the sum for all link. Therefore, standard normal z variable can be calculated by the following equation and compared with the critical z value [6].

$$\begin{aligned} z &= (S - 1) / [\sqrt{\text{Var}(S)}]; \text{ if } S > 0 \\ z &= 0; \quad \text{ if } S = 0 \\ z &= (S + 1) / [\sqrt{\text{Var}(S)}]; \text{ if } S < 0 \end{aligned} \quad (4)$$

Two -sided test is applied at the level of significance using alpha for a selected z . Based on the H_0 hypothesis, accepting ($k \neq j$) for all ($k, j \leq n$) in the series, distribution of X_j and X_k value is independent from time and similar

distributed random variables. Based on the H1 hypothesis, accepting ($k \neq j$) for all ($k, j \leq n$) in the series, distribution of X_j and X_k value is not similar, so there are linear trend in the series. If $|z| \geq z_{\alpha/2}$, the H0 hypothesis is not accepted. If the calculated value of S is positive, it is an increasing trend; otherwise decreasing trends [6].

b. İkizcetepeler Dam

İkizcetepeler dam was built on the Kille stream aiming for irrigation and flood prevention between 1986-1991 years. Being earth-filled type dam, its body volume is 1.115 million m³, the height from the stream bed is 52,00 m, the volume of lake is 164.56 hm³ and the lake area is 9.60 km². While dam services irrigation for 1,700 hectares area, it also provide drinking water as 72 hm³ per year. The dam coordinates is 39°27'53"N 27°56'29"E its view is given in Figure 1 and 2. The data used in this study have been obtained from DSI and Meteorology agencies in the region [4].



Figure 1: The location of the dam in the Balkesir



Figure 2: Aerial view of the dam

2. TREND ANALYSIS

Trend analysis is done by examining the trends over time using the items contained in the table. While trend analysis is made, trends are examined in the years following the base year in respect the items contained in the table [4].

The most important point in the trend analysis is selection of the base year. The year to be selected as the base year could not be very successful or very unsuccessful year, it could be normal and a typical year. This is because, when base year as the resort's very successful period selected, as may be agreed to erroneous conclusions about the developments in the following years, if the base year selected in a period of disastrous, it may be wrong case that the dam had a very successful period in the following year. The base year should not be included any critical period. After determining the base year, the table of items for base year is accepted to be 100 such as an index. After this, table of items is multiplied by 100 for the years follow the base year. Thus, the trend of the facility for a long term changes may be examined [4].

2.1 Trend Analysis Results

Seasonal Kendall Method was used in trend analysis. In this method, using mean values of consecutive five year data for precipitation, inflow and total water consumption with volume of the dam, obtained results was given in Figure 3-6. Using these data, the trend analysis were performed employing Seasonal Kendall Method and the results were presented in Table 2-5. The data used in the trend analysis is data obtained between 01.01.2010 and 31.12.2014. Data for volume and height were obtained from DSI. Data for Precipitation and evaporation were obtained from MET. Data are recorded in this government agencies in daily, but monthly and yearly average data were used in this study [4].

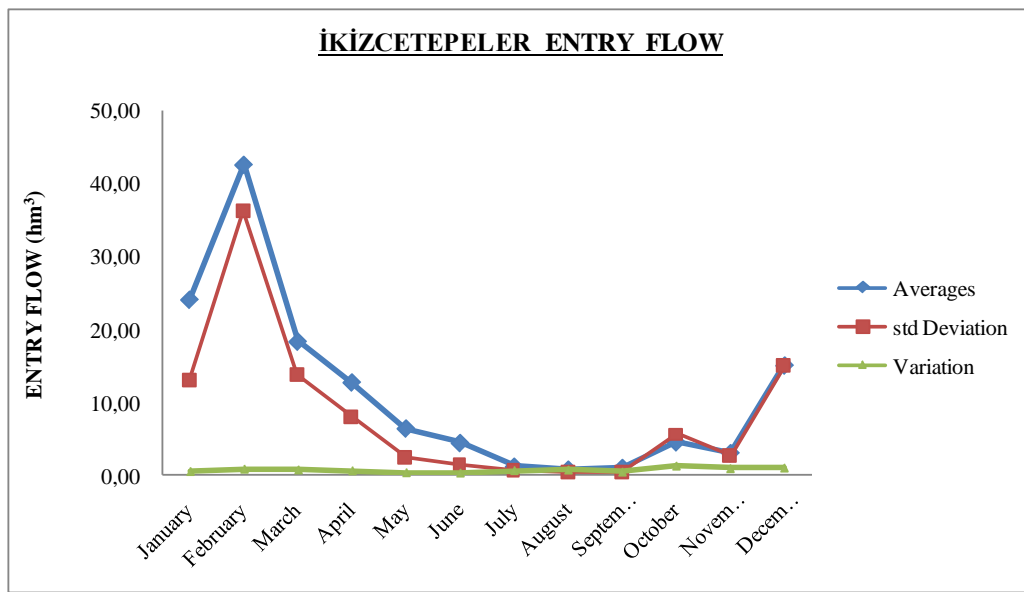


Figure 3: The entry flow to İkizcetepeler dam

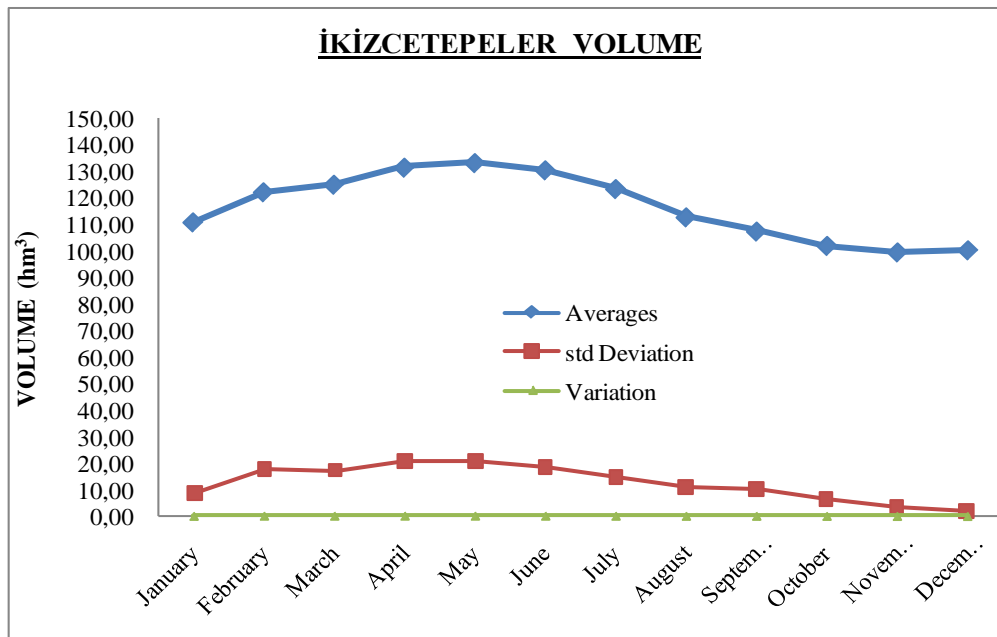


Figure 4: The volume of İkizcetepeler Dam based on months

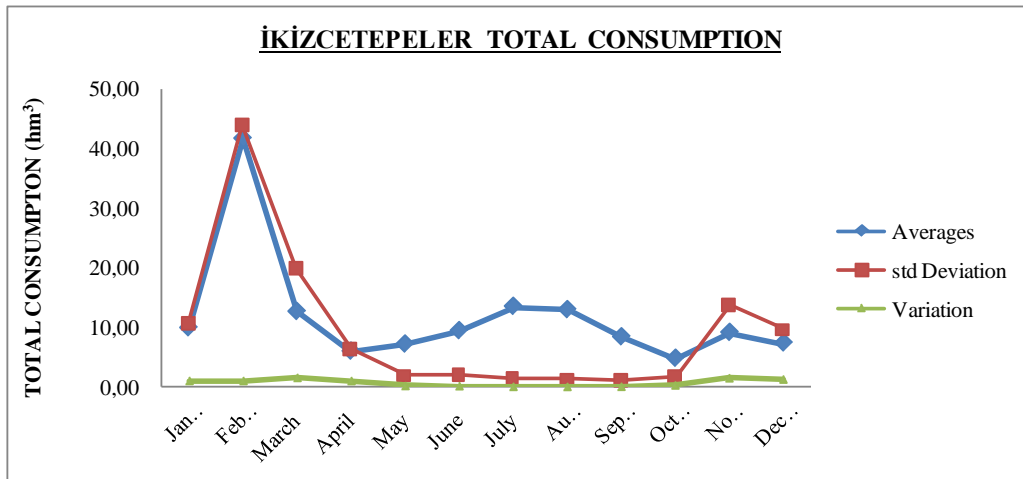


Figure 5: The total water consumption from İközçetepeleler Dam based on months

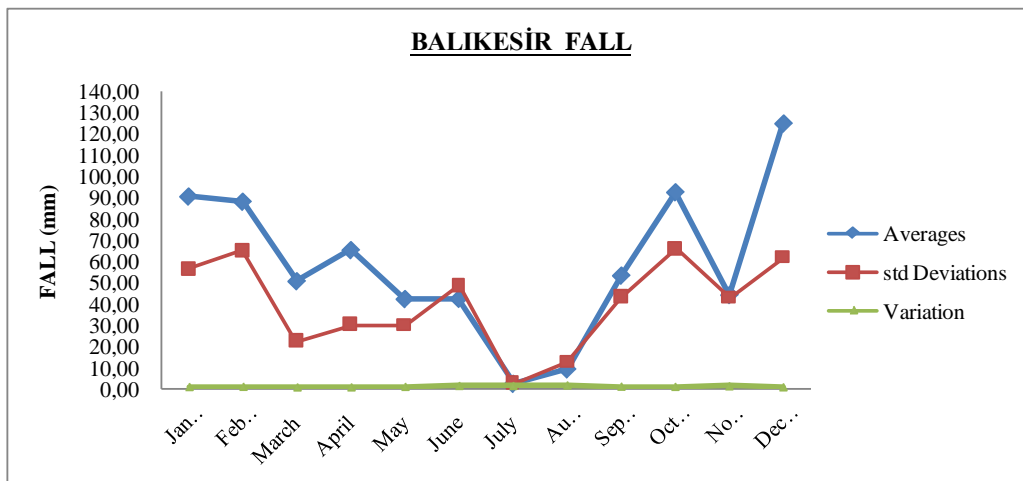


Figure 6: The total fall in Balıkesir based on months

Table 2: Kendall analysis of entry flow

		Seasonal Kendall				
		VAR(S')	S'	Zr	Interpretation	
12 Month	Total Period	200,000	-28,000	-1,909	NO TREND	-
	Winter	50,000	-14,000	-1,838	NO TREND	-
3 Month	Spring	50,000	2,000	0,141	NO TREND	-
	Summer	50,000	-8,000	-0,990	NO TREND	-
	Autumn	50,000	-8,000	-0,990	NO TREND	-

Table 3: Kendall analysis of total volume change

		<i>Seasonal Kendall</i>				
		VAR(S')	S'	Zr	Interpretation	
3 Month	Total Period	200,000	-38,000	-2,616	TREND YES	DECREASING TREND
	Winter	50,000	-10,000	-1,273	NO TREND	-
	Spring	50,000	-6,000	-0,707	NO TREND	-
	Summer	50,000	-16,000	-2,121	TREND YES	DECREASING TREND
	Autumn	50,000	-6,000	-0,707	NO TREND	-

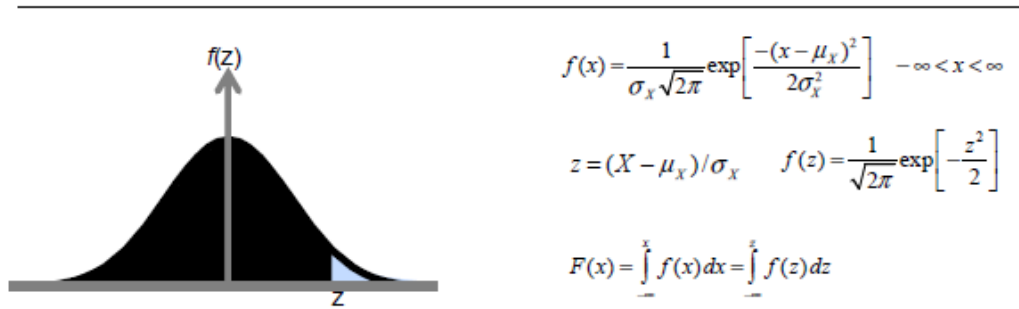
Table 4: Kendall analysis of total consumption

		<i>Seasonal Kendall</i>				
		VAR(S')	S'	Zr	Interpretation	
3 Month	Total Period	200,000	2,000	0,071	NO TREND	-
	Winter	50,000	-10,000	-1,273	NO TREND	-
	Spring	50,000	6,000	0,707	NO TREND	-
	Summer	50,000	10,000	1,273	NO TREND	-
	Autumn	50,000	-4,000	-0,424	NO TREND	-

Table 5: Kendall analysis of fall

		<i>Seasonal Kendall</i>				
		VAR(S')	S'	Zr	Interpretation	
3 Month	Total Period	200,000	-38,000	-2,616	TREND YES	DECREASING TREND
	Winter	50,000	-10,000	-1,273	NO TREND	-
	Spring	50,000	-6,000	-0,707	NO TREND	-
	Summer	50,000	-16,000	-2,121	TREND YES	DECREASING TREND
	Autumn	50,000	-6,000	-0,707	NO TREND	-

Table 6: Unexceeding probability table in standart normal distribution



z	0.00	0.01	0.02	0.03	0.04	0.05	0.06	0.07	0.08	0.09
0.0	0.5000	0.5040	0.5080	0.5120	0.5160	0.5199	0.5239	0.5279	0.5319	0.5359
0.1	0.5398	0.5438	0.5478	0.5517	0.5557	0.5596	0.5636	0.5675	0.5714	0.5753
0.2	0.5793	0.5832	0.5871	0.5910	0.5948	0.5987	0.6026	0.6064	0.6103	0.6141
0.3	0.6179	0.6217	0.6255	0.6293	0.6331	0.6368	0.6406	0.6443	0.6480	0.6517
0.4	0.6554	0.6591	0.6628	0.6664	0.6700	0.6736	0.6772	0.6808	0.6844	0.6879
0.5	0.6915	0.6950	0.6985	0.7019	0.7054	0.7088	0.7123	0.7157	0.7190	0.7224
0.6	0.7257	0.7291	0.7324	0.7357	0.7389	0.7422	0.7454	0.7486	0.7517	0.7549
0.7	0.7580	0.7611	0.7642	0.7673	0.7704	0.7734	0.7764	0.7794	0.7823	0.7852
0.8	0.7881	0.7910	0.7939	0.7967	0.7995	0.8023	0.8051	0.8078	0.8106	0.8133
0.9	0.8159	0.8186	0.8212	0.8238	0.8264	0.8289	0.8315	0.8340	0.8365	0.8389
1.0	0.8413	0.8438	0.8461	0.8485	0.8508	0.8531	0.8554	0.8577	0.8599	0.8621
1.1	0.8643	0.8665	0.8686	0.8708	0.8729	0.8749	0.8770	0.8790	0.8810	0.8830
1.2	0.8849	0.8869	0.8888	0.8907	0.8925	0.8944	0.8962	0.8980	0.8997	0.9015
1.3	0.9032	0.9049	0.9066	0.9082	0.9099	0.9115	0.9131	0.9147	0.9162	0.9177
1.4	0.9192	0.9207	0.9222	0.9236	0.9251	0.9265	0.9279	0.9292	0.9306	0.9319
1.5	0.9332	0.9345	0.9357	0.9370	0.9382	0.9394	0.9406	0.9418	0.9429	0.9441
1.6	0.9452	0.9463	0.9474	0.9484	0.9495	0.9505	0.9515	0.9525	0.9535	0.9545
1.7	0.9554	0.9564	0.9573	0.9582	0.9591	0.9599	0.9608	0.9616	0.9625	0.9633
1.8	0.9641	0.9649	0.9656	0.9664	0.9671	0.9678	0.9686	0.9693	0.9699	0.9706
1.9	0.9713	0.9719	0.9726	0.9732	0.9738	0.9744	0.9750	0.9756	0.9761	0.9767
2.0	0.9772	0.9778	0.9783	0.9788	0.9793	0.9798	0.9803	0.9808	0.9812	0.9817
2.1	0.9821	0.9826	0.9830	0.9834	0.9838	0.9842	0.9846	0.9850	0.9854	0.9857
2.2	0.9861	0.9864	0.9868	0.9871	0.9875	0.9878	0.9881	0.9884	0.9887	0.9890
2.3	0.9893	0.9896	0.9898	0.9901	0.9904	0.9906	0.9909	0.9911	0.9913	0.9916
2.4	0.9918	0.9920	0.9922	0.9925	0.9927	0.9929	0.9931	0.9932	0.9934	0.9936
2.5	0.9938	0.9940	0.9941	0.9943	0.9945	0.9946	0.9948	0.9949	0.9951	0.9952
2.6	0.9953	0.9955	0.9956	0.9957	0.9959	0.9960	0.9961	0.9962	0.9963	0.9964
2.7	0.9965	0.9966	0.9967	0.9968	0.9969	0.9970	0.9971	0.9972	0.9973	0.9974
2.8	0.9974	0.9975	0.9976	0.9977	0.9977	0.9978	0.9979	0.9979	0.9980	0.9981
2.9	0.9981	0.9982	0.9982	0.9983	0.9984	0.9984	0.9985	0.9985	0.9986	0.9986
3.0	0.9987	0.9987	0.9987	0.9988	0.9988	0.9989	0.9989	0.9989	0.9990	0.9990

3. CONCLUSION

- According to results of the trend analysis, a decreasing trend have been obtained in the volume of the dame for the summer periods.
- Most of the precipitation and current range was determined to be homogeneous according to five year data for inflow and precipitation. Randomization was found to be deteriorated in current series as a result of strong downward trend depending on decrease occurred in the number of departure.

- In results of the trends analysis, it was found that most of the seasonal current series show decreasing trends and especially from the beginning of 2013, it was started to increase strongly in draught conditions. Most of the decreasing trends in seasonal inflow is statistically significant. Precipitation in Akhisar region, except dominant but statistically insignificant decrease in winter season, there was no obvious or significant trend in all seasons.
- According to trend analysis in respect to the consecutive five year data, it was evaluated that the water reservoir in the İkizcetepeler dam have sufficient amount of water when assessing reservoir for irrigation, drinking and potable water except abnormal increase in population, agricultural and industrial activities.

REFERENCES

- [1] Akyürek, M. "Turkey Annual Flow Trend Analysis," MSc. thesis, Institute of Science, Istanbul, Turkey, 2003
- [2] F. Malkoç, M. Arslan, M. Diren ve A. H. Sargin, "The Investigation of Probable Effects of Climate Change on Çatalan Dam Flows," III. Turkey Climate Change Congress, June, 2013.
- [3] F. Malkoç, B. Bektaşoğlu, E. Eminoğlu, "The Estimation of Fall to be Flowing from Snowmelts in Bahçecik Dam Fall Region by Snowmelt Runoff Model (SRM), III. National Dam Security Semposium, October, Eskişehir, 2012.
- [4] C. Özmetin, E. Özmetin, O. Avcı, O. Alkan, M. Can, E. Beşelma, "Water Work of İkizcetepeler Dam", Graduation Complete Report, 2015.
- [5] H. Bulut, B. Yeşilata, M. I. Yeşilnacar, "The Determination of Effect of Atatürk Dam Lake on Local Climate by Trend Analysis" GAP V. Engineering Congress, April, 2006.
- [6] E. Şen, N. Başaran, Trend Analysis of Temperature and Fall Row of Konya Closed River Basin" 5th World Water Forum Konya Closed River Basin Groundwater and Drought Conference, İstanbul 2009.

The Effects of Particle Size (Fine) on Flotation: A Short Overview

Cengiz Karagüzel¹, Oktay Sahbaz²

Abstract

Flotation is a physicochemical process which is used for separation of hydrophobic materials from hydrophilic ones. This method is often used in mineral processing for the selective separation of minerals, it is also used in waste water treatment and recycling processes. In the flotation of minerals, hydrophobic particles forms bubble-particle aggregates because of micro-events (collision, attachment and detachment). The aggregates are floated to the top of flotation cell while the hydrophilic particles, which are not attached to bubbles, are taken from bottom of the flotation cells. For the high flotation recovery, particle should be attached to bubble and stay stable or non-detach during flotation process. The most important parameter affects the stability of particle-bubble aggregate is particle size. It is known that the highest recovery has been obtained in the commercial flotation devices with particles size between 250 and 38 micrometer. The recovery diminishes for the coarser and finer particle feeding in the flotation due to the high turbulence and low collision of bubble-particle, respectively. It is observed that many researchers have studied to develop new technologies and techniques for providing the increase of recovery in coarse and fine particle flotation. In this study; the development of new technologies to increase the efficiency of the flotation of fine were investigated. As the results of this study, the most appropriate techniques were determined industrial applicability of the fine particle flotation.

Keywords: Mineral Processing, Flotation, Particle Size, Fine particle

1 INTRODUCTION

Low grad-fine particles which cannot be enriched with physical methods can be benefited by flotation technique using physico-chemical characteristic differences of particles after milling process in mineral processing industry. Flotation is a method that enables the optional separation of hydrophobic particles with the help of air bubbles [1]. In this method, particles should create air-particle aggregates colliding with air bubbles. To reach the aggregate formed from the concentrate of non-detachment are required. The realization of these events which are known as micro events of flotation are related with the sizes of particle and bubbles and these events occur within certain limits in existing flotation technologies [2]. In flotation devices that are used commercially; while the particles that are below 25 micrometer is removed, the particles that are above 150 micrometer are sent to grinding stage again. While high efficiency is achieved in stated particle size ranges (-150+38 micrometer), if the rates are above or below these ranges, low efficiency is achieved as it is stated in Figure 1 [eg. 3,4]. It is known that this range is -600+50 micrometer for coal [5]. As it is seen in Figure 1, while the flotation efficiency decreases because of a decrease in collision probability of fine size particles with air bubble, in coarse particles, an increase in the probability of particles detach from bubble because of the effect of high particle mass and turbulence, decreases the flotation efficiency.

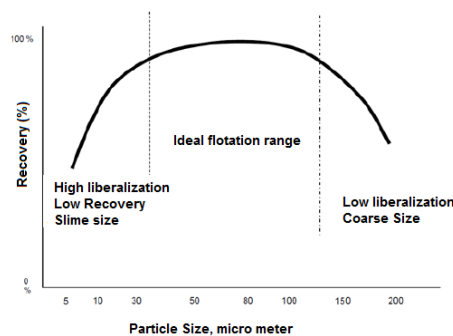


Figure 1. The effect of Particle Size on Flotation Efficiency [6]

¹Corresponding author: Dumlupinar University, Mining Engineering Department, 43270, Kütahya-Turkey
cengiz.karaguzel@dpu.edu.tr

²Dumlupinar University, Mining Engineering Department, 43270, Kütahya-Turkey
oktay.sahbaz@dpu.edu.tr

Today, studies are carried out in labs (bench scale) with modern flotation devices that generates fine bubbles to enrich fine particles with flotation but it is seen that the industrial applications of the mentioned devices are limited [eg.7,8].

In this study, the studies that aim to increase the flotation efficiency in fine particle sizes, flotation technologies and techniques have been analyzed in detail. According to results of examinations, the methods and studies have been identified which have industrial applicability towards fine particle flotation.

2 THE METHODS OF FINE PARTICLE FLOTATION

In the world, a rapid decrease in the number of mineral which are liberated in coarse size, very fine size wastes (slime) that are removed from concentration plants and especially the integration of clay minerals into developing technologies (especially nano-technologies) make the enrichment of fine particles necessary.

The flotation efficiencies of fine particles is quite low because of their low masses, momentums and high interfacial energies [eg.9,10,11,12,13]. In flotation process, the particles' adhering to air bubble depends on solid, liquid and gas contact phases and interaction of particle bubble includes the processes of encountering, collision, attachment and stability [eg. 14,15,16]. Sivomohan (1990) [9] published an article about the problems of the enrichment of fine particles in mineral processing and in this article he identified the methods which ground on surface characteristics for future studies. In the same study, it is also shown that the reason of losing efficiency in flotation technique which is among the methods that ground on surface characteristics of minerals, is fine particles' remaining incapable in encountering, collision and attachment events to air bubble. Yoon and Luterell (1989) [17] formularized the collision probability of particle and air bubble as $P_c = d_b^2/d_p^2$ and they also indicated that P_c is proportional directly with the square of particle size and indirectly with the square of bubble size. Dai et al. [10] compared many models related to the particle bubble encountering models in their review study (2000) and indicated that collision efficiency increased with particle size in all models. In his 2000 dated review which expressed the effect of bubble size on coarse and fine particle flotation, Tao explained the decrease in flotation efficiency of fine particles with the low collision probability of bubble particle and he indicated that detachment effective in flotation efficiency's decrease of coarse particles. In the same study, author also indicated that with the background studies he did, the collision probability of fine bubbles would increase and detachment would decrease. All these studies show that particle size must be enlarged or bubble size must be minimized for the optional flotation of fine particles.

One of the techniques used for the optional separation of fine particle is enlargement of particle optionally. The polymeric flocculation, coagulation, oil agglomeration and shear (with the effect of high rupturing power) flocculation are commonly used techniques for the optional particle enlargement [eg. 18,19,20,21,22]. While flocculation occurs with anionic or cationic polymers in polymeric flocculation, inorganic salt is used for coagulation. In oil agglomeration technique, particle size grows by means of constituting an oil bridge between hydrophobic particles. The polymeric flocculation, coagulation, oil agglomeration and shear flocculation studies conducted in recent years, have been done for fine sized energy raw material minerals [eg.22,23,24,25,26,27] industrial minerals [eg.22,24,28,29,30] metallic minerals [eg.31,32,33,34,35,36,37] and precious minerals [38] and the separation of these minerals of which particle size is enlarged, from accompanying minerals is achieved with screening, flotation, magnetic separation and sedimentation. Carrier flotation technique which is also known as the buoying of fine sized minerals with the help of an appropriate carrier mineral, is also used in enrichment of fine particles [eg.39,40,41].

The other techniques used in increasing the efficiency of fine particles' flotation are dissolved air flotation (DAF), gas aphon (CGA), pico bubble, electro flotation, electrostatic air spray, effervescent atomizer techniques in which fine bubbles are generated [eg.11,42,43,44,45,46,47,48]. Most of these techniques have been used with the purpose of water purification like clarification of water from oil and heavy metal [eg.49,50,51,52,53]. Rubio et al. (2002) [54] narrated several flotation techniques as treatment of waste water technique in their review. Some of the mentioned techniques have been used with conventional techniques to increase the efficiency of flotation [eg. 11,47,55]. With the electro flotation technique in which 22-50 μm bubble is produced, production of bubble is provided with water's electrolyze [eg.44,45]. While Ketkar et al. (1991) [56] were working on the flotation of fine quartz particles with this technique, Lierena et al. (1996) [57] were working on fine sphalerite particles' pH effect on electro flotation. Pico bubble flotation which was made by use of pico bubble (-1 μm), achieved by means of hydro dynamic cavitation tube, was used by Tao et al. (2006) [55] to develop coal flotation and it was seen that in the presence of pico bubble, the efficiency of column flotation increased but the content of coal did not change significantly. In a similar study by Yalçın et al. (2002) [11], adverse flotation of magnetite ore was applied to column with the use of DAF method which produces 10-100 μm (average 40 μm) bubble. While comparing the traditional system and DAF, the combinations of both systems were also compared. At the end of the study it is seen that silicate efficiency has increased in column+DAF system while Fe grade has decreased when compared to conventional and DAF systems. Another technique by which fine bubble is produced is CGA. In this technique, bubbles are minimized (an average of 50 μm) with the effect of shear force in high speed (> 5000 rpm). In a study by Waters et al. (2008) [42], flotation was performed in CGA column and Denver cell by use of copper oxide and silicon dioxide (-10 μm). In this study, bubbles which are loaded anionic reagent (SDS) used as a reagent.

It is seen that when compared to conventional system, modified CGA is the affirmative one. In a study performed by Cillers and Bradshaw in 1996 [58], pyrite minerals separated from quartz below 38 μm . In this study, GCA and conventional batch system was compared. Consequently, sulphur recovery rate was obtained 50% with GCA and 35% conventional system. Patil and Laskowski [47] enhanced the flotation efficiency by modifying effervescent

atomizer and batch flotation cell in 2008. Geroge et al. (2004) [59] mentioned about the importance of three function in fine particle flotation. These are true flotation, entrapment and entrainment. While entrapment occurs with fine particles' forming agglomerate with coarse particles in the event that fine particles and coarse particles are together, entrainment is known as the carrying of fine particles with coarse air bubbles in an environment only fine particles exist. In the same study, it is stated that fine bubble can not drag the particle back to it as it is in coarse bubble because in such a condition a very little slipstream will accompany.

Almost all of the aforesaid methods and devices have been performed in laboratory scale. Having developed through the end of 1980s, Jameson Cell [60] is a flotation device which gained success in fine particle flotation in industrial dimension. Nowadays, Jameson Cell which is used more than 300 flotation plant is used in a wide range of fields such as coal mines, metallic mines, industrial raw materials, waste cleaning etc. [8]. It is also known that this device which has important superiorities in fine particle optional separation has been used for oil sand flotation since 2009 [61]. Today, this device has 341 applications most of which are in Australia and America continents.

The most important reason of Jameson Cell is successful performance in fine particle is its compact design and its generating finer air bubbles than other conventional flotation devices [62,8]. Fine air bubbles (400-600 μm) generated in the device enables to a superior particle-bubble collision and nozzle-downcomer also enables fast collection [8, 63].

3 DISCUSSION

Flotation is a technique that is successfully applied to the 250-38 μm size ranged liberalized minerals which are unable to be enriched efficiently with physical methods. But today, flotation is becoming compulsory for the ore that is below and above the stated size because of the changing characteristics of the ores that are coming from the mines [64].

The flotation of fine size liberalized particles cannot be achieved efficiently with commercial flotation devices because of the encountering, collision and attachment problems which are explained in micro events of flotation. It is seen that new techniques and technologies are utilized by several researchers for the solution of these problems. When proposed methods are examined, it is concluded that the industrial application of some methods like electro flotation is limited because some of their cost is high and some of them are complex methods. However, in the environments that includes low solid, the industrial application of the techniques in which fine bubbles are used, seems possible with Jameson Flotation Technique.

Especially, metallic ores' liberalization at below 38 μm and the liberalized ores' tendency of extinction above this size, have directed researchers to the subject field of fine particle flotation. The optimum (high grade and recovery) enrichment that will perform in fine size will increase the product's sale price and also will reduce the cost of metallurgy process which is the next phase. In this context, the most widely used device for fine particle enrichment in industrial dimension is Jameson Cell. The devices and technologies that are performed out of cell have generally left in lab scale.

4 CONCLUSION

Today, the economical separation of the -38 micrometer particles that liberalized in fine sized has become necessary. For this purpose, flotation technology is widely utilized. In accordance with this purpose, it is known that techniques like DAF in which the size of air bubble is minimized and techniques like flocco-flotation in which particle size is enlarged optionally are being developed.

When the literature studies about fine particle flotation, it is obvious that the research/study conducted has generally been in laboratory scale. Nevertheless, it is believed that flotation techniques (DAF etc.) that generate fine bubble and Jameson flotation are appropriate for the enrichment of some ore examples that are liberalized in fine size in industrial scale.

REFERENCES

- [1] Wills, B., *Mineral Processing Technology*, Sixth Edition, Published by Butterworth-Heinemann,(1997)
- [2] Gontijo, C.F., Fornasiero, D., Ralston, J., *The limits of fine and coarse particle flotation*, The Canadian Journal of Chemical Engineering, 85(2007), pp. 739-747.
- [3] Trahar, W.J., *Int. Journal of Mineral Processing*, 8,(1981), pp. 289-327.
- [4] Karagüzel, C., Çobanoğlu, G., *Stage-wise flotation for the removal of colored minerals from feldspathic slimes using laboratory scale Jameson cell*, Separation and Purification Technology, 74(1), (2010), pp. 100-107.
- [5] Fan, M., Tao, D., Honaker, R., Luo, Z., *Nanobubble generation and its applications in froth flotation(Part IV) mechanical cells and specially designed column flotation of coal*, Mining Science and Technology, 20,(2010),pp.641-671.

- [6] Battersby M., Battersby R., M., Flatman S., Imhof R., Sprenger H., Bragado T., Recovery of Ultra fines using imhoflot pneumatic flotation two pilot plant case studies recovering nickel and zinc from tailings streams, MEI Conference, Cape Town, South Africa.(2011).
- [7] Karagüzel, C., Selective separation of fine albite from feldspathic slime containing colored minerals (Fe-min) by batch scale dissolved air flotation (DAF), *Minerals Engineering*, 23, (1), (2010), pp. 17-24.
- [8] O.Şahbaz, A.Uçar, B.Öteyaka, *Velocity gradient and maximum floatable particle size in the Jameson cell*, *Minerals Engineering (ISI)*, (2013), pp. 79-85.
- [9] Sivomohan, R., *The problem of recovering very fine particles in mineral processing - A Review*, *International Journal of Mineral Processing*, 28, (1990), pp. 247-288
- [10] Dai, Z., Fornasiero, D. and Ralston, J., *Particle-bubble collision models – a review*, *Adv. Colloid Interface Sci.*, 85(2-3), (2000), pp.231-256.
- [11] Yalçın, T., Byers, A. and Ughadpaga, K., *Dissolved gas method of generating bubbles for potential use in ore flotation*, *Mineral Processing and Extractive Metallurgy Review*, 23, (2002), pp. 181-197.
- [12] Tao, D., *Role of bubble size in flotation of coarse and fine particles- A review*, *Separation Science and Technology*, Vol. 39, No. 4, (2004), pp. 741-760.
- [13] Rodrigues, R. T., Rubio, J., DAF–dissolved air flotation: Potential applications in the mining and mineral processing industry, *Int. J. Miner. Process.* 82, (2007), pp. 1–13.
- [14] Gaudin, A. M., *Flotation*, New York, McGraw-Hill, (1957).
- [15] Nguyen, A. V. and Schulze, H. J., *Colloidal science of flotation*. New York, Marcel Dekker. (2004).
- [16] Binks, B. P. and T. S. Horozov, Eds. *Colloidal particles at liquid interfaces*. Cambridge, Cambridge University Press. (2006).
- [17] Yoon, R.H., and Luterell, G.H., *The effect of bubble size on fine particle flotation*, *Mineral Processing and Extractive Metallurgy Review*, Vol.5, (1989), pp. 101-122.
- [18] Attia, Y. A., *Fine Particle Separation by Selective Flocculation*, *Separation Sci. and Technology*, Vol. 17, (1982), Issue 3, pages 485-493.
- [19] Patil, D.P., Andrews, J.R.G., Uhlherr P.H.T., *Shear flocculation-kinetics of floc coalescence and breakage.*, *Int. J. Miner. Process.*, 61(3), (2001), pp. 171-188.
- [20] Song, S and Valdivieso, A.L., *Parametric aspect of hydrophobic flocculation technology*, *Mineral Processing and Extractive Metallurgy Review*, 23,(2002), pp.101-127.
- [21] Rosa, J.J., and Rubio, J., *The FF (flocculation-flotation) process*, *Minerals Engineering*, 18, (2005), pp. 701-707.
- [22] Ozkan, A., Ucbeyiay, H. and Duzyol, S., Comparison of stages in oil agglomeration process of quartz with sodium oleate in the presence of Ca(II) and Mg(II) ions, *Journal of Colloid and Interface Science* 329, (2009), pp. 81–88.
- [23] Laskowski, J. S., Yu, Z., *Oil agglomeration and its effect on beneficiation and filtration of low-rank/oxidized coals*, *International Journal of Mineral Processing*, Volume 58, Issues 1-4, (2000), pp. 237-252.
- [24] Laskowski, J.S., *Aggregation of fine particles in mineral processing circuits*, *Proceedings of the VIII. International Mineral Processing Symposium-Balkema, Antalya, Turkey*, (2000), pp.139-147.
- [25] Cebeci, Y. and Sönmez, I., The investigation of coal-pyrite/lignite concentration and their separation in the artificial mixture by oil agglomeration, *Fuel*, 81(2002), pp. 1139-1146.
- [26] Abakay, H., Ayhan, F.D. and Kahraman, F., *Selective oil agglomeration in Şırnakasphaltite beneficiation*, *Fuel*, 83, (2004), pp. 2081-2086.
- [27] Song, S., Experimental studies on hydrophobic flocculation of coal fines in aqueous solutions and flotation of flocculated coal, *Int. J. Oil, Gas and Coal Technology*, Vol. 1, Nos. 1/2,(2008), pp. 180- 193.
- [28] Sadowski, Z and Polowczyk, I., Agglomerate flotation of fine oxide particles, *Int. J. Miner. Process.*, 74, (2004), pp. 85– 90
- [29] Sönmez, I. and Cebeci, Y., *A study on spherical oil agglomeration of barite suspensions*, *Int. J. Miner. Process.*, 71, (2003), pp. 219– 232.
- [30] Cebeci and Sönmez, *Investigation of spherical oil agglomeration properties of celestite*, *Journal of Colloid and Interface Science* 273(2004), pp.198–204.
- [31] Vergouw, J.M., Difeo, A., Xu, Z., And Finch, J.A., *An agglomeration study of sulphide minerals using zeta potential and retting rate. part I pyrite and galene*, *Minerals Engineering*, Vol. 11, No. 2, (1998a), pp. 159-169.
- [32] Vergouw, J.M., Difeo, A., Xu, Z., And Finch, J.A., *An agglomeration study of sulphide minerals using zeta potential and retting rate. part II: sphalerite/pyrite and sphalerite/galena*, *Minerals Engineering*, Vol. 11, No. 7, (1998b), pp. 605-614,
- [33] Song, S., Lopez-Valdivieso, A., Ding, Y., *Effects of nonpolar oil on hydrophobic flocculation of hematite and rhodochrosite fines*, *Powder Technology*, 101, (1999), pp.73–81.
- [34] Song, S., Lopez-Valdivieso, A., Reyes-Bahena, J.L., Lara-Valenzuela, C., *Floc flotation of galena and sphalerite fines.*, *Minerals Engineering* 14, (2001), pp.87–98.
- [35] Song, S., Lu, S., Lopez-Valdivieso, A., *Magnetic separation of hematite and limonite fines as hydrophobic flocs from iron ores*, *Minerals Engineering*, 15, (2002), pp. 415–422
- [36] Sadowski, Z., *The role of surfactant salts on the spherical agglomeration of hematite suspension*, *Colloids and Surfaces A: Physicochemical and Engineering Aspects* 173, (2000), pp. 211–217.
- [37] Rubio, J., Capponi, F., Rodrigues, R.T., Matiolo, E., *Enhanced flotation of sulfide fines using the emulsified oil extender technique*, *Int. J. Miner. Processing*, 84, (2005), pp. 41-50.
- [38] Sen, S., Seyrankaya, A., Cilingir, Y., *Coal–oil assisted flotation for the gold recovery*, *Minerals Engineering* 18, (2005), pp. 1086–1092.
- [39] Valderrama, L. and Rubio, J., High intensity conditioning and the carrier flotation of gold fine particles, *Int. J. Miner. Processing*, 52, (1998), pp. 273-285.

- [40] Liang, R., Numata, Y. and Fujita, T., *Studies on carrier flotation of ultrafine wolframite*, Journal of the mining and materials processing institute of Japan, 115, 3, (1999), pp. 164-171. Abstract.
- [41] Ateşok, G., Boylu, F., Çelik, M.S., *Carrier flotation for desulfurization and deashing of difficult to float coals*, Minerals Engineering, 14, 6,(2001), pp. 661-670
- [42] Waters, K.E., Hadler, K., Cilliers, J.J., *The flotation of fine particle using charged microbubbles*. Miner. Eng., 21(12-14), (2008),pp. 918-923.
- [43] Tao, Y., Liu, J., Yu, S., Tao, D., *Picobubble Enhanced Fine Coal Flotation*, Separation Science and Technology, 41, pp. (2006), pp.3597–3607.
- [44] Khosla N.K., Venkatachalam, S., Somasunduran, P., *Pulsed electrogeneration of bubbles for electroflotation*, Journal of Applied Electrochemistry, 21, (1991), pp. 986-990.
- [45] Burns, S.E., Yiacomou, S., Tsouris, C., *Microbubble generation for environmental and industrial separation*, Separation and Purification Technology, 11,(1997), pp. 221-232.
- [46] Rodrigues, R.T., Rubio, J., *DAF-dissolved air flotation: potential applications in the mining and mineral processing industry*, International Journal of Mineral Processing 82, (2007), pp. 1–13.
- [47] Patil, D.P., Laskowski, J.S., *Development of zero conditioning procedure for coal reverse flotation*, Minerals Engineering, 21, (2008), pp. 373-379.
- [48] Englert, A.H., Rodrigues, R.T., Rubio J., *Dissolved air flotation (DAF) of fine quartz particles using an amine as collector*. Int. J. Miner. Process., 90(1-4), (2009), pp. 27-34.
- [49] Mostefa, N.M., Tir, M., *Coupling flocculation with electroflotation for waste oil/water emulsion treatment. Optimization of the operating conditions*. Desalination, 161, (2004), pp. 115-121.
- [50] Feris, L.A., De Leon, A.T., Santander, M., Rubio, J., *Advances in the adsorptive particulate flotation process*, Int. J. Miner. Process. 74(2004), pp. 01-106.
- [51] Chen, G., *Electrochemical Technologies in wastewater treatment*, Separation and Purification Technology, 38(2004), pp. 11-41.
- [52] Gao, P., Chen, X., Shen, F., Chen, G. *Removal of chromium(VI) from wastewater by combined electrocoagulation–electroflotation without a filter*, Separation and Purification Technology 43(2005), pp. 117–123.
- [53] Casqueira, R.G., Torem M.L., Kohler, H.M., *The removal of zinc from liquid streams by electroflotation*, Minerals Engineering 19(2006), pp. 1388–1392.
- [54] Rubio J., Souza, M.L., Smith, S., *Overview of flotation as a waste water treatment technique*, Minerals Engineering, 15, (2002), pp. 139-155
- [55] Tao, Y., Liu, J., Yu, S., Tao, D., *Picobubble enhanced fine coal flotation*, Int. J. of Coal Preparation and Utilization, 41, (2006), pp. 3597-3607.
- [56] Ketkar D.R., Mallikarjunan, R and Venkatachalam, S., *Electroflotation of quartz fines*, Int. J. Miner. Process., 31, (1991), pp. 127-138.
- [57] Lierena, C. Ho, J.C.K. and Piran, D.L., *Effect of pH on electroflotation of sphalerite*, Chem. Eng. Commun., 155, (1996), pp.217-228.
- [58] Cilliers, J.J., Bradshaw, D.J., *The flotation of fine pyrite using colloidal gas aphrons*, Minerals Engineering, 9, 2(1996), pp. 235-241.
- [59] George, P., Nguyen, A.V., Jameson, G.J., *Assesment of true flotation and entrainment in the flotation of submicron particle by fine bubbles*, Minerals Engineering, 17 (7-8), (2004), pp. 847-853.
- [60] Jameson, G.J., *New directions in flotation machine design*, Minerals Engineering, 23, (2010), pp. 835-841.
- [61] (2015) Website. [Online]. Available: <http://www.jameson.com/>
- [62] Evans, E., and Jameson, G.J., *Hydrodynamics of a plunging liquid jet bubble column*, Trans ChemE, Vol 73, Part A, August 1995, Australia.
- [63] Harbort, G.J., Manlapig, E.V. veDeBono, S.K., *Particle collection within the Jameson cell downcomer*, Trans. IMM Section C, V. 111/Proc. Australas IMM, V. 307. (2002).
- [64] Cowburn, J., Harbort, G., Manlapig, E. and Pokrajcic, *Improving the recovery of coarse coal particles in Jameson cell*, Minerals Engineering, Vol. 19(2006), pp.609-618.

Determination of the Best Growing Medium in Float System for Improving Germinability and Seedling Production of Tobacco (*Nicotiana Tabacum* L.), Coker 347

Gokhan Ipek¹, Amir Rahimi², Sina Siavash Moghaddam²

Abstract

The direct-seeded of tobacco with float system has taken the attention of many farmers for seedling production. Peat is an important component of culture medium which is mainly imported. In order to study growing medium to replace peat in float system for improving germinability and seedling production, a research was carried out in the seedling nursery of Rasht Tobacco Research Institute. This experiment was conducted in completely randomized design with 8 treatments and 3 replications. The treatments were peat, vermiculite, field soil, manure, sand, tree cortex compost and tea residue. Results indicated that there were significant differences between growing mediums in terms of germination percentage, germination rate, germination vigour, seedling length vigour, seedling weight vigour, collar diameter, radicle dry weight and seedling dry weight. The highest germination percentage, germination rate, germination vigour and seedling length vigour were observed in treatment of peat 50%+vermiculite 25%+field soil 25%. The highest collar diameter, radicle dry weight, seedling dry weight and seedling weight vigour were found in treatment of tree cortex compost 50%+ field soil 25%+ manure 25%. To sum up, peat utilization can be diminished through employing existing local medium.

Keywords: Seedling production, Float system, Peat, Vermiculite, Germination Speed.

1 INTRODUCTION

Tobacco with the scientific name of *Nicotiana tabacum*, is self-pollinated annual plant [1]. The ideal seedling production has an important role in the production of high quality tobacco. Because tobacco seeds are so small, they need special environment for germination. That's why instead of direct planting, seeds are produced in the nursery and seedlings are then transplanted to the field. Hence, under these circumstances, shortening the growing season, harvesting and drying leaves in proper time before the onset of autumn rain will be possible [2]. Floating method is the most common method of seedling production without shocking and damaging roots during transplanting. Tobacco growing media in trays can be included various materials such as peat, perlite, vermiculite, sand or sandy loam and sandy loam soil with ample organic matter [3]. Nowadays, the whole tobacco seedling production in the US and 60% in Brazil takes place through the flotation system [4, 5]. The main advantage of float-system compared with conventional methods are to reduce production costs, environmental control condition, increased uniformity and consistency of seedlings and decrease the utilization of toxins [6,7]. The most important issues related to floating system are appropriate medium to fill the tray [8]. Three components of the media that are being utilized as substrates include peat, perlite and vermiculite. Peat has the capacity to maintain water and nutrients as the main media in combination with other media [9]. Since the late 1970s, around the world searching for a suitable replacement for peat began [10]. Due to environmental hazards and the requirement for recycling organic wastes, investigating the possible applying organic waste is taken into consideration. Studies show that after the right process of composting organic residues, can be utilized as a substitution of peat substrates [10, 11, 12]. Mainly peats consumption in Iran is provided through imports from other countries. Therefore, combining or using other local resources can be considered as a key issue.

Ranjbar and Taghavi, (2007), [13] reported employing perlite, vermiculite and manure as tobacco floating nursery media for Burley 21, were an effective substitute for imported Peat. Masaka et al., (2007), [14] also concluded that the combination and particle size of medium has a noteworthy effect on the quality of tobacco seedlings. Hence, the objectives of the study were using existing local media in the region to replace imported peat and determine the best medium in flotation system to enhance germination and seedling production in tobacco.

¹Corresponding author: Çankırı Karatekin University, Yapraklı Vocational School, Çankırı, Turkey, gokhanipek@karatekin.edu.tr

²Dep of Agronomy, Faculty of Agriculture, Urmia University, Iran

2 MATERIALS AND METHODS

The experiment was conducted in the nursery of the Rasht Tobacco Research Station as a completely randomized design with 8 treatments and 3 replications. The treatments in this study are presented in Table 1.

Table 1. The treatments studied in this research

Treatment Number	Treatment
(1)	Peat (Control)
(2)	Peat 50%+Vermiculite 25%+Field Soil 25%
(3)	Manure 50%+ Field Soil 25%+Sand 25%
(4)	Manure 50%+ Field Soil 25%+ Vermiculite 25%
(5)	Manure 75%+ Field Soil 25%
(6)	Tree Cortex Compost 50%+ Field Soil 25%+ Manure 25%
(7)	Tree Cortex Compost 50%+ Vermiculite 25%+ Manure 25%
(8)	Tree Cortex Compost And Tea Residue 50%+ Vermiculite 25%+ Field Soil 25%

Indices and equations used are provided in Table 2.

Table 2. Equations of germination indices

Equation Number	Index	Equation	References
(1)	Germination percentage	$GP = \frac{n}{N} \times 100$	Panwar and Bhardwaj, 2005
(2)	Germination rate	$GR = \sum \frac{n_i}{t_i}$	Kulkarni <i>et al.</i> , 2007
(3)	Germination vigour	$GV = \frac{GR \times \text{Mean}(PL+RL)}{100}$	Bayat <i>et al.</i> , 2014
(4)	Seedling length vigour	$SLV = GP \times SL$	Reddy and Khan, 2001
(5)	Seedling weight vigour	$SWV = GP \times SW$	Reddy and Khan, 2001

n = Total of germinated seeds during period, n_i = The number of germinated seeds at an interval of distinct period;
 t_i , t_j = The number of days after the start of germination, N = Number of sowed seeds, PL = Plumule Length, RL
 = Radicle Length, SL = Seedling Length, SW = Seedling Dry Weight

In this study, floating system for tobacco seed germination and seedling production was used. Floating system containing pitted styrofoam trays, growth media and seed. Coated seeds were placed into each of the holes. The water depth, 12 cm was considered. Ridomil Mancozeb, 36 grams and 400 grams of fertilizer (NPK) per 10 meters was applied [15, 13]. Tobacco seeds were Coker 347 (flue-cured) that provided by Rasht Tobacco Research Institute.

3 RESULTS AND DISCUSSION

Results and discussion

Germination percentage: according to the analysis of variance, it was found that different medium has significant effect on germination percentage in the level of the 1%. Based on the results, the highest percentage of germination were (average 78.83%) in treatment 2 (Peat 50%+Vermiculite 25%+Field Soil 25%). It seems that retaining moisture by peat contributed to the increase of tobacco seed germination. Peat magnitude as part of the medium ingredients is related to high capacity water holding, optimum air holding and cation exchange capacity [16]. Vermiculite is kind of aluminosilicate minerals that has high water holding capacity and can be employed as medium [17].

The germination rate

The results indicated that the different media have a significant effect on the germination rate. The highest rate of germination (41.58) obtained in treatment 2 (Peat 50%+Vermiculite 25%+Field Soil 25%). Bahmani et al., (2014) [18], also reported that type of medium and soil texture has a significant effect on germination rate.

Vigour

Results of this study showed that the effect of medium on seed vigour was significant. Highest vigour was observed in treatment 2 (Peat 50%+Vermiculite 25%+Field Soil 25%). Ayan et al., (2006) [19], reported similar results which use of the peat in combination with other medium enhanced the quality of tobacco seeds.

Seedling length and weight vigour: Results indicated that the effect of medium on seedling vigour was significant. The highest seedling length vigour was observed in treatment 2 (Peat 50%+Vermiculite 25%+Field Soil 25%). Analysis of variance showed that the effect of medium on seedling weight vigour was significant. The highest seedling weight vigour in treatment 6 (Tree Cortex Compost 50%+ Field Soil 25%+ Manure 25%) was observed.

Plumule, root and seedling length

In this study the effect of different medium on the plumule, root and seedling length was not significant. However, the results of Ranjbar et al., (2007) [13], showed significant effect of medium (perlite, vermiculite and manure) on root length that demonstrates dependency of seed vigour and medium type.

Collar Diameter

Analysis of variance showed a significant effect of medium on collar diameter. Highest average collar diameter (5.98) was observed in the treatment 6 (Tree Cortex Compost 50%+ Field Soil 25%+ Manure 25%).

Plumule, root and seedling dry weight

The effect of different medium on plumule dry weight was not significant. However, analysis of variance showed a significant effect of medium on root dry weight. The highest root dry weight (9.4 g) was obtained in treatment 6 (Tree Cortex Compost 50%+ Field Soil 25%+ Manure 25%). The effect of different medium on seedling dry weight was significant. The highest seedling dry weight was found in treatment 6 (Tree Cortex Compost 50%+ Field Soil 25%+ Manure 25%). Tree cortex compost is a good medium for production of high quality of seedlings and can be one alternative for peat. In tree cortex compost significant reduction in the C/N was observed [20].

Conclusion

The outcomes demonstrated that distinctive sort of medium has ability to be choices instead imported peat and peat usage can be diminished by utilizing existing medium in the region. Further experiments using various local media are needed to find appropriate alternative or combination for peat. Therefore, relying on inexpensive local medium results into keeping dollars inside the country in connection to tobacco and other plants which require imported peat. Indeed, Iran could appreciate the value of their currency simply by not buying any more stuff (such as peat) that needs foreign currency (dollar or Euro).

REFERENCES:

- [1]. Ahifar, H. 1988. Botanic of tobacco and Iranian tobacco profile. Iranian Tobacco Company.
- [2]. Peksüslü, A., Gencer, S (2002). Tobacco Production (in Turkish). Aegean Agricultural Research Institute publications, 105, 151–168.
- [3]. Davis, D.L. & Nielsen, M.T. (1999). Tobacco, Production Chemistry and Technology. Pub, Blackwell Science, (CORESTA), P, 467.
- [4]. FAO (2001). Global report on validated alternatives to the use of methyl bromide for soil fumigation. <http://www.fao.org/DOCREP/004/Y1809E/Y1809E00.HTM>
- [5]. Fowlkes, D.J. (2001). Burley tobacco production in Tennessee. The float system for tobacco transplants. <http://economics.ag.utk.edu/budget/BurleyProductionGuide2001.pdf>
- [6]. Peek, D.R. & Reed, T.D. (2002). Burley tobacco production guide. Greenhouse transplant production. <http://www.ext.vt.edu/pubs/tobacco/436-050/436-050.html>
- [7]. Smith, W.D., Boyette, M.D., Moore, J.M. & Sumner, P.E. (2002). Transplant production in greenhouses. S.M. Jeter, 1981. "Maximum conversion efficiency for the utilization of direct solar radiation", Solar Energy, vol. 26(3), pp. 231–236.
- [8]. Peace, B., Palmer, G., Nesmith, W. & Tomansend, L. (2002). Management of tobacco float systems. <http://www.ca.uky.edu/agc/pubs/id/id132/id132.htm>
- [9]. Sales, L.A. (2002). Effective alternative to methyl bromide in Brazil. FAO Production and Protection Paper, 166, 13–24.
- [10]. Raviv, M., Chen, Y. & Inbar, Y. (1986). Peat and peat substitutes as growth media for container-grown plant. PP.257-287. In: Chen, Y. and Y. Y. Avnimelech (Eds.). The Role of Organic Matter in Modern Agriculture, MartinisNijhoff, Dordrecht.
- [11]. Chen, Y., Inbar, Y. & Hadar, Y. 1988. Composted agricultural wastes as potting media for ornamental plants. Soil Science, 145, 298-303.
- [12]. Garcia-Gomez, A., Bernal, M.P. & Roig, A. (2002). Growth of ornamental plants in two composts prepared from agroindustrial wastes. Bioresource Technology, 83, 81-87.
- [13]. Ranjbar, R., & Taghavi, R. (2007). Possibility of using perlite, vermiculite and manure tobacco Burley 21 in the floating method. The Tenth Congress of Soil Science Iran, Karaj, Tehran University College of Agriculture and Natural Resources.
- [14]. Masaka, J., Musundire, R. & Gondongwe, L. (2007). The effect of float seedling growth media combination and particle size distribution on germination and biometric characteristics of tobacco seedlings (*Nicotinatabacum*). International Journal of Agricultural Research, 2(5), 459-467.
- [15]. Assimi, M.H., Barzegarkho, M.H. & Jabarzadeh, A.R. (2010). Evaluation of substrates in the production of tobacco seedlings in the floating method. Congress Crop Sciences, Tehran, ShabhidBeheshti University.
- [16]. Mami, Y., Peyvast, Gh., Bakhshi, D. & Samizadeh, H. (2008). Effect of different substrates on tomato production in soilless culture. Journal of Horticultural Science, 22(2), 39-48.
- [17]. Abad, M., Noguera, P., Puchades, R., Maqueira, A., & Noguera, V. (2002). Physico-chemical and chemical properties of some coconut coir dusts for use as a peat substitute for containerised ornamental plants. Bioresource Technology, 82, 241-245.
- [18]. Bahmani, F., BanjShafiei, A., Eshaghi Rad, J. & Pato, M. (2014). Effect of sowing bed, irrigation period, seed provenance, seed cover and Effect of sowing bed, irrigation period, seed provenance, seed cover and sowing date on germination rate of Black pine seeds. Case study: Darlak nursery, Mahabad. Iranian Journal of Forest and Poplar Research, 22(3), 423-433.
- [19]. Ayan, A.K., Çalişkan, Ö. & Çirak, C. (2006). Seedling quality of flue-cured tobacco as affected by different types of peat. Commun. Biometry Crop Science, 1(1), 56-62.
- [20]. Padasht, M.N. & Khalighi, A. (2000). Medium effects of bark, tea waste, rice hull and replace Pittin the growth of Azolla as Marigold (*Tagetes patula* (Golden Boy)). Iran Agricultural Sciences, 31(3), 557-566.

Use of Dried Persian Lime (*Citrus latifolia* Tanaka) as a Flavoring in Food and Medicinal Plant in Iran

Gokhan Ipek¹, Amir Rahimi², Neset Arslan³

Abstract

Persian Lime, Tahiti lime or Bears Lime (Citrus latifolia Tanaka) belongs to the family Rutaceae and is a variety of lime. The Persian lime is believed to be a native to the old Iran region of the Middle East. It may be then spread to the Middle East and other tropical and subtropical countries as Brazil via Australia. It is believed that the Persian lime was introduced to the USA via Tahiti, hence one of its three common names. This fruit is widely produced in Iran right now.

Persian Lime is one of the most important citrus trees and used mainly in fresh drinks, as well as a part of salads and is chief source of carbohydrates, protein, oil and vitamin C. Dried fruit of Persian lime lost its water content, usually after having spent a majority of their drying time in the sun. Dried fruit of the Persian lime in Middle East, especially in Iran, is used as a flavoring in foods, whole, sliced or ground. In traditional medicine of Iran the dried fruits used as Stomach tonic, Carminative, appetizing, Antiseptic and etc. In this review paper, production and drying of the fruits and different uses of Persian lime in Iran are discussed.

Keywords: Persian lime, drying, fruit, Iran, flavoring.

1. INTRODUCTION

Iran and Plant Diversity

Islamic Republic of Iran, with 1,640,000 square kilometers area, in the south west of Asia of the northern hemisphere, has its specific combination of different elements of life and a special ecosystem and biodiversity due to various factors including different climatic conditions, high mountains all around and a large desert in center. Different phytogeographic regions of Iran's plateau cause massive genetic flow in this area which result in a variety of plant species and in comparison with neighbor countries and some others has very interesting points. Some plant species have been walled beyond the natural fences (as endemic), and some are scattered in other lands. Most part of Iran is occupied by deserts and semi-deserts. Residents of these areas have always been strongly dependent on vegetation cover, and where the vegetation cover could create good micro climate. Due to the diversity of climate, topography and edaphic conditions, limited areas of vegetation in Iran, are very different and heterogenous. About 1,900 endemic species have been described in Iran. Forests cover 12.4 million hectares, and mangrove swamps cover about 10,000 hectares along the Persian Gulf. The country can be considered the place of origin of many of the world's genetic resources, being the home of the original stocks of plant species of great commercial [1,2].

Important of Medicinal Plants

Since ancient times, plants have been one of the first and most available resources usable for treating illnesses. There has always been a close relationship between man and plants, and the medicinal effects of plants and their uses have been known by everybody. Medicinal plants contain plant materials such as leaf, root, flower and seed using in the form of their extracts and chemical compounds to produce human drugs or veterinary medicine. Properties of medicinal plants are due to the presence of various complex chemical substances from different composition which named secondary metabolites.

¹Corresponding author: Çankırı Karatekin University, Yapraklı Vocational School, Çankırı, Turkey, gokhanipek@karatekin.edu.tr

²Dep of Agronomy, Faculty of Agriculture, Urmia University, Iran

³Field Crops Department, Agriculture Faculty Ankara University, Ankara, Turkey

They are categorized as alkaloids, glycosides, flavonoids, saponins, tannins, carbohydrate and essential oils. Medicinal and aromatic plants form a large group of economically important plants that provide the basic raw materials for indigenous pharmaceuticals, perfumery, flavor and cosmetic industries. Essential oils and extracts of various species of edible and medicinal plants, herbs, and spices constitute of very potent natural biologically active agents. Use of essential oils as antimicrobial agents in food systems may be considered as an additional intrinsic determinant to increase the safety and shelf life of foods [3,4,5]. The genus *Citrus* (Rutaceae) includes several species of plants that produce some of the most cultivated fruits in the world and Persian lime is one of them.

Persian lime

Persian lime (*Citrus latifolia* Tanaka) which also known as Tahiti lime or Bearss lime is of hybrid origin, most likely from a cross between key lime (*Citrus aurantiifolia*) and either lemon (*Citrus limon*) or citron (*Citrus medica*). Its identity has been in doubt and only in recent years has it been given the botanical name. The plant is widely produced in Iran and is economically significant for the country but lacks the long history. Persian limes were first grown commercially in what is today southern Iraq and Iran, hence their name, although important varieties were developed in the U.S. (the common name "Bearss lime" refers to the seedless variety developed in 1895 by John T. Bearss in California), and Florida used to be the major producer of these limes. Persian lime rose to prominence after southern Florida's key lime orchards were destroyed by a hurricane in 1926. However, the 1992 Hurricane Andrew then devastated Florida's Persian lime orchards, virtually stopping U.S. production of the fruit. Mexico is now the primary grower and exporter of Persian limes for the American, European and Asian markets.

Limes originate from the Middle East, and were first grown on a large scale in Iran and probably southern Iraq; but some botanists say that the origin of the Persian Lime is uncertain. Recent genetic analysis of citrus suggests the origin of this lime is southeast Asia, specifically east and northeastern India, north Burma (Myanmar), southwest China, and eastward through the Malay archipelago [6]. It is known only in cultivation. It is cultivated commercially in Iran, Tahiti, New Caledonia, Florida, California, Mexico, Brazil, Venezuela, Portugal and Australia. It is believed that the lime was introduced into the Mediterranean region by way of Iran (formerly called Persia) from Tahiti.

The plant is grown throughout warm, subtropical and tropical areas of the world. The name "lime" may, in the U.K., also refer to the unrelated, non-citrus linden tree, *Tilia* species. Persian lime is the most commonly cultivated lime species for commercial use, and accounts for the largest share of the fruits sold as limes. The plant is typically a medium sized tree with 4.5 to 6.0 meter tall, wide spreading, drooping branches. In contrast to many other citrus species, is often without thorn. The flowers are white, tinged with purple, and have no viable pollen. The fruit is oval or oblong fruit that is 4 to 6.25 cm wide and 5 to 7.25 cm long, often with nipped or elongated ends, generally seedless or few seeded. The plant is larger and has thicker skins, with less intense citrus aromatics than those of its parent as key lime. The fruit is yellowish green or yellow when fully ripe. The fruit has a uniquely fragrant, spicy aroma and tart flavor, but the aroma and flavor are less intense than those of key lime. However, it has various advantages over the key lime for the purposes of commercial agriculture larger size, absence of seed, hardness, thorn less on the bushes, and longer fruit shelf life that have combined to make it more widely cultivated [7]. Persian lime is less acidic than key limes and do not have the bitterness that lends to the key lime's unique flavor. Persian limes are commercialized primarily in six sizes, known as 110's, 150's, 175's, 200's, 230's and 250's. Once grown primarily in Florida in the U.S, it rose to prominence after key lime orchards were wiped out there by a hurricane in 1926, according to the American Pomological Society; subsequently Persian lime orchards themselves were devastated by Hurricane Andrew in 1992 [8]. Large numbers of Persian limes are grown, processed, and exported every year primarily from Mexico to the American, European and Asian markets. U.S. Persian lime imports from Mexico are handled mostly through McAllen, Texas [9, 10, 11].

Persian Lime Adaptation

About climatic adaptation, in general, damage to Persian lime leaves occurs at temperatures below -2°C ; wood damage occurs below about -3°C , and severe damage or death occurs below -4°C . 'Tahiti' lime trees grow best in the warmest areas.

The plant can be grown successfully in a variety of soils. However, well drained soils are essential for good fruit production and growth. It is growing in high-pH, calcareous soils may be more susceptible to minor element deficiencies. The plant should be planted in full sun for best growth and fruit production. Select a part of the landscape away from other trees, buildings and other structures and power lines. Select the warmest area of the landscape that does not flood (or remain wet) after typical summer rainfall events [12].

Irrigation

Newly planted Persian lime trees should be watered at planting and then every other day for the first week or so and then once or twice a week for the first couple of months. During prolonged dry periods, newly planted and young lime trees should be well watered twice a week. Once the rainy season arrives, irrigation frequency may be reduced or stopped. Once Persian lime trees are four or more years old, irrigation will be beneficial to plant growth and crop yields during prolonged dry periods. Specific water requirements for mature trees have not been determined. However, as with other tree crops, the period from bloom through fruit development is important. Drought stress should be avoided at this time with periodic watering [12].

Dried Persian Lime

Dried fruit of Persian lime is a lime that lost its water content, usually after having spent a majority of their drying time in the sun. Unlike with fresh limes, you can't just squeeze the juice or micro plane the peels. Drying of Persian lime fruits developed in Oman at first, so dried limes named Limou Amani (Ommani limes) in Iran. Dried Persian lime also known as black lime, Noomi Basra in Iraq (Lemon from Basra) and Limo Oman [13]. The fruits are boiled briefly in salt brine, and then they are laid out in the sun to dry over the course of several weeks. But the simplicity of the process belies the alchemy that takes place under that desert sun. Over the weeks, the limes turn black or dusky brown on the outside and lose so much weight that they feel hollow; inside, the juicy green flesh turns a glossy, maroon-tinged black. The first stage of drying produces dried white limes – the black limes are a result of an elongated drying period, which allows them to develop stronger musky, fermented notes. Few people in the West seem to know they exist. If there's one culinary treasure that continually amazes me, it's dried limes [14, 15, 16, 17].

Uses

Persian limes are used similarly to key limes, occasionally as a fresh fruit generally, lime wedges are served as an accompaniment to salads, avocados, or Asian dishes, but more commonly processed into juice, for use in limeade and other non-alcoholic beverages, as well as cocktail beverages, including popular summertime drinks such as daiquiris, Cuban mojitos, and Brazilian caiparinhas. In the Middle East, these limes are most often added whole to soups and stews. You simply wash them well, pierce them a couple of times with a sharp knife or a fork, and drop three of four of them into the pot. As the cooking liquid sluices through the limes, they add an evocative tang and a subtle complexity to the entire dish [18].

Dried Persian limes are used to add a sour flavor to dishes, through a process known as souring. In Iranian cuisine, they are used to flavor stews and soups. Across the Persian Gulf, they are used cooked with fish, whereas in Iraq they are powdered and added to rice dishes and stuffing. Dried Persian lime is the perfect balance to all kinds of proteins. Their acidity cuts the fat in red meats; their sweetness enlivens poultry; their sultry funk adds nuance to fish. As for legumes, well, they haven't had an ally like this since onions and garlic came on the scene. The powder is not as easy to locate. Since the limes begin to lose their volatile oils the moment they are pulverized, it's much better to grind your own. Just cut them in half (a serrated knife is helpful), remove any seeds, and then grind them in a clean coffee grinder (best) or blender (acceptable) until very fine. Also, they're made into a warm drink called Hamidh (sour). Powdered dried lime is also used as an ingredient in Persian Gulf-style baharat (a spice mixture which is also called kabsa or kebsa) [19].

It is a traditional ingredient of Arabic and Iranian cooking although they are used whole, sliced or ground, as a spice. Dried Persian limes are strongly flavored. They taste sour and citrusy like a lime but they also taste earthy and somewhat smoky and lack the sweetness of fresh limes. Because they are preserved they also have a slightly bitter, fermented flavor, but the bitter accents are mainly concentrated in the lime's outer skin and seeds. As water passes through their glossy black internal chambers, they soften up and give up all the flavor of their sun-dried zest and flesh. When it's time to serve, they can be squeezed of their final juices and neatly discarded. Though their flavor is distinct, it doesn't overwhelm so experiment with abandon [10, 11].

Medicinal Property

The genus *Citrus* includes several species of plants that produce some of the most cultivated fruits in the world, including oranges and lemons, which have an appreciable content of essential oil. In folk medicine, they are used as a cholagogue and for their digestive, tonic, antipyretic, anti-inflammatory, sedative, and antitoxic effects [20, 21, 22]. Essential oils of plants from the genus *Citrus* have monoterpenes and sesquiterpenes as their constituents [23, 24].

The literature indicates the presence of 50 or more different compounds obtained from citrus peel, whereas limonene is the main compound [25]. Since ancient times, Lemon essential oil has been used for its antiseptic, carminative, diuretic, and eupeptic effects [21]. Some of its compounds, including β -caryophyllene, LIM, and linalool, have anti-inflammatory effects [26, 27, 28]; α -pinene and β -pinene inhibit the synthesis of nitric oxide (NO), suggesting an antioxidant effect [29], and recent reports showed that β -pinene exerts an antispasmodic effect on the rat ileum and provokes antinociceptive actions [30].

LIM is one of the most common terpenes in nature and has been used as a flavoring agent in common food items, such as fruit juices, soft drinks, and ice cream, and in the cosmetics and pesticide industries [27, 31]. LIM has been shown to exert antiulcerogenic, gastroprotective, chemopreventive, antiproliferative, insecticide, antimicrobial, and immunomodulatory effects [32, 33, 34, 35].

This compound has also been shown to have anti-inflammatory effects by reducing eosinophil chemotaxis and MCP-1 production [27]. It effectively inhibited lipopolysaccharide- (LPS-) induced NO and prostaglandin E2 (PGE2) production in macrophages [31] and decreased interleukin-1 α (IL-1 α) levels in normal human undifferentiated NCTC 2544 keratinocytes [36]. Citrus flavonoids have a large spectrum of biological activity including antibacterial, antifungal, antidiabetic, anticancer and antiviral activities. Preparation from peel, flowers and leaves of bitter orange (*Citrus aurantium* L.) are popularly used in order to minimize central nervous system disorders. The fiber of citrus fruit also contains bioactive compounds, such as polyphenols, the most important being vitamin C [37, 38, 39]. In traditional medicine of Iran the dried Persian lime used as stomach tonic, carminative, appetizing, antiseptic and etc.

REFERENCES:

- [1]. Anonymous, 2016a. <http://medomed.org/2010/iran-biodiversity-conservation-data>
- [2]. Anonymous, 2016b. <http://flora-iran.com>.
- [3]. Najafi Sh, SadeghiNejad B, Deokule SS, Estakhr J., 2010. Phytochemical screening of *Bidaria khandalense* (Sant.) *Loranthuscipitellatus* Wall., *Viscum articulatum* burm.F. and *Vitex negundo* Linn. Research Journal of Pharmaceutical, Biological and Chemical Sciences, 1: 388-393.
- [4]. Nejad Ebrahimi S, Hadian J, Mirjalili MH, Sonboli A, Yousefzadi M., 2008. Essential oil composition and antibacterial activity of *Thymus caramanicus* at different phenological stages. Food Chemistry; 110: 927-931.
- [5]. Nikbakht A, Kafi M, 2004. The history of herbal medicine and medicinal plants in Iran. Proceeding of the 8th international plant-people relationship symposium (IPPS), Hyogo, Japan.
- [6]. Moore, G.A. 2001. Oranges and lemons: clues to the taxonomy of Citrus from molecular markers. Trends in Genetics, 17: 536-540.
- [7]. Anonymous, 2016c. <http://eol.org/pages/5619784/overview>.
- [8]. Anonymous, 2016d. <http://www.thenibble.com/reviews/main/fruits/types-of-lime.asp>.
- [9]. Lorestani, A.N. and Tabatabaeifar, A., 2006. Modelling the mass of Kiwi fruit by geometrical attributes. International Agrophysics 20(2): 135-139.
- [10]. Basan, Ghillie, 2007. Middle Eastern Kitchen. NY, USA: Hippocrene Books Inc. p. 78.
- [11]. Mallos, Tess, 2007. Middle Eastern Cooking. VT, USA: Periplus Editions. p. 16.
- [12]. Crane, J.H. and Osborne, J.L., 2013. Growing 'Tahiti' Limes in the Home Landscape, University of Florida, IFAS extension.
- [13]. Anonymous, 2016e. <http://www.bonappetit.com/people/chefs/article/yotam-ottolenghi-dried-limes>.
- [14]. Anonymous, 2016f. <http://www.souschef.co.uk/dried-black-lime.html>.
- [15]. Lorestani, A.N., Jaliliantabar, F., and Gholami, R., 2012. Mass and volume modelling of Persian lime (*Citrus aurantifolia*) with geometrical attributes, Journal of Agricultural Technology, Vol. 8(5): 1537-1543.
- [16]. Anonymous, 2016g. <http://thepaleodiet.com/persian-inspired-dried-lime-chicken/>.
- [17]. Anonymous, 2016h. <http://www.nytimes.com/2010/06/02/dining/02power>.
- [18]. Anonymous, 2016i. https://en.wikipedia.org/wiki/Dried_lime.
- [19]. Anonymous, 2016j. <http://www.seriousseats.com/2010/10/spice-hunting-iranian-limu-loomi-omani-dried-limes.html>.
- [20]. B. A. Arias and L. Ramón-Laca, 2005. "Pharmacological properties of citrus and their ancient and medieval uses in the Mediterranean region," Journal of Ethnopharmacology, vol. 97, no. 1, pp. 89-95.
- [21]. A. A. García, 1998. Fitoterapia: Vademecum de Prescripción, Masson, Barcelona, Spain.
- [22]. M. P. Leite, J. Fassin, E. M. F. Baziloni, R. N. Almeida, R. Mattei, and J. R. Leite, 2008. "Behavioral effects of essential oil of *Citrus aurantium* L. inhalation in rats," Brazilian Journal of Pharmacognosy, vol. 18, pp. 661-666.
- [23]. A. Astani, J. Reichling, and P. Schnitzler, 2010. "Comparative study on the antiviral activity of selected monoterpenes derived from essential oils," Phytotherapy Research, vol. 24, no. 5, pp. 673-679.
- [24]. H. S. Choi, 2006. "Lipolytic effects of citrus peel oils and their components," Journal of Agricultural and Food Chemistry, vol. 54, no. 9, pp. 3254-3258.
- [25]. M. L. Lota, D. De Rocca Serra, F. Tomi, C. Jacquemond, and J. Casanova, 2002. "Volatile components of peel and leaf oils of lemon and lime species," Journal of Agricultural and Food Chemistry, vol. 50, no. 4, pp. 796-805.
- [26]. A. F. Bento, R. Marcon, R. C. Dutra, 2011. "β-caryophyllene inhibits dextran sulfate sodium-induced colitis in mice through CB2 receptor activation and PPARγ pathway," American Journal of Pathology, vol. 178, no. 3, pp. 1153-1166.
- [27]. R. Hirota, N. N. Roger, H. Nakamura, H. S. Song, M. Sawamura, and N. Sukanuma, 2010. "Anti-inflammatory effects of limonene from yuzu (*Citrus junos tanaka*) essential oil on eosinophils," Journal of Food Science, vol. 75, no. 3, pp. H87-H92.
- [28]. A. T. Peana, P. Rubattu, G. G. Piga, 2006. "Involvement of adenosine A1 and A2A receptors in (-)-linalool-induced antinociception," Life Sciences, vol. 78, no. 21, pp. 2471-2474.
- [29]. J. S. Baik, S. S. Kim, J. A. Lee, 2008. "Chemical composition and biological activities of essential oils extracted from Korea endemic citrus species," Journal of Microbiology and Biotechnology, vol. 18, no. 1, pp. 74-79.
- [30]. A. L. Rozza, T. D. M. Moraes, H. Kushima, 2011. "Gastroprotective mechanisms of Citrus lemon (Rutaceae) essential oil and its majority compounds limonene and β-pinene: involvement of heat-shock protein-70, vasoactive intestinal peptide, glutathione, sulfhydryl compounds, nitric oxide and prostaglandin E2," Chemico-Biological Interactions, vol. 189, no. 1-2, pp. 82-89.
- [31]. W. J. Yoon, N. H. Lee, and C. G. Hyun, 2010. "Limonene suppresses lipopolysaccharide-induced production of nitric oxide, prostaglandin E2, and pro-inflammatory cytokines in RAW 264.7 macrophages," Journal of Oleo Science, vol. 59, no. 8, pp. 415-421.
- [32]. D. C. Arruda, D. C. Miguel, J. K. U. Yokoyama-Yasunaka, A. M. Katzin, and S. R. B. Uliana, 2009. "Inhibitory activity of limonene against Leishmania parasites in vitro and in vivo," Biomedicine and Pharmacotherapy, vol. 63, no. 9, pp. 643-649.
- [33]. S. Del Toro-Arreola, E. Flores-Torales, C. Torres-Lozano, 2005. "Effect of D-limonene on immune response in BALB/c mice with lymphoma," International Immunopharmacology, vol. 5, no. 5, pp. 829-838.
- [34]. T. M. Moraes, H. Kushima, F. C. Moleiro, 2009. "Effects of limonene and essential oil from Citrus aurantium on gastric mucosa: role of prostaglandins and gastric mucus secretion," Chemico-Biological Interactions, vol. 180, no. 3, pp. 499-505.
- [35]. T. Parija and B. R. Das, 2003. "Involvement of YY1 and its correlation with c-myc in NDEA induced hepatocarcinogenesis, its prevention by d-limonene," Molecular Biology Reports, vol. 30 (1): 41-46.

- [36]. F. C. Kummer, R. Fachini-Queiroz, C. F. Estevão-Silva et al., 2012. "Effects of thymol and carvacrol, constituents of *Thymus vulgaris* L. essential oil, on the inflammatory response," *Evidence-Based Complementary and Alternative Medicine*, vol. 2012, Article ID 657026, 10 pages.
- [37]. Mohanapriya, M., Ramaswamy, L., and Rajendran, R., 2013. Health and Medicinal Properties of Lemon (*Citrus limonum*), *International Journal of Ayurvedic and Herbal Medicine*, 3(1): 1095-1100.
- [38]. Pultrini, A.M., Galindo, L.A., and M. Costa, 2006. "Effects of the essential oil from *Citrus aurantium* L. In experimental anxiety models in mice", *Life Sci.*, 78(15): 1720-1725.
- [39]. Sharafzadeh, Sh., and Alizadeh, O., 2012. Some Medicinal Plants Cultivated in Iran, *Journal of Applied Pharmaceutical Science* 02 (01): 134-137.

The Use Of Chitosan As Clarification Agent

Halil Ibrahim Kahve¹, Ayhan Duran²

Abstract

Clarification is an important step in the processing of fruit juice mainly in order to remove pectin and other carbohydrates which are present in the juice. Most often achieved through microfiltration enzymic treatment or by using common clarifying aids like gelatin bentonite, silica sol, polyvinyl pyrrolidone or a combination of these compounds. However, these processes can be labor-intensive, time-consuming and discontinuously operated. Chitosan (poly-b (1-4) N-acetyl-glucosamine) has been reported to have a number of potential industrial uses such as an adhesive, a paper-sizing agent, a chelating agent for metal ions, and as fruit-juice clarifying aids. Chitosan (deacetylated chitin), being polycationic in nature, nontoxic and biodegradable, has been found to be an effective coagulating agent in aiding the separation of suspended particles from beverages. Several works have reported the successful application of chitosan as a clarifying aid for apple, grape, lemon, orange, and bayberry juices, besides wine, and greentea.

Keywords: Clarification, chitosan, agent, juice.

1 INTRODUCTION

Although the method for producing clear and stable juices has been well known for years, problems with turbidity in juices and concentrates occasionally occur. Clarification is more important step in juice, milk, wine and tea production. For more fluid juices where cloud or turbidity is not acceptable primary extracted juice must be treated further. Natural fruit juices are complex multicomponent systems, opalescent or turbid due to the presence of insoluble solids in suspension [1]. These solids are mainly composed of carbohydrates and proteins, which are insoluble at the juice pH. The proteins have acid and basic groups whose degree of ionization depends on the pH and ionic strength of the liquid medium [2]. The pectin present both in solution and coating of the particles prevents the contact between them, providing stability to the juice. To elaborate clarified juices the native pectin must be degraded and removed since it complicates the clarification process [3]. The importance of polysaccharides and metal ions in juice turbidity (haze) and sediment formation is well established. A settling step can help, if the juice can be held refrigerated for a few hours but at ambient high temperatures holding is not recommended. Rapid methods such as centrifugation and filtration used produce a clear juice. Recently, another method which is using chitosan it began to be used.

2 CHITIN AND CHITOSAN

Chitin, a naturally abundant mucopolysaccharide, and the supporting material of crustaceans, insects, etc., is well known to consist of 2-acetamido-2-deoxy-b-D-glucose through a $\beta(1\rightarrow4)$. Chitin can be degraded by chitinase. Its immunogenicity is exceptionally low, in spite of the presence of nitrogen. It is a highly insoluble material resembling cellulose in its solubility and low chemical reactivity. It may be regarded as cellulose with hydroxyl at position C-2 replaced by an acetamido group. Like cellulose, it functions naturally as a structural polysaccharide. Chitin is a white, hard, inelastic, nitrogenous polysaccharide and the major source of surface pollution in coastal areas.

Chitosan is the N-deacetylated derivative of chitin, although this N-deacetylation is almost never complete. A sharp nomenclature with respect to the degree of N-deacetylation has not been defined between chitin and chitosan [(4), (5), (6)].

Chitin and chitosan are of commercial interest due to their high percentage of nitrogen (6.89%) compared to synthetically substituted cellulose (1.25%). This makes chitin a useful chelating agent [5].

Like cellulose, chitin functions naturally as a structural polysaccharide, but differs from cellulose in its properties. Chitin is highly hydrophobic and is insoluble in water and most organic solvents. It is soluble in hexafluoroisopropanol, hexafluoroacetone, chloroalcohols in conjugation with aqueous solutions of mineral acids [7].

The nitrogen content of chitin varies from 5 to 8% depending on the extent of deacetylation, whereas the nitrogen in chitosan is mostly in the form of primary aliphatic amino groups. Chitosan, therefore, undergoes reactions typical of

¹Corresponding author: Aksaray University, Department of Food Engineering, 68000, Aksaray Turkey. hibrahimkahve@gmail.com

²Aksaray University, Department of Food Engineering, 68000, Aksaray Turkey.

amines, of which N-acylation and Schiff reaction are the most important. Chitosan derivatives are easily obtained under mild conditions and can be considered as substituted glucans [8].

3 THE USE OF CHITOSAN IN FOOD INDUSTRY USE A CLARIFICATION AGENT

Chitosan films have been successfully used as a packaging material for the quality preservation of a variety of foods [11]. Antimicrobial films have been prepared by including various organic acids and essential oils in a chitosan matrix, and the ability of these bio-based films to inhibit the growth of indigenous (lactic acid bacteria and Enterobacteriaceae) or inoculated bacteria (*Lactobacillus sakei* and *Serratia liquefaciens*) onto the surfaces of vacuum packed cured meat products have been investigated.

In a study on carrots, carrots coated with edible chitosan films and the chitosan concentration is 5 mL/L. Consequently; during storage (at 4 ° C for 12 days), the color quality is maintained and whitening on surface is decreased [9].

Reference [10] investigated the effectiveness of water-soluble chitosan (0.03%) to minimize the microbial (bacterial and yeast) spoilage of processed milk. Complete inhibition of microbial growth was observed in the banana-flavored milk containing chitosan, in contrast to that observed in control milk (without chitosan), during storage for 15 d at 4 and 10 °C. The banana-flavored milk containing chitosan also maintained relatively higher pH than that of control milk during storage for 15 d at both temperatures.

Reference [12] investigated the effects of addition of chitosan ($M_w = 37$ kDa) on shelf life and quality of wet noodle. Chitosan dissolved in 1% acetic acid was added to wheat flour at 0.0%, 0.17%, 0.35%, 0.52%, and 0.7% concentrations. During storage at 18 °C for 6d, moisture content of wet noodle, irrespective of chitosan concentrations, slightly decreased with increasing storage periods. Increasing chitosan concentration from 0% to 0.70% decreased the numbers of viable cells during storage at 18 °C for 6 d. The shelf life of wet noodle containing 0.17%, 0.35%, 0.52%, and 0.70% chitosan was extended by 1, 2, 3, and 3 d, respectively, compared with that of the control. The wet noodle containing 0.35% chitosan had the most desirable sensory quality compared with other wet-noodle samples.

4 USE A CLARIFICATION AGENT CONCLUSION

In another study, the use of chitosan as a clarifying agent in the production of clear pomegranate juice was evaluated and its effects on quality characteristics of juice were investigated. The three factors were concentration of chitosan (10–120 mg/100 ml), process temperature (10–20°C), and process time (30–90 min) and their effects on turbidity and a' values were investigated. Chitosan can be proposed as an alternative clarification agent for production of pomegranate juice with an excellent clarity. The obtained results showed that clarification of pomegranate juice using chitosan can be a suitable, easily applicable, and fast method [15].

Reference [16] studied beer clarification and flocculation. Flocculation plays a central role in the way beer is produced. The primary function of flocculation is particle removal that can impart color to beer, create turbidity, and/or retain bacterial organisms. This study was carried out to investigate if carbon chitin and chitosan can be used as heterogeneous flocculants in the treatment of beer. Both chitin and chitosan demonstrated the ability to flocculate colloidal particles in the beer. Of all the tested flocculants, chitosan (5 mg/L) was found to be the most effective.

The largest single use of chitosan is the clarification of waste and effluent water [17]. The use of commercially available chitosan for drinkable water purification has been approved by the United State Environmental Protection Agency (USEPA) up to a maximum level of 10 mg/L [18]. Chitosan is more efficient activated charcoal for the clarification of polychlorinated biphenyls from contaminated water [19].

Zhi and other scientist studied that clarification of chitosan on green tea juice and the result showed that chitosan was a good clarifier, it could improve the light transmittance and stability of green tea juice without no undesirable effect on its main flavour material [20]. Chitosan have many advantages. Further, chitosan being nontoxic and biodegradable, it may be used as an alternative agent for refining of fruit juices. The use of chitosan in this respect is hindered due to its solubility in organic acids [13].

In a study using the chitosan agent, to 50 ml of different fruit juices taken in 250 ml erlenmeyer flask, 5ml of 2% chitosan solution in water was added. Grape, lemon and apple juices were used in this study. The optical density (OD) of the juices was measured at 540 nm in a spectrophotometer (Model Hitachi 2000) after filtering through cheesecloth. Results shown are Five milliliter of 2% chitosan solution was used to clarify 50 ml of fruit juices. A further increase in chitosan concentration did not improve the extent of clarification [14].

5 CONCLUSION

As a result, chitosan can be proposed as an alternative aid for juice clarification with high performance and low cost, since it is a natural abundant polymer. The present study suggests that treatment has no impact on the biochemical

parameters of the juices .Chitosan is a natural and abundant polymer, and due to its high performance and low cost, it can be a suitable and a more economic process for juice clarification. In that sense, further detailed physiological and sensory studies are required to determine the mechanisms of these effects.

REFERENCES

Degraded Image Restoration Using Neural Networks

Ibrahim Ipek¹, Nihan Kahraman²

Abstract

Image processing systems are used in different applications. Many methods have been developed to reduce adverse effects of blurred and noisy images formed for various reasons. However, sometimes it is very difficult to converge to original image due to high degradation. In order to determine this degradation rate and improve the quality of the picture, a neural network based system has performed including a database of various statistical statements. Three different interferences which are gaussian, blurring and speckle have been applied to eight different images which are used in literature commonly like Lena, photographer, Baboon etc. The inputs of neural network are some measures of degraded images such as peak signal to signal noise ratio (PSNR), mean absolute error (MAE), signal to signal noise ratio (SNR), universal image quality index (UIQI), Enhancement Measurement Error (EME), Pearson Correlation Coefficient (PCC), mean squared error (MSE), root mean squared error (RMSE). Output of neural network gives what is the original of the degraded image even it has much blurring effects or much noise. Furthermore, if degraded image is not in the database, the output is undefined. System proposed in this paper learned different algorithms of back propagation neural network including Levenberg-Marquardt training. One of the important matters is that the database has such images that have very low UIQI which means that a human being cannot predict the original image. 20 images were used as test images and the neural network has 90% accuracy.

Keywords: *Image restoration, neural networks, blurring*

1 INTRODUCTION

Image capturing devices sometimes cause errors of the scanning system like blur, distortions and imbalanced brightness distribution. These irregularities can otherwise lead to difficulties during further processing of the images like recognition. In general renovation performances are concerned with the recovery of the real image by applying a restoration process to its degraded version [1-4]. Some common methods for image restoration include the inverse filter, the Wiener filter, the moving-average filter, the parametric Wiener filter, the mean-squared-error filter, the band-pass filter and the singular value decomposition technique, as well as, the regularization filter. One of the oldest methods is a research using central weighted filter by Yang at al. Pitas and friends determined the difference between linear and nonlinear filters effect on noisy images. Xiao and Li studied central weighted filter including different dimensioned convolution masks, however they succeeded on little images that have very low noise distribution. Chan at al. used edge preserve approach on salt-pepper noise. This study has a good accuracy on simple noises whereas bad accuracy in Gaussian noise. Hillery at al. suggested iterative Wiener filter algorithm for restoration of noisy images. Wiener filters are thriving methods but they need prior knowledge of original image [3-4]. Polat and Yıldırım [5] have also used artificial neural networks in restoration of low impulse noise and they achieved more success than median filters.

In this work, we have used artificial neural networks for deblurring and restoration of artificially blurred images. There are some studies in the literature for denoising images using neural networks [6-13]. We have applied image quality measurements for defining the noise or blur effect to neural network [14]. We have trained the neural network with quality measurement values of 302 artificially degraded images and tested with highly noised or blurred ones. We have used 12 different training algorithms for MultiLayer Perceptron [15-16].

This paper first explains the quality measurements in images, the neural network architecture that used in this work in section two and three respectively. Last part gives the simulation result with comparisons. Finally the paper concludes with discussions and future works.

2 NOISE AND QUALITY MEASUREMENTS

Image noise rises because of unpredictable processes results going on capturing and production of the real signal depending on its source. In this paper, three different interferences which are Gaussian noise, blurring and speckle have been applied to eight different images which are used in literature commonly like Lena, photographer, Baboon etc.

¹Arçelik A.S, Cumhuriyet Mah. E5 Yanyol No:1 Beylikdüzü, İstanbul

² Corresponding author: Yıldız Technical University, Department of Environmental Engineering, 34220, Esenler/İstanbul, Turkey.
nicoskun@yildiz.edu.tr

Gaussian noise can be defined as Eq. 1. Here x is the grey level index, μ is the center and σ is the variance of the Gaussian noise. It can be reduced using spatial filtering techniques including mean filtering or median filtering. However, it must be noticed that when smoothing an image, we reduce not only the noise, but also the image details because they also correspond to blocked high frequencies.

$$P(x) = \frac{1}{\sigma\sqrt{2\pi}} e^{-\frac{(x-\mu)^2}{2\sigma^2}} \quad (1)$$

Blurring images may not seem like a useful operation, but actually is very useful for generating background effects and shadows. It is an integral part of image resizing, though a different method of blurring, which is restricted to within the boundaries of a single pixel of the original image. The blurring is characterized by a Point-Spread Function (PSF) or impulse response. The PSF is the output of the imaging system for an input point source. Figure 1 shows the blurring effects on 'Baboon' image.

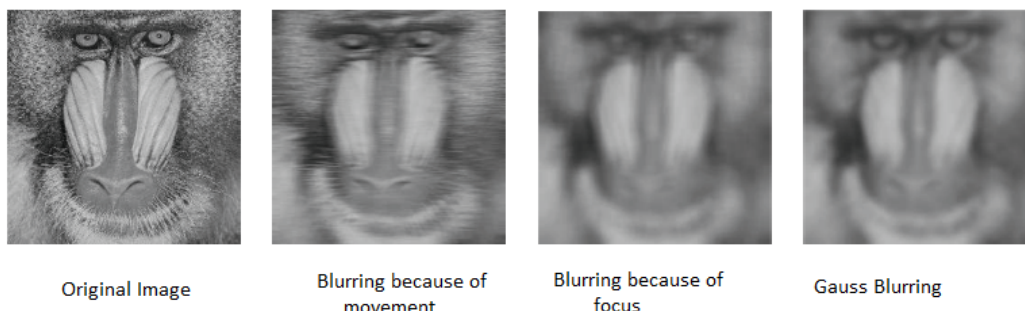


Figure 1. Some simple images for different blurring effects

Speckle is a particular type of noise which degrades the fine details and edges definition and limits the contrast resolution by making it difficult to detect small and low contrast lesions in body.

There are some quality measurements on degraded images [14]. These are peak signal to signal noise ratio (PSNR), mean absolute error (MAE), signal to signal noise ratio (SNR), and universal image quality index (UIQI), Enhancement Measurement Error (EME), Pearson Correlation Coefficient (PCC), mean squared error (MSE), root mean squared error (RMSE). MSE is usually used in statistical approaches but here it gave one of the degradation rates for images. The little MSE shows the little similarity between degraded image and original image. Equation 2 and 3 give the MSE and PSNR values respectively. Here, x is the original image and y is the test image where N is the pixel number [14].

$$MSE = \frac{1}{N} \sum_{i=1}^N (x_i - y_i)^2 \quad (2)$$

$$PSNR = 10 \log \frac{255^2}{MSE} \quad (3)$$

RMSE is obtained by taking the square root of MSE. Usually it is expected to be low. MAE is the mean of total absolute difference between two images. It can be calculated using Equation 4 [14].

$$MAE = \frac{1}{n} \sum_{i=1}^n |f_i - y_i| = \frac{1}{n} \sum_{i=1}^n |e_i| \quad (4)$$

Instead of using traditional error summation methods, Universal Image Quality Index, UIQI, has a combination of three factors: loss of correlation, luminance distortion, and contrast distortion. Figure 2 shows the measurements values on MATLAB using one of the images in this work.

```

Command Window
noisyImage is NOT type: uint8
PSNR = +20.40353 dB
MSE = 597.20915
RMSE = 24.43786
Universal Image Quality Index = 0.09208
EME (original image) = 9.99675
EME (noisy image) = 1.54032
PearsonCorrelationCoefficient (originalImage vs noisyImage) = 301468.31328
PearsonCorrelationCoefficient (originalImage vs originalImage) = 393215.00000
The noise is NOT relevant.
SNR = -3.71004 dB
MAE = 17.57570
fx >> |
    
```

Figure 2. The measurements values on MATLAB

Below, the images used in this work can be seen from Figure 3. They are well known images in literature like Lenna, cameraman, Baboon etc.

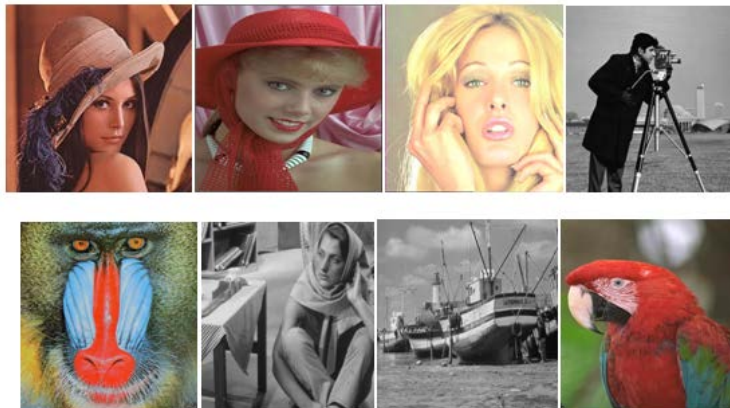


Figure 3. The database sample images

3 ARTIFICIAL NEURAL NETWORK BASED RESTORATION

We have used MultiLayer Perceptron architecture for classifying the degraded images into original ones. The inputs of neural network are some measures of degraded images such as peak signal to signal noise ratio (PSNR), mean absolute error (MAE), signal to signal noise ratio (SNR), universal image quality index (UIQI), Enhancement Measurement Error (EME), Pearson Correlation Coefficient (PCC), mean squared error (MSE), root mean squared error (RMSE). Output of neural network gives what is the original of the degraded image even it has much blurring effects or much noise. Figure 4 shows the structure of neural network. Furthermore, if degraded image is not in the database, the output is undefined. System proposed in this paper learned different algorithms of back propagation neural network including Levenberg-Marquardt training.

Here, we have applied image quality measurements for defining the noise or blur effect to neural network. We have trained the neural network with quality measurement values of 302 artificially degraded images and tested with highly noised or blurred ones. We have used 12 different training algorithms for MultiLayer Perceptron [15-16]. These training algorithms are `trainlm`, `traingd`, `traingda`, `traingdx`, `trainrp`, `trainbfg`, `trainbr`, `traincgb`, `traincgf`, `traincgp`, `trainscg` and `trainoss`. The details about the differences for algorithms can be found in MATLAB.

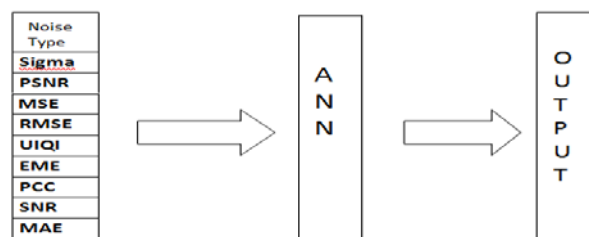


Figure 4. Inputs for ANN

For MLP parameters, learning rate and momentum coefficient are chosen as 0.1 and 0.9 respectively. After 100 iterations in 1.12 minutes for training we have applied test images and we obtained 90% test accuracy. Figure 5 shows some samples for test images. First image for each sample in Figure 5 is the original image where the second is degraded. It can be seen that the degradation rate is so high that even for a person it is very difficult to understand which image it belongs to.

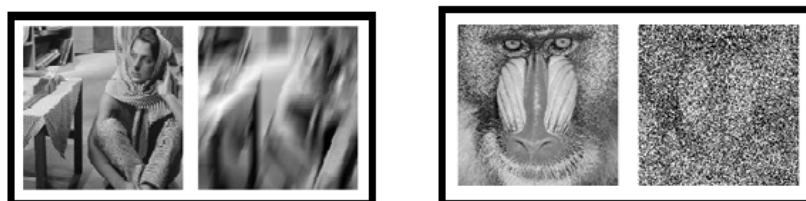


Figure 5. Some samples for test images

Table 1: Test images recognition accuracies after restoration via neural networks

#	Image name	UIQI	True (T) / False (F)	#	Image name	UIQI	True (T) / False (F)	Training Algorithm	Test Accuracy
								trainlm	%90
								trained	%20
1	Papagan	0,010	T	11	Boat	0,055	T	traineda	%30
2	Papagan	0,251	T	12	Yellow	0,029	T	trainedx	%15
3	Lena	0,186	T	13	Red	0,034	T	trainrp	%35
4	Red	0,021	T	14	Papagan	0,040	T	trainbfg	%30
5	Elaina	1,000	F	15	Cameraman	0,175	T	trainbr	%15
6	Yellow	0,133	T	16	Lena	0,067	T	traincgb	%15
7	Cameraman	0,189	T	17	Lena	0,032	T	traincxf	%10
8	House	1,000	T	18	Monkey	0,058	T	traincgp	%20
9	Monkey	0,241	T	19	Barbara	0,163	T	trainscg	%25
10	Barbara	0,056	F	20	Red	0,092	T	trainoss	%30

4 CONCLUSION AND FEATURE WORKS

This paper proposes an artificial intelligence method for restoration of the degraded image due to errors of image capturing devices. The methodology depends on the quality measurements in images and uses them as inputs to neural network architecture. MultiLayer Perceptron architecture is used for classifying the degraded images into original ones. For MLP parameters, learning rate and momentum coefficient are chosen as 0.1 and 0.9 respectively. After 100 iterations in 1.12 minutes for training we have applied test images and we obtained 90% test accuracy. For future work of image degradation, another artificial intelligence methods can be used or the database can be widened by variations of blurring effects.

REFERENCES

- [1] M. Bertero, P. Boccacci, "Introduction to Inverse Problems in Imaging", Philadelphia, Bristol, 1998.
- [2] R.C. Gonzalez, R.C. Woods, "Digital Image Processing", New York, Addison Wesley, 1992.
- [3] Akar, E.O., (2006). Tarihi görüntülerin kalitesinin görüntü işleme teknikleri kullanılarak artırılması, Yüksek Lisans Tezi, Selçuk Üniversitesi Fen Bilimleri Enstitüsü, Konya.
- [4] Saba, T., Rehman A. ve Sulong G., (2010). "An Intelligent approach to image denoising", Journal of Theoretical and Applied Information Technology, 17(No1): 32-36.
- [5] Polat, Ö. ve Yıldırım T., (2005). "Yapay sinir ağları ile sayısal görüntülerdeki yüksek yoğunluklu dürtü gürültüsünün azaltılması", IEEE 13. Sinyal İşleme ve İletişim Uygulamaları Kurultay kitabı, 16-18 Mayıs, Kayseri.
- [6] Kung, C., Yang W., Huang, C. ve Kung, C.(2010). "Investigation of the Image Quality Assessment using Neural Networks and Structure Similarity", Proceedings of the Third International Symposium on Computer Science and Computational Technology, 219-222, Jiaozuo, 14-15 Ağustos 2010.
- [7] Cho, C.M. ve Don, H.S., (1991). "Blur Identification and Image Restoration Using a Multilayer Neural Network", Neural Networks, 1991 IEEE International Joint Conference, 3: 2558 – 2563, 18-21 Kasım 1991.
- [8] Subashini, P., Krishnaveni, M. ve Singh, V., (2011). "Image Deblurring Using Back Propagation Neural Network", World of Computer Science and Information Technology Journal, 1(6): 277-282.
- [9] Ming, J. ve Zhenkang, S., "A novel neural network for object recognition with blurred shapes" Circuits and Systems, (1992). ISCAS '92. Proceedings., 6: 2901 – 2904.

- [10] Aizenberg, I., Paily, D. ve Astola J.T., (2006). "Multilayer Neural Network based on Multi- Valued Neurons and the Blur Identification Problem" 2006 International Joint Conference on Neural Networks, Temmuz 16-21, 2006, Vancouver.
- [11] Aizenberg, I., Jacob, J. ve Alexander, S.,(2011). "Classification of Blurred Textures using Multilayer Neural Network Based on Multi-Valued Neurons", Proceedings of International Joint Conference on Neural Networks, 31 Temmuz- 5 Ağustos 2011, San Jose.
- [12] Liu, Z.W. ve Zhao, P.,(2011). "Parameters Identification for Blur Image Combining Motion and Defocus Blurs using BP Neural Network" ,Image and Signal Processing (CISP), 2011 4th International Congress, 2 : 798 – 802 15-17 Ekim.
- [13] Dangeti, S.,(2003). Denoising Techniques – A Comparison, Master Thesis, Graduate Faculty of the Louisiana State University, Baton Rouge.
- [14] Chan M., (2010), Image Error Measurements, <http://www.mathworks.com/matlabcentral/fileexchange/29500-image-error-measurements>, 10 Şubat 2012.
- [15] Coşkun N. ve Yıldırım T., (2003). " The Effects of Training Algorithms in MLP Network on Image Classification ", International Joint Conference on Neural Networks (IJCNN), 2:1223-1226, Temmuz 20-24 2003, Portland.
- [16] Kiran I., Devi M.P. ve Lakshmi G.V., (2011). "Training Multilayered Perceptrons for Pattern Recognition: A Comparative Study of Five Training Algorithms", Proceedings of the International Multiconference of Engineers and Computer Scientists 2011,1,Mart 16-18, Hong Kong.

Experimental Modal Analysis of a Polyurethane Sandwich Panel

Murat Sen¹, Orhan Cakar²

Abstract

Polyurethane (PU) sandwich panels are widely used in engineering applications because PU foam has good vibration and acoustic properties as well as favorable thermal properties. Moreover, the top and bottom layers of the panel are corrugated in order to improve its strength properties. Depending on its place and type of application, different densities and reinforcement thicknesses of PU foam may be preferred and currently a variety of PU sandwich panels can be found on the market. In this study, the vibration characteristics of a standard PU foam sandwich panel, with corrugated top and bottom steel layers, are investigated. The modal properties of an example sandwich panel, which currently exists on the market, are determined by using experimental modal analysis (EMA). Additionally, ANSYS finite element software is used to determine the natural frequencies and mode shapes of this test sample. The results have been comparatively presented.

Keywords: natural frequency, modal damping, modal test, polyurethane foam, vibration isolation

1. INTRODUCTION

Due to various reasons, unwanted vibrations may occur on the dynamic systems. These unwanted vibrations can damage the system and affect the performance of the system adversely. Therefore, the dynamic properties of the system, namely natural frequency, mode shape and damping should be determined by performing dynamic analysis and necessary precautions should be taken. Plate structures are used in many areas of engineering. In order to improve the strength and the vibration properties of the plates, the sandwich panels are preferred. Sandwich structures consist of a number of layers that can be made different materials. Basically a sandwich panel consists of two face sheets and a core material. The face sheets are usually thin but it is corrugated with different forms in order to improve the strength properties. The core material is used to gain additional properties such as thermal properties, strength and vibration damping. The PU (polyurethane) foam material is preferred for vibration isolation applications due to the advantages of low production cost, light in weight and easy implementation to the systems. Hence the PU foam is widely used in the sandwich panel production. Therefore, it is very important to determine the dynamic characteristics of these structures.

There are many studies on the determination of dynamic properties of PU foam materials due to the mentioned advantages above. Davies et al. [1] studied the estimation of parameters of PU foam experimentally. They used a test system and modelled the system with a single degree of freedom foam-mass system and formulated a system identification procedure. They modelled PU foam as a linear viscoelastic material. They built their study on modelling the free response of the system with Prony series and by fitting them to the data. They used this estimated response model for estimating the parameters of the system model. Considering the presence of weak components and experimental noise, they improved the robustness of their test procedure by making some modifications on the system. They obtained the stiffness, viscous and viscoelastic parameters of the system by applying the procedure to the experimental data. Then, Davies et al. [2] gave a hereditary model and a fractional derivative model, by combining nonlinear elastic (represented by a polynomial function of compression) and linear viscoelastic (represented by a hereditary integral with a relaxation kernel consisting of two exponential terms in the hereditary model and by a fractional derivative term in the fractional derivative model) properties into the models, for the dynamic properties of flexible PU foams used in automotive seat cushions. They obtained the direct nonlinear optimization based formulations of the system identification procedures and a suboptimal method. They compared the performances of two models for the data with different compression and the input excitation levels, and they investigated the role of the viscous damping term in both types of models.

Patel et al. [3] investigated the suitability of low density PU foams for mimicking human osteoporotic cancellous bone by performing quasi-static compression tests on PU foam cylinders of different lengths and densities to determine the Young's modulus, yield strength and energy absorbed to yield. After their experimental studies, they presented that 16g/cm³ PU foam may prove to be suitable as an osteoporotic cancellous bone model.

Scarpa et al. [4] studied on analyzing the static and dynamic characteristics of conventional open cell, negative Poisson's ratio and iso-density PU foams. For the conventional form, they used gray open-cells PU foam with 30-35

¹ Corresponding author: Dept. of Mechanical Eng., Firat University, 23200, Elazığ, Turkey. msen@firat.edu.tr

²Dept. of Mechanical Eng., Firat University, 23200, Elazığ, Turkey. cakaro@firat.edu.tr

pores/inch and 0.0027 g/cm^3 density. They measured Poisson's ratio under quasi-static conditions by using a servo hydraulic test machine and a video image acquisition system. They performed the transmissibility tests in accordance with the ISO 1753 procedure for anti-vibration glove materials. In their study, they founded the transmissibility was greater than 1 within the frequency range from 10 to 31.5 Hz and it was less than 1 for the frequencies greater than 31.5 Hz. They suggested that the resilient behavior of glove isolation materials should be evaluated in terms of the indentation properties. Also, they suggested that foams with negative Poisson's ratio offered a significant decrease in compressive stresses with respect to convenient PU foams.

Barbieri et al. [5] investigated the physical parameters of sandwich beam made from association of hot-rolled steel, PU rigid foam and high impact polystyrene used for the assembly of refrigerators by using measured and numerical Frequency Response Functions (FRFs). In their study they utilized the finite element method (FEM) and the Timoshenko Beam Theory for mathematical models. They estimated Young's modulus and the loss factor of the PU rigid foam and the high impact polystyrene by using the amplitude correlation coefficient and genetic algorithm.

Havaldar and Sharma [6] presented an experimental study on the determination of the dynamic characteristics of multilayer polyurethane foam glass/fiber composite sandwich panels. They determined the natural frequencies, mode shapes and damping ratio of rectangular sandwich panels with 56, 82 and 289 kg/m^3 PU foam in different boundary conditions. They verified their experimental results with those of FEM, with good agreement. They presented in their study that there was a significant variation in the dynamic parameters in the case of multilayer sandwich panels for the same core density as compared to a monolayer sandwich panel.

In this study, the vibration characteristics of a standard PU foam sandwich panel, with corrugated top and bottom steel layers, are investigated. The modal properties of an example sandwich panel, which currently exists on the market, are determined by using EMA. Additionally, ANSYS finite element software is used to determine the natural frequencies and mode shapes of this test sample.

In this study, the effects of polyurethane foam which is widely used as sandwich structures in vibration isolation for plate vibrations have been investigated by using experimental modal analysis(EMA). For this aim, the experimental modal analysis of a standard 80 mm thickness of PU foam reinforced corrugated sandwich panel, used in engineering applications, with 38 kg/m^3 and $1000 \times 1000 \text{ mm}^2$ dimensions has been performed. Also, the structure has been modelled by using ANSYS finite element software and vibration analysis has been performed. The results have been comparatively presented.

2. MATERIALS AND METHODS

In this study, experimental modal analysis and FE methods were used to determine the dynamic characteristics of the sandwich panel. In EMA, the investigated system is excited by a measured force and the response of the system is measured. From these measurements, Response/Impulse ratio of the system is determined. This ratio is called Frequency Response Function (FRF) in vibration theory.. The FRF specifies the dynamic characteristic of the system and expresses the relationship between input and output of the linear system.

The measured FRFs can be used to determine the dynamic characteristics (natural frequency, mode shape and damping) of the system. In addition, FRFs are utilized for the verification of the results obtained from numerical solutions and the structural modifications.

In the modal test, the structure under investigation is excited by a modal hammer or a shaker and the applied force and the responses of the structure are measured using force transducer and accelerometer(s), simultaneously. The frequency response functions (FRFs) are calculated by using a frequency analyzer. A typical modal test setup using modal hammer is seen in Figure 1. Usually the test piece is suspended by elastic cords to satisfy free boundary conditions, which is reasonably easier and more trustworthy for comparing other boundary conditions.

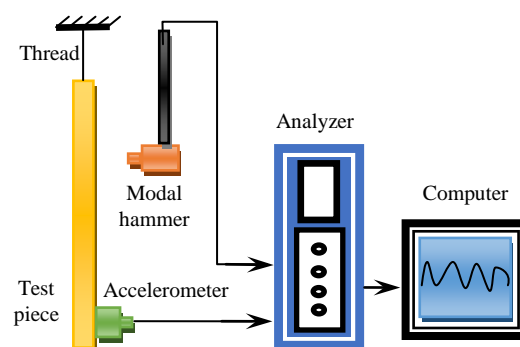


Figure 1. The Schematic of Modal Testing System

3. EXPERIMENTAL STUDIES

In this study, EMA of a standard 80 mm thickness of PU foam reinforced corrugated sandwich panel, used in engineering applications, with 38 kg/m^3 and $1000 \times 1000 \text{ mm}^2$ dimensions was performed. Experimental studies were carried out at Firat University, Machine Theory and Dynamics Laboratory. The sandwich panel was partitioned with 200 mm intervals and 36 measurement points on the panel were determined as shown in Figure 2. Then the plate was hinged to a stand from its two corners by using fiber strings to ensure free boundary conditions



Figure 2. PU Reinforced Corrugated Sandwich Structure

In the testing process, to excite the structure, a modal hammer (KISTLER, Model: 9724A2000 S/N 2069942) and to measure the response of the plate an ICP accelerometer (DYTRAN, Model: 3097A2 S/N2373) were used. For data acquisition and signal processing an OROS OR36 vibration analyzer and for the identification of modal parameters OROS Modal software were used. The test system are seen in Figure 3.



Figure 3. The Experimental Modal Analysis Test System

Before the measurements, some calibration tests such as repeatability and reciprocity checks were performed. Also, the time response of the system was observed and it was seen that the vibration was died in the measurement time, (Figure 4). Therefore, a windowing function was not applied to the signals, and so the additional damping effect, would be caused due to windowing function, has been eliminated.

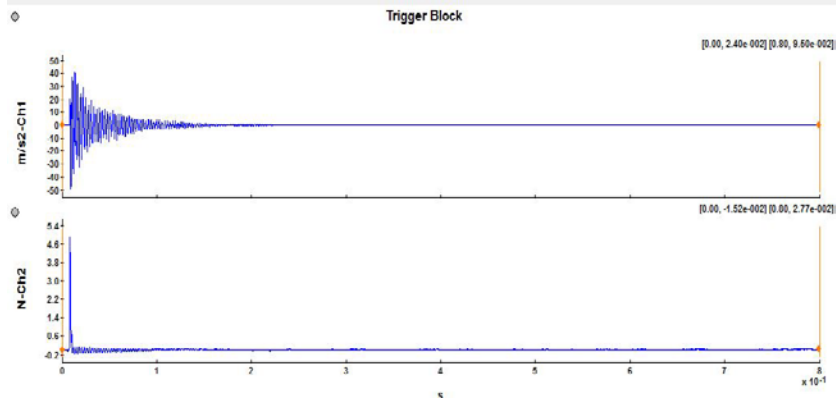


Figure 4. Time Signals Obtained From Force and Accelerometer Transducers

The accelerometer was located at the first node of the test piece (by using wax) because this node is very suitable for determining the dynamic properties of the panel over a wide frequency bandwidth for free boundary conditions. The test piece was sequentially hit at nodes 1 to 36 with the modal hammer and 36 FRFs were measured. The Measurement parameters used for the test of the PU reinforced sandwich structure are given in Table 1.

Table 1. Measurement Parameters of Experimental Study of PU Reinforced Sandwich Structure

Parameter	
Frequency Bandwidth	0-2000 Hz
Frequency Resolution	1.25 Hz
Sampling Number	1600
Measurement Time	0.8 s
Windowing (response/impulse)	(uniform/uniform)

Measured FRFs were analyzed and the modal properties were determined. Obtained natural frequencies and modal damping values are given in Table 2.

Table 2. Natural Frequencies and Damping Ratios for the first five modes

Mode	Experimental (Hz)	Damping (%)	ANSYS (Hz)	Difference (%)
1	114.29	1.06	113.93	0.31
2	139.60	1.08	142.68	2.15
3	174.56	0.17	174.65	0.05
4	198.27	1.18	198.98	0.35
5	217.96	1.20	231.28	5.75

For the comparison, the sandwich panel was also analyzed by using ANSYS FE software. FE model of the sandwich panel is seen in Figure 5 and the properties of PU foam material used for ANSYS model are given in Table 3. In the model 73725 nodes and 15136 elements were used. The natural frequencies obtained from ANSYS are compared in Table 2. The largest difference is 5.75% for 5th mode, the model is very satisfactory.

Table 3. Mechanical and Physical Properties of PU Material

Modulus of Elasticity (E)	Shear Modulus (G)	Poisson Ratio (ν)	Density (ρ)
4 MPa	2 MPa	0.45	38 kg/m ³

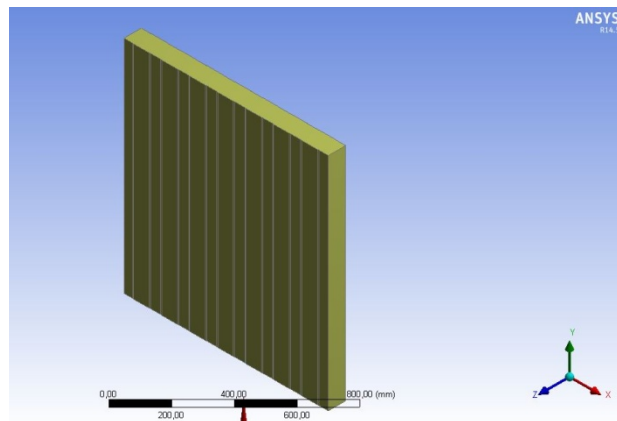


Figure 5. The ANSYS Model of PU Reinforced Corrugated Sandwich Structure

Also the first five mode shapes of the sandwich panel obtained from both EMA and FE (lower site in the figure) methods are compared in Figures 6-15.

Figure 6. Experimental mode 1

Figure 7. Numerical (ANSYS) mode 1

Figure 8. Experimental mode 2

Figure 9. Numerical (ANSYS) mode 2

BroBand : Mode 3 - Freq. 174.56Hz, Damp. 0.17%

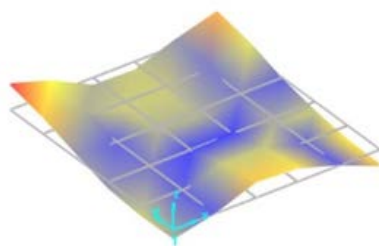


Figure 10. Experimental mode 3

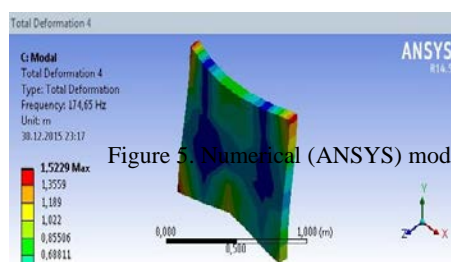


Figure 11. Experimental mode 3

BroBand : Mode 4 - Freq. 198.27Hz, Damp. 1.18%

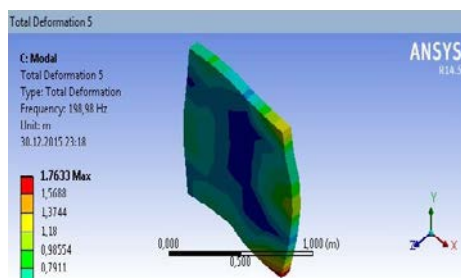
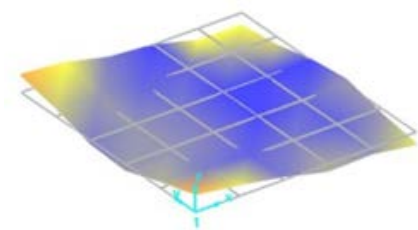


Figure 12. Experimental mode 4 Figure 13. Numerical (ANSYS) mode 4

BroBand : Mode 5 - Freq. 217.96Hz, Damp. 1.20%

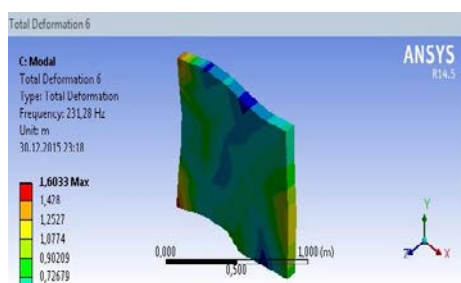
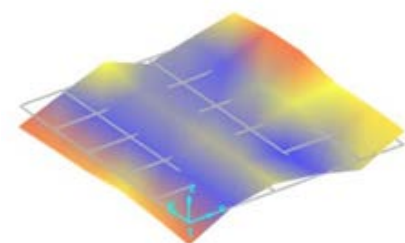


Figure 14. Experimental mode 5 Figure 15. Numerical (ANSYS) mode 5

4. CONCLUSIONS

PU reinforced sandwich structures are widely used in engineering applications. According to application place and type, different density and different reinforcement thickness of polyurethane foam can be preferred. In this study, the dynamic characteristics of a standard, 80 mm PU reinforced corrugated sandwich panel with 38 kg/m^3 density and $1000 \times 1000 \text{ mm}^2$ dimensions have been examined by using experimental modal analysis method. The experimental results are given with those of ANSYS finite element software comparatively. The results obtained from experimental and numerical methods are very close to each other as seen in Table 2. The highest difference is obtained in the fifth natural frequency with 5.75% and the lowest difference is obtained in the third natural frequency with 0.05%. Also, for the first five modes, third mode has the lowest damping ratio with 0.17% and the fifth mode has the highest damping ratio with 1.20%.

REFERENCES

- [1] Singh R., Davies P. and Bajaj A. K. Estimation of the dynamical properties of polyurethane foam through use of Prony series. *Journal of Sound and Vibration*, 264, 1005–1043, 2003.
- [2] Deng R., Davies P. and Bajaj A. K. Flexible polyurethane foam modeling and identification of viscoelastic parameters for automotive seating applications, *Journal of Sound and Vibration*, 252, 391–417, 2003. S. Zhang, C. Zhu, J. K. O. Sin, and P. K. T. Mok, "A novel ultrathin elevated channel low-temperature poly-Si TFT," *IEEE Electron Device Lett.*, vol. 20, pp. 569–571, Nov. 1999.
- [3] Purvi SD Patel, Duncan ET Shepherd and David WL Hukins. Compressive properties of commercially available polyurethane foams as mechanical models for osteoporotic human cancellous bone, *BMC Musculoskeletal Disorders*, doi:10.1186/1471-2474-9-137, 2008. R. E. Sorace, V. S. Reinhardt, and S. A. Vaughn, "High-speed digital-to-RF converter," U.S. Patent 5 668 842, Sep. 16, 1997.
- [4] Scarpa F., Giacomini J., Zhang Y. and Pastorino P. Mechanical performance of auxetic polyurethane foam for antivibration glove applications, *Cellular Polymers*, 24 (5), 253-268, 2005. M. Shell. (2007) IEEEtran webpage on CTAN. [Online]. Available: <http://www.ctan.org/tex-archive/macros/latex/contrib/IEEEtran/>
- [5] Barbieri N., Barbieri R. and Winikes L. C., Parameters estimation of sandwich beam model with rigid polyurethane foam core, *Mechanical Systems and Signal Processing* 24-406-415, 2010. "PDCA12-70 data sheet," Opto Speed SA, Mezzovico, Switzerland.
- [6] Havaladar S. S. and Sharma R. S., Experimental investigation of dynamic characteristics of multilayer PU foam sandwich panels,

Comparing Dynamic Response of an Euler-Bernoulli Beam under a Concentrated Moving Load on Linear Viscoelastic Foundation between FEM and Galerkin Method

Muzaffer Metin¹, Arif Ulu¹, Ozgur Demir¹, Rahim Can Peker¹, Aytac Arikoglu²

Abstract

In this paper a balastless track with continuous support is modeled as simply supported Euler-Bernoulli beam on linear viscoelastic foundation. A concentrated moving load effects on the beam to represent the axle load of the moving train on the track. Two different solution methods are implemented, including Galerkin Method and Finite Element Method (FEM) to compare the responses. With the use of Galerkin Method, equation of motion is turned from PDEs to ODEs. Displacement of the midpoint of the beam is plotted in Mathematica by solving equation of motion. On the other hand, this system is modeled in FEM for the same conditions. Finally, dynamic behaviors of the beam under concentrated moving load are investigated in consideration the effect of various simulation scenarios like different rail pads, different train velocities and different support lengths by comparing Galerkin Method and FEM.

Keywords: Euler - Bernoulli beam, Galerkin Method, FEM, moving load, balastless track

1 INTRODUCTION

In railway engineering for recent decades moving load problems has been studying increasingly. In moving load problems immense investigations mainly was carried on and a lot of problems was investigated in terms of different cases [1]. It was studied that historical background and special cases of applications of the practical solutions in railway engineering. Their models had good compatibility with rail, tie and wheel set in wide range of frequency [2]. An extensive finite element model was studied for train-track interaction. In track model it was used Timoshenko beam theory and discrete supports. Also, non-linear effects such as rail lift-off, tie lift off and loss of wheel-rail contact were studied. In time domain, a new cutting and merging method, which finite long track can be modeled as infinite long track, was presented [3]. For moving mass and moving load, two models on Pasternak foundation were presented. For these cases normalized deflection and bending moment in terms of variation of velocity, stiffness and shear modulus were investigated [4]. A uniform beam, resting on elastic foundation under moving load with invariant speed was modeled and in the solution Fourier transform method was used in the article. It was presented that numerical results for maximum deflection [5]. Decreasing effect of the boundary conditions track model long was taken between 22.5 - 60 meters [6]. It was described that all kinds of railway structures and their analysis methods. Historically, track structures were showed and additionally train-track interaction models was mentioned. Then for different cases two track models were analyzed and it was suggested for future works [7]. For train-track structure issues dynamic models were studied and in frequency domain the several solutions of these problems were showed. A discrete support model was transformed into continuous support model and analyzed in frequency domain [8]. In the thesis it was investigated that ballastless and ballasted railway track models. Dynamic behavior of these track structures was studied by using analytical and numerical methods. In analytical method it was used that an Euler-Bernoulli beam resting on Winkler foundation model and moving force. In numerical method discrete support model was used in Ansys finite element package program [9]. Maximum deflections of an Euler-Bernoulli beam resting on linear and non-linear foundation with comparing between FEM and Galerkin method was investigated [10]. The transverse vibrations of passenger seat in a railway vehicle is studied in terms of different speeds for ballasted and ballastless track. In time domain it was studied that displacements and accelerations of the rail [11]. For the responses of a simply supported finite length Euler-Bernoulli beam, acted on moving mass, a dynamic Green function approach was used to find [12].

In this study, it is considered that a real train vehicle axle load and verified track properties. Real track is discrete support but in this work it transformed into continuous support model and analyzed. Rail, rail pads and track structure was modeled Euler-Bernoulli beam, continuous support and rigid structure, respectively. A closed form of mathematical model is discretized by Galerkin method. In Mathematica 9.0, ODEs are solved. In the next sections, it

¹Muzaffer Metin: Yildiz Technical University, Department of Mechanical Engineering, 34349, Beşiktaş/İstanbul, Turkey.
mmetin@yildiz.edu.tr

²Aytac Arikoglu: Istanbul Technical University, Department of Aeronautical Engineering, 34469, Ayazağa/İstanbul, Turkey.
arikoglu@itu.edu.tr

is introduced FEM for this study and compared with Galerkin method solutions. Track parameters is taken from a real railway track in Istanbul metro line (Figure 3).

2 DYNAMIC MODELING

A model of railway balastless track shows in Figure 1. Rail modeled as Euler-Bernoulli beam which is constant cross-section, homogeneous and simply-supported. At that time rail pads modeled as linear viscoelastic foundation that consist of spring and damping elements. This modeled railway track is a slab railway track which consist of rail and rail pads. In addition force is thought as an axle force of rail vehicle.

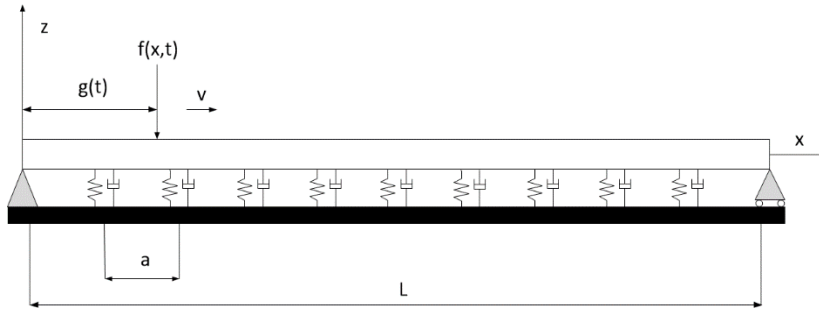


Figure 1. Discrete Supported Ballastless Track Model

Spring and damping terms of viscoelastic foundation added in Euler-Bernoulli beam theory. Equation is shown in (1);

$$EI \frac{\partial^4 z(x,t)}{\partial x^4} + \rho A \frac{\partial^2 z(x,t)}{\partial t^2} + k_L y(x,t) + c \frac{\partial z(x,t)}{\partial t} = \delta(x-vt) P_0 \quad (1)$$

where EI , ρ , A , c , k_L and $z(x,t)$ are flexural rigidity the density, the cross-sectional area, the damping coefficient, linear foundation stiffness, and transverse displacement of beam at point x and time t , respectively.

Right hand of equation is axial force represented by Dirac-delta function (2). P_0 is constant value of axial force. $g(t)$ represents kinematics of moving force as ϑ is constant speed of force (3).

$$f(x,t) = \delta(x-g(t)) P_0 \quad (2) \quad g(t) = vt \quad (3)$$

Dirac-delta function $\delta(x)$ is thought as a unit centered force acting at point $x=0$. Dirac-delta function is defined in equation (4).

$$\int_a^b \delta(x-vt) f(x) dx = f(\xi) \quad \text{for } a < \xi < b \quad (4)$$

Rail was modeled as simply-supported. So at $x=0$ and $x=L$ for boundary conditions are given in (5) and (6). Initial conditions are shown in (7) at $t=0$.

$$z(0,t) = z(L,t) = 0 \quad (5)$$

$$\frac{\partial^2 z(0,t)}{\partial x^2} = \frac{\partial^2 z(L,t)}{\partial x^2} = 0 \quad (6)$$

$$z(x,0) = \frac{\partial z(x,0)}{\partial t} = 0 \quad (7)$$

3 GALERKIN METHOD

By using Galerkin method transverse function $z(x,t)$ is transformed into two separate function (8). It is selected a sinus function $\sin\left(\frac{i\pi x}{L}\right)$ depending on x , in order to satisfy boundary conditions.

$$z(x,t) = \sum_{i=1}^N Q_i(t) \sin\left(\frac{i\pi x}{L}\right) \quad (8)$$

To imply separated $z(x,t)$ in equation 1, we differentiate depending on both x and t . Then differentiated $z(x,t)$ functions are relocated in equation 1, shown in (9).

$$\sum_{i=1}^N \int_0^L \left[EI \left(\frac{i\pi}{L} \right)^4 + k_L \right] Q_i(t) + \rho A \ddot{Q}_i(t) + c \dot{Q}_i(t) \sin\left(\frac{i\pi x}{L}\right) \sin\left(\frac{j\pi x}{L}\right) dx = P_0 \int_0^L \delta(x-vt) \sin\left(\frac{j\pi x}{L}\right) dx \quad (9)$$

Equation 9 is integrated from 0 to L, length of beam and simplified as following form

$$\left[EI \left(\frac{j\pi}{L} \right)^4 + k_L \right] Q_j(t) + \rho A \ddot{Q}_j(t) + c \dot{Q}_j(t) = 2 \frac{P_0}{L} \sin\left(\frac{j\pi vt}{L}\right), j=1,2,3,\dots,N \quad (10)$$

Initial conditions are shown in equation 11.

$$Q_j(0) = \dot{Q}_j(0) = 0 \quad j=1,2,3,\dots,N \quad (11)$$

4 FINITE ELEMENT METHOD

This chapter deals with the modeling techniques that are used to analyze the railway track in the commercial software ANSYS. The software performs the FEM analysis using the input data provided by the user. The development of the model and the definition of the simulation parameters are done using ANSYS Parametric Design Language (APDL). The finite element models were created in ANSYS Mechanical which includes the Graphical User Interface (GUI). This method of creating models is easier than coding an input file, especially when the models are large, as in the case with 3D models. The program includes a post-process tool capable to generate time dependent results for displacements, accelerations and forces of any element in the model.

After modeling the CAD model of the rail and foundation system, finite element model is prepared in ANSYS Mechanical. Schematic model of the track structure is shown in Figure 2. The effects of moving load are evaluated only for two direction, which are the force acting and moving directions. For this reason, FEM model is reduced to 2 dimensions, x and z (Figure 3).

There are several element types for finite element models to describe the engineering problems in ANSYS Mechanical. Two element types are used in this model. First, COMBIN14 (Figure 4) is used for damping and spring coefficients of viscoelastic foundation. BEAM188 is used for properties of the rail. Analysis type is considered as Transient Structural Analysis. To achieve the FEM model, the rail and viscoelastic foundation are discretized to 100 elements and 1 element, respectively. This model is shown Figures 3 and 5.

Simply support is applied both end of the rail and one side of the viscoelastic foundations. In this way it is fixed to the ground.

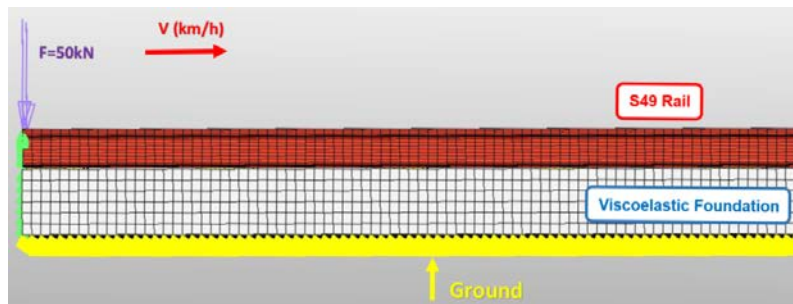


Figure 2. Schematic FE Model of Track Structure

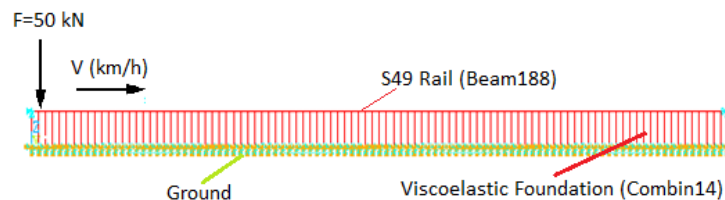


Figure 3. 2D-FE Model of Track Structure

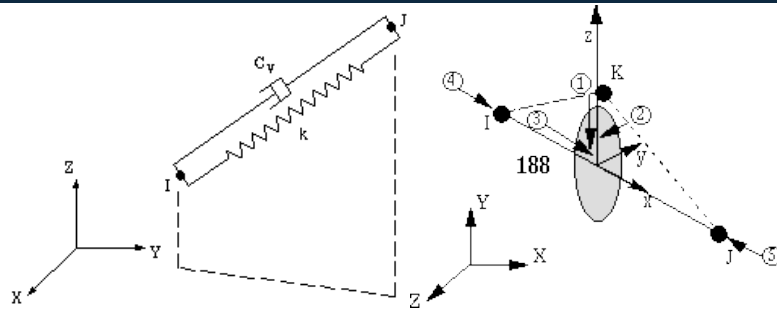


Figure 4. COMBIN14 and BEAM188 element models [13]

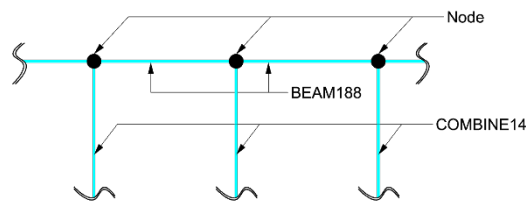


Figure 5. A section of FE Model of the Track Structure

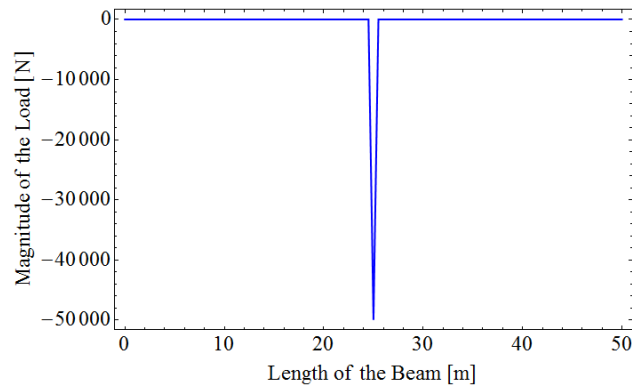


Figure 6. Magnitude of the loading along the railway

The function of moving axle load depends on time and location. It is applied to Beam188 element like distributed force (Eq. 12). Time-varying amplitude of this applied moving load function is shown in Figure 6. In equation 12, 'a' represents the force application gap.

$$F(x,t) = F_0 \sqrt{\frac{a}{\pi}} e^{-a(x-vt)^2} \quad (12)$$

5 COMPARASION OF THE METHODS IN VARIOUS SIMULATION CASES

Table 16. Properties of railway track components[9]

Properties of Track Components	
Young's modulus (N/m ²)	2.1x10 ¹⁰
Area moment of inertia (m ⁴)	1819x10 ⁻⁸
Cross sectional area (m ²)	
Density of the material (kg/m ³)	6297x10 ⁻⁶
Length of the beam (m)	7850
Linear spring stiffness (Linear foundation) (N/m)	50
Moving load (N)	90x10 ⁶
Support Length "a" (m)	50000
	0.75



Figure 7. ABB Railway Vehicle in working metro line



Figure 8. Ballastless Rigid Structure of Istanbul M1 metro line [9]

The moving load, which is used before measurements [9], is taken from axle load of real ABB railway vehicle for empty condition, shown in Figure 7. In Figure 8, investigated track structure in this paper is shown. In this section, it is tried to find that how the deflection at the midpoint of the beam is changed in time domain by comparing methods. Maximum deflections are investigated for several rail pads (Fc14, Fc864, 1403-N), speeds of load as 80 km/h (22 m/s), 40 km/h (11 m/s), 5 km/h (1.38 m/s) and support lengths (0.5 m, 0.6 m, 0.75 m).

5.1 Different Rail Pads

Maximum deflections of the rail, using different types and properties of rail pad, is shown in Figure 9. Bigger stiffness and damping coefficients of rail pads, less deflections of the midpoint of the beam is occurred. These rail pads, which properties are presented in Table 2, are usually used in Istanbul metro lines. The best solution between these pads for minimum deflection of the rail is 1403-N type as seen in figures. Maximum deflection is decreased about %38.2, when 1403-N type is used in railway track. In this simulation scenario, velocity and support length was taken 80 km/h and 0.75 m, respectively. Also, maximum deflections of the used methods are almost the same.

Table 2. Different Rail Pad Properties [9]

Rail Pad Types	Stiffness Coefficient (10^6 N/m)	Damping Coefficient (10^3 Ns/m)
Fc 14	90	4,1
Fc 864	125	8
1403 - N	171	17,1

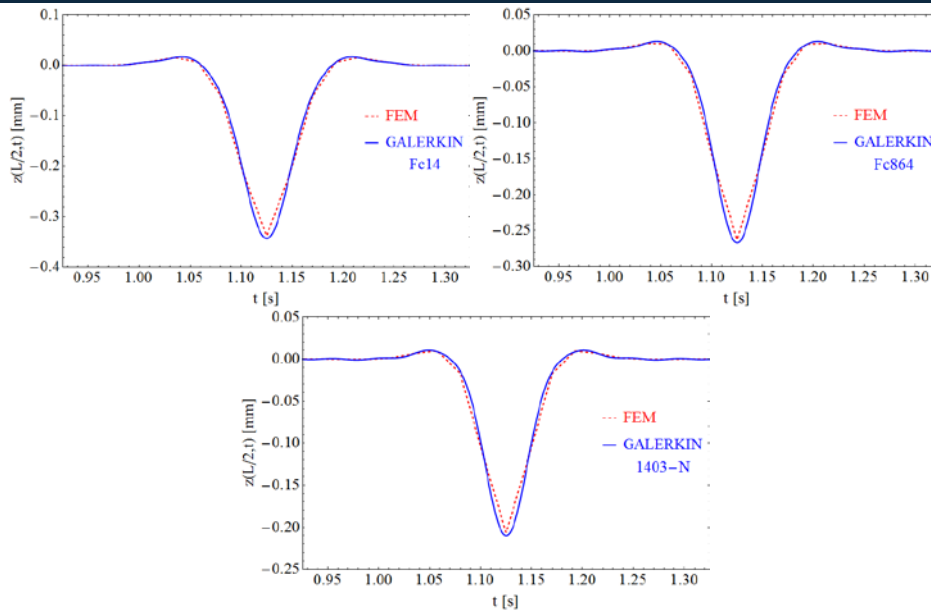


Figure 9. Deflection at the center of the beam for different rail pads (a) Fe14 (b) Fe864 (c) 1403-N

5.2 Different Train Velocities

Maximum deflections of midpoint of the beam depending on speed is shown in Figure 10. Train vehicle maximum design speed is 80 km/h, average train speed is 40 km/h and average closing the station speed is 5 km/h. Variant of the speed has no big effects on the deflection in linear modelling. The important effect of speed may be seen at non-linear modelling [10] or critical speed [4]. In this simulation scenario, support length and rail pad was taken 0.75 m and Fe 14, respectively. Also, maximum deflections of the used methods are almost the same.

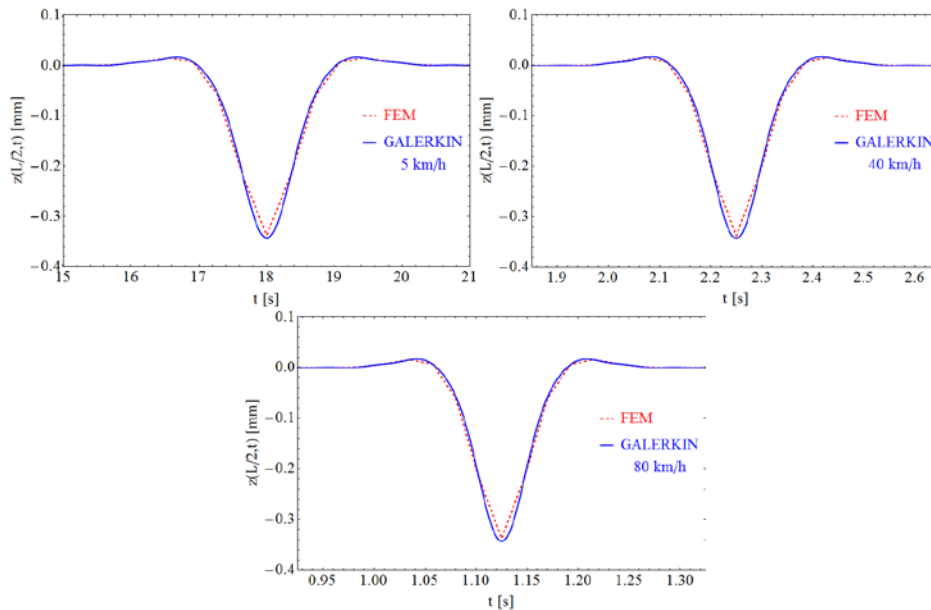


Figure 10. Deflection at the center of the beam for variable speeds (a) 5 km/h (b) 40 km/h (c) 80 km/h

5.3 Different Support Lengths

Maximum deflections of midpoint of the beam for different support lengths is shown in Figure 11. Using the longer support lengths, the bigger deflections are occurred at the center of the beam. Difference between 0.5 m and 0.75 m support lengths is approximately %26.5. For minimum deflection, in case of putting too many supports, it may be increased the total amount of track project. By taking into account dynamic and financial effects, an optimization is needed. In this simulation scenario, velocity and rail pad was taken 80 km/h and Fe 14, respectively. Also, maximum deflections of the used methods are almost the same.

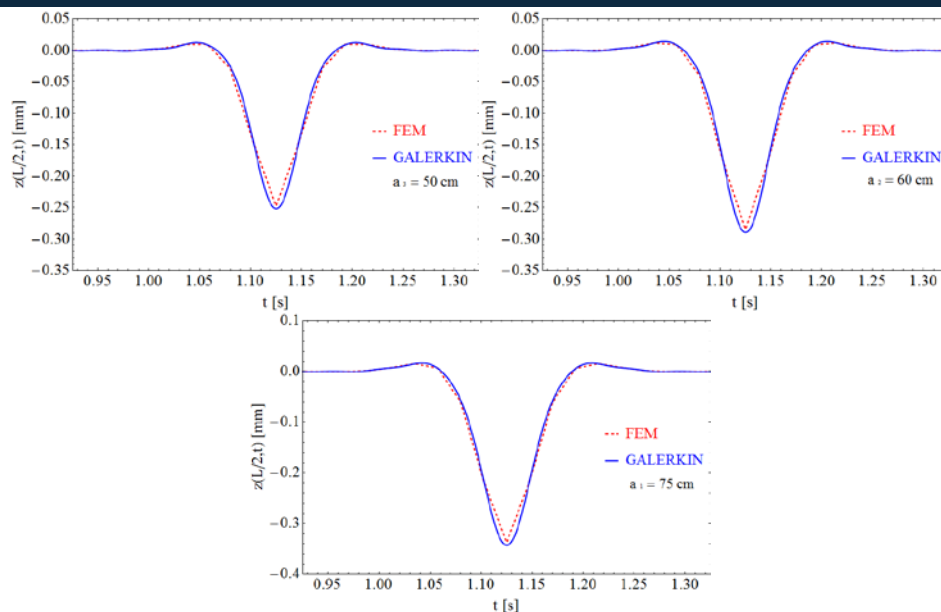


Figure 11. Deflection at the center of the beam for variable support lengths (a) 50 cm (b) 60 cm (c) 75 cm

6 CONCLUSIONS

A discrete support ballastless railway structure is modelled as continuous support Euler-Bernoulli beam theory in this study. Galerkin method is implied to discrete railway and ODEs are solved by using Mathematica package program, after gathering general equations of motion. Effects of the track elements on the dynamic response are investigated while changing track parameters. Used all track parameters was verified both analytical and numerical methods for dynamic and static analyses by Arlı [9]. Using 1403-N type rail pad and keeping shorter support length is minimizing maximum deflections of the rail. On the other hand, using shorter support lengths, for the smallest deflection, may increase price of the track for per length. So, it is need to be optimized between dynamic analysis and price. For the velocities, now it is no remarkable effect on deflection. Maybe in non-linear modelling or taking bigger speeds than critical speed [4] or more accurate modelling, it is supposed that surprising results will be revealed [10]. For all different cases, results are compared with Galerkin and FEM each other. So, analytical model and Galerkin method is verified by this way. In results, FEM graphics are not smoother because of the number of elements. When increasing the number of elements, the responses will be getting more sensitive.

In this paper, the effects of various dynamic scenarios on track modelling is showed and compared methods. Decreasing support length and using softer rail pads are effective ways to minimize deflections in ballastless tracks. Also, it is concluded that optimization problem between rail pads and price or more accurate modelling will be investigated in future works, where critical speeds will be considered.

ACKNOWLEDGMENT

The financial support of the Program for Scientific and Technological Research Projects (1001) by the Scientific and Technical Research Council of Turkey (TUBITAK) under Project No: 115M586 is gratefully acknowledged.

REFERENCES

- [1] Fryba, L., "Vibration of solids and structures under moving loads, third edition", Thomas Telford Ltd, Prague, Czech Republic, 1999.
- [2] Knothe, K., and Grassie, S.L., "Modeling of railway track and vehicle/track interaction at high frequencies", Vehicle System Dynamics, 22, pp 209-262, 1993.
- [3] Dong, R.G., "Vertical dynamics of railway vehicle-track system," Ph.D. Thesis, Dept. of Mechanical and Industrial Engineering, Concordia University, Montreal, Canada, 1994.
- [4] Uzzal, R., Analysis of A Three-Dimensional Railway Vehicle - Track System and Development of A Smart Wheelset, PhD Thesis, Concordia University, 2012.
- [5] Mallik, A. K., Chandra, S., and Singh, A. B., "Steady-state response of an elastically supported infinite beam to a moving load" Journal of Sound and Vibration, 291, pp 1148-1169, 2006.
- [6] Zakeri, J. A., Xia, H., Application of 2D-infinite beam elements in dynamic analysis of train-track interaction, Journal of Mechanical Science and Technology, 23, 1415-1421, 2009.
- [7] Yılmaz, V., Demiryolu Üstyapısının Dinamik Davranışı, Yüksek Lisans Tezi, YTU, 2004
- [8] Yalçın, S., Demiryolu Üstyapısının Dinamik Analizi, Yüksek Lisans Tezi, YTU, 2006.
- [9] Arlı, V., Demiryolu Titreşimlerinin Model Hat Üzerinde Çok Yönlü Analizi, Doktora Tezi, İTÜ, 2009.
- [10] Senalp, A. D., Arıkoğlu, A., Özkol, I., Doğan, V., "Dynamic response of a finite length Euler-Bernoulli beam on linear and nonlinear viscoelastic foundations to a concentrated moving force", Journal of Mechanical Science and Technology, 24, pp 1957-1961, 2010.

- [11] Yalcin, S., Guclu, R., Metin, M., & Yazici, H. ,” Analyses of Railway Induced Vibrations for Different Track Types”, The 36th International Congress & Exhibition on Noise Control Engineering, Inter-Noise, 2007.
- [12] Foda, M. A., and Abduljabbar, Z., “A dynamic green function formulation for the response of a beam structure to a moving mass”, Journal of Sound and Vibration, 210(3), pp 295-306, 1998.
- [13] Ansys Tutorials. [Online]. Available:http://www.ansys.stuba.sk/html/elem_55/chapter4/ES4-14.htm

A Novel Tool for Mining Access Patterns Efficiently from Web User Access Logs

Resul Das¹, Doygun Demiroglu², Gurkan Tuna³

Abstract

Almost all computer and information systems keep the records of transactions performed. These records can be utilized for many purposes such as detecting a web based attack, solving juridical cases, reconstructing electronic commerce web sites to develop product pages according to user behavior, and improving web application performance. On the other hand, log files store a great deal of information and it is not easy to process them. In this regard, the purpose of this study is to develop a new software tool which shows high performance in pruning web user logs stored in different forms on web servers. Using this tool, access log files can be quickly processed and unnecessary data can be removed. In this way, useful data can be obtained from access logs for information extraction and pattern analysis. Using this useful data, web designers and web administrators can improve their websites.

Keywords: Information extraction, log analysis, software development, web user access logs, Web usage mining

1 INTRODUCTION

In recent years, Internet usage has increased due to the variety of emerging communication tools, possibilities to keep personal and corporate information in digital environment and reduction in communication costs. The Internet has become a part of our lives since it is used to send/receive information and for social activities and official transactions. In addition, some private companies and governmental institutions perform a variety of applications through the Internet such as information/document sharing, education, electronic trading and banking. Therefore, compared to the past, not only service continuity but also information security has become much more important.

The users surfing the Internet leave traces on web servers, namely access logs. Analysis of these text-based logs provides useful data to system administrators for enhancing system performance and securing information. The analysis is typically carried out via web mining technique. Web mining allows converting distributed and huge data on the internet into meaningful and ordered one, which will lead eventually to discovery and analysis of a pattern [1, 2]. Through web usage mining, analysis of access logs of the users surfing on the internet, a lot of useful information can be obtained to improve existing web sites or develop more functional web sites which can increase marketing ability and determine visitor statistics [3-5].

In this paper, an effective and high performance software tool to prune access logs is proposed. By means of the proposed tool, log files can be read and unnecessary data can be removed quickly. In this way, statistical data can be obtained via various information extraction and pattern analysis techniques. For this objective, in this study, web mining pre-processing is performed and useful data which can help web designers and web administrators to improve their websites is provided. The proposed tool provides the following information and stores them in tables of a Microsoft SQL Server database.

- Statistical information about site traffic.
- Activity statistics of users at the web site.
- The distribution of users accessing the web site based on.
- The distribution of users accessing the web site based on month.
- Most accessed web pages by users.
- Most entered and exited web pages.
- The file extensions mostly accessed by accessing visitors.
- User request distributions based on web browsers, operating systems and accessing mobile devices.
- Statistics according to HTTP status code.
- Information about dangerous access.

¹ Corresponding author: Department of Software Engineering, Technology Faculty, Firat University, Elazığ, Turkey, resuldas@gmail.com

²Department of Computer Programming, Bingöl University, Bingöl, Turkey, doygundemiroglu@gmail.com

³Department of Computer Programming, Trakya University, Edirne, Turkey, gurkanatuna@trakya.edu.tr

The rest of the paper is organized as follows. Literature review is presented in Section 2. Section 3 explains the details of the proposed system. Finally, Section 4 concludes the paper.

2 RELATED WORK

Log files in which traces of transactions are recorded keep important and critical information about IT systems they are generated on. Especially, they play a key role in information security and business continuity. Computer Emergency Response Team (CERT) defines logs as activities or events recorded on computer systems [6]. It also presents detailed information about storing and managing log files generated by common database management systems such as Windows and Linux Web servers, Oracle and Microsoft SQL Server 2005 [6]. National Institute of Standards and Technology (NIST) defines log files as event records originating within a system or network of an enterprise or organization [7] and in [7] presents information about log file management and computer security in organizations.

Traditional access log analyzing tools provided similar functionalities as far as document accesses, even some early ones such as WebViz [8] provided path analysis and visualization. For log analysis tools, the absence of any a priori knowledge makes it difficult to obtain user profiles due to the enormous amount of historical data stored in access logs [9]. In this respect, unsupervised classification or clustering methods are well suited to analyse the semi-structured log data of user accesses. For this purpose, clustering user sessions based on pair-wise dissimilarities using a robust fuzzy clustering algorithm is proposed in [10]. Due to the emerging web-based applications, in recent years, analysis of log files has started to attract the attention of researchers more. In [11] Grace et al. present a detailed discussion about web log files and related information such as formats, uses, access procedures, and parameters. They also provide the idea of creating an extended log file and learning web user behavior through various algorithms used in web mining processes. Tyagi et al. in [12] investigate methods to collect and analyze log files. As they prove, access log statistics can be retrieved by various methods and by using web mining techniques, meaningful information that can help web designers and system administrators can be extracted. In [13] a novel method for the pre-processing step of web usage mining is proposed. Using this technique, data cleaning and transaction definition steps take less time compared to traditional methods.

Web usage mining can be described as the application of data mining methods to discover the knowledge hidden in web log files, such as user access patterns [14]. One of its emerging uses is to assess public response by analyzing web-based data such as Twitter and Google Trends [15]. However, the data stored in web log files consists of a great deal of misleading, erroneous, and incomplete information. In this respect, pre-processing step enables to transform logs into a set of web user sessions that are suitable for analyses. In [14] the importance of the preliminary phase of web mining procedure is discussed, methods which can be used for session identification are presented, and a sample evaluation study is carried out by using a web log file collected from a web server at NASA Kennedy Space Center. In a similar study [16] Daş et al. analyse user access logs of Firat University and proves that valuable information for system administrators and web designer can be obtained from log files using various approaches such as path analysis method [17] and genetic algorithms [18]. In this respect, with the example of Eindhoven University [19], Romero et al. show that web sites can be personalized with the data obtained from log files. Arbelaitz et al. in [20] presents the design of web mining system, which was built using the content of a tourism company website and the information from the log files stored in Common Log Format. The system they propose generates user navigation profiles in order to provide information for future web designs [20].

In addition to personalizing web sites [21], analysis of log files can serve for many other different purposes including commonly used purpose of securing e-commerce web sites and less used ones such as surveillance of illnesses and ascertaining the behavior of users accessing a website [22, 23, 24, 25]. Last but not least, analysis of log files can be used to investigate trends and suggest better search engine capabilities [26]. Although log analysis is typically carried out on servers, rather than server-side log analysis, a novel client-side tool to identify usage patterns based on client-side event logs is proposed in [27].

Different from the above-mentioned studies, rather than presenting the advantages of web log analysis and web usage mining techniques, in this study we present the details of the design steps of a tool which has an easy-to-use graphical user interface (GUI) and can quickly prune access logs stored in different forms on web servers. In this regard, the tool described in this paper both can enable system administrators to read access logs and remove un-necessary data in order to extract the information they need to improve the quality of provided services and can help developers to develop innovative tools for web log analysis.

3 PROPOSED TOOL

In this study, a data pruning tool for web user access logs is proposed. To ensure its efficiency and continuity, traditional software development life cycle was followed and the tool was developed using Visual C# and Microsoft SQL Server. When the tool is run, the first step of web usage mining is to obtain access log files from web servers and generate a session file. To run the tool successfully, the users can either use an existing database or create a new database. If a new database is created, its tables include information about data cleaning, user definition and session definition phases received from pre-processing step. In this way, it is possible to gain access to the statistics of the web sites under consideration. Pre-processing step is a prerequisite for discovering patterns in web usage mining since it improves the quality and efficiency of the later steps of web usage mining process [28, 29].

To transfer files into the database, freely available Microsoft Log Parser 2.2 software was used. When Microsoft Log Parser is installed in a directory, two files are created, namely “LogParser.dll” and “LogParser.exe”. “LogParser.exe” is an application which can be executed by sending parameters from command line. “LogParser.dll” is an Active X object and can easily be integrated into C# applications. The ActiveX object is saved to the registry as “MS Utility 1.0 Type Library - LogParser Interfaces Collection” key. “LogParser.dll” ActiveX object can be used with popular programming languages such as VBScript, C#, and JavaScript. With “MSUtil.LogQuery” class it is possible to create a LogParser object within the script languages. The overall architecture and GUI of the proposed tool are shown in Fig. 1 and Fig. 2.

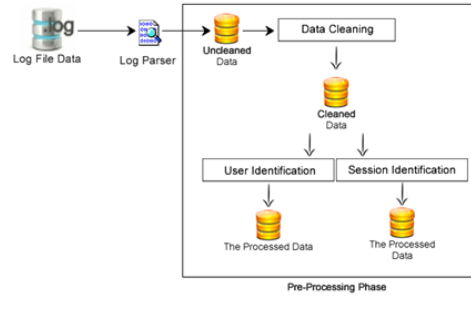


Figure 18. Overall architecture of the proposed tool.

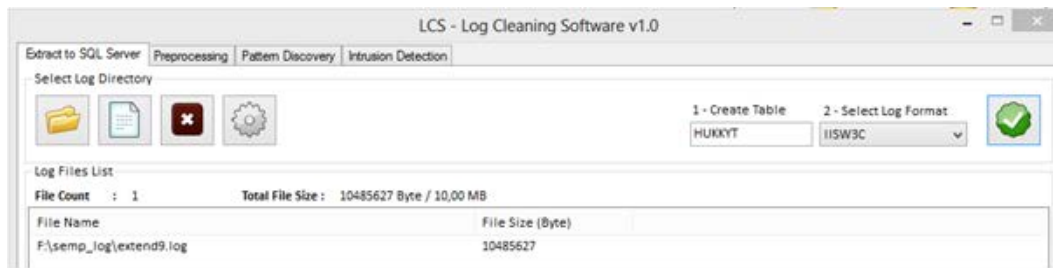


Figure 19. GUI interface of the proposed tool.

a. A. Transferring Access Logs

When a log file or a group of log files is selected in the tool’s GUI, its contents are splitted into fields and saved in a table. The splitting process is done by the “LogParser.dll” ActiveX object. Different log file formats including W3C, IIS, ODBC, and NCSA log files are fragmented by the

ActiveX object and the fragmented data is converted into pro-cess table systems like data tables. The lines of the log files transferred into the tables are processed through the preliminary phases of web usage mining. Fig. 3 shows a set of access logs transferred into the database.

	date	time	clp	csMethod	csUriStem	csUriQuery	scStatus
1	2007-03-30 00:00:00.000	09:01:20	65.55.208.93	GET	/robots.txt	NULL	404
2	2007-03-30 00:00:00.000	09:01:21	65.55.208.93	GET	/Default.asp	195f80004005[Microsoft][ODBC_Microsoft_Access_S...	500
3	2007-03-30 00:00:00.000	10:07:52	88.229.205.159	GET	/STYLES.CSS	NULL	200
4	2007-03-30 00:00:00.000	10:07:52	88.229.205.159	GET	/letism.asp	NULL	200
5	2007-03-30 00:00:00.000	10:07:52	88.229.205.159	GET	/stbkgde.gif	NULL	404
6	2007-03-30 00:00:00.000	10:07:52	88.229.205.159	GET	/images/topnav_bg.gif	NULL	200
7	2007-03-30 00:00:00.000	10:07:52	88.229.205.159	GET	/images/1_03.gif	NULL	200
8	2007-03-30 00:00:00.000	10:07:52	88.229.205.159	GET	/images/1_02.gif	NULL	200
9	2007-03-30 00:00:00.000	10:07:52	88.229.205.159	GET	/images/1_04.gif	NULL	200
10	2007-03-30 00:00:00.000	10:07:53	88.229.205.159	GET	/images/1_05.gif	NULL	200

Figure 20. Raw (unpruned) access logs in the database.

b. B. Pre-processing Step

The data transferred into the tables is first processed by the pre-processing step's phases, namely data cleaning, user identification and session identification. After the cleaning phase, unnecessary information eliminated from the data is transferred into a new table. As shown in Fig. 4, after each pre-processing phase, a new table is created and processed data is stored in these tables.

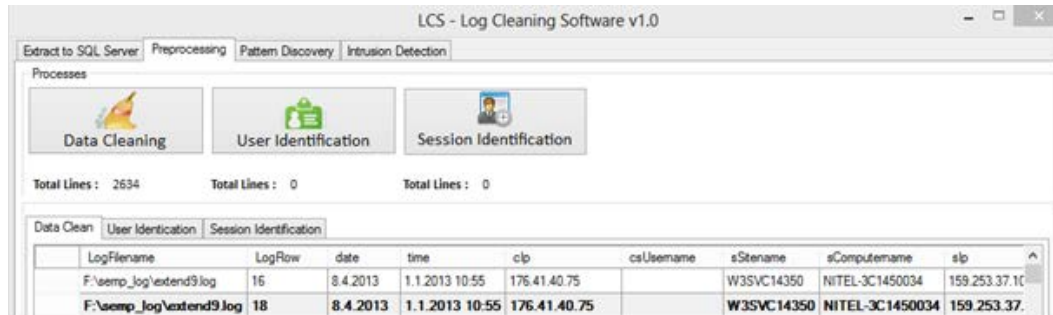


Figure 21. Pre-processing phases of the proposed tool.

Data cleaning

Raw data in access logs are not suitable for the web usage mining processes. Before the mining process, it must be processed to eliminate the records that are not usable or irrelevant to the mining process. When users access a web site, they do not just visit the site but also the embedded sources. Therefore, all objects such as images, videos, audios, and style and script files which carry information related to the design of the website are recorded in the log file after user access. The data on these lines must be removed since they are meaningless to the mining process. In the proposed tool, unnecessary lines are removed using a SQL query and resulting pruned data is added to a new table. The table with pruned data is a reference for other operations in the mining process. The above-mentioned process is illustrated in Fig. 5 and Fig. 6.



Figure 22. Pruning raw log data.

	date	time	clp	csMethod	csUriStem	csUriQuery	scStatus
1	2007-03-30 00:00:00.000	2013-01-01 10:07:52.000	88.229.205.159	GET	/letsim.asp	NULL	200
2	2007-03-30 00:00:00.000	2013-01-01 14:01:48.000	65.54.188.55	GET	/letsim.asp	NULL	200
3	2007-03-30 00:00:00.000	2013-01-01 14:01:53.000	65.54.188.55	GET	/yonetim.asp	NULL	200
4	2007-03-30 00:00:00.000	2013-01-01 14:19:11.000	88.245.65.22	GET	/misyon.asp	NULL	200
5	2007-03-30 00:00:00.000	2013-01-01 14:19:29.000	88.245.65.22	GET	/letsim.asp	NULL	200
6	2007-03-30 00:00:00.000	2013-01-01 16:07:29.000	88.64.151.239	GET	/misyon.asp	NULL	200
7	2007-03-30 00:00:00.000	2013-01-01 16:07:50.000	88.64.151.239	GET	/misyon.asp	NULL	200
8	2007-03-30 00:00:00.000	2013-01-01 16:08:17.000	88.64.151.239	GET	/misyon.asp	NULL	200
9	2007-03-30 00:00:00.000	2013-01-01 16:08:26.000	88.64.151.239	GET	/letsim.asp	NULL	200
10	2007-03-30 00:00:00.000	2013-01-01 17:06:35.000	88.244.22.1	GET	/misyon.asp	NULL	200

Figure 23. Pruning access logs in the database.

User identification

The purpose of the user identification phase is to identify the users, that is, to determine to which user the data belongs after the data cleaning phase. Due to the issues such as network address translation, instead of using IP address alone, cookies or user factor information is used along with the IP address. The flowchart of the user identification phase is shown in Fig. 7 and its pseudo code is listed below. A sample output of the user identification phase is shown in Fig. 8. The users are differentiated from each other via the pruned data in the table which includes

user factor information, cookie info and IP address. The obtained data is transferred into a table and recorded in the database.

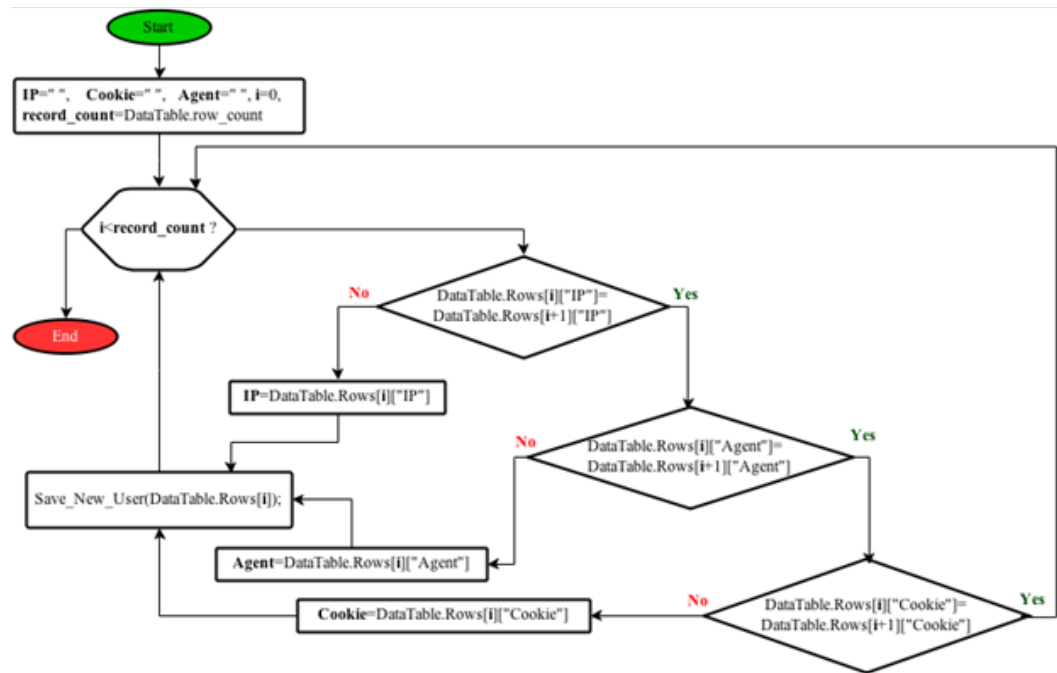


Figure 24. Flowchart of the User Identification phase.

Table 17. Pseudo Code of the User Identification Phase

Start
← ← IP "", i 0, Cookie ← "", Agent ← "", record_count ← DataTable.Rows.Count
i ← 0 to record_count
if DataTable.Rows[i]["IP"] = DataTable.Rows[i+1]["IP"]
if DataTable.Rows[i]["Agent"] = DataTable.Rows[i+1]["Agent"]
if DataTable.Rows[i]["Cookie"] != DataTable.Rows[i+1]["Cookie"]
Cookie ← DataTable.Rows[i]["Cookie"]
Save_New_User(DataTable.Rows[i])
Endif
Else
Agent ← DataTable.Rows[i]["Agent"]
Save_New_User(DataTable.Rows[i])
Endif
Else
IP ← DataTable.Rows[i]["IP"]
Save_New_User(DataTable.Rows[i])
Endif
Endfor

End

clp	csUserAgent
4	85.106.229.0 Mozilla/4.0+(compatible;+MSIE+6.0;+Windows+NT+5.1;+SV1)
5	88.226.0.194 Mozilla/4.0+(compatible;+MSIE+6.0;+Windows+NT+5.1;+SV1;+NET+CLR+2.0.50727)
6	88.229.186.66 Mozilla/4.0+(compatible;+MSIE+7.0;+Windows+NT+5.1)
7	88.229.205.159 Mozilla/4.0+(compatible;+MSIE+6.0;+Windows+NT+5.1;+SV1)
8	88.231.143.36 Mozilla/4.0+(compatible;+MSIE+6.0;+Windows+NT+5.1;+SV1)
9	88.244.22.1 Mozilla/4.0+(compatible;+MSIE+6.0;+Windows+NT+5.1;+SV1)
10	88.245.65.22 Mozilla/4.0+(compatible;+MSIE+7.0;+Windows+NT+5.1;+NET+CLR+1.1.4322;+InfoPath.1)
11	88.64.151.239 Mozilla/4.0+(compatible;+MSIE+7.0;+Windows+NT+5.1;+NET+CLR+1.0.3705;+NET+CLR+1.1.4322;+Media+Center+PC+4.0;+NET+CLR+2.0.50727)

Figure 25. Records resulting from the User Identification phase.

Session Identification

A session can be defined as a set of all transactions realized on a web site [30]. In the session identification phase, session time, visiting time and reference based various intuitive methods can be used [23]. In this study, a session based intuitive approach is used and session time is limited to 30 min. The flowchart of the session identification phase is shown in Fig. 9 and its pseudo code is listed below. A sample output of the session identification phase is shown in Fig. 10.

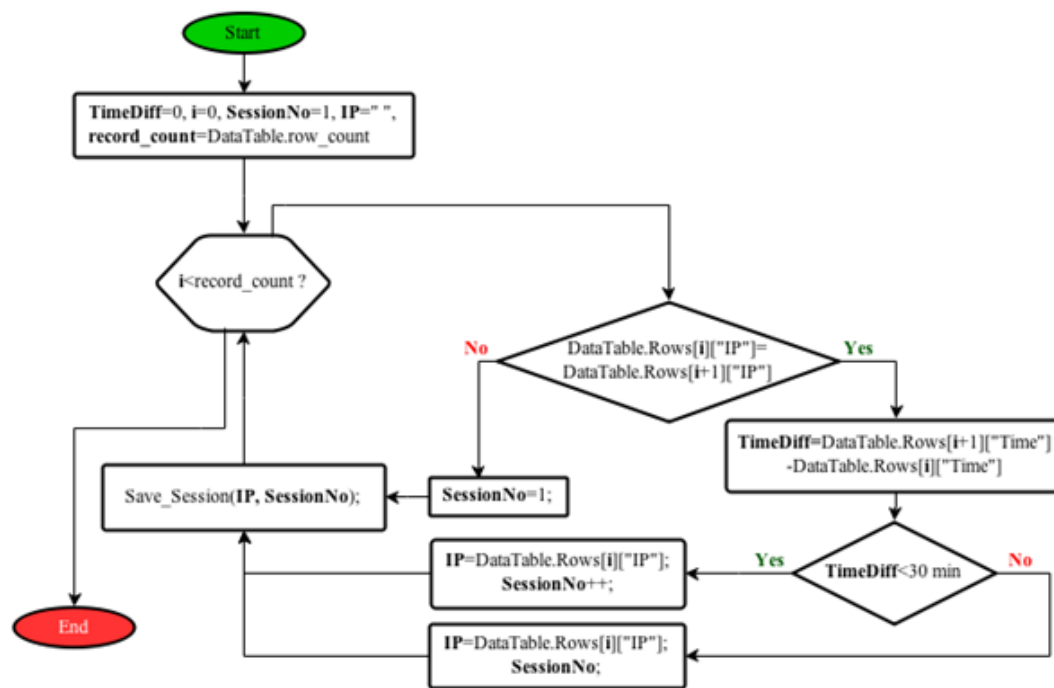


Figure 26. Flowchart of the Session Identification phase.

Table 18. Pseudo Code of the Session Identification Phase.

Start
TimeDiff ← 0, i ← 0, SessionNo ← 1, IP ← "", record_count ← DataTable.Rows.Count
i ← 0 to record_count
if DataTable.Rows[i]['IP'] = DataTable.Rows[i+1]['IP']

```

TimeDiff ← DataTable.Rows[i+1]["Time"] - DataTable.Rows[i]["Time"]
-----
if TimeDiff < 30 minute
-----
IP ← DataTable.Rows[i]["IP"]
-----
SessionNo = SessionNo+1
-----
Save_Session(IP, SessionNo)
-----
Else
-----
IP ← DataTable.Rows[i]["IP"]
-----
Save_Session(IP, SessionNo)
-----
Endif
-----
Else
-----
SessionNo ←
-----
Save_Session(IP, SessionNo)
-----
Endif
-----
Endfor
-----
End

```

	Date	Time	IP	Domain Address	Referer	Session No	User No
1	16/05/2008	09:15:35	10.1.1.212	A	NULL	1	1
2	16/05/2008	17:12:04	10.1.2.104	A	NULL	1	2
3	16/05/2008	17:27:17	10.1.2.104	B	A	1	2
4	16/05/2008	17:01:45	10.1.2.105	A	NULL	1	3
5	16/05/2008	05:31:09	10.1.2.106	B	A	1	4
6	16/05/2008	05:31:16	10.1.2.106	C	B	1	4
7	16/05/2008	12:24:45	10.1.2.106	D	C	2	4
8	16/05/2008	12:24:48	10.1.2.106	A	D	2	4
9	16/05/2008	12:24:58	10.1.2.106	C	A	2	4
10	16/05/2008	11:49:36	10.1.2.124	C	NULL	1	5

Figure 27. Records resulting from the Session Identification phase.

4 CONCLUSION

Log files must be carefully stored and regularly analyzed by system administrators. It is not only a legal obligation in some countries, but also it plays an important role in terms of standards and system performance. Moreover, in terms of information security, the collection, analysis and reporting of log records play a key role.

In this paper, a user-friendly and effective tool which can prune access logs stored in different forms on web servers has been proposed. The proposed tool enables system administrators to read access logs and remove unnecessary data quickly. Web mining preprocessing technique is used to obtain important statistical information from raw access logs about web sites. Using the information provided by the proposed tool, web de-signers and system administrators can improve the quality of services provided by their websites. After final improvements currently going on, the tool developed in this study with its full source code will be made freely available to the research community.

REFERENCES

- [9]. P.-N. Tan, M. Steinbach, and V. Kumar. Introduction to Data Mining, (First Edition). Addison-Wesley Longman Publishing Co., Inc., Boston, MA, USA, 2005.
- [10]. R. Cooley, B. Mobasher, and J. Srivastava, "Data preparation for mining world wide web browsing patterns," Knowledge and Information Systems, vol. 1, no. 1, pp. 5-32, 1999.
- [11]. Q. Yang and H. H. Zhang, "Web-Log Mining for Predictive Web Caching," IEEE Transactions on Knowledge and Data Engineering, vol. 15, no. 4, pp. 1050-1053, 2003.

- [12]. O. Nasraoui, M. Soliman, E. Saka, A. Badia, and R. Germain, "A Web Usage Mining Framework for Mining Evolving User Profiles in Dynamic Web Sites," *IEEE Transactions on Knowledge and Data Engineering*, vol. 20, no. 2, pp. 202-215, 2008.
- [13]. J. Srivastava, R. Cooley, M. Deshpande, and P.-N. Tan, "Web usage mining: discovery and applications of usage patterns from Web data," *ACM SIGKDD Explorations Newsletter*, vol. 1, no. 2, pp. 12-23, 2000.
- [14]. Guidelines for Auditing and Logging. India: Computer Emergency Response Team, 2008.
- [15]. K. Kent and M. Souppaya, *Guide to Computer Security Log Management*, Gaithersburg, USA: National Institute of Standards and Technology, 2006.
- [16]. J. E. Pitkow and K. A. Bharat, "WEBVIZ: A Tool for World Wide Web Access Log Analysis," *Proc. of the First International WWW Conference*, 1994.
- [17]. A. Joshi, K. P. Joshi, and R. Krishnapuram, "On Mining Web Access Logs," *Technical Report*, University of Maryland Baltimore County, 1999.
- [18]. O. Nasraoui, R. Krishnapuram, and A. Joshi, "Mining Web Access Logs Using a Fuzzy Relational Clustering Algorithm Based on a Robust Estimator", *Proc. of the 8th International World wide Web Conference (WWW8)*, Toronto, Canada, 1999.
- [19]. L. K. Joshila Grace, V. Maheswari, and D. Nagamalai, "Analysis of Web Logs and Web User in Web Mining," *International Journal of Network Security & Its Applications*, vol. 3, no. 1, pp. 99-110, 2011.
- [20]. N. K. Tyagi, A. K. Solanki, and M. Wadhwa, "Analysis of Server Log by Web Usage Mining for Website Improvement," *IJCSI International Journal of Computer Science Issues*, vol. 7, no. 4, pp. 17-21, 2010.
- [21]. J. Vellingiri and S. C. Pandian, "A Novel Technique for Web Log mining with Better Data Cleaning and Transaction Identification," *Journal of Computer Science*, vol. 7, no. 5, pp. 683-689, 2011.
- [22]. T. Pamutha, S. Chimphee, C. Kimpan, and P. Sanguansat, "Data Preprocessing on Web Server Log Files for Mining Users Access Patterns," *International Journal of Research and Reviews in Wireless Communications*, vol. 2, no. 2, pp. 92-98, 2012.
- [23]. Y. K. Cha and C. A. Stow, "Mining web-based data to assess public response to environmental events," *Environmental Pollution*, vol. 198, pp. 97-99, 2015.
- [24]. R. Daş, İ. Türkoğlu, and M. Poyraz, "Bir Web Sitesine Ait Kullanıcı Erişim Kayıtlarının Web Kullanım Madenciliği Yöntemiyle Analizi: Fırat Üniversitesi Örneği (in Turkish)," *e-Journal of New World Sciences Academy*, vol. 3, no. 2, pp. 310-320, 2008.
- [25]. R. Daş and İ. Türkoğlu, "Creating Meaningful Data From Web Logs For Improving The Impressiveness of a Website By Using Path Analysis Method," *Expert Systems with Applications*, vol. 36, no. 3, pp. 6635-6644, 2009.
- [26]. R. Daş, İ. Türkoğlu, and M. Poyraz, "Genetik Algoritma Yöntemiyle İnternet Erişim Kayıtlarından Bilgi Çıkarılması (in Turkish)," *Sakarya Üniversitesi Fen Bilimleri Enstitüsü Dergisi*, vol. 10, no. 2, pp. 67-72, 2006.
- [27]. C. Romero, S. Ventura, A. Zafra, and P. de Bra, "Applying Web Usage Mining For Personalizing Hyperlinks In Web-Based Adaptive Educational Systems," *Computers & Education*, vol. 53, no. 3, pp. 828-840, 2009.
- [28]. O. Arbelaitz, I. Gurrutxaga, A. Lojo, J. Muguerza, J. M. Pérez, and I. Perona, "Web usage and content mining to extract knowledge for modelling the users of the Bidasoa Turismo website and to adapt it," *Expert Systems with Applications*, vol. 40, no. 18, pp. 7478-7491, 2013.
- [29]. P. Batista and M. J. Silva, "Mining Web Access Logs of an On-line Newspaper," *Proc. the 5th WSEAS International Conference on Artificial Intelligence, Knowledge Engineering and Data Bases*, 2002.
- [30]. S. E. Salama, M. I. Marie, L. M. El-Fangary, and Y. K. Helmy, "Web Server Logs Preprocessing for Web Intrusion Detection," *Canadian Center of Science and Education*, vol. 4, no. 4, pp. 123-133, 2011.
- [31]. R. Daş, *Web Kullanıcı Erişim Kütüklerinden Bilgi Çıkarımı (in Turkish)*, PhD Dissertation, Fırat Üniversitesi, Elazığ, Türkiye, 2008.
- [32]. H. A. Johnson, M. M. Wagner, W. R. Hogan, W. Chapman, R. T. Olszewski, J. Dowling, and G. Barnas, "Analysis of Web access logs for surveillance of influenza," *Stud Health Technol Inform.*, vol. 107, pp. 1202-1206, 2004.
- [33]. N. Goel and C. K. Jha, "Analyzing Users Behavior from Web Access Logs using Automated Log Analyzer Tool," *International Journal of Computer Applications*, vol. 62, no. 2, pp. 29-33, 2013.
- [34]. M. Taghavi, A. Patel, N. Schmidt, C. Wills, and Y. Tew, "An analysis of web proxy logs with query distribution pattern approach for search engines," *Computer Standards & Interfaces*, vol. 34, no. 1, pp. 162-170, 2012.
- [35]. V. F. de Santana and M. C. C. Baranauskas, "WELFIT: A remote evaluation tool for identifying Web usage patterns through client-side logging," *International Journal of Human-Computer Studies*, vol. 76, pp. 40-49, 2015.
- [36]. Z. Ansari, S. A. Sattar, A. V. Babu, and M. F. Azeem, "Mountain density-based fuzzy approach for discovering web usage clusters from web log data," *Fuzzy Sets and Systems*, 2015. DOI: 10.1016/j.fss.2015.01.021
- [37]. G. Petz, M. Karpowicz, H. Fürschuß, A. Auinger, V. Striteský, and A. Holzinger, "Computational approaches for mining user's opinions on the Web 2.0," *Information Processing & Management*, vol. 50, no. 6, pp. 899-908, 2014.
- [38]. R. Geng and J. Tian, "Improving Web Navigation Usability by Comparing Actual and Anticipated Usage," *IEEE Transactions on Human-Machine Systems*, vol. 45, no. 1, pp. 84-94, 2014.

An Evaluation for the Effect of the Number of Holes on the Blast-Induced Ground Vibrations in Open Cast Blasting Operations

Sahin Yuvka¹, Onder Uysal²

Abstract

In this study, effect of number of holes on blast induced vibrations has been investigated in open pit mines. The studies performed on an overburden panel in Garp Lignite Enterprise, Kutahya, Turkey. The number of holes of the blasts in this panel classified and blasting results evaluated by statistical methods. Drill-hole patterns of all blasting were the same form and charge amount of the blast holes was the same for all cases. Explosive charges are equal for all holes. It has been used the non-electric detonator for the ignition during blasting studies. For measuring of the vibration of the blasts, seismographs have been used. The study has been performed in two steps. Firstly, the data obtained have been analyzed for each hole groups. Secondly, the all data has been analyzed together. Scaled distance- peak particle velocity graphs have been created for the statistical evaluation. In this way, equations and regression coefficients were obtained and these data have been compared.

Keywords: Vibrations, number of holes, blasting

1. INTRODUCTION

Blasting is one of the fundamental elements of various engineering activities including civil work, quarry mining, dam and tunnel construction, in addition to mining. Although blasting is an unavoidable operation, problems such as ground vibration, airblast and flyrocks are sometimes seen to be serious drawbacks. These factors cause significant problems, particularly during activities carried out near residential areas. In recent years, environmental issues due to blasting operations have become one of the most important issues for the technical staff employed in these sectors (Felice 1993, Özdemir et al. 2004, Tuncer et al. 2003, Uysal et al. 2004). In these situations, the main public concern is on the amount of explosives used. Although many researchers reported that the amount of explosives did not have remarkable affect on the blast-induced ground vibration, some claimed that the amount of explosives did have an impact (Singh et al. 2000). In mining activities, the operators are sometimes forced to decrease the total number of blast holes either due to lack of knowledge or psychological reasons. This study investigated the effect of number of blast holes and, therefore, the amount of explosives onto the blast-induced ground vibration. The tests were conducted at a panel (bench) of the Garp Lignite Enterprise (GLE) owned by Turkish National Coal Board (TKI). A total of 50 blasts were performed and vibration measurements were made using a seismograph at various distances. The number of blast holes were classified into two groups as ">50" and "<50", and a statistical analysis was then carried out.

2. EXPERIMENTAL SITE

The study was conducted at a panel at the Garp Lignite Enterprise (GLE) open pits. The mine is situated in western Turkey approximately 50 km from Kutahya and 10 km from Tavşanlı (Figure 1). The bench height was 9 m and the boreholes drilled were 10 m long. The distance between holes and the burden were 6 m. Each hole was charged with 75 kg ANFO and 625 g dynamite (Figure 2). Non-electric blasting caps were used for detonations, and the delay intervals between holes and burdens were 25 ms and 42 ms, respectively.

¹ Corresponding author: Dumlupinar University, Department of Mining Engineering, Kutahya, Turkey. sahin.yuvka@dpu.edu.tr

² Dumlupinar University, Department of Mining Engineering, Kutahya, Turkey. onder.uysal@dpu.edu.tr



Figure 1. Location map of Garp Lignite Enterprise

3. FIELD WORK

In the scope of the field work, the routine blasting operations of the mine were evaluated. In order to demonstrate the effect of number of blast hole and, therefore, the amount of explosives, the number of holes in each blast was classified into two groups as more than 50 holes and less than 50 holes. At this stage, a total of 50 blasts were performed and the vibrations induced by the blasts were recorded for various distances. A total number of 50 vibration readings were recorded of which 29 readings belong to >50 hole group and 21 readings belong to <50 hole group. Scaled distance (SD) and peak particle velocity (PPV) were used in the data analysis. Scaled distance is calculated using the formula given below, which considers the distance between blast and measurement points, and the maximum amount of explosive per delay. The data and measurements of the blasts for >50 holes and < 50 holes were given in Table 1 and Table 2, respectively.

$$SD=R/W^{0.5} \quad (1)$$

Where;

SD : Scaled distance

R : Distance between the blast and the measurement points (m)

W : Maximum amount of explosive per delay (kg).

Table 1. Measurements for blasts with more than 50 blast holes

No	Number of Holes	Maximum amount of explosive	Maximum amount of charge per delay	Distance	Scaled Distance	Particle velocity and frequency							
						Transverse		Vertical		Longitudinal		PPV	
						mm/s	Hz	mm/s	Hz	mm/s	Hz	mm/s	Hz
1	120	6240	52	664	92.10	0.76	17	1.02	19	0.64	13	1.02	19

2	91	5460	60	270	34.84	5.58	8.3	4.064	21	8.64	9.1	8.64	9.1
3	67	3685	55	737	99.41	2.032	7.3	1.143	6.3	3.175	6.1	3.175	6.1
4	133	7980	60	118	15.25	8.76	9.5	3.94	13	10.16	9.8	18	9.8
5	75	3750	50	591	83.58	2.28	3.8	1.14	5.3	2.79	5.6	2.79	5.6
6	130	8125	62.5	302	38.21	6.99	6.8	6.9	6	7.36	9.8	7.36	9.8
7	70	4812.5	68.75	327	39.49	22.61	10	28.19	6.9	27.66	6.9	6	6.9
8	80	5496	68.7	167	20.17	8.38	7.1	7.36	13	13.59	5.5	13.59	5.5
9	150	9750	65	507	62.82	1.39	4.4	2.28	4	2.79	4.5	2.79	4.5
10	120	6240	52	161	22.33	8.51	4.6	12.95	5.6	10.67	5.3	12.95	5.6
11	91	4732	52	212	29.40	2.92	5.1	1.78	3.2	1.68	3.2	8	3.2
12	65	4062.5	62.5	478	60.46	2.16	7.4	2.16	43	3.57	6.7	3.57	6.7
13	65	4062.5	62.5	250	31.62	5.08	12	8	11	8.38	9.7	8.38	9.7
14	80	5000	62.5	386	48.83	5.84	12	4.7	12	7.493	10	7.493	10
15	100	6250	62.5	372	47.05	2.54	20	3.55	32	2.92	11	3.55	32
16	70	4375	62.5	468	59.20	3.12	9.1	2.03	7.4	2.79	9.8	3.12	9.1
17	60	3750	62.5	399	50.47	2.16	20	3.05	39	3.3	23	3.3	23
18	80	5000	62.5	228	28.84	3.81	26	7.49	20	4.7	13	7.49	20
19	110	6875	62.5	263	33.27	5.72	23	6.35	47	6.86	27	6.86	27
20	65	4062.5	62.5	319	40.35	3.68	21	4.95	26	9.14	13	9.14	13
21	60	3750	62.5	281	35.54	3.56	12	4.06	34	4.45	13	4.45	13
22	55	3437.5	62.5	312	39.47	3.56	19	4.45	10	9.1	9	9.1	9
23	80	5000	62.5	391	49.46	3.43	11	3.81	10	6.85	12	6.85	12
24	175	10885	62.2	560	71.01	4.32	5.7	2.16	4.6	3.05	6.9	4.32	5.7
25	150	10605	70.7	420	49.95	3.3	9.1	2.87	14	3.56	7.6	3.56	7.6
26	120	7500	62.5	421	53.25	0.43	8	3.55	9.3	5.33	7.6	5.33	7.6
27	54	4044.6	74.9	342	39.52	3.56	8.3	3.18	7.4	5.21	4.7	5.21	4.7
28	100	7300	73	460	53.84	3.18	23	3.68	23	3.05	7.8	3.68	23
29	120	7500	62.5	421	53.25	3.43	8	3.56	9.3	5.33	7.6	5.33	7.6

Table 2. Measurements for blasts with equal to or less than 50 blast holes

Event No	Number of Holes	Total amount of explosive	Maximum amount of charge per delay	Distance	Scaled Distance	Particle velocity and frequency							
						Transverse		Vertical		Longitudinal		PPV	
						mm/s	Hz	mm/s	Hz	mm/s	Hz	mm/s	Hz
1	50	3125	62.5	268	33.94	6.99	6.1	7.24	6.6	9.02	5.4	9.02	5.4
2	25	1562.5	62.5	161	20.36	11.56	10	11.94	11	16.26	13	16.26	13
3	25	1562.5	62.5	394	49.84	22.99	13	31.04	14	22.86	10	5	10
4	50	3125	62.5	179	22.64	10.79	11	8.76	15	18.54	11	18.54	11
5	40	2500	62.5	454	57.43	2.67	3.7	1.78	4	1.52	5	2.67	3.7
6	31	1937.5	62.5	94	11.89	15.62	16	22.1	15	22.73	16	22.73	16
7	42	2625	62.5	184	23.27	5.72	17	6.35	25	7.87	15	7.87	15
8	42	2625	62.5	286	36.18	3.048	16	4.32	19	5.84	14	5.84	14
9	40	2500	62.5	226	28.59	6.22	15	7.87	17	10.03	15	10.03	15
10	35	2187.5	62.5	224	28.33	5.46	10	6.86	23	8.64	10	8.64	10
11	40	2500	62.5	252	31.88	6.86	14	7.75	19	7.24	17	7.75	19
12	45	2812.5	62.5	255	32.26	5.08	32	4.45	47	6.6	12	6.6	12
13	35	2187.5	62.5	344	43.51	3.18	57	5.72	34	3.56	9.7	5.72	34
14	50	3125	62.5	332	42.00	4.12	19	4.57	32	4.32	17	4.57	32
15	45	2812.5	62.5	367	46.42	4.57	12	4.32	26	4.32	11	4.57	12
16	24	1351.2	56.3	426	56.77	2.41	9.7	2.54	11	3.05	12	3.05	12
17	46	2589.8	56.3	309	41.18	4.32	12	5.72	28	4.7	16	5.72	28
18	40	2252	56.3	365	48.65	3.05	13	3.18	27	2.67	19	3.18	27
19	40	2500	62.5	424	53.63	1.65	14	2.03	12	2.54	7.4	2.54	7.4
20	46	3118.8	67.8	471	57.20	3.3	11	2.16	9.3	4.57	9.5	4.57	9.5
21	50	3540	70.8	549	65.25	2.87	8.8	1.98	9.3	3.43	7.5	3.43	7.5

The results of the measurements conducted to determine the effect of the number of blast holes onto blast-induced ground vibrations were statistically analyzed. Scaled distance-PPV graphs were plotted using the measurements; the equations and regression coefficients were obtained (Figure 3). As it is seen from Figure 3, there are three groups of analysis namely; analysis for >50 holes, analysis for <50 holes, and the overall analysis. Thus, a comparison could be made between the groups, as well as having an overall analysis. The equations and regression coefficients obtained from the graphs are given below. The regression coefficients from the separate analysis of the two groups were

calculated as 0.83 and 0.75, while it was found as 0.79 from the overall analysis without making any distinction between the groups.

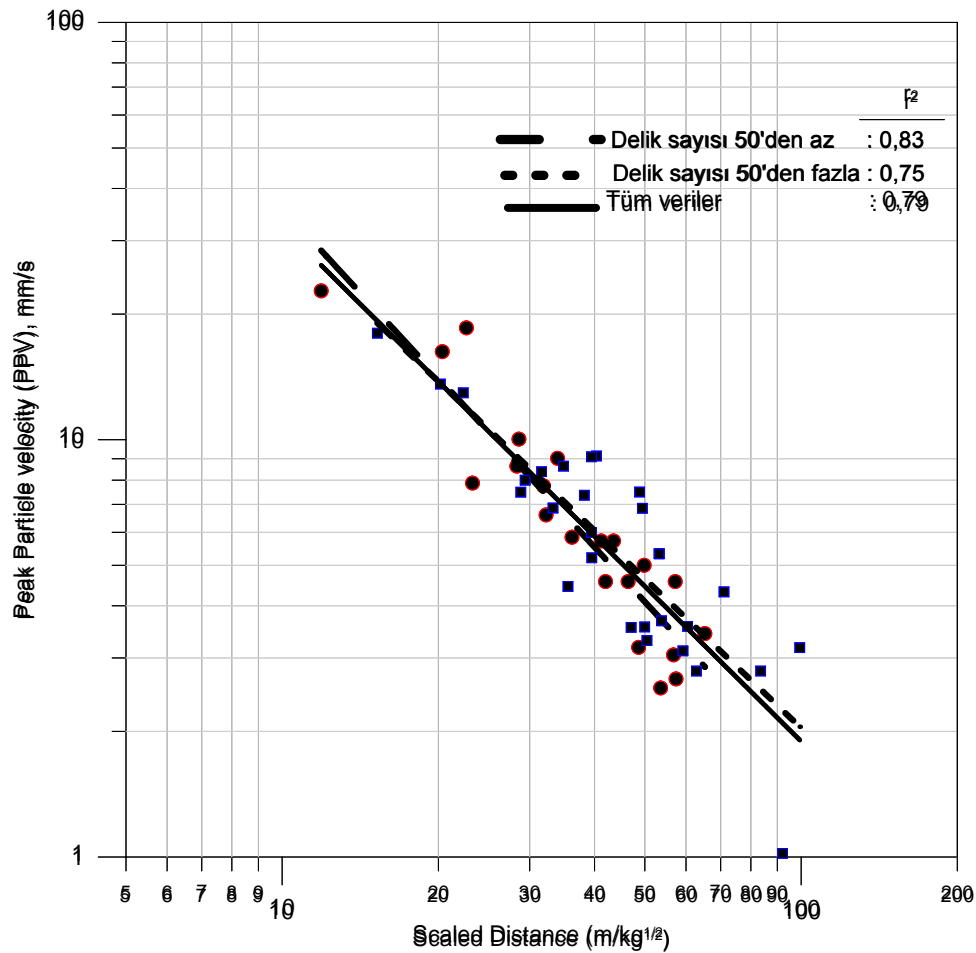


Figure 3. The Graphs of Scaled distance-PPV

Blasts with less than 50 holes;

$$PPV = 803.077 \times SD^{-1.350} \quad (R^2 = 0.83) \quad (2)$$

Blasts with more than 50 holes;

$$PPV = 485.857 \times SD^{-1.188} \quad (R^2 = 0.75) \quad (3)$$

Overall;

$$PPV = 555.078 \times SD^{-1.234} \quad (R^2 = 0.79) \quad (4)$$

4. CONCLUSION

In this study, the effect of the number of blast holes and, therefore, the amount of explosives onto blast-induced ground vibration was investigated. The investigation was mainly based on the number of holes blasted at a stripping panel of a coal mine. The blasting operations were classified into two groups as operations with more than 50 holes and operations with less than 50 holes with respect to the number of holes in each blast. A total of 50 blasts were evaluated of which 29 of the blasts belong to >50 hole groups and 21 of the blasts belong to <50 hole groups. Non-electric delaying capsules were used in all the detonations. Blast-induced ground vibrations were recorded at various distances with a blasting seismograph. The data collected were statistically analyzed; the scaled distance-peak particle

velocity (PPV) graphs were plotted and the correlation coefficients were calculated. Blasts with less than 50 holes and with more than 50 holes were analyzed both separately and together. The regression coefficients for each groups were calculated as 0.83 and 0.75 for <50 hole groups and >50 holes group, respectively, while the overall analysis produced an regression coefficient of 0.79. The correlation coefficients are quite similar to each other which indicates that there is no significant difference between the evaluations of the data separately or together. The same result can also be observed in Figure 3. The scaled distance-PPV graphs plotted were also found to be in good conformity.

As a result, it can be said that the number of blast holes and, therefore, the total amount of explosives does not have a significant effect on the blast-induced ground vibrations as long as each hole is detonated by using a separate delaying capsule. The results of this study reemphasized the importance of the amount of explosives per delay in the formation of blast-induced ground vibration.

REFERENCES

- [1]. Felice JJ, Applications of Modelling to Reduce Vibration and Airblast Levels. 4th International Symposium on Rock Fragmentation by Blasting, Vienna, 5–8 July 1993.
- [2]. Ozdemir K, Kahrman A, Tuncer G, Akgu'ndogdu A, Elver E, Uc'an, O.N., Fragmentation Assessment Using a New Image Processing Technique Based on Adaptive Neuro Fuzzy Inherence Systems. In: 30th Annual Conference on Explosives and Blasting Technique, Louisiana, Vol II, pp 181–187, 1–4 February, 2004.
- [3]. Tuncer G, Kahrman A, Ozdemir K, Guven S, Ferhatoglu A, Gezbul T., The Damage Risk Evaluation of Ground Vibration Induced by Blasting in Naipli Quarry. In: 3rd International Conference: Modern Management of Mine Producing, Geology and Environmental Protection, SGEM-2003, Varna, Bulgaria, pp, 67–75, 9–13 June 2003
- [4]. Uysal O, Eelevli B, Akcakoca H., Environmentally Sensitive Drilling and Blasting Design for a Surface Mining. 13th International Symposium on Mine Planning and Equipment Selection, 1–3 September, Wroclaw, Poland, 2004.
- [5]. Singh TN, Singh V., An Intelligent Approach to Prediction and Control Ground Vibration in Mines. *Geotech Geol Eng* 23:249–262, 2005

Predictive Perspective on Resonance Problem by Testing with Rotating Elements

Salih Seckin Erol¹

Abstract

In this research, resonance condition which is a common problem for mechanical constructions has been studied within perspective of oil starving failure in a bearing. A test setup designed, constructed and located in laboratory conditions. A bearing in the electrical motor, that is one of the compounds in the test setup, has been chosen for gathering data in acoustic, vibration and electrical consumption during the test. The aim of the research is testing condition monitoring of oil starving failure and resonance for studying comparison in different predictive maintenance approaches. Test has been implemented under the electricity frequency of 40.5 Hz that induced the electrical motor for identifying the rotation speed. According to the analysis results, inspecting of oil starving failure and resonance problem has been detected as the most clearly by vibration analysis.

Keywords: acoustic, electrical consumption, oil starving, resonance, vibration

1. INTRODUCTION

Mechanical systems require maintenance due to failures occurred or will occur. Main maintenance techniques implemented in manufacturing industries are breakdown maintenance, periodic maintenance and predictive maintenance. Predictive is the maintenance technique that is based on collecting symptomatic data about health of the machine. Organs of the predictive maintenance are such as vibration, acoustics, heat, lubrication, electrical consumption and etc. consisting of the data that has characteristics about the condition of the machine health. Resonance is one of the catastrophic problem for mechanical systems and oil starvation is an crucial factor for eliminating the resonance problem. In this research, effect of oil starvation on resonance problem has been researched in the perspective of acoustics analysis, vibration analysis and electrical consumption and results are presented.

Main idea of the condition monitoring technology is following the machine health by using certain type of sensors and evaluating the signals collected [1]. Fundamental of the condition monitoring technique is reading sensor measurements of the mechanical system that is in the failure process and understanding the root causes of the failure respect to machine health [2]. Breakdown maintenance requires unplanned stoppages and these stoppages are one of the reasons for high production losses and high economical costs due to repairing, renewing elements of the machine [3].

Beginner level cracked or broken rotor bars, small bearing damages and axial misalignments may cause increase in the electrical current consumption [4]. Time/resistance, temperature, acoustic emissions [5] and ultrasonic inspection, electrical current density changes take place in wide implementations as well. Traditional signal processing techniques are used in evaluating these parameters and consequently prognostic approach has been limited mainly in that area [6]. Failures of the machines that has rotating elements mainly causes vibrational symptoms. These failures are evaluated mostly by vibrational analysis[7].

2. MATERIALS AND METHODS

Test setup designed as consisting of double inlet fan, AC induction motor, five feet of flexible coupling and frequency inverter. The test construction is mounted on a steel sheet and a steel tripod. The test setup is mounted on a double-decker rubber sheet that is located between the test system and the tripod; also, a vacuum rubber under each foot of the tripod stands over the floor. This system with a data acquisition card and an induction motor is connected to monitoring system through a computer. Testing system in Figure 1 presents an actual view.

¹ Corresponding author: Kilis 7 Aralik University, Department of Mechanical Engineering, 79000, Kilis, Turkey. sserol@kilis.edu.tr

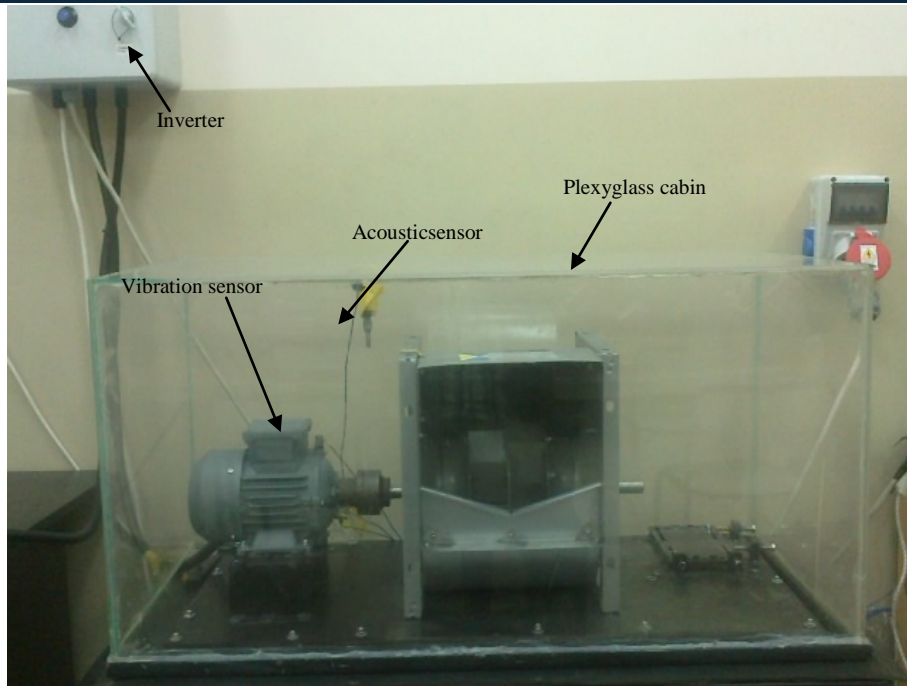


Figure 1. A view from the test setup

Frequencies used in the test (T) and measured (M) are identified in Table 1. Theoretical frequencies shows the value set on the digital frequency changer; according to data gained during the application, actual frequency ranging suffered some losses. 1x expressed as a frequency that is known as fundamental frequency; 2x, 3x and the upper orders are harmonics of fundamental frequency. In Table 1, the frequency is shown with the symbol of f for frequency changer and harmonic order presented with symbol of h.

Table 1. Harmonics

(h)	1x		2x		3x		4x		5x	
	T	M	T	M	T	M	T	M	T	M
40.5	40.5	39.06	81	78.12	121.5	117.18	162	156.24	202.5	241.56

Measurements were made during the tests at electrical frequency 40.5 Hz and rotational period was measured as 2350 min⁻¹. Frequencies of failures and harmonics are taken into account when calculating the bearing and fan-induced vibrations of the test apparatus.

Bearing related equations with the basic failure frequency calculations and respect to measurements are presented in Table 2.

Table 2. Fault frequencies

f (Hz)	ω_s (Hz)	ω_{bpf} (Hz)	ω_c (Hz)	ω_{bpfo} (Hz)	ω_{bpfi} (Hz)	ω_{bsf} (Hz)
40.5	39.06	390.6	14.84	118.74	193.76	76.69

ω_{bpfo} : Outer ring passing frequency (Hz), ω_{bpfi} : Inner ring passing frequency (Hz),

ω_{bsf} : Ball spin frequency (Hz), ω_c : Cage frequency (Hz), ω_s : Shaft frequency (Hz),

ω_{bpf} : Fan blade passing frequency (Hz)

In order to practice condition of oil starving failure, oil is completely removed from the tested bearing; in order to manage fast deterioration, 0.55 g oil has been applied on bearing. Tested bearing has been presented in Figure 2.



a) Tested bearing lubricated b) Tested bearing non-lubricated

Figure 2. Tested bearing

In order to evaluate measurements, the raw data from acoustics and vibrational techniques have been processed with FFT (Fast Fourier Transform) method and data has been transferred making analysis. Electrical consumption data has been processed according to the algorithm of the device software and analysis are based on PSD (Power Spectrum Density) and trend indicators.

3. EXPERIMENTAL

Vibration measurements are implemented in radial (vertical) direction during the tests. Acoustic measurements are done in omni-directional over the test setup in plexyglass cabin. Vibrational and acoustic data captured with sensors connected to a DAQ (Data Acquisition Card) and processed with its software. In order to identify natural frequencies for comparison, damping tests are practised on test setup when the system is not in rotational movement. Data relevant with electrical consumption has been captured through an electronic device connected to electrical circuit of the motor and analyzed with its software.

a. Acoustic Analysis

Frequencies of acoustic data received based on rotation of shaft and bearing elements has been presented in Figure 3 and the highest five amplitudes are given. The main rotation frequency is 39.06 Hz and the highest amplitude signal has been detected at 0.5x (19.53 Hz). An other order of the main frequency has been detected at 351.6 Hz (9x) that is the third dominant signal in the spectrum domain.

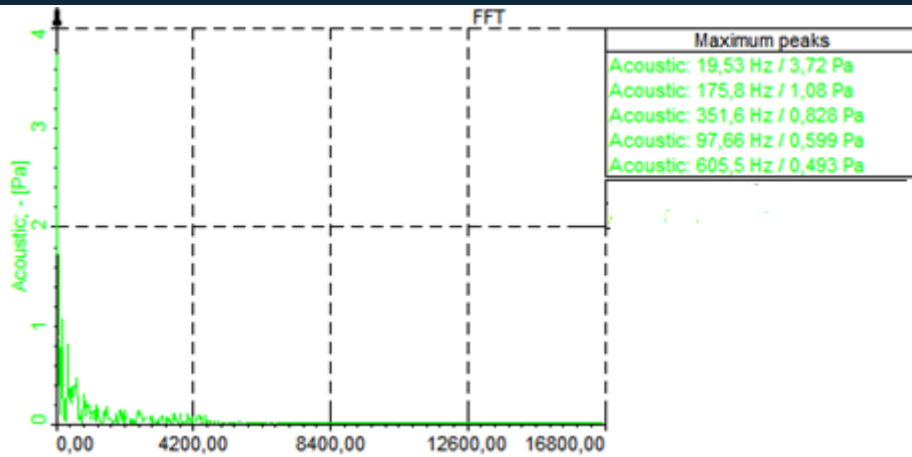


Figure 3. Spectrum in acoustic data

According to the Figure 3, resonance frequencies are detected at frequencies of 175.8 Hz (second dominant), 97.66 Hz (fourth dominant) and 605.5 Hz (fifth dominant).

b. Vibration Analysis

In radial direction, signal at 860.72 Hz that is the upper harmonics of cage frequency ($58x\omega_c$) excited a signal at the frequency 866.7 Hz which is a natural frequency and consequently superharmonic resonance has been observed with the highest signal amplitude as 0.613 m/s^2 . 1x unbalance harmonic has been explored as second dominant signal in radial direction. The other resonance effects are detected at the fourth and fifth dominant signal in frequencies of 948.5 Hz and 120.8 Hz. Signal in upper order of cage frequency at 949.76 Hz ($64x\omega_c$) has excited the natural frequency at 948.5 Hz and subharmonic resonance has been appeared with the amplitude of 0.314 m/s^2 . Signal at 117.18 Hz (3x) has excited the natural frequency at 120.8 Hz and superharmonic resonance has been detected with the amplitude of 0.277 m/s^2 . Signal at harmonic 2x has been appeared as the third dominant signal.

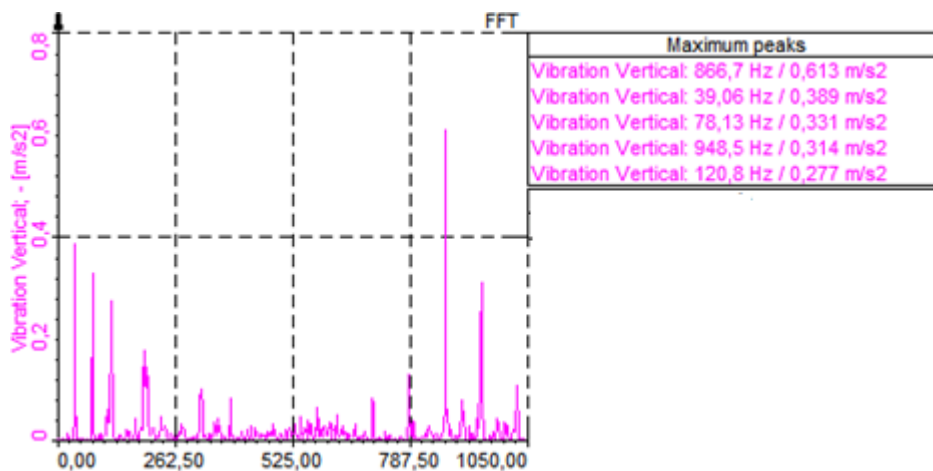


Figure 4. Spectrum in vibration data

Respect to the Figure 4 and Table 3, oil starvation increased the vibration magnitude of signals at the element passing zone.

Table 3. Harmonics respect to dominant vibration signals (S:Signal)

MEASUREMENT	1.S	2.S	3.S	4.S	5.S
Oil starving	f_n ($58x\omega_c$)	1x	2x	f_n ($64x\omega_c$)	f_n (3x)

c. Electrical Consumption Analysis

Standard deviations in measurements are evaluated in perspective of electrical consumption, data is given in PSD analysis and trend analysis. Respect to PSD analysis in Figure 5, peaks can be seen at the orders of 40.5 Hz. Highest three amplitudes are on 40.5 Hz, 81 Hz and 121.5 Hz. According to the methodological approach of device software, band at the main frequency represents the condition of the rotor, band at the second order represents the condition of bearing and band at the third order represents the any other failure. The PSD analysis takes attention to rotor and bearing.

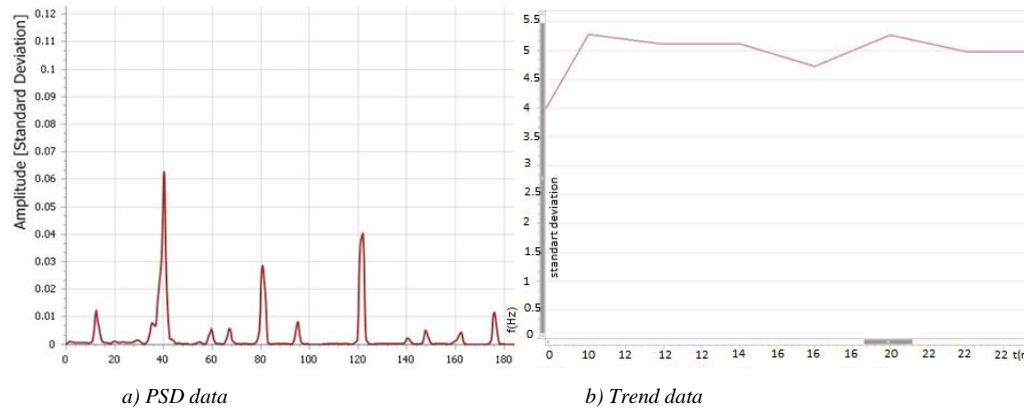


Figure 5. Electrical consumption data

According to evaluation of trend analysis in Figure 5, bearing indicator has detected fluctuation in the condition of the bearing respect to the oil starvation failure.

4. RESULTS AND DISCUSSION

In this experimental research, resonance features of a test setup have been studied under the oil starving conditions of a bearing. Approaching with predictive maintenance perspective; techniques of acoustics, vibration and electrical consumption analysis are studied in order to identify the condition of a tested bearing.

According to analysis results of acoustic measurement on effect of oil starving failure, bearing frequency and resonance frequencies are found in the acoustic data.

Respect to vibration analysis, bearing failure frequencies and resonance frequencies are detected in spectrum data under the oil starvation failure.

Electrical consumption analysis is successful in detection of oil starving failure in PSD and trend analysis. On the other hand, it is detected that analysis programme of the measuring device is not designed for detection of resonance. But resonance effect studied may be in the band of rotor or bands of other; not exist enough data about it.

In comparison of acoustic, vibration and electrical consumption analysis results; vibration analysis has been decided as the most informative and accurate tool for inspecting the resonance features of the tested system in the condition of oil starving.

5 CONCLUSIONS

Amount of resonance quantity and magnitude of the deterioration may increase and reach catastrophic failures respect to the oil starvation. Oil need of the bearings may differ according to external and internal effects; so that, oil need of the bearings should be checked periodically or predictively and sufficient lubrication should be fulfilled continuously.

REFERENCES

- [1] Lebold, M., Reichard, K., Boylan, D., 2003: Using DCOM in an open system architecture framework for machinery monitoring and diagnostics. *IEEE AerospaceConference*, 1227–1235.
- [2] Sudhar, G.N.D.S., Sekhar, A.S., 2011: Identification of unbalance in rotor bearing system. *Journal of Sound and Vibration*, 330, 2299-2313.
- [3] Collacott, R.A., 1977: *Mechanical Fault Diagnosis*, Chapman&Hall, London, s405.
- [4] Velarde-Suarez S., Ballesteros-Tajadura R., Hurtado-Cruz J.P., 2006: A predictivemaintenance procedure using pressure and acceleration signals from a centrifugal fan, *Applied Acoustics*, 67, 49-61.
- [5] Hardman, W., Hess, A., Sheaffer, A., 2000: A helicopter powertrain diagnostics andprognostics demonstration, in: *IEEE Aerospace Conference Proceedings*, 6, 355–366.
- [6] Acosta, G.G., Verucchi, C.J., Gelso, E.R., 2006: A current monitoring system fordiagnosing electrical failures in induction motors. *Mechanical Systems and Signal Processing*, 20, 953–965.
- [7] Goodenow, T., Hardman, W., Karchnak, M., 2000: Acoustic emissions in broadbandvibration as an indicator of bearing stress, in: *IEEE AerospaceConference Proceedings*, 6, 95–122.

BIOGRAPHY

Salih Seckin Erol was born in year 1976 in Afyonkarahisar/Turkey. He completed high school education at Salihli Sekine Evren Anatolian High School in Manisa/Turkey in year 1994. He received B.Sc. degree from Hacettepe University / Ankara-Turkey in year 2000. He received M.Sc. degree in Total Quality Maintenance from Vaxjö (Linnaeus) University / Sweden in year 2009 and received Ph.D. degree in Mechanical Engineering from Pamukkale University - Denizli / Turkey in year 2015. His research and expertise areas are predictive maintenance, prognostics, diagnostics, vibration analysis, lean six-sigma implementations and grant funding projects. He had job experiences at private companies about manufacturing, quality control, export-import departments. Also, he worked at Denizli Chamber of Commerce as a Project Task Manager in the name of Enterprise Europe Network. He is currently working as an Assistant Professor and Head of Mechanical Engineering Department at Kilis 7 Aralik University in Turkey.

Accuracy Assessment of Commercial GPS Processing Software as a Function of Baseline Distance and Occupation Time: A case study in Turkey

Sermet Ogutcu¹, Ibrahim Kalayci¹

Abstract

This paper investigates the accuracy of constrained adjustment of the two commercial GPS processing software with different length of baselines and occupation time. National Continuously Operating Reference Stations (CORS) also known as TUSAGA-Aktif was used to determine five different networks. Each network consists of four CORS stations. For each network, the same CORS station was taken as an unknown point and the others were taken as control points, and the unknown point's three-dimensional coordinates were determined with respect to the other three CORS stations (control points). The different networks provide the baseline distances, 50 to 465km, from control points to the unknown point. Five different occupation time were determined for the unknown point and three days of GPS data were processed for each network. Two commonly used commercial processing software, Trimble Spectra Precision Survey Office and Leica Geo Office, were used to perform the constrained adjustment to obtain final coordinates of the unknown point for each network. The difference between the Earth Centered Earth Fixed (ECEF) Cartesian coordinates (obtained after the constrained adjustment) and the already established ECEF coordinates of the unknown point were transformed to topocentric coordinates (north, east, up). The results show that three-dimensional millimeter level accuracy, up to 100km baseline, is possible for each commercial software. For the baselines more than 100km, several centimeter and in some cases decimeter level accuracy is obtained. The results also show that the longer occupation time does not always improve the accuracy especially for the baselines longer than 200km. The authors strongly recommend that in static relative positioning in Turkey, baseline distances between stations should not exceed the inter-station distances (~50-130km) of national CORS network if surveyors prefer to use commercial GPS processing software.

Keywords: Constrained Adjustment, GPS, Static relative positioning, Post-processing

1 INTRODUCTION

Static relative positioning GPS (Global Positioning System) technique has been playing an increasingly important role in many applications which require highly accurate positioning. Static relative positioning employs at least two GPS receivers (base receiver and roving receiver) simultaneously tracking the same satellites to determine their relative coordinates. Base receiver remains stationary at a site with accurately known coordinates while the remaining receivers occupy the points whose coordinates are unknown [1]. Generally, carrier phase measurements are used for precise static relative positioning [2], [3].

In static relative positioning, resolution of the carrier phase integer ambiguity plays an essential role for positioning accuracy and precision [4]. Carrier phase differencing algorithm has been applied to resolve this ambiguity. In most cases, the double differenced carrier phase observable is used to mitigate errors associated receivers and satellites which are essential part to successful ambiguity resolution [5].

This investigation was motivated by the need to evaluate the estimated coordinate accuracy by using the national CORS stations known as Tusaga-Aktif (Fig. 1) with commercial GPS processing software which performs static relative positioning. Tusaga-Aktif consists of 147 CORS stations, located across the country. Trimble Zephyr Geodetic II triple-frequency antenna has been used for the all CORS stations. The distances between the CORS stations are in the range of 50-130km. This coverage defines the minimum baseline distances for this study.

¹ Corresponding author: Necmettin Erbakan University, Department of Surveying Engineering, 42100, Meram/Konya, Turkey.
sermetogutcu@konya.edu.tr



Figure 1. Locations of Tusaga-Aktif CORS stations (Yildirim et al. 2011)

Since commercial GPS processing software are easy to use and requires no advanced skills, many government institutions and private sectors are widely using this kind of software in surveying application. After the establishment of national CORS station, static relative positioning is no longer a labor-intensive and time consuming task. 24 hours rinex data of the Tusaga-Aktif CORS stations are available online. There is only roving station requires to perform static relative positioning.

We address in this paper how the accuracy of the estimated three-dimensional coordinates, constrained to the national CORS stations, depend on the baseline distance and occupation time. One CORS station which is approximately the center of the national CORS sites was taken as an unknown point. Five different networks (Fig. 2) whose baselines distances approximately 50 to 380km were determined to assess the accuracy of the constrained adjustment of the two commonly used commercial software, Trimble Spectra Precision Survey Office (version 3.30) and Leica Geo Office (version 8.3) in Turkey. Fig. 2 shows the unknown point (CIHA) and other CORS stations.

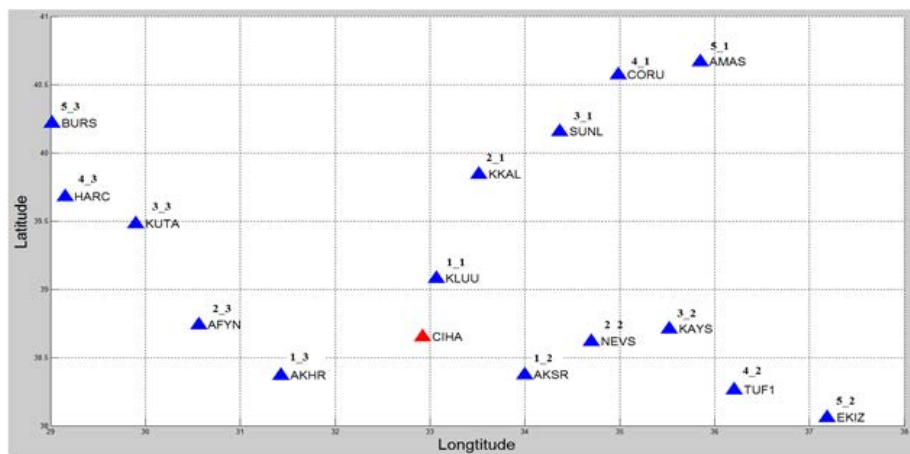


Figure 2. The location of the unknown point and the other CORS stations

CORS stations and their distances to unknown point for each network are given in Table 1.

Table 1. Inter-Station distances for each network

Network 1	
CORS stations	Distances to unknown point (CIHA)
KLUU	~49km
AKSR	~98km

AKHR	~134km
Network_2	
KKAL	~142km
NEVS	~155km
AFYN	~205km
Network_3	
SUNL	~208km
KAYS	~226km
KUTA	~277km
Network_4	
CORU	~277km
TUFI	~290km
HARC	~345km
Network_5	
AMAS	~336km
EKIZ	~378km
BURS	~379km

2 METHODOLOGY AND DATA PROCESSING

For each network, three days of observation data (DOY 60, 61, 62) in March 2015 was chosen. Only GPS observations were used for processing. 24 hours rinex data of the unknown point was divided as 00-02, 00-06, 00-12, 00-18, 00-24 hours for each chosen day. Each divided rinex data of the unknown point, was processed in each software for each network and each day.

There are several limitations associated with this study. The processing data only involves GPS observations by the fact that for the some baselines, phase initial ambiguities associated with GLONASS satellites could not be fixed especially for long baselines. Therefore to maintain the consistency between the adjustments, GLONASS satellites were removed from the processing. Only three days of data during March 2015 was processed thus seasonal, long-term effects and precision are not considered. 24 hours rinex data of the unknown point was divided from 00.00 UTC hours thus accuracy from short observation times (especially for 2h-6h) are likely be correlated with the geometric dilution of precision (GDOP) (Richard 1997). In according with Turkish survey regulation, at least two CORS stations can be used to perform network adjustment. In this paper we used three CORS stations which encloses the unknown point for each network adjustment. This is the most preferred way for surveyors. As a result of this, the effect of number and the geometry of reference stations is neglected.

Each CORS station's rinex data has been recorded at 30 seconds interval thus we selected this default time interval for all processed data. Since low elevation cut-off angles (0-10) increases the double-differenced observations residuals which affects tropospheric and ionospheric corrections [6] elevation cut-off angle of 15 degree was selected for all data. For each software, NGS absolute antenna calibration model was used for antenna phase center variations which if ignored could introduce several centimeters error especially in height component for long baselines even for the same type of receiver and antenna [7-10].

Generally, mathematical models used for baseline processing and network adjustment do not publish for the commercial software. Users can select some models related tropospheric and ionospheric corrections. For Trimble, users cannot select any correction model. For tropospheric modelling, Neill mapping function [11, 12] is used as a default model by Trimble. For Leica, several tropospheric modelling can be selected by the users. We selected Hopfield tropospheric model (Hopfield 1969) for all processed data. Ionospheric effect was mitigated by using double frequencies linear combinations for each software. Precise ephemerides of GPS satellites [13] used for all processed data which is compulsory for network adjustment in according with Turkish survey regulation.

The same processing steps were carried out by each software. For each network, three CORS stations' established ECEF Cartesian coordinates (ITRF96, reference epoch: 2005) are held fixed then three baselines from these CORS

stations to the unknown point were processed. Only the phase ambiguity fixed solutions are accepted from these baseline processing for each network and each day. Trimble was processed all baselines with fixed phase ambiguity but Leica cannot resolve phase ambiguity for each baselines and each day. Unresolved phase ambiguity for Leica exist in network 3, baseline from KAYS station to the unknown point cannot be resolved to fixed phase ambiguity for each day therefore only two baselines were processed to the unknown point. After the baseline processing, constrained adjustment was performed for each network and each day. The obtained three-dimensional coordinates of the unknown point after the constrained adjustment is taken as final coordinates.

To investigate the accuracy of the adjustment, the differences between three-dimensional coordinates obtained after the adjustment and already established three-dimensional coordinates of the unknown point were resolved into north, east, up components for all processed data for each software. The results were given in section 3. Published three-dimensional coordinates which we assumed true coordinates of Tusaga-Aktif CORS stations were computed by using GAMIT/GLOBK scientific software. This computation consists of three main processes. In the first process, coordinate time series of CORS stations were computed in ITRF08 datum w.r.t. IGS stations which are evenly distributed in azimuth. Second process involves computing ITRF velocity (no-net rotation) of CORS stations' Cartesian coordinates. Final process involves the ITRF transformation between ITRF08 and ITRF96 (national datum).

3 RESULTS

The divided rinex data (00-02, 00-06, 00-12, 00-18h) for each three-day was processed for the five different networks with each software to investigate the estimated coordinates' accuracy dependence on the baseline distance and occupation time. For each network and each day, resolved topocentric coordinates were tabulated in Table 2 with respect to the occupation time.

Table 2. North, east, up differences (mm) of Trimble and Leica software for each network and each day

Network 1, DOY 60								
TRIMBLE					LEICA			
Time	North	East	Up	3D	North	East	Up	3D
00-02	3	-5	-2	9	3	0	6	7
00-06	2	-6	-3	7	2	0	-3	3
00-12	2	-5	-1	5	2	-1	3	4
00-18	3	-5	2	6	2	-1	3	3
00-24	2	-3	0	3	2	-1	3	3
Network 2, DOY 60								
TRIMBLE					LEICA			
Time	North	East	Up	3D	North	East	Up	3D
00-02	-2	-18	-33	38	4	-6	2	7
00-06	-3	-19	-2	19	3	-6	-11	13
00-12	-2	-12	-3	12	-4	-7	-16	18
00-18	-2	-13	-2	13	-2	-3	-7	8
00-24	-3	-10	-6	12	3	-7	-17	18
Network 3, DOY60								
TRIMBLE					LEICA			
Time	North	East	Up	3D	North	East	Up	3D
00-02	-1	-15	-3	15	-4	24	-200	201
00-06	-2	-19	-3	17	3	2	-60	60
00-12	-2	-31	-5	17	13	21	4	25
00-18	-2	-16	-11	19	14	21	3	25

00-24	-3	-16	5	17	0	17	5	18
Network 4, DOY60								
TRIMBLE					LEICA			
Time	North	East	Up	3D	North	East	Up	3D
00-02	1	29	8	30	4	-20	5	21
00-06	0	-3	-7	7	2	-19	-13	23
00-12	1	-24	-10	26	2	-19	-18	26
00-18	-3	-24	-9	25	2	-19	-23	30
00-24	-4	-25	-9	27	0	-21	-27	34
Network 5, DOY60								
TRIMBLE					LEICA			
Time	North	East	Up	3D	North	East	Up	3D
00-02	2	-37	26	52	-15	-40	35	55
00-06	-6	-40	-9	41	-13	-35	12	39
00-12	-11	-34	-24	43	-13	-32	-7	35
00-18	-11	-38	-23	46	-10	-34	-5	36
00-24	-13	-39	-20	46	2	-44	10	45
Network 5, DOY61								
TRIMBLE					LEICA			
Time	North	East	Up	3D	North	East	Up	3D
00-02	-1	-44	36	57	-12	-42	16	46
00-06	-7	-42	-4	43	-19	-32	0	37
00-12	-9	-40	-21	46	-17	-34	6	38
00-18	-11	-41	-16	45	-22	-29	21	42
00-24	-12	-42	-12	45	-16	-33	18	41
Network 1, DOY62								
TRIMBLE					LEICA			
Time	North	East	Up	3D	North	East	Up	3D
00-02	-3	-9	8	12	0	-2	5	5
00-06	0	-8	-7	10	0	-3	4	5
00-12	2	-3	5	6	1	-2	3	4
00-18	3	-4	7	9	2	-2	5	6
00-24	2	-2	4	5	2	-2	5	6
Network 2, DOY62								
TRIMBLE					LEICA			
Time	North	East	Up	3D	North	East	Up	3D
00-02	-4	-16	31	35	2	-8	7	11
00-06	-5	-17	7	19	1	-7	-6	9

00-12	-3	-8	4	9	3	-7	-16	18
00-18	-3	-10	10	14	3	-8	18	20
00-24	-4	-6	3	10	3	-8	18	20
Network 3, DOY62								
TRIMBLE					LEICA			
Time	North	East	Up	3D	North	East	Up	3D
00-02	0	-19	39	43	17	22	23	36
00-06	-3	-23	9	25	15	21	18	31
00-12	-1	-16	9	18	1	17	8	19
00-18	-1	-18	21	28	2	17	7	18
00-24	-3	-18	18	26	10	21	5	24
Network 4, DOY62								
TRIMBLE					LEICA			
Time	North	East	Up	3D	North	East	Up	3D
00-02	2	-31	34	46	1	-21	23	31
00-06	1	-34	-2	34	1	-20	2	20
00-12	-1	-26	-7	27	0	-22	-16	27
00-18	-1	-28	-5	28	0	-22	-18	28
00-24	-3	-28	-7	29	-40	-38	3	55
Network 5, DOY62								
TRIMBLE					LEICA			
Time	North	East	Up	3D	North	East	Up	3D
00-02	4	-40	31	51	-17	-44	63	79
00-06	-7	-46	-7	47	-15	-40	25	49
00-12	-8	-42	-21	48	-14	-41	11	45
00-18	-9	-46	-22	52	-14	-39	2	41
00-24	-12	-44	-21	50	-15	-42	10	46

As it can be seen from the Table 2, the strong correlation is observed between the inter-station distances and the accuracy of the estimated coordinates of the unknown point. Generally, millimeter level accuracy is obtainable for network 1 (whose baseline distances are the shortest one) for each day with the occupation time longer than 2 hours. Long inter-station distances badly affect the baseline processing and the network adjustment. For long baselines, (more than 100km) long occupation time cannot always produce better accuracy as it seen from network 3, 4, 5. For the baselines longer than the 100km, centimeter-level accuracy is obtainable for each software.

Generally, up to 6 hours observation time is chosen for the surveyors in Turkey thus accuracy graphics for 2 and 6 hours adjustment w.r.t. the coordinates' component is given in Figure 3 to save the space in the manuscript.

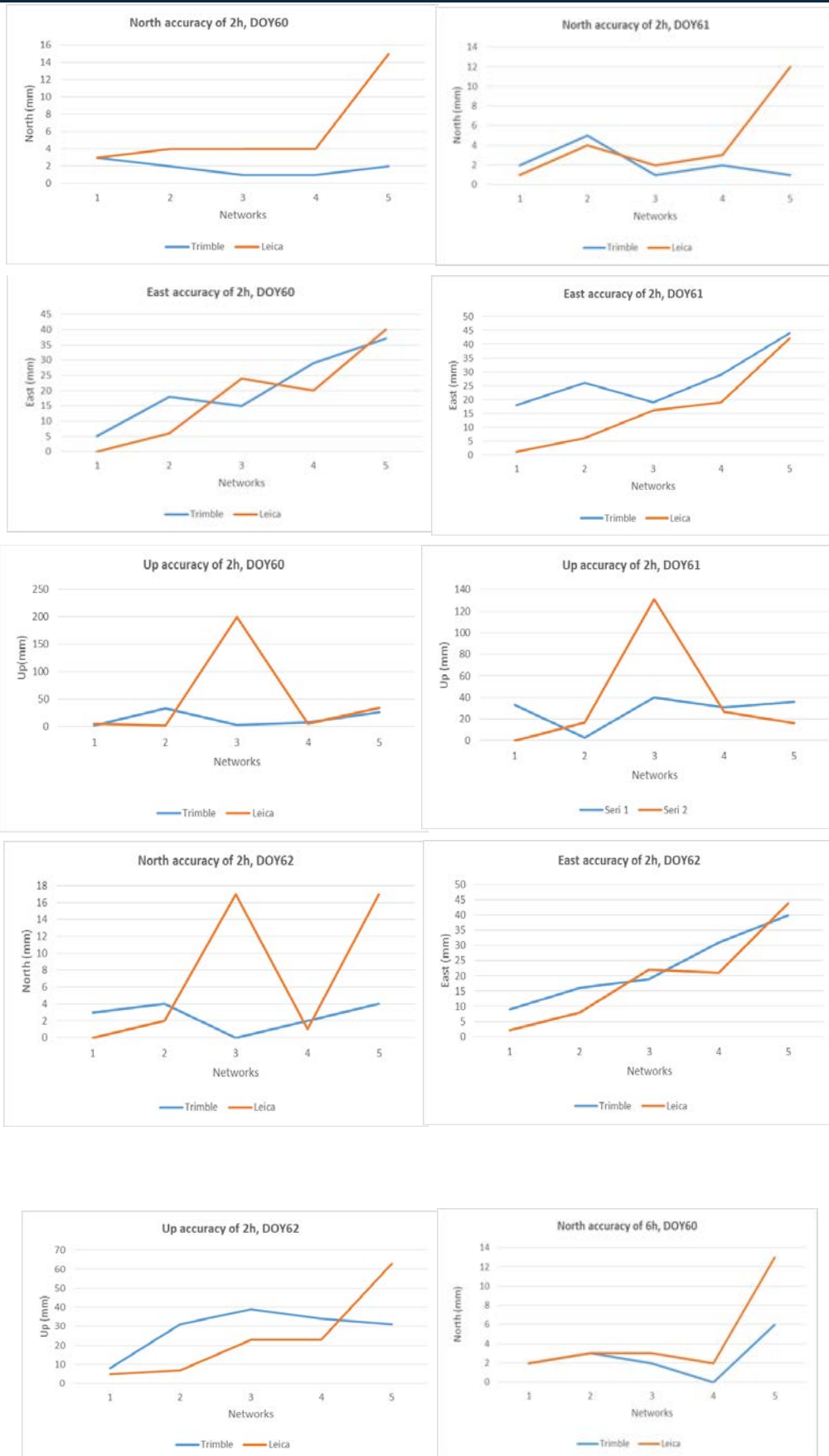




Figure 3. Accuracy of the coordinates' components for 2 and 6 hours adjustment w.r.t. the networks

For DOY 60 (00-02h) and 61 (00-02h, 00-06h, 00-12h), the difference in up component is reached 13-20cm after the adjustment with Leica for network 3. These differences are assumed outliers for the estimated position and further investigation needs to be carried out to find out the reason of these large differences. For each network and each software, the east difference is much higher than the north especially for long baselines on each day. As it is shown in Fig. 2, the east component accuracy increases dramatically comparing with east component when baselines length increases. Since accuracy of east component is more sensitive to ambiguity resolution than north component, it proves that for long baselines, ambiguity resolution decreases. That is the main reason for low accuracy of east component. Since ambiguity resolution percentage of baselines cannot be taken from each software, we conclude this assumption from the accuracy results.

CONCLUSIONS AND RECOMMENDATIONS

Since the establishment of Tusaga-Aktif national CORS system, surveyors can use CORS stations as a base station while they perform static relative positioning. In this study, accuracy analysis of the two commonly used commercial software for static relative positioning was carried out within the national CORS network whose inter-station

distances are in the range of ~50-130km. This distance is the typical minimum inter-station distance for the surveyors who use national CORS stations for static relative positioning.

In this study, baseline processing and constraint adjustment were performed to obtain final three-dimensional coordinates of the unknown point with the two commonly used commercial GPS software. The results show that for the baselines whose distances are in the range of 100km, millimeter level accuracy is achievable for each software with the occupation time longer than 2 hours. For the longer baselines, three-dimensional accuracy is degrading and centimeter level accuracy is possible. Due to the satellite geometry and movement which affects the ambiguity resolution, the eastward component can be estimated several times less accurate than the northward component.

The results also show that for the baselines longer than 100km, to increase occupation time cannot always improve the accuracy and the results would be unpredictable. The authors strongly recommend that in static relative positioning in Turkey, baseline distances between stations should not exceed the inter-station distances (~50-130km) of national CORS network if surveyors prefer to use commercial GPS processing software.

ACKNOWLEDGMENT

This work is supported by scientific research development department of Necmettin Erbakan University.

REFERENCES

- [1] M. Berber, A. Üstün, M. Yetkin., "Comparison of accuracy of GPS techniques", *Measurement.*, 45:1742-1746, 2012.
- [2] J. Wang, C. Satirapod, C. Rizos., "Stochastic Assessment of GPS carrier phase measurements for precise static relative positioning". *Journal of Geodesy*76: 95-104, 2001.
- [3] P. Teunissen., "GPS Carrier Phase Ambiguity Fixing Concepts". *GPS for Geodesy* 319:388, 1998.
- [4] G. Blewitt., "Fixed point theorems of GPS carrier phase ambiguity resolution and their application to massive network processing: Ambizap". *Journal of Geophysical Research* 113: B12410, 2008.
- [5] S. Feng, W. Ochieng, T. Moore, C. Hill, C. Hide., "Carrier Phase-based integrity monitoring for high-accuracy positioning". *GPS Solutions* 13:13-22, 2009.
- [6] S. Jin, J. Wang, P.H. Park., "An improvement of GPS height estimations: stochastic modeling". *Earth Planets Space* 57:253-259, 2005
- [7] A. El-Hattab., "Influence of GPS antenna phase center variation on precise positioning". *NRIAG Journal of Astronomy and Geophysics* 2:272-277, 2013.
- [8] R. Schmid, M. Rothacher., "Estimation of elevation-dependent satellite antenna phase center variations of GPS satellites". *Journal of Geodesy*77: 440-446, 2003.
- [9] K. Dawidowicz., "Antenna phase center variations corrections in processing of GPS observations with use of commercial software". *Technical Sciences*13: 120-132, 2010.
- [10] R. Bruce, Schupler, A.C. Thomas., "Characterizing the Behavior of Geodetic GPS Antennas". *GPS World*, February 48-55, 2001.
- [11] A.E. Neill., "Global mapping functions for the atmospheric delay at radio wavelengths". *Journal of Geophysical Research*111:3227-3246, 1996.
- [12] Neill A.E., "Improved atmospheric mapping functions for VLBI and GPS". *Earth Planets Space*52:699-702, 2000.
- [13] J.M. Dow, R.E. Neilan and G.Gendt., "The International GPS Service: celebrating the 10th anniversary and looking to the next decade". *Advances in Space Research* 36:320-326, 2005.

Experimental study on effects of die geometry and temperature on limit drawing ratio

*Cebeli Ozek¹, Vedat Tasdemir^{*2}*

Abstract

Accurate determination of process parameters are important in deep drawing. The aim is to draw faultless and higher cups in one step. Thus, the Limit Drawing Ratio (LDR) is very important parameter for deep drawing process. The objective of the present study is to determine the effects of the die face angle and forming temperature on the Limit Drawing Ratio (LDR) and wall thickness of AA5754-O Al-Mg alloy in deep drawing dies. For this, die surfaces were formed in four different angles -- 0°, 5°, 10° and 15° -- and experiments were conducted at room temperature, 100°C, 175°C, and 250°C. In experiments, the die cavity was kept stable at 1.35 mm, MoS₂ of high temperature, high compressive strength, and low friction coefficient was used as lubricant. As a result, it was determined that LDR increased from 2.14 to 2.80 when at optimum temperature and die geometry was used. It was observed that the effect of die geometry on wall thickness is limited and the effect of temperature is relatively more significant.

Key Words: Warm deep drawing, Limit drawing ratio, Die geometry, Wall thickness

1. INTRODUCTION

Deep drawing process is a plastic forming method in which a metal blank is given form by the mechanical action of a punch. In this method, three dimensional products with certain depth and profile are obtained from two-dimensional work pieces of planar geometry with the help of elements called drawing dies. Cups produced may be formed by multiple operations. This method has an important place in industrial practices because many simple and complex shaped parts can be manufactured easily [1 –3]. In recent years, light and high strength materials have been increasingly used. Some of these materials are aluminium alloys. AA 5754 Al-Mg alloys are widely-used, particularly in the automotive industry due because of to their properties such as high ductility and strength, good weldability and low density [4, 5]. However, formability of these alloys is low compared to steel blanks because of their microstructure at room temperature [6]. The aforementioned Limit Drawing Ratio (LDR) increases substantially at temperatures below recrystallization temperature. Behaviour of Al-Mg alloy at room temperature is independent of the deformation rate however -- its yield strength starts decreasing at temperatures above 100°C. This in turn increases the deformation rate sensitivity index (*m*). The decrease in yield strength caused by temperature increase becomes more apparent above 175°C [7]. Experimental studies showed that yield strength decreases when the *m* index value is positive and dynamic deformation hardening occurs when it is negative [8]. The locking caused by the dislocation movements of Mg atoms lead to dynamic deformation hardening [9, 10]. Deformation hardening decreases as the temperature increases and the formability ratio increases due to uniform temperatures. The highest effect on this rate of increase is caused by the temperature distribution [11]. In a study, Boogard increased LDR of AA 5754 alloy from 2.1 at room temperature to 2.6 by cooling the punch and increasing the temperature in the flange area of the blank to 250°C [7]. In another study by Bolt et al., LDR of AA 5754 alloy was increased to 2.7 as a result of the deep drawing test performed at 250 °C [12].

Another factor affecting formability is die design and geometry. Die geometry should be designed to facilitate flowing of the blank into the die cavity. O. Secgin and V. Savas created angled die surfaces with the new die system they designed and determined that LDR of a DIN 10130-99 steel blank increased from 1.75 to 2.175 and that the thinning in the cup's wall thickness was reduced by 11% based on face angle of the die. Schoichiro et al. increased LDR of Mg alloys from 2.1 to 5 by using local heating and cooling technique in a study they conducted [14]. The aforementioned studies revealed that die design is an important parameter that affects the formability of products. In addition, factors such as structural and mechanical properties of the material, material geometry, friction, lubricant type, blank holder force, die cavity and punch speed are other important parameters that affect formability.

In the present study, different from the existing literature, 0°, 5°, 10° and 15° angles were formed on die and blank holder surfaces and the effects of parameters such as die geometry and room temperature, 100°C, 175°C and 250°C temperatures on the limit drawing ratio (β) and wall thickness were studied experimentally.

¹Firat University, Technology Faculty, Mechanical Engineering Department, Elazığ, Turkey.

cozek@firat.edu.tr

²Corresponding author: Kahramanmaraş Sütçü İmam University, Elbistan Vocational School, Kahramanmaraş, Turkey.

vtasdemir@ksu.edu.tr

2. EXPERIMENTAL PROCEDURE

2.1. Material

Commercially available EN AW-5754-H111 (AlMg3) blank of 1 mm thickness was used in the experiments. Specimens were subjected to heat treatment at 380°C for 4 hours before the process. The chemical composition of the material used is shown in Table 1.

The mechanical properties of the specimens were determined by drawing to three different hot forming directions at 0°, 45° and 90° angles at a fixed drawing rate of 5mm/min in a SHIMATZU drawing test machine with 5000 kN capacity. Hardness values were measured by using a DIGIROCK Macro hardness measuring device. Hardness and mechanical test readings are provided in Table 2.

- a.
- b.
- c.

d. **Table 1. Chemical analysis of EN AW-5754 (AlMg3) blank, %**

Chemical Composition, %												
Si	Fe	Cu	Mn	Mg	Cr	Ni	Zn	Ti	Ga	V	Al	
0.13	0.3	0.019	0.14	2.72	0.005	0.005	0.022	0.018	0.01	0.013	Remaining	

e. **Table 2. Mechanical properties of test specimen at room temperature**

Rolling direction (°)	Yield strength (N/mm ²)	Tensile strength (N/mm ²)	Elongation (%)	Young's modulus (GPa)	Hardness (HRB)
0	167.748	248.544	10,321	66	26,6
45	163.257	235.162	12,826		26,4
90	165.643	240.119	11,684		26,8

2.2. Test Procedures

In the present study, the effects of forming temperature and die geometry on LDR were studied experimentally. Tests were conducted by giving 0°, 5°, 10° and 15° angles to die and blank holder surfaces at room temperature, 100°C, 175°C and 250°C temperatures. A fixed value of 8 mm was used as the punch corner radius and die corner radius, and the blank holder force was applied at 1.2 kN, 2.4 kN and 3.6 kN. MoS₂ (3-4 μm) was used as a lubricant for the purpose of reducing friction between surfaces. Figure 1 shows a schematic design of the testing apparatus.

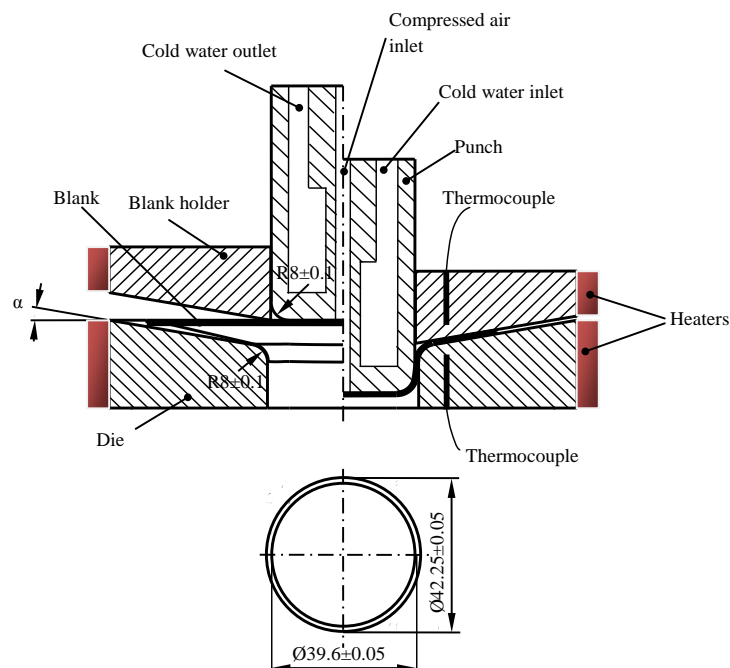


Figure 1. Schematic design of the testing apparatus

The die and blank holder were heated by using heating coils. The punch was cooled by using water and the blank material by using compressed air during the drawing process. Temperatures were measured with thermocouples placed in the dies. Temperature values were checked by using digital thermostats. Tensile forces were measured by a CAS LS -20 T, single-axis load cell with a capacity of 20 tons. Punch speed was kept stable at 4mm/sec. Specimens were heated for 30 to 90 seconds based on their LDR values. Heating was applied at the blank holder force that would be used in each test. Figure 2 shows the testing apparatus. Variations in the thickness of specimens were measured in the direction of forming by using a digital micrometer with an accuracy of 1 μ m following the drawing process.

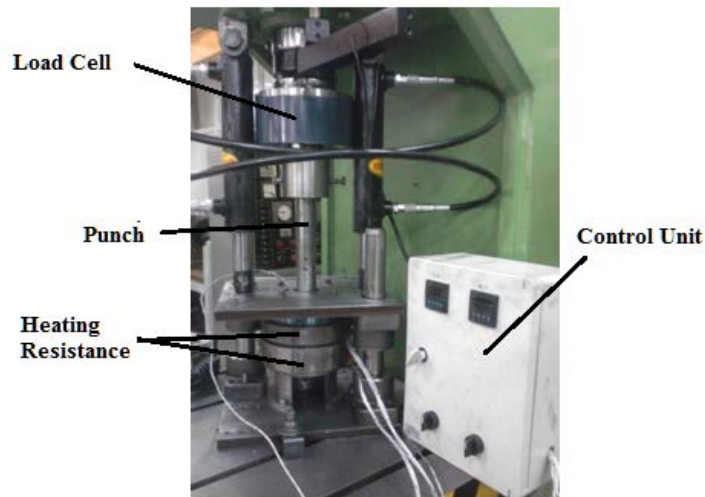


Figure 2. Testing apparatus

3. RESULTS AND DISCUSSION

3.1. Measurement Results for Limit Drawing Ratio (LDR)

One of the most important criteria in deep drawing method is determining the LDR value, which is important for reducing production costs. Figure 3 shows the effects of forming temperature and die angle on LDR. As is seen in the Figure, LDR tends to increase based on the temperature increase at all angle values. This increase becomes more apparent at temperature values particularly above 100 $^{\circ}$ C. This situation may be associated with the yield strength decrease and formability increase that occur as the temperature increases. Similar results were obtained by Boogaard [7]. LDR increases from 2.14 to 2.75 when the temperature is increased from room temperature to the highest value (250 $^{\circ}$ C) at 0 $^{\circ}$ die angle. This increase is approximately 22%. LDR increases from 2.17 to 2.80 at all values if the die angle is different than 0 $^{\circ}$. Figure 4 shows the cups obtained as a result of the drawing process that was applied at fixed blank holder force, different die angles and temperature values. As is seen in the figure, the effect of die angle on LDR is not as significant as the effect of temperature. LDR increased from 2.14 to 2.17 when the angle is increased from 0 $^{\circ}$ to 15 $^{\circ}$ at room temperature. However, LDR increased from 2.75 to 2.80 at 250 $^{\circ}$ C.

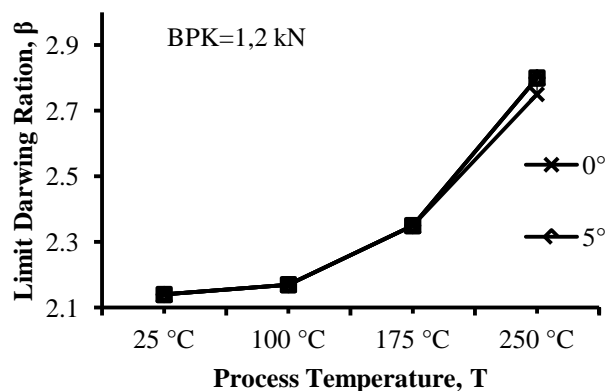


Figure 3. The effects of α and T on β

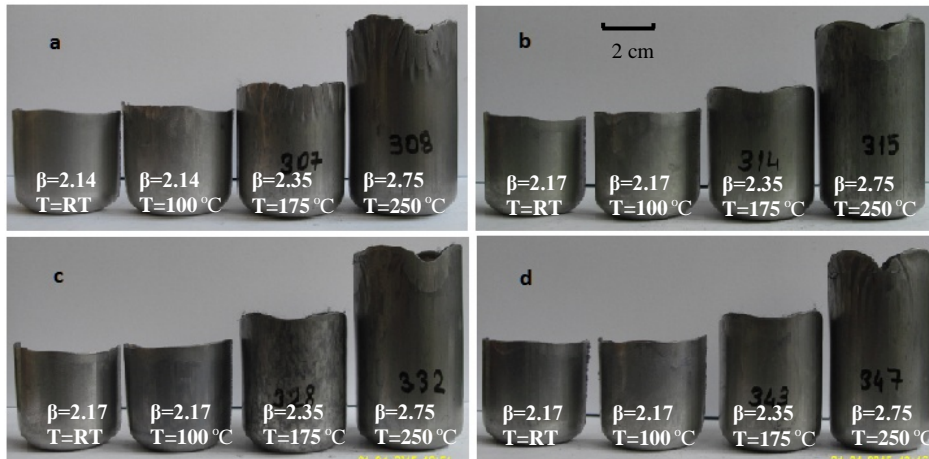


Figure 4. Specimens drawn at 1.2 kN BHF. a) $\alpha=0^\circ$, b) $\alpha=5^\circ$, c) $\alpha=10^\circ$, d) $\alpha=15^\circ$

3.2. Measurement Results for Wall Thickness

Multiple tensile forces apply on the cup drawn through the deep drawing process. These tensile forces are directly related to the wall thickness of the cup [13]. Variation in the cup wall thickness affects the quality of the work piece to an important degree. Figure 5 shows the effect of die angle on wall thickness at stable room temperature and die holder force. Detailed analysis of the figure reveals that the wall thickness does not vary along a length of 10 mm starting from the cup bottom, and significant variations occur for all angle values from that point on. However, at room temperature, die angle does not have a substantial effect on wall thickness. Measurement results on wall thickness of cups obtained after the tests conducted at 250°C temperature are provided in Figure 6. The effect of die angle on wall thickness increases in proportion to the temperature increase. This effect is particularly significant in the upper areas of the cups. This situation may be associated with the fact that flow of the material in the die cavity gets easier when the angle values are increased -- particularly at high temperatures. When analysed in combination with the graphics, no substantial variation is observed on the bottom part due to die angle, and thinning is seen in the radius areas and thickening in the upper parts of the cup walls. Similar results were obtained by Unal [15].

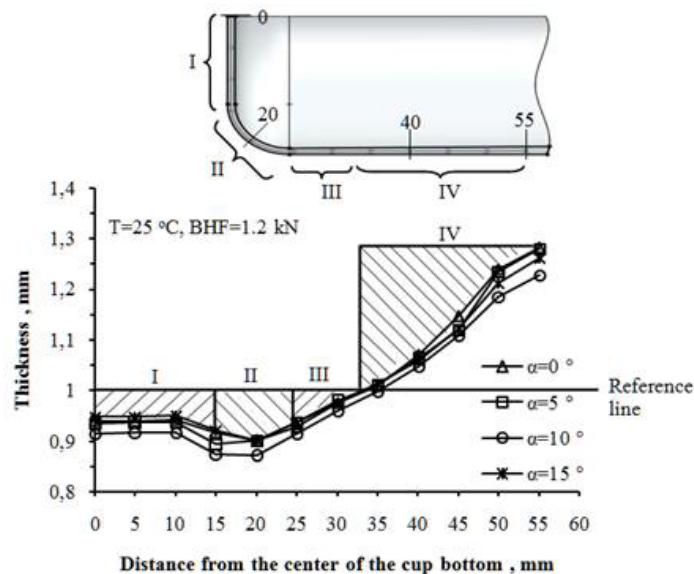


Figure 5. Effect of die angle on wall thickness at room temperature (LDR: 2.14)

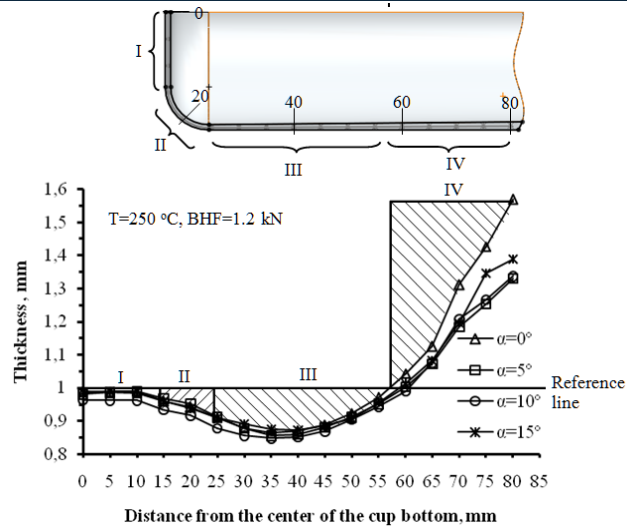


Figure 6. Effect of die angle on wall thickness at 250°C (LDR: 2.75)

Figure 5 shows that thinning occurs in the height range of 0-33 mm and thickening occurs in the height range of 33-55 mm. Figure 6 shows that wall thickness is reduced (thinning) in the height range of 10-57 mm and it is increased (thickening) in the height range of 57-80 mm. Thickness variations that are shown in the figures were analysed by dividing into four zones. Zone I is the contact zone where the effect of the punch on the deep drawing process is limited. In this zone, blank material elongates with the effect of force. Tension force increases to a very high value as a result of increase in the friction forces due to the contact that occurs with the action of the punch between the punch radius and blank material. Consequently, thinning occurs in the cup as shown for Zone II. The tension force increases in proportion with the deformation caused by the punch. This situation leads to excessive deformation of the cup which in turn causes important reduction in the thickness as shown for Zone III. In the last step, as a result of the insufficient blank holder force, the thickness increases due to material concentration, as is seen in zone IV. Figures also show that the length of the zone where thinning occurs is an important factor determining the cup height and LDR. As a result of the tests performed at room temperature, it was determined that the wall thickness on the bottom of the cup decreased significantly and approximately 8% thinning occurred. On the other hand, at 250°C, the thinning on the bottom was reduced substantially down to approximately 3%. This situation may be explained by the reduction in the flow strength of the material at 250°C, easier flow of the material in the die cavity as a result of re-increasing the strength on the cup bottom by cooling the cup bottom, and contact area of the punch and the resultant reduction in the tensile force. Variation of the punch force based on temperature is shown in Figure 7. The figure shows that temperature is an important parameter that affects the punch force. It was determined that the punch force that was 24.68 kN at 25°C decreased to 19.15 kN at 250°C, which corresponds to a variation of 22.4%

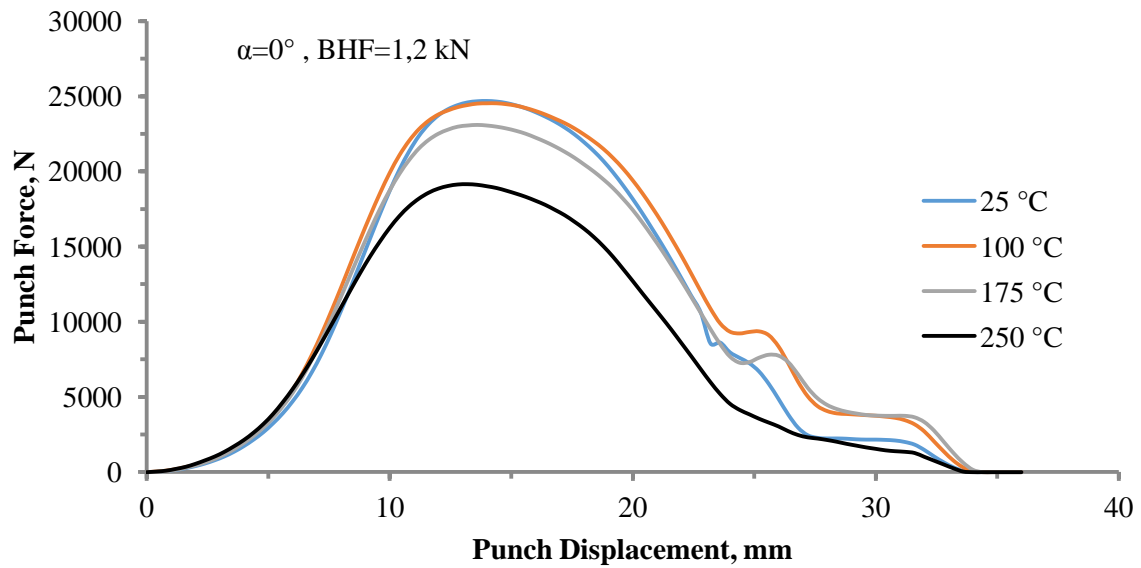


Figure 7. Variation of the punch force based on temperature

Figure 8 shows the effect of die angle on punch force at room temperature. Analysis of the graphic indicates that variation in the punch force is not significant at any of the angle values. The variation that occurs in the punch force when the temperature is increased to 250°C is given in Figure 9. It is observed that a substantial increase occurs in ironing force in the experiment performed with the die that has $\alpha=0^\circ$. This situation may be explained by material concentration on the upper parts of the cup due to insufficient blank holder force applied while forming with the die that has $\alpha=0^\circ$. In addition, it can be argued that the ironing force and concentration is very low as the angle makes material flow easier at all other die angle values. As the concentration damages the cup, it affects the degree of usability of the cup to a substantial degree. Figure 10 shows specimens that were drawn at stable die holder force and temperature of 250°C based on the die angle. In the figure, it is observed that the wrinkle in the upper parts of the cup is high when the die angle is 0° and that it is eliminated at 5° and 10° , but that it occurs again when the die angle is increased to 15° .

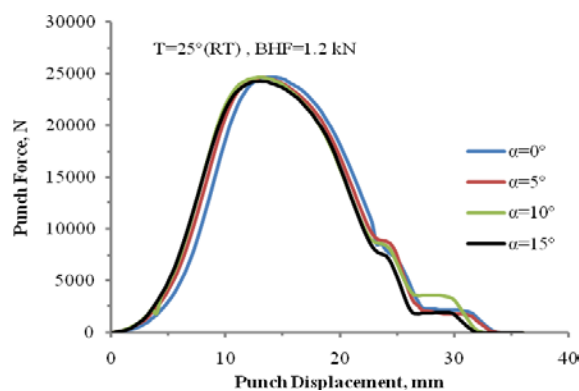


Figure 8. Effect of die angle on punch force at room temperature (LDR: 2.14)

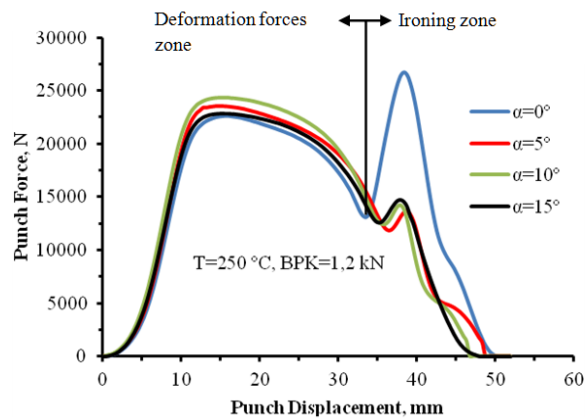


Figure 9. Effect of die angle on punch force at 250 °C (LDR: 2.75)

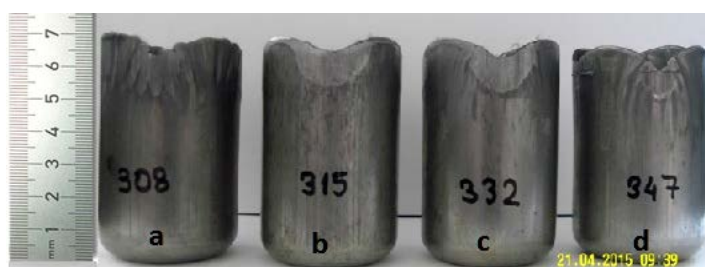


Figure 10. Specimens for 250°C temperature, 1.2 kN and 2.75 LDR a) $\alpha=0^\circ$ b) $\alpha=5^\circ$ c) $\alpha=10^\circ$ d) $\alpha=15^\circ$

Forming applied under the effect of temperature substantially correlates with the temperature distribution. Uniform temperature distributed on the entire surface area of the sample leads to tearing. For the purpose of preventing that, both the contact area between the sample and punch and the punch itself were cooled. It was determined that cooling reduces tearing damages significantly. Figure 11.a shows the cup torn as a result of the experiment conducted through uniform heating. Figure 11.b shows the specimens produced by using the temperature distribution method.



Figure 11. Experiments conducted by using uniform heating (a) and temperature distribution (b) method

4. CONCLUSION

The present study was performed for the purpose of determining the effect of die geometry and forming temperature on LDR and wall thickness with deep drawing dies of AA 5754 Al-Mg. General results obtained from the study are as follows.

- LDR of cups produced as a result of warm deep drawing (250°C) increased by 22.18% when compared with the cups obtained at room temperature; however the effect of die geometry was found to be very limited.
- Both the contact area between the sample and punch and the punch itself must be cooled for a successful warm deep drawing process.
- Experiments show that an effective testing apparatus must be established and improved further based on the technological requirements, particularly for alloys that have difficult formability at room temperature.

- It was observed that the wrinkle that occurs in the drawn cups is reduced substantially by increasing the die angle, but wrinkle occurred again at $\alpha=15^\circ$. This situation shows that 5° - 10° die angle is ideal. In addition, it was determined that the usable length of the cup decreased by approximately 20% due to wrinkle.
- It was determined that the most important factor affecting the punch force is temperature, and the force decreases by 22.4% with temperature.
- Results showed that die geometry does not have significant effect on wall thickness at room temperature; however, the effect becomes more significant based on the die angle at high temperature and LDR.

REFERENCES

- [1] Ethiraj, N., Senthilkumar, V. S., (2010). Experimental Investigation on Warm Deep Drawing of Stainless Steel AISI 304. *Applied Mechanics and Materials*, Vol. 26-28, pp 436-442.
- [2] Güneş, A.T., (2002). *Pres İşleri Tekniği Cilt 2*. Makine Mühendisleri Odası, Ankara.
- [3] L. Jayahari, P.V. Sasidhar, P. Prudvi Reddy, B. BaluNaik, A.K. Gupta, S. Kumar Singh, (2014). Formability studies of ASS 304 and evaluation of friction for Al in deep drawing setup at elevated temperatures using LS-DYNA. *Journal of King Saud University – Engineering Sciences* 26, 21–31.
- [4] H. Gedikli, Ö. N. Cora, M. Koç, (2011). Comparative investigations on numerical modeling for warm hydroforming of AA5754-O aluminum sheet alloy. *Materials and Design* 32 2650–2662.
- [5] H. Laurent, R.Grèze , M.C.Oliveira, L.F.Menezes, P.Y.Manach, J.L.Alves, (2010). Numerical study of springback using the split-ring test for an AA5754 aluminum alloy. *Finite Elements in Analysis and Design* 46 751–759.
- [6] N. Abedrabbo, F. Pourboghrat and J. E. Carsley, (2005). Warm Forming of Aluminum Alloys using a Coupled Thermo-Mechanical Anisotropic Material Model. CP778 Volume A, Numisheet 2005.
- [7] A. van den Boogaard, (2002). Thermally enhanced forming of aluminum sheet—modeling and experiments. Ph.D. thesis, Twente University, Enschede, The Netherlands.
- [8] F. Öztürk, H. Pekel, and H. S. Halkacı, (2011). The Effect of Strain-Rate Sensitivity on Formability of AA 5754-O at Cold and Warm Temperatures. *Journal of Materials Engineering and Performance*, 20:77–81.
- [9] J. Coër, C. Bernard, H. Laurent, A. Andrade-Campos, and S. Thuillier, (2010). The effect of temperature on anisotropy properties of an aluminium alloy. *Experimental Mechanics*.
- [10] H. Halim, D.S. Wilkinson, and M. Niewczas, (2007). The Portevin-Le Chatelier (PLC) Effect and Shear Band Formation in an AA5754 Alloy. *Acta Mater.*, 55, p 4151–4160
- [11] R. Grèze, P.Y.Manach, H. Laurent, S. Thuillier and L.F.Menezes, (2010). Influence of the temperature on residual stresses and springback effect in an aluminium alloy. *International Journal of Mechanical Sciences* 52 1094-1100.
- [12] Bolt PJ, Lamboo NAPM, Rozier PJCM. (2001). Feasibility of warm drawing of aluminum products. *J Mater Proc Technol* 115:118–21.
- [13] Seçgin, O., Savaş, V., (2010). An experimental investigation of forming load and side-wall thickness obtained by a new deep drawing die. *Int J Mater Form* 3:209–213.
- [14] Shoichiro, Y., Hisashi, N., Hirokuni, Y. and Ken-ichi, M., (2003). Formability Enhancement in Magnesium Alloy Stamping Using A Local Heating and Cooling Technique: Circular Cup Deep Drawing Process. *Journal of Materials Processing Technology* 142, pp. 609–613.
- [15] Özek, C., Ünal, E., (2012). Kare kapların derin çekilmesinde kalıp/baskı plakası açısının limit çekme oranı ve et kalınlığı üzerindeki etkisi. *Journal of the Faculty of Engineering and Architecture of Gazi University*, Vol 27, No 3, 615-622.

Investigation of Stator and Rotor Slit Effects on Medium Powered Induction Motor

Asim Gokhan Yetgin¹, Mustafa Turan², Mehmet Murat Tezcan³, Ali Ihsan Canakoglu⁴

Abstract

To improve the performance of the induction motors, several techniques are used. Especially in recent years, optimization of the stator and rotor slot geometrical parameters to stand out in academic publications. Furthermore, studies on magnetic and electrical design parameters, airgap length optimization, control techniques, cooling systems, using of efficient materials, using of different winding topologies are conducted for improve the performance of the induction motors.

In this study, different from these techniques, for decreasing the influence of armature reaction and for increasing the performance of the motor, a new approach is used. Object of the technique is using modified stator and rotor structure which have slitted stator and rotor teeth. Lengths of the slits are the same with stator and rotor slots height. Widths of the slits are designed at 0.1mm. For these analyses, 13.5 kW squirrel cage induction motor and FEA based simulation package program is used. Magnetic analyze, performance values, harmonic analyze are compared for reference motor and slitted motor.

Keywords: Induction Motor, Slits, Performance Analysis

1. INTRODUCTION

Three phase induction motors are the most frequently used machines in various electrical drives. About 70% of all industrial loads on a utility are represented by induction motors. Recently oil prices, on which electricity and other public utility rates are highly dependent, are rapidly increasing. It, therefore, becomes imperative that major attention be paid to the efficiency and operating cost of induction motors. To achieve minimum energy cost or maximum efficiency, the induction motor should either be redesigned or fed through an inverter [1].

In general, there are two broad approaches to improve the induction motor efficiency, namely optimal design (OD) and optimal control (OC). Many researchers have been reported several techniques on both the broad approaches. Some OC algorithms uses slip speed, rotor flux, power input and voltage as variables to optimize the motor performance. Some of the evolutionary algorithms for OD are available in the literatures [1]. Jagiela ve Garbiec have investigated that the effect of the solid rotor induction motor's stack length on the motor efficiency. They have shown that the solid rotor induction motor rotor stack length is 40 mm as experimentally and theoretically. Also slitting reduces the equivalent surface impedance of the rotor by increasing the penetration depth by the magnetic field in radial direction [2]. Pyrhonen and friends have examined the solid rotor induction motor with slits and without slits. They expressed that the best torque is reached when the slitting depth is 60% of the rotor radius. The rated per unit slip of the motor with 60% deep slits is 0.8% [3]. Power factor and torque of synchronous reluctance motors with a slit rotor are studied. In there stators, divided teeth made of powder magnetic core are adopted and windings are improved to get high space factor of stator windings and to shorten coil ends. In there rotors, stainless sheets are inserted among soft magnetic metal sheets with adhesive to strengthen the rotors and rotor structure is improved to enlarge the saliency ratio (L_d/L_q). As the result, the power factor 0.78 and 1.6 times torque at same motor size are attained [4]. Their paper presents an eddy current loss analysis for a transverse flux rotary machine (TFRM) with laminated stator cores, which consist of inner and outer cores whose laminated directions are perpendicular to each other. Although the TFRM is laminated to reduce eddy current losses, it still exhibits rapidly increasing core losses as the frequency increases. To solve this problem, slits are introduced to the stator outer core. Experimentally and analytically it was confirmed that slits are an efficient method to reduce eddy current loss in TFRMs with ring shaped steel sheets. The core loss decreases when the number of slits is increased [5]. Kondo and friends opened the slits the permanent magnet synchronous motor's (PMSM) teeth parts. The triangle slits types graphic are given in Figure 1. They expressed that the efficiency value is improved the 5 points with proposed slit construction [6].

¹ Corresponding author: Dumlupinar University, Department of Electrical and Electronics Engineering, 43100, Kutahya, Turkey. gokhan.yetgin@dpu.edu.tr

² Sakarya University, Department of Electrical and Electronics Engineering, 54000, Sakarya, Turkey. turan@sakarya.edu.tr

^{3,4} Dumlupinar University, Department of Electrical and Electronics Engineering, 43100, Kutahya, Turkey. murat.tezcan@dpu.edu.tr, aihsan.canakoglu@dpu.edu.tr

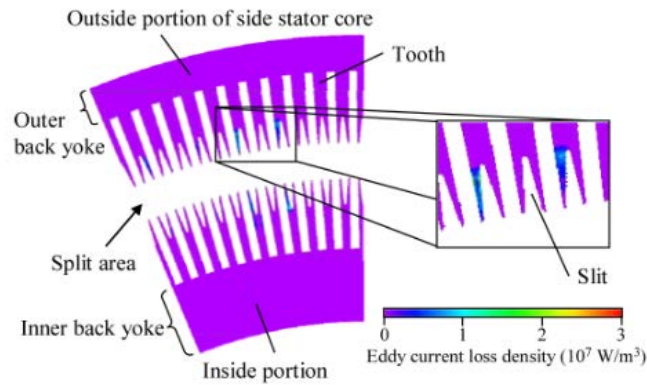


Figure 1. PMSM with slits

Aho and friends investigated that the effect of slit depth on the solid rotor induction motor performance. The solid rotor induction motor model with slits is given in Figure 2. They have explained that give a better field distribution but rotor's mechanical strength reduces by using slitted motor structure and also analytically solution is difficult [7].

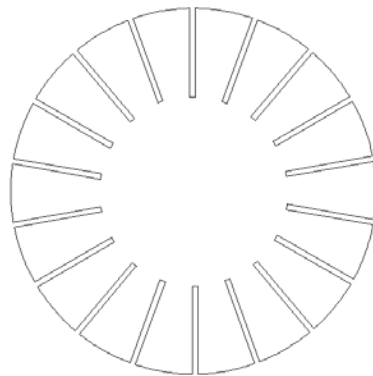


Figure 2. Solid rotor induction motor with slits

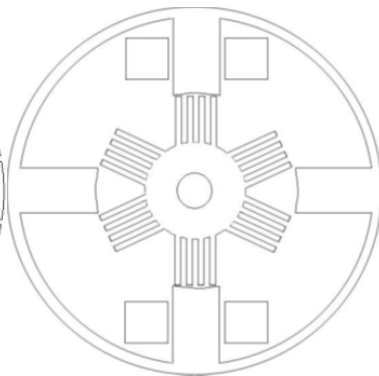


Figure 3. SRM with slits

Chan and Hamid in their paper, they investigated to the switched reluctance motor (SRM) model using FEM. They analyzed that changing of the magnetic flux density, torque and current value by opening the different number of the slits on the rotor construction. Their motor model is given in Figure 3. They obtained that both current and torque graphics which are a flat waveform and the output power is increased by 16% (without increase of the current peak value) using five slitted motor construction. They also expressed the saturation can be controlled by changing the number of slits in the rotor [8]. Li et al. suggested slitted structure model in order to prevent the armature reaction in hybrid excitation synchronous machine. They stated that the effect of armature reaction could be reduced by making flux line longer with slitted structure. Hybrid excitation synchronous machine with slitted construction is given Figure 4. This kind of methods has also been explored for claw pole machine application in stator teeth and in claw poles [9].

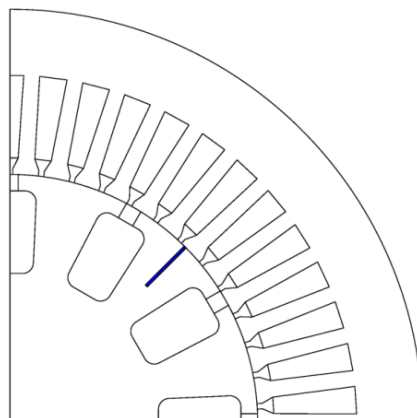


Figure 4. Hybrid excitation synchronous machine with slit

Figure 5. Claw pole machine with slits [10]

Rajagopalan and Murty in their paper, they expressed to the composite permeability method is unable to bring out, quantitatively, the influence of number, depth, and width of the slits. This implies that the performance of the 38 slits rotor should be better than the 6 slits rotor. Increase in the depth of the slits results the rotor impedance falls down and I_r rotor current increases, resulting in better performance [11].

In this paper, the slits opened between the stator and rotor teeth of three phase squirrel cage induction motor. The aims of the slits are reducing the armature reaction and improve the motor performance. The reference motor and slitted motor are modelled using FEMM (Finite Element Method Magnetics) package program. Distribution of magnetic flux density, graphics of performance and harmonic values are investigated for reference and slitted motor models.

2 MOTOR AND ITS SPECIFICATIONS

The nameplate values are given in Table 1 for the motor which is modelled reference and slitted construction.

Table 1. Induction motor nameplate values

Parameters of motor	Values
Power (kW)	13.5
Voltage (V) (L-L)	460
Number of poles (2p)	2
Stator winding connection type	Wye
Frequency (Hz)	60
Number of phases (m)	3

The advantages of slitted construction according to reference motor are [12]:

- The more effective using of the magnetic flux for all the working areas: reduction of saturation, properly distribution of flux at the teeth, reduction of rotor reaction
- Decreasing additional losses: a properly flux distribution
- The reduction of loss values: loss values improve due to decreasing saturation and iron losses
- The reduction of slip: decreasing rotor copper loss
- The improvement of efficiency: the efficiency increases because of decreasing losses
- The improvement of performance at the nominal operating points
- The improvement of leakage reactance: the improvement of speed-torque characteristic
- For big power motors, there will be no extra cost due to the new mold to be created for mass production

The disadvantage of the slitted construction is:

- For small power motors, the initial construction cost is slightly high owing to cut off the core with laser
- Solution time is longer than reference motor

The stator and rotor slots types and slits which is opened between the stator and rotor teeth for slitted motor model are given in Figure 6. The slit depth is chosen in stator and rotor slot height, the slit width is chosen 0.1 mm. The slit width and depth is determined according to the results obtained from the author's previous studies [12-14].

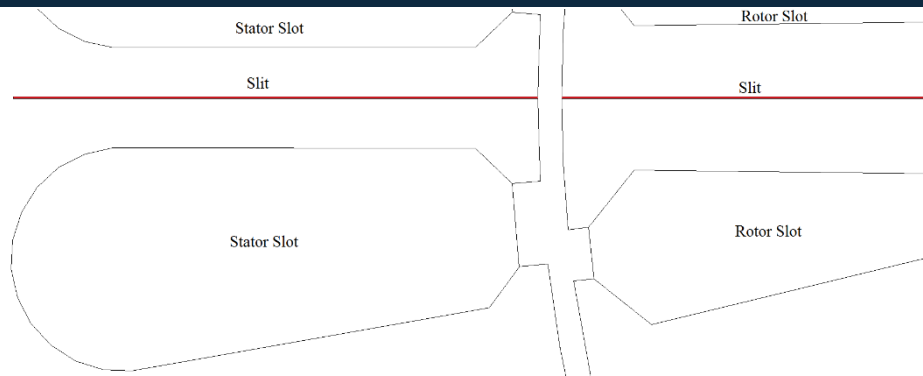


Figure 6. Stator and rotor slot types and slits

The motor models which have double and triple slits and have different slit heights are given in Figure 7. It was observed that magnetic flux density is increased due to the increase of the number of the slits and decrease of the distance of the stator and rotor teeth. For this reason, it was determined that this affects adversely the performance of the motor. In case of different heights of the slits, it was found that the magnetic flux lines complete their circuit from through of the stator and rotor slots.

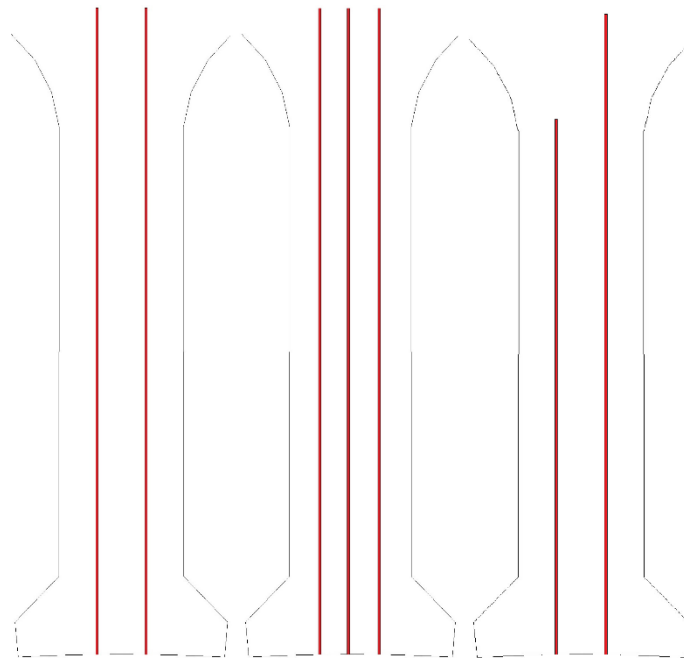


Figure 7. The other slitted motor models

3 RESULTS

The distribution of air gap magnetic flux of both motors are given in Figure 8. Figure 8 (a) is for the reference motor, Figure 8 (b) is the slitted motor model. The field distribution is analyzed that a reduction in magnetic flux density value is observed in the yoke part of the stator and rotor. However, a decrease was observed in the magnetic flux distribution in the shaft part. Only, an increase in magnetic flux density values in the bottom part of the slits was observed in the slitted structure.

In the FEMM [15] models, 131806 nodes and 263420 elements are used for the reference motor; 251140 nodes and 502092 elements are used for the slitted motor. The analysis time of the slitted motors is long according to the reference motor model. It is due to the more number of elements and the number of triangles.

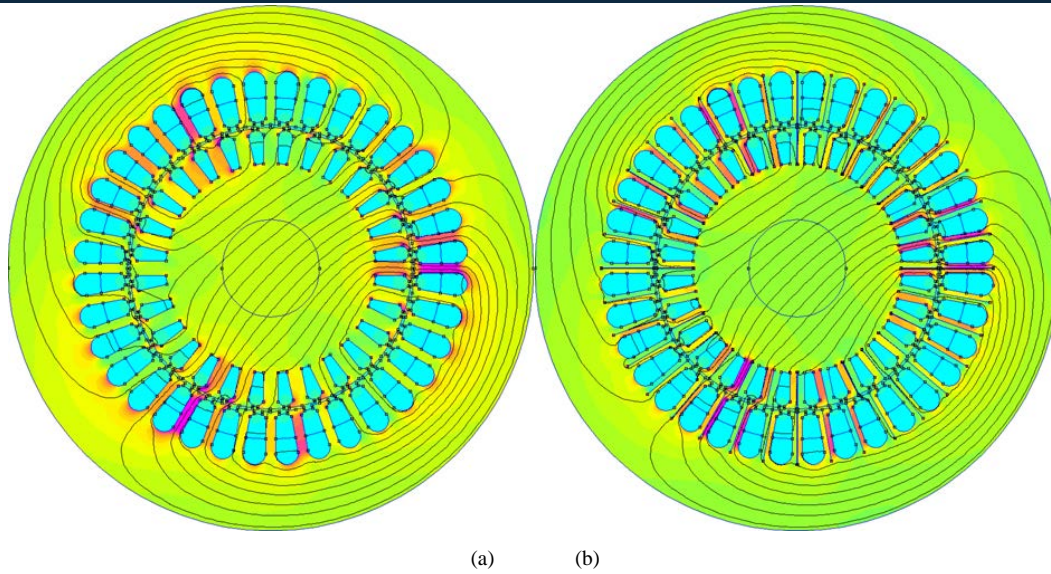


Figure 8. Distribution of magnetic flux density for (a) reference motor and (b) slitted motor

The slip-torque graphic is given in Figure 9 for reference and slitted motor models. This graphic is plotted to results which are obtained from FEMM analysis. The figure is examined; the starting torque is increase by 0.45% for slitted motor construction and the maximum torque and the nominal torque values also increase by 4.97% and by 2.6% respectively. The slip-efficiency graphic is given in Figure 10 for both motor models.

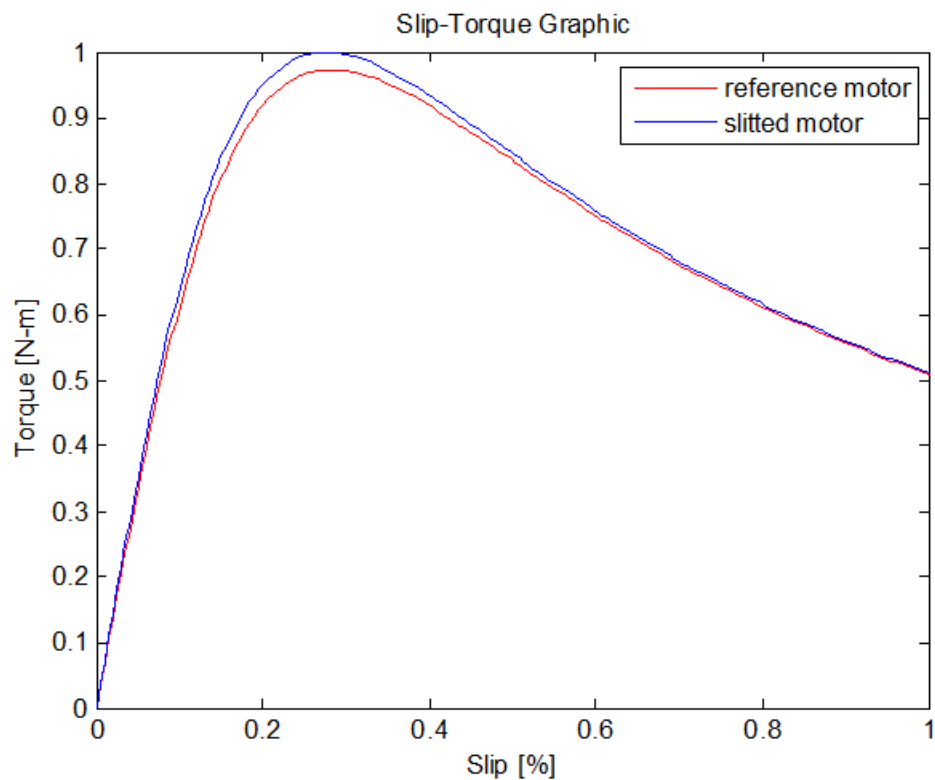


Figure 9. Torque-slip graphic for both motors

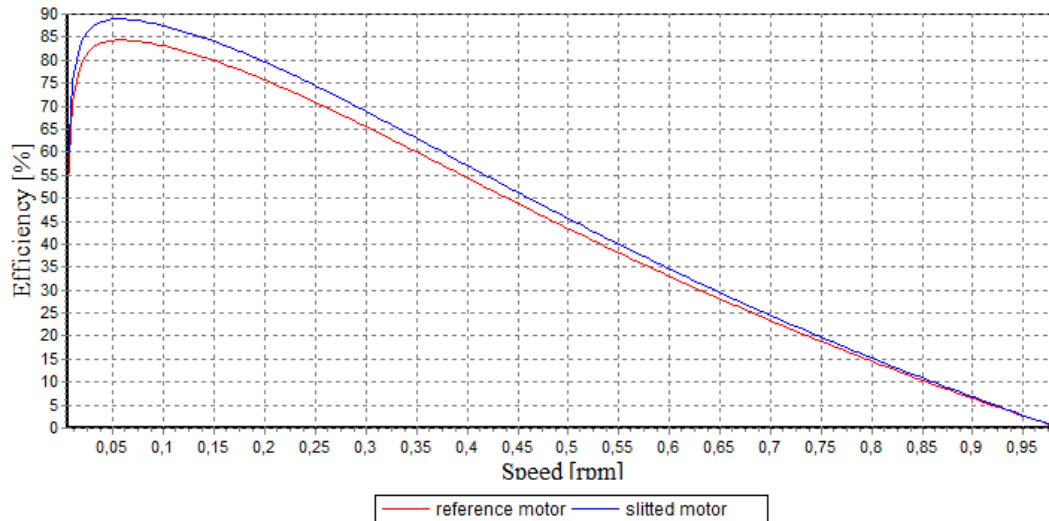


Figure 10. Efficiency-slip graphic for both motors

The Figure 10 is examined; the efficiency value is increased by 5.61% for slitted motor model in nominal operating point.

Distribution of magnetic flux and harmonic values for reference motor are given in Figure 11.

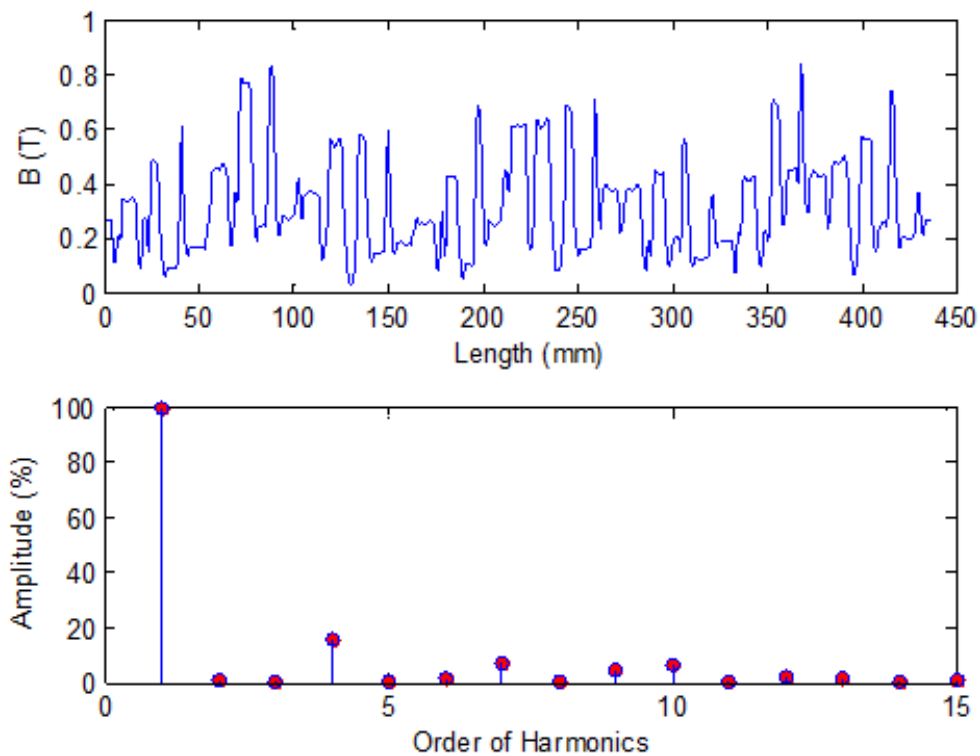


Figure 11. Distribution of air-gap magnetic flux and harmonics for the reference motor

Distribution of magnetic flux and harmonic values for slitted motor model are given in Figure 12.

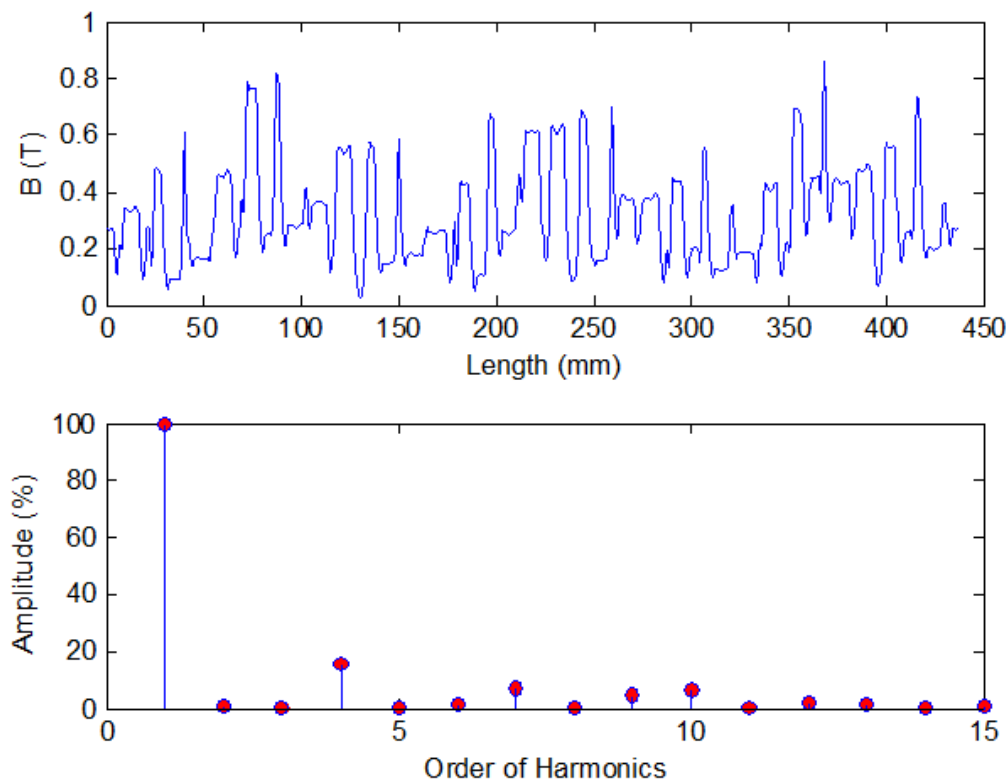


Figure 12. Distribution of air-gap magnetic flux and harmonics for the one slitted motor

Harmonic values for reference and slitted motor models are given in Table 2. The table is examined; the fifth harmonic value is decreased by 23.75%, and ninth harmonic value is decrease by 1.2%. The 7th harmonic value is increased by 0.46% for slitted motor construction.

Table 2. Harmonic values for both motor

Order of harmonic	Reference motor	Slitted motor	Difference [%]
5 th harmonic	0.2	0.1525	- 23.75
7 th harmonic	7.16	7.1935	+ 0.46
9 th harmonic	4.9055	4.8471	- 1.2

CONCLUSIONS

In this study, the slits are opened between the stator and rotor teeth of a 3-phase induction motor. The FEMM and harmonic analysis of reference and slitted motors are performed. The results can be listing as follows:

1. The magnetic flux in the yoke of the rotor in slitted motor is reduced.
2. The torque values are increased as a result of the decreasing the slot leakage fluxes and air gap zig-zag fluxes and increase the useful flux.
3. As a results of harmonic analysis, especially the value of 5th harmonic are decreased about 23.75%.
4. The analysis time of the slitted motors is took a long.
5. Increased the number of slit is affected the motor performance negatively.

REFERENCES

- [1]. C. Thanga Raj, S. P. Srivastava, and P. Agarwal, "Induction motor design with limited harmonic currents using particle swarm optimization," *International Journal of Electrical, Computer, Energetic, Electronic and Communication Engineering*, vol. 2, no. 10, pp. 2348-2354, 2008.
- [2]. M. Jagiela, and T. Garbiec, "Determination of best rotor length in solid-rotor induction motor with axial slitting," *Archives of Electrical Engineering*, vol. 61, no. 2, pp. 267-276, 2012.

- [3]. J. Pyrhonen, J. Nerg, A. Mikkola, J. Sapanen, and T. Aho, "Electromagnetic and mechanical design aspects of a high-speed solid-rotor induction machine with no separate copper electric circuit in the megawatt range," *Electr Eng*, vol. 91, pp. 35–49, 2009.
- [4]. N. Masayuki, I. Yoshimitu, K. Youichi, Y. Takanori, S. Akiyoshi, and O. Shigeru, "Improvements of power factor and torque of a synchronous reluctance motor with a slit rotor," *IEEJ Transactions on Industry Applications*, vol. 126, no. 2, pp. 116-123, 2006.
- [5]. J. Y. Lee, D. H. Koo, D. H. Kang, and J. P. Hong, "Stator core with slits in transverse flux rotary machine to reduce eddy current loss," *Journal of Magnetism*, vol. 17, no. 1, pp. 51-55, 2012.
- [6]. K. Kondo, T. Maekawa, and S. Kusase, "A new multi air gap motor with trench shaped coil for hev applications," SAE International, 2014, pp. 67-74.
- [7]. T. Aho, J. Nerg, and J. Pyrhonen, "Influence of rotor slit depth on the performance of the solid rotor induction motor," *Energy Efficiency in Motor Driven Systems Conference Proceedings*, Sep, 2005, vol. 1, pp. 81–89.
- [8]. S. Chan, and M. N. Hamid, "Finite element study on a two-phase switched reluctance motor with split rotor poles," *Power Electronics and Drives Systems PEDs 2005 International Conference*, Nov-Dec, 2005, pp. 1156-1160.
- [9]. L. Li, A. Foggia, A. K. Lebouc, J. C. Mipo and L. Kobylansky, "Some armature reaction compensation methods numerical design of experiments and optimization for a hybrid excitation machine," in *Int. Electric Machines and Drives Conf.*, Miami, United States, 2009, pp. 832-838.
- [10]. Y. Tamto, "Determination des paramètres de la machines griffes: application au domaine automobile (Determination of claw pole generator parameters: for vehicle application)," Ph.D. Dissertation, Grenoble Electrical Engineering Laboratory, Inpg, France, 2008.
- [11]. P. K. Rajagopalan and V. B. Murty, "Effects of axial slits on the performance of induction machines with solid iron rotors," *IEEE Transactions on Power Apparatus and Systems*, vol. Pas-88, no. 11, pp. 1695-1709, Nov. 1969.
- [12]. A. G. Yetgin, "Performance improvement of induction motor with slitted core design," Ph. D. Dissertation, Dept. Electr. and Electron. Eng., Sakarya Univ., Sakarya, Turkey, 2010.
- [13]. A. G. Yetgin, M. Turan, and E. Unlukaya, "Analyzing the effect of slit depth and width on the electrical performance of a squirrel cage induction motor," *The Second International Symposium on Engineering, Artificial Intelligence and Applications (ISEAIA 2014)*, 5-7 Nov. 2014, Girne, North Cyprus, pp. 24.
- [14]. A. G. Yetgin, and M. Turan, "Optimization efficiency of slitted-core induction motor," *Journal of Electrical Engineering-Elektrotechnicky Casopis*, nol. 65, no. 1, pp 60-64, 2014.
- [15]. D. Meeker, "Induction motor example," 2002.

Influences of Winding Topology and Turn Number on Induction Motor Performance and Space Harmonics

Mehmet Murat Tezcan¹, Asim Gokhan Yetgin¹, Ali Ihsan Canakoglu¹

Abstract

Magnetic design and electrical design are the two of the most important parameters on designing the electric motors. Two of the parameters are directly affect the performance and efficiency of the electric motor. Especially the winding topology and distribution of the coils to the stator slots are affect not only the airgap magnetic flux distribution but also the back electromotive forces on windings. Other important parameters that affect the airgap space harmonics and torque ripple are whole coiled winding type or half coiled winding type, cross section and number of conductors in slots. In this study, influence on a 1.5 kW induction motor performance when modifying the winding type and turn number is investigated. Furthermore, harmonic analyses of each type of motor are studied. For these analyses, FEA based simulation package program is used. Equivalent circuit parameters, magnetic analyze parameters, physical and electrical parameters and performance values (torque, efficiency etc.) are compared for different winding turn numbers and different winding topologies. Comparing of the analytical and numeric solutions, optimum design parameters are determined.

Keywords: *Induction Motor, Winding Topology, Finite Element Method, Harmonic Analysis*

1. INTRODUCTION

The squirrel cage induction motor has been used in all kinds of electric drives more often than other electric motors because of its reliability, robustness and simplicity of its construction. The classical theory of this electromechanical component is based on the assumption that the rotating mmf produced by stator winding excitation is sinusoidally distributed in space and that the rotor mmf due to the slip frequency induced currents is similarly distributed. This condition would only exist, however, if the surfaces of the stator and rotor were both smooth, and the windings were sinusoidally distributed on them. In the real machine, windings are placed in slots and therefore the resulting mmf and flux density distributions are not sinusoidal and contain apart from the fundamental wave, a series of space harmonics. The space harmonics effects must be considered precisely during the design process of the induction machine to achieve good motor performance. These effects are of many kinds: asynchronous crawling, locking and synchronous crawling, magnetic noise, vibration and speed ripples. On the other hand the space harmonics have also a great influence on the harmonic content of stator currents [1].

Three-phase stator winding is one of the most important construction parts of these motors. Main energy interchange processes take place in this winding therefore it essentially determined the operation of the motor. When electric currents forming the symmetric three phase system of the currents flow through the three phase winding of induction motor they create non-sinusoidal magnetic fields which move in space and periodically change their shape in the course of time. Usually only odd space harmonics except for the multiples of three exist in the harmonic spectrum of these non-sinusoidal magnetic fields. There are many different constructions of the three phase windings of induction motors and each of them have distinctive parameters. Therefore harmonic spectrum of the magnetic fields created by these windings and at the same time the electromagnetic properties differ and they in turn determine the power indexes and operation quality of induction motors. Electromagnetic efficiency factor is used to evaluate electromagnetic properties of three-phase windings [2]. The influence of the space harmonics must be considered precisely during the design process of induction machines to achieve good motor performance by minimizing the vibrations and the undesirable asynchronous, synchronous crawling and synchronous locking torques. On the other hand, the space harmonics have also a great influence on the harmonic content of the stator currents. It is possible to use this information to estimate the rotor speed for control purpose or to monitor some mechanical defaults like rotor eccentricity, broken rotor bars, cracked rotor end-rings or shorted windings [3]. The instantaneous magnetic fields in induction motors include both space and time harmonics. They are caused respectively by the geometrical effect of winding and slots and by the saturation and static converters. If the motor is driven by sinusoidal voltage sources, the phase-belt harmonics and slot harmonics of the stator and rotor cause relatively large harmonic copper and core losses and breaking forces, which may decrease the torque of the motor [4]. Rotating machines are considered a source of harmonics because the windings are embedded in slots which can never be exactly sinusoidally distributed so that the mmf is distorted. Low-order harmonics have a larger impact on the three-phase induction motor than that

¹Corresponding author: Dumlupinar University, Department of Electrical and Electronics Engineering, 43100, Kutahya, Turkey. murat.tezcan@dpu.edu.tr

of high-order harmonics [5]. Quispe and friends have examined the three phase induction motor when supplied by unbalanced and harmonics voltage. They have showed that a poor quality voltage has bad effects over the motor performance such as loss, temperature rise, rated output power, efficiency, magnetic noise and reliability [6]. Mirzamani and Choobari have investigated the effect of harmonics on temperature rise of induction motors with using steady state model and thermal model. They have showed that temperature rise of induction motor due to harmonics is approximately between 4-6 °C, and this impact of harmonics on induction motors must be take into account in selecting the motor insulation class and life assessments. Also they have showed that the harmonics below 5th have significant impact on temperature rise and can cause more loss of life [7]. Birbir and Nogay have explained the effect of chording (fractional pitch) on three phase squirrel cage induction motors fed from a three phase inverter [5]. Yamazaki has proposed and investigated a method of calculating the losses of induction motors involving iron loss, considering the effects of the slot harmonics and the rotational magnetic field. He has applied to four types of induction motors, which are the solid rotor induction motors with/without slot and the cage induction motors with/without skew [8]. Rata and friends paper presents a solution for the estimation of induction machine rotor speed utilizing harmonic saliencies created by rotor and stator slotting. Their solution purposes to add a carrier-signal voltage at the fundamental excitation [9]. Their paper deals with the design of irregular AC windings by a new method. Their new method is based on the notion of local density of conductors. They stated that this type of winding can be used to reduce higher harmonic components of magnetic flux density in the air gap, mainly the fifth and the seventh harmonic [10]. Zhang and friends' paper presents several methods for stator winding design of induction motors to obtain higher efficiency. They are analyzed the configuration and connection form of stator windings [11]. Buksnaitis has presented a new approach for evaluation of electromagnetic properties of three-phase windings, on the basis of which it is easy to compare different type windings of different parameters and to determine the optimal one [12].

2. TYPES OF WINDINGS AND PHYSICAL-ELECTRICAL SPECS OF INDUCTION MOTOR

2.1. Types of Three Phase Stator Windings

Windings which produce the rotating magnetic field are the most important part of the machine. In general, windings are prepared half coiled or whole coiled in conventional induction machines. These windings are distributed in stator slots with the 120 mechanical degrees for creating the three phase [13]. In another point of view, these winding topologies have electrical differences. For example, a half coiled winding topology has a lower iron loss but it has a bigger power factor so far as whole coiled topology. Despite that, coil pitch reduction is limited with only one slot for half coiled topology but it is not limited for whole coiled topology [14].

2.1.1. Single Layer Windings

Single layer winding is common in small ac machines of power rating below 15 HP, though this mainly depends on the manufacturer. And such machines have large number of conductors per slot. Single layer windings have higher efficiency and quieter operations due to the openings of their narrow slots. Single layer windings are highly insulated because of the end connections that are separated by large air spaces which make them suitable for high voltages. The absence of inter layer separator is due to higher space factor [15]. Single layer windings may be concentric, lap or wave type. Single layer windings have a few advantages. One of them is higher efficiency and quieter operation because of narrow slot openings, the other is space factor for slots is higher owing to absence of inter layer separator [16]. Schematic diagram of 36 slots, 4 poles and half coil winding motors is given in Figure 1.

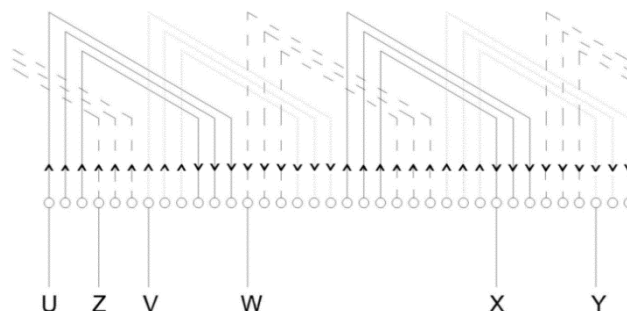


Figure 1. $N_s=36$, $2p=4$, $m=3$, half coil winding diagram

2.1.2. Double Layer Windings

This topology is used for big powered induction machines. To decrease the high level winding harmonics, it should be used coil reduction for wide edges [13]. Double layer windings have many advantages over single layer windings: easier to manufacture and lower cost of coils, fractional-slot can be used, chorded-winding is possible, lower leakage reactance and therefore, better performance of the machine [17]. The double layer windings are the most widely used class of windings. Though both lap and wave types are possible, because of inherent problems of wave windings, it is now an accepted practice to use the lap type for double layer AC windings [18]. Schematic diagram of 36 slots, 4 poles and whole coil winding motors is given in Figure 2.

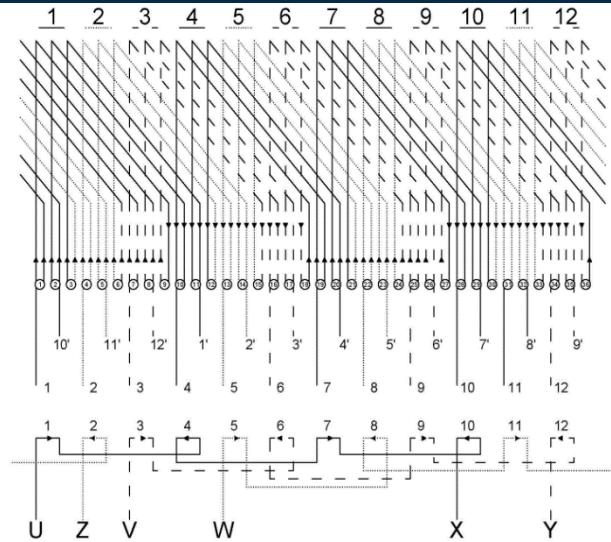


Figure 2. $N_s=36$, $2p=4$, $m=3$, whole coil winding diagram

2.2. Geometrical and Electrical Specs of Induction Motors

In Table 1 basic geometrical and electrical parameters of 36-28 slot, 4 pole, induction motor are given. Total circulating power in induction motor is 1.5 kW at 1500 rpm shaft speed. Figure 3 shows the general 2D geometry description of induction motor.

Table 1. Physical dimensions and nameplate of the six motors

Parameters of motors	Values
Stator core inner diameter	80 mm
Stator core outer diameter	136 mm
Rotor core inner diameter	24 mm
Rotor core outer diameter	79.4 mm
Air gap length	0.3 mm
Stack length	96.3 mm
Shaft diameter	24 mm
Voltage (L-L)	380 V
Number of poles (2p)	4
Stator winding connection type	Star
Frequency	50 Hz
Number of phases (m)	3
Output Power	1.5 kW

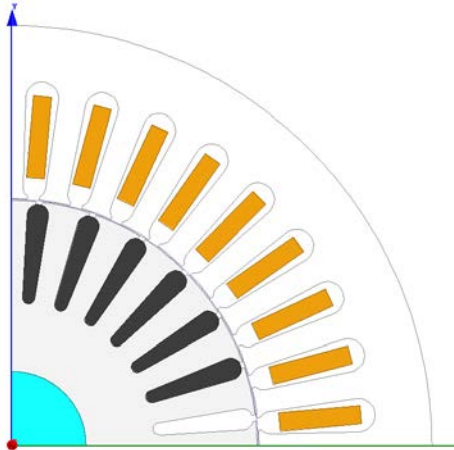


Figure 3. The general 2D geometry description of induction motor

3. AIRGAP FLUX HARMONICS OF STATOR WINDINGS

Given that a sinusoidal variation of air gap flux density is required then harmonic analysis becomes of immense value and the harmonic flux density that it extracts become a useful vantage point for assessing the efficacy of a machine design. But harmonic analysis can provide more information of equal value, it can indicate the presence of negative sequence (reverse rotating), and less commonly zero sequence fields, and can also indicate how well each harmonic couples into the machine (harmonic winding factors) [19].

Two types of winding topology are used in this study. One of them is half coiled distributed winding topology; the other one is whole coiled winding topology. The difference between two types is the coil pitch of whole coil winding is one slot greater than half coiled winding. In practice, this situation decreases the airgap flux density distribution harmonics. Therefore induced back EMF's in phases are more sinusoidal. As expected, efficiency of the motor will be increased. On the other hand, various winding turn numbers affect the performance of the motor. Both of the winding topologies were simulated by FEA program and influence of total magnetomotor forces on motor performance analyzed carefully.

In Figure 5 (a) and (b), winding arrangements of half coiled and whole coiled distributed winding topologies are shown respectively.

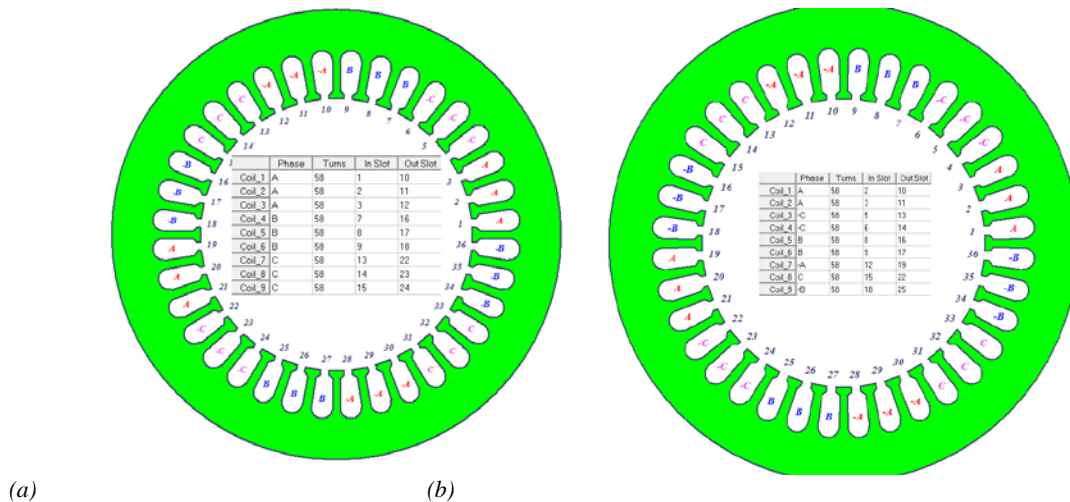


Figure 5. (a) Half coiled distributed winding, (b) whole coiled distributed winding

Manufacturers prefer 50 percent of stator slot fill factor to practical coiling to phase windings. Therefore, it is necessary to do an optometric analysis to observe the suitable slot fill factor for 1.5 kW output power. In terms of 1.5 kW output power for 1430 rpm of different turn numbered half coiled windings, there is increase of output power according to increasing of turn number. Figure 6 shows that the increasing output power for lower speeds and higher slot fill factor (48 turns near %45 slot fill factor, 58 turns near %50 slot fill factor) of the half coiled machine for suitable slot fill factor.

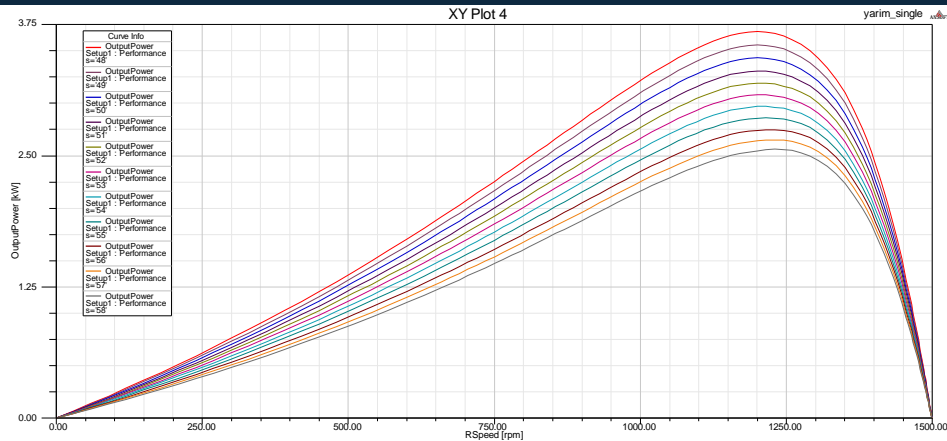


Figure 6. Increasing output power for lower speeds of the half coiled machine for suitable fill factor

Similarly for whole coiled winding topology, Figure 7 shows the variation of the phase winding turn number influence on output power.

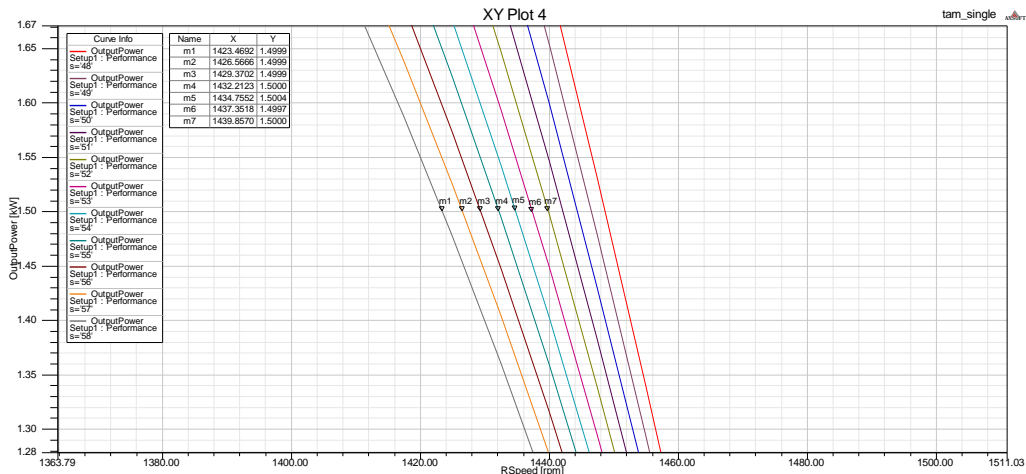


Figure 7. Variation of the phase winding turn number influence on output power for speed range

On the other hand, Figure 8 and 9 shows the comparing of motor efficiencies with different turn numbers of half coiled and whole coiled winding topologies respectively at 1447 rpm constant speed.

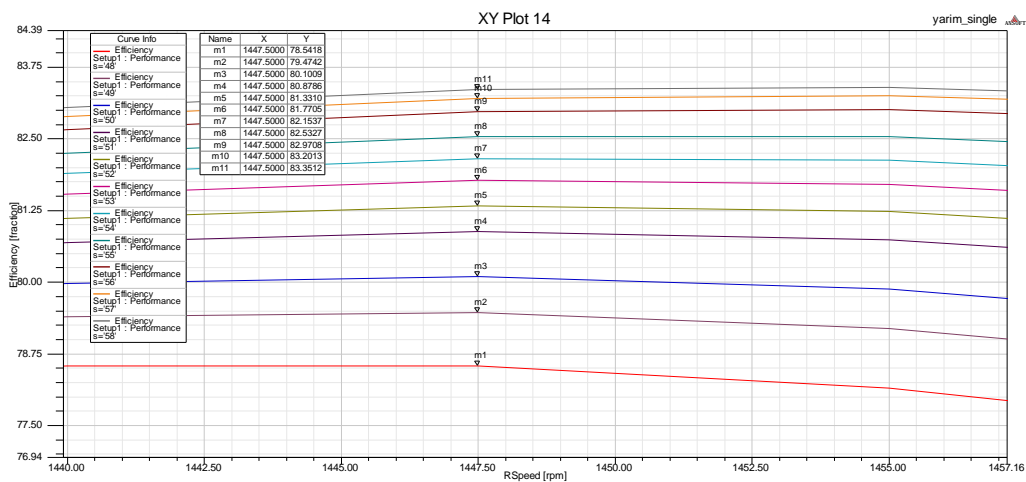


Figure 8. Comparing of motor efficiencies with different turn numbers of half coiled winding topology

Different turn numbers directly affects the total magnetomotor force in airgap. An optimum analysis has performed for optimum turn number in a slot for both of the winding topologies. Therefore, increasing turn number to near of 58 turns for a slot, gives high performance for motors. Figure 8 shows the increasing of efficiency for half coiled distributed winding topology according to suitable slot fill factor (%50). Similarly Figure 9 shows the increasing of

efficiency for whole coiled distributed winding topology according to suitable slot fill factor (%50). Comparing two winding topologies, whole coiled winding topology gives %1-2 better efficiency performance for similar motor structures. Motor core frames are similar therefore core losses are stable for 50 Hz frequency.

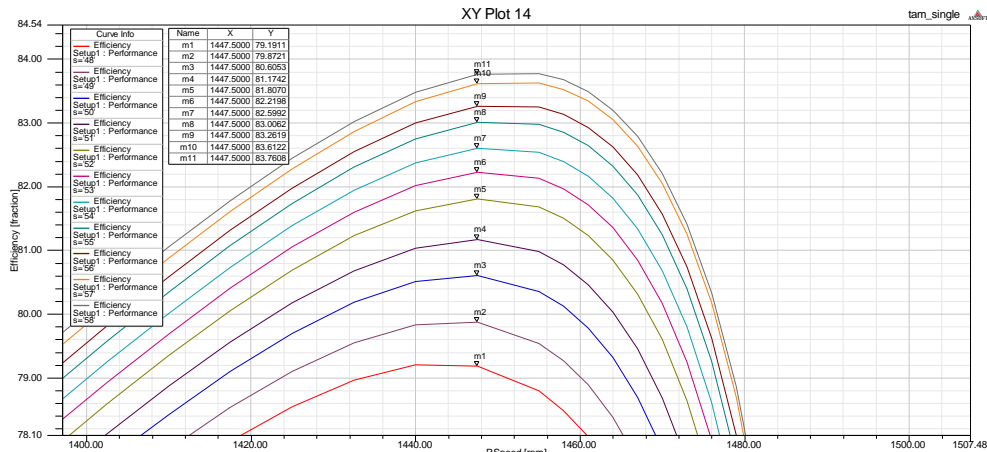
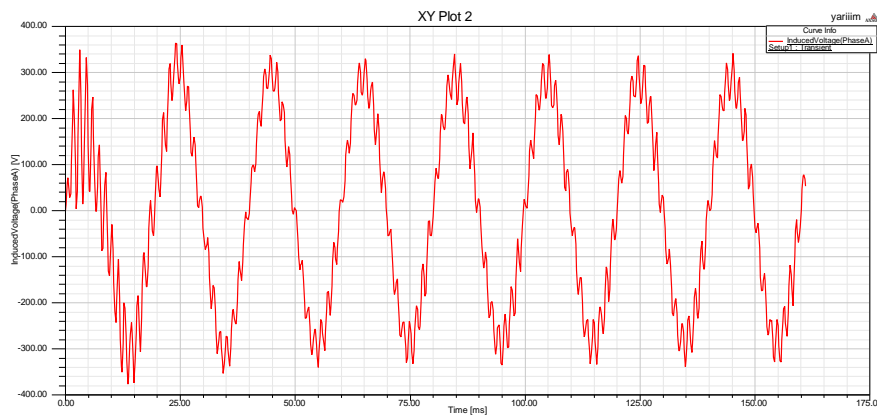
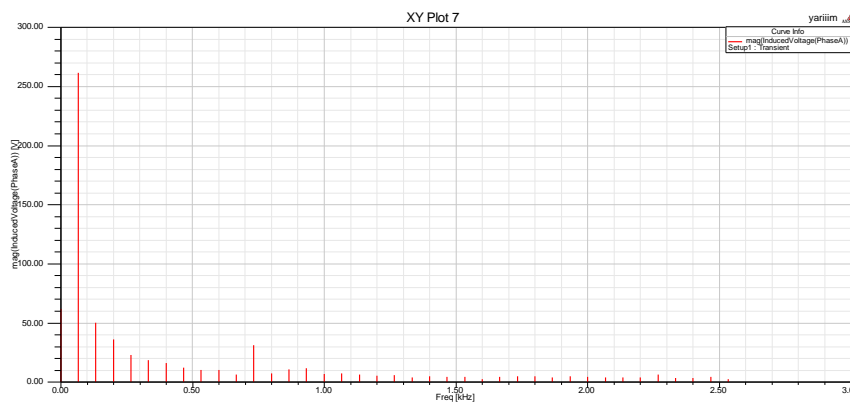


Figure 9. Comparing of motor efficiencies with different turn numbers of whole coiled winding topology

Looking the motor torque from induced phase back EMF's and its harmonics, both of the winding topologies are compared, Figure 10 shows the phase back EMF's and their harmonic values respectively. Whole coiled winding topology is also same back EMF characteristic with half coiled one. Layer situation is same for both topologies. Therefore similar harmonic and torque ripple performance for two types of motors is achieved.



(a)



(b)

Figure 10. The phase a back EMF (a) and its harmonic spectrum (b) of half coiled winding.

Similarly, induced torque values powered by half coiled and whole coiled windings are quite similar. Both of the torque ripple values are shown in Table 2. In Equation (1), calculation of torque ripple is shown.

$$\% T_{ripple} = \frac{T_{max} - T_{min}}{T_{avg}} \quad (1)$$

The whole coiled winding's steady state output torque graphic is shown in Figure 11. In the figure maximum value of output torque is 13.25 Nm, minimum value of output torque is 9.2 Nm and mean value of the output torque is 11.25 Nm. Therefore the torque ripple value is % 12.

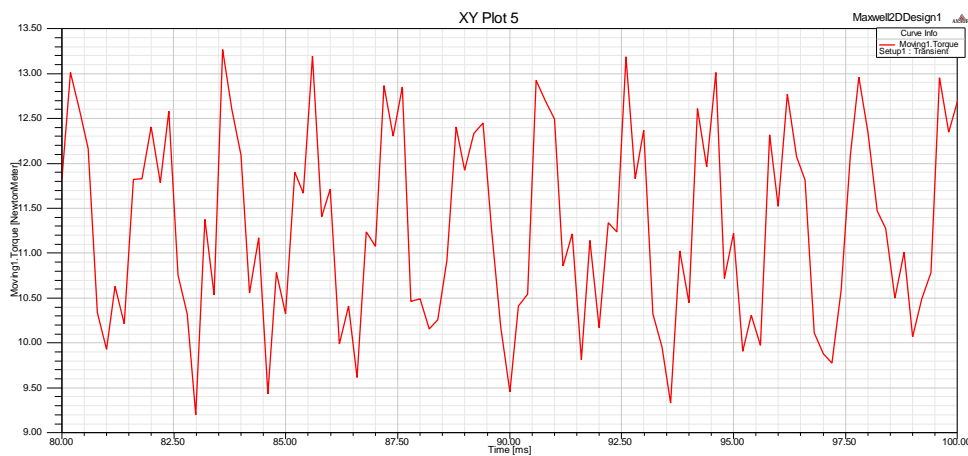


Figure 11. The whole coiled winding's steady state output torque graphic

The half coiled winding's steady state output torque graphic is shown in Figure 12. In the figure maximum value of output torque is 10.25 Nm, minimum value of output torque is 6.56 Nm and mean value of the output torque is 8.25 Nm. Therefore the torque ripple value is %9.25.

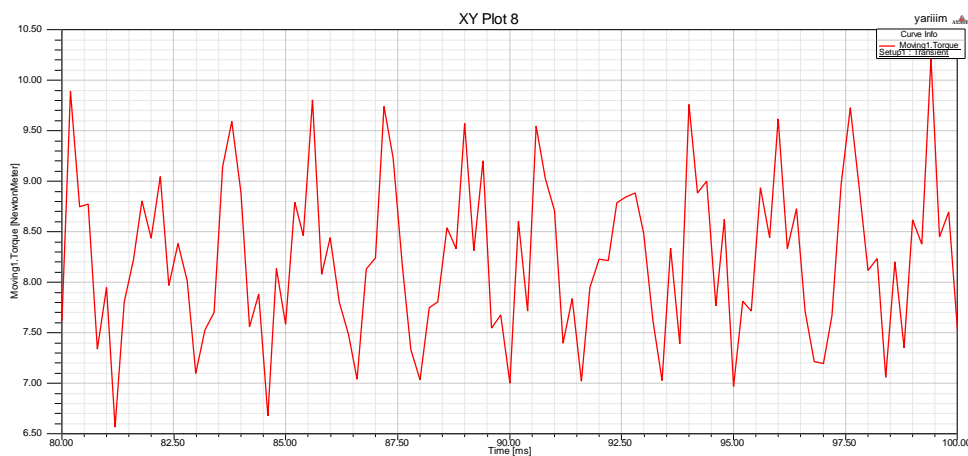


Figure 12. The half coiled winding's steady state output torque graphic

Comparing two output torques, whole coiled winding generates required torque value but it has a bit bigger ripple value at same speeds.

4. CONCLUSION

Winding topology is one of the most important performance parameter for induction machines. For half coiled or whole coiled winding topology, slot fill factor is necessary for airgap magnetomotor force and efficiency. In practical, manufacturers choose the %50 fill factor for easy coiling. An optimetrics analysis has done for suitable turn number for 50 percent fill factor. Both of half coiled and whole coiled windings best efficiency performance achieved with 58 turns in a slot for 1450 rpm shaft speed. Whole coiled winding topology gives better efficiency performance for suitable turn number. Whole coiled winding topology is also same back EMF characteristic with half coiled one. Layer situation is same for both topologies. Therefore similar harmonic and torque ripple performance for two types of motors is achieved. Comparing two output torques, whole coiled winding generates required torque value but it has a bit bigger ripple value at same speeds.

REFERENCES

- [1] M. Y. Kaikaa, F. Babaa, A. Khezzar, and M. Boucherma, "Analytical analysis of rotor slot harmonics in the line current of squirrel cage induction motors," *Journal of Electrical Engineering*, vol. 57, no. 1, pp. 12-19, 2006.
- [2] J. Buksnaitis, "Power indexes of induction motors and electromagnetic efficiency their windings," *Electronics and Electrical Engineering*, vol. 4(100), pp 11-14, 2010.
- [3] R. B. Stincescu, P. Viarouge, J. Cros, and I. Kamwa, "A general approach of space and time harmonics interactions in induction motors," *Electric Machines and Drives. International Conference IEMD '99*, Seattle, WA, May 1999 pp. 366-368.
- [4] Y. Ouazir, "Computation of the effect of space harmonics on starting process of induction motors using TSFEM," *Journal of Electrical Systems*, Special Issue no. 01, pp. 48-52, 2009.
- [5] Y. Birbir, and H. S. Nogay, "Harmonic variations in three-phase induction motors fed by pwm inverter with different stator coil pitches," *Proceedings of the 6th WSEAS International Conference on Applications of Electrical Engineering*, Istanbul, Turkey, May 27-29, 2007, pp. 195-199.
- [6] E. Quispe, G. Gonzalez, and J. Aguado, "Influence unbalanced and waveform voltage on the performance characteristics of three-phase induction motor," pp. 1-5.
- [7] H. O. Mirzamani, and A. L. Choobari, "Study of harmonics effects on performance of induction motors," 8th WSEAS International Conference on Circuits, CSCC 2004, Greece, 2004, pp. 487-837.
- [8] K. Yamazaki, "Loss calculation of induction motors considering harmonic electromagnetic field in stator and rotor," *Electrical Engineering in Japan*, vol. 147, no. 2, pp. 63-73, 2004,
- [9] G. Rata, M. Rata, I. Graur, and D. L. Milici, "Induction motor speed estimator using rotor slot harmonics," *Advances in Electrical and Computer Engineering*, vol. 9, no. 1, pp. 70-73, 2009.
- [10] R. Cipin, and M. Patocka, "Electromagnetic design of irregular three phase windings," *15th European Conference on Power Electronics and Applications (EPE)*, Lille, 2-6 Sept. 2013, pp. 1-10.
- [11] L. Zhang, Y. Huang, J. Dong, B. Guo, and T. Zhou, "Stator winding design of induction motors for high efficiency," 17th International Conference on Electrical Machines and Systems (ICEMS), Hangzhou, China, Oct. 22-25, 2014, pp. 130-134.
- [12] J. Buksnaitis, "New approach for evaluation of electromagnetic properties of three-phase windings," *Electronics and Electrical Engineering*, no. 3(75), pp. 31-36, 2007.
- [13] I. Coskun, and Y. Korkmaz, "Effects of the structure of asynchronous motor winding on the performance of 3 phase motor fed by public supply," *Journal of The Faculty of Engineering and Architecture of Gazi University*, vol. 22, no. 4, pp. 927-932, 2007.
- [14] Y. Korkmaz, "Performance effect of inverter fed on the different wounded induction motors," Ph. D. Dissertation, Institute of Science and Technology, Gazi University, Ankara, Turkey, 2005.
- [15] E. A. Yahaya, "Single layer winding of three phase induction motor," *The International Journal of Engineering and Science*, vol. 2, no. 4, pp. 8-13, 2013.
- [16] <http://www.ustudy.in/node/2159>, 2016 (Accessed 15.01.16)
- [17] B. Kundrotas, A. Petrovas, R. Rinkeviciene, and A. Smilgevicius, "Research of six-phase induction motor windings," *Elektronika Ir Elektrotechnika*, vol. 20, no. 1, pp. 15-18, 2014.
- [18] <http://www.ustudy.in/node/2160>, 2016 (Accessed 15.01.16)
- [19] C. G. Hodge, F. Eastham, and A. C. Smith, "The harmonic analysis of machine excitation," INEC 2012 Conference, Edinburgh, 15-17 May 2012, pp. 1-12.

Effect of Storage Temperature on Shelf Life of Sliced Mushroom (*Agaricus Bisporus*)

Fatih Tarlak^{1*}, *Murat Ozdemir*¹, *Mehmet Melikoglu*¹

Abstract

*Mushrooms have been consumed as food and medicine for centuries, because of their high protein, mineral and bioactive compound content. The cultivated button mushroom (*Agaricus bisporus*) is the most common edible mushroom in the world. *Agaricus bisporus* has a very short shelf life because it has no cuticle to protect it from physical or microbial attacks. In addition, mushrooms can easily be contaminated with microorganisms during their growth and processing. *Pseudomonas spp.* has frequently been isolated from sliced mushrooms, ranging from 6.9 to 7.8 logCFU/g. Mushrooms are delivered to consumers under variable environmental conditions such as temperature and humidity from production to consumption. Temperature is the main environmental factor that is most likely to change during processing and storage. Even a slight change in temperature dramatically affects microbial load, appearance, colour, taste and texture of *Agaricus bisporus*. Therefore, it is crucial to determine how the change in temperature affects the quality of *Agaricus bisporus*. The main objective of this work was to investigate the effect of different storage temperatures (4, 12, 20 and 28°C) on the shelf life of sliced mushrooms. For this purpose, the changes in microbial load, pH, weight loss, colour, texture and gas composition in packages were measured throughout the shelf life. The change in the quality parameters of *Agaricus bisporus* with respect to temperature provided important data to simulate and model the growth kinetics of *Pseudomonas spp.* and thereby the shelf life of sliced mushrooms at different storage temperatures could be predicted.*

Keywords: Colour, Shelf Life, Sliced Mushroom, Storage Temperature, Texture

1. INTRODUCTION

Mushrooms have been consumed as food and medicine for centuries, because of their high protein, mineral and bioactive compound content [1]. They are also consumed as a diet food since they contain low cholesterol and carbohydrate contents. The cultivated button mushroom (*Agaricus bisporus*) is the most common edible mushroom in the world. *Agaricus bisporus* has a very short shelf life because it has no cuticle to protect it from physical or microbial attack [2]. Therefore, it can be easily contaminated with microorganisms during growth and processing. If *Agaricus bisporus* is contaminated by any microorganism, especially pathogen microorganism it may cause serious health problems. But until now, outbreaks caused by consumption of contaminated mushrooms containing pathogen microorganisms such as *E. coli* O157:H7 and *L. monocytogenes* have not been reported [3]. On the other hand, the initial counts of microorganism on cultivated button mushroom are quite high. *Pseudomonas spp.* is the most abundant bacterial genus at harvest time and was highly isolated from mushrooms, ranging from 6.9 to 7.8 logCFU/g [4], [5].

Mushrooms are marketed under different environmental conditions such as temperature and humidity. Temperature is the main environmental factor that is most likely to change during processing and storage. Even a slight change in temperature dramatically affects microbial load, appearance, colour, taste and texture of *Agaricus bisporus*. Because mushroom quality is defined by a combination of parameters, including whiteness, texture and microbial counts, it is crucial to determine how the change in temperature affects the quality of *Agaricus bisporus*. But until now, the detail research about the effect of temperature on quality parameters of *Agaricus bisporus* has not been reported. Therefore, it is necessary to investigate the effect of temperature on quality parameters of *Agaricus bisporus*.

The main objective of this work was to investigate the effect of different storage temperatures (4, 12, 20 and 28°C) on the shelf life of sliced mushrooms. For this purpose, the changes in colour, microbial load, texture weight loss, pH and gas composition in packages were measured throughout the shelf life.

2. MATERIALS AND METHODS

2.1. Food

The cultivated button mushrooms (*Agaricus bisporus*) were obtained from MUPA Agriculture and Industry Incorporated Company (Izmit, Kocaeli, Turkey). The mushrooms were harvested at the closed cap stage with the cap diameter of 3.5–4.5 cm. After harvesting, mushrooms were immediately transported to the laboratory. After

¹Department of Chemical Engineering, Gebze Technical University, 41400, Gebze, Kocaeli, Turkey

*Corresponding author. E-mail address: ftarlak@gtu.edu.tr

mushrooms cleaned with distillate water, stapeses were trimmed at 1 cm and they were sliced carefully (thickness of 5 mm) using manual equipment. The slices were placed in polystyrene trays (100 g/tray) with the dimension of 22.5 x 13.5 x 3 cm³. The trays were overwrapped polyvinyl chloride (PVC) film. Packaged sliced mushrooms were stored four different temperatures (4, 12, 20 and 28°C) during their shelf life.

2.2. Colour Measurement

The colour of sliced mushrooms in each package was determined using a Chroma Meter (CR-400, Konica Minolta Inc., Tokyo, Japan) equipped with D₆₅ illuminant. Prior to colour measurements, the chroma meter was calibrated with its white calibration tile (Y=86.6 x=0.3188 y=0.3364). The L*a*b* colour analysis was performed randomly via twenty different measurements from the internal surfaces of sliced mushrooms in each package. Generally, visual colour degradation of procedure is expressed with respect to colour values (L*, a* and b*) individually, or their combination such as browning index (BI) and total colour difference (Δe_{ab}^*) [6], [7]. Browning index of sliced mushrooms was calculated using Equation (1):

$$BI = \frac{100 * (x - 0.31)}{0.17} \quad (1)$$

where $x = (a^* - 1.75 * L^*) / (5.645 * L^*) + (a^* - (3.012 * b^*))$, L*, a* and b* colour values are measured with Chroma Meter. The total colour difference in sliced mushroom was also calculated using Equation (2):

$$\Delta e_{ab}^* = \sqrt{(L_i^* - L_t^*)^2 + (a_i^* - a_t^*)^2 + (b_i^* - b_t^*)^2} \quad (2)$$

where Δe_{ab}^* is the total colour change at t time. L_i^{*}, a_i^{*} and b_i^{*} are the initial colour values. L_t^{*}, a_t^{*} and b_t^{*} are the final colour values at t time. The results were given as the average of twenty measurements with the standard deviations.

2.3. Microbiological Analyses

Twenty-five grams of mushrooms were aseptically weighed and homogenized using Stomacher (Interscience, Bag Mixer 400VW, USA) at high speed for 2 min by adding 0.1% 225 ml of sterile peptone water. Serial dilutions (10⁻¹-10⁻¹⁰) were made in serial tubes by taking 1 ml sample with 9 ml 0.1% of sterile peptone water. *Pseudomonas* spp. which already exists on natural microflora of mushrooms was determined in King's B medium [8], with an incubation temperature of 25°C for 48 hours. Each experiment was repeated three times and the average of three measurements was expressed as the colony forming units per gram sliced mushroom (log₁₀ CFU/g).

2.4. Texture Measurement

The firmness of sliced mushrooms was measured with a TAPplus texture analyser (TA1, Lloyd, USA) equipped with a load cell of 250N. Compression platen, a diameter of 5 cm was used with the constant speed of 10 mm/s and the contact force of 0.5 N. The firmness of sliced mushroom was expressed as the maximum force to obtain 1 mm deformation, which corresponds to compression of 20% sliced mushroom. Due to the hardness of stipe, this was removed each piece, the firmness was measured using cap of mushrooms. Seven samples were analysed from each packed. The results were given as the average of seven measurements with the standard deviations.

2.5. Weight Loss

The initial and final weight of sliced mushrooms in each tray was measured by using electronic balance (Mettler Toledo, PB03-S) during their shelf life. Weight loss was calculated as the percentage weight loss with respect to the initial weight (Equation (3)):

$$w_l = \frac{w_i - w_t}{w_i} * 100 \quad (3)$$

where w_l is the amount of weight loss (%), w_i is the initial weight (g) and w_t is the final weight (g) of sliced mushroom in each tray.

2.6. pH and Gas Composition Analyses

Sliced mushrooms were homogenized using a kitchen type blender (Tefal, MB450, Turkey) and homogenised mushroom was filtered with a muslin cloth. The pH value of obtained mushroom solution was measured using a digital pH meter (Mettler Toledo, S-20K, US). The results were given as the average of three measurements of the same solution.

Oxygen and carbon dioxide levels were determined using an O₂ and CO₂ head space gas analyser Checkmate model 9900 (PBI Dansensor, Check Mate-II). Samples were taken with a syringe through a septum. Three replicate was performed for each package from different parts and three packages were analysed for each gas composition experiment. The results were given as the average of nine measurements with the standard deviations

2.7. Statistical Analysis

Experiments were performed using a completely randomized design. Data were subjected to one-way analysis of variance (ANOVA). Mean separations were performed using Tukey's least significant difference (LSD) procedure in Matlab 7.12.0 (R2011a) software (MathWorks Inc., 130 Natick, MA, USA). Differences at $p < 0.05$ were considered significant.

3. RESULT AND DISCUSSION

Sliced mushrooms were separated into four groups with respect to their storage temperatures (4, 12, 20 and 28°C) and following quality parameters of mushrooms were analysed; i) colour, ii) microbial quality, iii) texture, iv) weight loss, v) pH and vi) gas composition in package during their shelf life. Details of the results were explained in the following subsections.

3.1. Colour Measurement

The colour of mushrooms is the first used key response to determine easily their shelf life in industry, and for this purpose especially L* value is used. If L* value of mushrooms is less than 80, wholesalers cannot accept them [9].

Generally, visual colour degradation of procedure is expressed with respect to colour values (L*, a* and b*) individually, or their combination such as browning index (BI) and total colour difference (Δe_{ab}^*) [6], [7]. In this regards, to determine the effects of storage temperatures on colour quality of mushrooms, L*, BI and Δe_{ab}^* were assessed during their shelf life. Figure 1 shows the change of L* values on sliced mushrooms at different temperatures (4, 12, 20 and 28°C).

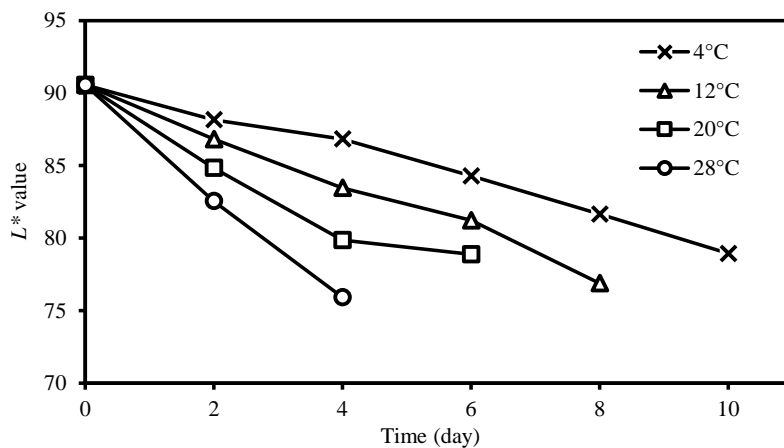


Figure 1. The effect of different storage temperatures on L* values of sliced mushrooms

L* values decreased with the increasing storage temperature and progressing storage period. There was a significant difference between different storage temperatures for L* values ($p < 0.05$). The L* values of sliced mushrooms highly reduced as the storage temperature developed. Additionally, the lowest L* value was observed in sliced mushrooms, which were stored at 28°C and it decreased to lower than 76 at the end of the just four days. On the other hand, L* values of sliced mushrooms which were preserved at 4°C were higher than 78 even at the end of the ten days.

The BI value is used to determine how much food get dark. If BI value is high, it means that the darkening of sliced mushroom is high. Figure 2 shows the change of BI values of sliced mushrooms stored at different temperatures (4°C, 12°C, 20°C and 28°C).

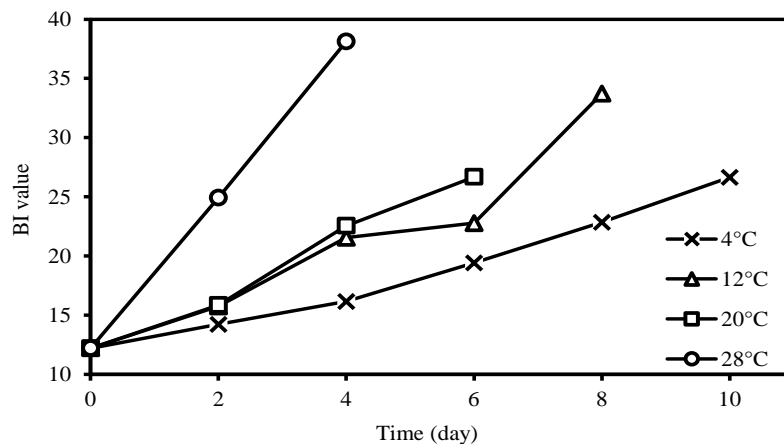


Figure 2. The effect of different storage temperatures on BI values of sliced mushrooms

BI values increased with increasing storage temperature and developing storage period. There was a significant difference between different storage temperatures for BI values ($p < 0.05$). The BI values of sliced mushrooms highly increased as the storage temperature increased. The highest BI value was observed in sliced mushrooms, which were preserved at 28°C and it reached to higher than 38 at the end of the just four days. On the other hand, BI value of sliced mushrooms which were preserved at 4°C were lower than 31 even at the end of the ten days.

The Δe_{ab}^* between two different colours corresponds to colour difference perceived by the human eye. If this value is high, the colour difference is easily perceived by the human eye. If this value is small, human eye has the difficulty in distinguishing the difference between two colours. Therefore, the Δe_{ab}^* values were calculated for all sliced mushrooms. Figure 3 shows the change of Δe_{ab}^* values of sliced mushrooms stored at different temperatures (4, 12, 20 and 28°C).

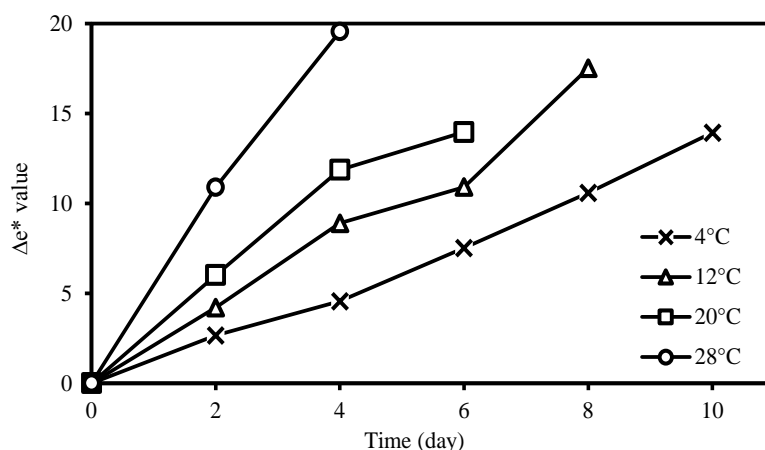


Figure 3. The effect of different storage temperatures on Δe_{ab}^* values of sliced mushrooms

The Δe_{ab}^* values also increased with increasing storage temperature and proceeding storage period. There was also a significant difference between different storage temperatures for Δe_{ab}^* values ($p < 0.05$). The Δe_{ab}^* values of sliced mushrooms highly increased as the storage temperature increased. The highest Δe_{ab}^* value was observed in sliced mushrooms, which were preserved at 28°C and it reached to higher than 19 at the end of the just four days. On the other hand, Δe_{ab}^* value of sliced mushrooms which were preserved at 4°C were lower than 14 even at the end of the ten days. These colour results (L^* , BI, and Δe_{ab}^*) simply mean that sliced mushrooms should be stored in 4°C, to keep colour of mushrooms in fresh form.

3.2. Microbiological Analyses

The microbial load on mushrooms is one of the most important parameters affecting their shelf life. According to [10], the microorganism usually responsible for spoilage of mushrooms are gram-negative bacteria, belonging particularly to the *Pseudomonas* spp. Therefore, the load of *Pseudomonas* spp. was determined during shelf life of mushrooms. Figure 4 shows the load of *Pseudomonas* spp. on sliced mushrooms which were stored four different temperatures (4, 12, 20 and 28°C).

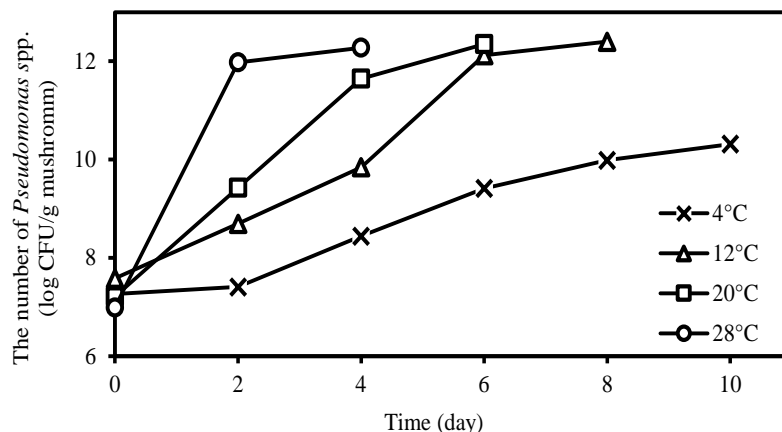


Figure 4. The effect of different storage temperatures on load of *Pseudomonas* spp. on sliced mushrooms

As can be seen from Figure 4, the initial bacterial count of *Pseudomonas* spp. on mushrooms was 7.26 ± 0.21 log CFU/g. This result is in agreement with published data for sliced mushroom and the initial bacterial count of *Pseudomonas* spp. on sliced mushroom was reported 6.90 by [5] and 7.80 by [4]. On the other hand, at the end of the shelf life of mushrooms the final population of *Pseudomonas* spp. was almost 10 log CFU/g for 4°C, and roughly 12 log CFU/g for 12°C, 20°C and 28°C. These results indicated that the growth rate of *Pseudomonas* spp. on mushrooms increased with increasing storage temperatures from 4°C to 28°C. Therefore, in order to extend shelf life of mushrooms, they should be kept in 4°C.

3.3. Texture Measurement

Texture analysis is a testing of physical characteristics of food products, and it gives valuable information about their tactile properties such as firmness. Because tactile properties of mushroom affect consumers' sensory perception and their acceptance, texture analysis was performed to evaluate freshness of mushroom. The results are the average of seven analyses and error bars are the standard deviations of these seven analyses (Figure 5).

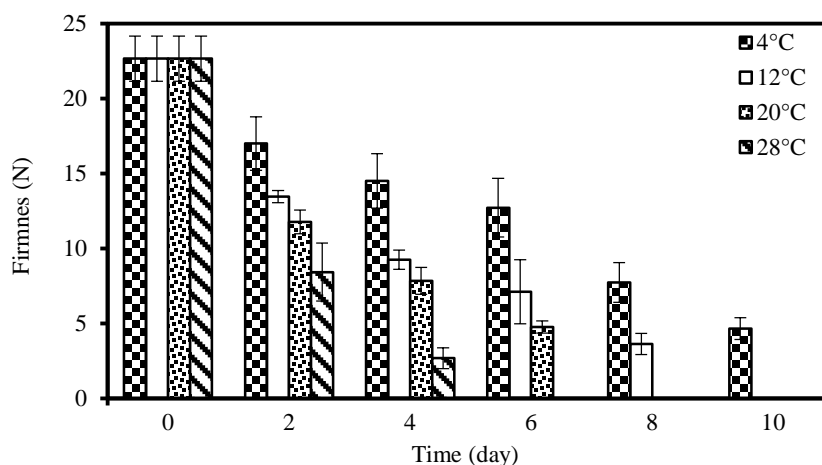


Figure 5. The effect of different storage temperatures on texture of sliced mushrooms

The initial firmness of sliced mushrooms was found to be 22.66 N (Figure 5). Firmness of sliced mushroom decreased with proceeding storage period for all different storage temperatures and there was a significant difference between the different storage temperatures ($p < 0.05$). The firmness of sliced mushrooms highly reduced, as the storage temperature increased. Additionally, the lowest firmness was observed in sliced mushrooms, which were preserved at 28°C and it decreased to lower than 2.70 at the end of the just four days. On the other hand, firmness of sliced mushrooms, which were preserved at 4°C were higher than 4.60 even at the end of the ten days. Texture analyses show that sliced mushrooms should be stored in 4°C, to decrease the softening rate of mushrooms.

3.4. Weight Loss

Sliced mushroom were preserved four different temperatures (4, 12, 20 and 28°C) during their shelf life. Weight loss increased with progressing storage period for all different storage temperatures. The results are the average of three analyses and error bars are the standard deviations of these three analyses (Figure 6). There was a significant difference between the different storage temperatures ($p < 0.05$). Additionally, the weight loss highly increased as the storage temperature increased. The highest weight loss was observed in sliced mushrooms, which were preserved at

28°C and it reached to 11.97% at the end of the just four days. On the other hand, the lowest weight loss was observed in sliced mushrooms, which were preserved at 4°C and it reached to 9.04% at the end of the ten days.

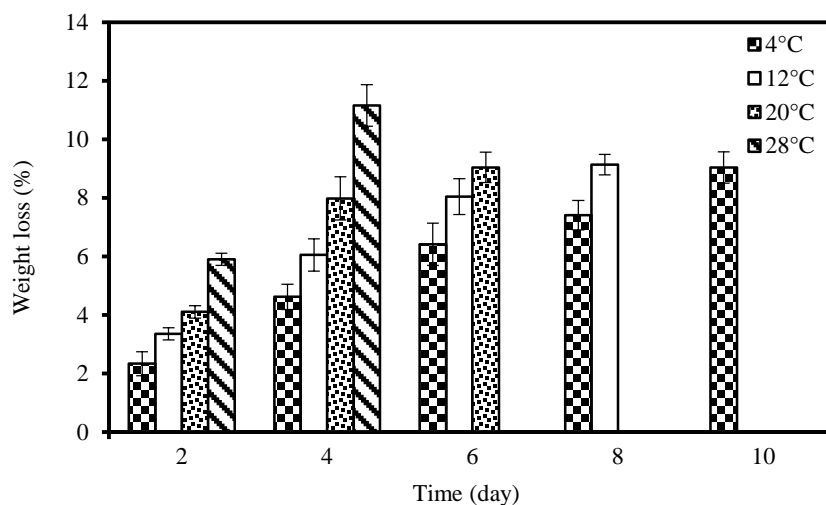


Figure 6. The effect of different storage temperatures on weight loss of sliced mushrooms

In [11] was reported that the weight loss of sliced mushroom (5 mm thickness) was almost 6% after six days at 4°C. In [7] it was obtained that the weight loss of sliced mushrooms (5 mm thickness) was almost 9% after six days at 15°C. So all these results obtained in this study are in agreement with published literature and to decrease weight loss of sliced mushroom, they must not be kept at high temperatures.

3.5. pH and Gas Composition Analysis

The initial pH values of sliced mushroom were 6.40 ± 0.1 and there was no significant difference ($p > 0.05$) between the different temperatures (4, 12, 20 and 28°C) for pH values of sliced mushroom. This result is an agreement with [12], they reported that the initial pH values of homogenised mushrooms were 6.50 ± 0.1 . The pH values of sliced mushrooms, which was stored different temperatures (4, 12, 20 and 28°C) increased to 7.00 ± 0.2 during the first two days, and then decreased to 6.5 ± 0.2 with a fluctuating manner for all temperatures. This result corresponds with [13], they reported that aerobic mesophilic bacteria are natural contaminants in mushrooms, which grow in presence of O_2 . This growth helps decreasing pH which ultimately inhibits the growth of certain communities.

In addition to pH values, there was no significant difference ($p > 0.05$) between different storage temperatures for gas composition in package. While the CO_2 concentration increased to 5.4 ± 2.6 , the O_2 concentration decreased to 7.2 ± 3.2 at the end of the 2 days and after two days later gas concentration in packages reached to roughly equilibrium. This means that for the first 2 days, the respiration rate of mushrooms was high, then this value progressively decreased. Similar results have been previously reported by [14], who observed that an increase in CO_2 concentration caused an inhibitory effect on respiration rate of mushrooms and after a while gas concentration in package reached to equilibrium.

4. CONCLUSIONS

In this work, the effects of storage temperature on shelf life of mushrooms were investigated. Compared to different storage temperatures (4, 12, 20 and 28°C), 4°C appeared to be the most suitable storage temperature for keeping the quality of mushrooms such as colour, texture, and this temperature has also delayed growth of *Pseudomonas* spp. on mushrooms. The change in the quality parameters of *Agaricus bisporus* with respect to temperature provided important data to simulate and model the growth kinetics of *Pseudomonas* spp. and thereby the shelf life of sliced mushrooms at different storage temperatures could be predicted.

ACKNOWLEDGEMENT

This work was financially supported by Gebze Technical University through Scientific Research Projects (BAP) 2014 A-25 and 2015 A-40. Fatih Tarlak would like to thank The Scientific and Technology Research Council of Turkey (TUBITAK) for granting PhD scholarship (2211-C).

REFERENCES

- [1]. B.A. Wani, R.H. Bodha, and A.H. Wani, "Nutritional and medicinal importance of mushrooms", *J. Med. Plants Res.*, vol. 4, pp. 2598-2604, 2010.
- [2]. M. Brennan, G.L. Port, and R. Gormley, "Post-harvest with citric acid or hydrogen peroxide to extend the shelf life of fresh sliced mushrooms", *Food Sci. Technol.-LEB.*, vol. 33, pp. 285-289, 2000.
- [3]. W. Guan, X. Fan, and R. Yan, "Effects of UV-C treatment on inactivation of *Escherichia coli* O157:H7, microbial loads, and quality of button mushrooms", *Postharvest Biol. Tec.*, vol. 64, pp. 119-125, 2012.
- [4]. E. Gonzalez-Fandos, A. Simon, and V. Pardo, "Quality and shelf life of packaged fresh sliced mushrooms stored at two different temperatures", *Agri. Food Sci.*, vol. 15, pp. 414-422, 2006.
- [5]. A. Simon, E. Gonzalez-Fandos, and V. Pardo, "The sensory and microbiological quality of fresh sliced mushroom (*Agaricus bisporus* L.) packaged in modified atmospheres", *Int. J. Food Sci. Tech.*, vol. 40, pp. 943-952, 2005.
- [6]. M. Maskan, "Kinetics of colour change of kiwifruits during hot air and microwave drying", *J. Food Eng.*, vol. 48, pp. 169-175, 2001.
- [7]. F. Oliveira, M.J. Sousa-Gallagher, P.V. Mahajan, and J.A. Teixeira, "Development of shelf- life kinetic model for modified atmosphere packaging of fresh sliced mushrooms", *J. Food Eng.*, vol. 111, pp. 466-473, 2012.
- [8]. E.O.King, M.K. Ward, and R. Ranzy, "Two simple media for the demonstration of pyocyanin and fluorescein", *J. Lab. Clin. Med.*, vol. 44, pp. 301-307, 1954.
- [9]. T.R.Gormley, "Chill storage of mushrooms", *J. Sci. Food Agr.*, vol. 26, pp. 401-411, 1975.
- [10]. D. Eastwood, and K. Burton, "Mushrooms – a matter of choice and spoiling oneself", *Microbiology Today*, vol. 29, pp. 18-19, 2002.
- [11]. K.M. Kim, A.J. Ko, J.S. Lee, H.J. Park, and M.A. Hanna, "Effect of modified atmosphere packaging on the shelf-life of coated, whole and sliced mushrooms", *Food Sci. Technol.- LEB.*, vol. 39, pp. 364-371, 2006.
- [12]. Y.Masson, P. Ainsworth, D. Fuller, H. Bozkurt, and Ş. İbanoğlu, "Growth of *Pseudomonas fluorescens* and *Candida sake* in homogenized mushrooms under modified atmosphere", *J. Food Eng.*, vol. 54, pp. 125-131, 2002.
- [13]. S. Zivanovic, R. Buescher, and S.K. Kim, "Growth of *Pseudomonas fluorescens* and *Candida sake* in homogenized mushrooms under modified atmosphere", *J. Food Sci.*, vol. 68, pp. 1860-1865, 2003.
- [14]. C. Lagnika, M. Zhang, and J. Nsor-Atindana, "Effects of ultrasound and chemical treatments on white mushroom (*Agaricus bisporus*) prior to modified atmosphere packaging in extending shelf-life", *J. Food Sci. Technol.*, vol. 51, pp. 3749-3757, 2012.

BIOGRAPHY

Fatih Tarlak received his B.Sc. in 2009 from Department of Chemical Engineering, Gazi University, and he received his M.Sc. Department of Chemical Engineering, Gebze Technical University three days later. He is a Ph.D. student and research assistant in Department of Chemical Engineering, Gebze Technical University at present. His main research areas are optimization and modelling of food microbiology and shelf life.

Tensile Strength of Double Lap Joints Bonded with a Micro-Particle-Reinforced Adhesive

Mehmet Akif Kutuk¹, Nurettin Furkan Dogan², Omar Al-Dulaimi³

Abstract

Adhesive bonding of structures has significant advantages over conventional fastening systems. Bonded joints are considerably more fatigue resistant than mechanically fastened structures because of the absence of stress concentrations that occur at fasteners. Therefore, the need to improve adhesives used for bonding has acquired utmost importance. The present work aims to strengthen double-lap adhesive joints. In order to improve the tensile lap shear strength of adhesively bonded joints, micro-particles (45µm and below) of sewage sludge ash were mixed with the adhesive. Glass fiber/epoxy composite laminates with 10 layers were chosen as adherents and the adhesive was produced from different amount of micro-particles added into epoxy. The mechanical properties of adhesively bonded double-lap joint geometry with same configurations and thicknesses of lower and upper adherents under tensile loading were investigated experimentally to assess the effect of different weight content of micro-particles on the mechanical properties of the adhesive. After mechanical tests, failure loads and effect of additive ratio were presented for each mass rated adhesive with some conclusions.

KeyWords: Double Lap Joints, Adhesive, Composite Materials, Bonding, Micro-particles

1. INTRODUCTION

The development of reliable joining methods for composite structures has become an important research area because large or complex composite structures usually have other metallic or ceramic parts which are joined to the composites to improve their performance. The efficiency of composite structures with joints is largely dependent on the joint rather than on the structure itself, because the joint is usually the weakest part among the components of assembled structures [1–3].

Generally, joining methods for composite structures are classified into adhesive bonding and mechanical joining. A mechanical joint is created by fastening the adherents with bolts or rivets while an adhesive joint uses an adhesive interlayer between the adherents. An adhesive joint distributes the load over a larger area than a mechanical joint, requires no holes, adds very little weight to the structure and has superior fatigue resistance. However, the strength of the adhesive joint is highly dependent on the mechanical property of adhesive and thermal residual stresses generated during the curing process of the joint due to large difference in coefficient of thermal expansion between the adhesive and composite adherents [1].

Kahraman et al. (2008) dealt with single-lap joints bonded with aluminium powder filled epoxy. These bonds fail in a cohesive mode (failure within the adhesive) due to the high stress levels generated in the adhesive which indicates that the adhesion to the metal surface is stronger than that of the interior part of the adhesive. Kavak and Altan (2012) investigated epoxy resins filled with particles of 63/37 Sn-Pb. Their experimental results show that bonds prepared by adhesive which was modified, adding the amount of 5 wt% of 63/37 Sn-Pb powder, are of higher mechanical strength than bonds which are prepared by adding aluminium powder with different ratios as 5, 25, 50 wt%. Kilik and Davies (1989) determined the used adhesive as a toughened, single part epoxy which contained various amounts of admixed copper and aluminium powders.

Zhai et al. (2006) demonstrated that incorporating epoxy adhesive with nanoparticles (nano-Al₂O₃ homogeneously dispersed in epoxy adhesive) could distinctly increase the adhesion strength of epoxy adhesive. Bahattab et al. (2011) increased shear adhesion strength values of polyurethane bonds by filling with nanosilicas of different particle size from the value 14.2 ± 0.1 MPa to the value 15.3 ± 0.3 MPa (100 nm, 30 wt%). Inorganic micro-particles need not to serve only for optimizing the adhesive and cohesive characteristics of bonds but they can also according to authors (Valášek and Müller, 2013a) increase other mechanical properties. In the practice hard inorganic particles (SiC, Al₂O₃) are used which should increase the ability of the system to resist to the abrasive wear. Then these systems serve for repair of damaged machine parts such as shafts, boxes, keyways for tongues and flanges or of damaged parts such as casts and pipes. The glass powder also increases the resistance of epoxides to the abrasive wear (Valášek and Müller, 2013b). The aim of the reference paper is to describe the influence of the variable concentration

¹ Corresponding author: University of Gaziantep, Department of Mechanical Engineering, 27310, Şehitkamil/Gaziantep, Turkey. kutuk@gantep.edu.tr

² University of Gaziantep, Department of Mechanical Engineering, 27310, Şehitkamil/Gaziantep, Turkey. nfurkandogan@gantep.edu.tr

³ Iraqi Ministry of Education, Educational Directorate of Al-Anbar, Al-Anbar, Iraq. o_aldulaimy@yahoo.com

of the glass powder to the lap-shear tensile strength of rigid adherents created with some types of high-strength epoxy adhesives.

In the given studies above and many others different particles are used to increase the strength of adhesive. Therefore, in this work, the epoxy adhesive was reinforced with micro-sized particles to improve the tensile lap shear strength of adhesively bonded double lap joint. The effect of micro-particles on the mechanical properties of the adhesive was measured with respect to weight content of micro-particles. Also, the tensile load capability of the adhesively bonded double lap joint composed of unidirectional glass/epoxy composite and micro-particle-reinforced adhesive was measured to investigate the effect of micro-particles on the lap shear strength of the joint.

In the current study, sewage sludge ash (SSA) is used as additive in epoxy adhesive. SSA is already a waste and the amount of it increases in the world rapidly. As a result of rapid increase in urbanization, population growth and amount of waste water has led to increase in waste water treatment plant together. The increase of plants causes to increase sewage sludge. There are many methods existed for disposal of sewage sludge such as landfill, thermal drying, discharging into the sea, agricultural use, cement production and incineration. However, in any method aside from incineration, some problems arise in time. For this reason, incineration of sewage sludge is preferred in the leading countries and other developed countries. By this way while the major source of environmental problem is eliminated, electrical energy is produced and a harmless waste generated as ash [11]. In Turkey, annual amount of waste water is 3.5 billion m³ [12]. This amount shows that Turkey has about 140 million tons of sewage sludge potential and is a sign of the importance of the disposal sewage sludge ash (SSA). The sewage sludge incineration system was first founded in Gaziantep city, Turkey, which generates electric energy by burning 150 tons/day sewage sludge [13]. About 15 tons ash remains at the end of combustion. Many studies are being conducted to assess the various sectors of the usage of SSA. M. A. Kutuk et al [14] studied the effect of SSA on the mechanical properties of composite materials and published experimental results. Also, studies of SSA used in cement production are available in literature.

The present study represents a sample for evaluation of SSA and aimed to determine the mechanical properties of SSA reinforced epoxy adhesive on bonding of composites.

2. MATERIALS AND EXPERIMENTAL PROCEDURES

The glass fiber/epoxy composite plates were manufactured from unidirectional S2-glass fabrics and epoxy resin by hand lay-up method. An epoxy resin matrix based on Momentive-MGS L285 epoxy polymer and Momentive-H285 hardener was used in the production of the composite plates. The mixing ratio for resin to hardener was 100:40. The glass/epoxy composite plates were cured in a lamination press, at a constant pressure of 0.4MPa pressure and 75°C temperature for 2 hours. Then, the composite plates were cooled down to room temperature. After manufacturing process, the composite plates were cut by guillotine in proper dimension.

The sewage sludge ash of which chemical content is given in Table 1, was provided from Gaziantep Metropolitan Municipality Directorate of Water and Sewerage Works (GASKI). The SSA was classified from 45 µm and below by sieve. By sieving procedure, it was intended that the uniform sized particles used in adhesive. Otherwise, ash in different sizes, different adhesion behaviour will be exhibited on the adhesion strength [15, 16].

Table 1. Sewage sludge ash chemical composition. [17]

Oxide	percentages %	Oxide	percentages %	Oxide	percentages %
Al ₂ O ₃	5,727	Fe ₂ O ₃	7,461	PbO	0,031
BaO	0,206	K ₂ O	4,874	SO ₃	8,533
Br	0,063	MgO	8,221	SiO ₂	16,602
CaO	19,588	MnO ₂	0,188	SrO	0,049
Cl	0,539	Na ₂ O	0,442	TiO ₂	1,079
Cr ₂ O ₃	0,354	NiO	0,068	ZnO	2,096
CuO	0,189	P ₂ O ₅	23,655	ZrO ₂	0,036

Epoxy adhesive with different weight ratios (Table 2) of sewage sludge ash was used in the bonding operation of composite samples. Before bonding process, sample surfaces were cleaned with acetone, abraded with a fine abrasive paper and then cleaned with acetone again.

Table 2. Weight value of the sample mixture to be applied for tensile test

Sample	Epoxy+Hardener (%)	Ash (%)
--------	--------------------	---------

T 0	100	0
T 5	95	5
T 10	90	10
T 15	85	15
T 20	80	20
T 25	75	25

3. EXPERIMENTS

In the experiments, samples were cut in proper dimensions shown in Figure 1 by guillotine and were all joined with double lap formation by particle filled adhesive. Three samples were prepared for each mass rate.

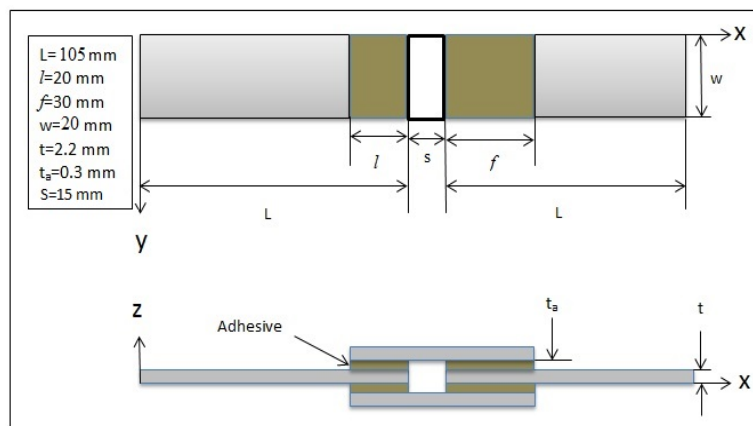


Figure 1. Double-lap bonding joint and geometric properties

3.1 Axial Tensile Test

Axial tensile test was performed according to ASTM D 3528 standard test mechanism shown in Figure 2 (a). A total of 18 samples (3 samples per mass ratio) prepared in accordance with each mass rate, were tested with Shimadzu AG-X 300 kN tensile testing machine with 1 mm/min speed at room conditions.

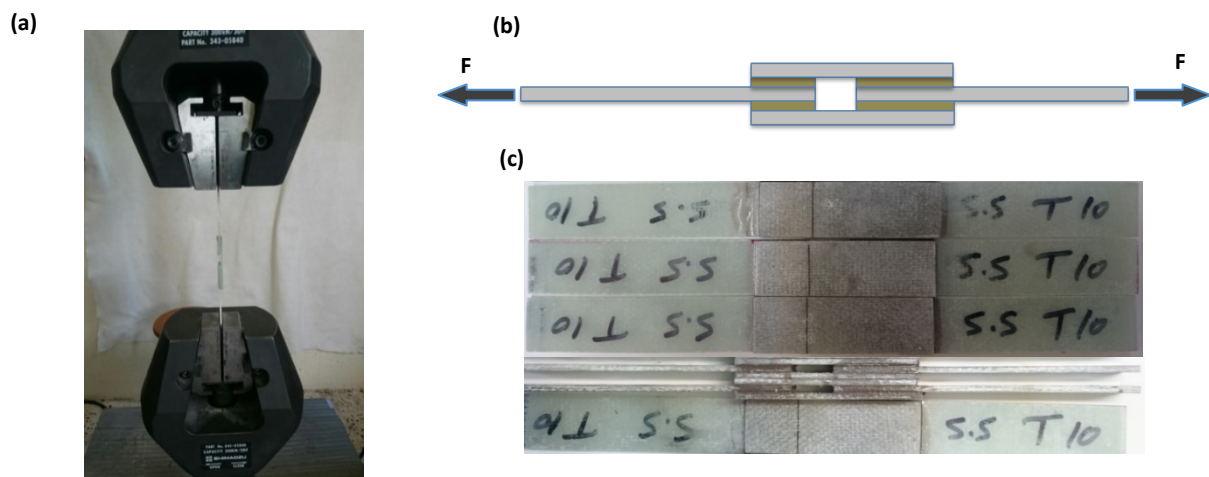


Figure 2. Tensile test mechanism for double lap bonding. (a) Connecting to test machine, (b) Axial loading simulation, (c) Test samples.

4. RESULTS

The results of the axial tensile test are given in the following charts. As shown in Figure 3 and Figure 4, when ash content in the mixture is 5-10%, load carrying capacity of the adherent is decreased, then ash content is increased to 15 and 25%, load carrying capacity is increased. The reduction of load capacity with 25% filler content is related to decreasing in the distance between particles causes irregularities in the material and stress concentration. In Figure 5, lap shear stress of the particle filled adhesive is increased according to increasing load capacity.

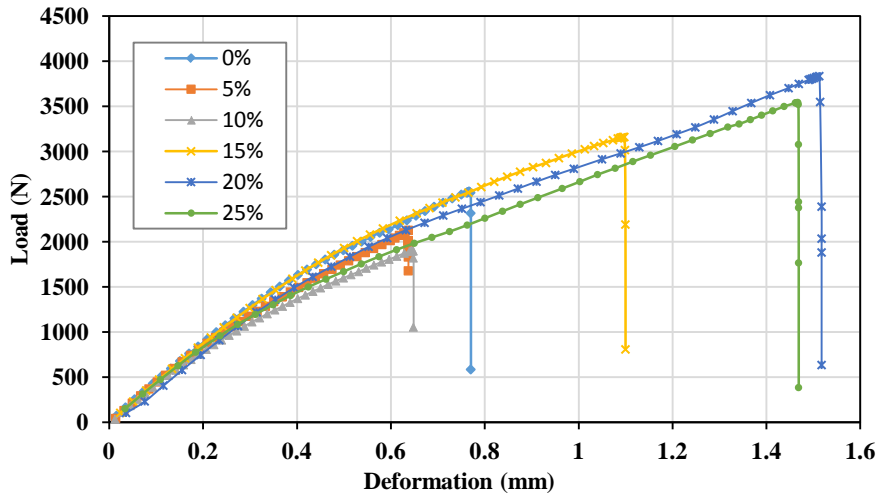


Figure 3. Force-Displacement distribution for different mass ratios.

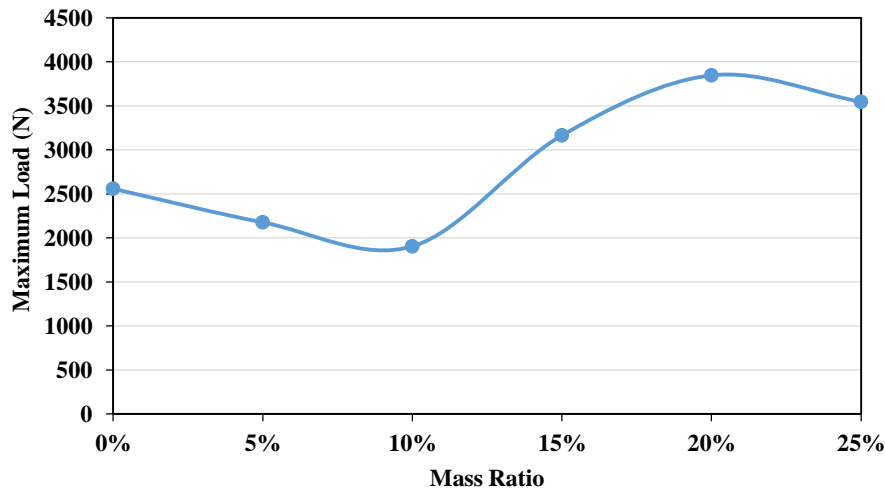


Figure 4. Load capacity for different mass ratios.

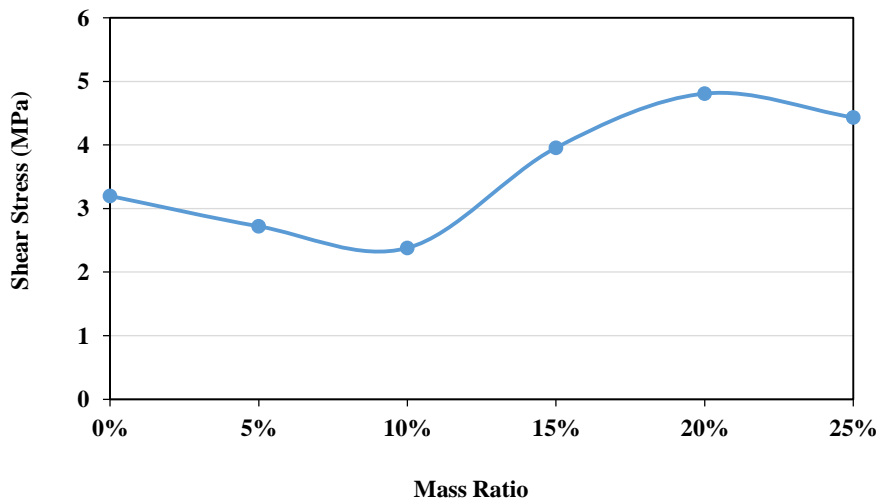


Figure 5. Lap shear strength distribution of the test samples.

5. CONCLUSION

In this study, it is shown that sewage sludge ash increases the adhesion performance of epoxy adhesive as it has been studied in a tensile test. Adhesive bonding with sewage sludge ash additive mass rate is significantly affect the adhesive performance. In the tensile test results, the mass rate of additive is determined to be 20%, compared to pure epoxy adhesive has reached the maximum load carrying capacity by about 50%, and it showed a tendency to decrease in the load capacity after 20% filler content.

As a result, when the final product of the sewage sludge incineration process SSA is used in proper rate as a filler material of adhesive, bonding performance of the epoxy adhesive increases considerably.

REFERENCES

- [1]. D. G. Lee and N. P. Suh, "Axiomatic Design and Fabrication of Composite Structures", Application in Robots, Machine Tools and Automobiles, pp. 14–61. Oxford University Press, Oxford ,2006.
- [2]. Hart-Smith L.J., In: Reinhart TJ, editors. in Composites. Ohio: ASM International, p. 479-495 (1987).
- [3]. J. R. Vinson and R. L. Sierakowski, "The Behaviour of Structures Composed of Composite Materials", pp. 239–283. Martinus Nijhoff, Dordrecht ,1987.
- [4]. R. Kahraman, M. Sunar, B. Yilbas, "Influence of adhesive thickness and filler content on the mechanical performance of aluminium single-lap joints bonded with aluminium powder filled epoxy adhesive", Materials Science Forum, 205: 183–189, 2008.
- [5]. N. Kavak, E. Altan, "Influence of filler amount and content on the mechanical performance of joints bonded with metal powder filled adhesive", In: 15th International Conference on Advances in Materials and Processing Technologies, AMPT, Wollongong, NSW; Australia, 773–774: 226–233, 2012.
- [6]. R. Kilik, R. Davies, "Mechanical properties of adhesive filled with metal powders", International Journal of Adhesion and Adhesives, 9(4): 224–228, 1989.
- [7]. L. Zhai, G. Ling, J. Li, Y. Wang, "The effect of nanoparticles on the adhesion of epoxy adhesive", Materials Letters, 60(25–26): 3031–3033, 2006.
- [8]. M. A. Bahattab, J. B. Donate-Robles et al., "Characterization of polyurethane adhesives containing nanosilicas of different particle size", International Journal of Adhesion and Adhesives, 31(2): 97–103, 2001.
- [9]. P. Valašek, M. Muller, "Polyurethane resins filled with inorganic waste particles", Manufacturing Technology, 13: 241–247, 2013a.
- [10]. P. Valašek, M. Muller, "Polymeric composite based on glass powder – Usage possibilities in agro complex", Scientia Agriculturae Bohemica, 2: 107–112, 2013b.
- [11]. Z. Ayvaz, "Atıksu arıtma çamurlarının değerlendirilmesi", ÇEVKOR, 9:35 , pp. 3-12, 2000.
- [12]. TÜİK: Municipals Waste Water Statistics (2010)
- [13]. M. A. Kütük, M. Aksoy, "A Case Study On Sewage Sludge Incineration Plant: GASKI", Proceedings of the Second International Conference on Water, Energy and the Environment Kuşadası/Turkey (2013), Sept. 21-24.
- [14]. M. A. Kütük and Z. A. Oğuz, "Research on Effect of Sewage Sludge Ash on the Mechanical Properties of Composite Material", ICSENM'16, Czech Republic.
- [15]. A. Nourbakhsh, A. Karegarfard, A. Ashori, A. Nourbakhsh, "Effects of Particle Size and Coupling Agent Concentration on Mechanical Properties of Particulate-filled Polymer Composites", Journal of Thermoplastic Comp. Materials, 23, pp. 169 originally published online, 30 July 2009, DOI: 10.1177/0892705709340962, 2010.
- [16]. F. Shao-Yun, F. Xi-Qiao, L. Bernd, M. Yiu-Wing, "Effects of particle size, particle/matrix interface adhesion and particle loading on mechanical properties of particulate-polymer composites", ScienceDirect, Composites: Part B 39, pp.933–961, 2008.
- [17]. Türkiye Bilimsel ve Teknolojik Araştırma Kurumu Marmara Araştırma Merkezi Çevre Enstitüsü 07.07.2011 tarihli B.02.1.TBT.5.01.14.00 - 181.06.03 - 2049 Nolu Analiz Raporu

BIOGRAPHY

M. Akif KÜTÜK – was born in Gaziantep, Turkey in 1973. He received the B.S. degree in Mechanical Engineering from the Gaziantep University, Gaziantep, Turkey in 1995, the M.S. degree in Mechanical Engineering from the Gaziantep University, Gaziantep, Turkey in 1997, and the Ph.D. degree in Mechanical Engineering from the Gaziantep University, Gaziantep, Turkey in 2003. Since 2003 he has been Assistant and Associate Professor in the Department of Mechanical Engineering, Engineering Faculty, Gaziantep University, Gaziantep, Turkey.

N. Furkan DOĞAN –was born in 1988, Osmaniye, Turkey. He received BSc degree in 2012 and MSc degree with the thesis topic is "Elasto-Plastic Analysis of Thick Beams Using Meshfree Methods" in 2015 at Gaziantep University Mechanical Engineering Department. The researcher has also served as Research Assistant and continued PhD education at the same department in Gaziantep.

Omar Al-Dulaimi - was born in 1986, Baghdad, Iraq. He received BSc degree in 2008 from University of Mosul. The researcher has continued MSc education at Gaziantep University Mechanical Engineering Department.

The Effects of Heavy Metals on Germination of Scots Pine (*Pinus sylvestris* L.) Seeds

Halil BarisOzel¹, Handan Ucun Ozel², Halil Ibrahim Caylak³, Mehmet Efe⁴

Abstract

In this study, in order to determine the effects of the solutions prepared for various heavy metals (10%, 30%, 50%, 70% and control) on germination percentages of scots pine seeds, the seed samples were exposed to germination test in germination media. When the results of statistical analyses were analyzed in detail, it was observed that the lowest germination percentage (15.6%) at 10% concentration level was obtained with Co solution, while the highest germination percentage (88.9%) at the same concentration level was achieved with Zn solution. At 30% concentration level, the lowest germination levels (4.3% and 5.8%) were obtained with Co and Pb, while the highest germination percentage (63.7%) was obtained with Cu solution. At %50 concentration level, the lowest level of germination (11.7%) was observed in Ni solution, while the highest germination percentage (42.8%) was obtained with Cr. At the highest concentration level (70%), the lowest germination percentages were observed to be 10.6% and 17.5% with Cu and Cr.

Keywords: Heavy Metal, Germination Percentage, Scots Pine, Seed

1. INTRODUCTION

Formed and shaped by many factors, the ecological balance lays the foundation of life concept. Continuity of vital activities is the most fundamental component of the social life. Protecting this system and passing it down to next generations are the main responsibility of human beings. But the never-ending demands and requests of people have deteriorated and even demolished the most important components of fundamental life cycle, especially the natural resources, because the rapidly increasing population, irregular urbanization, excessive consumption, and rapidly increasing technology require meeting the uninterrupted need for raw material and energy. The semi-finished products manufactured during these activities, especially the gas, solid and liquid pollutants, pollute firstly the soil and then the air and water resources, which are the fundamental components of life cycle. These factors, which are named pollutant or pollutant factor, lead to global problem, which is named environmental pollution, deteriorating the ecological balance [1]. Leading one among these pollutant factors deteriorating the ecological balance and causing generally irreversible damages is the heavy metals [2], [3]. As well as heavy metals can lead to pollution in soil and water resources, they also have significant damages on the anatomical and physiological structures of the plants and lead individual and mass destruction by weakening them [4], [5]. On the other hand, by damaging the genital organs of the plants, the heavy metals also decrease the pollination and prevent the formation of healthy generations. This also jeopardizes the continuity of many species of plants. Hence, it has been determined in many studies that heavy metals play significant role in limiting the high growth performance and genetic quality and yield of seed sources in early developmental phases of many agricultural products and forest trees [6], [7], [8].

In this study, Kars-Sarkamış-origin scots pine (*Pinus sylvestris* L.) seeds were exposed to various concentrations of (10%, 30%, 50%, 70% and control) heavy metal (Cu, Zn, Ni, Co, Cr and Pb) solutions, and it was attempted to examine the effects of these solutions on the mean germination percentage. During these analyses, it was aimed to determine upper levels of heavy metal concentrations that the seeds could tolerate in terms of their vital activities (germination).

2. MATERIAL AND METHOD

2.1. Material

The scots pine seeds used in this study were originated from Kars-Sarkamış (TM167), and collected in year 2015 from the clonal seed orchard established in Erzurum center at the altitude of 1850 m. The 102 number of scots pine seed orchard has been established in year 1990 on 5.5 ha land by using 30 clones and 1130 seedlings planted with

¹ Corresponding author: Bartın University, Faculty of Forestry, Department of Silviculture, Agdaci Campus, 74100, Bartın, Turkey. halilbarisozel@yahoo.com

² Bartın University, Faculty of Engineering, Kutlubey Campus, 74100, Bartın, Turkey hanucun@yahoo.com

³ Bartın University, Faculty of Forestry, Department of Silviculture, Agdaci Campus, 74100, Bartın, Turkey, muhendis_halil_25@hotmail.com

⁴ Bartın University, Faculty of Forestry, Department of Silviculture, Agdaci Campus, 74100, Bartın, Turkey, efemehmet@yahoo.com

7x7m distances [9]. Within this context, considering the aims of this study and the number of heavy metal sorts, 20kg seed was collected from each of the clones.

2.2. Method

2.2.1. Preparation of Seed Samples for Germination Tests

During this study, germination tests were performed in order to determine the effect of various concentrations of heavy metals. Within this context, 10%, 30%, 50%, and 70% solutions of each of the heavy metal sorts were prepared, besides the control sample (not containing any heavy metal). For this purpose, the triplicated solution trials were performed each of the heavy metal solutions, and 300 seeds were used in each of the replicates. Hence, a total of 900 seeds were used for each of heavy metal solution concentration levels. On the other hand, also the control samples were prepared in triplicated, and again 300 seeds were used in each of replicates (a total of 900). Thus, in order to achieve accurate results, it has been reported in previous studies that at least 300 seeds should be used in each of replicates [10], [11]. In this parallel, as well as in previous studies, where the germination tests have been performed, 300 seeds were used in each of replicates in our study.

2.2.2. Preparation of Heavy Metal Solutions

In this study, 4 different concentration (10%, 30%, 50%, 70% and control) levels of 6 heavy metal various (Cu, Zn, Ni, Co, Cr and Pb) were examined in terms of the effect on germination percentage of scots pine seeds. In preparing these solutions, the similar studies were utilized, and the chemical in those studies were used [12]. Within this context, the solutions were prepared in Silviculture Department Laboratory of Forestry Faculty of Bartın University. Accordingly, the $\text{Cu}(\text{NO}_3)_2$ for Cu solutions, $\text{Zn}(\text{NO}_3)_2$ for Zn solutions, $\text{Ni}(\text{NO}_3)_2$ for Ni solutions, CoCl_2 for Co solutions, $\text{K}_2\text{Cr}_2\text{O}_7$ for Cr solutions, and $\text{Pb}(\text{NO}_3)_2$ for Pb solutions were used, and the chemicals were procured from Sigma-Aldrich. All the solutions were prepared in glass containers.

2.2.3. Germination Tests

In this study, in order to determine the effects of the solutions prepared for various heavy metals (10%, 30%, 50%, 70% and control) on the mean germination percentages of scots pine seeds, the seed samples were exposed to germination test in germination media. Within this context, for each solution concentration level of each heavy metal sort, the scots pine seeds were exposed to germination test, in 3 replicates, within plastic containers on filter paper at 20°C temperature under 70% light intensity for 30 days. By using the formula reported by Genç [11] and Yılmaz [13], the mean germination percentage and germination power parameters were calculated.

$$MGP (\%) = \frac{\sum n_i}{N} \times 100(1)$$

MGP (%): Mean Germination Percentage, n_i : the number of seeds germinated on i^{th} day, N: Total number of seeds in trial.

2.2.4. Statistical Analyses

In this study, where the effects of various concentrations of heavy metal solutions on mean germination percentages of scots pine seeds, random block experimental pattern was utilized. For this purpose, in order to determine if the raw data calculated after the germination tests exhibited normal distribution, the Kolmogorov-Smirnov Test was performed. And then, in order to determine the statistical differences between the different concentrations of heavy metal solutions in terms of mean germination percentage and germination power, the variance analysis (ANOVA) was performed. After the variance analysis, Duncan Test was used in grouping the statistical differences at both of heavy metal and concentration levels. SPSS package software was used in statistical analyses in this study.

3. RESULTS AND DISCUSSION

The results of variance analyses and Duncan test performed for the mean germination percentage values found during germination tests are presented in Table 1. In calculation of mean germination percentage values for heavy metal sorts and concentration levels, the results on 30th day were used, and the mean germination percentage values, which were obtained in triplicated, were exposed to variance analysis and Duncan test after Arc. Sin. transformation.

Table 1. Variance analysis and Duncan test results of mean germination percentage values

Heavy Metal Sorts	<i>F=118.34**</i>				
	Control (%)	10%	30%	50%	70%
Cu	94.2 ^a	86.5 ^a	63.7 ^a	38.9 ^b	10.6 ^a
Zn	95.4 ^a	88.9 ^a	59.6 ^c	15.9 ^c	-
Ni	100.0 ^a	75.3 ^b	48.4 ^{cd}	11.7 ^d	-
Co	100.0 ^a	15.6 ^d	4.3 ^d	-	-

Cr	100.0 ^a	66.4 ^c	61.9 ^b	42.8 ^a	17.5 ^a
Pb	100.0 ^a	18.2 ^d	5.8 ^d	-	-
	A	B	C	D	E

**: Significant difference at $P < 0.01$ confidence level

According to the variance analysis and Duncan test results in Table 1, statistically significant differences were between both of the heavy metal sorts and heavy metal concentrations in terms of mean germination percentage ($P < 0.01$). Within this scope, as a result of Duncan test at the confidence level of $P < 0.05$, 4 different groups emerged among the heavy metal sorts at 10%, 30%, and 50% concentrations, while no different groups emerged for 70% concentration. On the other hand, among the concentrations and control samples, 5 different groups emerged at the confidence level of $P < 0.05$. When the results of statistical analyses were analyzed in detail, it was observed that the lowest germination percentage (15.6%) at 10% concentration level was obtained with Co solution, while the highest germination percentage (88.9%) at the same concentration level was achieved with Zn solution. At 30% concentration level, the lowest germination levels (4.3% and 5.8%) were obtained with Co and Pb, while the highest germination percentage (63.7%) was obtained with Cu solution. At %50 concentration level, the lowest level of germination (11.7%) was observed in Ni solution, while the highest germination percentage (42.8%) was obtained with Cr. At the highest concentration level (70%), the lowest germination percentages were observed to be 10.6% and 17.5% with Cu and Cr. At this concentration level, no high germination percentage was observed (Table 1). According to these results, the upper limits of scots pine seeds in terms of mean germination percentage were determined to be 7% for copper, 50% for zinc, 30% for cobalt, 70% for chromium, and 30% for lead (Table 1).

The number of studies carried out in our country on the effects of heavy metals on the mean germination percentage of the seeds of forests trees is limited. For this reason, it was attempted to examine the results of this study by utilizing the study results, where the germination and growth of agricultural plants under the effects of heavy metals. Hence, in a study in Donana National Park, the effects of heavy metals, which are observed in soil, such as copper, zinc, cadmium and soil on the distribution and growth performance of certain needle-leaved and broad-leaved climax species were examined. According to the result of that study, it has been determined that, in proportion to other heavy metal sorts, the cadmium and lead heavy metals have negatively affected the natural germination path of both of needle- and broad-leaved species and the formation of their natural youth [14]. In another study on the seeds of tomato plant, it has been reported that the cobalt heavy metal has decreased the germination percentage of seeds by 45.6% [15]. On the other hand, in another study on the effects of chromium on the germination of various wheat genotypes, it has been reported that this heavy metal sort has decreased the mean germination percentage and rates of the seeds by 41.7% and 36.4%, respectively [16]. In another study, where the effects of copper heavy metal on the ipomoea, it has been determined that the copper has significantly delayed the flowering and development of the plant [17]. It has been reported that, as a result of exposure to nickel heavy metal pollution, the young individuals of *Triticum aestivum* L. species have been eliminated by 52.8% [18]. In another study, where the effects of lead heavy metal on growth of different corn genotypes, it has been determined that even the lowest concentration of lead (10%) has deteriorated the enzymatic activities of plants and decreased the growth by 65.7% [19]. In another study on the effects of zinc on germination and growth of bean seeds, it has been determined that 5% and 20% solutions have decreased the germination percentage of seeds by 8.3% and 15.4%, and that the highest level of effects has started from the dose of 40% [20]. Even though the plant species used as study object were different, it can be said that the results of our study significantly overlap with similar studies carried out before. From this aspect, it can be emphasized that some heavy metal sorts, which were used in examining the Kars-Sarikamış-origin scots pine seeds, have significantly decreased the mean germination percentage up to 50% concentration but the seeds have kept their ability of germinating.

4. CONCLUSION

According to the results obtained from this study, where the effects of various concentrations of heavy metal solutions on mean germination percentages of scots pine seeds, it should be reminded that, in parallel with the increase in environmental pollution level, also the heavy metals accumulating in soil and received from irrigation water lead to significantly unsuccessful results from arboricultural activities. This may significantly affect the success of silvicultural studies to be carried out in forestation areas by using natural forest resources. Within this context, it would be very useful to periodically analyze the samples taken from irrigation water and soil material of open nursery units, where the saplings of forest trees were grown, from the aspect of heavy metal accumulation. On the other hand, the heavy metal accumulation to occur in soil environment should be decreased by using plans having high bioremediation abilities. Moreover, use of origins and clones resistant to heavy metal pollution, which occurs as a result of air pollution, in artificial regeneration, rehabilitation, restoration, and forestation activities to be performed near the industrial facilities, especially at medium and high altitudes, would be very useful for establishing the forests that are resistant to this environmental problem.

REFERENCES

- [1] N. Çepel, *Ecological Problems and Solutions*, 1st ed., Ankara, Turkey: TUBITAK Publications, 2003.
- [2] A. Arruti, I. Fernandez-Olmo and A. Irabien, "Evaluation of the contribution of local sources to trace metals levels in urban PM_{2.5} and PM₁₀ in the Cantabria region (Northern Spain)," *Journal of Environmental Monitoring*, Vol. 12(7), pp. 1451-1458, 2010.
- [3] B.R. Stern, "Essentiality and toxicity in copper health risk assessment: overview, update and regulatory considerations," *Toxicol Environmental Health*, Vol. 73(2), pp. 114-127, 2010.
- [4] L. Taiz and E. Zeiger, *Plant Physiology*, 2nd ed., Sinauer Associates, Sunderland, Mass, USA, 2002.
- [5] N. Çepel, *Ecology, Worlds of Natural Life and Human*, 1st ed., Ankara, Turkey: Palme Publisher, 2007.
- [6] N. Saglam and N. Cihangir, "Biosorption studies of heavy metals by biological processes," *Journal of Faculty of Education of Hacettepe University*, Vol. 11, pp. 157-161, 1995.
- [7] A. Patlolla, C. Barnes, C. Yedjou, V. Velma, P.B. Tchounwou, "Oxidative stress, DNA damage and antioxidant enzyme activity induced by hexavalent chromium in Sprague Dawley rats," *Environmental Toxicology*, Vol. 24(1), pp.66-73, 2009.
- [8] G.U. Chibuike and C. Obiora, "Heavy metal polluted soils: Effect on plants and bioremediation methods," *Applied and Environmental Soil Science*, Vol. 14, pp. 1-12, 2014.
- [9] Anonymous. *Seed orchards of Turkey*, 1st ed., Ankara, Turkey: Directorate of Research Institute of Forest Trees and Seed Improvement, 2014.
- [10] ISTA, *International rules for seed testing*, 10th ed., Zurich, Switzerland: Association International Seed Testing, 2015.
- [11] M. Genc, *Seedling standardization*, 1st ed., Isparta, Turkey: Suleyman Demirel University, Faculty of Forestry, Publishing Number: 75, 2007.
- [12] H. Terzi and M. Yildiz, "Heavy metals and phytoremediation: physiological and molecular mechanisms," *Journal of Natural Sciences of Afyon Kocatepe University*, Vol. 11, pp.1-22, 2011.
- [13] M. Yilmaz, "Germination behavior of oriental beechnuts (*Fagus orientalis* Lipsky.) at different temperatures," *Journal of Forestry Faculty of SDU University*, Vol. 1, pp.1-8, 2010.
- [14] L. Ramos, M. Hernandez and M.J. Gonzalez, "Sequential fractionation of copper, lead, cadmium and zinc in soils from or near Donana National Park," *Journal of Environmental Quality*, Vol.23 (1), pp. 50-57, 1994.
- [15] K. Jayakumar, M. Rajesh, L. Baskaran and P. Vijayarangan, "Changes in nutritional metabolism of tomato (*Lycopersicon esculantum* Mill.) plants exposed to increasing concentration of cobalt chloride," *International Journal of Food Nutrition and Safety*, Vol.4(2), pp. 62-69, 2013.
- [16] D.C. Sharma and C.P. Sharma, "Chromium uptake and its effect on growth and biological yield of wheat seedlings," *Cereal Research Communications*, Vol.21 (4), pp. 317-322, 1993.
- [17] C. Kjaer and N. Elmegaard, "Effects of copper sulfate on black bindweed (*Polygonum convolvulus* L.)," *Ecotoxicology and Environmental Safety*, Vol.33(2), pp. 110-117, 1996.
- [18] T. Pandolfini, R. Gabbriellini and C. Comparini, "Nickel toxicity and peroxidase activity in seedlings of *Triticum aestivum* L.," *Plant, Cell and Environment*, Vol.15(6), pp. 719-725, 1992.
- [19] A. Hussain, N. Abbas and F. Arshad, "Effects of diverse doses of lead (Pb) on different growth attributes of *Zea mays* L.," *Agricultural Sciences*, Vol. 4(5), pp. 262-265, 2013.
- [20] R. Manivasagaperumal, S. Balamurugan, G. Thiyagarajan and J. Sekar, "Effect of zinc on germination, seedling growth and biochemical content of cluster bean (*Cyamopsis tetragonoloba* (L.) Taub)," *Current Botany*, Vol.2(5), pp.11-15, 2011.

A Novel S-box Algorithm Based on Physical Entropy Sources

Fatih Ozkaynak¹

Abstract

In the symmetric encryption systems, Substitution boxes (S-boxes) are an important part. Since this structures are the only nonlinear part of many block cipher. Therefore, the S-box should be constructed such that, its nonlinearity is as high as possible. This paper discusses an efficient S-box design based on continuous measurement of soil radon gas. The main contribution of this paper is proposed entropy source. Natural and geophysical observations are not usually regular and, these observations can be used as entropy source. Security evaluations of the proposed design strategy show that generator can provide high quality random bit sequences.

Keywords: *Substitution Boxes (S-boxes), Entropy Source, Soil Radon Gas, Computer Application of Natural and Geophysical Observations*

1. INTRODUCTION

Substitution boxes (S-boxes) are critical components for designing robust encryption systems. In this paper, an S-box construction method based on physical entropy sources has been presented. Main purpose of proposed method is that to find S-boxes with high nonlinearity. We employ continuous measurement of soil radon gas to find substitution boxes with desired cryptographic properties. The analysis results proved the feasibility of finding substitution boxes with the desired properties.

Many various criteria have been developed for the design strong S-boxes. References [] can be used for detailed description of these test criteria. The most commonly used criteria are:

- Bijective property: If f_i boolean function satisfies the condition $wr(\sum_{i=1}^n a_i f_i) = 2^{n-1}$ then it is bijective.,
- Nonlinearity: Walsh spectrum is carecterized nonlinearity of a boolean function.
- Strict avalanche criterion: If the function satisfies the strict avalanche criterion, it is possible that half of each output bit might change if there is a change in a single input bit. An effective method in order to check whether a complete S-box satisfies the strict avalanche criterion is given in [49].
- Output bits independence criterion: all avalanche variable couples must be independent for the set of avalanche vectors generated by the inverse of the bits of a single plaintext.
- Equiprobable input/output XOR distribution: Output variations can be obtained from input variations. The XOR value of each output must have equal probability with the XOR value of each input.

The proposed method used for construction of the 8-bit lookup table (S-box) with fixed entries transforms from the output of the nonlinear observation into numbers between 0 and 255. The structure of the study is as follows. In the next section, we describe the proposed new construction method in detail. The test results of the proposed method are given in Section 3. Finally, we give concluding remarks.

2. PROPOSED METHOD

Noise-based methods are the most common method for designing cryptographic modules. Proposed S-box generator method is an approach that generates lookup tables based on employ continuous measurement of soil radon gas. The basic approach of the method is that physical values obtained by periodic sampling of the analog value and these analog values converted to cell of lookup table.

The proposed algorithm is described below step by step.

Step1. A lookup table is created with the length of 256. The value of each cell in the table range from 0 to 255. The following steps are used to create the table.

Step2. Measurement value of soil radon is normalized to the range 0-255 by applying the mod 256.

Step3. The normalized value is added into the table if it is not already present, otherwise has been used another new measurement value of soil radon.

¹Corresponding author: Firat University, Department of Software Engineering, 23119, Elazig, Turkey, ozkaynak@firat.edu.tr

Step4. The process goes on until all cell values of the table are filled.

The sample S-box designed by using the proposed algorithm and the output of continuous measurement of soil radon gas is given in Table 1.

Table 1. Generated S-box

61	0	78	211	104	176	36	220	87	155	186	73	90	133	145	19
151	237	10	182	32	42	164	204	14	62	71	229	66	117	181	239
122	183	29	76	232	65	163	240	146	223	6	178	193	225	189	174
68	100	218	177	119	54	207	137	153	46	106	139	125	255	26	219
4	91	2	111	116	40	55	18	170	58	160	140	236	115	13	242
128	70	159	37	118	31	200	222	175	167	67	81	86	233	217	20
89	43	41	250	197	105	44	162	127	75	7	114	53	57	188	34
166	95	110	16	12	194	130	141	50	196	15	74	206	47	52	158
249	205	59	24	243	8	51	224	202	185	56	228	79	63	135	247
113	244	168	64	3	187	98	157	172	94	154	131	245	241	165	38
121	109	30	148	22	227	161	212	230	235	215	85	180	126	210	231
93	246	33	248	120	195	138	88	35	156	97	99	5	191	221	48
142	107	23	173	226	1	216	171	112	21	234	25	92	143	136	60
152	169	179	150	144	49	134	129	103	101	102	149	17	132	108	190
199	192	123	27	77	72	80	39	198	147	254	28	82	124	96	83
9		208	214	45	84	253	69	201	184	203	251	252	209	11	238
213															

3. ANALYSIS RESULTS

Security of substitution box is generally tested using five criteria (bijective property, nonlinearity, strict avalanche criterion, output bits independence criterion and equiprobable input/output XOR distribution). The analysis results in Table 2 show that any generated lookup table based on proposed method meets all design criteria and it is better than a randomly generated lookup table.

4. CONCLUSIONS

In the literature, there are many algorithms based on random selection. One of the most common example is the use of chaos systems. The main features of chaosbased S-box construction methods is that these methods, uses chaotic systems as a source of randomness. This study shows that other randomness sources such as continuous measurement of soil radon gas can be used for generating S-box structures. Test results of proposed method show that obtained better performance than that in previous studies.

Table 2. Analysis results of generated S-box

S-Box	Nonlinearity			SAC			BIC-SAC	BIC-Nonlinearity	Maximum I/O XOR
	min	max	Avg	min	max	avg			
Proposed method	94	108	104.8	0.4218	0.5937	0.5100	0.5019	103.5	12
standard rand() function	94	108	102.5	0.4062	0.6093	0.5083	0.4726	104.2	12

Table 3. Performance comparison for chaotic S-boxes

S-Box	Nonlinearity			SAC			BIC-SAC	BIC-Nonlinearity	Maximum I/O XOR
	min	max	Avg	min	max	avg			
Ref. [4]	100	106	103.2	0.4218	0.5937	0.5048	0.5009	103.7	10
Ref. [5]	98	108	103	0.4062	0.5937	0.5012	0.4988	104.1	12
Ref. [6]	96	106	103	0.3906	0.625	0.5039	0.5010	100.3	12
Ref. [7]	102	108	104.7	0.3906	0.5937	0.5056	0.5021	104.1	12
Ref. [8]	101	106	103.8	0.4140	0.6328	0.5036	0.5037	103.4	10
Ref. [9]	102	106	104	0.4825	0.5175	0.5018	0.5019	103.5	10
Ref. [10]	108	112	109	0.4531	0.5156	0.5012	0.5012	104	8
Ref. [11]	104	110	108	0.4258	0.5175	0.5007	0.5006	112	12
Ref. [12]	84	106	100	0.125	0.625	0.4812	0.4962	101.9	16
Ref. [13]	98	108	104	0.4218	0.6093	0.5039	0.5078	104	12
Ref. [14]	84	106	100	0.125	0.625	0.4812	0.4962	101.9	16
Ref. [15]	100	108	104.75	0.4218	0.6093	0.4978	0.5009	103.6	12
Ref. [16]	98	110	105.5	0.4062	0.5937	0.4926	0.4994	105.7	32
Proposed method	94	108	104.8	0.4218	0.5937	0.5100	0.5019	103.5	12

REFERENCES

- [1] Katz, J., Lindell, Y., Introduction to modern cryptography: principles and protocols, Chapman & Hall, (2008).
- [2] Knudsen, L. R., Robshaw, M. J. B., The Block Cipher Companion, Springer-Verlag Berlin Heidelberg (2011).
- [3] Cusick, T. W., Stanica, P., Cryptographic Boolean Functions and Applications, Elsevier, (2009).
- [4] Özkaynak, F., Özer, A. B., A method for designing strong S-Boxes based on chaotic Lorenz system. *Physics Letters A.* 374, 3733–3738 (2010).
- [5] Khan, M., Shah, T., Mahmood, H., Gondal, M. A., An efficient method for the construction of block cipher with multi-chaotic systems. *Nonlinear Dyn.* 71(3), 489–492 (2013).
- [6] Khan, M., Shah, T., Mahmood, H., Gondal, M. A., Hussain, I., A novel technique for the construction of strong S-boxes based on chaotic Lorenz systems. *Nonlinear Dyn.* 70, 2303–2311 (2012).
- [7] Hussain, I., Shah, T., Gondal, M. A., A novel approach for designing substitution-boxes based on nonlinear chaotic algorithm. *Nonlinear Dyn.* 70, 1791–1794 (2012).
- [8] Özkaynak, F., Yavuz, S., Designing chaotic S-boxes based on time-delay chaotic system. *Nonlinear Dyn.* 74, 551–557 (2013).
- [9] Hongjun L., Abdurahman K., Yujun N., Chaos-based color image block encryption scheme using S-box. *AEU - International Journal of Electronics and Communications.* 68(7), 676–686 (2014).
- [10] Dragan L., A novel method of S-box design based on chaotic map and composition method. *Chaos, Solitons and Fractals.* 58, 16–21 (2014).
- [11] Xuanping Z., Zhongmeng Z., Jiayin W., Chaotic image encryption based on circular substitution box and key stream buffer. *Signal Processing: Image Communication.* 29(8), 902–913 (2014).
- [12] Majid K., Tariq S., Syeda Iram B., Construction of S-box based on chaotic Boolean functions and its application in image encryption. *Neural Computing and Applications.* 27(3), 677–685 (2016).

- [13] Majid K., Tariq S., Syeda Iram B., A new implementation of chaotic S-boxes in CAPTCHA. *Signal, Image and Video Processing*. 10(2), 293–300 (2016).
- [14] Majid Khan, A novel image encryption scheme based on multiple chaotic S-boxes. *Nonlinear Dyn.* 82(1), 527–533 (2015).
- [15] Majid K., Tariq S., An efficient construction of substitution box with fractional chaotic system. *Signal, Image and Video Processing*. 9(6), 1335–1338 (2015).
- [16] Majid K., Tariq S., A novel image encryption technique based on Hénon chaotic map and S8 symmetric group. *Neural Computing and Applications*. 25(7), 1717–1722 (2014).

BIOGRAPHY

Fatih Özkaynak: Fatih Ozkaynak is an assistant professor of Software Engineering at Firat University. He received his Bachelor of Science degree in Computer Engineering from Firat University, Elazig, Turkey in 2005, Master of Science degree from Computer Engineering from Firat University in 2007, and Doctor of Philosophy in Computer Engineering from Yildiz Technical University in 2013. Dr. Ozkaynak's research interests are cryptography, information security, and chaotic systems. He has co-authored over 30 refereed scientific journal and conference papers. His work has cited more than 200 times. His h-index is 7. He serves as a reviewer for scientific journals including *Cryptography and Communications - Discrete Structures, Boolean Functions and Sequences, Information Sciences, IEEE Transactions on Very Large Scale Integration Systems, IET Information Security, Security and Communication Networks, Computers & Electrical Engineering, Applied Soft Computing, Physics Letter A, Applied Mathematical Modelling...*

Cryptanalysis of A New Image Encryption Scheme Based on A Chaotic Function

Fatih Okaynak¹, Ahmet Bedri Ozer²

Abstract

Cryptography based on nonlinear systems and chaos theory has been developed a model which is a new and efficient way to cope with the security problems of image encryption. However, cryptanalysis works of proposed new model show that proposed chaos based image encryption schemes is not secure. François et al. proposes a novel chaos-based bit-level permutation scheme for secure and efficient image cipher. To overcome the drawbacks of conventional permutation-only type image cipher, the proposed scheme introduced a procedure through a bit-level shuffling algorithm. The encryption operations are realized by chaotic function and XOR operator. In this study, we analyze the security weaknesses of the proposal. Both theoretical analysis and experimental simulation indicate that the plain image can be recovered exactly from the cipher image without the secret key.

Keywords: Chaos; Cryptography; Cryptanalysis; Chosen-plaintext Attack

1. INTRODUCTION

Chaos theory has been developed to model complex behavior using quite simple mathematical models. This theory has captured the attention of the scientific community for to explain and predict the behavior of systems in real world. For cryptography applications, there is a relationship between chaos and cryptography. The main characteristics of chaotic dynamics (dependency to initial conditions and control parameters, ergodicity) are connected to the requirements of cryptography (confusion and diffusion of information) [1, 2]. Consequently, many chaos based image encryption algorithm proposed using this relationship [3-13]. However, some schemes have been found to be insecure from the viewpoint of cryptography, and some general recommendations have been drawn to facilitate the design of more secure encryption schemes [14-24].

In this study, we cryptanalyze the image cryptosystem recently proposed in [3]. The cryptosystem uses the chaotic function to shuffle plain image sequences. The cryptosystem performs the encryption process with bitwise XOR operation. However, this is not enough to make the cryptosystem secure. Secret parameters of cryptosystem have been obtained using only a few a pair of plaintext/ciphertext.

The outline of the study is as follows. In the next section we describe the proposed encryption algorithm. In Section 3, we demonstrate a chosen-plaintext attack that reveals all the secret parameters. Finally, we give concluding remarks.

2. DESCRIPTION OF THE ENCRYPTION ALGORITHM

In this section, we describe the encryption algorithm. Before starting encryption process, original image of $M \times N$ dimensions is transferred into one-dimensional bit sequence (I_B). Encryption algorithm produces two different bit sequences to encrypt original image. The first sequence (Z_1) is a copy of the form which was transferred from original image into one-dimensional bit series. Original bit series is shuffled to form second series (Z_2). For shuffling process, the equality in Eq. (5) is used. The chaotic structure of algorithm is caused by Eq. (1). XOR process is applied to the two generated series which are produced to form encrypted image (Z_3). These processes are repeated for the number of rounds (R).

$$X_{n+1} = \left[[X_n^2 \bmod S] \times X_n + X_g \right] \bmod S \quad (1)$$

$$0 < r < R \quad (2)$$

$$j \leftarrow i + 1 + X \quad (3)$$

$$Z_1 \leftarrow I_{r-1}^b[i] \quad (4)$$

$$Z_2 \leftarrow I_{r-1}^b[j] \quad (5)$$

¹Corresponding author: Firat University, Department of Software Engineering, 23119, Elazığ, Turkey, ozkaynak@firat.edu.tr

$$Z_3 \leftarrow Z_1 \oplus Z_2 \quad (6)$$

3. CHOSEN PLAINTEXT ATTACK

In the chosen-plaintext attack, the attacker chooses a plain image and somehow obtains the corresponding ciphered image. By analyzing the plain/ciphered image pair, he tries to reveal the secret parameters. Before the chosen-plaintext attack, some explanations used in the attack are given below.

Many useful algorithms are recursive in structure: to solve a given problem, they call themselves recursively one or more times to deal with closely related subproblems. These algorithms typically follow a divide-and-conquer approach: they break the problem into several subproblems that are similar to the original problem but smaller in size, solve the subproblems recursively, and then combine these solutions to create a solution to the original problem.

Plain images which were chosen to be used in attack were selected according to the logic of divide-and-conquer. The number of plain images to be used in the attack is $\lceil \log_2 L \rceil$ for $L=8 \times M \times N$. In the plain image selected initially, it is desired that half of its bits is to be 0 and the rest is to be 1. For the other plain image which will be selected, former bit series is divided into two and, again, it was desired that first half is to be 0, second half to be 1. Division process is continued until one bit remains.

For ease of understanding, plain images which will be selected to encrypt an image of 2×2 dimensions were shown in Table 1. The corresponding pixels of these images are $\{0,0,255,255\}$, $\{15,15,15,15\}$, $\{51,51,51,51\}$, $\{85,85,85,85\}$, respectively.

Table 1: Bit sequence for selected 2×2 plain images

0	0	0	0	0	0	0	0	0	0	0	0	0	0	0	0	1	1	1	1	1	1	1	1	1	1	1	1	1	1	1	1	1	1	1	1	1	1	1	1		
0	0	0	0	0	0	0	0	0	1	1	1	1	1	1	1	0	0	0	0	0	0	0	0	1	1	1	1	1	1	1	1	1	1	1	1	1	1	1	1	1	
0	0	0	0	1	1	1	1	0	0	0	0	1	1	1	1	0	0	0	0	1	1	1	1	0	0	0	0	1	1	1	1	1	1	1	1	1	1	1	1	1	
0	0	1	1	0	0	1	1	0	0	1	1	0	0	1	1	0	0	1	1	0	0	1	1	0	0	1	1	0	0	1	1	0	0	1	1	0	0	1	1	1	1
0	1	0	1	0	1	0	1	0	1	0	1	0	1	0	1	0	1	0	1	0	1	0	1	0	1	0	1	0	1	0	1	0	1	0	1	0	1	0	1	0	1

As a consequence of attack nature, encrypted images which correspond to these selected plain images are obtained. As explained in the second section, encrypted image was obtained by applying XOR process to the bit series which were obtained from chaotically shuffled image and from original image, as shown in Eq. (6). Since cryptanalyst has both original image and encrypted image, it can obtain the image chaotically shuffled. At this stage, X values which are the output of chaotic function showing the obtainment of shuffled image by taking values of which positions the original image has accordingly, should be determined. For this purpose, plain/ciphered image pairs are utilized which were formed according to the logic of divide-and-conquer. For instance, first bits of the selected plain/ciphered images are examined to find that the first bit values of shuffled images are obtained with the bit value of which position the original image has accordingly. Since first bits of all selected plain images are equal to 0, the values of shuffled images determine the values of encrypted images. Since encrypted image obtained for the first plain image is 1, the first X value is in the left-down tree of the tree given in Figure 1. Since the encrypted form of the image corresponding to first bit of second plain image is also equal to 1, it is continued with the left bottom tree of bottom tree. Since the value of the encrypted image found for third plain image, it was again continued with the left bottom tree of bottom tree. Since the encrypted values obtained for the fourth and fifth plain images are 0, it is continued from right, bottom trees for these conditions and position data of the first X value is found. For all bit series, same processes are repeated and all X values are found. The X values which were found are equivalent to the key of encryption algorithm. Anyone who has this data can encrypt/decrypt a data. The chosen-plaintext requirement of the attack is only $2^{10} = \lceil \log_2 (8 \times 512 \times 512) \rceil$ for the 512×512 traditional Lena image.

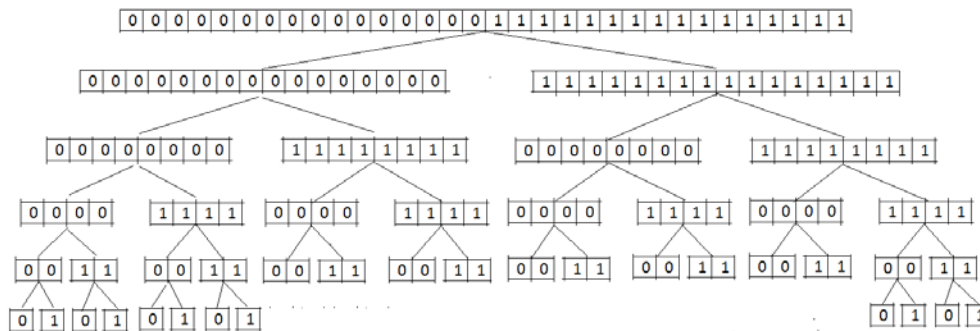


Figure 1: Attack tree for chosen plaintext attack

4. CONCLUSIONS

Computer science is developing rapidly; consequently, it is getting easier to attack a cryptosystem, for an attacker. There are many attack types introduced by cryptanalysts as well, from day to day. In this study, our goal is to find a weakness in the cryptosystem which can be exploited with a complexity lower than a brute force attack.

In many chaos based image encryption algorithms, the secret parameters are generated by iterating one or more chaotic systems starting with secret initial conditions and parameters. In attacking these algorithms, the attacker aims to reveal the intermediate secret parameters rather than the chaotic system parameters. A novel image encryption method based on a chaotic function is proposed by François et al. Although it has a lot of advantages, such as large key space, low encryption time and high key sensitivity and so on, unfortunately, we find this method is vulnerable to chosen plaintext attack.

REFERENCES

- [1] M. Amigo, L. Kocarev, J. Szczapanski, Theory and practice of chaotic cryptography, *Physics Letters A* 366 (2007) 211-216.
- [2] G. Jakimoski, L. Kocarev. Chaos and cryptography: block encryption ciphers. *IEEE Trans Circ Syst—I* 48/2 (2001) 163-169.
- [3] M. François, T. Grosgees, D. Barchiesi, R. Erra, A new image encryption scheme based on a chaotic function, *Signal Processing: Image Communication* 27 (2012) 249-259.
- [4] X. Wang, W. Zhang, W. Guo, Jiashu Zhang, Secure chaotic system with application to chaotic ciphers, *Information Sciences* 221 (2013) 555-570.
- [5] A. Kalso, H. Yahyaoui, M. Almulla, Keyed hash function based on a chaotic map, *Information Sciences* 186/1 (2012) 249-264.
- [6] C. Chen, C. Lin, C. Chiang, S. Lin, Personalized information encryption using ECG signals with chaotic functions, *Information Sciences* 193 (2012) 125-140.
- [7] Z. Zhu, W. Zhang, K. Wong, H. Yu, A chaos-based symmetric image encryption scheme using a bit-level permutation, *Information Sciences* 181/6 (2011) 1171-1186.
- [8] J. Fridrich, Symmetric ciphers based on two-dimensional chaotic maps, *International Journal of Bifurcation and Chaos* 8/6 (1998) 1259-1284.
- [9] C. Zhu, A novel image encryption scheme based on improved hyperchaotic sequences, *Optics Communications* 285/1 (2012) 29-37
- [10] H. Hu, L. Liu, N. Ding, Pseudorandom sequence generator based on Chen chaotic system, *Computer Physics Communications* 184 (2013) 765-768.
- [11] Q. Zhang, L. Guo, X. Wei, Image encryption using DNA addition combining with chaotic maps, *Mathematical and Computer Modelling* 52 (2010) 2028-2035.
- [12] N. Bigdeli, Y. Farid, K. Afshar, A robust hybrid method for image encryption based on Hopfield neural network, *Computers and Electrical Engineering* 38, pp.356-369, 2012.
- [13] L. Liu, Q. Zhang, X. Wei, A RGB image encryption algorithm based on DNA encoding and chaos map, *Computers & Electrical Engineering*, 38/5 (2012) 1240-1248.
- [14] E. Solak, *Cryptanalysis of Chaotic Ciphers*, in: L. Kocarev, S. Lian (Eds.), *Chaos Based Cryptography Theory Algorithms and Applications*, Springer-Verlag, 2011, 227-256.
- [15] G. Alvarez, J. M. Amigo, D. Arroyo, S. Li, Lessons Learnt from the Cryptanalysis of Chaos-Based Ciphers, in: L. Kocarev, S. Lian (Eds.), *Chaos Based Cryptography Theory Algorithms and Applications*, Springer-Verlag, 2011, 257-295.
- [16] G. Alvarez, S. Li, Some basic cryptographic requirements for chaos-based cryptosystems. *International Journal of Bifurcation Chaos* 16/8 (2006) 2129-2151.
- [17] F. Özkaynak, S. Yavuz, Security problems of pseudorandom sequence generator based on Chen chaotic system, *Computer Physics Communications* 184 (2013) 2178-2181.
- [18] F. Özkaynak, A. B. Özer, S. Yavuz, Cryptanalysis of a novel image encryption scheme based on improved hyperchaotic sequences, *Optics Communications* 285 (2012) 4946-4948.
- [19] F. Özkaynak, A. B. Özer, S. Yavuz, Cryptanalysis of Bigdeli algorithm using Çokal and Solak attack, *International Journal of Information Security Science*, 1/3 (2012) 79-81.

- [20]F. Özkaynak, A. B. Özer, S. Yavuz, (2012). Analysis of Chaotic Methods for Compression and Encryption Processes in Data Communication, 20th IEEE Signal Processing and Communications Applications Conference.
- [21]F. Özkaynak, A. B. Özer, S. Yavuz, (2013). Security Analysis of An Image Encryption Algorithm Based on Chaos and DNA Encoding, 21th IEEE Signal Processing and Communications Applications Conference.
- [22]E. Solak, C. Çokal , Algebraic break of image ciphers based on discretized chaotic map lattices, Information Sciences, 181/1 (2011) ,227-233.
- [23]E. Solak, C. Çokal, O.T. Yildiz, T. Biyikoglu, Cryptanalysis of fridrich's chaotic image encryption. International Journal of Bifurcation and Chaos 20/5 (2010) 1405–1413.
- [24]F. Özkaynak, S. Yavuz, Analysis and improvement of a novel image fusion encryption algorithm based on DNA sequence operation and hyper-chaotic system, Nonlinear Dynamics: Volume, 78/2, 1311-1320, 2014.

BIOGRAPHY

Fatih Özkaynak: Fatih Ozkaynak is an assistant professor of Software Engineering at Firat University. He received his Bachelor of Science degree in Computer Engineering from Firat University, Elazig, Turkey in 2005, Master of Science degree from Computer Engineering from Firat University in 2007, and Doctor of Philosophy in Computer Engineering from Yildiz Technical University in 2013. Dr. Ozkaynak's research interests are cryptography, information security, and chaotic systems. He has co-authored over 30 refereed scientific journal and conference papers. His work has cited more than 200 times. His h-index is 7. He serves as a reviewer for scientific journals including Cryptography and Communications - Discrete Structures, Boolean Functions and Sequences, Information Sciences, IEEE Transactions on Very Large Scale Integration Systems, IET Information Security, Security and Communication Networks, Computers & Electrical Engineering, Applied Soft Computing, Physics Letter A, Applied Mathematical Modelling.

A Survey on MPC Widely Used Many Areas of the Industry

Ibrahim Celik¹, Mehmet Polat²

Abstract

This paper presents exhaustive information about Model Predictive Control (MPC) which is used in industry widespread. Although MPC opinion emerged in 1960's, interest to this field started with a study made by Richalet in 1978. Nowadays, it has been one of the most important methods for linear and non-linear plants. MPC consists a lot of control methods such as Generalized Predictive Control (GPC), Dynamic Matrix Control (DMC) etc. Main characteristic of these methods includes mathematical model of the plant. It is also created to control signal based on prediction moving horizon principle and response of plant. MPC has the ability that the input signals are currently optimized on mathematical model and it is observed that other control methods including Proportional-Integral-Derivative (PID), Linear Quadratic Regulator (LQR) in the same category do not have this predictive ability. By considering the results of the studies, the aim of this study is to determine the advantages and disadvantages of MPC by using a comparison between MPC and other control methods in the same class. Therefore, this study has an importance for researchers who want to work in this area.

Keywords: MPC, Comparison of MPC, Use Areas of MPC

1. INTRODUCTION

MPC is commonly used to control plant which has hundreds of inputs and outputs by depending on constraints in chemical applications [1]. The basic of MPC grounds to optimize predicts of the plant behavior and this predicts are obtained by dynamic model of the plant [2]. MPC which uses current state of the plant as initiate state at each sample time during finite horizon is a control approach applied by optimizing signals that obtained from mathematical model of the plant in open-loop. This optimization is a problem for MPC, since calculating a new input vector and also taking into consideration constraints for considered inputs and outputs are difficult.

As MPC used industrially in recent years has technically advanced, its application areas have increased significantly and it has been one of the most popular control methods. So this paper provides an overview to this approach by observing brief history of MPC and its industrial applications.

2. DEVELOPMENT

In the early 1960s, MPC approach firstly based on the works of Kalman who said that a linear control plant can be optimized [3]. Then, LQR is designed to minimize unconstrained quadratic functions of states and inputs. As LQR has infinite horizon, it has robust stability property. However, it is not used generally in real plants of industries since real plants are non-linear and there are not constraints of that.

In the late of 1970's, various applications of MPC is utilized in industry. There is a great effect to history of MPC in this applications of Model Predictive Heuristic Control (MPHC) and DMC respectively made by Richalet and Cutler, Ramaker [4,5]. The common property of them is used mathematical model of the plant to predict the influence of future control actions with constraints. Then, MPHC developed by Richalet is called as Model Algorithmic Control (MAC). These approaches create the input signal of the plant at each sample time by optimizing signals obtained from the mathematical model. Stability is not automatically provided in the first generation of MPC. However, if horizon is chosen higher than the settling time of the plant and plant is stabled, stability can be provided. Identification and Command (IDCOM) is proposed as solution to this problem. Inputs in this method are calculated by heuristic algorithm.

DMC was developed by engineers in Shell independently from the other methods in the early 1970's. Although first application was done in 1973, the development of unconstrained multivariable control algorithms was not reported until 1979 [6]. This method was presented by Cutler and Ramaker at the National AIChE Meeting and Joint Automatic Control Conference in 1979 and 1980, respectively [3]. In this approach, Least-Square Method (LSM) was utilized for optimizing data obtained from mathematical model. DMC approach was used by Prett and Gillette for Fluidized Catalytic Cracking Units (FCCU) [7]. Thus, IDCOM and DMC constitute the first generation of MPC.

¹ Corresponding author: Master Student, Firat University, Department of Mechatronic Engineering, 23119, Elazığ, Turkey. ibrahimcelik.04@gmail.com

² Assistant Professor, Firat University, Faculty of Engineer, Mechatronic Engineer, 23119, Elazığ, Turkey. mpolat@firat.edu.tr

Improvement of the adjustment capability of DMC is needed as online in applications. Therefore, Cutler firstly described Quadratic Dynamic Matrix Control (QDMC) at AIChE Conference in 1983 [8]. After few years, Carlos, Garcia, and Morshedi presented more comprehensive description. QDMC consists of online solution of a quadratic program that minimizes sum of quadratic difference to keep variables within the constraints [9]. QDMC creates to the second generation of MPC.

Grosdidier, Froisy, and Hammann who described needs of multivariable plants in industry proposed Identification and COMmand-Multi (IDCOM-M) controller in 1988. IDCOM-M is developed by SETPOINT Inc.. IDCOM-M, which has a structure which defines results obtained from dynamic model prior to process, is based on MPC technology developed by Adersa [10]. Shell Multivariable Optimizing Control (SMOC) was synchronously developed by Marquis and Broustail. In this application, MPC technology and State-space control are merged. As a consequence, State-space control provides a rich theoretical perspective to cope with complex feedback configurations. SMOC approach was implemented to hydro treating unit by Marquis and Broustail [11]. IDCOM-M, HIERarchical constraint CONtrol (HIECON), Shell Multivariable Control Algorithm (SMCA), and SMOC create the third generation of MPC. As well as, Predictive Control Technology (PCT) and Robust Model Predictive Control (RMPC) were developed by Profimatics and Honeywell, respectively.

In the late 1995s, Honeywell bought Profimatics and changed its name as Honeywell Hi-Spec Solutions. Therefore, current controller called as Robust Model Predictive Control Technology (RMPCT) occurs from the combination of RMPC and PCT developing by Profimatics. In the early 1996s, Aspen Technology constituted to DMC-plus merge technologies of SMCA and DMC by buying both SETPOINT Inc. and DMC Corporation [1]. DMC-plus and RMPCT are the fourth generation of MPC. The genealogy of MPC algorithms is shown in Figure 1.

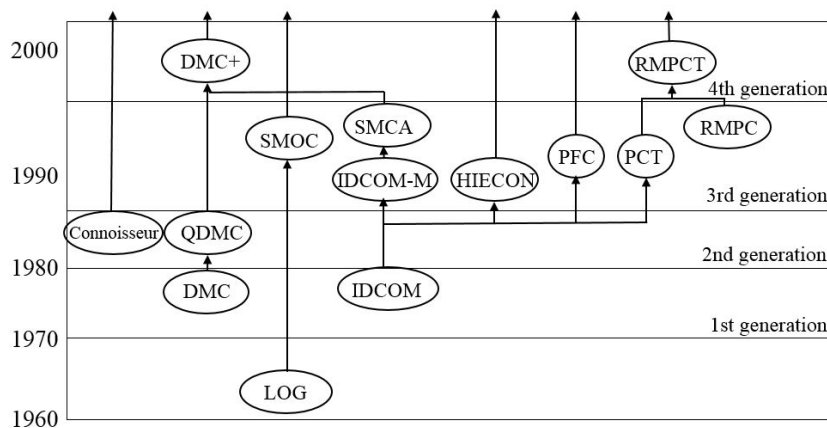


Figure 1. Genealogy of MPC algorithms [1]

Runge-Kutta Model Predictive Control (RKMPC) is proposed for the control of non-linear plants lately by Iplikçi [12]. Nowadays, MPC approach has been included in the adaptive control class and it continues to improve with developing technology.

3. USAGE AREAS OF MPC

Although MPC is generally developed for chemical applications, it is used in many areas of industry. In this chapter, the usage areas of MPC are classified by different scientific fields.

3.1. Chemical

MPC is used in the power management system. The system is prepared by integration of renewable energy conversion devices (Photovoltaic, PV), a high efficiency energy conversion programmable system (Fuel Cell, FC) and an electrochemical energy storage system (batteries). A control strategy purposing to optimize minimum energy consume is developed to provide the environmental comfort in the home. Results in [13] show the regulation comfort conditions of the home and lower consumption as average 14.5% of primary fossil energy. The reasons of that are both reduction the amount of requested energy and increasing the use of renewable energy supplies. Experiments are done in the periods of winter and summer. Results are compared with Rule Based Control (RBC). It is observed that consume of FC reduces in winter and summer conditions as 25% and 60%, respectively which means a great cost benefit for this type of applications [13].

The performance of MPC applied to a chemical reactor being one of the most important applications of chemical engineer is examined. The temperatures of reactor and propylene glycol occurring from reaction of water and propylene oxide are controlled by the adjustment of fluid flow. The temperatures of refrigerant water and propylene oxide are taken into consideration as aliasing. As a result, it is observed that MPC follows to the reference signal by lower overshoot and is faster than PID calculating with Ziegler-Nichols rules [6].

3.2. *Electric and Electronic*

Since linear MPC can not realize the control of non-linear plants, non-linear MPC is developed. However, the usage of this method is difficult in industry due to too much processing needs. As a consequence, algorithms facilitating design for controller of non-linear plants divided to linear sub-systems are advanced to reduce the number of processing. In this study, Fuzzy MPC (FMPC) structure which is alternative method to these algorithms is proposed. Proposed approach is applied to a non-linear plant on MATLAB and results are given. The plant actions of PT326 temperature kit are observed and compared with PID controller. It is shown that FMPC is more successful than PID [14]. Robust MPC approach is applied to PT326 temperature kit by using MATLAB-SIMULINK and MATLAB-XPCTARGET tools. The controller design provides to stability for changing whole parameters of the temperature kit. It is observed that there is not stable state error [15].

In [16], the linearization problem of the model is solved by merging MPC and Artificial Neural Network (ANN). As ANN has training and adaptation abilities in linear and non-linear plants, a MPC structure which has these abilities is created by ANNMPC approach. Therefore, the usage of matrix is not necessary to the contrary classic predictive controllers, which increase the speed of algorithm. is compared with Dynamic Matrix Algorithm (DMA) in terms of speed and it is observed that the performance of ANNMPC is better than the other method [16].

The aim of [17] is to regulate the torque while winding currents of Switched Reluctance Motor (SRM) and switching frequency of power converter are minimum. On the contrary standard current-based control, MPC is utilized to control the torque of SRM. MPC directly controls the switches of the dc-link power converter by non-linear model obtained [17].

Smart building technologies are improved to optimize usage of the energy in electric systems of residential and commercial facilities. The delay of feedback signal in the network based on the control reduces the ability to follow the reference trajectory in motor drive utilized for processes such as heating, cooling, refrigeration, and ventilation. The compensation of time delay is realized by MPC for connection delays decreasing the performance of networks in smart buildings [18].

The problem of production scheduling is taken into consideration continuously by parallel machines that have different speed and energy remanded on production lines. Total energy consumption is calculated properly considering the diversity of transport lines such as length and transport parts. An optimal control structure aimed to optimize total energy consumption and maximum production is presented in [19].

PID controller is generally utilized to control the asynchronous motor using widely in industry. However, it has some drawbacks such as adjustment of its parameters required to provide close-loop performance in different environment conditions, which is the most important one. MPC approach is utilized to increase the ability to follow the reference of asynchronous motor and eliminate disadvantages of PID. Linear dynamic model of asynchronous motor is obtained by using of vector control principle. It is shown that MPC is more stable than conventional PID when rotor resistance and load are taken as aliasing [20].

MPC is used for regulating the output voltage of full bridge dc-dc converter without ignoring to the peak current constraint. Integrated Perturbation Analysis and Sequential Quadratic Programming (InPA-SQP) method is proposed to solve the constrained optimal control problems. Dynamic model for full bridge dc-dc converter is improved. The peak current protection requirement is defined by the state and input constraints. Experimental results show that proposed control algorithm is successful [21].

3.3. *Machine*

Helicopters have abilities such as high maneuver ability, being able to fly at very low speed and to remain suspended in the air. In [22], to control the linear speed and the angular position of the unmanned helicopter is tackled. Non-linear dynamic model for 6 degrees of freedom helicopter is obtained and transferred to MATLAB. Both LQR and MPC are designed for model and various scenarios are considered. Besides, a lot of scenarios including the changing of the plant dynamic and aliasing are added for MPC. The error of the both is makeequaled by Integral Absolute Error (IAE). When results are compared, it is observed that the response of MPC is much faster than LQR [22].

Approximate Model Predictive Control (AMPC) which based on linearization including GPC techniques on Neural Network is utilized to control the shaft speed of gas turbine engine. Firstly, the non-linear model of gas turbine is examined, using NARMAX. The plant is controlled by giving randomly small and big step references and obtained results are compared with the results of PID. As a result, it is shown that AMPC is better response according to Integral of Time Absolute Error (ITAE) criteria [23].

GPC is designed to provide the following reference trajectory of six-axis robot arm. The dynamic model of the robot arm is created by utilized Lagrange-Euler method and trajectory scheduling is done according to sinusoidal trajectory criteria. The aim of the controller designed is to control the torque of the joints during reference trajectory. Linear model is obtained by Controlled Auto Regressive Integrated Moving Average (CARIMA) linear form and the input values of the plant are calculated by LSM. The controller obtaining the torque information of the joints in exchange for position data is designed. Predictive control approach being an advanced alternative to conventional controllers is yielded very successful results in applications which are knowing beforehand the reference trajectory [24].

4. THEORY OF MPC

Mathematic and significant parameters of MPC are examined in this chapter.

b. The Basic Parameters

The important parameters used in the design of MPC are considered. The choosing of those parameters directly affects the outputs of the plant. The basic structure of MPC is shown in Figure 2.

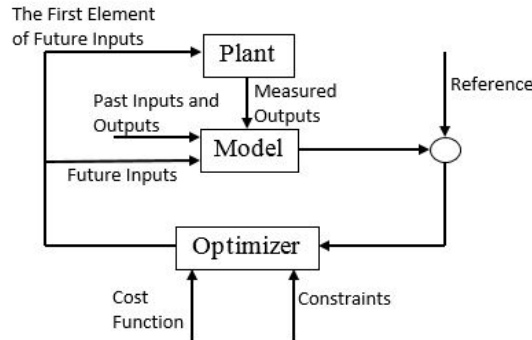


Figure 2. Basic structure of MPC [25]

i. Prediction Horizon

Prediction Horizon (N_p) determines how much each horizon will be when doing calculations in other words, the number of the input parameters obtained from model of plant. The value of N_p generally is chosen between 20 and 30; however, it can be chosen larger depending on the model. If predictive horizon is chosen as a great value, the plant is more stable. On the other hand, if predictive horizon is chosen as a small value, the plant becomes unstable to follow reference trajectory. When predictive horizon is increased, the number of processing rises for calculation.

ii. Control Horizon

Control horizon (N_c) is the number of variable to be calculate at how much sample time. Its value can choose between 1 and N_p . However, its value generally chooses much smaller than N_p to calculate fewer variables in quadratic program at each control range. The signal obtaining from controller accepts constant in remaining until the end of prediction horizon from the control horizon.

iii. Reference Trajectory

The one of advantages of MPC is also more stable in applications which know beforehand the reference trajectory. Besides, if the aliasing will be known when, MPC provides the advantage to control algorithm when reference is constant.

iv. Cost Function

The aim of control algorithm is to minimize the cost function (J). The cost function consist of the multiplying of the difference between output signal and reference signal, the difference between input signal and input signal waiting and weight matrix prearranged.

Example equation [26]:

$$J = \sum_{i=1}^{n_y} (r_{k+i} - y_{k+i})^2 + \sum_{i=0}^{n_u-1} W(u_k - u_{ss})^2 + (W_d \Delta u_k)$$

- (1)
- J : Cost function
 - r_{k+i} : Value of reference signal at $t=k+i$
 - y_{k+i} : Value of output signal at $t=k+i$
 - u_{ss} : Expected steady-state of the input
 - W, W_d : Weights

c. Strategy

The output signals of the plant predict by utilizing model at each k time during prediction horizon. These signals depend on the value of past input and outputs signals at t moment for $p : 1, \dots, N_p$ and the value of future input signals which calculated to be applied to the plant for $p : 0, \dots, N_p - 1$.

$\hat{y}(k+p|k)$: the value of prediction for $k+p$ moment at $t=k$ time

$u(k+p|k)$: the value of input signal giving the value of reference for $k+p$ moment at $t=k$ time

Future input signals calculate by optimizing to provide the following reference signal of the plant. MPC logic is shown in Figure 3.

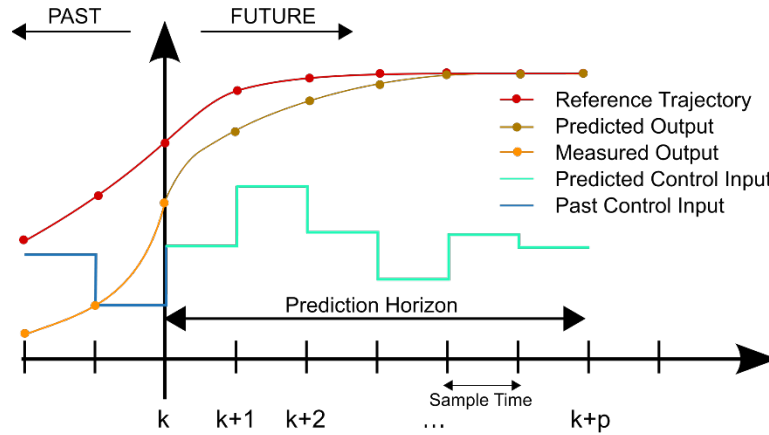


Figure 3. Model Predictive Control Logic

i. The Model Types Used in MPC

In this chapter, the some model types used in MPC is mentioned.

4.2.1.1. Transfer Function Model

$$A(z^{-1}) = 1 + a_{-1}z^{-1} + a_{-2}z^{-2} + \dots + a_{na}z^{-na} \quad (2)$$

$$B(z^{-1}) = b_0 + b_{-1}z^{-1} + b_{-2}z^{-2} + \dots + b_{nb}z^{-nb} \quad (3)$$

$$A(z^{-1})y(t) = B(z^{-1})u(t) \quad (4)$$

The expression of predicted output is defined in equation 5.

$$\hat{y}(k+p|k) = \frac{B(z^{-1})}{A(z^{-1})} u(k+p|k) \quad (5)$$

As this model needs a few parameters especially A and B polynomials, it which based on the knowledge of the pre-processing provide advantage and it is appropriate for unstable plants [25].

4.2.1.2. State-Space Model

$$x(k) = Mx(k-1) + Nu(k-1) \quad (6)$$

$$y(k) = Qx(k) \quad (7)$$

x , M , N and Q indicate state, plant, input and output, respectively. The prediction equation of model is described in equation 8.

$$\hat{y}(k+p|k) = Q\hat{x}(k+p|k) = Q[M^k x(t) + \sum_{i=1}^{N_p} M^{i-1} Nu(k+p-i|k)] \quad (8)$$

The one of advantages of this model is easily to implement the multivariable plants. Control rule is the feedback of linear combination of the state vector. If states can not be obtained, observer should be done the necessary adding to perform calculations.

4.2.1.3. Finite Sstep Response Model

FSR model is obtained by implementing unit step input to a plant which is stable state. The coefficients of plant create by output values. S_i indicate the step response for i th sample time. The output is changed according to changing in unit step response [27].

Step model is defined as the vector of step response coefficients.

$$S = [s_1 \ s_2 \ s_3 \ \dots \ s_N]^T \tag{9}$$

If the length of model is chosen tall enough, the value of coefficient is relatively approved.

5 COMPARISON

In comparison, DC motor is considered as the plant. The parameter of MPC which is N_p , N_c and W is taken 30, 29 and 0.001, respectively. Results are observed the response of controllers in reply to the changing of reference speed in Figure 4a. Load value is changed as aliasing at $t=10$ second for same plant and parameters and the responses is shown in return this changing in Figure 4b. Results in both is shown that MPC is arrived faster reference and is be influenced less from aliasing according to Fuzzy Logic Control (FLC).

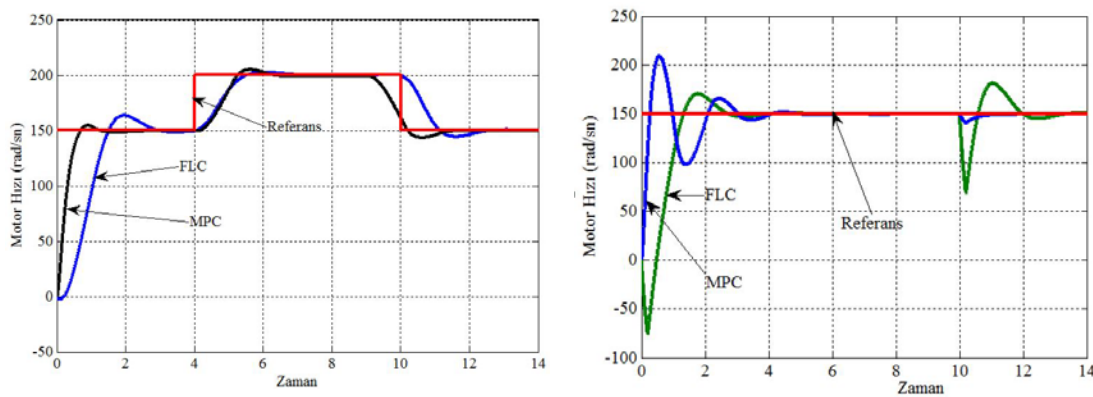


Figure 4a-4b. Comparisons of the MPC and FLC [28]

LQR and MPC are designed for difference scenarios including basic movements it did before helicopter remain suspended in the air. N_p and N_c is determined 50 and 5 for MPC design, respectively. In Figure 5a is shown that while MPC is merely made 6 swaying, LQR is swayed more than 20. They are utilized to control the pitch attitude of helicopter in Figure 5b. MPC is arrived the reference at $t=12$ second, while LQR is maintained to arrive the reference value at $t=18$ second.

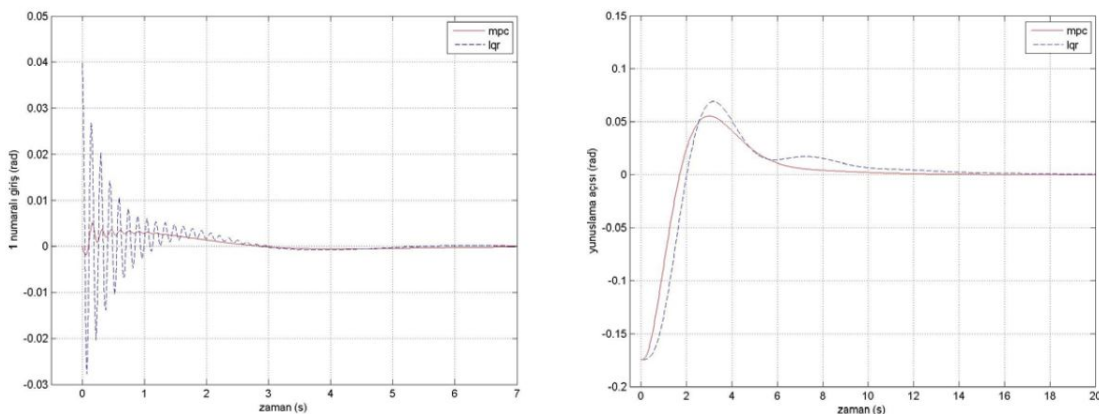


Figure 5a-5b. Comparisons of the MPC and LQR [21]

In addition to the above study, a lot of study which compare with MPC and PID are present. The controller characteristics, which are settling time, the response in exchange for aliasing and overshoot, of MPC is occurred to be superior to most in these studies.

6 RESULTS

This paper is presented a beneficial article about MPC to the resources. Nowadays, as the importance of MPC is increased better and better, the aim of this paper is to create awareness about it. In this study as is seen, MPC using a lot of application in industry is over towered the other control methods that in the same class. In future study, We are practically aimed MPC approach the utilizing for electric vehicle technology.

ACKNOWLEDGMENT

This work is supported by TUBITAK (The Scientific and Technological Research Council of Turkey) with the project, 113M090.

REFERENCES

- [1] S.J. Qin, Thomas A. Badgwell, *A Survey of Industrial Model Predictive Control Technology*, Control Engineering Practice, 11 (2003), pp733-764, 2003.
- [2] Rawlings James B., *Tutorial Overview of Model Predictive Control*, SPECIAL SECTION Industrial Process Control, IEEE Control Plant Magazine, 1053-5888/00, pp38-52, June 2000.
- [3] Ruchika, N. Raghu, *Model Predictive Control: History and Development*, International Journal of Engineering Trends and Technology (IJETT), Volume 4 Issue 6, ISSN: 2231-5381, pp2600-2602, June 2013.
- [4] Richalet J., Rault A., Testud J. L and Papon J., *Algorithmic control of industrial processes*, In Proceedings of the 4th IFAC symposium on identification and plant parameter estimation, pp1119-1167, 1976.
- [5] Cutler C.R, Ramaker B.C, *Dynamic Matrix Control – A Computer Control Algorithm*, Automatic Control Conference, 1980.
- [6] Kuzu E. Ö., *An Investigation on Model Predictive Controllers Applications of A Chemical Engineering Process*, Istanbul Technical University, M. Sc. Thesis, June 2006.
- [7] Prett D. M. And Gillette R. D., *Optimization and Constrained Multivariable Control of A Catalytic Cracking Unit*, In Proceedings of The Joint Automatic Control Conference, 1980.
- [8] Cutler C., Morshedi A. M. And Haydel J., *An Industrial Perspective on Advanced Control*, In AIChE annual meeting, October 1983.
- [9] Carlos E., Garcia C. E. And Morshedi A. M., *Quadratic Programming Solution of Dynamic Matrix Control (QDMC)*, Chemical Engineering Communications, December 27, pp073-087, 1985.
- [10] Grosdidier P., Froisy B., and Hammann M., *The IDOCOM-M Controller*, IFAC Model Based Process Control, Setpoint Inc., Georgia, USA 1988.
- [11] Marquis P. And Broustail J.P., *SMOC, A Bridge Between State Space And Model Predictive Controllers: Application to The Automation of A Hydrotreating Unit*, IFAC Model Based Process Control, Shell Recherche SA, Georgia, USA 1988.
- [12] Bahtiyar B., *FPGA ile Gerçek-Zamanlı Runge-Kutta Model Öngörülmesi Kontrolü*, Pamukkale University, Doctoral Thesis, May 2015.
- [13] Bruni G., Cordiner S., Mulone V., Rocco V. And Spagnolo F., *A study on the energy management in domestic micro-grids based on model predictive control strategies*, Energy Conversion and Management, 102(2015), pp50-58, 02-24-2015.
- [14] Kömürçü E., *Bulanık Model Öngörülmesi Kontrolü*, Istanbul Technical University, M. Sc. Thesis, June 2009.
- [15] Akçakaya H., *Dayanıklı Model Öngörülmesi Kontrolü*, Istanbul Technical University, M. Sc. Thesis, June 2006.
- [16] Şahin S., *Yapay Sinir Ağları Temelli Model Öngörülmesi Kontrolü*, Ege University, M. Sc. Thesis, 08-13-2013.
- [17] Peyrl H., Papafotiou G. And Morari M., *Model Predictive Torque Control of a Switched Reluctance Motor*, Industrial Technology, ICIT 2009, IEEE International Conference, pp1-6, Feb 2009.
- [18] McCann R., Anh T. Le and Traore D., *Model Predictive Control For Time-Delay Compensation of A Switched Reluctance Motor Drive In Smart Building Applications*, 978-1-4244-2279-1, IEEE 2008, pp1-4, 2008.
- [19] Cataldo A., Perizzato A. And Scattolini R., *Production Scheduling of Parallel Machines With Model Predictive Control*, Control Engineering Practice, 42(2015), pp28-40, June 2015.
- [20] Artar R., Ertuğrul Ş., *AC Asenkron Motorun Model Tabanlı Kontrolü*, İTÜ dergisi, pp157-167, Ekim 2010.
- [21] Xie Y., Ghanemi R., Sun J. And Freudenberg J. S., *Implicit Model Predictive Control Of A Full Bridge DC-DC Converter*, IEEE Transactions on Power Electronics, Vol.. 24, NO. 12, pp2704-2713, December 2009.
- [22] Franko S., *İnsansız Helikopterin Model Öngörülmesi Kontrolü*, Istanbul Technical University, M. Sc. Thesis, June 2010.
- [23] Junxia Mu and David Rees, *Approximate Model Predictive Control for Gas Turbine Engines*, Proceeding of the 2004 American Control Conference, Boston, Massachusetts, USA, pp5704-5709, June 30 – July 2, 2004.
- [24] Durmuş B., Temurtaş H., *Öngörülmesi Kontrolü ile Altı Eksenli Bir Robot Kolunun Eklem Esaslı Yörünge Kontrolü*, DPÜ Fen Bilimleri Enstitüsü Dergisi, August 2010.
- [25] Camacho E. F. And Bordons C., *Model Predictive Control*, ISBN 3-540-76241-8 Springer-Verlag Berlin Heidelberg New York, 1999.
- [26] Dughman S.S., Rossiter J.A., *A Survey Of Guaranteeing Feasibility And Stability In MPC During Target Changes*, International Federation of Automatic Control, pp813-818, IFAC 2015.
- [27] Wayne Bequette B., *Process Control-Modeling, Design and Simulation*, Prentice Hall International Series In the Physical and Chemical Engineering Sciences, ISBN 0-13-353640-8, 2003.
- [28] Danayiyen Y., *Model Öngörülmesi Kontrol Yönteminin Örneklerle Karşılaştırılması İncelenmesi*, Karadeniz Technical University, M. Sc. Thesis, September 2010.
- [29]

Aerodynamic Tailcone Shape Optimization for Autonomous Navigation Performance Maximization of Morphing Aerial Robot

Tugrul Oktay¹, Metin Uzun²

Abstract

The purpose of this conference article is to advance flight performance of an autonomous aerial robot via benefiting aerodynamic tailcone shape optimization experimentally and computationally. For this intention aerodynamic performance criteria (i.e. maximum fines) of a scaled model of our autonomous aerial robot named as Zanka-II manufactured in Erciyes University Faculty of Aeronautics and Astronautics Model Aircraft Laboratory is first examined in sub-sonic Wind Tunnel. Results found in this wind tunnel are validated using a computational fluid dynamics software package (i.e. Ansys). Tailcone of fuselage is optimized in order to maximize maximum fines of our autonomous aerial robot via applying Ansys. A novel scaled model using optimum data found by Ansys is then produced and placed in Wind Tunnel in order to validate computational results with experimental results. By using geometrical data of ultimate aerodynamically optimized aerial robot, improved autonomous flight performance is found both in simulation environment (i.e. Matlab and Simulink) and real time flights.

Keywords: *Aerial Robots, Autonomous Performance, Aerodynamics, Tailcone Shape Optimization*

1 INTRODUCTION

For around last four and five quarters *aerial robots* have been largely used for military tasks and also in commercial operations because of the fact that they have various superiorities with respect to the old-fashioned manned vehicles. Some of these advantages are economical manufacturing and operation, elastic configuration for customer demand and not risking the pilot's life on stiff missions.

Aerial robots have also been benefited in aerial agriculture for instance crop monitoring and spraying, photography for example film and video, coast guarding such as coastline and sea-lane, conservation such as pollution and land monitoring, etc. during civilian missions.

Aerial robots have also been benefited for military operations. For instance, they have been used for navy such as decoying missiles via the emission of artificial signatures and shadowing enemy fleets, army such as reconnaissance and surveillance of enemy activity and air force such as radar system jamming and destruction and airfield base security. Many different aerial robot uses is examined in detail by [1]. So many scientific study for aerial robot design, manufacturing and autonomous control have been lately examined (e.g. [2], [3], [4], [5]).

In order to obtain better performance several studies are done for aerodynamic shape optimization (e.g. [6], [7]). In [7] several tailcone shapes are used in order to minimize drag for example elliptical tailcone, conical tailcone and spherical tailcone.

This is the *first conference article* examining aerodynamic tailcone shape optimization for maximization of autonomous flight performance of morphing aerial vehicle during simultaneous design of a load-carrying morphing aerial robot and autopilot system. Moreover, for this motivation a stochastic optimization method (i.e. SPSA, simultaneous perturbation stochastic approximation) is *first time* benefited and using it, optimal results are found safely and fast. In addition to this, aerodynamic tailcone shape optimization advances autonomous flight performance considerably, therefore less overshoot, less settling time and less rise time are found during trajectory tracking.

2 OUR AUTONOMOUS AERIAL ROBOT

In Figure 1 below solidworks drawings of morphing aerial robot, side and upper view photos of Zanka-II are illustrated.

¹ Corresponding author: Erciyes University, Faculty of Aeronautics and Astronautics, 38039, Kayseri, Turkey, tugruloktay52@gmail.com,

² Erciyes University, Faculty of Aeronautics and Astronautics, 38039, Kayseri, Turkey, m.uzun2010@gmail.com

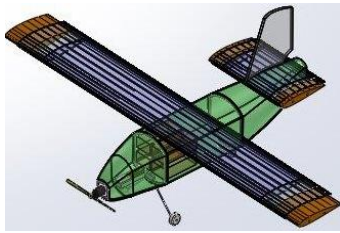


Figure 1. (a) Solidworks drawing of the Aerial Robot

(b) A photo of the Aerial Robot

(c) Another photo in which both non-morphing and morphing wings are put

Aircraft or aerial robot wings provide the aerial robot to satisfy the flight conditions, but by wings singly, the performance at each situation is not optimal. In order to achieve the optimal performance, mechanisms like deployable flaps, wing tips transferring the capability of a wing surface to change its geometry during flight has studied by researchers and designers. Since it is seen that studies can reduce the design compromises required, the researches have increased over the last years. Placing mechanical moving elements on the wing tips and remote control of wing tips to quantified values using them are developed. Thus, also wing area can be increased. Principal components of our wing system are reductive two equal number of gear teeth, micro motor, bidirectional mini brushing ESC, and M3 worm gear.

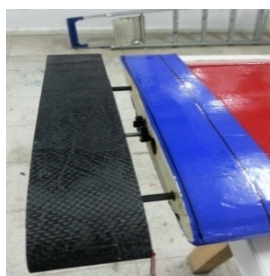
The system is comprised of the simple collaboration of the elements listed before. As seen in Figure 2 (a), micro motor is a DC motor and operating between ranges 6-9 V, creates a torque of 1.8 kg. The gear motor is placed on the shaft of the related motor. This gear works with a second gear placed on a bearing compatibly (see Figure 2 (c)).

In released state of the gear mounted on bearing, the gear has M3 tooth. For turning the engine right or left by the remote control, a bistable switch is used to sent signal to ESC. ESC is a bidirectional and brushed circuit and works in two sides according to the incoming signal through the remote control switch directly (see Figure 2(e)). The direction of rotation of gears which also determines the moving of motor, and hence mechanical systems lead worm screw in-or-outward (see Figure 2(f)). This movement results to moving of wing tips parts, produced by outer mold method, over main section so therefore to provide the alteration of the wing area.



Figure 2. Morphing mechanism: (a) and (b) DC Motor and gear motor mounted to shaft

(c) Placement of the Servo motor in the wing

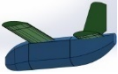
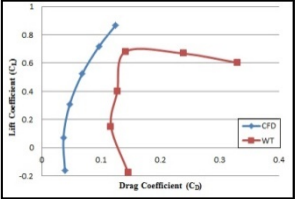
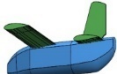

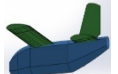
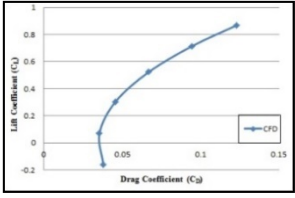
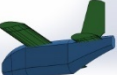
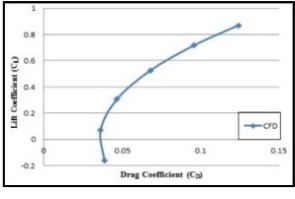


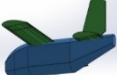
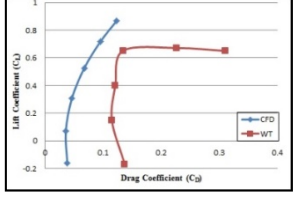


(d) Electronic speed controller

(e) Montage of the expanding parts of the wing

(f) 3D View of the Over-expanding part of the wing

Table 1. Optimization Results

Tailcone	CFD	C_L - C_D	E_{max}
Production Aircraft			7.72
Haack Series C=0.3			7,54
Parabolic			7.825
Inverse Parabolic			7.74
Elliptical			7.65
Conical			7.828

3 AERODYNAMIC SHAPE OPTIMIZATION

In this conference article several tailcone shapes are investigated in order to maximize the value of maximum fines (E_{max}) such as elliptical tailcone, conical tailcone, inverse-parabolic tailcone, parabolic tailcone, and haack series tailcone. In Table 1 for this tailcone shapes, CFD drawings, CFD and Wind Tunnel (WT) results and E_{max} values are presented. From this table it can be realized that the maximum value of E_{max} is obtained for conical tailcone shape. The maximum value for it is around 1.4% larger than the one for initial aerial robot. This amount seems smaller but it is very advantageous for performance characteristics such maximum range, endurance and autonomous performance. In Fig. 3 wind tunnel experiments for initial and optimum geometry is presented.



Figure 3. Wind Tunnel Test: (a) Conical Tailcone

(b) Initial Tailcone

4 AUTOPILOT SYSTEM AND AUTONOMOUS PERFORMANCE EVALUATION

a. Autopilot System

For our simulation environment (i.e. Matlab) conventional PID based hierarchical autopilot system is preferred (see [8] and [9]). In this structure, to achieve waypoint navigation, three layers PID controller is utilized (see Figure 4). More detailed version of PID-based hierarchical autopilot system is shown in Figure 5. The fuselage of autopilot equipped Zanka-II aerial robot is illustrated in Figure 6.

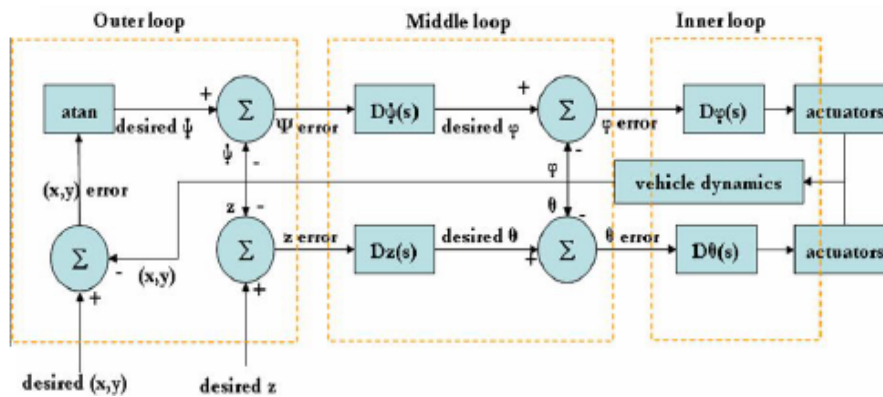


Figure 4. Hierarchical Autopilot System (taken from [9])

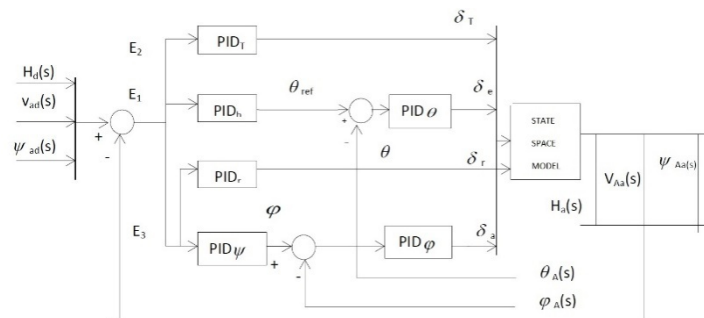


Figure 5. PID Based Autopilot Structure



Figure 6. Autopilot Equipment of ZANKA-II

b. Autonomous Performance Evaluation

In most general situation, PID-based hierarchical autopilot system lets to control height, yaw angle, and velocity for tracking a defined trajectory. Proposed system includes 6 P-I-D controllers with the 3 layers (outer, middle, inner). These PIDs have also upper and lower constraints and ensure trajectory tracking. Instead of general situation, to benefit from all of them, interested autopilot user needs to tune 18 parameters of PID (i.e. 6 P parameters, 6 I parameters and 6 D parameters). However, in this study for morphing aerial robot and autopilot design strategy simultaneously, two additional structural parameters are tuned (optimum extension ratios of horizontal tail and wing). For high-performance trajectory tracking, a cost function determined by settling time, rise time and overshoot is adequate choice (see Eq. (1)).

$$J = \sum g(T_{st} - T_{st_u})^2 + g(T_{rt} - T_{rt_u})^2 + g(\%OS - \%OS_u)^2 \quad (1)$$

The simultaneous optimization problem can be described as follows:

$\min \{J\}$ where

$$J = f(x_w_{morph}, x_{ht}_{morph}, K_{P_1}, K_{I_1}, K_{D_1}, K_{P_2}, K_{I_2}, K_{D_2}, \dots, K_{P_6}, K_{I_6}, K_{D_6}) \quad (2)$$

and it is function of 20 terms (2 aerial morphing parameters and 18 autopilot system design parameters). Terms of cost function is calculated in this conference article as below:

If $T_{st} \geq T_{st_u}$, T_{st} is non-defined else

$$T_{st} < T_{st_u}, T_{st} \text{ is its value} \quad (3)$$

If $T_{rt} \geq T_{rt_u}$, T_{rt} is non-defined else,

$$T_{rt} < T_{rt_u}, T_{rt} \text{ is its value} \quad (4)$$

If $\%OS \geq \%OS_u$, $\%OS$ is non-defined else

$$\%OS < \%OS_u, \%OS \text{ is its value} \quad (5)$$

After the simultaneous optimisation, the 1.4% improvement in maximum value of E_{max} results to 1% improvement in entire autonomous performance. This amount may seem small. However, it is obtained with a very small modification in aerial robot geometry. In future it will be combined with tail cone shape optimization in order to increase the amount of improvement in autonomous performance. In Figure 7 when Von Karman turbulence exists, trajectory tracking for aerial robot pitch angle is given and it is satisfactory.

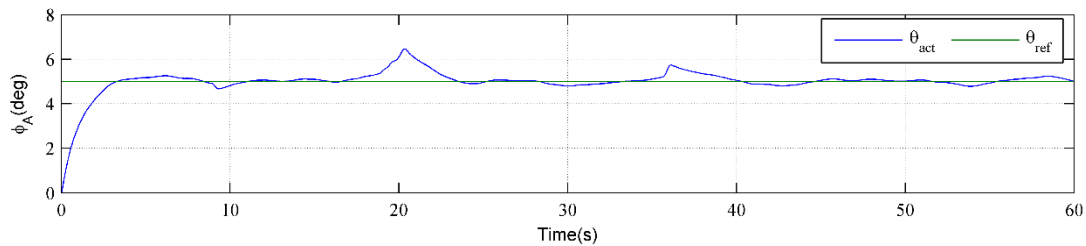


Figure 7. Trajectory Tracking for Resulting Aerial Robot

CONCLUSIONS

In order to improve flight performance of an autonomous aerial robot, aerodynamic tailcone shape optimization both experimentally and computationally was applied. Aerodynamic performance criteria (i.e. maximum fines) of a scaled model of our autonomous aerial robot called as Zanka-II produced in Erciyes University Faculty of Aeronautics and Astronautics Model Aircraft Laboratory was first observed in sub-sonic Wind Tunnel. Results obtained was validated using a computational fluid dynamics software (i.e. Ansys). Tailcone cone of fuselage was optimized in order to maximize maximum fines of our autonomous aerial robot by using Ansys. A novel scaled model using optimum data was then produced and placed in Wind Tunnel in order to validate Ansys results with experimental results. By using geometrical data of eventual aerodynamically optimized aerial robot, better autonomous flight performance was found both in simulation environment (i.e. Matlab) and real time flights.

Aerodynamic tailcone shape optimization for morphing autonomous aerial robot increased the maximum value of fines (around % 1.4). In entire autonomous performance, a minor improvement (around % 1) is obtained.

ACKNOWLEDGEMENT

This work was supported by Research Fund of The Scientific and Technological Research Council of Turkey (TUBITAK) under Project Number: 214M282.

REFERENCES

- [1] Austin, R., Unmanned aircraft systems, Wiley, 2010.
- [2] Ding, Y., Liu, Y. C., and Hsiao, F. B., The application of extended Kalman filtering to autonomous formation flight of small UAV system. *Aircraft Engineering and Aerospace Technology*. 1(2), 154-186, 2013.
- [3] Drak, A., Hejase, M., ElShorbagy, M., Wahyudie, A., & Noura, H., Autonomous Formation Flight Algorithm and Platform for Quadrotor UAVs. *International Journal of Robotics and Mechatronics*. 1(4), 124-132, 2014.
- [4] Luca De Filippis, Giorgio Guglieri, Fulvia B. Quagliotti, A novel approach for trajectory tracking of UAVs. *Aircraft Engineering and Aerospace Technology: An International Journal*. 86 (3), 198 – 206, 2014.
- [5] Hadi, G., Varianto, R., Trilaksono, B., and Budiyo, A., Autonomous UAV System Development for Payload Dropping Mission. *Journal of Instrumentation, Automation and Systems*. 1(2), 72-77, 2014.
- [6] Xuetao, Z., UAV Design and Manufacture, BS Thesis, 2010.
- [7] Lyu, Z., Kenway, G. K. W., Martins, J. R. R. A., Aerodynamic Shape Optimization Investigations of the Common Research Model Wing Benchmark. *AIAA Journal*, 2014.
- [8] Jang, J. S., Liccardo, D., Automation of small UAVs using a low cost mems sensor and embedded computing platform, 2006.
- [9] Chao, H., Cao, Y., and Chen, Y. Q., Autopilots for Small Fixed-Wing Unmanned Aerial Vehicles: A Survey. Paper presented at IEEE International Conference on Mechatronics and Automation, Harbin, China, 2007.

The Contributions of the Parks and Children's Playgrounds in the City of Malatya to the Green Area and Urban Open Green Area Systems

Atilla Atik^{1}, Furuzan Aslan¹, Bulent Yilmaz¹*

Abstract

Parks located in cities are accepted as one of the most important elements of the intracity open and green area systems. The green areas of the parks and children's playgrounds in a city have an important role on urban green areas. In this study, the size of the green areas in the 94 parks located in the city of Malatya, the influence of the green areas per capita, and the distribution of green areas in neighborhoods have been examined. According to the data obtained in the study, the total area of the 94 units consisting of parks and playgrounds in Malatya city center is 573519.82 m², the total green areas are 264781 m² and average green area of each units is 46.2%. In this context, active green area amount per capita in the city stemming from these two units has been determined as 0.45 m².

Keywords: *Urban Green Area, Urban Park, City, Malatya*

1. INTRODUCTION

Today, especially underdeveloped and developing countries face a fast and uncontrolled population increase. What is worst is the increase in the urban population due to the migration from rural areas to urban areas besides the increase in the population of countries. Cities face a fast construction process in order to cover the basic needs of the population like accommodation, work, health, and education, which are mainly based on concretion. According to the data from FAO, the population of the world was 2.5 billion in early 1950s, and has reached 7 billion in the 60-year process by an increase of 3 fold. What is more is that fact that this increase will continue in future 40 years as well as in the past, and according to FAO, exceed 9 billion in 2050 [1].

Especially the population in urban areas increase in a fast and unplanned manner and lead to a wild urbanization, and this prepares the ground for problems of infrastructure and social troubles. The horizontal and vertical growth of cities cause the destruction of the nature around cities in an increasing manner. First of all, in these areas, the forest areas, which has the duty of protecting the soil layer from erosion, which themselves have created the forest areas, providing numerous organisms in the soil with nutrients, and hosting wild life, and which have various functions that are not possible to recover, and the natural structure is destructed and destroyed. The water basins, water distribution ways, and agriculture areas are forced to change shapes and structures, and all of these are destroyed in time losing all of their basic functions.

The dense population and the dense construction makes it difficult and limit the possibility of the people to reach the nature. The urban mankind who are surrounded by internal and external areas are forced to live far from nature, and cannot cover the needs that are based on recreate activities, and as a result, may have physical and psychological problems [2, 3]. The urban open green area systems become even more important in this process on urban life quality. Urban open green areas are defined as the areas that response to the needs of the people like accommodation, working and other general activities [4]. The parks as well as natural or artificial forest areas surrounding the cities, orchards, street trees, and the trees in squares, road slope and refuge, trees, cemeteries, house gardens, school gardens, green roofs, gardens of the work places of the public or private sector, and sports complexes are included in this definition [5].

The current regulation related with urban open green area symbols in Turkey is the one that was enacted on 14.11.2015 with the number 29532 in Official Gazette with the title "Regulation on the Changes to be made on the Planned Area Types Building Regulation". The regulation includes the changes made in previous 15 regulations with the dates 02.11.1985 with the number 18916 in Official Gazette with the title "Planned Areas Type Building Regulation", the first one being on 12.08.1987 with the number 19542 released in the Official Gazette. In the 7th Item of the Regulation which has the title of "Urban Area Definitions and Area Use Conditions" and in "Social and

¹Inonu University Faculty of Fine Arts and Design Department of Landscape Architecture, 44280, Malatya-Turkey.

*Corresponding Author: atikatilla@hotmail.com

Cultural Infrastructure Areas” which is the 2nd Item, these areas are classified under 5 main groups, which are green areas, sports and game areas, socio-cultural facility areas, worshipping places, and cemeteries. The green areas in this classification are defined as “the total of game gardens, children’s gardens, recreational areas, travel areas, picnic areas, entertainment areas, recreation areas and coastal areas. The fairs, botanic and animal gardens and regional parks are also included in this classification”. These elements are given under 3 titles, which are fairs, botanic and animal gardens, regional parks, children’s gardens, parks and picnic and recreation areas at a metropolitan scale [6].

The physical, psychological and psycho-social benefits of the open and green areas in cities for the residents of the city have been examined and revealed with a great number of studies conducted by authors from various disciplines [2]. In this context, the physical influences of green areas on cities need to be handled under a separate title and is directly related with the sustainability of the city. In this context, Davies et al. (2011) and Paoletti et al. (2011) reported that urban open green areas and other vegetation have a duty like a carbon sink against the release of carbon stemming from industrial activities in the atmosphere of the city because of their carbon-binding property [7, 8]. Gidlöf-Gunnarsson & Öhrström (2007) reported that especially a vegetation form in which woody taxons are dense will have in influence to decrease the noise in a city [9]. Chiesura (2004) reported that natural areas had to be protected and developed in order to give a sustainable property to cities [10].

There have been a great deal of studies conducted in Turkey on open and green areas and the sufficiency of these areas for the city people. Generally in these studies, green areas are separated as active and passive, and the evaluations have been made generally over the active areas.

Boyacıgil and Altunkasa (2009) examined the existence of active green areas in Adana in terms of area values per capita and at neighborhood level [11]. Again, Boyacıgil and Altunkasa (2010) conducted a study in İskenderun (Hatay) to determine the public recreational opportunities [12]. Bağcı (2010) examined the existence of active green areas, which consist of parks, children’s gardens, and sports-games areas, in Yenişehir (Mersin) example per capita and at neighborhoods level [13]. Gilliland et al. (2006) examined the distribution of recreational areas in London in Canada at neighborhood level and indexed the existing opportunities according to the needs of the children and young population [14]. Giles-Corti et al. (2005) conducted a study in Perth city in Australia and examined the size, distance (pedestrian availability) and attractiveness of the active green areas over 8 decares (2 acres) [15].

Doygun and İltter (2007) examined the sufficiency, square meter rates per capita and the availability of the green areas by pedestrians in Kahramanmaraş in Turkey and the plans and actual practices [16].

In the scope of this study, the parks in Malatya have been examined in terms of active green areas. The rate of the parks per capita was examined by considering the current population of the city, and the parks have been indexed according to the green area amounts and rates. In this spectrum, the contributions of the parks in Malatya city center have been investigated.

2. MATERIALS AND METHODS

Malatya is located in the Upper Euphrates Basin of the Eastern Anatolia Region of Turkey, and its neighbors are Elazığ and Diyarbakir in the East, Adıyaman in the south, Kahramanmaraş in the west, Sivas and Erzincan in the north. 47% of the city area consist of meadows and ranges, 34% of it consist of agricultural areas [17, 18]. The total forest area in the city in general is 188127 ha (normal + disrupted) showing that 15% of the city area is covered with forest area. According to the Thornthwaite Climate Classification, continental climate, which is shown with D,B’2,s,b’2, subarid, mesothermal, water excess rate being in winter, vaporization rate in summer season is 58%, dominates the city [19].

According to the Address-Based Population Registry System, the total population of Malatya in 2014 is 769544. Malatya Centrum Municipality became metropolitan municipality in 2012, and the city center was divided into two as Battalgazi and Yeşilyurt Municipality. The total population of these municipalities was 583579 in 2014 [20].

The name list, total area size and address information of the 94 parks located in the city center of Malatya, which is the subject matter of the study, were obtained from the Malatya Metropolitan Municipality, Park and Gardens Management. The list was organized with the data obtained and constitutes the basis of the study. All the parks in the list were marked in the Google Earth Satellite Map and on the construction plan of the city, and the quality and quantity of the watery areas were determined. Then, all the parks and children’s playgrounds in the list were marked one-by-one on Google Earth Satellite Map and on the construction plan of the city, and the size, and were classified as green areas and hard ground. According to the data obtained, the total green area of the parks and children’s playgrounds and the active green areas were determined and they are listed according to their sizes and rates.

3. RESULT AND DISCUSSION

According to the data obtained in the study, the total surface area of the 94 units which consist of parks and children’s playgrounds in the city center of Malatya is 573519.82 m², and total green areas are 264781 m² and average green area of each unit is 46.2% (Figure 1). In this context, active green area amount per capita stemming from these two

units in the city is 0.45 m^2 . The average total area of these units is 6101.27 m^2 , and the average green area size is 2816.82 m^2 .

In 4 of these units, there are no green areas, and the unit with the biggest green area is Abdullah Gul Park which has a green area of 61250 m^2 . The rate of the green area of this park to total park area is 62.9%.

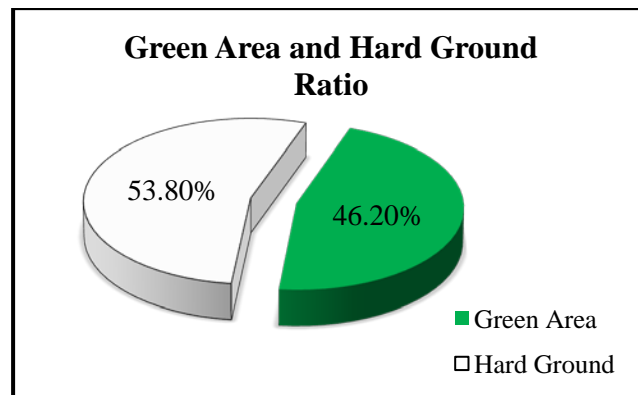


Figure 1. Total green area rate of the parks and children's playgrounds in the Malatya city center.

The parks and children's playgrounds in the city are classified under 3 groups according to their green area rates in Table 1. The ones that are at 1000 m^2 and below constitute the Group 1; those between $1001-5000 \text{ m}^2$ constitute Group 2; those and over 5001 m^2 constitute Group 3. According to Table 1, 53.2% (50) of the parks and children's playgrounds in the city are in the 1st Group; 40.4% (38) are in the 2nd Group; and 6.4% (6) are in the 3rd Group (Figure 2). In this context, the green areas of the majority of these units are below 1000 m^2 , and the rate of those over 5000 m^2 is extremely low.

Table 1. The Distribution of the parks and children's playgrounds in Malatya city center according to their green area sizes.

Group	Green Area Size	Number of the Units	Unit Percentage
1	<1000 m^2	50	53.2
2	1001-5000 m^2	38	40.4
3	>5001 m^2	6	6.4
Total		94	100

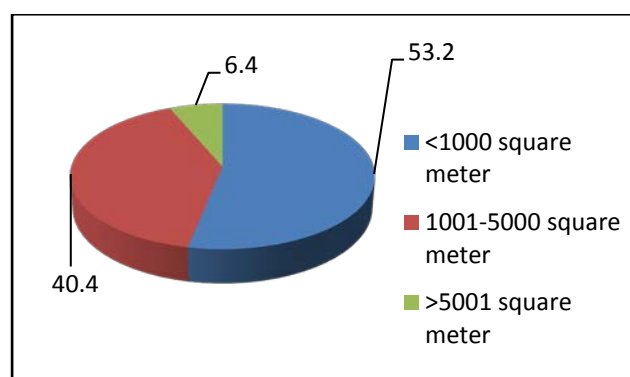


Figure 2. The distribution of the parks and children's playgrounds in Malatya according to the green area sizes.

The parks and children's playgrounds have been classified to 10 groups by considering the green area rates and given in Table 2. In this context, the number of the units with green area rates between 41-50% is 25; and this constitutes 26.6% of the all area. On the other hand, it has also been determined that there are no units with green area rates between 90-100%.

Table 2. The distribution of the parks and children's playground in Malatya city center according to their green area rates

Group	Green Area Percentage (%)	Number of the Units	Unit Percentage
1	0-10	6	6.4
2	11-20	4	4.3
3	21-30	10	10.6
4	31-40	19	20.2
5	41-50	25	26.6
6	51-60	14	14.9
7	61-70	11	11.7
8	71-80	3	3.2
9	81-90	2	2.1
10	91-100	0	0.0
	Total	94	100

When the units were examined in terms of the distribution of the green areas to the neighborhoods, it was determined that in 51 out of 85 neighborhoods in Malatya city center, there were green areas, and in the remaining 34 neighborhoods, there were no parks and/or active green areas. In this context, there are no parks and children's playgrounds with green areas in 40% of the neighborhoods in Malatya.

When the neighborhoods were classified according to their green areas, it was determined that the neighborhood with the biggest green area is the Inonu neighborhood with 71045 m² green area (parks and children's playground). Cevatpaşa neighborhood 30099 m² and Turgut Özalneighborhood follow this with 7575.94 m². The lowest green area rate was determined in Kernek neighborhood which has 126 m² green area in terms of parks and children's playgrounds.

In the Urban Audit Report, which was released by the European Union, the urban green areas are defined as "green areas in the city that are open for public use, for example parks", and the green area size per capita for 11 European cities (Berlin, Hamburg, Brussels, Milan, Palermo, Wien, Helsinki, Barcelona, Copenhagen, Birmingham and Liverpool) in 1996 is given as 41.2 m² [21]. However, at the end of this study which was conducted in Malatya city center, the total area of parks and children's playgrounds have been determined as 573519.82 m², green area existence has been determined as 264781 m², and the parks per capita has been determined as 0.98 m², and the active green area in these parks is about 0.45 m².

Boyacıgil and Altunkasa (2009) conducted an urban developmental study in Northwestern Adana and investigated the active green areas given by Bağcı (2010) for Yenişehir (Mersin) example, and reported similar results. In this context, it has been concluded that the active green areas in the area did not show an even distribution; and in neighborhoods where the active green areas were sufficient, the efficiency decreased because people from other areas where the active green areas were insufficient came to these areas [11, 13]. Similar results were obtained in the study that was conducted in İskenderun (Hatay) example to determine the public recreational areas. In this study, the distance of a neighborhood to the other neighborhoods where source values were higher leads to an increase in the activity in these areas; and the closeness to the areas where population was high and the opportunities were low led to the decrease in the efficiency due to excessive users [12].

According to Giles-Corti et al. (2005), there is an important relation between the usage level of the active green areas and their availability [15].

Doygun and İltter (2007) conducted a study to examine the sufficiency of the Present and Planned Active Green Areas in the City of Kahramanmaraş and reported that 386.6 ha area was planned as green areas in the construction plan, and according to the population projection in the construction plan 7.1 m² green area was planned per capita. On the other hand, it was also observed that the present active green areas covered 45.2 ha, and the up-to-date active green area per capita was 1.4 m². In addition, the size of the present and planned active green area per capita was found to be lower than ideal size, and the 68% of the study area was in walking distance to the planned green area parcels, and this rate was 41% for the present ones. In the light of these results, the authors expressed that the active green areas did not contribute to the city life due to their small surface areas and uneven distribution in the city [16].

4. CONCLUSIONS

In this study, which was conducted to determine the green area assets of the parks and children's playgrounds in the city center of the city of Malatya in Turkey, according to the data obtained, the green areas are extremely insufficient per capita in the light of the current population. In addition, the green areas in more than half of the parks is below 1000 m². When the distribution of the parks that have green areas in the city is examined, it was observed that in 40% of the neighborhoods in the city there are no parks or children's playgrounds.

It is recommended that the local administrations should revise the present construction plan in order to increase the quality of the city life. By so-doing and with the help of the planning and establishment works of new parks in the city center, the opportunities for increasing the green areas in present parks will be investigated. As a matter of fact, the amount of the parks and children's playgrounds, which constitute the basis of the active green area assets in the

city, is extremely low according to the European countries and according to many other cities in Turkey. In addition, the distribution of such areas in the city must be organized in a balanced manner. By doing so, it is considered that the green area usage activities stemming from imbalances in the city that lead to the decrease of the use of these areas, as it is stated in the literature, will be eliminated.

REFERENCES

- [1] FAO, United Nations, Department of Economic and Social Affairs, Population Division, World Urbanization Prospects: The 2011 Revision, CD-ROM Edition, 2012.
- [2] A. Atik, B. Yılmaz, E. Taçoral, Ş. İ. Bayazit and M. Kılıç, *Urban Forests and Their Contributions to Urban Sustainability*. Urban and Urbanization, St. Kliment Ohridski University Press Sofia, ISBN: 978-954-07-3772-0, pp. 134-148, 2014.
- [3] F. Aslan and A. Atik, Qualitative and Quantitative Evaluation of the Parks in Malatya City. Tourism, Environment and Sustainability, St. Kliment Ohridski University Press, Sofia, Bulgaria, Chapter 3, pp. 35-45, 2015.
- [4] M. Dil, "İstanbul'un yeşil alan sisteminin, planlama kriterleri açısından irdelenmesi," Master of Science Thesis, İstanbul Teknik Üniversitesi, Fen Bilimleri Enstitüsü, İstanbul, Turkey, 2004.
- [5] C. Konijnendijk, M. Annerstedt, A. B. Nielsen and S. Maruthaveeran, "Benefits of Urban Parks. A Systematic Review," A Report for IFPRA, 2-7, 2013.
- [6] Anonymous, "Planlı Alanlar Tip İmar Yönetmeliğinde Değişiklik Yapılmasına Dair Yönetmelik," Resmi Gazete, Tarih: 14.11.2015, Sayı: 29532.
- [7] Z. Davies, J. Edmondson, A. Heinemeyer, J. Leake and K. Gaston, "Mapping an urban ecosystem service: Quantifying above-ground carbon storage at a city-wide scale," *Journal of Applied Ecology*, vol. 48, no. 5, pp. 1125-1134, 2011.
- [8] E. Paoletti, T. Bardelli, G. Giovannini and L. Pecchioli, "Air quality impact of an urban park over time," *Procedia Environmental Sciences*, vol. 2011, no. 4, pp. 10-16, 2011.
- [9] A. Gidlof-Gunnarsson and E. Ohrstrom, "Noise and well-being in urban residential environments: The potential role of perceived availability to nearby green areas," *Landscape and Urban Planning*, vol. 83, pp. 115-126, 2007.
- [10] A. Chiesura, "The role of urban parks for the sustainable city," *Landscape and Urban Planning*, vol. 68, pp. 129-138, 2004.
- [11] O. Boyacıgil and M. F. Altunkasa, "A Case Study on Determining Effective Active Green Space Opportunities in Upper Northwest Urban Development Area of Adana," *Akdeniz Üniversitesi Ziraat Fakültesi Dergisi*, vol. 22, no. 1, pp. 59-67, 2009.
- [12] O. Boyacıgil and M. F. Altunkasa, "Determining Effective Public Recreation Opportunities: A Case Study in Yskenderun (Hatay)," *Ekoloji*, vol. 19, no. 74, pp. 110-121, 2010.
- [13] Ö. Bağcı, "The study of urban welfare in yenişehir (mersin) urban area within the discipline of landscape architecture," Master of Science Thesis, Çukurova University Institute of Natural and Applied Sciences Department of Landscape Architecture, Adana, Turkey, 2010.
- [14] J. Gilliland, M. Holmes, J. D. Irwin and P. Tucker, "Environmental, Equity is Child's Play: Mapping Public Provision of Recreation Opportunities in Urban Neighbourhoods," *Vulnerable Children and Youth Studies*, vol. 1, no. 3, pp. 256-268, 2006.
- [15] B. Giles-Corti, M. H. Broomhall, M. Knuiman, C. Collins, K. Douglas, K. Ng, A. Lange and R. J. Donovan, "Increasing walking: how important is distance to, attractiveness, and size of public open space?," *Am. J. Prev. Med.*, vol. 28, pp. 169-176, 2005.
- [16] H. Doygün and A. A. İlter, "Investigating Adequacy of Existing and Proposed Active Green Spaces in Kahramanmaraş City," *Ekoloji*, vol. 17, no. 65, pp. 21-27, 2007.
- [17] Anonymous 2010a, "Kayısı Araştırma Raporu," Fırat Kalkınma Ajansı, Malatya, TR. 63 p.
- [18] Anonymous 2010b, "Malatya Provincial Environmental Status Report," Malatya Governorship Provincial Directorate of Environment and Forestry, Malatya, 366 p.
- [19] (2015) The "Turkish State Meteorological Service" website. [Online]. Available: <http://www.meteor.gov.tr/>
- [20] (2015) The "Turkish Statistical Institute" website. [Online]. Available: <http://www.turkstat.gov.tr/>
- [21] Anonymous 2000, "The Urban Audit: Towards the benchmarking of quality of life in European cities, vol I, Office for Official Publications of the European Communities, Luxembourg, 13, 152-153, 2000.

Effects Of The Ejector On Vapour Compression Cooling System

Bahadır Acar¹, Alper Ergüün¹, Erdogan Kilicaslan¹

Abstract

In this study, getting more performance with using an ejector on vapor compression cooling system was aimed and a cooling system with ejector was designed and manufactured. At the end of the experiments and calculations the differences of two systems were examined in detail. The cooling systems which have been designed with ejector and without ejector were operated and experimental studies were performed. For each experiment, inlet and outlet temperatures of condenser, evaporator and compressor were measured by thermocouples. Minimum temperature in the system without ejector was -10 °C and in the system with ejector was -15°C. According to these findings, coefficient of performance (COP) were calculated for both systems. COP of the system without ejector was calculated as 3.61 and COP of system with ejector was calculated as 3.92. These results showed that there is a % 8 percent performance difference between the systems and ejector has a positive effect on the vapor compression system.

Keywords: Cooling, Ejector, Performance

1. INTRODUCTION

Cooling is a process that decreases the temperature of substance or environment below the temperature of surrounding volume and maintains both temperatures at same degree. According to the second law of thermodynamica, heat is transferred instinctively from the warm environment to the cold environment. On the other hand, cooling process is a reverse process of second law and heat is transferred from cold environment to the warm environment. According to the second law, in order to carry out the heat transfer from low temperature environment to the high temperature environment, energy must be given into the system. This energy is difference between absorbed heat power and discarded heat power[1]. Because of improving technology rapidly there have been many progresses in cooling field and using cooling technique and applications of its become widespread. Cooling is placed in food and medical fields. Cooling applications is widely used many fields from local applications to the central industrial applications

Recently, there have been many studies on the purpose of increasing cooling system performance. Da Wen Sun examined the efficiency of cooling system when the various cooling fluids were used[2]. Yapıcı and Yetişen used low pressure ejector that works with various energy sources such as solar energy, geothermal energy and discarded energy and R11 as working fluid. As a result of experiments, they mentioned that vapour generator temperature must be increased in order to obtain low vapour temperature and high cooling capacity[3]. Selvaraju and Mani examined performance of vapour ejector cooling system that has 0.5kW cooling capacity and used six different ejector models which have different geometries. They used the R134a working fluid[4]. Pridasawas and Lundqvist determined the performance of cooler with ejector. The investigated variable parameters such as sun radiation, cooling capacity, vapour temperature and five environment temperatures. As a result, they observed that the optimum working temperature of the system is approximately about 80 °C for those parameters[5]. Somchai and Disawas investigated the performance of two phases ejector cooling system that has ejectors and expansion valve and compared it with traditional cooling cycle. As a result of experiments, they determined that two phases system that has expansion valve and ejector supplied more cooling and improved the system performance as traditional cooling method. Besides, they mentioned that pressure ratio of compressor and temperature evacuation were lower[6]. Khan an Zubair performed thermodynamic analysis of vapour compressing cooling cycle. In this study, they developed a finite element thermodynamic model of cooling cycle simulation using real data of cooling cycle that uses the R22 working fluid. In this model, they changed the mass flow of fluid when the temperature of cooling fluid was constant In this way, they examined the effects of evaporator capacity, sub-cooling and sub-heating on system efficiency. As a result, they underlined that sub-heating has more influence on system efficiency than sub-cooling[7].

In this study, the use of ejector in vapour compressing cooling cycle and its influence on the system performance were investigated. For this purpose, a cooling cabinet which works according to vapour compressing cooling cycle method was designed and the performance was determined with and without ejector.

¹ Corresponding author: Karabük University, Energy Systems Engineering Department, Karabük, Turkey. bacar@karabuk.edu.tr

¹Karabük University, Energy Systems Engineering Department, Karabük, Turkey alperergun@karabuk.edu.tr,
ekilicaslan@karabuk.edu.tr

2 MATERIAL AND METHOD

In this study, a cabinet that has 0.33 m^3 cooling volume and isolation was designed and it was used as cooling room. The cooling system of cooling room works according to vapour compressing cooling cycle method. The technical properties of the system are given in Table 1.

Table 1. Technical properties of refrigerator test unit.

Fresh food volume	0.33 m^3
Voltage	190-220 V
Frequency	50 Hz
Number of doors	1
Refrigerant type	R134-a
Refrigerant charged	300 gr
Compressor capacity	246 W
Evaporator capacity	1/3 Hp
Condenser fan	60 W
Evaporator fan	60 W
Heat transfer coefficient of room	$0.0081 \text{ W/m}^2\text{K}$
Capillary tube length	3 m
Contactora	2
Selonoid valve	1
Manometer	2 (High and low pressure)
Digital thermostat	1

The designed experimental setup was built according to parts listed in Table 1 and was operated as a conventional BSSÇ in first stage. The ejector which seen cross-sectional shape in Figure 1 was added to system and the test was separately carried out for each station in the second stage.

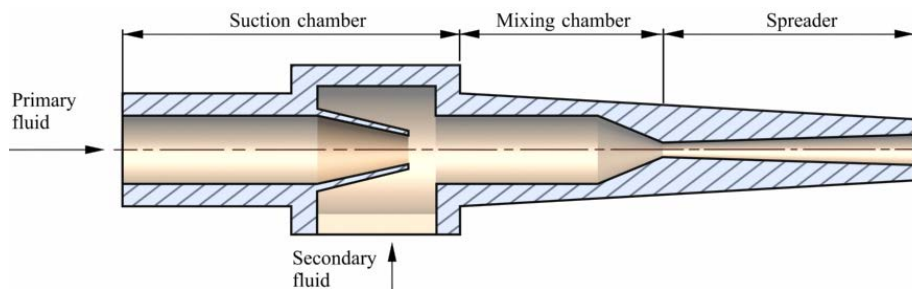


Figure 1. Section view of ejector

The ejector shown in Figure 1 is simple and functional device designed to be used at cooling cycle which converts to kinetic energy by creating low pressure area of pressure energy of the moving primary fluid. Thus, it pulls secondary fluid and mix the primary fluid with the secondary fluid and velocity energy of mixed fluid converts to pressure energy again [8].

Schematic view of system with ejector and without ejector is shown in Figures 2 and 3, respectively.

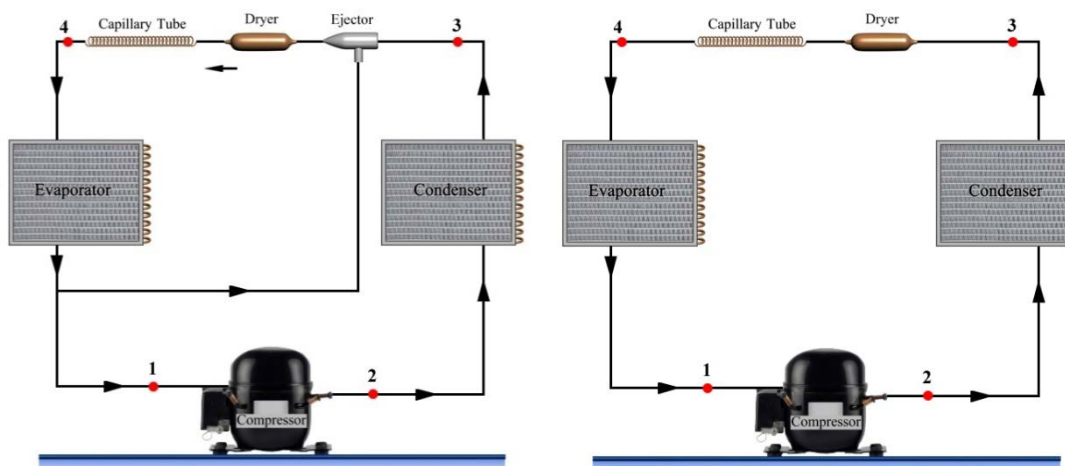


Figure 2. Schematic view of the system with ejector. Figure 3. Schematic view of the system without ejector

Ejector has three connected end. Linear ends were integrated into the system between the condenser and capillary tube and before dryer. Lower end was integrated into the system into a line drawn from the evaporator outlet.

Design and manufacturing of the final system is seen in figure 4.



Figure 4. Designed and manufactured system

Experiments of design and manufacturing was performed in Karabük University Energy laboratory. In the experiments, the compressor output, condenser output, evaporator input-output, indoor and set point temperatures were measured. Temperature measurement was taken with Fe-Const. thermocouple material and 12-channelled Elimko-6000 type temperature measuring device. The accuracy of the measuring instruments is determined $\pm 0.25\%$.

After the experimental data obtained, performance analysis of system was determined.

3 ANALYSIS OF THERMODYNAMIC SYSTEM

In this study, designed and manufactured a cold storage with/without ejector was tested. The most important parameters that determine the performance of the cooling system is the coefficient of performance (COP). The COP values of both systems were calculated.

Energy balance for a continuous-flow system can be calculated by the following equation.

$$q_{net} - w_{net} = \Delta h + \Delta ke + \Delta pe \quad (1)$$

Equation 1 shows the energy that occurs with heat and work. In the cooling cycle, the effect of kinetic and potential energies are very low and can be neglected [ICENS2015]. Thus, equation 1 can be transformed as follows;

$$(q_i - q_o) + (w_i - w_o) = h_o - h_i \quad (2)$$

Therefore, heat removed from condenser and absorbed from evaporator can be expressed as follows,

$$\dot{Q}_{evp.} = \dot{m}(h_1 - h_4) \quad (3)$$

$$\dot{Q}_{con.} = \dot{m}(h_3 - h_2) \quad (4)$$

The compressor work of the system can be calculated as follow;

$$\dot{W}_{comp.} = \dot{m}(h_2 - h_1) \quad (5)$$

Finally, COP values for both systems can be calculated from equation 6 in order to determine efficiency of both systems.

$$\begin{aligned} COP &= \frac{\dot{Q}_{evp.}}{\dot{W}_{comp.}} \\ &= \frac{h_1 - h_4}{h_2 - h_1} \end{aligned} \quad (6)$$

4 RESULTS AND DISCUSSIONS

All the experiments performed and examined into two parts as with and without ejectors. First stage, results of experiments without ejector is given in Table 2.

Table 2. Experiment results of system without ejector

Without Ejector	30.dk	60.dk	90.dk	120.dk
Compressor output	56,5	65,5	65	65,6
Condenser output	24,4	24,6	26,2	25,9
Evaporatorinput	-10,3	-10,8	-10,5	-10,9
Evaporatoroutput	-10	-10,1	-10,5	-10,9
Indoor temperature	-9,2	-9,6	-9,9	-10

In Figure 5, Evaporator output, input, cabin temperature and set value of system were given as a function of time.

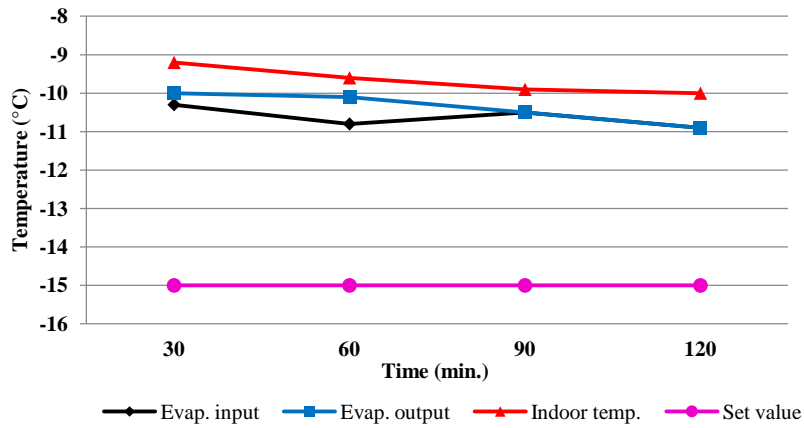


Figure 5. Temperature vs. time graphics of the system without ejector

Besides, output temperatures of compressor and condenser were given as a function of time in Figure 6.

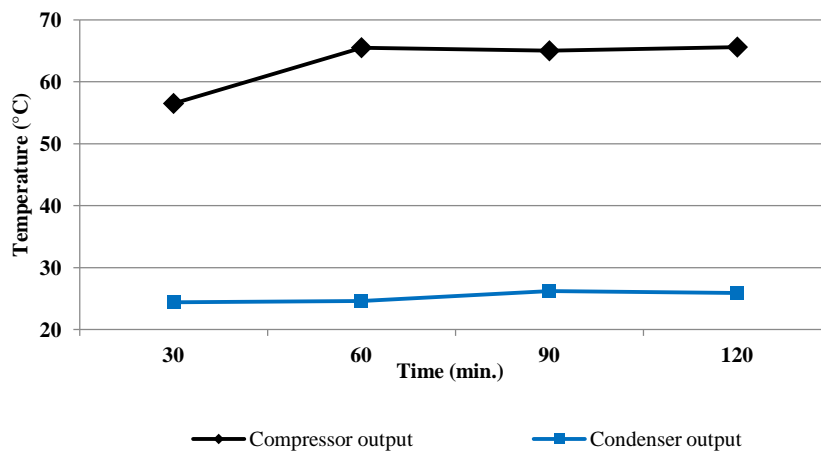


Figure 6. The variation of output temperatures of compressor and condenser without ejector

The variation of indoor temperature is important parameter in order to determine the system performance. The compressor output temperature of the system without ejector varied from 56.5°C to 65.6°C and the condenser output temperature varied from 24.4°C to 29.5°C. The lower indoor temperature of the system was -10°C.

In the second stage of the experiments, the ejector was mounted on the system. The results of the second stage are given in Table 3.

Table 3. Experiment results of system with ejector

With ejector	30.dk	60.dk	90.dk	120.dk
Compressor output	72,8	73	75	77,1
Condenser output	37,5	37,8	38	38,5
Evaporatorinput	-13,2	-13,9	-13,9	-15
Evaporatoroutput	-10,4	-11,9	-13,1	-13,6
Indoor temperature	-8	-10	-12,5	-15

In Figure 7, Evaporator output, input, cabin temperature and set value of system with ejector were given as a function of time.

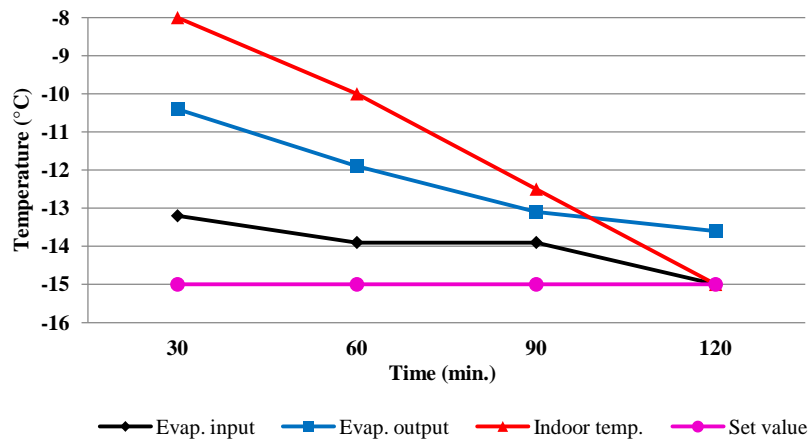


Figure 7. Temperature vs. time graphics of the system with ejector

In addition, output temperatures of compressor and condenser were given as a function of time in Figure 8.

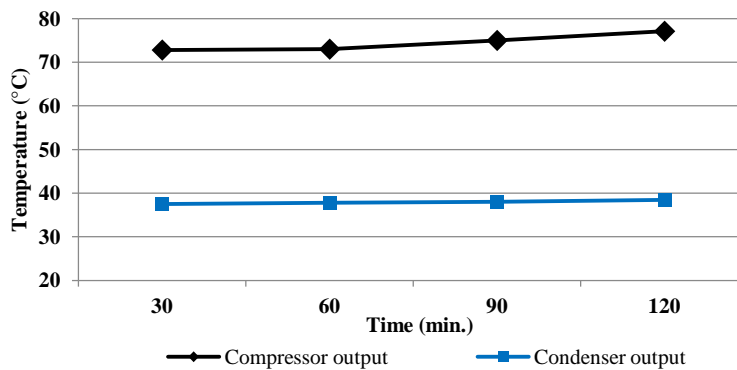


Figure 8. The variation of output temperatures of compressor and condenser with ejector

In the second stage experiments, the compressor output temperature of the system with ejector was varied from 72.8°C to 77.1°C and the condenser output temperature was varied from 37.5°C to 38.5°C. The lower indoor temperature of the system was measured as -15°C.

In figure 9, indoor temperature of the system with and without ejector were given as a function of time. Indoor temperature was varied from -8°C to -13°C in the ejector mounted system and the lowest temperature was measured as -13°C in 120th minutes. On the other hand, indoor temperature was varied from -9.2°C to -10°C in the system without ejector and the lowest temperature was obtained as -10°C. The system without ejector turned to be a stable after first 30 minutes and the decreasing of temperature was getting lower and becoming constant. Besides, the system with ejector behaved decreasing until 90th minutes and become stable after 120th minutes. In Figure 9, temperature distributions were given as a function of time both systems.

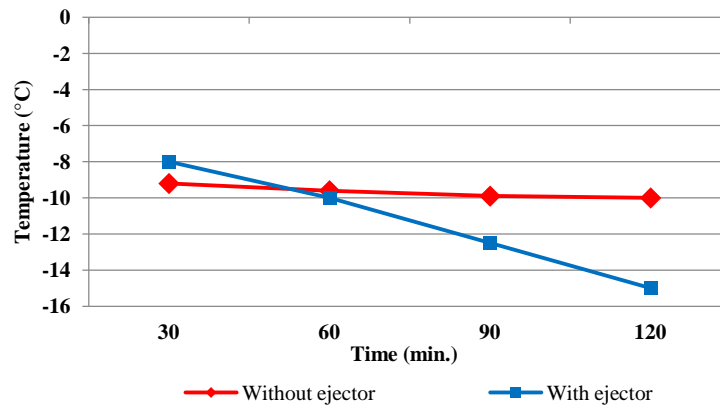


Figure 9. Indoor temperature distributions of the systems with and without ejector

On the purpose of determining performance analysis of the systems with and without ejector, COP values must be calculated. In Table 4, thermodynamic properties of the experimental results are given. Those values were determined from thermodynamic tables for R134a cooling fluid according to temperature and pressure values.

Table 4 Thermodynamic properties of the systems with and without ejector

Exp	T1	T2	T3	T4	P2=P3(bar)	P1=P4(bar)	h3=h4(kj/kg)	h1(kj/kg)	h2(kj/kg)
Without Ejector	-10	65,6	25,9	-10,9	11,98	1,95	250	380	430
With Ejector	-13,6	77,1	38,5	-15	13,25	1,65	271,14	389,41	432,22

COP values were calculated using thermodynamic properties are given in Table 4 and equations are given in chapter 3. COP value of the system without ejector was about 3.61 and it was 3.92 for the system with ejector. As seen in Figure 10, the using of the ejector was effected the performance of the system positively.

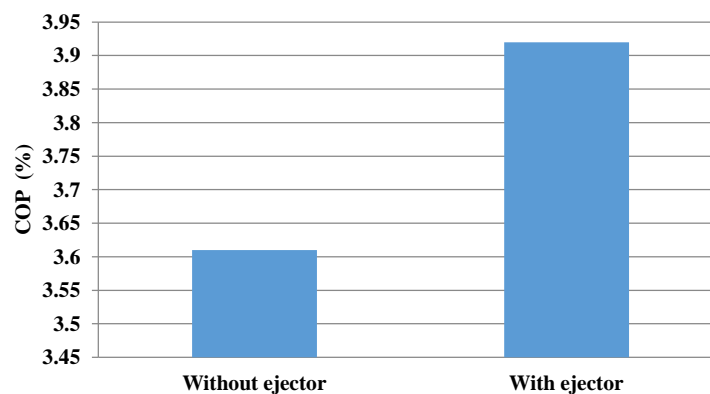


Figure 10. Her iki sistemde COP değerleri

CONCLUSIONS

As a result of experiments and comparison with calculations;

Indoor temperature was measured as -10°C at the lowest point in the system without ejector. As a result of calculations, COP was determined about 3.61. On the other hand, indoor temperature was obtained about -15°C at the lowest point in the system with ejector, COP was calculated about 3.92. According to these findings, it was determined that the system with ejector is more efficient about 8% than the system without ejector

It is observed that using ejector has positive influence on the efficiency of the system. Moreover, when the efficiency and energy conservation that gained by means of mounting ejector to the system compared with cost of ejector, it was seen that mounting an ejector is an economic and productive application.

In the future, it will be a significant progress that using ejector in small scale systems widely in terms of cooling process. In addition, using ejector will be an outstanding application in the sense of energy consumption around the world day by day.

ACKNOWLEDGMENT

The authors would like to thank the Karabük University Scientific Research Projects Unit, Karabük/TURKEY for providing the financial supports for this study under the KBÜ-BAP-16/1-YD-025 project.

REFERENCES

- [1]. N. Örün, Effect on energy consumption of dirty condensers of mechanical cooling system, *Master Thesis*, ZKÜ Natural And Applied Sciences Department of Mechanical Education, Karabük, 2007.
- [2]. S. Da-Wen, "Comparative study of the performance of an ejector refrigeration cycle operating with various refrigerants," *Energy Conversion & Management*, vol. 40, pp. 873-884, 1999.
- [3]. R. Yapıcı and C.C. Yetisen, "Experimental Study on Ejektör Refrigeration System Powered by Low Grade Heat," *Energy Conversion & Management*. vol. 48, pp. 1560–1568, 2007.
- [4]. A. Selvaraju and A. Mani, "Experimental Investigation on R134a Vapour Ejektör Refrigeration System," *International Journal of Refrigeration*, vol. 29, pp. 1160-1116, 2006.
- [5]. W. Pridasawas, and P. Lundqvist, "An Axergy Analysis of a Solar-Driven Ejektör Refrigeration System," *Solar Energy*, vol. 76, Issue 4, pp. 369–379, 2004.
- [6]. W. Somchai and S. Disawas, "Performance of The Two-Phase Ejektör Expansion Refrigeration Cycle," *International Journal of Heat and Mass Transfer*, vol. 48, pp. 4282-4286, 2005.
- [7]. J.R. Khan and S.M. Zubair, "Design and Performance Evaluation of Reciprocating Refrigeration Systems," *International Journal of Refrigeration*, vol. 22(3), pp. 235-243, 1999.
- [8]. H. Taş, N. Bilgin, U. Şentürk, A. Güngör, Soğutma Çevrimlerinde Ejektör Kullanımının Araştırılması, *TESKON Soğutma Teknolojileri Sempozyumu*, pp. 911-930, 2015.

Thermodynamic, Heat Transfer and Fluid Flow Analyses of Encapsulated Ice Thermal Storage System Used in A Shopping Center

Dogan Erdemir¹, Necdet Altuntop¹

Abstract

This study presents thermodynamic, heat transfer and fluid flow analyses of ice thermal storage system used in a shopping center. ITES can be used to shift electric demand from high demand period to low demand period. The electric load of cooling can be shift to peak-off period by ITES. Thus, cooling cost can be reduced and lower-capacity cooling systems can be used. The shopping center investigated in this study is located in Ankara, Turkey. It has 15000 m² closed-area. Total cooling load of the shopping center is 6589 kW/day. Peak time cooling load has been stored during off-peak time. In present study, thermodynamic, heat transfer and pressure drop calculations of the ice thermal energy storage unit have been performed. Energy and exergy efficiencies, pressure drop, center line temperature distribution for storage tank have been calculated and presented. Also hard-saving amount has been presented.

Keywords: Ice Thermal Energy Storage System, Encapsulated, Peak Load Storing

1. INTRODUCTION

Energy demand in the utility, commercial and industrial sectors vary on daily, weekly and seasonal bases. These demands can be matched and shifted with help of thermal energy storage (TES) systems. TES systems are used in space and water heating, cooling and air-conditioning (AC). TES systems have an advantageous to make the use of systems equipment more effective. Also TES systems supply hard-saving during systems utilization and systems setup. Advantageous of the TES systems can be ordered as below [1];

- Reduced energy consumption,
- Reduced energy cost,
- Shifting peak load to off-peak periods.
- Low initial and maintenance costs,
- Improved indoor air quality,
- Increased flexibility of operation,
- Reduced equipment size,
- Efficient and effective utilization of equipment,
- Conservation of fossil fuels,
- Reduced pollutant emissions

Ice thermal energy storage (ITES) systems is an innovative way of storing night-time off-peak energy for daytime peak use. In many cities, demand for electrical power peaks during summer. AC is the main reason for this peak electrical demand. Also AC systems are used in expensive and peak time. ITES systems can shift this cooling electric load from peak time to off-time. So cooling requirements are supplied cheaper. Also higher-capacity AC systems are used in buildings because of cooling-peak load. Lower-capacity AC systems can be used through ITES.

The most common method to use the low electricity rates during off-peak periods is using ice thermal energy storage (ITES) systems. The basic of ITES is in-expensive off-peak electricity is utilized during the off-peak hours to produce ice, and during the day this ice store is melted by absorbing the heat from buildings needing cooling [2]. MacPhee et al. [3] emphasized that spherical capsule shape had better heat transfer performance than the other capsule geometry. Ismail and Henriquez [4] investigated different capsule materials for spherical capsule. They used 1-D numerical model and they validated their study with experimental study. They found that PVC was better material for ice capsule. Kousksou et al. [5] studied out that the ice capsule storing tank should be stayed in vertical position. Erek and Dincer [6], investigated temperature changing through the flow direction. They emphasized that heat transfer coefficient decreased through the flow direction. Cho and Choi [7], used paraffin instead of water inside the capsule. Ismail et al. [8], used finite difference model for spherical encapsulated ITES. Chen and Yue [9,10]

¹ Corresponding author: Erciyes University, Department of Mechanical Engineering, 38030, Melikgazi/Kayseri, Turkey.
erdemir@erdemir.edu.tr

applied porous medium equation into encapsulated ITES. Ezan et al. [11], developed thermal resistant mesh model for heat transfer analysis. Ryu et al. [12] investigated super-cooling effect in ITES. Super-cooling was seen in inlet and outlet of the tank. Calvet et al. [13] added graphite inside the capsule. Amin et al. [14] developed a new model consists buoyancy forces and density changing with the temperature. Chaichana et al. [15] investigated the economic performance of ice-on-coil systems. ITES system saved 55 % in full storage, 15 % in partial storage.

Many studies are available in literature. All of these studies are about to heat transfer, thermodynamic, fluid flow and economic analyses of the ITES. These studies are laboratory-scale experimental applications or theoretical big-scale building applications. And there is no clear study consists all together heat transfer, thermodynamic, fluid flow and economic analyses. In this study, temperature distribution inside the storage tank, energy and exergy efficiencies and pressure drop for encapsulated ITES used in the shopping center have calculated. Also economic analysis for hard-save have been determined in terms of peak time cooling load storing.

2 MATERIAL AND METHODS

c. Details of the Shopping Center

The shopping center is located in Ankara, Turkey. It has 15.000m² closed-area. Hourly cooling load of the shopping center is seen in Figure 1. Total cooling load is 6589 kW. Also 20% fresh air heat gain has been added to total cooling load. Because, 20% fresh-air is given to the shopping center. Ankara has arid climate. According to metrological information for Ankara between 1950 and 2014 [16], Closed-volumes in Ankara need to cooling six months in a year.

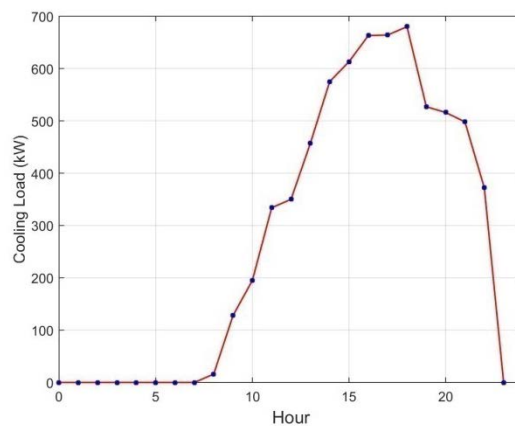


Figure 1. Hourly cooling load of the shopping center

Triple tariff is utilized in the shopping center. In this tariff, there are three different electric utilization fare depend on time. Details of the electric utilization fare are [17];

- Day time period, 6:00 – 17:00, 0.0644 USD/kWh
- Peak time period, 17:00 – 22:00, 0.1156 USD/kWh
- Off-peak time period, 22:00 – 6:00, 0.0258 USD/kWh

d. Details of the ITES System

ITES system used in the shopping center is seen in Figure 2. There three different using modes for ITES system. First is charging mode (green line). In this mode, -6°C heat transfer fluid (HTF) is obtain for the storage tank. So ice is gained, HTF is heated to -3°C and exit from the storage tank. Second mode is storing and normal cooling. In this mode, cooling unit directly cools the shopping center. Temperatures for this mode are 4°C and 10°C. Third mode is discharging. In this mode, ice is melted and the shopping center is cooled. Storage tank working temperatures are 4°C and 10°C as become in normal cooling mode. Building cooling cycling temperatures are 7 and 12°C. The storage tank diameter and height is 4 meters and 8 meters, respectively. There are nearly 85,000 ice capsules. Diameter of the capsule is 100 mm.

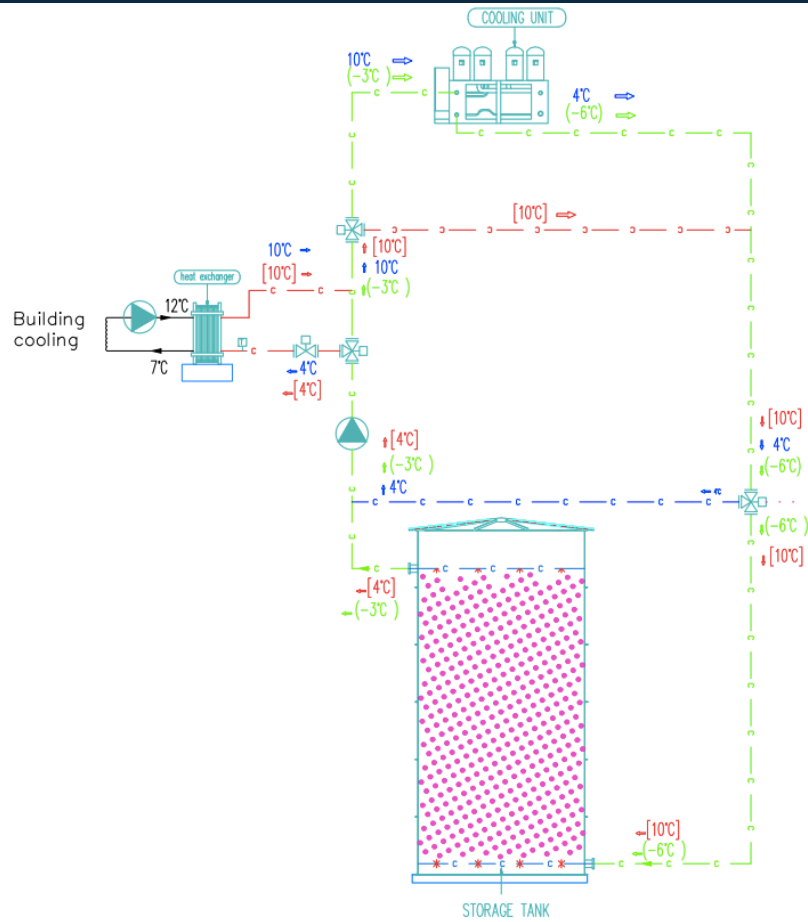


Figure 2. Schematic view of the ITES systems

e. Heat Transfer and Thermodynamics Analyses

2.3.1. Heat Transfer Analysis of the Storage Tank

Theoretical model of ice storage tank is seen in Figure 3. The following assumption are made before proceeding any further. The storage system is cylindrical, with diameter D and height H . This is due to the low surface area to volume ratio, which will be important when analyzing heat transfer to ambient. Buoyancy effects are negligible, since the bulk of heat transferred from the storage capsules will be a result of forced convection, and viscous dissipation within the storage system will be ignored. The heat transfer fluid is incompressible, the thermophysical properties of the system are constant and the velocity profile is regarded as fully developed plug flow in the y -direction. The ice capsules have a constant temperature equal to that of the phase change material freezing temperature. With the aforementioned assumption, the energy equation for heat transfer fluid, in cylindrical co-ordinates (Figure 3), can be written as

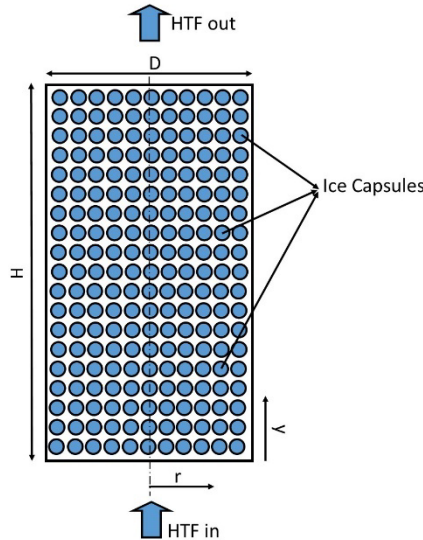


Figure 3. Schematic of the ITES storage system

$$\varepsilon \rho C u \frac{\partial T}{\partial y} = \frac{1}{r} \frac{\partial}{\partial r} \left(k r \frac{\partial T}{\partial r} \right) + \frac{\partial}{\partial y} \left(k \frac{\partial T}{\partial y} \right) + H A_{bed} (T_{PCM} - T) \quad (1)$$

Temperature changing in r-direction can be assumed as either plug, linear or quadratic, and using the integral method, the results will indicate which assumption is most suitable. As expressed earlier, the temperature profile at a point x in the system is assumed either linear or quadratic. To do so, the following boundary conditions are used in order to correctly evaluate the profiles:

$$T(x, 0) = T_c \quad (2)$$

$$\left. \frac{\partial T}{\partial r} \right|_{r=0} = 0 \quad (3)$$

$$\left. \frac{\partial T}{\partial r} \right|_{r=R} = -\frac{\dot{q}_w}{k} \quad (4)$$

Where Eq. (2) refers to the centerline temperature, Eq. (3) results from the system being symmetric about the y-axis, and Eq. (4) is a result of Fourier's law at the edge where $r=R$. Eq. (3) is not used as a boundary condition for the linear case, since only two boundary conditions are required (2) and (4). Again, using Fourier's law, the wall flux term in Eq. (4) can be further simplified as:

$$\dot{q}_w = \frac{T_{\infty} - T_w}{R_T} \quad (5)$$

$T_w = T(x, r=R)$, using the boundary conditions and rearranging, the temperature profiles for the linear case and quadratic case are displayed as Eq. (6) and (7) below, respectively.

$$T = T_c + \left(\frac{T_{\infty} - T_c}{-kR_T + R} \right) r \quad (6)$$

$$T = T_c + \left(\frac{T_{\infty} - T_c}{-2kR_T R + R^2} \right) r^2 \quad (7)$$

Heat transfer analysis and centerline temperature distribution inside the storage tank are calculated as described above.

2.3.2. Thermodynamic Analysis

The energy and exergy efficiencies during the ice storage process are now examined.

Energy analysis:

Energy balance for entire cycle of a cold capacity storage can be written as;

$$\text{Cold Input} - (\text{Cold Recovered} + \text{Cold Loss}) = \text{Cold Accumulation} \quad (8)$$

where "cold input" is gathering cold energy from HTF during charging period, "cold recovered" is gathering cold energy from storage medium during discharging period, "cold loss" is heat gain from environment to the storage medium during all periods and "cold accumulation" is the resultant change in energy of the storage fluid.

$$(H_b - H_a) - [(H_c - H_d) + Q_l] = -\Delta E \quad (9)$$

where H_a , H_b , H_c and H_d are enthalpies of the flows at points a, b, c and d given in Fig. 4. Q_l is the heat gain during charging, discharging and storing periods. ΔE is the change in energy of the storage fluid. If ITES undergoes a complete cycle, $\Delta E=0$. So, the energy changing is also defined as:

$$\Delta E = E_{final} - E_{initial} \quad (10)$$

The energy content of the solid and liquid portions of the storage fluid can be evaluated separately and summed as follows:

$$E = m[(1 - F)(u_s - u_o) + F(u_l - u_o)] \quad (11)$$

Here, u_s and u_l are specific internal energies of the solid and liquid portions of the storage fluid, respectively; u_o is specific enthalpy at environmental conditions; F is the melted fraction and m is the mass of storage fluid. Cold input can also be expressed as:

$$H_b - H_a = \dot{m}_{htf} C (T_a - T_b) \quad (12)$$

Here, " \dot{m}_{htf} " is the mass flow rate for HTF, " C " is the specific heat for HTF at the mean temperature. Cold output can be written as:

$$H_c - H_d = \dot{m}_{htf} C (T_c - T_d) \quad (13)$$

Heat loss is calculated as follows:

$$Q_l = R_t A \Delta T \quad (14)$$

Where " R_t " is overall thermal resistance, A is total surface area for the storage tank and ΔT is temperature difference between mean HTF temperature and environment. Energy efficiencies for ITES can be calculated as:

$$\eta = \frac{\text{Product cold recovered}}{\text{Cold input}} = \frac{\sum_{j=1}^{24} (H_c - H_d)_j}{\sum_{j=1}^{24} (H_b - H_a)_j} \quad (15)$$

$$\eta_{CH} = \frac{\Delta E_{CH}}{(H_b - H_a)} = \frac{(H_b - H_a) - Q_l}{(H_b - H_a)} \quad (16)$$

$$\eta_{ST} = 1 - \frac{Q_l}{\Delta E_{CH}} \quad (17)$$

$$\eta_{DIS} = \frac{(H_c - H_d)}{\Delta E_{CH}} = \frac{(H_c - H_d)}{(H_c - H_d) - Q_l} \quad (18)$$

Exergy analysis:

Exergy balance for a cold capacity storage undergoing a complete cycle of charging, storing and discharging can be written as:

$$Ex. input - (Ex. recovered + Ex. loss) - Ex. Consumption = Ex. Accumulation \quad (19)$$

Here, $Ex.$ is abbreviation of the exergy. Exergy loss is the quantity of exergy dissipated from the storage fluid through heat gain from the environment. Exergy consumption is the exergy loss due to irreversibility. The overall exergy balance:

$$(\varepsilon_a - \varepsilon_b) - [(\varepsilon_d - \varepsilon_c) - \varepsilon_{Q_l}] - I = \Delta \mathcal{E} \quad (20)$$

Where " ε_a ", " ε_b ", " ε_c " and " ε_d " are the exergy flows at points a, b, c and d in Fig. 4, " I " is the exergy consumption due to irreversibility and " $\Delta \mathcal{E}$ " is the change in non-flow exergy of the storage fluid. If the ITES is a complete cycle, $\Delta \mathcal{E}=0$. The exergy change can also be expressed as:

$$\Delta \mathcal{E} = \mathcal{E}_{final} - \mathcal{E}_{initial} \quad (21)$$

The exergy content of the storage fluid having solid and liquid phases can be determined as follows:

$$\mathcal{E} = m\{(1 - F)[(u_s - u_o) - T_o(s_s - s_o)] + F[(u_l - u_o) - T_o(s_l - s_o)]\} \quad (22)$$

Where T_o denotes the temperature of the reference environment; s_s and s_l are the specific entropies of the solid and liquid portions of the storage fluid, respectively; s_o is the specific entropy of the storage fluid at environmental conditions. The exergy transfer associated with the charging heat transfer fluid can be expressed as:

$$\mathcal{E} \varepsilon_a - \varepsilon_b = \dot{m}_{HTF} C [(T_a - T_b) - T_o \ln (T_a/T_b)] \quad (23)$$

Exergy efficiencies for ITES system can be calculated as follows:

$$\psi = \frac{\text{Exergy Recovered}}{\text{Exergy Input}} = \frac{\sum_{j=1}^{24} (\varepsilon_c - \varepsilon_d)_j}{\sum_{j=1}^{24} (\varepsilon_b - \varepsilon_a)_j} \quad (24)$$

$$\psi_{CH} = \frac{\Delta \mathcal{E}_{CH}}{(\varepsilon_b - \varepsilon_a)} = \frac{(\varepsilon_b - \varepsilon_a) - (\varepsilon_{Q_l} + I)}{(\varepsilon_b - \varepsilon_a)} \quad (25)$$

$$\psi_{ST} = 1 - \frac{Q_l}{\Delta E_{CH}} \quad (26)$$

$$\psi_{DIS} = \frac{(H_c - H_d)}{\Delta E_{CH}} = \frac{(H_c - H_d)}{(H_c - H_d) - Q_l} \quad (27)$$

RESULTS AND DISCUSSION

In present study, thermodynamic, heat transfer and economic analyses have been performed for an ITES systems used in the shopping center.

f. Results of Heat Transfer Analysis

The centerline temperature distribution can be obtained by solving the equations given in chapter 2.3.1. Energy equation has been solved as 1-D and with assuming linear temperature changing in radial direction. Because there is no significant difference between 1-D and 2-D and also between linear and quadratic case [18]. Centerline temperature changing with the tank height is seen in Figure 3.

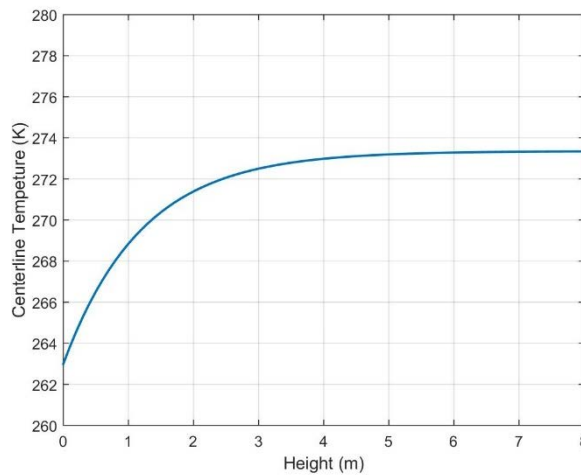


Figure 3. Centerline temperature distribution changing with the tank height

g. Results of Thermodynamic Analysis

Thermodynamic analysis has been performed with the equations given in chapter 2.3.2. Energy and exergy efficiencies have been calculated for charging, discharging and storing period. Before the calculation of thermodynamic efficiencies, heat gain should be found. Heat gain of the storage tank is 37 kW for a per hour. This heat gain has been added to storage medium. Beside of heat gain, 20% fresh air cooling load must be added to hourly cooling load. Energy efficiency for ITES in charging, discharging and storing periods have been calculated as 97.46%, 97.40% and 96.7%, respectively. Exergy efficiency of ITES in charging, discharging and storing periods have been calculated as 72.47%, 62.49% and 62.02%, respectively. As seen from these results, energy efficiencies do not give significant information about to system performance. However, as seen from exergy results, the highest exergy consumption is seen in discharging and storing period. Because of this result, discharging and storing periods working conditions can be enhanced.

h. Results of Economic Analysis

The shopping center cooling load and chiller usage are given in Table 1. Green color represents off-peak, yellow color represents day-time and red color represents peak-time periods in Table 1. In peak load storage mode, the cooling load and the heat gains of storage tank in peak-time is stored in off-peak period. Thus, cooling cost is reduced by ITES system. Daily electric usage cost for normal cooling mode, without ITES is 867 USD. When ITES is used, 450 USD, respectively. Besides this cost value, initial investment cost should be considered. Initial investment cost and ITES usage scenarios have great impact on payback period. Because fully storage requires bigger storage tank and larger-capacity cooling system. Because of these reason economic analysis should be performed carefully. All these factors are effected to pay-back period.

Table 1. Hourly cooling load and chiller usage

Hours	Cooling load (kW)	Normal cooling without ITES (kW)	Peak Load Storing (kW)
00:00 - 01:00	0	0	547

01:00 - 02:00	0	0	547
02:00 - 03:00	0	0	547
03:00 - 04:00	0	0	547
04:00 - 05:00	0	0	547
05:00 - 06:00	0	0	547
06:00 - 07:00	0	0	0
07:00 - 08:00	0	0	0
08:00 - 09:00	16	16	16
09:00 - 10:00	128	128	128
10:00 - 11:00	329	329	329
11:00 - 12:00	485	485	485
12:00 - 13:00	512	512	512
13:00 - 14:00	624	624	624
14:00 - 15:00	742	742	742
15:00 - 16:00	791	791	791
16:00 - 17:00	830	830	763
17:00 - 18:00	831	831	0
18:00 - 19:00	847	847	0
19:00 - 20:00	678	678	0
20:00 - 21:00	650	650	0
21:00 - 22:00	498	498	0
22:00 - 23:00	372	372	372
23:00 - 24:00	0	0	547

CONCLUSION

In this study as theoretical heat transfer, thermodynamic and economic analyses are performed for ITES used in the shopping center located in Ankara, Turkey. Since Ankara has arid climate, cooling is a requirement for closed volumes for thermal comfort. Because of triple tariff, cooling becomes expensive in day and peak time period. ITES system supplies cheaper cooling by shifting peak load to off-peak time. Energy efficiency for ITES in charging, discharging and storing periods have been calculated as 97.46%, 97.40% and 96.7%. Exergy efficiency of ITES in charging, discharging and storing periods have been calculated as 72.47%, 62.49% and 62.02%. As seen from these results, energy calculation hasn't give significant information about the systems. However, exergy analysis has shown that exergy consumption is higher in discharging and storing periods than charging period. Two different ITES utilization scenarios have been performed the shopping center. These are fully storage and partial storage. Energy consumption cost for cooling has been reduced nearly 40% with ITES.

REFERENCES

- [1.] Rosen, M.A., Dincer I., Pedinelli N., 2000. Thermodynamics Performance of Ice Thermal Energy Storage Systems. Journal of Energy Resources Technology, 122: 205-211.
- [2.] Beggs C., 1991. The economics of ice thermal storage, Buildings Research and Information, Vol. 19, No. 6, pp. 342-355.
- [3.] Ismail, K.A.R., Henriquez, J.R., 2002. Numerical and Experimental Study if Spherical Capsules Packed Bed Latent Heat Storage System. Applied Thermal Engineering, 22: 1705-1716.
- [4.] Kousksou, T., Bedecarrats, J.P., Dumas, J.P., Mimet, A., 2005. Dynamic Modelling of the Storage of an Encapsulated Ice Tank, 25: 1534-1548.
- [5.] MacPhee, D., Dincer, I., Beyene, A., 2012. Numerical Simulation and Exergetic Performance Assessment of Charging Process in Encapsulated Ice Thermal Energy Storage System. Energy, 41: 491 – 498.

- [6.] Chaichana, C., Charters W.W.S., Aye, L., 2001. An Ice Thermal Energy Storage Computer Model. *Applied Thermal Engineering*, 21: 1769 – 1778.
- [7.] Cho, K., Choi, S.H., 2000. Thermal Characteristics of Paraffin in a Spherical Capsule During Freezing and Melting Processes. *International Journal of Heat and Mass Transfer*, 43: 3183 – 3196.
- [8.] Ereğ, A., Dincer I., 2009. Numerical Heat Transfer Analysis of Encapsulated Ice Thermal Energy Storage Systems with Variable Heat Transfer Coefficient in Downstream. *International Journal of Heat and Mass Transfer*, 52: 851 – 859.
- [9.] Ezan, M.A., Ereğ, A., Dincer, I., 2011. Energy and Exergy Analyses of an Ice-on-Coil Thermal Energy Storage System. *Energy* 36: 6375 - 6386.
- [10.] Ismail, K.A.R., Henquez, J.R., da Silva, T.M., 2003. A parametric study on ice formation inside a spherical capsule. *International Journal of Thermal Sciences* 42: 881-887.
- [11.] Chen, S.L., Yue, J.S., 1991. Thermal performance of cool storage in packed capsules for air conditioning. *Heat Recovery Systems and CHP*, 11: 551-531.
- [12.] Chen, S.L., Yue, J.S., 1991. A simplified analysis for cold storage in porous capsules with solidification. *Energy Resources*, 113: 108-116.
- [13.] Ryu, H.W., Hong, S.A., Shin, B.C., Kim, A.D., 1991. Heat transfer characteristics of cool-thermal storage systems. *Energy* 16: 727-737.
- [14.] Calvet, N., Py, X., Olives, R., Bedecarrats, J.P., Dumas, J.P., Jay, F., 2013. Enhanced performances of macro-encapsulated phase change materials (PCMs) by intensification of the internal effective thermal conductivity. *Energy* 55: 956-964.
- [15.] Amin, N.A.M., Bruno, F., Belusko, M., 2014. Effective thermal conductivity for melting in PCM encapsulated in a sphere. *Applied Energy* 122: 280-287.
- [16.] <http://www.mgm.gov.tr/veridegerlendirme/il-ve-ilceler-istatistik.aspx?m=ANKARA#sfB>
- [17.] <http://www3.epdk.org.tr/index.php/elektrik-piyasasi/tarifeler>
- [18.] MacPhee D., Dincer I., 2008. Thermal modelling of a packed bed thermal energy storage system during charging. *Applied Thermal Engineering* 29: 695-705.

Time Predictable Model Applicability for Earthquake Prediction along the North Anatolian Fault Zone

Nilgun Sayil¹, Yasemin Beker²

Abstract

North Anatolian Fault Zone is located on the one of the seismically most active regions in the world, where a few large and several moderate earthquakes have occurred in the past. In this study the North Anatolian Fault Zone has been considered for an earthquake generation model using earthquake data in the historical period ($I_0 \geq 9.0$ corresponding to $M_s \geq 7.0$, before 1900) and in the instrumental period ($M_s \geq 5.5$, until 2015) earthquake catalogues reported by national and international data center. In this region, thirteen seismogenic sources were identified on the basis of certain seismological and geomorphological criteria. It is observed that the time interval between the two consecutive mainshocks depends upon the preceding mainshock magnitude (M_p). This result corroborates the validity of time-predictable model in the North Anatolian Fault Zone. A linear relation between the logarithm of repeat time (T) of two consecutive events and the magnitude of the preceding mainshock is established in the form $\text{Log}T = cM_p + a$, where “ c ” is a positive slope of line and “ a ” is function of minimum magnitude of the earthquake considered. The values of the parameters “ c ” and “ a ” are estimated to be 0.19 and 0.08 in the North Anatolian Fault Zone. For the region considered, the positive correlation between the time interval of the events and the magnitude of the preceding earthquake shows that the model is suitable. The result derived can be used for long term seismic hazard estimation in the delineated seismogenic regions.

Keywords: Time Predictable Model, Earthquake Prediction, North Anatolian Fault Zone

1. INTRODUCTION

In the time-predictable model, the time interval between two large earthquakes is proportional to the slip amount of the preceding earthquake and a large earthquake occurs when the stress has reached a limit value. The magnitude-predictable model gives the relation between the magnitudes of the preceding and the following earthquake and indicates that the larger the magnitude of the preceding mainshock, the smaller the magnitude of the following mainshock [1]. Therefore, the time-predictable and magnitude-predictable models were combined to a single one called the regional time and magnitude-predictable seismicity model, which applies to seismogenic sources including the main fault and other smaller faults [2]. Several scientists have applied this model at different seismogenic regions of world [3]-[5],[6]-[9].

In this study, we are testing the applicability of the time and magnitude predictable model for earthquake generation along the North Anatolian Fault Zone. In order to estimate the recurrence intervals for large earthquakes occurred along the North Anatolian Fault Zone (NAFZ), this region limited with the coordinates of 38°-42°N, 26°-44°E has been separated into thirteen seismogenic sources on the basis of certain seismological and geomorphological criteria (Figure 1).

¹ Corresponding author: Karadeniz Technical University, Department of Geophysical Engineering, 61080, Trabzon, Turkey. sayil@ktu.edu.tr

² Gumushane University, Department of Geophysical Engineering, 29100, Gumushane, Turkey. bekeryasemin@gmail.com

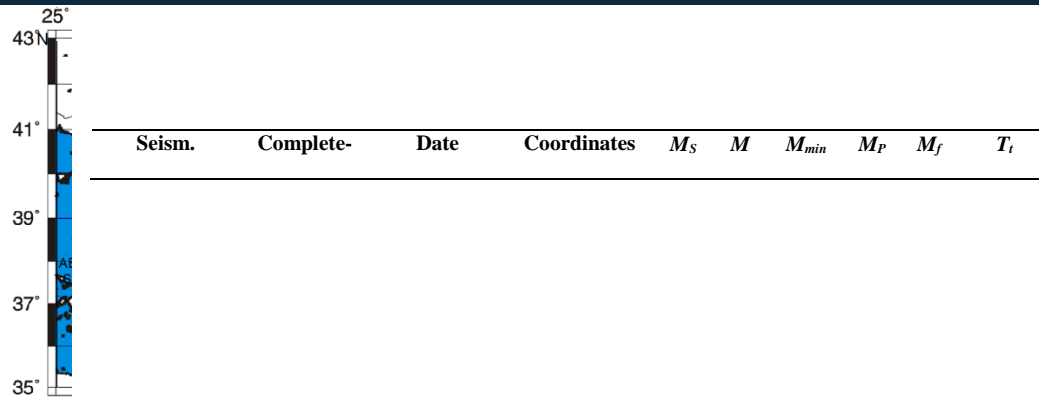


Figure 1 Tectonic and seismicity map of the North Anatolian Fault Zone and thirteen seismogenic sources. Filled and open circles show shallow main shocks and pre- or following main shocks, respectively.

2. METHODOLOGY APPLIED AND CALCULATION

The magnitude-predictable model implies that the magnitude of the preceding main shock which is the largest earthquake during a seismic excitation in a seismogenic source governs the time of occurrence and the magnitude of the expected main shock in this source. The data belonging to both instrumental period ($M_S \geq 5.5$) until 2015 and historical period ($I_0 \geq 9.0$ corresponding to $M_S \geq 7.0$) before 1900 have been used in the analysis. The interevent time between successive main shocks with magnitude equal to or larger than a certain minimum magnitude threshold were considered in each of 13 seismogenic sources within the study area. These interevent times as well as the magnitudes of the main shocks have been used to determine the following relations using the database given Table 1;

$$\text{Log}T_t = 0.29M_{min} + 0.19M_p - 0.34\log \dot{M}_0 + 7.07 \quad (1)$$

$$M_f = 0.82M_{min} - 0.14M_p + 0.18\log \dot{M}_0 - 1.96 \quad (2)$$

where T_t is the interevent time measured in years, M_{min} is the surface wave magnitude of the smallest main shock considered, M_p is the magnitude of the preceding main shock, M_f is magnitude of the following main shock, and \dot{M}_0 is the released seismic moment per year in each source. The multiple correlation coefficient and standard deviation are 0.76 and 0.32 for Eq. (1) and 0.66 and 0.43 for Eq. (2), respectively. The strong positive correlation between the interevent time and the magnitude of the preceding mainshock suggests that the time-predictable model is applicable in the considered region. $\text{Log} T^*$ is calculated by the Eq. (3) corresponding to each M_p . The relation between $\text{Log} T^*$ and M_p is shown in Fig. 2a. This equation has a smaller correlation coefficient than 0.40 (Fig 2a).

$$\text{Log}T^* = 0.19M_p + 0.08 \quad (3)$$

The value of M_f^* is computed using the equation Eq. (2) corresponding to each M_p . The relation between M_f^* and M_p is shown in Fig. 2b.

$$M_f = -0.14M_p - 0.09 \quad (4)$$

The above equation has a smaller correlation coefficient than 0.20 (Fig 2b). The observed negative dependence of the magnitude of the following mainshock on the magnitude of the preceding mainshock indicates that a large mainshock is followed by a small one and vice versa.

Table 1 Earthquake data used for Time- and Magnitude-Predictable Model; a: aftershocks, f: foreshocks, M: cumulative magnitude. (for examples, some seismogenic sources)

Sources	ness	dd.mm.yy	(°N)	(°E)	(years)						
1	1354, 7.0	01.10.1875	40.20	26.40	7.0	7.0	5.5	7.0	5.5	80.26	
Saros Gulf	1900, 5.5	06.01.1956	40.39	26.29	5.5	5.5	5.5	5.5	5.6	9.62	
		23.08.1965	40.51	26.17	5.6	5.6	5.5	5.6	6.7	9.50	
		17.03.1975	40.49	26.17	5.5	<i>f</i>	5.5	6.7	5.6	28.27	
		17.03.1975	40.48	26.08	5.9	<i>f</i>	5.5	5.6	5.5	7.32	
		27.03.1975	40.40	26.10	6.7	6.7	5.6	7.0	5.6	89.88	
		29.03.1975	40.42	26.00	5.5	<i>a</i>	5.6	5.6	6.7	9.50	
		06.07.2003	40.39	26.19	5.6	5.6	5.6	6.7	5.6	28.27	
		03.11.2010	40.42	26.34	5.5	5.5	6.7	7.0	6.7	99.48	
2	1010, 7.0	05.08.1766	41.00	27.50	7.7	7.7	5.5	7.7	7.3	146.01	
Tekirdag	1900, 5.5	09.08.1912	40.60	27.20	7.3	7.3	5.5	7.3	5.6	29.84	
		10.08.1912	40.60	27.10	6.3	<i>a</i>	5.5	5.6	5.5	17.11	
		10.04.1917	40.60	27.10	5.5	<i>a</i>	5.6	7.7	7.3	146.01	
		16.06.1942	40.80	27.80	5.6	5.6	5.6	7.3	5.6	29.84	
		26.07.1959	40.91	27.54	5.5	5.5	7.3	7.7	7.3	146.01	
3	325, 7.0	01.01.325	41.00	29.00	7.0	7.0	7.0	7.0	7.0	102.00	
Istanbul	1900, 5.5	01.01.427	41.00	29.00	7.0	7.0	7.0	7.0	7.5	20.84	
		08.11.447	40.90	28.50	7.5	7.5	7.0	7.5	7.0	29.87	
		25.09.477	40.90	28.80	7.0	7.0	7.0	7.0	7.6	77.88	
		16.08.555	41.04	28.98	7.5	7.6	7.0	7.6	7.4	185.19	
		14.12.557	40.90	28.80	7.0	<i>a</i>	7.0	7.4	7.0	124.55	
		26.10.740	41.00	28.30	7.4	7.4	7.0	7.0	7.2	198.35	
		16.05.865	41.00	29.00	7.0	7.0	7.0	7.2	7.2	281.00	
		23.09.1063	40.90	28.30	7.2	7.2	7.0	7.2	7.0	117.27	
		23.09.1344	41.00	29.00	7.2	7.2	7.0	7.0	7.0	197.10	
		01.01.1462	41.00	29.00	7.0	7.0	7.0	7.0	7.0	107.29	
		06.02.1659	41.00	29.00	7.0	7.0	7.2	7.5	7.6	107.76	
		22.05.1766	41.00	29.00	7.0	7.0	7.2	7.6	7.4	185.19	
								7.2	7.4	7.2	322.90
						7.2	7.2	7.2	281.00		
						7.4	7.5	7.6	107.76		
						7.4	7.6	7.4	185.19		
						7.5	7.5	7.6	107.76		
4	1509, 7.0	25.05.1719	40.70	29.50	7.0	7.0	5.5	7.0	7.0	35.27	
İzmit	1900, 5.5	02.09.1754	40.80	29.40	7.0	7.0	5.5	7.0	6.7	123.62	
		19.04.1878	40.80	29.00	6.7	6.7	5.5	6.7	5.5	29.33	
		21.08.1907	40.70	30.10	5.5	5.5	5.5	5.5	5.5	15.76	
		29.05.1923	41.00	30.00	5.5	5.5	5.5	5.5	6.3	40.3	

			18.09.1963	40.77	29.12	6.3	6.3	5.5	6.3	7.8	35.9
			17.08.1999	40.74	29.96	7.8	7.8	6.3	7.0	7.0	35.27
			13.09.1999	40.75	30.08	5.5	<i>a</i>	6.3	7.0	6.7	123.62
			20.09.1999	40.74	29.33	5.5	<i>a</i>	6.3	6.7	6.3	85.41
			11.11.1999	40.74	30.27	5.9	<i>a</i>	6.3	6.3	7.8	35.9
								6.7	7.0	7.0	35.27
								6.7	7.0	6.7	123.62
								6.7	6.7	7.8	121.32
								7.0	7.0	7.0	35.27
								7.0	7.0	7.8	244.95
5	1719, 7.0	24.01.1928	40.99	30.86	5.5	5.5	5.5	5.5	6.7	6.7	14.98
Adapazari	1900, 5.5	20.01.1943	40.80	30.50	6.6	6.7	5.5	6.7	7.2	7.2	14.35
		20.06.1943	40.84	30.60	6.2	<i>a</i>	5.5	7.2	7.3	7.3	10.15
		05.04.1944	40.84	31.12	5.6	<i>a</i>	5.5	7.3	7.5	7.5	32.3
		26.05.1957	40.70	30.90	7.2	7.2	6.7	6.7	7.2	7.2	14.35
		26.05.1957	40.60	30.74	5.5	<i>a</i>	6.7	7.2	7.3	7.3	10.15
		26.05.1957	40.76	30.81	5.9	<i>a</i>	6.7	7.3	7.5	7.5	32.3
		27.05.1957	40.73	30.95	5.8	<i>a</i>	7.2	7.2	7.3	7.3	10.15
		22.07.1967	40.67	30.69	7.3	7.3	7.2	7.3	7.5	7.5	32.3
		22.07.1967	40.70	30.80	5.5	<i>a</i>	7.3	7.3	7.5	7.5	32.3
		30.07.1967	40.72	30.52	5.6	<i>a</i>					
		17.08.1999	40.64	30.65	5.6	<i>f</i>					
		06.09.1999	40.76	31.07	5.7	<i>f</i>					
		12.11.1999	40.81	31.19	7.5	7.5					
		12.11.1999	40.74	31.05	5.5	<i>a</i>					

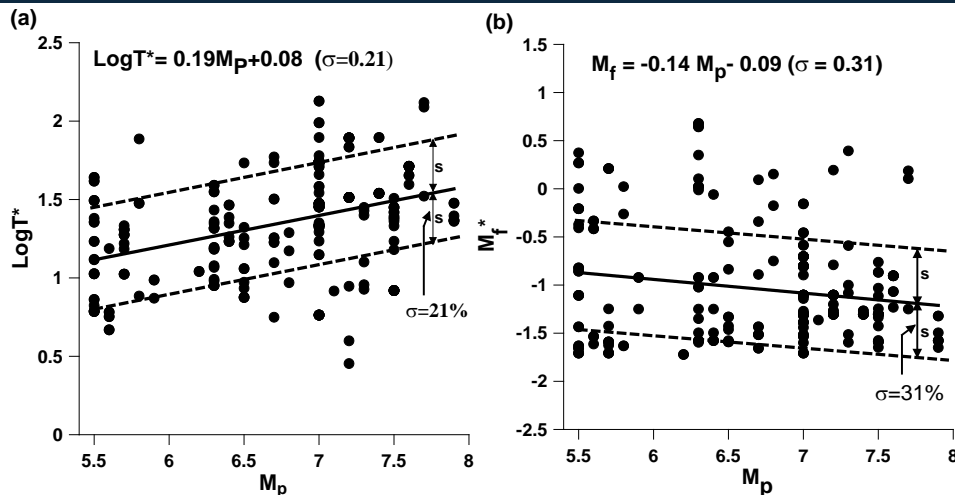


Figure 2 (a) The relation between the repeat time, T^* , and the magnitude of the preceding mainshock, M_p ; (b) The relation between the following mainshock, M_f^* , and the magnitude of the preceding mainshock, M_p . Broken lines show interval bands (s) for estimates of $\sigma = 21\%$ and $\sigma = 31\%$.

DISCUSSIONS AND CONCLUSIONS

The study of long-term characteristics of the earthquake generation processes in different seismogenic sources is of fundamental importance for the seismic hazard evaluation. In the present study, the identified 13 seismogenic sources in the North Anatolian Fault Zone show diverse seismotectonic environments. The strong positive correlation between the interevent time (T) and the magnitude of the preceding mainshock (M_p) suggests that the time-predictable model is applicable in the considered region. This is because the large earthquake releases the accumulated stress to a minimum level, but, the tectonic loading may remain the same. The observed negative dependence of the magnitude of the following mainshock (M_f) on the magnitude of the preceding mainshock (M_p) indicates that a large mainshock is followed by a small one and vice versa.

REFERENCES

- [1] B. C. Papazachos, "A time and magnitude predictable model for generation of shallow earthquakes in the Aegean area", *Pure Appl. Geophys.*, vol. 138, pp. 287–308, 1992.
- [2] B. C. Papazachos and Ch. "A. Papaioannou, Long-term earthquake prediction in Aegean area based on the time and magnitude predictable model". *Pure Appl. Geophys.* vol. 140, pp. 593–612, 1993.
- [3] K. Mogi, *Earthquake Prediction*, Academic Press, Tokyo, pp. 355, 1985.
- [4] B. C. Papazachos, "A time predictable model for earthquake generation in Greece", *Bull. Seismo. Soc. Am.*, vol. 79, pp. 77–84, 1989.
- [5] D. Shanker, Characteristic studies of tectonics, Seismicity and occurrences of major earthquakes in northeast India, PhD Thesis, Banaras Hindu University, Varanasi, India, pp. 117, 1990.
- [6] D. Shanker, and V. P. Singh, Regional Time- and Magnitude predictable Seismicity model for north-east India and vicinity, *Acta Geod. Geoph. Hung.*, vol. 31(1–2), pp. 181–190, 1996.
- [7] D. Shanker and H. N. Singh, Application of the time-predictable model in Peninsular India for future seismic hazard assessment, *Acta Geophysica*, vol. 55(3), pp. 302–312, 2007.
- [8] H. Paudyal, H. N. Singh, D. Shankar and V. P. Singh, Validity of Time-Predictable Seismicity Model for Nepal and its Adjoining Regions, *Journal of Nepal Geological Society*, vol. 38, pp. 15–22, 2008.
- [9] D. Shanker, A. Panthi and H. N. Singh, "Long-term seismic hazard analysis in Northeast Himalaya and its adjoining regions", *Geosciences*, vol. 2, pp. 25–32, 2012.

Usefulness of Slip Predictable Model for Earthquake Occurrence in Turkey

Nilgun Sayil¹, Kaan Hakan Coban²

Abstract

Turkey locates in the seismically most active section of the Alpine-Himalayan Belt in the eastern Mediterranean and involves several important tectonic structures. In this study, Turkey has been considered for an earthquake generation model using earthquake data in the historical period ($I_0 \geq 9.0$ corresponding to $M_S \geq 7.0$, before 1900) and in the instrumental period ($M_S \geq 5.5$, until 2015) earthquake catalogues reported by national and international data center. In this region, 33 seismogenic sources were identified on the basis of certain seismological and geomorphological criteria. It is observed that the repeat time (T^*) between the two consecutive mainshocks depends upon the following mainshock (M_f). The linear regression between the logarithm of repeat time of two consecutive events and the magnitude of the following mainshock was obtained as $\text{Log}T = kM_f + l$, where “ k ” is a positive slope of line and “ l ” is function of minimum magnitude of the earthquake considered. The values of the parameters “ k ” and “ l ” are estimated to be 0.05 and 0.95 for Turkey. The above equation has a smaller correlation coefficient than 0.15 and a standard deviation with $\sigma=0.1$. The positive slope graphically indicates that more time is needed for a large forthcoming earthquake, which is accordance with slip-predictable model. The slip-predictable model is applicable to the regions considered.

Keywords: Slip Predictable Model, Earthquake Prediction, Turkey

1. INTRODUCTION

Most of the studies related to seismicity and seismic hazard assessment are based on time-independent models [1]. These models are based on the Poisson distribution for time and Gutenberg-Richter formula for magnitude distribution. The researchers worked for and searched for a time-dependent seismicity model to fulfill the limitations and inadequacy of independent models. Two time-dependent seismicity models have been proposed by [2]: the slip-predictable model and the time-predictable model. With these models, the size and time of occurrence of future earthquakes can be predicted. Later on, the time-predictable model [3]-[6] and the slip-predictable model [4] was modified.

The earthquake recurrence models were proposed based on Reid’s concept of the elastic rebound theory, i.e. that successive earthquakes occur when stress reaches a critical value in a fault of seismogenic sources. Figure 1 shows the two levels of stresses, τ_1 and τ_2 , upper and lower level, respectively. These stresses are responsible for controlling the behavior of a fault in the earthquake generation process. When τ_1 is constant, the model is said to be time predictable (Fig. 1a). In this case, stress drop changes to different shocks. When τ_2 is constant, the model is said to be slip predictable. In this case, earthquakes start at variable states of stress (Fig. 1b).

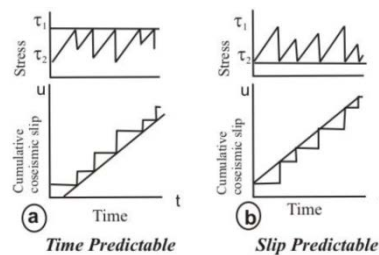


Figure 1. Earthquake Recurrence Model: (a) time-predictable model showing stress buildup to a certain value (τ_1) and non-uniform stress drop; and (b) slip predictable-model illustrating non-uniform stress buildup and stress drop to a certain minimum value (τ_2) [2].

In the time-predictable model, the time interval between two large earthquakes is proportional to the slip amount of the preceding earthquake and a large earthquake occurs when the stress has reached a fixed, limiting value. Similarly, in the case of the slip-predictable model, the time interval between two successive, large earthquakes is proportional

¹ Corresponding author: Karadeniz Technical University, Department of Geophysical Engineering, 61080, Trabzon, Turkey. sayil@ktu.edu.tr

² Karadeniz Technical University, Department of Geophysical Engineering, 61080, Trabzon, Turkey. h.coban@ktu.edu.tr

to the slip amount of the next large earthquake. In general, only the size of a future earthquake can be predicted by the slip predictable model and only the time of its occurrence can be predicted by the time predictable model. Several scientists have applied this model [7], [5], [8]-[11] at different seismogenic regions of world. In the present paper, we are testing the usefulness of the slip predictable model for earthquake occurrence in Turkey. An area bounded by 36-42°N and 25-45°E has been considered in this study (Fig. 2).

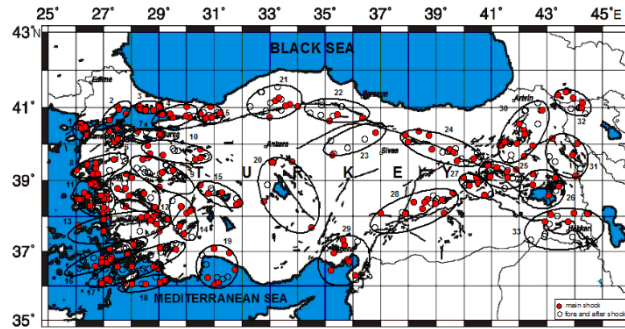


Figure 2. Earthquake plots with $M_s \geq 5.5$ for the instrumental period 1900-2015 and $M_s \geq 7.0$ the historical period (before 1900) in Turkey with thirteen seismogenic sources over major tectonic features of the area. The seismogenic sources are separated by shaded elliptical boundaries.

2 METHODOLOGY APPLIED AND CALCULATION

In this study, Turkey has been considered for an earthquake generation model using earthquake data in the historical period ($I_0 \geq 9.0$ corresponding to $M_s \geq 7.0$, before 1900) and in the instrumental period ($M_s \geq 5.5$, until 2015) earthquake catalogues reported by national and international data center. In this region, 33 seismogenic sources were identified on the basis of certain seismological and geomorphological criteria.

The database given Table 1 were used to obtain the relation between repeat time T and the following mainshock magnitude M_f ;

$$\text{Log}T = kM_f + l \quad (1)$$

The correlation coefficient of the above equation is 0.40. The value of l is affected by both k and M_{min} considered in each case. Therefore, to reduce $\text{log}T$ the value of constant l was calculated by using $k=0.05$ for all available data of T and M_f from Table 1. Then, the average value \bar{l}_m was calculated for all l . By applying the same method, different values of \bar{l}_m were calculated corresponding to the different sets of M_{min} and T and average, \bar{l}_m , was determined. The difference of $\bar{l}_m - \bar{l}_{mn}$ was added to $\text{log}T$ to obtain

$$\text{Log}T^* = \text{Log}T + \bar{l}_m - \bar{l}_{mn} \quad (2)$$

Where T^* gives the average time of the event for all the seismogenic sources. The regression line was obtained as:

$$\text{Log}T^* = 0.05M_f + 0.95 \quad (3)$$

The above equation has a smaller correlation coefficient than 0.35 (Fig 3a). The positive slope graphically indicates that more time is needed for a large forthcoming earthquake, which is contentious to slip-predictable model. The slip-predictable model is valid to the regions considered. Again, the same database and method was applied to obtain the relation between preceding mainshock magnitude M_p and the following mainshock magnitude M_f (Fig. 3b). The regression line was obtained as:

$$M_f^* = -0.01M_p - 0.10 \quad (4)$$

The above equation has a smaller correlation coefficient than 0.10. The negative slope graphically indicates that a large mainshock is followed by a small one and *vice versa*.

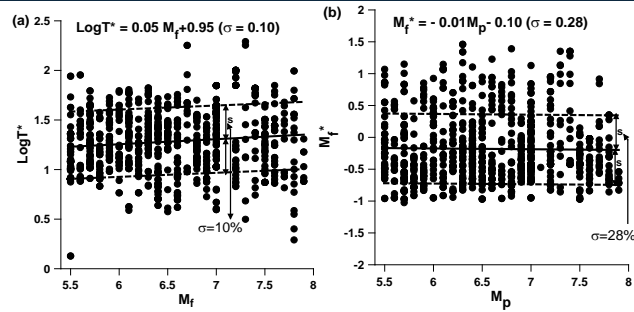


Fig. 3. (a) Plot of T^* (repeat time) against M_f (the following mainshock magnitude) and (b) M_p (the preceding mainshock magnitude) and M_f (the following mainshock magnitude) with their estimated regression lines (with residual, s and standard deviation, σ).

Figure 3 suggest that extreme vales are obtained only if the scattered data in a scattergram lie on a perfectly straight line that is, only if $LogT^*$ depending only on the sign of k (slope). In this case the $LogT^*$ and M_f are said to be perfectly correlated. The point estimates of parameters are also indicated in these figures with residual, s and standard deviation σ , denote the correctness of the data.

Table 1. Earthquake Data (for example, some seismogenic sources) having a magnitude of $M_s \geq 5.5$ used for testing the usefulness of Slip Predictable Model; a = aftershocks, f = foreshocks, M = cumulative magnitude.

Seismogenic Sources	Completeness	Date	Coordinates		M_s	M	M_{min}	M_p	M_f	T
			(°N)	(°E)						
1 Saros Gulf	1354, 7.0	01.10.1875	40.20	26.40	7.0	7.0	5.5	7.0	5.5	80.26
	1900, 5.5	06.01.1956	40.39	26.29	5.5	5.5	5.5	5.5	5.6	9.62
		23.08.1965	40.51	26.17	5.6	5.6	5.5	5.6	6.7	9.50
		17.03.1975	40.49	26.17	5.5	f	5.5	6.7	5.6	28.27
		17.03.1975	40.48	26.08	5.9	f	5.5	5.6	5.5	7.32
		27.03.1975	40.40	26.10	6.7	6.7	5.6	7.0	5.6	89.88
		29.03.1975	40.42	26.00	5.5	a	5.6	5.6	6.7	9.50
		06.07.2003	40.39	26.19	5.6	5.6	5.6	6.7	5.6	28.27
		03.11.2010	40.42	26.34	5.5	5.5	6.7	7.0	6.7	99.48
3 Istanbul	325, 7.0	01.01.325	41.00	29.00	7.0	7.0	7.0	7.0	7.0	102.00
	1900, 5.5	01.01.427	41.00	29.00	7.0	7.0	7.0	7.0	7.5	20.84
		08.11.447	40.90	28.50	7.5	7.5	7.0	7.5	7.0	29.87
		25.09.477	40.90	28.80	7.0	7.0	7.0	7.0	7.6	77.88
		16.08.555	41.04	28.98	7.5	7.6	7.0	7.6	7.4	185.19
		14.12.557	40.90	28.80	7.0	a	7.0	7.4	7.0	124.55
		26.10.740	41.00	28.30	7.4	7.4	7.0	7.0	7.2	198.35
		16.05.865	41.00	29.00	7.0	7.0	7.0	7.2	7.2	281.00
		23.09.1063	40.90	28.30	7.2	7.2	7.0	7.2	7.0	117.27
23.09.1344	41.00	29.00	7.2	7.2	7.0	7.0	7.0	197.10		

06.02.1659	41.00	29.00	7.0	7.0	7.2	7.5	7.6	107.76
22.05.1766	41.00	29.00	7.0	7.0	7.2	7.6	7.4	185.19
					7.2	7.4	7.2	322.90
					7.2	7.2	7.2	281.00
					7.4	7.5	7.6	107.76
					7.4	7.6	7.4	185.19
					7.5	7.5	7.6	107.76

Table 1. continue

Seismogenic Sources	Completeness	Date	Coordinates	M_S	M	M_{min}	M_P	M_f	T	
		dd.mm.yy	(°N) (°E)						(years)	
4 İzmit	1509, 7.0	25.05.1719	40.70 29.50	7.0	7.0	5.5	7.0	7.0	35.27	
	1900, 5.5	02.09.1754	40.80 29.40	7.0	7.0	5.5	7.0	6.7	123.62	
		19.04.1878	40.80 29.00	6.7	6.7	5.5	6.7	5.5	29.33	
		21.08.1907	40.70 30.10	5.5	5.5	5.5	5.5	5.5	15.76	
		29.05.1923	41.00 30.00	5.5	5.5	5.5	5.5	6.3	40.3	
		18.09.1963	40.77 29.12	6.3	6.3	5.5	6.3	7.8	35.9	
		17.08.1999	40.74 29.96	7.8	7.8	6.3	7.0	7.0	35.27	
		13.09.1999	40.75 30.08	5.5	<i>a</i>	6.3	7.0	6.7	123.62	
		20.09.1999	40.74 29.33	5.5	<i>a</i>	6.3	6.7	6.3	85.41	
		11.11.1999	40.74 30.27	5.9	<i>a</i>	6.3	6.3	7.8	35.9	
							6.7	7.0	7.0	35.27
							6.7	7.0	6.7	123.62
							6.7	6.7	7.8	121.32
							7.0	7.0	7.0	35.27
					7.0	7.0	7.8	244.95		
5 Adapazari	1719, 7.0	24.01.1928	40.99 30.86	5.5	5.5	5.5	5.5	6.7	14.98	
	1900, 5.5	20.01.1943	40.80 30.50	6.6	6.7	5.5	6.7	7.2	14.35	
		20.06.1943	40.84 30.60	6.2	<i>a</i>	5.5	7.2	7.3	10.15	
		05.04.1944	40.84 31.12	5.6	<i>a</i>	5.5	7.3	7.5	32.3	
		26.05.1957	40.70 30.90	7.2	7.2	6.7	6.7	7.2	14.35	
		26.05.1957	40.60 30.74	5.5	<i>a</i>	6.7	7.2	7.3	10.15	
		26.05.1957	40.76 30.81	5.9	<i>a</i>	6.7	7.3	7.5	32.3	
		27.05.1957	40.73 30.95	5.8	<i>a</i>	7.2	7.2	7.3	10.15	
		22.07.1967	40.67 30.69	7.3	7.3	7.2	7.3	7.5	32.3	
		22.07.1967	40.70 30.80	5.5	<i>a</i>	7.3	7.3	7.5	32.3	
		30.07.1967	40.72 30.52	5.6	<i>a</i>					
		17.08.1999	40.64 30.65	5.6	<i>f</i>					
		06.09.1999	40.76 31.07	5.7	<i>f</i>					

		12.11.1999	40.81	31.19	7.5	7.5					
		12.11.1999	40.74	31.05	5.5	<i>a</i>					
6	Bandirma	543, 7.0	04.01.1935	40.40	27.50	6.7	6.8	5.7	6.8	7.5	18.20
		1900, 5.5	04.01.1935	40.30	27.45	6.3	<i>a</i>	5.7	7.5	5.7	16.04
			18.03.1953	40.00	27.40	7.5	7.5	5.7	5.7	6.1	14.33
			18.03.1953	39.96	27.59	5.5	<i>a</i>	6.1	6.8	7.5	18.20
			03.03.1969	40.08	27.50	5.7	5.7	6.1	7.5	6.1	30.29
			05.07.1983	40.30	27.20	6.1	6.1	6.8	6.8	7.5	18.20
7	Bursa	715, 7.0	28.02.1855	40.18	29.10	7.5	7.5	5.8	7.5	6.5	50.13
		1900, 5.5	11.04.1855	40.20	29.10	6.7	<i>a</i>	5.8	6.5	5.8	43.57
			15.04.1905	40.20	29.00	6.5	6.5	5.8	5.8	7.0	15.89
			13.11.1948	40.23	29.02	5.6	5.8	6.5	7.5	6.5	50.13
			03.06.1953	40.28	28.53	5.5	<i>a</i>	6.5	6.5	7.0	59.47
			06.10.1964	40.24	28.16	5.6	<i>f</i>	7.0	7.5	7.0	109.60
			06.10.1964	40.30	28.23	7.0	7.0				
21	Bolu	968, 7.0	25.06.1910	41.00	34.00	6.5	6.5	5.5	6.5	5.7	9.04
		1900, 5.5	09.08.1918	40.89	33.41	5.8	<i>a</i>	5.5	5.7	5.5	17.44
			09.06.1919	41.16	33.20	5.7	5.7	5.5	5.5	7.5	7.02
			18.11.1936	41.25	33.33	5.5	5.5	5.5	7.5	5.7	33.89
			26.11.1943	41.05	33.72	7.2	7.5	5.5	5.7	5.7	22.66
			01.02.1944	41.41	32.69	7.2	<i>a</i>	5.7	6.5	5.7	9.04
			01.02.1944	41.40	32.70	5.5	<i>a</i>	5.7	5.7	7.5	24.46
			10.02.1944	41.00	32.30	5.5	<i>a</i>	5.7	7.5	5.7	33.89
			02.03.1945	41.20	33.40	5.6	<i>a</i>	5.7	5.7	5.7	22.66
			26.10.1945	41.54	33.29	5.7	<i>a</i>	6.5	6.5	7.5	33.41
			13.08.1951	40.88	32.87	6.9	<i>a</i>				
			07.09.1953	41.09	33.01	6.0	<i>a</i>				
			05.10.1977	41.02	33.57	5.7	5.7				
			06.06.2000	40.70	32.99	5.7	5.7				
22	Merzifon	1598, 7.0	29.08.1918	40.58	35.16	5.5	5.5	5.5	5.5	7.0	24.3
	(Tosya)	1900, 5.5	21.11.1942	40.82	34.44	5.5	<i>f</i>	5.5	7.0	6.1	54.21
			02.12.1942	41.04	34.88	5.5	<i>f</i>	6.1	7.0	6.1	54.21
			11.12.1942	40.76	34.83	5.9	<i>f</i>				
			20.12.1942	40.66	36.35	7.0	7.0				
			10.12.1943	41.00	35.60	5.6	<i>a</i>				
			30.09.1944	41.11	34.87	5.5	<i>a</i>				
			10.08.1996	40.74	35.29	5.6	<i>f</i>				
			10.03.1997	40.78	35.44	6.0	6.1				

DISCUSSIONS AND CONCLUSIONS

In the present study, the identified thirteen seismogenic sources in Turkey show diverse seismotectonic environments. For the region considered, the positive correlation between the time interval of the events (repeat time, T) and the magnitude of the following earthquake (M_f) shows that the model is suitable.

The correlation between the magnitude of the preceding event (M_p) of the earthquake and the magnitude of the following event (M_f) is weaker, suggesting that earthquake occurrences in the considered regions are different from those in plate boundary. This may be a matter of future discuss on the difference between the mechanisms of earthquake occurrence in plate boundary and that occurring in the continent.

The study of the applicability of the slip-predictable model for earthquake occurrence in different regions is significant for earthquake hazard evaluation. It is also helpful in understanding earthquake genesis under different tectonic environments. Such topics should be studied further both in theory and practice.

REFERENCES

- [1] B. C. Papazachos, E. E. Papadimitriou, and G. F.Karakaisis, "Time dependent seismicity in the zones of the continental fracturesystem", *Pro. XXIV General Assembly of European Seismological Commission*, Athens, Greece, pp. 1099–1107, 1994.
- [2] K. Shimazaki and T.Nakata, "Time predictable recurrence of great earthquakes", *Geophys. Res. Letters*, vol. 7, pp.279–282, 1980.
- [3] L.R. Sykes and R.C. Quittmeyer, *Repeat times of Great Earthquakes along simple plate boundaries*, Maurice Ewing Series, vol.4, pp. 297–332, 1981.
- [4] T. Anagnos and A. S.Kiremidjian, "Stochastic time-predictable model for earthquake occurrences", *Bull. Seismo. Soc. Am.*, vol. 74, pp. 2593–2611, 1984.
- [5] B. C. Papazachos, "A time predictable model for earthquake generation in Greece", *Bull. Seismo. Soc. Am.*, vol. 79, pp. 77–84, 1989.
- [6] B. C.Papazachos, "A time and magnitude predictable model for generation of shallow earthquakes in the Aegean area", *Pure Appl. Geophys.*, vol. 138, pp. 287–308, 1992.
- [7] K.Mogi, *Earthquake Prediction*, Academic Press, Tokyo, pp. 355, 1985.
- [8] D.Shanker, Characteristic studies of tectonics, Seismicity and occurrences of major earthquakes in northeast India, PhD Thesis, Banaras Hindu University, Varanasi, India, pp. 117, 1990.
- [9] D. Shanker, and V. P.Singh, Regional Time- and Magnitudepredictable Seismicity model for north-east India and vicinity, *Acta Geod. Geoph. Hung.*, vol. 31(1–2), pp. 181–190, 1996.
- [10]D. Shanker and H. N.Singh, Application of the time-predictable model in Peninsular India for future seismic hazard assessment, *Acta Geophysica*, vol. 55(3), pp. 302–312, 2007.
- [11]H. Paudyal, H. N. Singh, D. Shankar and V. P.Singh, Validity of Time-Predictable Seismicity Model for Nepal and its Adjoining Regions, *Journal of Nepal Geological Society*, vol. 38, pp. 15–22, 2008.
- [12]

Chaotically Initiated Flower Pollination Algorithm for Search and Optimization Problems

Sinem Akyol¹, Bilal Alatas²

Abstract

Metaheuristics algorithms are recently getting strong and becoming more popular due to their many advantages. In spite of the preponderance of plant life, surprisingly little inspiration has been drawn from botanical activities and processes for the design of novel metaheuristic algorithm for search and optimization problems. Flower Pollination Algorithm (FPA) is one of the recently proposed botanic based metaheuristic algorithm inspired by the flow pollination process of flowery plants. Although initial pollen population have great importance for the performance of the FPA, they have randomly generated in the studies. In this paper, Chaotically Initiated Flower Pollination Algorithm (CIFPA) has been proposed and sequences generated from different chaotic maps have been used for generating initial pollen population of FPA. By this way, enhancing the global convergence and preventing to stick on a local solution has been intended. The experimental results obtained from FPA and CIFPA for different benchmark functions show that the application of chaotic maps instead of random sequences in initial pollen population generation step may be a possible strategy to improve the performance of the original FPA in terms of convergence speed and accuracy. Different chaotic maps may also be used for different parameters of FPA and its variants with optimized parameters may be proposed for more efficient solutions in future works.

Keywords: *Chaos, Flower Pollination Algorithm, Metaheuristic Algorithms, Optimization, Performance*

1. INTRODUCTION

Metaheuristic optimization is subfield of computational intelligence and recently getting strong and becoming more popular due to their good computation power and easily transformations. They are adaptable and general purposed population based solution methods that can be applied to the high-scale combinatorial and non-linear search and optimization problems in case of concurrent different decision variables, objective functions, and constraints and they do not depend on the solution space type, the number of decision variables, and the number of constraint functions. Furthermore, they do not require very well defined mathematical models that are hard to derive. Their computation power is also good and they do not require excessive computation time. Their transformations and adaptations are easy. These algorithms do not require the assumptions that are hard to be approved to adapt a solution algorithm to a given problem and they do not require the alteration on the interested problem as done in classical algorithm. Due to these advantages, these algorithms are densely being used in many different fields [1-3].

General purposed metaheuristic methods are generally classified in different groups like biological based, social based, music based, sports based, chemistry based, and physics based. There are also hybrid methods formed with these methods [1]. In spite of the preponderance of plant life, surprisingly little inspiration has been drawn from botanical activities and processes for the design of novel metaheuristic algorithm for search and optimization problems. Flower Pollination Algorithm (FPA) is one of the recently proposed botanic based metaheuristic algorithm inspired by the flow pollination process of flowery plants [4-6].

Recently, chaotic number arrays have taken place of random number arrays and given better results in many real world problems due to their theoretically unpredictability, their spread spectrum characteristic and also ergodic features. The objective of this paper is to reveal the influence of chaotic sequence with distinct chaotic maps on computational performance of FPA for global optimization. Initializing step of FPA affects convergence success. Thus, different chaotic systems have been used instead of random number arrays in the first step of FPA. In this way, it has been tried to improve global convergence of the FPA and keep away from trapping in local solution. However, these parameters do not guarantee ergodic feature of the algorithm in the phase space; because they are random in the FPA.

The organization of the paper has been organized as follows. Section two introduces the FPA. Section three describes the works about FPA. Chaotically initiated FPA (CFPA) for search and optimization problems has been described in section four. Experimental results obtained from the proposed CFPA and FPA have been given in section five and finally section six concludes the paper.

¹ Corresponding author: Tunceli University, Department of Computer Engineering, 62000, Tunceli, Turkey. sakyol@tunceli.edu.tr

²Firat University, Department of Software Engineering, 23119, Elazig, Turkey. balatas@firat.edu.tr

2. FLOWER POLLINATION ALGORITHM (FPA)

FPA, inspired by the flow pollination process of flowery plants, was developed in 2012 by Xin-She-Yang [4-6]. The following 4 rules are used as a matter of convenience.

- (1) Biotic cross-pollination can be thought as global pollination process. Pollen-carrying pollinators move according to a Levy flight process (Rule 1).
- (2) Self-pollination and local pollination are used for local pollination (Rule 2).
- (3) Pollinators such as birds and bees can develop flower persistence (Rule 3).
- (4) A switch probability $p \in [0,1]$, which is slightly biased towards local pollination, can control the switching or interaction of global and local pollination (Rule 4).

The above rules must be converted to appropriate updating equations for formulation of updating formulas. For example, flower pollen gametes are moved by pollinators such as birds and bees in the global pollination process. Pollen can be transferred over a long distance, because pollinators can often fly and move over a much longer range. Therefore, Rule 1 and Rule 3 (flower persistence) can be represented mathematically as (1).

$$x_i^{t+1} = x_i^t + \gamma L(\lambda)(g_* - x_i^t) \quad (1)$$

x_i^t , is the pollen i , or x_i solution vector in iteration t , γ is a scale factor to control the step size. $L(\lambda)$ is the parameter corresponding to the pollination power, more specially it is the Levy-flights based step size, g_* is the current best solution found among all solutions at the current iteration/generation. Levy flight can be used effectively to simulate pollinators' movements [4-6].

$$L \sim \frac{\lambda \Gamma(\lambda) \sin(\pi\lambda/2)}{\pi} \frac{1}{s^{1+\lambda}}, (s \gg s_0 > 0) \quad (2)$$

Here $\Gamma(\lambda)$ is the standard gamma function and this distribution is valid for large steps $s > 0$. It must be $|s_0 \gg 0|$ in theory, but in practice, s_0 can be as small as 0.1. However, it is not trivial to generate pseudo-random step sizes which conform to the Levy distribution. There are a few methods for drawing these type pseudo-random numbers. One of the most efficient methods is using two Gaussian distributions U and V , which is the so-called Mantegna algorithm for drawing step size s .

$$s = \frac{U}{|V|^{1/\lambda}}, U \sim N(0, \sigma^2), V \sim N(0,1) \quad (3)$$

In (3), $U \sim (0, \sigma^2)$ means that the samples are drawn from a Gaussian normal distribution with a variance of σ^2 and a zero mean. The variance can be calculated as (4) [4-6].

$$\sigma^2 = \left\{ \frac{\Gamma(1+\lambda)}{\lambda \Gamma[(1+\lambda)/2]} \cdot \frac{\sin(\pi\lambda/2)}{2^{(\lambda-1)/2}} \right\}^{1/\lambda} \quad (4)$$

This formula seems complicated, but for a given λ value it is only a constant. For example, if $\lambda = 1$, then the gamma functions become $\Gamma(1 + \lambda) = 1, \Gamma([1 + \lambda/2]) = 1$.

$$\sigma^2 = \left\{ \frac{1}{1 \cdot 1} \cdot \frac{\sin(\pi \cdot 1/2)}{2^0} \right\}^{1/1} = 1 \quad (5)$$

It is proved mathematically that Mantegna algorithm can produce random samples which obey the required distribution (2) correctly [4-6].

Both of rules (2) and (3) can be represented as (6) for local pollination.

$$x_i^{t+1} = x_i^t + \epsilon(x_j^t - x_k^t) \quad (6)$$

Here x_j^t and x_k^t are pollens in different flowers of the same plant species. This essentially mimics flower constancy in a limited neighborhood. Mathematically, if x_j^t and x_k^t are selected from the same population or come from the same species; this equivalently becomes a local random walk if ϵ is drawn from a uniform distribution in $[0, 1]$.

In principle, flower pollination activities can occur both local and global, at all scales. However, substantially, the flowers in the not-far-away or adjacent flower patches are more likely to be pollinated by local flower pollen than those far away. Therefore, value of the switch probability can be taken as $p = 0.8$. The pseudo code of FPA is shown in Figure 1.


```

Flower Pollination Algorithm
Objective function min or max  $f(x)$ ,  $x=(x_1, x_2, \dots, x_d)$ 
Initialize a population of  $n$  flower/pollen gametes with random solutions.
Find the best solution in the population
Define a switch probability
Define a stopping criterion
While ()
  For  $i=1 : n$  (all  $n$  flowers in the population)
    If  $rand < p$ ,
      Draw a ( $d$ -dimensional) step vector  $L$  which obeys Levy distribution
      Do global pollination via Eq. (1)
    Else
      Draw from a uniform distribution in  $[0,1]$ 
      Do local pollination via Eq. (6)
    End If
  Evaluate new solutions
  If new solutions are better, than update them in the population
  Find current best solution
End While
Output is the best solution found
    
```

Figure 1. Pseudo code of FPA

3. STUDIES WITH FPA

Yang et al. used FPA for solving multi-objective optimization problems. Proposed algorithm was tested in multi-objective test functions and it was seemed that this algorithm has a better convergence speed compared to other algorithms [4, 5]. Lenin et al., proposed a hybrid algorithm, which is a combination of chaotic harmony search algorithm and FPA, for solving reactive power dispatch problem. Standard FPA was integrated with the harmony search algorithm to improve the search accuracy [7].

Wang and Zhou proposed dimension by dimension improvement based FPA, for multi-objective optimization problem. They also applied local neighborhood search strategy in this improved algorithm for enhancing the local searching ability [8]. Yang et al. indicated that it is important to balance exploration and exploitation for any metaheuristic algorithm. Because, interaction of these two components could significantly affect the efficiency. Therefore, they studied FPA with Eagle Strategy [5].

Abdel-Raouf et al. used FPA with chaos theory for solving definite integral [9]. Additionally, they proposed a hybrid method which was a combination of FPA and Particle Swarm Optimization for improving search accuracy. They used it for solving constrained optimization problems [10]. They also proposed a new hybrid algorithm combined with FPA and chaotic harmony search algorithm, to solve Sudoku puzzles [11]. Sundareswaran et al. proposed a modification for steps of traditional Genetic Algorithm, used for PVM inverter, by imitating flower pollination and subsequent seed production in plants [12]. Prathiba et al. set the real power generations using FPA, for minimizing the fuel cost, in economic load dispatch, which is the main optimization task in power system operation [13].

Lukasik et al., studied FPA for continuous optimization and they compared solutions with Particle Swarm Optimization [14]. Platt used FPA in the calculation of dew point pressures of a system exhibiting double retrograde vaporization. The main idea was to apply a new algorithmic structure in a hard nonlinear algebraic system arising from real-world situations [15]. Kanagasabai and RavindhranathReddy proposed a combination of FPA and Particle Swarm Optimization for solving optimal reactive power dispatch problem [16]. Sakib et al. compared FPA with Bat Algorithm. They tested these two algorithms on both unimodal and multimodal, low and high dimensional continuous functions and they observed that FPA gave better results [17].

4. METHODS AND MODIFICATIONS

Convergence feature of the FPA seems to be based on its stochastic nature that uses random number array for the parameters during run. Because different random number arrays are used in the FPA, obtained results in different runs may not equal and may be very closer to each other. Different number of iterations may be needed in order to obtain same optimum values. However, as like in other evolutionary algorithms, there is not analytical result that guarantees improvements in performance of FPA according to a special number generator.

Recently, chaotic number arrays have taken place of random number arrays and given better results in many real world problems. Popularity of using chaotic number arrays has been increased due to their theoretically unpredictability, their spread spectrum characteristic, and also ergodic features related to them. The objective of this paper is to reveal the influence of chaotic sequence with distinct chaotic maps on computational performance of FPA for global optimization. Initializing step of FPA may affect convergence success. Thus, different chaotic systems have been used instead of random number arrays in initializing step of FPA. Thus a chaotically initialized FPA called CFPA has been proposed in this paper. In this way, it has been tried to improve global convergence of the FPA and keep away from trapping in local solutions. However, these parameters do not guarantee ergodic feature of the

algorithm in the phase space; because they are random in the FPA. Different chaotic versions of FPA using different chaotic maps may also be proposed for future works.

Maps, which are used for FPA parameters in order to generate chaotic numbers, are listed as follows:

Circle Map

Circle Map [18] equation is shown in Equation (7).

$$X_{n+1} = X_n + b - (a/2\pi)\sin(2\pi X_n) \text{ mod}(1) \quad (7)$$

Logistic Map

It is one of the simplest chaotic maps [19]. It is appeared in non-linear dynamics of biological populations that show chaotic behaviors. Equation of the Logistic Map is given in Equation (8).

$$X_{n+1} = aX_n(1 - X_n) \quad (8)$$

Tent Map

Tent Map is like Logistic Map [19]. It generates number in (0, 1) interval and expressed as shown in Equation (9).

$$X_{n+1} = f(x) = \begin{cases} X_n/0.7, & X_n < 0.7 \\ 10/3X_n(1 - X_n), & \text{otherwise} \end{cases} \quad (9)$$

Chaotic number series generated from these maps with 0.8 as initial number for 150 iterations have been shown in Figure 2. Chaotic initialization step of FPA has been demonstrated in Figure 3.

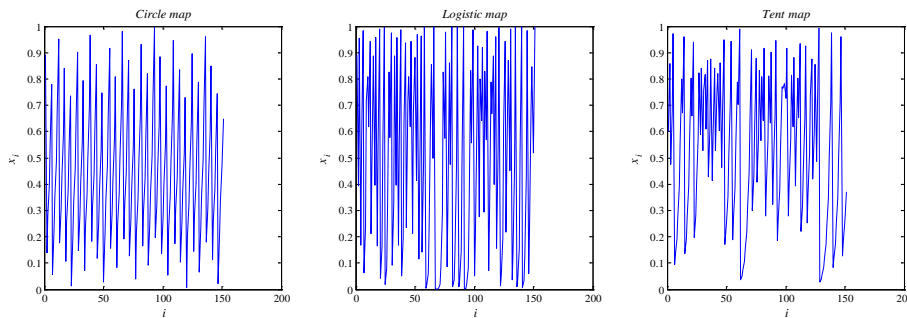


Figure 2. Chaotic numbers generated from the chaotic maps with

```

ci = maximum number of iteration for chaotic maps
i = 0
While (i ≤ number of flowers)
    Take the initial number for chaotic map
    j = 0
    While (j ≤ number of decision variable)
        Generate chaotic number cni,j according to the selected chaotic map
         $x_{i,j} = x_j^{\min} + cn_{i,j}(x_j^{\max} - x_j^{\min})$ 
        j = j + 1
    End While
    i = i + 1
End While
    
```

Figure 3. Pseudo code of CFPA

Table 1. Selected benchmark functions

Function No	Function Name	Definition	Interval
1	Sphere	$f_1(x) = \sum_{i=1}^n x_i^2$	$-5.12 \leq x_i \leq 5.12$
2	Griewank	$f_2(x) = 1 + \frac{1}{4000} \sum_{i=1}^n x_i^2 - \prod_{i=1}^n \cos\left(\frac{x_i}{\sqrt{i}}\right)$	$-600 \leq x_i \leq 600$

Table 2. Results of Sphere function obtained from FPA and CFPA using different chaotic maps

Run no	FPA	CFPA-Circle	CFPA-Logistic	CFPA-Tent
1	3.6063	0.0003	0.0049	0.0040
2	4.0752	0.0031	0.0053	0.0050
3	2.9196	0.0043	0.0031	0.0019
4	3.1932	0.0011	0.0067	0.0047
5	2.8778	0.0002	0.0082	0.0033
6	3.2499	0.0007	0.0104	0.0063

7	2.3139	0.0025	0.0072	0.0036
8	1.4623	0.0007	0.0034	0.0053
9	3.3187	0.0031	0.0074	0.0000
10	2.9672	0.0012	0.0043	0.0000
11	3.9367	0.0032	0.0067	0.0077
12	3.5617	0.0041	0.0074	0.0006
13	3.3896	0.0000	0.0041	0.0063
14	3.4039	0.0008	0.0069	0.0015
15	2.4913	0.0000	0.0026	0.0008
16	1.7459	0.0006	0.0048	0.0054
17	3.6325	0.0056	0.0041	0.0032
18	2.0563	0.0059	0.0083	0.0014
19	3.3652	0.0013	0.0039	0.0048
20	3.2157	0.0025	0.0058	0.0008
21	3.0982	0.0004	0.0061	0.0025
22	2.6779	0.0020	0.0071	0.0021
23	3.5083	0.0010	0.0054	0.0083
24	2.9708	0.0014	0.0022	0.0016
25	3.3932	0.0050	0.0068	0.0031
26	2.5616	0.0033	0.0071	0.0042
27	4.3044	0.0016	0.0078	0.0049
28	3.3906	0.0005	0.0008	0.0042
29	3.8661	0.0044	0.0026	0.0066
30	2.3972	0.0021	0.0120	0.0033
<i>Average</i>	3.0984	0.0021	0.0058	0.0036
<i>Best</i>	1.4623	0.0000	0.0008	0.0000

5. EXPERIMENTAL RESULTS

Generally, benchmark test functions are used to evaluate and compare the characteristics of optimization algorithms in terms of convergence, precision, robustness, and general performance as a rule. The nature, complexity and other properties of these benchmark functions can be easily obtained from their definitions. The difficulty levels of most benchmark functions are adjustable by setting their dimensions and intervals of decision variables [20]. The selected benchmark functions and its properties have been demonstrated in Table 1. The dimensions for all functions have been determined as 30. Sphere function is unimodal with less complexity and it can be used to evaluate the converging behaviors of algorithms [21]. Griewank function is multi-modal function with many local optima and it can be used to test the global search ability of the algorithms in avoiding premature convergence [22].

Their graphs with two dimensions have been shown in Figure 4 (a) and Figure 4 (b).

Table 3. Results of Griewank function obtained from FPA and CFPA using different chaotic maps

Run no	FPA	CFPA-Circle	CFPA-Logistic	CFPA-Tent
1	14.5908	0.9852	1.0112	1.0196
2	12.8850	0.3191	0.9052	0.2988
3	11.0015	0.6149	0.9690	0.4817
4	14.2432	0.7211	0.9865	0.9648
5	7.2978	0.9463	1.0408	0.0060
6	8.1552	0.8322	0.3380	0.9614
7	9.2171	0.1181	1.0276	0.9854
8	7.3108	0.6703	1.0349	1.0021
9	14.4701	0.9145	0.6664	1.0029
10	8.5830	0.7130	0.5901	0.8378
11	12.0910	0.7549	1.0239	1.0194
12	11.8666	0.9602	0.9568	0.9133
13	10.3712	0.9902	1.0312	0.5628
14	12.5243	0.9287	0.6328	0.2535

15	11.4344	0.7635	0.8209	0.8411
16	16.6047	0.6710	1.0167	0.8257
17	10.8818	0.4672	0.3648	0.1525
18	16.5389	0.4816	0.9768	0.9705
19	9.9144	0.8407	0.1337	0.9258
20	16.5370	0.6396	0.9089	0.7889
21	17.5166	0.6177	0.9564	0.3946
22	12.6505	0.6305	1.0037	0.9953
23	13.5100	0.0754	1.0259	0.6927
24	12.2525	0.9394	1.0215	1.0172
25	14.3334	0.6451	0.9968	0.9881
26	9.8402	0.3290	0.8701	0.9674
27	12.5468	0.9329	0.9633	0.9844
28	12.3439	0.8451	1.0380	0.8842
29	9.7284	0.8973	0.9518	0.9482
30	11.2142	0.6640	1.0238	0.6583
Average	12.0818	0.6970	0.8763	0.7781
Best	7.2978	0.0754	0.1337	0.0060

Classical FPA and CFPA using different chaotic maps have been run 30 times with 1000 iterations and 100 flowers and cost function $f(x)$ results have been stored. Experimental results for Sphere function obtained from these algorithms have been demonstrated in Table 2. It can be seen that CFPA using different maps have outperformed the classical FPA and CFPA using circle map has the best performance in average. Experimental results for Griewank function obtained from these algorithms have been demonstrated in Table 3. It can be seen that CFPA using different maps have outperformed the classical FPA and CFPA using circle map has also the best performance for this benchmark function.

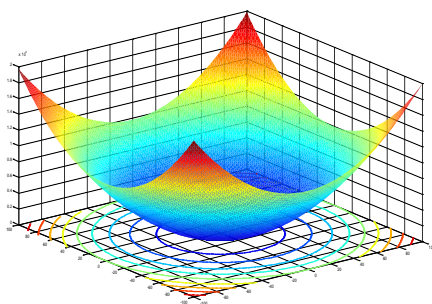
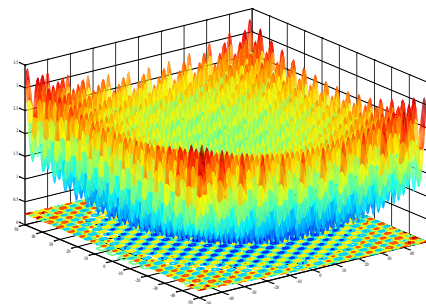


Figure 4. (a) Sphere function with two variables



(b) Griewank function with two variables

Table 5 reports the obtained test results for Griewank function. From the experimental results, It can be seen that the observed difference between the sample means is convincing enough to say success of CFPA using all different maps differs significantly. It can be concluded that combining results appeared in different fields like FPA and complex dynamics can increase quality in some optimization problems and the chaos can be a wanted process.

Table 4. Wilcoxon rank-sum test for Sphere function

	CFPA-Circle	CFPA-Logistic	CFPA-Tent
<i>t Stat</i>	25.54645193	25.50142	25.54397
<i>t Critical two-tail</i>	2.045229642	2.04523	2.04523

Table 5. Wilcoxon rank-sum test for Griewank function

	CFPA-Circle	CFPA-Logistic	CFPA-Tent
<i>t Stat</i>	22.45653	22.8058	22.63883
<i>t Critical two-tail</i>	2.04523	2.04523	2.04523

6. CONCLUSIONS

FPA is one of the newest botanic based general purposed metaheuristic optimization algorithm. Like as other evolutionary algorithms, to obtain rapid global convergence and accuracy rates; getting stuck of FPA on local points should be prevented. In this study, chaos theory has been applied to initial step of FPA for the first time to remove the disadvantages of the algorithm. Although there is not any analytical results that guarantees improvements in performance of FPA according to a special number generator, from the experimental results, it can be concluded that combining results appeared in different fields like FPA and complex dynamics can increase quality in optimization problems and the chaos can be a wanted process. Different chaotic maps may also be simply embedded to different steps of FPA and efficient result may be obtained for different types of search and optimization problems.

REFERENCES

- [1] S. Akyol and B. Alatas, "The Current Swarm Intelligence Optimization Algorithms", *Nevsehir Universitesi Fen Bilimleri Enstitüsü Dergisi*, vol. 1, pp. 36-50, 2012.
- [2] S. Akyol and B. Alatas, "A New Field in Social based Computational Intelligence: Social Impact Theory based Optimization", in *1st International Conference on Engineering Technology and Applied Sciences ICETAS*, 2016.
- [3] S. Akyol and B. Alatas, "Fizik Tabanlı En Güncel Yapay Zekâ Algoritması "Elektromanyetik Alan Optimizasyonu" nun Performansının İncelenmesi" (in Turkish), *1st International Conference on Engineering Technology and Applied Sciences ICETAS*, 2016.
- [4] X. S. Yang, "Flower Pollination Algorithm for Global Optimization". *Unconventional Computation and Natural Computation*. Springer, vol. 7445, pp 240-249, 2012.
- [5] X. S. Yang, M. Karamanoglu and X. He, "Multi-Objective Flower Algorithm for Optimization", *Procedia Computer Science*, vol. 18, pp. 861-868, 2013.
- [6] X. S. Yang, M. Karamanoglu and X. He, "Flower Pollination Algorithm: A Novel Approach for Multiobjective Optimization", *Engineering Optimization*, vol. 46, pp. 1222-1237, 2014.
- [7] K. Lenin, "Shrinkage of Active Power Loss by Hybridization of Flower Pollination Algorithm with Chaotic Harmony Search Algorithm", *Control Theory and Informatics*, vol. 4, pp. 31-38, 2014.
- [8] R. Wang and Y. Zhou, "Flower Pollination Algorithm with Dimension by Dimension Improvement", *Mathematical Problems in Engineering*, 2014.
- [9] O. Abdel-Raouf, M. Abdel-Baset and I. El-henawy, "An Improved Flower Pollination Algorithm with Chaos", *International Journal of Education and Management Engineering (IJEME)*, vol. 4, pp. 1-8, 2014a.
- [10] O. Abdel-Raouf, M. Abdel-Baset and I. El-henawy, "A New Hybrid Flower Pollination Algorithm for Solving Constrained Global Optimization Problems", *International Journal of Applied Operational Research*, vol. 4, pp.1-13, 2014b.
- [11] O. Abdel-Raouf, M. Abdel-Baset and I. El-henawy, "A Novel Hybrid Flower Pollination Algorithm with Chaotic Harmony Search for Solving Sudoku Puzzles", *International Journal of Modern Education and Computer Science (IJMECS)*, vol. 6(3), pp. 38-44. 2014c.
- [12] K. Sundaeswaran, P. S. Nayak, P. Sankar and V. V. Kumar, "Inverter Harmonic Elimination through Flower Pollination Enhanced Genetic Algorithm", *International Journal of Advanced Trends in Computer Science and Engineering*, vol. 3, pp. 342-348, 2014.
- [13] R. Prathiba, M. B. Moses and S. Sakthivel, "Flower Pollination Algorithm Applied for Different Economic Load Dispatch Problems", *International Journal of Engineering and Technology*, vol. 6, pp. 1009-1016, 2014.
- [14] S. Łukasik and P. Kowalski, "Study of Flower Pollination Algorithm for Continuous Optimization", *Intelligent Systems'2014, Advances in Intelligent Systems and Computing*. Springer International Publishing, vol 322, pp 451-459, doi: 10.1007/978-3-319-11313-5_40, 2015.
- [15] G. M. Platt, "Computational Experiments with Flower Pollination Algorithm in the Calculation of Double Retrograde Dew Points", *International Review of Chemical Engineering (IRECHE)*, vol. 6, 2014.
- [16] L. Kanagasabai and B. RavindhranathReddy, "Reduction of Real Power Loss by Using Fusion of Flower Pollination Algorithm with Particle Swarm Optimization", *Journal of the Institute of Industrial Applications Engineers*, vol. 2, pp. 97-103, 2014.
- [17] N. Sakib, M. Kabir, M. Subbir and S. Alam, "A Comparative Study of Flower Pollination Algorithm and Bat Algorithm on Continuous Optimization Problems", *International Journal of Applied Information Systems (IJ AIS)*, vol. 7, pp. 19-20, 2014.
- [18] W. M. Zheng, "Kneading Plane of the Circle Map", *Chaos Soliton Fract*, vol. 4, pp. 1221-1233, 1994.
- [19] R. M. May, "Simple Mathematical Models with Very Complicated Dynamics", *Nature*, vol. 261, pp. 459-467, 1976.
- [20] B. Alatas, E. Akin and A. B. Ozer, "Chaos Embedded Particle Swarm Optimization Algorithms", *Chaos, Solitons & Fractals*, vol. 40, pp. 1715-1734, 2009.
- [21] (March 2016) GEATbx: Examples of Objective Functions. Available: <http://www.pg.gda.pl/~mkwies/dyd/geadocu/fcnfun1.html>
- [22] (March 2016) GEATbx: Examples of Objective Functions. Available: <http://www.pg.gda.pl/~mkwies/dyd/geadocu/fcnfun8.html>

BIOGRAPHY

Sinem Akyol: She received her BSc in Computer Engineering from Ege University, Turkey in 2009. She completed her MSc in Electrical and Electronics Engineering at Tunceli University. At present she is pursuing Ph. D. in Computer Engineering, Firat University, Turkey. She is a Research Assistant in the Department of Computer Engineering at the Tunceli University. Her research interests include social network analysis, data mining, and metaheuristic optimization.

Bilal Alatas: He received his B.S., M.S., and Ph.D. degrees from Firat University. He has been working as Head of Software Engineering Department at Firat University in Elazig, Turkey. His research interests include artificial intelligence, data mining, and metaheuristic computation. Dr. Alatas has published over 50 papers in many well-known international journals and proceedings of refereed conference since 2001. He has been editor of nine international journals and reviewer of twenty international journals.

Chassis Analysis and Parametric Optimizations of Concept Vehicle

M. Umut Karaoglan¹, N. Sefa Kuralay²

Abstract

A concept vehicle chassis and suspensions have been designed for fuel cell hybrid drive. Chassis includes circular and rectangular shape structural steel (st-70) profiles with welding assembly. In this study, structure analysis and optimizations of chassis design has been performed. Structure analysis of chassis is performed by Ansys Workbench which is working with Solidworks. Forces acting on chassis from the road are calculated separately for different road conditions. For each road condition, forces acting on chassis determined by structure analysis of suspension systems. Chassis analysis has been achieved for these forces. Based on stresses on profiles of chassis, thickness optimization of critical profiles performed for optimum values. Yield stress of material, chassis mass and standard profile requirements are considered for determining optimum values. Vehicle chassis manufacturing is aimed with optimization on minimum cost.

Keywords: *Chassis Analysis, Optimization, Vehicle Body*

1. INTRODUCTION

Motor vehicle structures are changing every decade base on their propulsion types and purposes of usage. Hybrid and electric vehicle powertrains cause reconsiderations about the structures. Concept vehicles that use electric motor with a single speed gearbox at front and simple solid axle at rear, are designed shown in figure 1. Independence of internal combustion engine provides small track width and simple front suspension design at front. Front wheel drive concept car has Mc Pherson Suspension at front. Non driven rear suspension carries the weight of batteries and fuel cell stack which are about 180 kg. Total weight of vehicle is taking into considered as 650 kg. Vehicle has designed as solid model by Solidworks which its chassis consist of rectangular profiles as main body at bottom and circular profiles at top of main body with weldment [3,4,5].

Structural analysis has been performed by Ansys Workbench software with quasi-static approach [3]. Finite element method is used for analysis [3-11]. Similar works about chassis analysis and optimization take place in literatures. Structural analysis of car, truck and articulated bus chassis had been performed for the purpose of determining critical points, weight reduction and topology optimization [5]. Parametric optimization is used to calculate optimum profile thicknesses of chassis by response surface methodology [10,12]. Chassis shall also meet precise stiffness requirements in order to allow a safe drive under various road conditions [3]. Different values of forces could occur on tires as the direction of lateral, longitudinal and vertical under each road condition. Suspension systems and chassis of vehicle should resist the most critical conditions of road. Also stresses on vehicle body should remain under yield stress of their material. Determination critical profiles of chassis and profile thickness optimization of its provide increasing the ability of bending resistant. The major challenge of hybrid drive concept vehicle is to overcome the increasing demands for lower weight in order to satisfy fuel economy requirements [11].

¹ Corresponding author: Dokuz Eylul University, Department of Mechanical Engineering, 35397, Buca/Izmir, Turkey. mustafa.karaoglan@deu.edu.tr

² Dokuz Eylul University, Department of Mechanical Engineering, 35397, Buca/Izmir, Turkey. kuralay@deu.edu.tr



Figure 1. Concept vehicle layout

2 VEHICLE MODEL AND METHODOLOGY

Different road conditions cause changing forces acting upon tire. These conditions of road include continuously strength (CS), bump passing (BP), rough and holed road (RH), acceleration (AC), blocking brake (BB). As a result of various road conditions, pulsed forces act on tires. These forces shown in table 1 as three dimensional vector for 175/70 R13 82T tires. Suspension analysis results also shown is table 1 which maximum stress occurs in bump passing at both front and rear suspensions.

Table 1. Forces acting on suspension systems and maximum stresses

	Road Condition	Vertical Force [N]	Lateral Force [N]	Longitudinal Force [N]	Max Stress [MPa]
Front	CS	4217,1	318,83	651,1	87,996
	BP	5811,2	318,83	651,1	119,31
	RH	4217,1	1020,2	651,1	97,604
	AC	4217,1	-	651,1	91,461
	BB	4217,1	-	1275,3	109,72
Rear	CS	4217,1	318,83	-	154,66
	BP	5811,2	318,83	-	208,95
	RH	4217,1	1020,2	-	178,88
	BB	4217,1	-	1275,3	202,8

Front suspension system has designed as independent Mc Pherson strut. Front suspension model has 7 mm mesh which is generate 37060 nodes and 117371 elements. Lower arm connection with chassis is defined as revolute body-ground. Front lower arm strut connection is defined spherical body-ground with chassis. Connection between wheel carrier and lower arm is also defined spherical body-body which means rotations around all directions are free. Boundary conditions and acting forces based road conditions shown in left picture of figure 2. Maximum stress is 119.31 MPa in bump passing road conditions (figure 2).

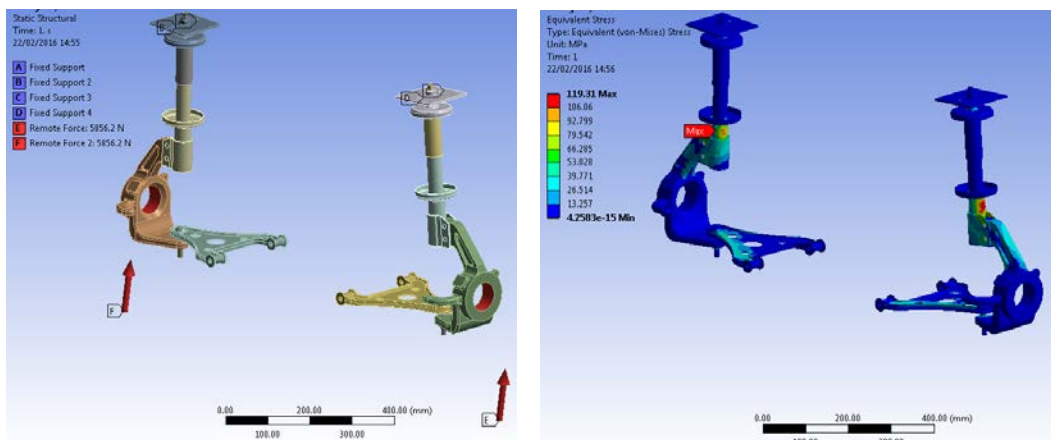


Figure 2. Front suspension model and analysis

Rear suspension has designed as solid axle with panhard rod for its simple construction characteristics. Panhard rod connection is defined as revolute joint body-ground to chassis. U-shape circular profile is connected to brackets as revolute joint body-body and the brackets have fixed support. Also suspension springs are defined body to ground in each suspensions. Because of the vehicle has front wheel drive, acceleration condition haven't examined. Maximum stress is 208.95 MPa in bump passing road conditions which is the same critical condition with front suspension (figure 3).

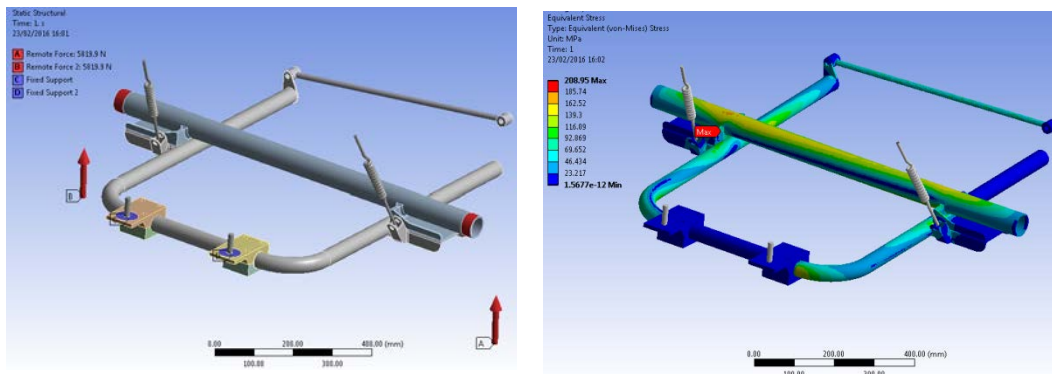


Figure 3. Rear suspension model and analysis

Stress results are far from the yield stress of material so suspension design is proper to use without any modifications on it. Reaction forces on suspension systems are used to chassis analysis. Connection points of front suspension systems are A, B, C₁, C₂, D₁, D₂ and rear suspension systems are E₁, E₂, F₁, F₂, G shown in figure 4. Forces (F) and moments (M) act on X, Y and Z directions based on right side of figure 4 and their values are shown in left side of figure 4.

	A		B	
	F [N]	M [Nm]	F [N]	M [Nm]
X	609,2	4,13	552,1	-20,9
Y	4337	1,12	4293	-0,13
Z	-1615	6,31	-1998	5,01
	D ₁		D ₂	
	F [N]	M [Nm]	F [N]	M [Nm]
X	-218	0	-672	0
Y	-8,06	-11,6	-8,91	-13,1
Z	-360	-2,4	-1389	-0,8
	C ₁		C ₂	
	F [N]	M [Nm]	F [N]	M [Nm]
X	16,22	0	-888	0
Y	-15,9	10,3	-17,2	13,6
Z	-153	-2,9	-1872	-0,1
	F ₁		F ₂	
	F [N]	M [Nm]	F [N]	M [Nm]
X	-1070	-64,7	8458	-64,1
Y	-248	93,3	-1542	91,5
Z	-1045	-54,2	-1008	161,5
	E ₁	E ₂	G	
	F [N]	F [N]	F [N]	M [Nm]
X	-6392	-6347	-28,1	0
Y	6583	6537	174,8	23,5
Z	1607	-1596	1409	52,2

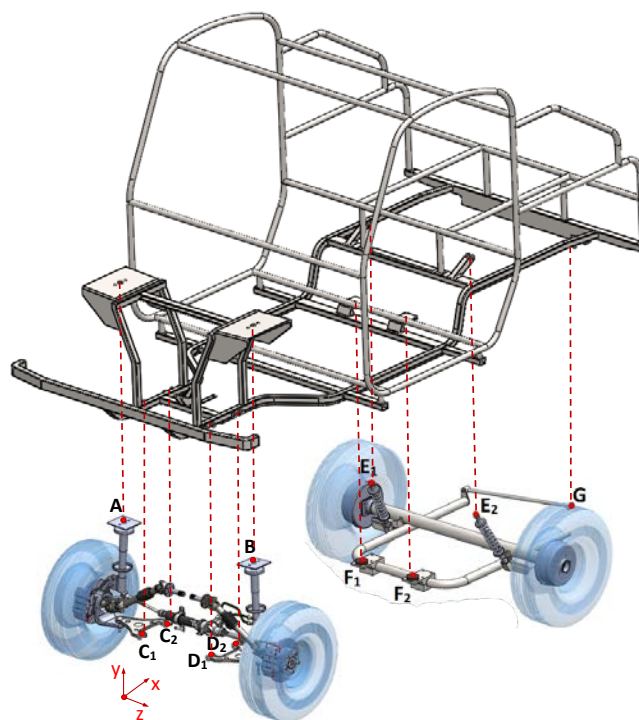


Figure 3. Rear suspension model and analysis

Vehicle chassis has two main carriers which are 30x30 square section with 3 mm thickness and five lateral profile which are 30x40 with same section. Sheet support has welded under main carriers to increase moment of inertia for bending stress. The most critical operating condition have been chosen for chassis under bending stress. The operating condition, which its values of reaction moment and forces shown in the left side of figure 3, is continuously strength for front and bump passing for the rear suspension. Suspension springs are also defined body to ground in Ansys software which means chassis to fixed ground.

3 ANALYSIS RESULTS AND OPTIMIZATION

Stress results are obtained based on the suspension reaction forces that acts on chassis connection points shown in figure 3. Finite element model of chassis have 189972 nodes and 570737 with 7 mm mesh dimensions. Equivalent stress and total deformation results are shown in figure 4 and 5.

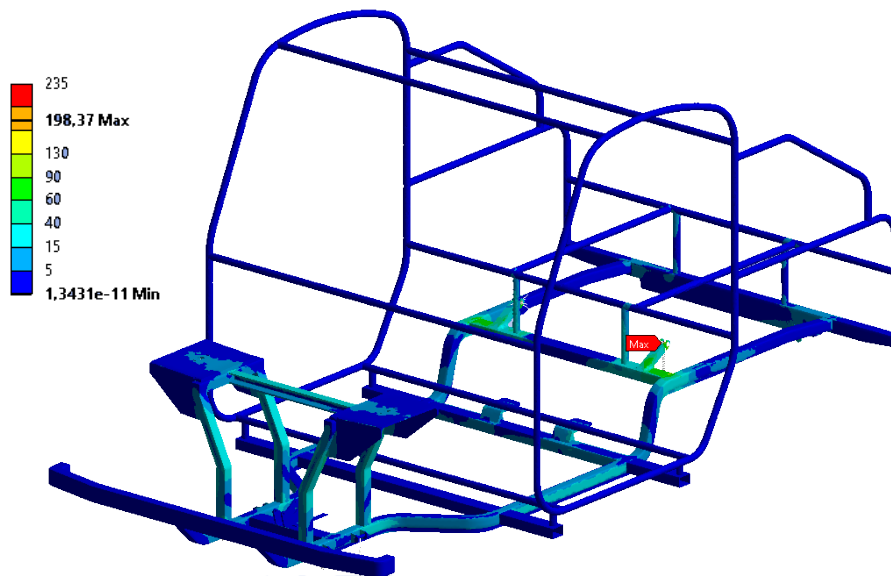


Figure 4. Equivalent stress results of chassis

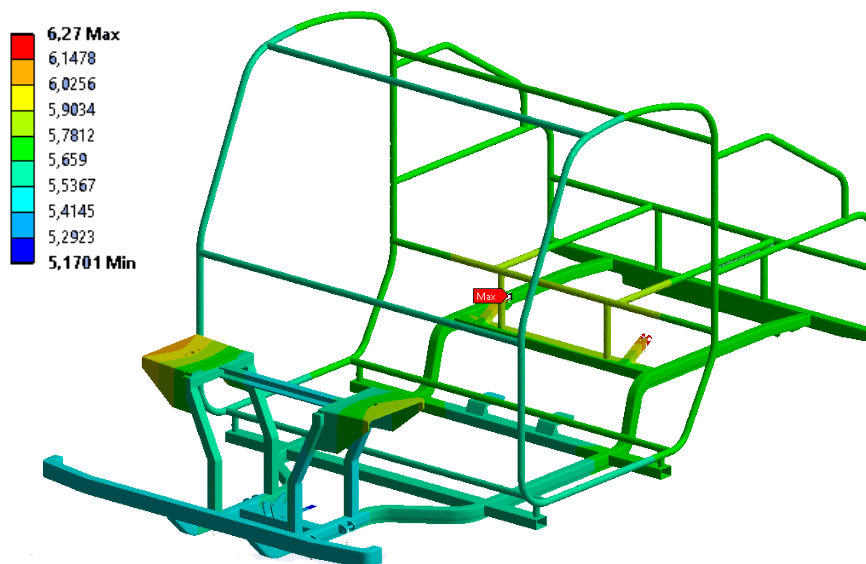


Figure 5. Total deformation results of chassis

Maximum equivalent stress is 198.37 MPa and maximum total deformation is 6.27 mm including with the spring deformations of chassis that has 3 mm thickness. Figure 4 shows also critical part of chassis. Maximum stress and deformation occurs on this part of chassis which is designed parametrically for profile thickness. Thickness parameter (δ_a) is shown in the figure 6. Optimization study investigates stress total deformation results for mass reducing with focused on just critical part. If critical part is strength for reaction forces, other parts of chassis maintain their strength condition. Welding distortions could be occurred on chassis so minimum allowable value of profile thickness is decided as 2 mm to avoid distortions. Welding locations of chassis are defined for all connections but heat or distortion effects of welding are neglected in analysis.

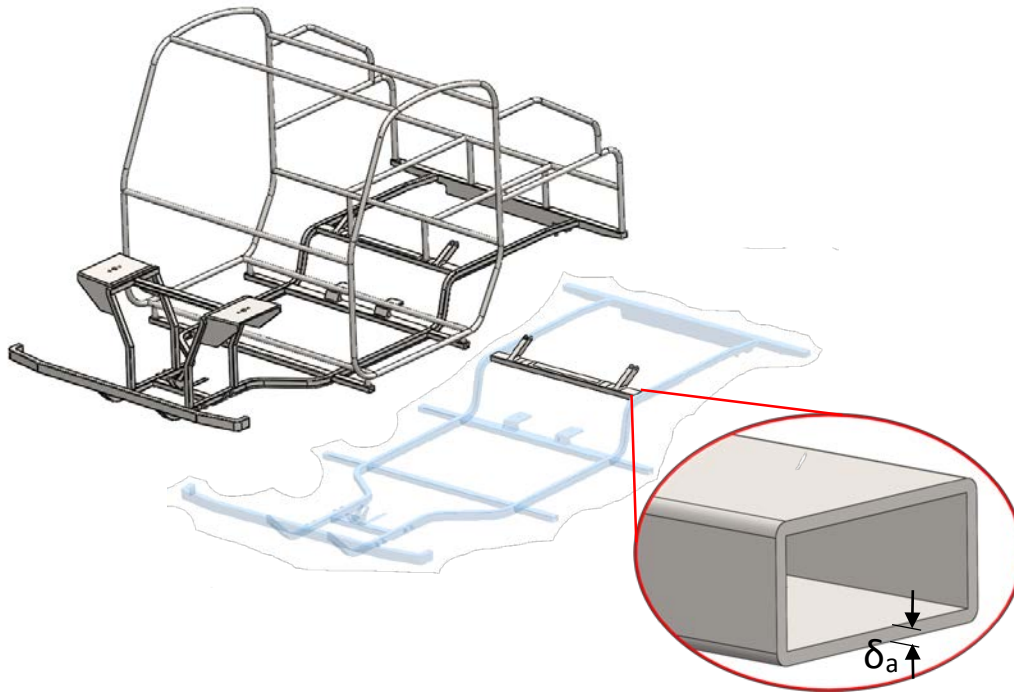


Figure 6. Parametric thickness design for critical part of chassis

Stress and deformation results are shown in figure 7 and figure 8 based on δ_a which is changed between 2 and 4. Stress are increased by changing of thickness parameter.

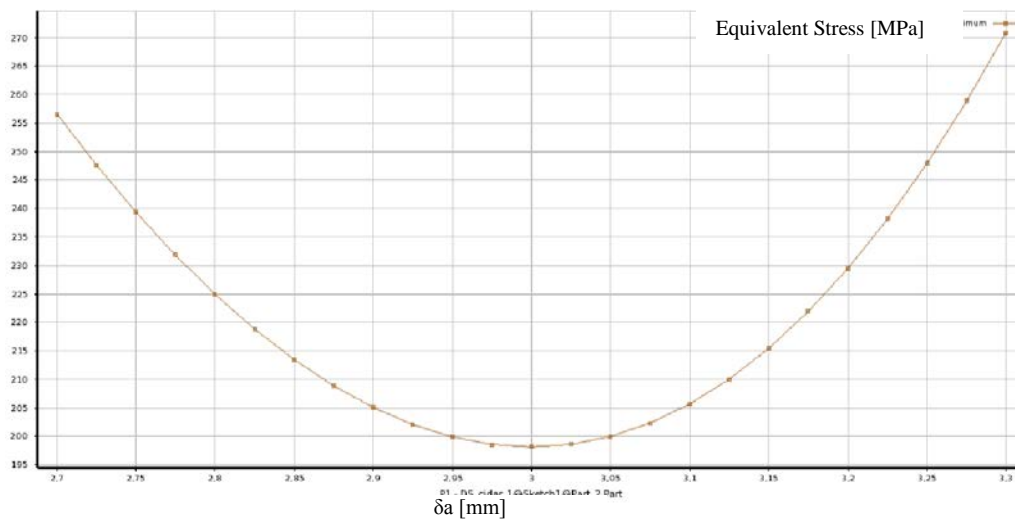


Figure 7. Stress results based on thickness variation of critical part

Stress distributions on chassis are shown in figure 8 when critical part of the chassis has 2 mm thickness. Maximum equivalent stress was located at left rear suspension spring joints as 198.37 MPa which is shown in figure 4. Unlike the stress distributions at first design in figure 4, 323.76 MPa maximum stress is located right part of profile at welding points shown in figure 8. Other profiles of chassis have not higher stresses akin yield stress of the material.

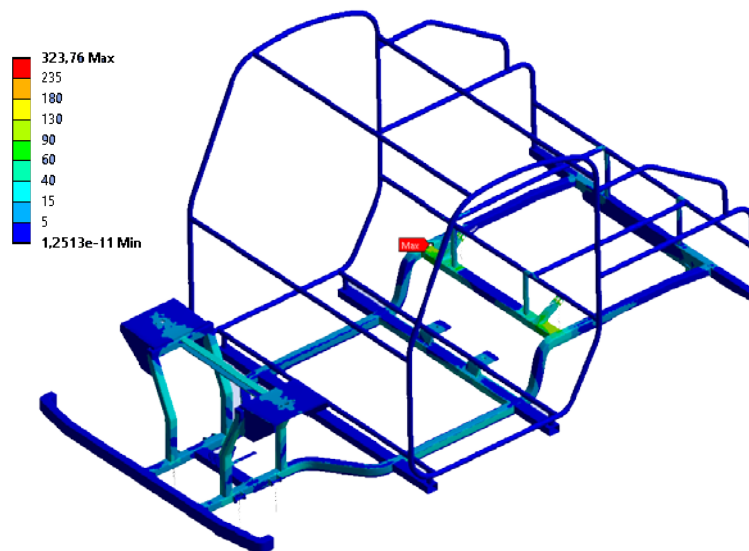


Figure 8. Equivalent stress results of chassis with 2mm thickness of critical profile

CONCLUSIONS

Stress distributions on chassis after the optimization shows maximum 323.76 MPa stress is occurred on welding location of left side of critical profile. Relatively high stress could be decreased by changing welding parameters. On the other hand, 2 mm thickness of profiles achieve for required stress based on material properties. Vehicle mass can reduced that is important parameter for hybrid and electric vehicle. Total weight of carrier chassis and circular profile cabin chassis have 95 kg for the first design. If critical part of chassis, which is 5.5 kg, still remain 3 mm thickness, total weight with other part of carrier chassis is 82 kg for 2 mm profile thickness. Thus 13 kg mass reduction could be achieved after optimization compared to first design.

ACKNOWLEDGMENT

Authors are grateful for the support of **International Conference on Engineering and Natural Science** for helping make this conference possible. The precious contributions of Okan KIRIL, Uğur POLAT and Ömer Y. TURNALI are also acknowledged.

REFERENCES

- [1] N. S. Kuralay, *Motorlu Taşıtlar; Temel ve Tasarım Esasları, Yapı Elemanları, Cilt 1; Tahrik ve Sürüş Sistemleri*, İzmir: TMMOB Makina Mühendisleri Odası, MMO/2008/484, 2008. (In Turkish).
- [2] J. Reimpell, H. Stoll and J. W. Betzler, *The Automotive Chassis: Engineering Principles*, Warrendale, PA: Society of Automotive Engineers, Inc, 2001.
- [3] D. Crococolo, M. D. Agosinis and N. Vincenzi, "Structural Analysis of an Articulated Urban Bus Chassis via FEM: a Methodology Applied to a Case Study," *Strojinski Vestnik- Journal of Mechanical Engineering*, vol. 57, pp. 799-809, 2011.
- [4] R. A. Rahman, M. N. Tamin and O. Kurdi, "Stress Analysis of Heavy Duty Truck Chassis as a Preliminary Data for its Fatigue Life Prediction using FEM," *Jurnal Mekanikal*, vol. 26, pp. 76-85, 2008.
- [5] H. Patel, K. C. Panchal and C. S. Jadav, "Structural Analysis of Truck Chassis Frame and Design Optimization for Weight Reduction," *International Journal of Engineering and Advanced Technology*, vol. 2, pp. 665-668, 2013.
- [6] P. A. Renuke, "Dynamic Analysis of a Car Chassis," *International Journal of Engineering Research and Applications*, vol. 2, pp. 955-959, 2012.
- [7] H. B. Patil, S. D. Kachave and E. R. Deore, "Stress Analysis of Automotive Chassis with Various Thicknesses," *Journal of Mechanical and Civil Engineering*, vol. 6, pp. 44-49, 2013.
- [8] D. Meznar and M. Lazovic, "The Strength of the Bus Structure with the Determination of Critical Points," *Strojinski Vestnik- Journal of Mechanical Engineering*, vol. 56, pp. 544-550, 2010.
- [9] R. H. Myers, D. C. Montgomery and C. M. Anderson-Cook, *Response Surface Methodology, Process and Product Optimization Using Design of Experiments*, 3rd ed., Hoboken, New Jersey: John Wiley & Sons, Inc, 2009.
- [10] M. M. Topaç, H. E. Enginar and N. S. Kuralay, "Reduction of Stress Concentration at the Corner Bends of the Anti-roll Bar by using Parametric Optimization," *Mathematical and Computational Applications*, vol. 16, pp. 148-158, 2011.
- [11] M. S. Agrawal and M. Razik, "Finite Element Analysis of Truck Chassis," *International Journal of Engineering Sciences & Research*, vol. 12, pp. 3432-3438, 2013.
- [12] H. K. Çelik, M. Uçar and A. Cengiz, "Parametric Design, Stress Analysis and Optimization of the housing in Gear Pumps," *Engineer and Machinery*, vol. 49, pp. 15-24. 2008. (In Turkish with an abstract in English).

- [13] S. M. Metev and V. P. Veiko, *Laser Assisted Microtechnology*, 2nd ed., R. M. Osgood, Jr., Ed. Berlin, Germany: Springer-Verlag, 1998.
- [14] J. Breckling, Ed., *The Analysis of Directional Time Series: Applications to Wind Speed and Direction*, ser. Lecture Notes in Statistics. Berlin, Germany: Springer, 1989, vol. 61.
- [15] S. Zhang, C. Zhu, J. K. O. Sin, and P. K. T. Mok, "A novel ultrathin elevated channel low-temperature poly-Si TFT," *IEEE Electron Device Lett.*, vol. 20, pp. 569–571, Nov. 1999.
- [16] M. Wegmuller, J. P. von der Weid, P. Oberson, and N. Gisin, "High resolution fiber distributed measurements with coherent OFDR," in *Proc. ECOC'00*, 2000, paper 11.3.4, p. 109.
- [17] R. E. Sorace, V. S. Reinhardt, and S. A. Vaughn, "High-speed digital-to-RF converter," U.S. Patent 5 668 842, Sep. 16, 1997.
- [18] (2007) The IEEE website. [Online]. Available: <http://www.ieee.org/>
- [19] M. Shell. (2007) IEEEtran webpage on CTAN. [Online]. Available: <http://www.ctan.org/tex-archive/macros/latex/contrib/IEEEtran/>
- [20] *FLEXChip Signal Processor (MC68175/D)*, Motorola, 1996.
- [21] "PDCA12-70 data sheet," Opto Speed SA, Mezzovico, Switzerland.
- [22] Karnik, "Performance of TCP congestion control with rate feedback: TCP/ABR and rate adaptive TCP/IP," M. Eng. thesis, Indian Institute of Science, Bangalore, India, Jan. 1999.
- [23] J. Padhye, V. Firoiu, and D. Towsley, "A stochastic model of TCP Reno congestion avoidance and control," Univ. of Massachusetts, Amherst, MA, CMPSCI Tech. Rep. 99-02, 1999.
- [24] *Wireless LAN Medium Access Control (MAC) and Physical Layer (PHY) Specification*, IEEE Std. 802.11, 1997

Neural Network Approach for Inverse Kinematic of a 4-DOF Lighting Manipulator

Nihat Cabuk¹, Veli Bakircioglu², Faruk Sen³

Abstract

Inverse kinematic is a challenging problem of robots. The inverse kinematics in robotic is the determination of joint angles for a desired position of the end effector. This paper proposes an Artificial Neural Network (ANN) model to find Inverse kinematic solution of a 4-DOF manipulator, which is designed instead of a manually lighting system that is used in surgery rooms. After obtaining forward kinematic equations, these equations were used to derive training data of ANN. Manipulator was designed in a computer aided design (CAD) program and this CAD model transferred to Simulink environment for a realistic and visual simulation purpose. To evaluate the trained ANN performance visually, this Simulink model were used. A test input set is introduced to the trained ANN. Results are discussed and demonstrated graphically. It was observed that obtained results are satisfactory, and the error of ANN for a reference position is acceptable.

Keywords: CAD, ANN, Inverse kinematic

1. INTRODUCTION

Inverse kinematic (IK) is a challenging problem in robotics. Schematic representation of IK is illustrated in Fig.1. For redundant manipulators, to obtain IK problem solution is more complex and difficult. Complexity of the IK problem is related to manipulators geometry and redundancy. Redundant manipulators have more degrees of freedom than required for position and orientation. Thus, there are multiple solutions for this problem and this leads to manipulator control challenges. Generally, there are three methods to solve IK problems. First one is the algebraic method, second one is the iterative method, and finally third one is the geometric method [1-12]. Each method has advantages and

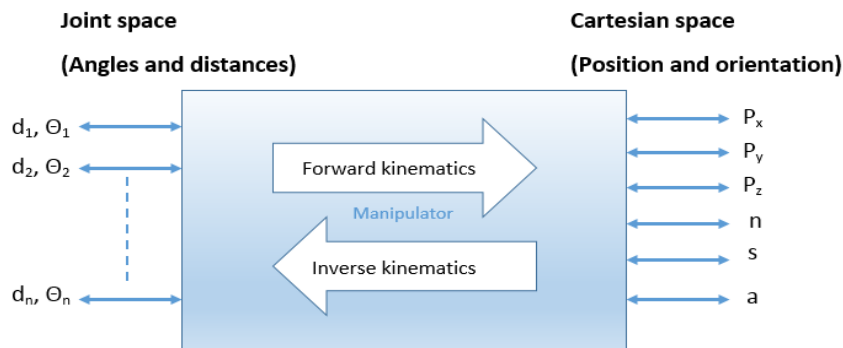


Figure 1. Schematic representation of IK

disadvantages. Algebraic method doesn't guarantee the closed-form solution. Geometric method only guarantees closed-form solution of first three joint of the manipulator. Iterative methods returns one solution related to starting point and has high computational cost. Therefore many researchers focused on Artificial Neural Network (ANN) to solve IK problems. In the literature, there are many papers studied on ANN based IK solution of redundant manipulators. [1-15] ANNs have been widely used in many different fields [15-16-17-18] and they are very powerful tool to represent correlation between inputs and outputs. Especially, ANNs have been used for highly non-linear and uncertain systems. In robotics, ANNs have been used to redundancy, singularities and complex inverse kinematic problems. [8-10]

2 PROBLEM DEFINITION

¹ Corresponding author: Aksaray University, Technical Science VA&T School, 68100, Aksaray Turkey. nihatcabuk@aksaray.edu.tr

²Aksaray University, Technical Science VA&T School, 68100, Aksaray Turkey. vbakircioglu@aksaray.edu.tr

³Muğla Sıtkı Koçman University, Technology Faculty, Department of Energy Systems Engineering, 48100, Muğla Turkey. faruksen@mu.edu.tr

The manipulator under studied in this paper is an industrial and medical robot consists of a set of rigid links connected together by four rotational joints. 3D model of the manipulator is shown in Fig.2. Each joints are actuated by individual motors. Each joint working ranges given in Table.1. The lighting robot could be used in medical operation rooms for surgical operations.

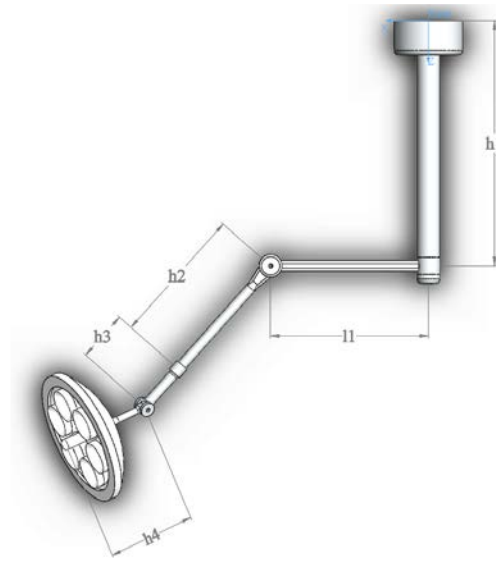


Figure 2. Automatically positioning lighting manipulator.

Denavit-Hartenberg parameters for the manipulator are given in Table.1. The forward kinematic equations for the manipulator that are derived by D-H parameters are given in Eq.1-3.

Table 1. D-H Parameters for the manipulator.

Link i	α_{i-1} (rad)	a_{i-1} (m)	d_i (m)	θ_i (rad)	Variable	Joint Angle Range
1	0	0	0.486	θ_1	θ_1	$\pi/6 - \pi/3$
2	$-\pi/2$	0.690	0	θ_2	θ_2	$0 - \pi/6$
3	$\pi/2$	0	0.572	θ_3	θ_3	$0 - \pi/6$
4	$-\pi/2$	0	0.254	θ_4	θ_4	$0 - \pi/6$
5	$\pi/2$	0	0.318	0	-	-

$$P_x = l_1 c\theta_1 - h_4 (s\theta_4 (s\theta_1 s\theta_3 - c\theta_1 c\theta_2 c\theta_3) - c\theta_1 c\theta_4 s\theta_2) + h_2 c\theta_1 s\theta_2 + h_3 c\theta_1 s\theta_2 \quad (1)$$

$$P_y = l_1 s\theta_1 + h_4 (s\theta_4 (c\theta_1 s\theta_3 + c\theta_2 c\theta_3 s\theta_1) + c\theta_4 s\theta_1 s\theta_2) + h_2 s\theta_1 s\theta_2 + h_3 s\theta_1 s\theta_2 \quad (2)$$

$$P_z = h_1 + h_4 (c\theta_2 c\theta_4 - c\theta_3 s\theta_2 s\theta_4) + h_2 c\theta_2 + h_3 c\theta_2 \quad (3)$$

Eq.1-3 define the coordinates of the end-effector in the base frame attached to the base of the manipulator. Generally, end effector performs tasks in the Cartesian coordinate system, which is controlled by joint coordinate system. For positioning the manipulator at a desired position in the workspace, each joint angles must derived by IK.

3 METHODOLOGY

This study presents a solution for the inverse kinematics problem based on ANN. A feed-forward multi-layer perceptron with backpropagation neural network is selected for this research. An IK solution for a lighting robot is developed by training the neural network with the robot's end-effector Cartesian coordinates at base frame and its corresponding joint configurations. Training data set for ANN was obtained in the MATLAB environment from forward kinematic relations which is given in Eq.1-3. Points obtained from forward kinematic were used for inputs and corresponding joint angles were used for outputs. These points were obtained for the entire workspace of the manipulator with a joint angle resolution of 0.05π . Finally, 296352 different points in the Cartesian coordinate are obtained as inputs of ANN and same amount of the angle values in the joint space was used as targets of the ANN.

ANN implementation was performed in MATLAB environment. Neural Fitting app is a powerful built-in tool in MATLAB to solve input-output fitting problems with a two-layered feed-forward neural networks. This tool uses Levenberg-Marquardt backpropagation algorithm to train network and has sigmoid hidden neurons for the hidden layer and linear output neurons for the output layer [7-9]. Simple schematic representation of the ANN structure is shown in Fig.3. ANN model consists 3 inputs and 4 outputs with 296352 samples. %70 of samples were used for training data and %15 for validation data and %15 for test data which was needed for the Neural Fitting app.

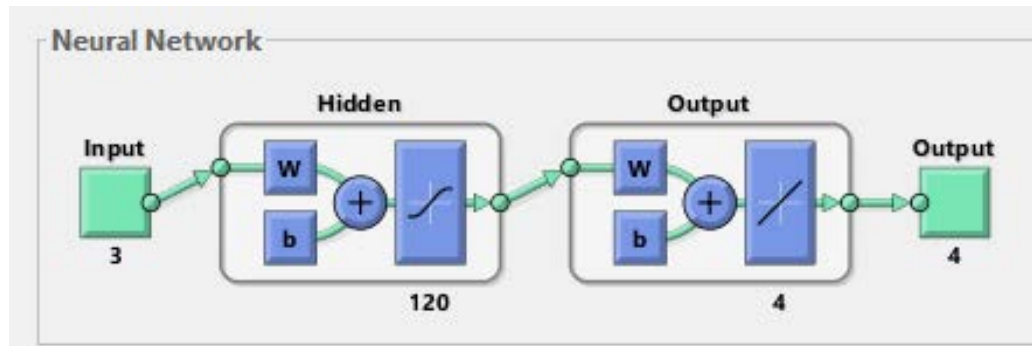


Figure 3. Schematic Representation of the ANN structure.

4 RESULTS

For a comparative study, training was performed for different neuron numbers in the hidden layer. Comparisons of the neural networks with different neuron numbers in the hidden layer are given in Table.2. As seen in the Table.2, while neuron numbers are increased, better training performance is obtained as expected. After a trial and error study, the network that has 120 neuron numbers in the hidden layer offers acceptable errors. Thus, this network used for IK predictions in this paper. In Figure 4, Regression graphics of the network is presented, which compares the target values and the network output values.

Table.2 Neural Network Training Results Comparison

Neuron Numbers in Hidden Layer	12	24	36	72	96	110	120
Overall Mean Square Error	0.0230	0.0224	0.0221	0.0217	0.0216	0.0216	0.0215
Training Performance	0.0230	0.0224	0.0221	0.0217	0.0216	0.0216	0.0215
Testing Performance	0.0230	0.0223	0.0219	0.0219	0.0218	0.0217	0.0215
Validation Performance	0.0228	0.0225	0.0222	0.0220	0.0215	0.0217	0.0217
Overall Regression Value	0.9513	0.9525	0.9532	0.9538	0.9542	0.9542	0.9543

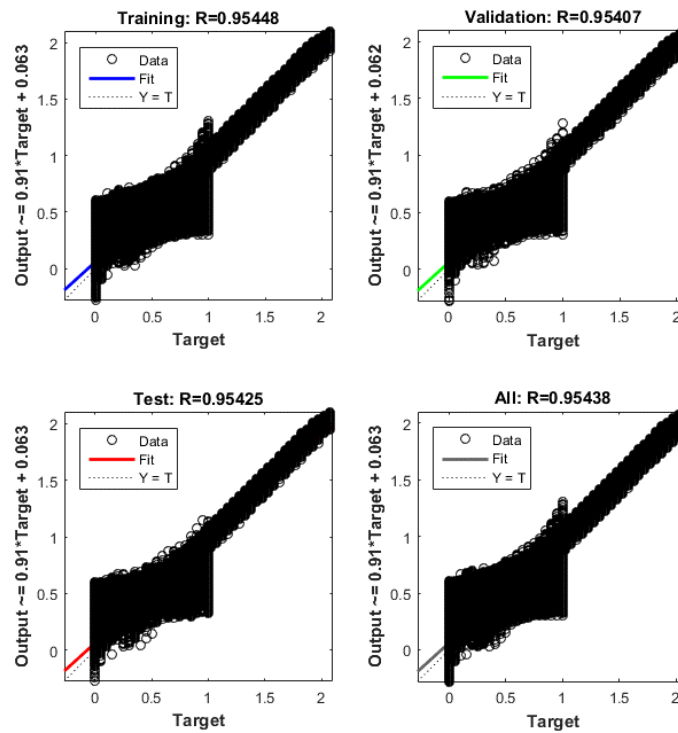


Figure 4. Regression Graphic

Once the network is trained, a test input set is introduced to the trained networks to predict the joint angles. Joint angle prediction results and position errors are given for different sample points in Table.3

Table.3. Predicted Joint Angles and Position Errors

Theta	Cartesian Position (m)			Predicted Angle (rad)	Predicted Position (m)			Error (mm)		
	X	Y	Z		X	Y	Z	X	Y	Z
θ_1				0.7975						
θ_2	0.8935	0.9947	1.4070	0.5162	0.8931	0.9984	1.4045	0.4	-3.7	2.5
θ_3				0.4845						
θ_4				0.4048						
θ_1				0.6045						
θ_2	0.9834	0.7752	1.4462	0.4094	0.9895	0.7765	1.4424	-6.1	-1.3	3.8
θ_3				0.5054						
θ_4				0.5200						

After achieved reliable predictions for a set of sample points, a desired trajectory in Cartesian space introduced to trained network to simulate. A rectangle-shaped path in the manipulator workspace was chosen as trajectory. Simulation performed in MATLAB/Simulink environment. In Fig.5, Simulink block diagram is presented. In the Simulink model, trained network executes joint angle prediction for a reference trajectory input. Output of the network is used as controller input. Simulink model output and reference trajectory for the manipulator are represented in Fig.6. As seen in Fig.6, tracking error for actual trajectory is satisfactory.

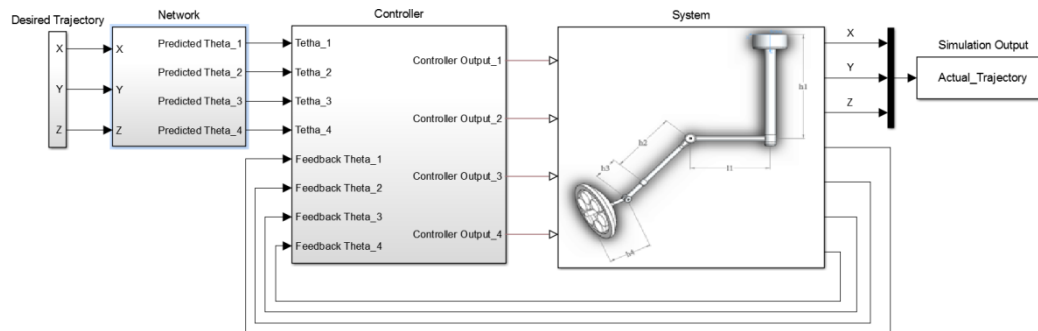


Figure 5. Block diagram of the Simulink model

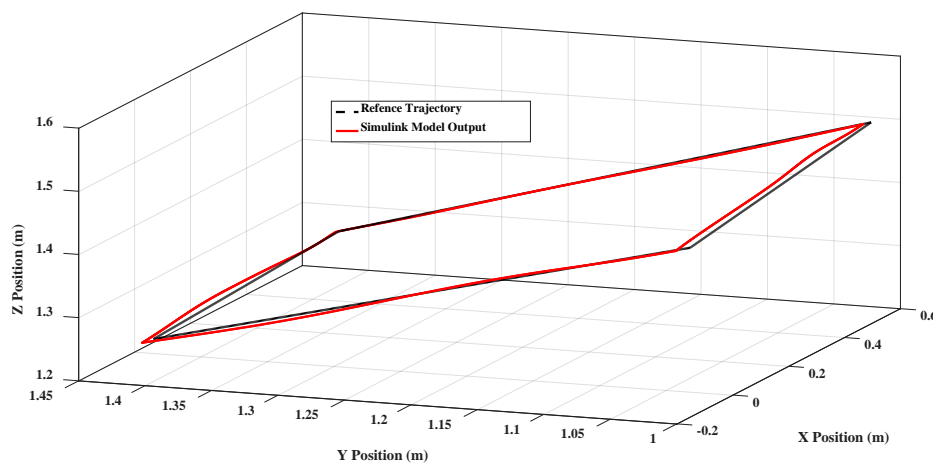


Figure 6. Desired Trajectory and Actual Trajectory

7 CONCLUSION

This paper aim is to find IK solution of a 4-DOFs lighting manipulator that is designed for medical operation lighting. In this context, an ANN trained for the IK solution of the manipulator. Training performed in MATLAB environment with 296352 samples. Neural Fitting App was used to construct the network which is a MATLAB built-in app. After testing different neuron numbers in the hidden layer, the network with 120 neuron numbers in the hidden layer was used to predict joint angles. After achieved reliable predictions, for the desired trajectory of the manipulator, the networks can generate the IK solutions of this pre-specified trajectory. Simulation results show that the presented approach can do the locomotion with a good performance of track error.

ACKNOWLEDGMENT

This study was conducted from Nihat Çabuk's Master of Science Thesis "Design of Robot Arm Following Manually Controlling Medical Lighting".

REFERENCES

- [1] S. Alavandar, M.J. Nigam “Inverse Kinematics Solution of 3DOF Planar Robot using ANFIS” Int. J. of Computers, Communications & Control, Vol. III Suppl. issue: Proceedings of ICCCC, pp. 150-155, 2008
- [2] Z. Bingul, H.M. Ertunc, C. Oysu “Applying Neural Network to Inverse Kinematic Problem for 6R Robot Manipulator with Offset Wrist” Adaptive and Natural Computing Algorithms, pp. 112-11, 2005
- [3] Ş. Yildirim, I. Eski, “A QP Artificial Neural Network Inverse Kinematic Solution for Accurate Robot Path Control” Journal of Mechanical Science and Technology Vol. 20, No. 7, pp. 917-928, 2006
- [4] R. Köker “A Genetic algorithm approach to a neural-network-based inverse kinematics solution of robotic manipulators based on error minimization” Information Sciences 222 pp 528-543, 2013
- [5] R. Köker “A neuro-genetic approach to the inverse kinematics solution of robotic manipulators” Scientific Research and Essays Vol. 6 (13), pp. 2784-2794, 4 July, 2011
- [6] A.V. Duka “Neural network based inverse kinematics solution for trajectory tracking of a robotic arm” Procedia Technology 12 The 7th International Conference Interdisciplinarily in Engineering (INTER-ENG 2013) pp. 20 – 27, 2014
- [7] Z. Bingül, O. Karahan “A Fuzzy Logic Controller tuned with PSO for 2 DOF robot trajectory control” Vol. 38, Issue 1, pp. 1017–1031, January 2011
- [8] S. Yahya, M. Moghavvemi, “Artificial neural networks aided solution to the problem of geometrically bounded singularities and joint limits prevention of a three dimensional planar redundant manipulator” Neuro Computing 137, pp. 34-36, 2014
- [9] S. Küçük, Z. Bingül “Inverse kinematic solutions for industrial robot manipulators with offset wrists” Applied Mathematical Modeling 38 pp. 1983-1999, 2014
- [10] L. Aggarwala, K. Aggarwala, R. J. Urbanica “Use of artificial neural networks for the development of an inverse kinematic solution and visual identification of singularity zone(s)” Procedia CIRP 17 pp. 812 – 817, 2014
- [11] Ş. Yıldırım “Adaptive robust neural controller for robots” Robotics and Autonomous Systems 46 pp. 175–184, 2004
- [12] Y. I. Al Mashhadany “ANFIS-Inverse-Controlled PUMA 560 Workspace Robot with Spherical Wrist” International Symposium on Robotics and Intelligent Sensors 2012 (IRIS 2012) Procedia Engineering 41 pp. 700 – 709, 2012
- [13] R. Köker, C. Öz, T. Çakar, H. Ekiz “A study of neural network based inverse kinematics solution for a three-joint robot” Robotics and Autonomous Systems 49 pp. 227–234, 2004
- [14] H. Chaudhary, R. Prasad, N. Sukavanum “Position analysis based approach for trajectory tracking control of scrobot-er-v plus robot manipulator” International Journal of Advances in Engineering & Technology, Vol. 3, Issue 2, pp. 253-264, May 2012.
- [15] N-B. Hoang, H-J Kang “Neural network-based adaptive tracking control of mobile robots in the presence of wheel slip and external disturbance force” Neuro computing 188, pp. 12-22, 2016
- [16] M. Karaatlı, M. Albeni “Forecasting rose flower planting areas using artificial neural networks” Akdeniz University International Journal of Alanya Faculty of Business, Vol.3, No.2, pp.137-149, 2011
- [17] B. Karlık, S. Cemal “Diagnosing diabetes from breath odor using artificial neural networks” Türkiye Klinikleri J Med Sci 32(2):331(6), 2012
- [18] Ş. Çakır, H.M. Ertunç, H. Ocak “A Case Study for Identification of Texture in Carbonate Rocks Using Artificial Neural Networks: Akveren Formation” Uygulamalı Yerbilimleri Vol. 2, pp.71-79 Oct-Nov 2009

Analysis of desiccant cooling systems with various configurations for different locations in Europe

Arif Ozbek¹, Ertac Hurdogan, Osman Kara, Orhan Buyukalaca

Abstract

Solid desiccant cooling systems has become suitable for typical hot and humid climate in the world, especially Turkey. The development of the technology was caused by the contribution of refrigerants used in conventional cooling systems to the depletion of the ozone layer. The desiccant cooling systems composed mainly of a desiccant wheel, heat exchangers, humidifier and fans. In this study, different configurations of desiccant cooling systems are evaluated by using model developed by the authors. Performance of the systems are investigated and compared with each other for different locations in Europe and results are considered.

Keywords: *Dehumidification, Air conditioning, COP, Desiccant*

1. INTRODUCTION

Increasing energy consumption in cooling applications is one of the prime concerns of the present age all over the world. Environmental issues associated with the production of high grade electrical energy and increasing demand for cooling applications have thrown researchers to investigate newer technologies for air conditioning. Desiccant cooling is an approach for air conditioning towards resolving the environmental and economic issues of the conventional vapor compression cooling systems [1]. In addition, evaporative and desiccant cooling technologies for air conditioning systems have increased as an alternative or as an addition to conventional vapor compression systems. These systems are mainly used in places where thermal energy sources are easily found, where the price of electrical power is high, the latent heat percentage is high or the needed dew point of the air is low [2]. Desiccant air conditioning systems can be classified into two categories, solid and liquid desiccant air conditioning systems. These technologies have been used widely; because of being advantageous in handling latent heat load [3]. Desiccant cooling systems were studied experimentally and theoretically by several researchers. In these studies, it was shown that desiccant cooling systems is suitable for hot and humid environment conditions [4-6]. Desiccant air-conditioning systems do not use harmful to the environment refrigerants, neither do they consume electrical energy for the cooling process, but thermal energy, in temperature levels that favor the use of solar energy, and more specifically flat plate solar collectors [7].

Desiccant cooling systems can be categorized based on operating cycles, such as ventilation, recirculation, dunkle cycles and etc. [3]. Performance of desiccant cooling systems with different operation cycle was evaluated by many researchers. Jain et al. [8] investigated various solid desiccant cycles (the ventilation cycle, the recirculation cycle, the Dunkle cycle and the wet surface heat exchangers cycle (SENS cycle)) for various outdoor conditions of many cities in India. It was shown that performance (COP) is 2.63 for wet surface heat exchangers cycle, while it is 0.46 for Dunkle cycle. Meckler [9] has proposed a two-stage solid desiccant air conditioning system integrating with a HVAC system. It was reported that 30–50% of the dehumidification task could be accomplished by the enthalpy exchanger. Sheridan and Mitchell [10] have analyzed the performance of a hybrid desiccant cooling system for hot-humid and hot-dry climates. The results showed that the energy savings ranged from 20% to 40% in high sensible heat load applications and the hybrid system saved more energy in a hot-dry climate than that in a hot-humid climate, where it might even use more energy than a conventional system. In another study, Hong et al.[11] were studied the performances of the two different hybrid cycles (vapor compressor and desiccant cooling system; vapor compressor, desiccant and direct evaporative cooler cooling system) in China. They showed that more energy was saved in hot, dry climates and less was saved in hot, humid climates for the conventional hybrid cycles, while the solar hybrid cycles always saved more energy than conventional vapor compression cycles.

In this study, two different desiccant cooling systems (which are the most used [12-13]) were evaluated. In the analysis, EES (Engineering Equation Solver) and FORTRAN Programing Language were used. Performance of the systems are evaluated and compared with each other for different locations in Europe.

¹Corresponding author: Cukurova University, Ceyhan Engineering Faculty, Mechanical Engineering Department, 01330 Adana, Turkey. arozbek@cu.edu.tr

2. MATERIAL AND METHOD

Desiccant Cooling Systems (DCS) mainly consists of rotary desiccant dehumidifier, heat exchangers, humidifier (evaporative coolers), fans, control units and channels. In this study, two different desiccant cooling systems (DCS1 and DCS2) are considered.

Figure 1 shows the schematic view of DCS1. This system is known as Pennington cycle in the literature [3]. In the system, two separate air channels are used for fresh (process 1-5) and regeneration (process 6-11) air streams. Fresh air channel is used to supply fresh air to the air-conditioned room. Regeneration air channel is used to remove moisture of desiccant wheel. The rotary desiccant wheel is followed by heat exchanger to pre-cool the fresh air in the fresh air channel. After heat exchanger, humidifier-1 is utilized to cool the fresh air to the blowing temperature. Humidity of the fresh outside air (state 1) is absorbed by the desiccant material of the wheel. The fresh air leaves the process side of the desiccant wheel (state 2) hotter, and much drier than when entering the system. The dry fresh air is pre-cooled by the regeneration air in heat exchanger (process 2-3) where it is further pre-cooled by the evaporatively cooled waste air, and then fresh air enters into humidifier-1 (process 3-4) in which it is cooled down to blowing conditions and supplied to the conditioned room (state 5). The air sucked from the indoor (state 6) into the regeneration air duct is evaporatively cooled before entering into heat exchanger in order to increase the cool recovery (process 7-8). In heat exchanger (process 8-9), due to the heat transfer from the fresh air to the waste air, temperature of the fresh air decreases and that of the regeneration air increases. After regeneration air is leaved from the heat exchanger, electric heater is used for heating the regeneration air (state 9). Hot regeneration air is used for removing moisture at the desiccant wheel (process 10-11). After the regeneration air passes from the desiccant wheel, its moisture contents increase and finally it is discharged to atmosphere. In this model, evaporative cooling is integrated in process air stream that prepare cooled and comfort air for indoor, cools to a temperature at or near the wet bulb temperature depending on its effectiveness before entering the heat recovery in order to improve the cooling performance [13].

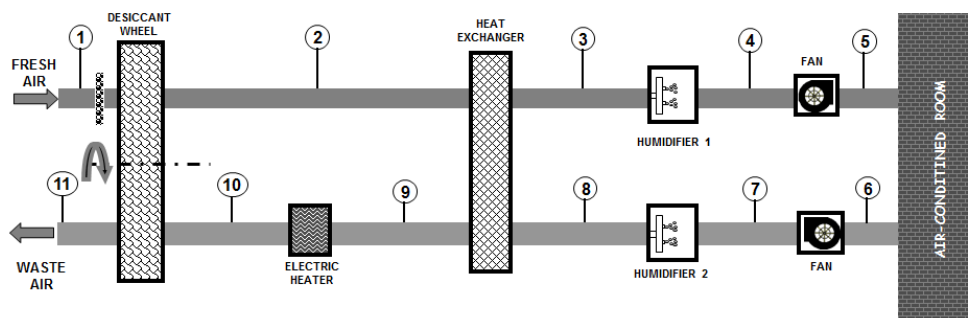


Figure 1. Schematic representation of DCS1.

Figure 2 illustrates the schematic view of DCS2. There are two main differences between DCS1 and DCS2 in terms of main equipment. Firstly, three air channels which is composed fresh air (process 1-6), waste air (process 7-10) and regeneration air (process 11-17) are used in DCS2. Secondly, vapor compression refrigeration (heat exchangers 3) is placed in DCS2. Sensible cooling of the fresh air is carried out (process 4-5) in a cooling coil, which is fed by chilled water from a chiller unit. However, the fresh air is passed through two recuperative type heat exchangers (heat exchangers 1 and 2) before coming to the cooling coil for cool recovery. In the recuperators, only sensible heat is removed from the fresh air, and therefore, humidity ratio of the air remains constant. The desired blowing temperature of the fresh air (state 6) is obtained in the cooling coil. The surface temperature of the cooling coil is always kept higher than the dew point temperature of the fresh air entering into the cooling coil. Therefore, only sensible cooling is performed in the coil (dry coil application). Moisture from the fresh air (latent cooling) is removed only in the desiccant wheel and there is no change in the humidity ratio of the fresh air after the desiccant wheel [12].

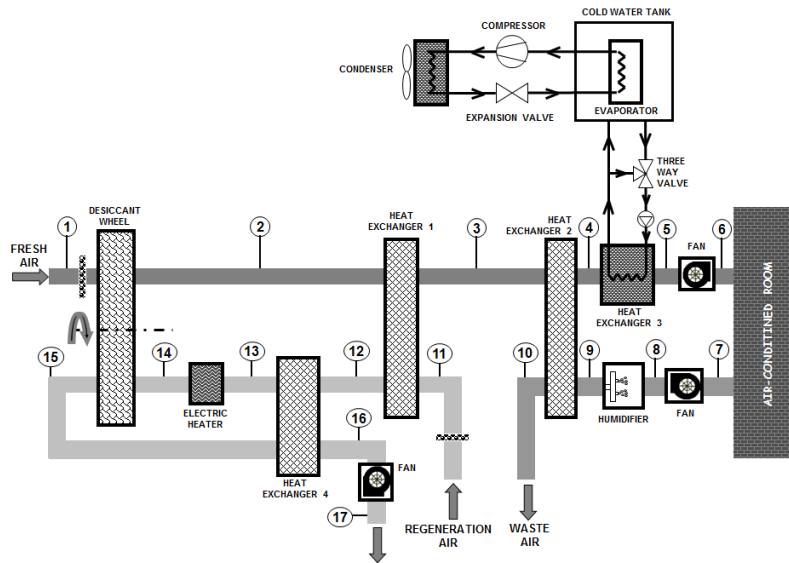


Figure 2. Schematic representation of DCS2.

2.1. Performance Calculations

In the analysis, various calculations (effectiveness of the heat exchangers and humidifier, cooling capacity, COP, etc) are carried out to determine the performance of the system and its components.

The effectiveness of the heat exchangers (η_{HE}) are determined by;

$$\eta_{HE} = \frac{\dot{Q}}{\dot{Q}_{max}} \quad (1)$$

where \dot{Q} is the amount of actual heat transfer and \dot{Q}_{max} is the maximum possible heat transfer:

$$\dot{Q} = \dot{m}_p (T_i - T_o) \quad (2)$$

$$\dot{Q}_{max} = \dot{C}_{min} (T_{hi} - T_{ci}) \quad (3)$$

\dot{C}_{min} is the minimum of the capacitance rate of cold (\dot{C}_c) and hot (\dot{C}_h) air streams:

$$\dot{C}_h = \dot{m}_h c_{ph} \quad (4)$$

$$\dot{C}_c = \dot{m}_c c_{pc} \quad (5)$$

The effectiveness of humidifier (η_{EC}) is determined by [14]:

$$\eta_{EC} = \frac{T_i - T_o}{T_i - T_{wi}} \quad (6)$$

where T_{wi} is the wet bulb temperature of the air at the inlet of humidifier; T_i and T_o is the dry bulb temperature of the air at the inlet and outlet of humidifier.

Electric heater capacity of a desiccant cooling system \dot{Q}_E is obtained from:

$$\dot{Q}_E = \dot{m}_r (h_{eo} - h_{ei}) \quad (7)$$

where \dot{m}_r is the mass flow rate of the regeneration air stream; h_{eo} and h_{ei} is the enthalpy of the air at the inlet and outlet of electric heater.

Cooling capacity of a desiccant cooling system \dot{Q}_{CC} is obtained from:

$$\dot{Q}_{CC} = \dot{m}_f (h_b - h_f) \quad (8)$$

where \dot{m}_f is the mass flow rate of the fresh air stream, h_b is the enthalpy of the air at the inlet of air-conditioned room and h_f is the enthalpy of the ambient air.

The coefficient of performance (COP) of the systems is defined as the ratio between the cooling capacity obtained and total energy input (\dot{E}_{tot}) to the system:

$$COP = \frac{\dot{Q}_{CC}}{\dot{E}_{tot}} \quad (9)$$

\dot{E}_{tot} is the sum of energy consumption of regeneration heat (\dot{Q}_{reg}), fans (\dot{W}_{fan}), compressor of the vapor compression refrigeration cycle (\dot{W}_{com}) for configuration3 and other electrical components (\dot{W}_{oth}):

$$\dot{E}_{tot} = \dot{Q}_{reg} + \dot{W}_{fan} + \dot{W}_{com} + \dot{W}_{oth} \quad (10)$$

In this study, since electric heaters are used to simulate regeneration heat source, the heat input for the regeneration is almost same as power consumption of electric heaters (\dot{W}_{eh}) when the daily total values are considered ($\dot{Q}_{reg} = \dot{W}_{eh}$).

3. RESULTS AND DISCUSSION

DCS1 and DCS2 were selected to investigate the performance of system under different climatic conditions (Nice, Napoli and Sarajevo) for Europe. Cooling design values for Nice (France), Napoli (Italy) and Sarajevo (Bosnia and Herzegovina) are taken from [15]. Moreover, some values used in the calculations as input data are given Table 1. The obtained results for Nice, Napoli, and Sarajevo are given in Figure 3-8 for DCS1 and DCS2 on psychometric chart.

Table 1. The values used in the calculations

Parameter	Value
Total cooling load of the air-conditioned room (kW)	10
Design dry bulb temperature (°C) and relative humidity (%) of the air-conditioned room	26 - 50
Flow rate of the fresh air (m ³ /h)	4000
Flow rate of the exhaust air (m ³ /h)	4000
Flow rate of the regeneration air (m ³ /h)	4000
Effectiveness of the recuperators (%)	65
Effectiveness of the regenerator (%)	85
Sensible heat ratio of the air-conditioned room	0.9
Effectiveness of the evaporative cooler (%)	90
Efficiency of the fans (%)	60
Powers of the fans (kW) (Fresh-Waste-Regeneration)	3-1-4

Figure 3 shows all the processes of DCS1 on psychometric chart for Nice. Fresh ambient air (28°C dry bulb temperature, 60 % relative humidity) is sucked into the desiccant wheel. After the dehumidification process, the dry bulb temperature of fresh air increases to 51.8°C and relative humidity decreases to 8.29 %. The fresh air leaves heat exchanger at 26.16°C. The fresh air enters into humidifier in order to obtain the desired blowing temperature (18.96°C). The waste air is humidified (92.96 % relative humidity) in order to increase saving during heat exchanger. In the humidifier the waste air cools down to 19.79°C. The dry bulb temperature of regeneration air is increased to 40.62°C in heat exchanger. In order to remove moisture in the desiccant wheel, the dry bulb temperature of the air is increased to 70°C with the help of electric heaters. Regeneration air leaves the desiccant wheel at 46.48°C, before discharged to the outdoors. Similar results were obtained for Napoli (Figure 4) because cooling design values in Nice and Napoli are close each other. As can be seen from Figure 5, dehumidification process is very short because of low ambient humidity ratio in Sarajevo. Moisture of ambient air must be removed before enter to the conditioned room, because air cools down to blowing conditions by humidification process. Figure 6 presents results for DCS2 on psychometric chart for Nice. The fresh air leaves heat exchanger 1 and 2 at 33.05°C and 24.21°C, respectively. After heat exchanger 2, the fresh air enters into heat exchanger 3 in order to obtain the desired blowing temperature (18.96°C). The air, which is sucked from the air-conditioned room, gets hotter (26.3°C) while passing through the fan. The waste air is humidified (93.28 % relative humidity) in order to increase saving during heat exchanger 2. In the humidifier the waste air cools down to 19.56°C. The waste air leaving the heat exchanger 2 is rejected to the outdoors (28.33°C dry bulb temperature and 55.05 % relative humidity). In regeneration process; the dry bulb temperature of regeneration air is increased to 37.33 in heat exchanger 1 and to 53°C in the rotary regenerator. Regeneration air leaving the desiccant wheel comes to the rotary regenerator and cools down to 41.34°C, before discharged to the outdoors. Similar results were obtained again for DCS2 in Napoli. As it is shown from Figure 8, it is not require humidification and dehumidification process due to the low humidity value of the ambient air in Sarajevo. In this case, the characteristics of the points 1-3 and 11-17 are the same.

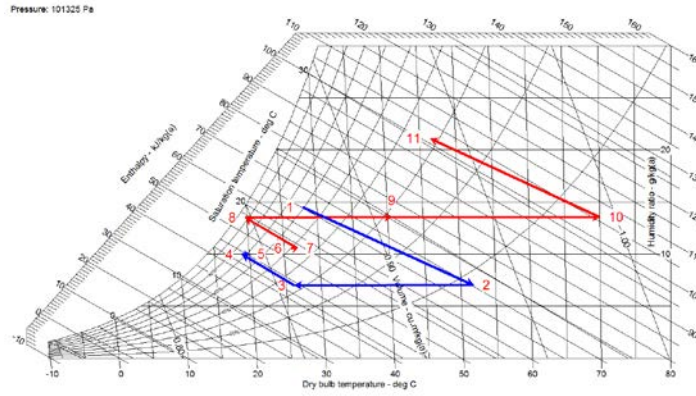


Figure 3. DCS1 psychrometric chart for Nice

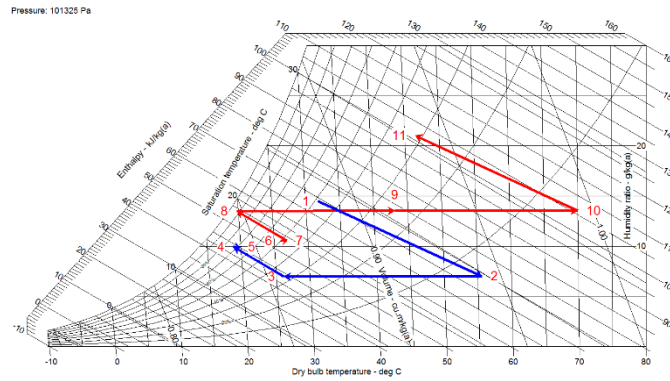


Figure 4. DCS1 psychrometric chart for Napoli

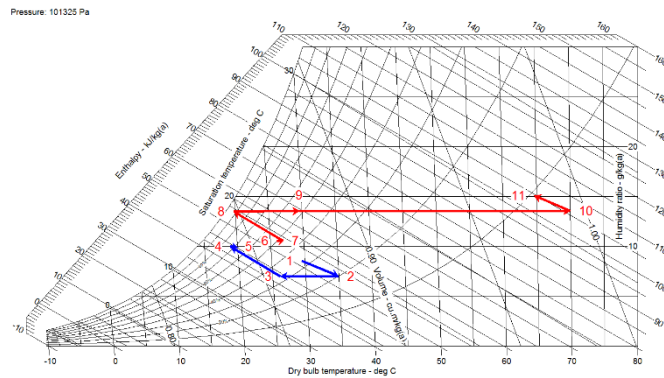


Figure 5. DCS1 psychrometric chart for Sarajevo

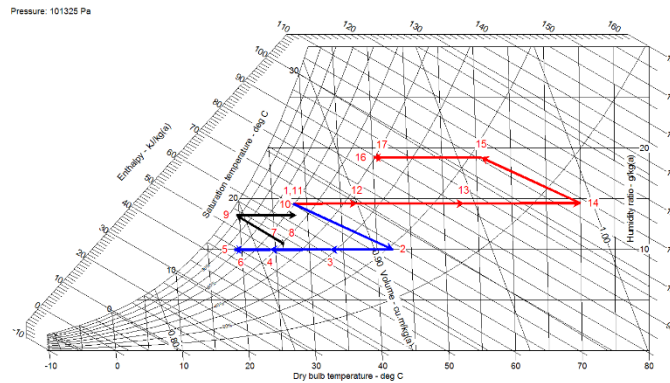


Figure 6. DCS2 psychrometric chart for Nice

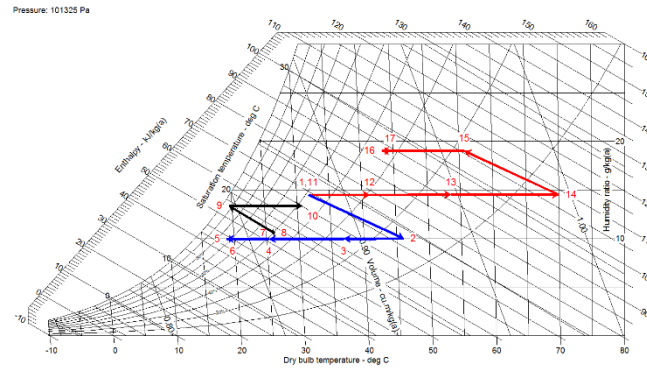


Figure 7. DCS2 psychrometric chart for Napoli

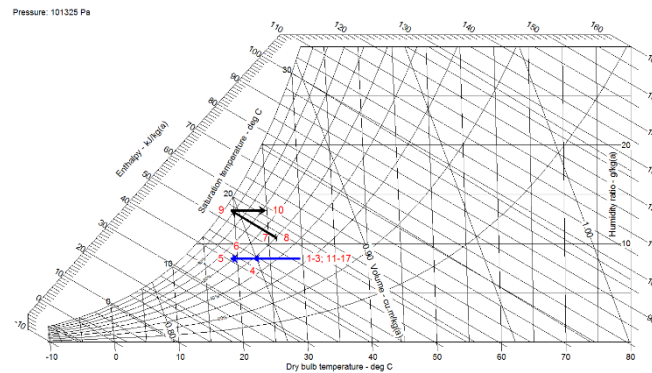


Figure 8. DCS2 psychrometric chart for Sarajevo

Table 2 presents the results obtained from the model for different locations in Europa. In this table, COP values, the total energy consumptions, capacity of the electric heaters and cities design dry bulb temperature ($T(^{\circ}\text{C})$), absolute humidity ($W(\text{g}/\text{kg})$) values for DCS 1 and DCS2 are shown. COP is 0.55 and 0.74 respectively for DCS1 and DCS2 in Nice, 0.70 and 0.90 respectively for DCS1 and DCS2 in Napoli and 0.55 and 0.73 respectively for DCS1 and DCS2 in Sarajevo.

Table 2. Results obtained from the model for different locations in Europa

	DCS1			DCS2		
	W_T (kW)	W_{elk} (kW)	COP	W_T (kW)	W_{elk} (kW)	COP
Nice, France ($T=28.05^{\circ}\text{C}$; $W=14.83\text{ g}/\text{kg}$)	47.16	39.58	0.55	34.95	22.77	0.74
Napoli, Italy ($T=31.88^{\circ}\text{C}$; $W=14.41\text{ g}/\text{kg}$)	43.84	36.26	0.70	34.11	21.66	0.90
Sarajevo, Bosnia and Herzegovina ($T=29.55^{\circ}\text{C}$; $W=8.47\text{ g}/\text{kg}$)	61.92	54.34	0.13	13.76	0	0.73

4. CONCLUSION

New approaches to space conditioning of buildings are required to resolve economic, environmental, and regulatory issues. One of the alternative systems that is brought to agenda is the desiccant cooling systems, which may provide important advantages in solving air conditioning problems. In this study, different desiccant cooling systems for various locations in Europe are discussed by using EES and Fortran Programming Language. It was shown that COP of the systems is related to ambient conditions. It is also shown that desiccant cooling systems are suitable in hot and humid regions in Europe. COP of the systems can be increased with usage of waste heat or renewable energy sources.

REFERENCES

- [1]. D.B. Jani, M. Mishra, P.K Sahoo, Performance studies of hybrid solid desiccant-vapor compression air-conditioning system for hot and humid climates, *Energy and Buildings* vol.102, pp. 284-292, 2015.
- [2]. J.R. Camargo, C.D. Ebinuma, J.L. Silveira, Thermoeconomic analysis of an evaporative desiccant air conditioning system, *Applied Thermal Engineering* vol.23, pp. 1537-1549, 2003.
- [3]. D. La, Y.J. Dai, Y. Li, R.Z. Wang, T.S. Ge, Technical development of rotary desiccant dehumidification and air conditioning: A review, *Renewable and Sustainable Energy Reviews* vol.14, pp. 130-147, 2010.
- [4]. K. Daou, R.Z. Wang, Z.Z. Xia, Z.Z. Desiccant, Cooling air conditioning: a review, *Renewable and Sustainable Energy Reviews* vol.10, pp. 55-77, 2006.
- [5]. L. Yong, K. Sumathy, Y.J. Dai, J.H. Zhong, R.Z. Wang, Experimental study on a hybrid desiccant dehumidification and air conditioning system, *J. Sol. Energy Eng.* vol.128, pp. 77-82, 2006.
- [6]. M. Dezfouli, M.H. Bakhtyar, K. Sopian, A. Zaharim, S. Mat, A. Rachman, Experimental investigation of solar hybrid desiccant cooling system in hot and humid weather of Malaysia, in: 3rd International Conference on Development, Energy, Environment, Economics, pp. 172-176, 2012.
- [7]. Panaras G., Mathioulakis E., Belessiotis V., Kyriakis N., Theoretical and experimental investigation of the performance of a desiccant air-conditioning system, *Renewable Energy* vol. 35, pp. 1368-1375, 2010.
- [8]. S. Jain, P.L. Dhar, S.C. Kaushik, Evaluation of solid desiccant based evaporative cooling cycles for typical hot and humid climates, *International Journal of Refrigeration* vol. 18 (5), pp. 287-296, 1995.
- [9]. G. Meckler, Two-stage desiccant dehumidification in commercial building HVAC systems. *ASHRAE Transactions* vol.95(2), pp.1116-23, 1989.
- [10]. J.C. Sheridan, J.W. Mitchell, A hybrid solar desiccant cooling system, *Solar Energy* vol.34(2), pp.187-93, 1985.
- [11]. H. Hong, F. Guohui, W Hongwei, Performance research of solar hybrid desiccant cooling systems. *Procedia Environmental Sciences* vol.12, pp.57-64, 2012.
- [12]. E. Hurdogan, O. Buyukalaca, T. Yilmaz, A. Hepbasli, Experimental investigation of a novel desiccant cooling system, *Energy and Buildings* vol.42, pp.2049-2060, 2010
- [13]. G. Heidarinejad, H. Pasharshahi, Potential of a desiccant-evaporative cooling system performance in a multi-climate country, *International journal of refrigeration* vol.34, pp.1251-1261, 2011.
- [14]. Kreider J. F., Rabl A., *Heating and Cooling of Buildings*, McGrawHill. 1994.
- [15]. *Ashrae Handbook Fundamentals*, Chapter 14, Climatic Design Information, 2009.

The Effect of Micro-particle-Reinforced Adhesive on Tensile Strength of Double lap Joints

Ahmet Erklig¹, Yousif Jaber AL-Ani², Mehmet Bulut³, M. Akif Kutuk⁴

Abstract

In this study, the influence of microscale particles Borax filler dispersion in the epoxy adhesive on tensile lap shear strength of adhesively bonded double-lap joints was experimentally investigated. Borax filler was used as additive material within the epoxy, having different mass ratios (5, 10, 15, 20, 25% wt). Test samples were produced by woven and plain S-glass fiber and they have same adhesive thicknesses for all interphases of two adjacent laminates. Tensile strength and load carrying capacities of them were determined by a series of mechanical tests using ASTM standards, then resulting failure and fractured surfaces were visualized and compared with each other.

Keywords: *Double Lap Joint, Adhesive, Composite Materials, Borax-micro-particles*

1. INTRODUCTION

Adhesive bonding is widely used in various engineering industries because of its several advantages such as lower structural weight, lower fabrication cost, improved damage tolerance and possibility of joining dissimilar materials. There are many applications in aerospace, railway, automobile, aircraft, wind turbine and marine industries, for investigation of the adhesive bonding and joining performances during the manufacturing of parts. The usage of adhesive bonding joint is more favorable compared with the other types of mechanical joints like welding, rivets and bolts, in consideration of reduction in stress concentration.

Filler is the most commonly used in the reinforcement of polymer matrix composite materials. Many studies related with the effect of particulate filler on mechanical properties of polymer composites can be found from literature [1-3], indicating that stiffness can be improved by the inclusion of the micro or nano scale particles. **Sumita et al. [4]** indicated the effect of particle size by replacing micro scale silica with its nano scale counterpart. They found that incorporation of nanoparticles resulted the higher mechanical properties to the polymer composites. Several researchers [5-8] have shown the improvement of the strength of adhesive joints such as adding powders, particles, random and woven fibers to the adhesive layer. **Kunz-Douglass et al. [5]** studied crack propagation in epoxy-rubber composites and revealed that the adhesive toughness increased with increase of the volume fraction of rubber toughening particles. **Lange and Radford [6]** investigated the effects of alumina trihydrate particles on the fracture energy of epoxy-composite systems. They found that the fracture energy considerably increased by selecting the appropriate particle size and volume fraction. **Moloney et al. [7]** reported the fracture properties of epoxy resins filled with silica, dolomite and alumina particles. The results showed that there was a linear relationship between the volume fraction of the filling particles and the critical stress intensity factor. **Kahraman et al. [8]** tested single lap joints having an adhesive modified by aluminum powder and investigated the effect of the adhesive thickness and the volume fraction of aluminum powder on the strength of the joints.

It is evident from literature survey that mechanical properties of polymer matrix composites were significantly affected by particle content, particle size and particle/matrix adhesion. Present study aims to investigate the mechanical performance of S-glass fiber reinforced composite laminates having adhesively bonded double lap joints. Adherent of epoxy was modified by incorporating microscale borax filler for different epoxy/borax filler mixing

¹Corresponding author: University of Gaziantep, Department of Mechanical Engineering, 27310, Şehitkamil/Gaziantep, Turkey. erklig@gantep.edu.tr

² University of Gaziantep, Department of Mechanical Engineering, 27310, Şehitkamil / Gaziantep, Turkey. mbulut@gantep.edu.tr

³ Iraqi Ministry of Industry and Minerals, Iraqi state company for cement, Iraq –Baghdad yousif_1975@yahoo.com

⁴University of Gaziantep, Department of Mechanical Engineering, 27310, Şehitkamil/Gaziantep, Turkey. kutuk@gantep.edu.tr

ratios. The load bearing capacity of samples was explored in terms of force-deflection relation and results were compared with each other.

2. EXPERIMENTAL STUDIES

2.1. Material Production

Composite plates were produced with 10 layers by woven and plain S-glass fiber having 200gr/m² areal density. MOMENTIVE-MGS L285 epoxy resin with MGS MOMENTIVE-H285 hardener (supplied from Dost Kimya Co.) was used in the production of composite plates. Epoxy (MOMENTIVE-MGS L285) was used as an adhesive for joining of composite laminates.

Micro sized (45 μ) Borax particles were used as additive in the epoxy adhesive with different weight fractions. Also epoxy adhesive is used at the interface during the bonding of the double lap Joints; different weight ratios at the micro level (45 μ) Borax particles having inhomogeneous joining adhesives are prepared. The schematic illustration of a double lap joints is illustrated in Figure 1.

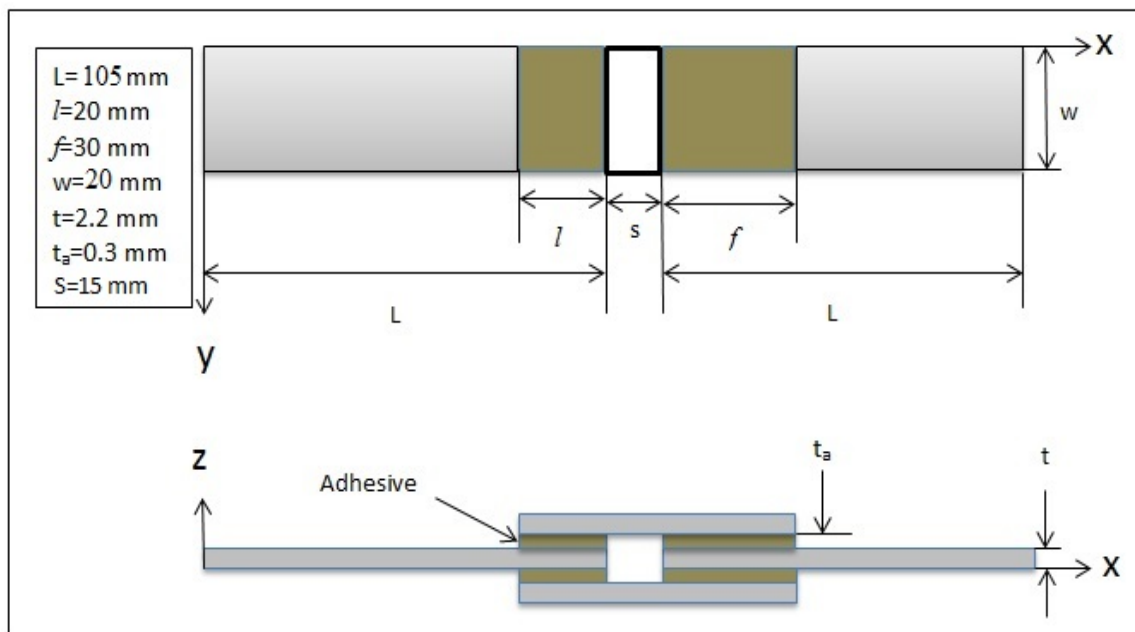


Figure 1. Double lap Joints geometric properties

2.2. Sample Preparation

Bonding surfaces of the laminates were abraded with P120 sandpaper and cleaned with acetone. Adhesive thickness of the lap joints was set to 0.3 mm. Mixing ratios of Borax and epoxy resin are presented in Table 1. Chemical composition of Borax is also provided in Table 2.

Table 1. Epoxy and mixing ratio of Borax

Epoxy and hardener (g)	Borax particles (g)
100	0 pure
95	5
90	10
85	15
80	20
75	25

Table 2. Chemical composition of Borax

Chemical composition	
Chemical formula	$\text{Na}_2\text{B}_4\text{O}_7 \cdot 10\text{H}_2\text{O}$ or $\text{Na}_2[\text{B}_4\text{O}_5(\text{OH})_4] \cdot 8\text{H}_2\text{O}$
Molar mass	381.38(decahydrate) ,201.22(anhydrate)
Appearance	White solid
Density	1.73g/cm ³ (solid)
Melting point	743 °C(1.369 °F; 1.016 K), anhydrate
Boiling point	1.575 °C (2.867 °F; 1.848 K)

2.3. Axial Tensile Tests

Axial tensile tests were conducted according to ASTM D 3528 standard [9] test mechanism as shown in Figure 2. Experiments were performed with **Shimadzu AG-X 300 kN** tensile testing machine. In order to provide the axial loading linearly, the end of the samples was bonded with a tap material made of S-glass fiber/epoxy laminates. All tests were performed at room temperature, with cross head speed of 1mm/min. To obtain the reliability of results, three samples were tested and their resulting average value was taken as final result.

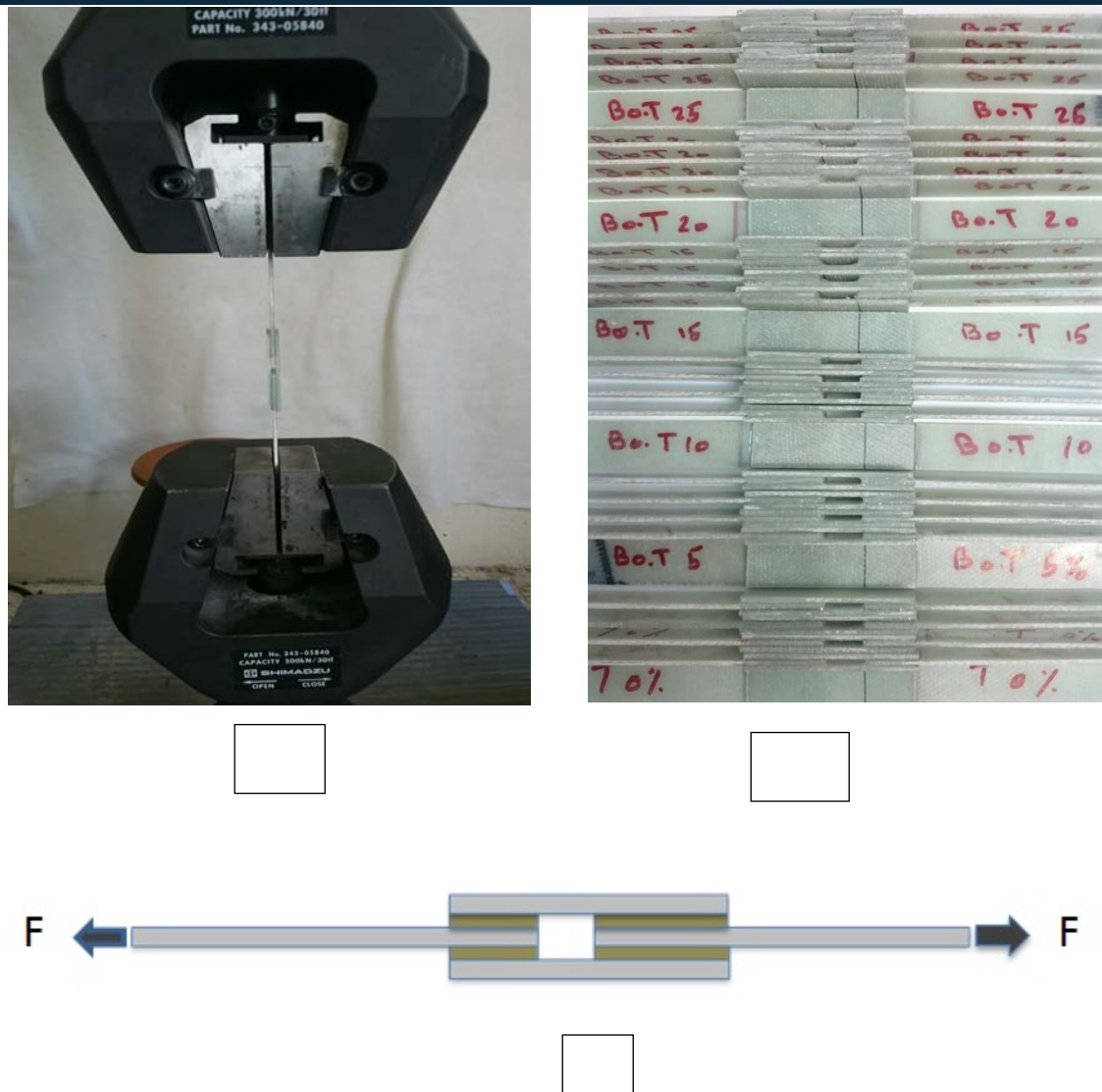


Figure 2. One-way tensile testing mechanism for trapping. (A) Binding to the extruder, (b) produced samples, (c) representation of axial loading

3. RESULTS AND DISCUSSION

In this study, it was examined the effects of epoxy adhesive and tensile strength of the Borax particles mixing with epoxy additives. Results from this study were shown in Figure (3) and Figure (4) in terms of forces and deformation. As can be seen from the results, incorporation of borax particles with micro scale was resulted the significantly increase in tensile strength, while further increase in borax content in the epoxy resin caused the reverse effect, showing the decreasing trend of tensile strength. All curves showed the similar trend. Maximum tensile force has been increased up to 10%wt content of Borax, then the value decreased rapidly. This is attributed the distribution and weight percentages of particles in the epoxy, resulting the higher strength between particle-matrix interphases. According to test results, maximum improvement in tensile force (10% wt content of Borax particles) was recorded as 49% with reference to the pure epoxy adhesive. This is attributed the distribution and weight percentages of particles in the epoxy, resulting the higher strength between particle-matrix interphases.

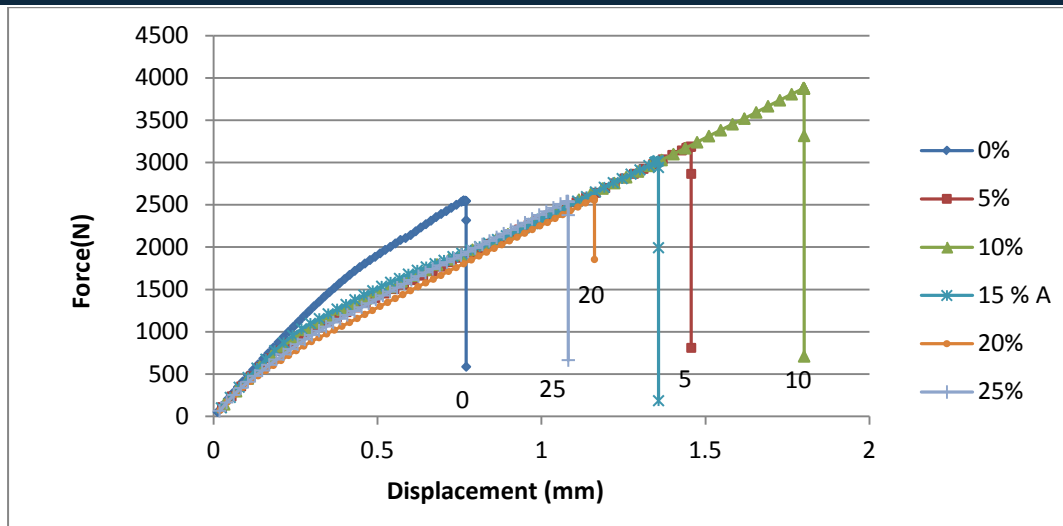


Figure (3) Force Displacement distribution of the tensile test results

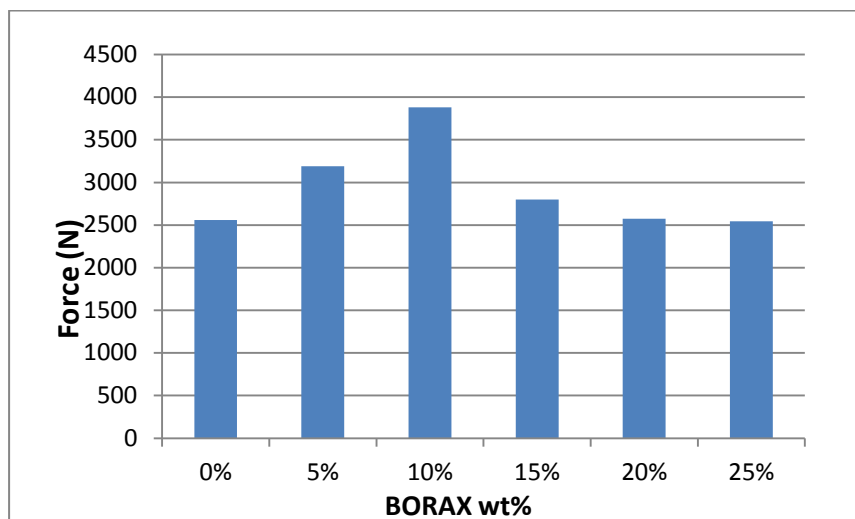


Figure (4) Effect of Borax content ratio

4. CONCLUSION

In this study, the effect of the contribution of different particle subjected to tensile loads and the results obtained are as follows:

- A lower content of particulate additive significantly increases tensile strength and further increase in borax content causes the reverse effect, resulting the decrease of load carrying capacity,
- In the case of Borax filler content is at 10% Borax, tensile strength reaches its maximum value due to the improved particle matrix interphase strength.
- Consequently, joining performance of composite laminates can be improved by mixing of borax filler with an adhesive epoxy at low weight percentage of borax filler, contributing the resolve an important engineering problem during the service.

REFERENCES

- [1]. Zhu ZK, Yang Y, Yin J, Qi ZN. Preparation and properties of organosoluble polyimide/silica hybrid materials by sol-gel process. J Appl Polym Sci 1999;73:2977-84.

- [2]. Fu SY, Lauke B. Characterization of tensile behaviour of hybrid short glass fibre calcite particle ABS composites. Composite Part A 1998;29A:575–83.
- [3]. Radford KC. The mechanical properties of an epoxy resin with a second phase dispersion. J Mater Sci 1971;6: 1286–91.
- [4]. Sumita M, Shizuma T, Miyasaka K, Ishikawa K. Effect of reducible properties of temperature, rate of strain, and filler content on the tensile yield stress of nylon 6 composites filled with ultrafine particles. J Macromol Sci 1983; B22:601–18.
- [5]. Kunz-Douglass S, Beaumont PWR, Ashby MF. A model for the toughness of epoxy–rubber particulate composites. J Mater Sci 1980;15:1109–23.
- [6]. Lange FF, Radford KC. Fracture energy of an epoxy composite system. J Mater Sci 1971;6:1197–203.
- [7]. Moloney AC, Kausch HH, Stieger HR. Interfacial properties of filled epoxy resin. Org Coat Appl Polym Sci Proc 1982;47:402–6.
- [8]. Kahraman R, Sunar M, Yilbas B. Influence of adhesive thickness and filler content on the mechanical performance of aluminum single-lap joints bonded with aluminum powder filled epoxy adhesive. J Mater Process Technol 2008;205:183–9.
- [9]. ASTM D3528 - 96(2008). Standard Test Method for Strength Properties of Double Lap Shear Adhesive Joints by Tension Loading

BIOGRAPHY

AHMET ERKLIĞ – was born in Iskenderun, Turkey in 1974. He received the B.S. degree in Mechanical Engineering from the Gaziantep University, Gaziantep, Turkey in 1996, the M.S. degree in Mechanical Engineering from the Gaziantep University, Gaziantep, Turkey in 1999, and the Ph.D. degree in Mechanical Engineering from the Gaziantep University, Gaziantep, Turkey in 2004. In 1996, he started to work as a research assistant, in the department of mechanical engineering in Gaziantep University, the task is continued with Assistant in 2004 and Associate Professor in 2014. He is married and has two children.

YOUSIF JABER SHAKER AL-ANI- Yousif Jaber Shaker Al-Ani was born in Iraq, Al –Anbar in 06.11.1975. First, middle and high school education completed in Al Anbar. B.Sc Mechanical Engineering (University of Al Anbar –Iraq) in July 1997. Member of Iraqi Engineers Union in 1997, Employee in Iraqi Ministry of Industry and Minerals /Iraqi Cement State Company from 2000, Job title : Assistant Chief Engineer, M.SC. Researcher in the Mechanical Engineering Department of Gaziantep University 2015-2016. He is married and has four children.

MEHMET BULUT – Res. Asst. Mehmet Bulut was born in Sivas at 1980. After completing his primary and secondary education in Kayseri, he completed his high school education in Sivas. After graduating with a license degree from Balikesir University in 2002, he completed a master's degree in mechanical engineering department in Gaziantep University at 2013. He has continued in the same section of the doctoral program. In 2010, he started to work as a research assistant in the department of mechanical engineering in Gaziantep University, the task is still continued in this section. He is married and has one child.

M. Akif KÜTÜK – was born in Gaziantep, Turkey in 1973. He received the B.S. degree in Mechanical Engineering from the Gaziantep University, Gaziantep, Turkey in 1995, the M.S. degree in Mechanical Engineering from the Gaziantep University, Gaziantep, Turkey in 1997, and the Ph.D. degree in Mechanical Engineering from the Gaziantep University, Gaziantep, Turkey in 2003. Since 2003 he has been Assistant and Associate Professor in the Department of Mechanical Engineering, Engineering Faculty, Gaziantep University, Gaziantep, Turkey.

Effect of Abrasive Waterjet Machining Parameters on Inconel 718 Nickel-Based Super Alloy

Mustafa Ay¹, Ahmet Hasçalık²

Abstract

In this study, the effect of machining parameters (traverse speed, pressure and standoff distance) on abrasive waterjet machining (AWJM) of Inconel 718 nickel-based super alloy was experimentally investigated. In the experiments, effects of these three parameters on cutting performance (surface roughness, kerf width and kerf taper angle) are investigated. For this purpose, in order to save in cost and time, a Taguchi L9 (34) orthogonal array was chosen instead of full factorial experimentation. The each cutting parameters were changed at three levels in order to explore their effects on the measured responses. In present study, Analysis found that varying parameters are affected in different way for different response.

Keywords: AWJM, Inconel 718, Traverse Speed, Water Pressure, Standoff Distance

1. INTRODUCTION

Nickel-based super alloys are used frequently in spacecrafts, rocket engines, nuclear reactors, submarines, the high-temperature parts of airplane, marina and industrial gas turbine engines, pressure tanks, steam turbine generators and in other heat treatments. [1-5]. Inconel 718 is one of the most frequently used alloys among the nickel-based super alloys. In addition to this, some unique characteristic of this material such as low thermal conductivity, hardness, process stiffening and existence of abrasive carbide particles make the machining hard [6, 7]. Non-traditional manufacture methods are known as appropriate methods for the shaping of materials that are hard to machine. Abrasive Water Jet Machining (AWJM) is one of the non-traditional machining methods. AWJM has obvious differences than other cutting technologies; it can make versatile and flexible cutting without causing any thermal tensions and without any high cutting forces. Therefore, AWJM is proved to have an efficient technology in the machining of different engineering materials. AWJM can easily cut hard and fragile material such as steel, non-iron material such as Ti, Ni; polymers, metal matrix composites (MMC), ceramic matrix composites (CMC), concrete, rock, wood, plastic, metal polymer laminates and glass fiber metal laminates [8]. Having the proper cutting mechanism and material lifting rate with AWJM depends on the type and size of abrasive, flow rate of abrasive, and the rate of cutting parameters such as standoff distance and cutting speed [9, 10]. This study has examined the changes of the Inconel 718 nickel based super alloy's cutting with AWJM; that depend on parameters such as upper and lower kerf width, kerf taper angle and surface roughness.

2. EXPERIMENTAL WORK

This study has used commercially obtained Inconel 718 nickel alloy with AMS 5596 standard number and 4.76 mm of width. The chemical compound of this material is given in Table 1.

Table 1. Chemical composition of Inconel 718

Element	Ni	Cr	Nb	Mo	Ti	Al	C	B	Si	S	P	Fe
Composition (wt. %)	53.60	18.20	5.06	3.04	0.97	0.44	0.052	0.003	0.10	<0.002	<0.005	Balance

¹Corresponding author: Mustafa AY, Firat University, Technology Faculty, Department of Mechatronics Engineering, 23119 Elazığ, Turkey. mustafaay@firat.edu.tr

²Ahmet Hasçalık, Firat University, Technology Faculty, Department of Mechanical Engineering, 23119 Elazığ, Turkey. ahascalik@firat.edu.tr

Experimental work was conducted in CT (Cutting Technologies & Machinery) CNC AWJ machine. Parameters of Pressure (bar), traverse speed (mm/min), nozzle standoff distance (mm) are selected as variables in experimental studies. Depending on these cutting parameters and levels; Taguchi L9 experimental design method was considered as base and total of 9 experiments were implemented. Table 2 indicates the parameters used in experiments and their levels and Table 3 indicates the experiment desing.

Table 2. Cutting parameters and levels of AWJ

Parameters	Units	Level 1	Level 2	Level 3
Working pump pressure	bar	3000	3300	3600
Traverse speed	mm/min	80	200	350
Nozzle Standoff distance	mm	2	4	6
Water nozzle orifice diameter	mm	0.28	fix	fix
Focusing nozzle diameter	mm	1.1	fix	fix
Abrasive type	mesh	80 (garnet)	fix	fix
Abrasive flow rate	g-l	500	fix	fix

Table 3 Design experiment of TaguchiL9 orthogonal array

Exp. No	Preasure	Traverse speed	Standoff distance
1	3000	80	2
2	3000	200	4
3	3000	350	6
4	3300	80	4
5	3300	200	6
6	3300	350	2
7	3600	80	6
8	3600	200	2
9	3600	350	4

Experiments implemented by AWJ are limited by 20 mm. for each experiment's cutting transaction on the sample with 110 x 30 mm dimensions; as seen in Figure 1. In order to have more accurate measures, cutting experiments were done three times.

Effect of Abrasive Waterjet Machining Parameters on Inconel 718 Nickel-Based Super Alloy and Mustafa Ay, Ahmet Hasçalık

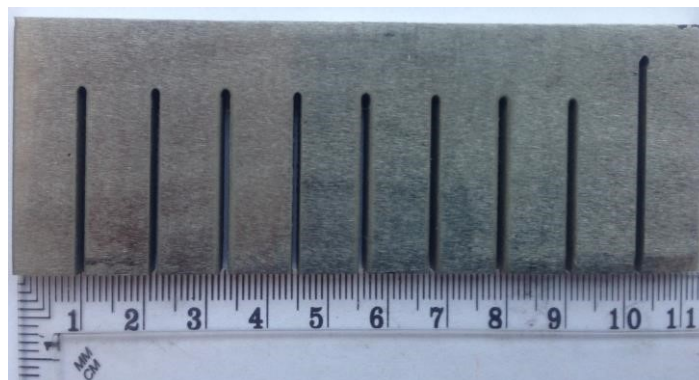


Figure 1. Inconel 718 cut with abrasive water jet

As a result of experiments; lower and upper kerf width for each cutting were measured in five different points through the kerf by a profile measuring microscope (Model 98-0001, SCHERR TUMICO, U.S.A) of 0.002 sensitivity in order to determine the kerf width and angle characteristics that set the cutting quality; and the average values of these measures are obtained, thereby the kerf width value and kerf taper angle were detected. Depending on the obtained lower and upper kerf width values; the formula 1 below was used and kerf taper angle (Ta) was calculated.

$$T_a(deg) = \frac{(T_w - B_w) \times 180}{2\pi \times t} \quad (1)$$

where T_w is the top kerf width, B_w is the bottom kerf width, and t is the material thickness. Average surface roughness values of the samples were measured with the help of portable Mitutoyo SurfTest SJ-210 device. 3 different measures were obtained from each sample and the average of these measures are considered as the average surface roughness.

3. RESULTS AND DISCUSSION

3.1. Effect of Process Parameters on Kerf Taper Angle

Measurement results of kerf quality characteristics are listed in Table 3. In this table, the corresponding terms are top kerf width (T_w), bottom kerf width (B_w), kerf taper angle (Ta) and surface roughness (Ra) respectively. Also main effect plots of kerf taper angle is given in Figure 2.

Table 3. Experimental result of performance characteristics using L9 Orthogonal array.

Exp. No	Pressure	Traverse speed	Standoff distance	T_w (mm)	B_w (mm)	Ta (mm)	Ra (°)
1	3000	80	2	1.366	1.106	1.564	3.06
2	3000	200	4	1.494	0.942	3.322	3.21
3	3000	350	6	1.518	0.74	4.682	4.21
4	3300	80	4	1.526	1.004	3.141	3.05
5	3300	200	6	1.668	0.908	4.574	3.54
6	3300	350	2	1.364	0.828	3.226	3.95
7	3600	80	6	1.716	1.012	4.237	2.96
8	3600	200	2	1.348	0.88	2.816	3.01
9	3600	350	4	1.432	0.814	3.719	4.13

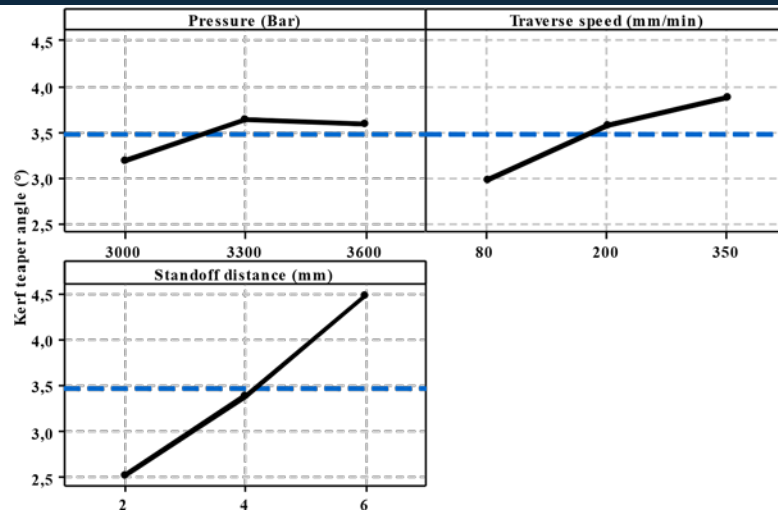


Figure 2. Main effects of process parameters on kerf taper angle

As it can be seen in Figure, as the pressure increases, so does the kerf taper angle. This can be explained by kinetic energy theory. As the pressure increases, the abrasive particles with high kinetic energy begin to cut off more parts from the initial area of hitting; and the cutting off ability of particles from the material decrease closer to the exit. Therefore, upper kerf is wider than lower kerf. This causes the increase of kerf width on the piece that is being cut. It is seen that as the pressure increases to 3600 bar, kerf taper angle decreases. Increase of pressure will cause the abrasive particles to have higher kinetic energy. As a result of this, difference between upper and lower width decreases. Increase of traverse speed increases kerf taper angle as shown in Fig. 2. Increase of kerf taper angle is a direct result of material's exposure time to AWJ impact. Depending on the increasing traverse speed, kerf taper angle also increases as the lesser amount of abrasive particles take part in cutting through the cutting line on the material. Referring to Fig. 2; it is seen that as standoff distance increases, so does the kerf taper angle. As it can be seen in Figure 3, jet caliber extends from the nozzle output and its impact decreases. Depending on this, kerf taper angle increases with the increase of standoff distance. Obtained results are consistent with the previous facts [10-12].

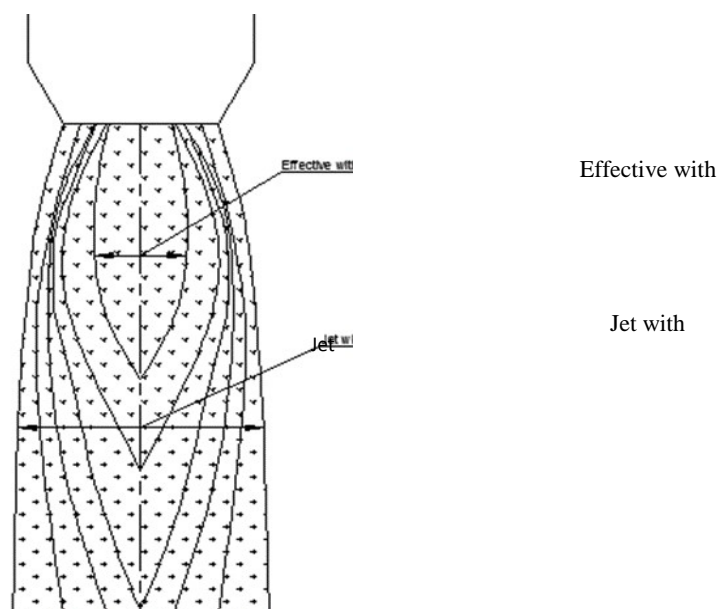


Figure 3. Relative strength zones in a waterjet [11]

Effect of Abrasive Waterjet Machining Parameters on Inconel 718 Nickel-Based Super Alloy and Mustafa Ay, Ahmet Hasçalık

3.2. Effect of Process Parameters on Surface Roughness

The effect of process parameters on surface roughness is shown in Figure 4. It is seen that as pressure increases, surface roughness decreases. Increase of pressure provides the required high energy for the abrasive particles to cut-off parts from the material. The abrasive particles which obtain the necessary energy increase their cutting capacities and cut-off more pieces from the material without jet deviations. This helps the cutting surfaces to be more smooth. It is also seen that when traverse speed increases, surface roughness increases as well. Increase of traverse speed causes a certain point on the material being cut to be exposed to less abrasive particles within the unit time. This will prevent the contact of abrasive particles which will follow the impacting abrasive particles and to remove the anomalies generated after the first impact. Therefore, material cutting surface will be more rough with the increasing cutting speed. It is seen that as standoff distance increases, surface roughness increases too (Fig. 4). Increase of standoff distance will also increase the jet caliber and this means that the abrasive particles inside the jet will contact with a wider area on the material. As the abrasive particles are scattered and execute the cutting, the possibility of existence of collective and orderly cutting surfaces will decrease. Therefore, the cutting surfaces will not be in an order and a the surface generated will be more rough. Previous studies have reported that increase of cutting speed and standoff distance also increase the kerf taper angle and surface roughness; and as the pressure increases, the kerf taper angle will increase whereas roughness will decrease [13, 14].

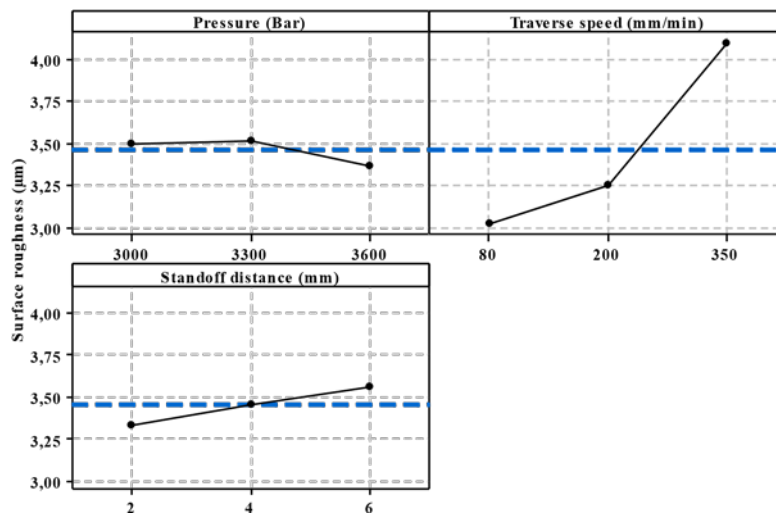


Figure 4. Main effects of process parameters on surface roughness

4. RESULTS

Results stated below were obtained from the studies and reviews conducted.

1. During the transaction of cutting with AWJ; increase of pressure decreases the surface roughness; but increases the kerf width and kerf taper angle.
2. It has been determined that speed of progress and standoff distance have significant impact on kerf taper angle and roughness; and as these parameters increase, characteristics that determine the kerf quality decrease.
3. For minimum kerf taper angle lowest levels of water pressure, transfer speed and standoff distance at 3000 bar, 80 mm/min and 2mm emerged as optimal settings.
4. Based on the test conditions a combination of high pressure, low traverse speed and low standoff distance is recommended to minimize surface roughness.

REFERENCES

- [1].E. Kose, A. Kurt, U. Seker, The effects of the feed rate on the cutting tool stresses in machining of Inconel 718, *Journal of Materials Processing Technology*, 2008,196, p.165.
- [2].I.A. Choudhury, M.A. El-Baradie, Machinability of nickel-base super alloys: a general review, *Journal of Materials Processing Technology*, 1998, 77, p. 278.
- [3].M. Ay U. Çaydaş A. Hasçalık, Optimization of micro-EDM drilling of inconel 718, *Int J Adv Manuf Technol*. 2013, 66:1015–1023.
- [4].M. Ay, U. Çaydaş, A. Hasçalık, Effect of Traverse Speed on Abrasive Waterjet Machining, of Age Hardened Inconel 718 Nickel-Based Superalloy, *Materials and Manufacturing Processes*, 25: 1–6, 2010
- [5].E.O. Ezugwu, Z.M. Wang, A.R. Machado, The machinability of nickel-based alloys: A review. *Journal of Materials Processing Technology* 1999, 86, 1–16.
- [6].A. Altin, M. Nalbant, A. Taskesen, The effects of cutting speed on tool wear and tool life when machining Inconel 718 with ceramic tools. *Materials and Design* 2007;28:2518–22.
- [7].E.O. Ezugwu, Key improvements in the machining of difficult-to-cut aerospace superalloys, *International Journal of Machine Tools & Manufacture* 45 (2005) 1353–1367
- [8].D.K. Aspinwall, S.L. Soo, A.E. Berrisford, G. Walder, Workpiece surface roughness and integrity after WEDM of Ti6Al-4V and Inconel 718 using minimum damage generator technology, *Ann. CIRP*. 57 (1), 187–190.
- [9].D. Arola, M. Ramulu, Mechanism of Material Removal in Abrasive Waterjet Machining of Common Aerospace Materials, *Proceedings of the 7th American Waterjet Conference*, Seattle WA, 1993; 43–64.
- [10].D.K. Shanmugam, S.H. Masood, An investigation on kerf characteristics in abrasive waterjet cutting of layered composites, *journal of materials processing technology* 2 0 9 (2 0 0 9) 3887–3893
- [11].J. Wang, W.C.K. Wong, A study of abrasive waterjet cutting of metallic coated sheet steels, *International Journal of Machine Tools & Manufacture* 39 (1999) 855–870
- [12].M. A. Azmir, A. K. Ahsan, A. Rahmah, Effect of abrasive water jet machining parameters on aramid fibre reinforced plastics composite, *Int J Mater Form* (2009) 2:37–44
- [13].J. Kechagias, G. Petropoulos, N. Vaxevanidis, Application of Taguchi design for quality characterization of abrasive water jet machining of TRIP sheet steels *Int J Adv Manuf Technol* (2012) 62:635–643
- [14].Y. W. Seo, M. Ramulu, D. Kim, Machinability of titanium alloy (Ti-6Al-4V) by abrasive waterjets, *PROC INST MECH ENG B-J ENG MA* 2003; 217(12):1709-1721

Survey for Control Strategies and Application Areas of PWM Rectifiers

Baran Yildiz¹, Mehmet Polat²

Abstract

PWM rectifier is ac to dc rectifiers which have switches to rectify and regulate output voltage. There are so many application areas of PWM rectifiers like telecommunication, power electronics and electrical machine drivers because of higher input power factor and allowable output harmonics. So, in last decades there are so many researches for PWM rectifiers. This paper is one of them. It analyzes the mathematical model of PWM rectifiers and helps researchers to choose inductor and capacitor values and switching strategies of PWM rectifiers. While analyzing PWM rectifiers, table contents and graphics are used for optimizing output values. After analyze and conclude some results from PWM rectifiers explained some disadvantages of PWM rectifiers. These disadvantages are higher cost and complexity when it is compared with other ac-dc converters. Moreover there are two types of PWM rectifiers. These are three phase and one phase rectifiers and they are analyzed and compared with other single phase and three phase converters. To control PWM rectifier microprocessors are used so we also consider control strategies and control techniques with microprocessors for PWM techniques. As a result this paper is prepared for researchers to find almost everything about PWM rectifiers when they need.

Keywords: *PWM rectifier, Rectifier Control Strategies, Rectifier Application Areas*

1. INTRODUCTION

PWM rectifier is continuously switched and controllable rectifier. When compared with the other ac/dc rectifiers, PWM rectifiers have less undesired effects like much amount of current/voltage total harmonic distortion (which causes increased losses in transmission lines), unwanted ripples and low power factor. It provides solution to the problems with 2 types three phase and single phase rectifiers. These rectifiers consist of power transistors with anti-parallel diodes, input inductance and output capacitance and resistance. Different from other ac/dc rectifiers PWM rectifier has distributive switching. It provides fast and continuous switching with this property. This provides to converter controllable dc output and bidirectional power flow[1,2,3] and it makes this converter the best solution for many application areas including interruptible power supplies[4,5], adjustable-speed drives[6,7,8], battery management[9,10], active filters[13,14], etc. Because of these properties for last decades, PWM rectifier has become an indispensable element of distributed power generation systems (DGS) and renewable energy systems including wind energy and photovoltaic grid tied systems. This paper presents a comprehensive survey on PWM rectifiers, their types, mathematical models, control strategies, advantages and disadvantages and application areas.

2. APPLICATIONAREAS

PWM rectifier has better performances when it is compared with conventional thyristor rectifier. Indeed, the power transistors are capable to operate at high switching frequency which allows reducing the input/output harmonics while providing a high quality of the input currents and DC voltage. Therefore, this PWM rectifier has a better power density and reduced cost. On the other hand, it allows also a perfect regulation of the reactive power injected in the grid leading to a near unity input power factor operation [6].

This rectifier is also used in Energy storage systems which are widely used in power distribution sectors like renewable energy sources and electrical vehicles. The AC/DC converter which operates as an active rectifier should provide a regulated dc voltage with minimized ripple and the currents flowing through the electric supply need to be sinusoidal and in phase with the grid circuit voltages[9]. So, all of these properties are provided only by PWM rectifier efficiently.

Speed applications are another application area for PWM rectifiers, especially traction systems. When we want to control ac machines like these traction systems, we should use firstly a rectifier for generating dc source. In general, the DC source is constructed from a full wave diode bridge rectifier but we can also use PWM rectifier for this

¹Corresponding author: Firat University, Department of Mechatronic Engineering, 23000, Merkez/Elazig, Turkeyb.yildiz@firat.edu.tr

²Asistant Professor Dr. Mehmet POLAT mpolat@firat.edu.tr

application. With this rectifier we can provide an appropriate modulation scheme. For this purpose we can use Voltage Source Inverter (VSI) control technique to supply the AC machine by a controllable frequency and amplitude output voltage [7,8]. If we want to use fewer components, bidirectional power flow and less size, we can also choose matrix converter for this AC-AC purpose. Because, when we use inverter, we must use also a structure like PWM rectifier to provide same advantages and properties of matrix converters.

3. MATHEMATICAL MODELS

To use and control PWM rectifiers, we must know about its mathematical model and also control strategies and what changes while we control and changes switches continuously. So in this chapter I try to explain mathematical model of three-phase PWM rectifiers. Before the mathematical model a figure which belongs to PWM rectifier is shown below on Figure 2.

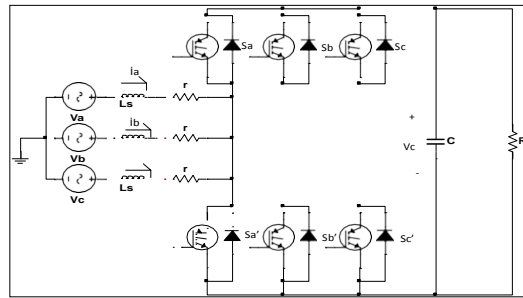


Figure 1. AC/DC voltage source three phase PWM rectifier

(1) Power is the sinusoidal three-phase voltage source, and in the equilibrium condition, namely:

$$e_a + e_b + e_c = 0 \quad (1)$$

$$i_a + i_b + i_c = 0 \quad (2)$$

(2) Filter inductance L is linear, and considered it is not saturated. Definition of the three-phase switching function are s_a, s_b, s_c : $s_x = 1$ ($x=a, b, c$) on behalf of turn on the higher switch while turn off the lower one in the same bridge; $s_x = 0$ is just the other way round, on behalf of turn off the higher switch while turn on the lower one.

Three-phase model for the VSR as below:

$$C \frac{dV_c}{dt} = i_a s_a + i_b s_b + i_c s_c - \frac{V_{dc}}{R_L} \quad (3)$$

$$L \frac{di_a}{dt} + r i_a = e_a - V_{dc} s_a - V_{on} \quad (4)$$

$$L \frac{di_b}{dt} + r i_b = e_b - V_{dc} s_b - V_{on} \quad (5)$$

$$L \frac{di_c}{dt} + r i_c = e_c - V_{dc} s_c - V_{on} \quad (6)$$

The model for figure of the rectifier in the two-phase synchronous rotation d-q coordinate is:

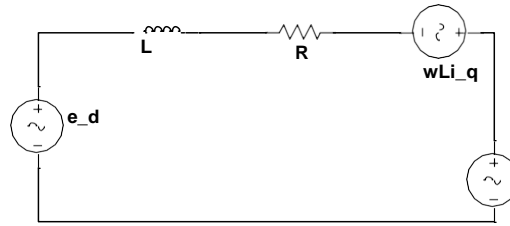


Figure 2. Equivalent circuit of rectifier in the d-axis

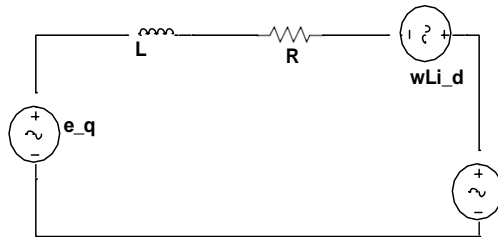


Figure 3. Equivalent circuit of rectifier in the q-axis

$$\frac{di_d}{dt} = \frac{-R}{L} i_d - \omega i_q - \frac{S_d}{L} V_{dc} + \frac{e_d}{L} \quad (7)$$

$$\frac{di_q}{dt} = \frac{-R}{L} i_q - \omega i_d - \frac{S_q}{L} V_{dc} + \frac{e_q}{L} \quad (8)$$

$$\frac{dV_{dc}}{dt} = \frac{S_d}{C} i_d - \frac{S_q}{C} i_q - \frac{1}{RL} V_{dc} \quad (9)$$

In the above equations, i_d and i_q are active and reactive current component in d-q coordinate system; S_d and S_q are switching function in d-q coordinate system; e_d and e_q are representative of active and reactive voltage source in d-q coordinate system; ω represents of the synchronous rotation angular frequency; R represents of the summation of equivalent resistance of switching power devices and the equivalent resistance of inductance.

4. PROS AND CONS

Researchers have used PWM rectifiers in a large area for last decades. So, this paper is prepared to give information about this rectifier. But this rectifier has also some disadvantages. So, this rectifier's advantages and disadvantages and also control techniques and these techniques' advantages and disadvantages are discussed in this chapter. Furthermore a table which explains control techniques' advantages and disadvantages is prepared for this chapter.

4.1 Control Techniques of PWM Rectifier

After PWM rectifier was started to use, various control strategies have been developed. These strategies also have advantages and disadvantages according to each other. So we can use these control strategies for various applications which are different according to control strategies. Table1 shows these pros and cons of control strategies.

	Advantages	Disadvantages
voltage-oriented control (VOC)	switching frequency is fixed (design of the input filter is easier) PWM strategies can be used According to other A/D converters, It is cheaper. There is no sensitivity to line inductance variation	Coordinate transformation and decoupling between active and reactive components are required it has complex algorithm Input power factor is lower than V-DPC
voltage-based direct power control (V-DPC)	There is no separate PWM voltage modulation block There is no current regulation loops There is no coordinate transformation Dynamic performance is good It has decoupled active and reactive power control Instantaneous variables are estimated with all harmonic components (we can improve power factor and efficiency)	High values of the inductance and sampling frequency are needed (it is important for the estimator, because smooth shape of the current is needed) Power and voltage estimation should be avoided at the moment of switching (it returns high errors) switching frequency is variable Fast microprocessor and A/D converters are required
virtual flux-oriented control (VFOC)	switching frequency is fixed Advanced PWM strategies can be used. It is cheaper A/D converters There is no sensitivity to line inductance variation	Coordinate transformation and decoupling between active and reactive components are required it has complex algorithm Input power factor is lower than VF-DPC
virtual flux-based direct power control (VF-DPC)	Simple and noise-resistant power estimation algorithm that easy to implement in a DSP It has lower sampling frequency than V-DPC There is low THD of line currents at a distorted and unbalanced supply voltage There is no separate PWM voltage modulation block There is no current regulation loops There is no coordinate transformation Dynamic performance is good It has decoupled active and reactive power control	switching frequency is variable Fast microprocessor and A/D converters are required

As we see from table1, if we want to use PWM rectifier for not advanced applications, we can choose VOC and VFOC which are cheaper than the others. But if we want to use this rectifier for advanced applications in which we want less THD and good performance, we should choose V-DPC and VF-DPC.

4.2 PWM Rectifiers

The most important advantage of using the pulse width modulation rectifier is the reduction of higher order harmonics. In addition to this, PWM rectifier can control the magnitude of the output voltage, and improve the power factor by forcing the switches to follow the input voltage waveform. And another advantages of PWM rectifier's power flow is bidirectional. This property makes it possible to perform regenerative braking for input and output.

If we want to mention disadvantages of PWM rectifier, it is more complex than the other rectifier and this property makes it possible to generate radio frequency interference. It has high cost when compared the other rectifiers. It has less speed than others.

CONCLUSION

The PWM rectifier gives potential solutions to the low power factor and high harmonic distortion problems in power converters industry. It is usually the best choice for a variety of industrial applications such as machine drives, battery management, active filters, renewable power generation, etc. So in this paper, PWM rectifiers are studied because of this reasons. From application areas chapter, it is concluded that PWM rectifier is used in large area especially where low harmonic distortion and high power factor and bidirectional power flow are needed. After that mathematical model of single phase and three phase PWM rectifier is explained. In addition to these conclusions, control strategies and their advantages and disadvantages are discussed also PWM rectifier's advantages and disadvantages are discussed. And concluded from these discussions we should choose rectifier's control strategy for what we will use rectifier and they should be used if or not it used for advanced applications. And also provided an explanation about PWM rectifier's pros and cons. So also we have seen from this discussion that if we use rectifier for simple situations

PWM rectifier shouldn't be chosen because of high cost and complexity but if we work more sensitive situations PWM rectifiers are best solution.

REFERENCES

- [1]. A. Marzouki, M. Hamouda, and F. Fnaiech, "Sensorless Nonlinear Control for a Three-Phase PWM AC-DC Converter," in *Industrial Electronics (ISIE)*, 2010 IEEE International Symposium, Bari, Italy, pp.1052-1057, July 2010.
- [2]. A. Marzouki, M. Hamouda, and F. Fnaiech, "Nonlinear Control of a Three-Phase Active Rectifiers Based L and LCL Filters," *Electrical Engineering and Software Applications (ICEESA)*, 2013 International Conference, Hammamet, Tunisia, pp. 1-5, March 2013.
- [3]. B., Singh; B. N., Singh; K., Al-Haddad; A., Pandey; and D. P., Kothari, "A Review of Three-Phase Improved Power Quality AC-DC Converters," *IEEE Trans. on Industrial Electronics*, Vol.51, pp.641-660, June 2004.
- [4]. T., Kommers Jappe; T., Brunelli Lazzarin; C.A.; Arbugeri; and S.A., Mussa, "Control strategy for three-phase four- wire PWM VSI parallel connected in UPS applications," in *Industrial Electronics (ISIE)*, 2014 IEEE International Symposium, Istanbul, pp. 443-448, 2014.
- [5]. H., Lei; E., Xiao; J., Xiong; X., Lin; and Y., Kang, "Modeling and Analysis of Three-Phase Four-Leg PWM Boost- Type Rectifier for Double Conversion Transformerless UPS," *IECON 2011 - 37th Annual Conference on IEEE Industrial Electronics Society*, pp. 1444 - 1449, 2011.
- [6]. H.F., Bilgin; K.N., Köse; G., Zenginobuz; M., Ermis; E., Nalçacı; I. Çadirci; and H., Köse, "A Unity Power Factor Buck Type PWM Rectifier for Medium/High Power DC Motor Drive Applications," *Industry Applications, IEEE Transactions on*, Vol.38, No. 5, pp.1412-1425, October 2002.
- [7]. M.H., Hedayati; A.B., Acharya; and V., John, "Common-Mode Filter Design for PWM Rectifier-Based Motor Drives," *Power Electronics, IEEE Transaction. On*, Vol.28, No. 11, pp.5364-5371, November 2013.
- [8]. K., Hatua and V. T. Ranganathan "A Novel VSI- and CSI-Fed Active- Reactive Induction Motor Drive with Sinusoidal Voltages and Currents," *Power Electronics, IEEE Transactions On*, Vol. 26, No. 12, pp. 3936- 3947, December 2011.
- [9]. M. P., Akter, S., Mekhilef, N. M. L., Tan, and H., Akagi, "Model Predictive Control of Bidirectional AC-DC Converter for Energy Storage System," *Journal of Electrical Engineering & Technology*, Vol. 10, No. 1, pp. 165-175, 2015.
- [10]. L., Maharjan; S., Inoue; H., Akagi; and J., Asakura, "State-of-Charge (SOC)-Balancing Control of a Battery Energy Storage System Based on a Cascade PWM Converter," *Power Electronics, IEEE Transactions on*, Vol.24(6), pp.1628- 1636, 2009.
- [11]. B., Singh; K., Al-Haddad; and A., Chandra, "A review of active filters for power quality improvement," *Industrial Electronics, IEEE Transactions on*, Vol. 46, No.5, pp. 960-971, 1999.
- [12]. R., Hou; J., Wu; Y., Liu; and D., Xu, "Generalized Design of Shunt Active Power Filter with Output LCL Filter [13]. V. Blasko, and V. Kaura, "A new mathematical model and control of a three-phase AC-DC voltage source converter," *IEEE Trans. Power Electron.*, vol. 12, no. 1, pp. 116-123, 1997.
- [13]. M. Malinowski, M.P. Kazmierkowski, A. Trzynadlowski, "Review and comparative study of control techniques for three-phase PWM rectifiers"

Activities of Some Natural Mineral Waters from Gumushane Region of Turkey

Selim Sen¹ Mesut Yalcin², Mehmet Oz³

Abstract

*We investigated the antifungal effects of some natural mineral waters obtained from Gumushane region of Turkey against to white-rot (*Coriolus versicolor*, MAD-697) and brown-rot (*Gloeophyllum trabeum*(Mad-617-R) , fungus (*Basidiomycetes*). Fungal experiments were performed on Scots pine sapwood (*Pinus sylvestris* L.) We used non-concentrated mineral water and concentrated mineral water (increased concentration of active components via evaporation) in ratios of 10%, 25%, 50%, and 75%. To evaluate the results, we measured the amount of specific minerals in the mineral waters such as calcium (Ca), sodium (Na), potassium (K), magnesium (Mg) chloride(Cl) and small amounts of boron (B), copper (Cu), iron (Fe), manganese (Mn). Results indicated that the rich minerals in underground spring waters could not achieve sufficient antifungal activities. Moreover, the concentration levels obtained after 90% evaporation could not give reasonable antifungal properties in the development of wood-damaging, white and brown decay fungus. Mineral salts in natural mineral waters – including anti-toxic effects to protect woods from damage –should be enriched by adding some salts of copper, boron and chrome*

Keywords: *natural mineral water, C. versicolor, G. trabeum, scots pine, wood protection*

1. INTRODUCTION

Wood material, which has been used around our surroundings for centuries, still maintains its importance in the present day. It is used as parquet, wainscot, ceiling, and framework materials and is preferred in the furniture industry because of its various esthetics and decorative appearance. It is a preferred construction material because it can easily be obtained and processed with desired dimensions and forms and because of its low labor and repair costs. Despite all the advantages of wood material, it must be treated with some preservative materials using necessary methods to preserve it from wood-damaging insects and other harmful external factors to increase its service life [1].

Wood materials are subject to degradation, rot, and damage under external environmental conditions. One way to slow this process is to impregnate wood with chemical preservatives, however, many such substances have become targets of environmental organizations [2], and those containing heavy metals are now restricted in Japan, the USA, and European countries because they are toxic to plants and animals including mammals [3]. Hence, some studies have focused on identifying environmentally-friendly and efficient wood preservatives [4], such as geothermal fluids [5].

While various preservative materials including heavy metals have been used for many years in the wood-preservation technology, environmentally friendly and less harmful, new wood-preserving materials have been researched [6]. Impregnating materials used nowadays are categorized into three groups: lubricated, organic solvent based, and water-soluble impregnating materials. When the formulations of water-soluble impregnating materials are examined, it is observed that they include copper, chrome, arsenic, and boron minerals.

Ilgar et al. indicated in his study “The view of dualist approach on geothermal sources” that geothermal fluids are renewable and environmentally friendly natural resources and they are used in numerous countries for a variety of purposes [7]. In the article as in [8] “Evaluation of Geothermal Energy Sources”, stated that geothermal fluids in the forms of hot water, and wet or dry steam include chemicals dissolved in higher levels and rich mineral salts.

It is mentioned the article as in [9]“The amounts of potential impregnate materials in geothermal fluids and convenience of those to wood impregnation process” that although Turkey is among the first six countries in the world in terms of its geothermal resources, these resources are not used enough in industry. On the basis of results of geothermal chemical analyses conducted by the Mineral Research & Exploration General Directorate (MTA), it gave the amounts (in ppm levels) of basic elements and their ions – present in geothermal liquids in molten state – in the thermic solution. It conducted chemical analyses of geothermal waters taken from Ankara, Afyon, Denizli, and Eskişehir and investigated their antifungal properties by concentrating them. Boron (B) and arsenic (As) elements, which are important in terms of antifungal properties, were present among those mineral waters used in that study. it

¹Corresponding author: Department of Forestry and Forest Products, Gumushane Vocational School, Baglarbasi Location, Gumushane University, 29100, Gumushane, Turkey. selimsen@gumushane.edu.tr

²Department of Industrial Forest Engineering, Faculty of Forestry, Duzce University, Konuralp Campus, 81620, Duzce, Turkey, mesutyalcin@duzce.edu.tr

³Department of Forestry and Forest Products, Gumushane Vocational School, Gumushane University, Baglarbasi Location, 29100, Gumushane, Turkey, mehmetoz@gumushane.edu.tr

studied fungus using Kraft paper and Scotch pine wood samples and found considerable antifungal activities among wood samples impregnated with mineral waters having concentration levels of 25, 50, and 75%, respectively [5]. Gümüşhane province, located in the northeast of Turkey, is one of leading counties having underground minerals and waters. Some of rich minerals in this region are gold, silver, and copper, which are also mined. There are mineral water resources in several regions of Gümüşhane, which has an altitude of 1150 meters. These waters have blurry, bitterish, and rusty characteristics and they produce gas if bottled. Mining has continued in some regions of Gümüşhane. Water resources having rich metallic substances [10] are present, as well. Some elements that can be toxic in terms of wood-preservation, such as boron, copper, and sodium, are present in such waters. In this study, it was investigated whether these waters can be potential sources to preserve wood samples when they are used as received or after evaporation.

2. MATERIALS AND METHOD

2.1. Preparation of Wood-Preserving Solutions

To determine which minerals in those waters can be effective against wood-damaging species series of studies was conducted within the project suggested to Gümüşhane University, Directorate of Scientific Researchers. In this study, firstly, the contents of minerals in water resources were analyzed. Results showed that the amounts of minerals in the water had lower concentration levels compared to those in impregnating materials specified in standards. Five different concentration levels were obtained by evaporating 10, 25, 50, 75, and 90% of them and then using these concentrations for the impregnation of Scotch pine sapwood samples.

2.2. Preparation of Experimental Samples and Impregnation Process

Experimental wood samples were prepared using Scotch pine in 5 x 2.5 x 1.5 cm dimensions. The filled cell method was used to impregnate samples. The first step in the impregnation process is to withdraw the air inside the cell pores of wood samples by applying a pre-vacuum treatment of 600 mm-Hg for 30 min. The second step is to apply a pressure of 8 kp/cm² for 60 min after filling the boiler with impregnating material. Solution amounts absorbed by impregnated samples were calculated as follow [11, 12]

$$\text{Retention, } R = \frac{(M_1 - M_0) \cdot C}{V} \quad R = \frac{(M_1 - M_0) \cdot C}{V} \text{ g/cm}^3$$

In this equation, M_0 is the specimen weight before treatment (g), M_1 is the specimen weight after treatment (g), C is the mineral concentration of mineral waters, and V is the volume of wood blocks (cm³).

2.3. Experimental Fungi

Two different wood-decay fungi obtained from the USDA Forest Service, Forest Product Laboratory (Madison, Wisconsin, USA) were vaccinated with *Coriolus versicolor* (*C.v*) white-rot and *Gloeophyllum trabeum* (*G.t*) brown-rot and then their antifungal activities were determined.

The blocks were sterilized by autoclaving at 100±2°C for 20 min. Petri dishes with potato dextrose agar (4% for 500 mL jars) were inoculated with a mycelium agar disk taken from sub-margin old cultures of *G.t* and *C.v* when the mycelia reached the edge of the Petri dish. The wood blocks were placed in the Petri dish medium under laminar airflow conditions. The petri dishes were incubated for 16 weeks at 22±1°C and 75±5% RH to evaluate the efficacy of the treatments. After incubation, the wood blocks were removed, conditioned, and dried at 60°C for 24 h to determine the mass loss of wood blocks. The percent mass loss (ML) was calculated as follows,

$$\text{Mass Loss (\%)} = \frac{(M_1 - M_2) \cdot 100}{M_1}$$

where M_1 represents the weight of specimens before the fungal test (g) and M_2 is the weight of specimens after the fungal test (g).

3. FINDINGS

3.1. Chemical analyses of mineral waters

Mineral waters taken from five distinct regions of Gümüşhane – Tekke town, and İkisü town, City Forest, Yeşildere village, and Zigana village – were chemically analyzed. Mineral water samples having the highest water amounts, which included those taken from Tekke, Yeşildere and Zigana mineral waters were used in experimental studies.

The mineral water taken from Tekke, which causes drying of trees and grasses in rural areas, has a slightly tattleale grey color; when it is bottled, a slight gas formation inside the bottle is observed. The mineral water obtained from Yeşildere mineral water has a straw yellowish and brown color through its flowing paths, as well as blurry, rusty characteristics. As in the case of mineral water taken from Tekke, a gas formation is observed after bottling. The mineral water taken from Ziganawater has a mineral water taste, clear appearance, and gas formation if it is in a plastic bottle. The mineral substance contents of these waters are shown in Table 1.

Table 1. Analysis results of mineral waters taken from the regions of Gümüşhane (mg/L)

Region	Ca	Na	K	Mg	Cl	B	As	Cd	Fe	Cu	Mn	Ni	Co	Zn	Pb
Tekke	479	276	11,8	50,3	4,12	<0,1	<0,001	<0,05	<0,09	<0,07	0,35	<0,08	<0,06	<0,05	<0,1
Yeşildere	93,2	49,0	1,28	28,9	6,03	<0,1	<0,001	<0,05	<0,09	<0,07	0,21	<0,08	<0,06	<0,05	<0,1
Zigana	480	86,1	2,60	43,7	1,13	<0,1	<0,001	<0,05	<0,09	<0,07	1,42	<0,08	0,11	<0,05	<0,1

Results of chemical analysis of the waters showed that the amounts of mineral salts in these waters were substantially lower than those in the preservatives necessary for the impregnation of wood samples. The concentrations of impregnating materials vary depending on their CCA (copper-chrome-arsenic) uses. For instance, copper sulfate and potassium dichromate salts are used at concentration levels of 1-3%, while boron salts are used at concentration levels of 10-15% [1]

3.2. The samples impregnated with concentrated mineral waters

Antifungal activities of mineral waters to be used for the impregnation process were investigated after concentrating them by evaporation. Impregnated samples using the CCA impregnating material at a concentration level of 1% were prepared for comparisons. One white-decay and one brown-decay fungus were used in experimental studies, and the results are shown in Tables 2 and Table 3.

Table 2. Findings of damage caused by white wood-decay fungus (*C.v*)

Samples	Evaporation level (%)	Weight losses (%)	Homogen. groups	Standard deviation	Min	Max
CCA	-	0,01	a	0,01	0,00	0,01
Tekke mineral water	original	9,49	de	1,07	8,33	10,92
	25	10,28	de	3,65	7,06	15,17
	50	11,64	ef	4,12	7,15	16,24
	75	11,10	ef	1,08	10,13	12,45
	90	14,06	fg	2,64	12,16	17,88
Yeşildere mineral water	original	3,31	b	0,59	2,58	3,95
	25	4,28	bc	0,70	3,37	5,07
	50	6,10	cd	0,94	5,23	7,09
	75	5,15	cd	1,63	3,37	6,55
	90	8,06	cde	2,27	5,94	11,12
Zigana mineral water	original	12,41	fg	5,43	6,94	18,68
	25	14,73	fg	2,26	11,62	16,68
	50	16,00	g	3,54	13,22	20,90
	75	13,61	fg	3,47	10,91	18,66
	90	15,21	g	3,66	10,25	19,07

When the mass losses of Scotch pine wood samples caused by white wood-decay fungus (*C.v*) were examined, it was observed that fungi developed much more when the level of water evaporation was increased up to 90%, resulting in higher mass losses. This result shows that the contents of mineral waters and evaporation levels were not at toxicity concentrations for fungi, but instead positively affected the development of fungi and mass losses. There were no statistically significant mass loss differences between the mineral waters of Tekke, Yeşildere, and Zigana mineral waters villages and the control samples having concentration levels evaporated up to 75%. No mass loss was observed in wood samples impregnated with 1% CCA

Table3. Findings of damage caused by brown wood-decay fungus (*G.t*)

Samples	Evaporation level (%)	Weight losses (%)	Homogen. groups	Standard deviation	Min	Max
CCA	-	0,01	a	0,01	0,00	0,01
Tekke mineral water	original	10,06	de	2,38	7,22	12,96
	25	7,65	d	2,09	5,38	10,06
	50	10,23	de	1,37	8,80	12,09
	75	18,39	g	4,25	13,19	23,37
	90	23,06	g	6,28	16,37	31,05
Yeşildere mineral water	original	1,77	b	0,67	0,81	2,31
	25	3,67	bc	1,56	1,69	5,08
	50	7,77	d	1,13	6,63	9,34
	75	11,22	e	1,56	9,07	12,50
	90	9,08	de	0,97	8,23	10,26
Zigana mineral water	original	13,90	f	0,91	13,02	15,05
	25	18,07	gf	4,83	15,38	25,30
	50	16,64	g	5,18	11,74	22,64
	75	21,64	h	3,22	18,79	26,25
	90	17,68	gh	3,13	15,70	22,35

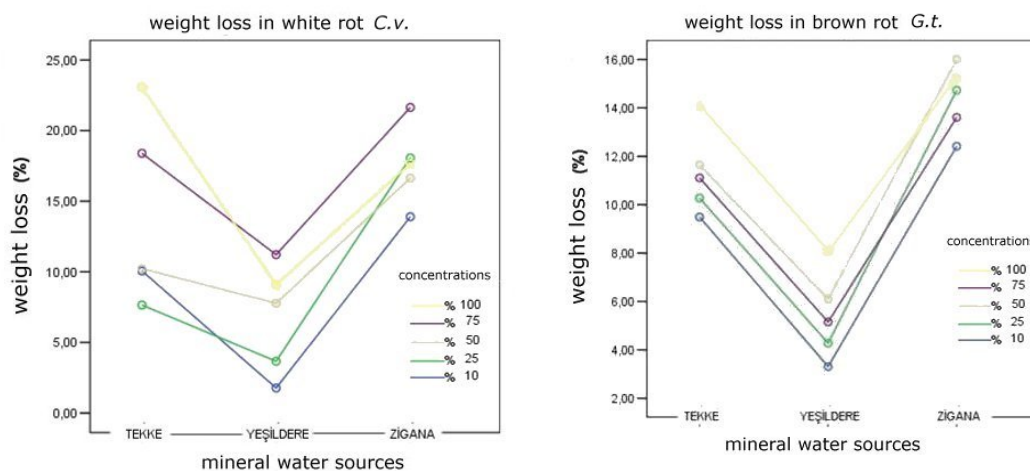


Figure1. Findings of weight losses caused by white rot fungi *C.v* and brown rot fungi *G.t*

When the mass losses of Scotch pine wood samples caused by brown wood-decay fungus (*G.t*) were examined, it was observed that mass losses and fungi developed more when the level of evaporation was increased up to 90% (Figure 1a and b). Similar to the results observed in white wood-decay fungus, mineral waters and evaporation levels were not enough to cause toxicity effect for this type of fungus. On the contrary, they contributed to the development the fungus and increased mass loss.

Differences between the mass losses among samples impregnated using mineral waters with three different concentrations – two of them with 25 and 50% evaporation and one of them without any evaporation – were not statistically significant. Moreover, there were no important differences among samples using concentration levels of 75 and 90%.

4. DISCUSSION AND CONCLUSION

Mineral waters without any evaporation were not sufficient to have antifungal effects for both white and brown wood-decay fungi. Concentration levels obtained after 90% evaporation accelerated both the development of fungi and mass losses of wood samples. It is reported as in [5], their study on Kraft papers and wood samples using minerals in geothermal fluids that the wood-preserving effects of mineral waters were at sufficient levels after evaporation.

It was determined by laboratory studies that almost all types of fungi need C, O, H, N, P, K, Mg, S, B, Mn, Cu, Mo, Fe, and Zn elements, and some need Ga and Ca elements [13]. The presence of some elements like copper, chrome, and boron – having toxic effects against fungus and insects to preserve the wood – in mineral waters in small quantities and insufficient concentration levels obtained from evaporation showed that these mineral waters could not be used in wood-preserving practices for a while. Increasing the evaporation rate and obtaining higher concentration levels in mineral waters are not cost-effective because of higher energy consumption. Instead, the addition of mineral salts, which are toxic for fungi, into solutions will be sufficient. Furthermore, development of new formulas by adding chrome minerals to impart adherence characteristics is necessary.

ACKNOWLEDGMENT

This research was financially supported by BAP (Directory of Scientific Research Projects of Gumushane University).

REFERENCES

- [1] Bozkurt, A.Y., Göker, Y., Erdin, N., *Emprenye Tekniği*, İÜ. Yayınları No: 3779/425, p 429, İstanbul, 1993.
- [2] Kartal, S.N. and Kantay, R., *Emprenye Maddelerinin Piknik Masaları ve Çocuk Oyun Alanı Elemanlarında Kullanımı*, DÜ Orman Fakültesi Dergisi, 56 (2), 43-51, 2006.
- [3] Kartal, S.N., Kakitani, T. and Imamura, Y., *Bioremediation of CCA-C treated wood by Aspergillus niger fermentation*, Holz als Roh- und Werkstoff 62, pp. 64-68, 2004a
- [4] Kartal, S.N., Munir, E., Kakitani, T. and Imamura, Y., *Bioremediation of CCA-treated wood by brown-rot fungi Fomitopsis palustris, Coniophora puteana, and Laetiporus sulphureus*, Journal of Wood Science 50, pp. 182-188, 2004b.
- [5] Var, A.A., Yalcin, M., Şen, S., Tascioglu C, *Antifungal Activity of Geothermal Fluids From Different Regions of Turkey*, BioResources 7(3), 4226-4236, 2012.
- [6] Sen and Yalcin, *Activity of Commercial Still Waters from Volatile Oils Production Against Wood Decay Fungi*, Maderas Ciencia Y Tecnologia, 12(2):127-133, 2010.
- [7] Ilgar, R., *Ekolojik Bakışla Jeotermal Kaynaklara Dualist Yaklaşım*, Elektronik Sosyal Bilimler Dergisi, C.4, S.13: 88-98, 2005.
- [8] Gürü, M., 2005. *Jeotermal Enerji Kaynaklarının Değerlendirilmesi*, Çevreye Genç Bakış, Mart 2005/ Sayı 7.
- [9] Var, A.A., *Jeotermal Akışkanlarda Potansiyel Emprenye Maddelerinin Miktarı Ve Bunların Ahşap Emprenye İşlemine Uygunluğu*, Süleyman Demirel Üniversitesi, Orman Fakültesi Dergisi, Seri: A, Sayı: 1, ISSN: 1302-7085, Sayfa: 184-197, 2009.
- [10] Gültekin, F., Dilek, R., *Gümüşhane Yöresi Mineralli Su Kaynaklarının İz Element ve Radyoaktivite İçerikleri*, KTÜ, Jeoloji Mühendisliği Dergisi, 29 (1) 37-43, 2005.
- [11] TS ENV 839/2006. Turkish standards. *Wood preservatives—determination of the preventive efficacy against wood destroying Basidiomycetes fungi*.
- [12] European Standard (1996) EN 113. *Wood preservatives—method of test for determining the protective effectiveness against wood destroying basidiomycetes—determination of the toxic values*, CEN, technical committee TC 38.
- [13] Bozkurt, A.Y., Erdin, N., Ünlügil, H., *Odun Patolojisi*, İÜ. Yayınları No: 3878/432, p 398, İstanbul, 1995

Corrosion Behaviour Of AlCuMg/B₄C Nanocomposites Produced By Powder Metallurgy Method

S.Ozkaya¹, A.Canakci¹, T.Varol¹, F.Erdemir¹

Abstract

Metal matrix composites that exhibit superior mechanical and physical properties combine the advantages of both the matrix and the reinforcing materials. Different metals have been used as matrix materials to develop new composites, such as the aluminum matrix composites used for aircraft, automotive and military applications. The important properties of Al alloys of high strength-to-weight ratio, high ductility, high stiffness and high wear resistance increase the use of Al alloys in the fabrication of metal matrix composites or metal matrix nanocomposites. The corrosion behaviour and mechanical strength of Al alloys can be improved by adding ceramic particles, such as B₄C, SiC, Al₂O₃ and TiC. B₄C is one of the most promising ceramic materials, due to its appealing properties, such as high strength, low density, exceptionally high hardness, good chemical stability and neutron absorption capability. In this study, AlCuMg-B₄C nanocomposites reinforced with the B₄C particles were produced using the mechanical alloying and hot pressing method. The AlCuMg-B₄C nanocomposite powders were milled for up to 25 h and then hot pressed in vacuum at 560 °C and 600 MPa. The effect of milling time of AlCuMg/B₄C nanocomposites on the corrosion behaviour was investigated. The corrosion performances of composites were evaluated by potentiodynamic polarization scans in 3.5% NaCl solution.

Keywords: Composites, Corrosion, AlCuMg, B₄C

1. INTRODUCTION

Most aluminium (Al) alloys possess a comparatively high specific strength, making them suitable for a wide range of engineering applications. However, their use often remains limited in many applications due to their low corrosion resistance [1-3]. In recent studies, researchers have been successful at improving corrosion resistance and mechanical properties of Al alloys separately. However, studies to develop alloys with improved corrosion resistance and strengths exceeding the current strength of commercial Al alloys have not yet been reported. This deficiency has drawn the attention of the scientists to the metal matrix composites (MMCs). These materials have the ability to combine the properties of ceramics with those of metals and alloys, thus showing significant improvements compared with monolithic metal and alloys [1,2]. Aluminum is a low density element useful for a large number of industrial applications such as aeroplane, automotive, military and space industries. On the other hand, B₄C is chemically inert and corrosion resistant material which also provides interior mechanical and tribological properties [3-5]. Thus, B₄C-reinforced Al alloys are being developed as promising engineering candidates for industrial applications [6]. They offer superior mechanical and tribological properties. Problems come up with composite preparation by melting and casting routes due to the non-wettability of B₄C by liquid Al; density differences and undesirable interfacial reactions induced by temperature. For MMNCs preparation a homogeneous distribution of the reinforcing phase is the most important requirement. To overcome unhomogeneous distribution problem mechanical alloying (MA) is an important processing. Moreover, by MA technique the mechanical and tribological properties of final product can be improved by hardening and strengthening of powders before compacting process [7,8].

In the present work, in order to improve the mechanical properties and the corrosion resistance of AlCuMg alloy, the B₄C particles were added to the matrix by mechanical alloying technique. Reinforced AlCuMg-B₄C samples were prepared using a solid state route complemented with powder metallurgy techniques. The focus of this study is to explore the possibility of improving the corrosion and mechanical properties of Al alloys simultaneously. In this paper, the effect of mechanical alloying on the corrosion behaviour on AlCuMg-B₄C nanocomposites composites is presented.

2. EXPERIMENTAL STUDY

As received AlCuMg aluminum alloy powders (d₅₀:25 μm) with a chemical composition of (in wt.%) 4.85 Cu, 1.78 Mg, 0.312 Mn, 0.005 Ti and 0.138 Zn, 92.114 Al (Gundogdu Exhoterm Company), and B₄C(d₅₀:5 μm)(Alfa-Aesar) powders were used as starting materials to produce AlCuMg-B₄C nanocomposites reinforced with 5 wt% B₄C. The

Corresponding author: Serdar Özkaya, Karadeniz Technical University, Metallurgy and Materials Engineering, Trabzon, Turkey.
sozkaya@ktu.edu.tr

particle sizes of as-received and milled powders were examined using a particle size analyzer (Malvern, model 'Mastersizer Hydro 2000e'). To produce the Al-Cu-Mg/B4C nanocomposites, Al-Cu-Mg alloy powders with 5 wt.% of B4C particles were milled with tungsten carbide balls (5mm) in tungsten carbide vial using a Retsch PM 200 mill. The milling speed of 400 rpm and ball-to-powder weight ratio of 10:1 were used. Mechanical milling was performed at the durations of 0, 6, 15 and 25h respectively. Then the milled powders were hot pressed at 5600C and 600 MPa pressure under argon gas atmosphere to obtain bulk samples. The Brinell hardness of the nanocomposites were determined using a 32.5 kgf load for 10s. The density measurements were done by Archimed's method. The corrosion performances of composites were evaluated by potentiodynamic polarization scans in 3.5% NaCl solution. For the potentiodynamic polarization measurement, machined samples (square cube shaped samples with an average size of 6 mm 10 mm) were mounted on copper rod using epoxy resin for electrical connection, and open surfaces of all samples were cleaned with deionized water followed by rinsing with methanol and then dried. Before potentiodynamic polarization measurements, an initial delay of 45 min was employed in order to measure the open circuit potential between working and reference electrodes. Corrosion tests were conducted within a range of ± 500 mV of open circuit potential at a scan rate of 1 mV/s. Electrolytic corrosion behavior of the samples was evaluated according to corrosion potential and corrosion current density. Each data point for potentiodynamic polarization tests represents at least an average of three different measurements

3.RESULTS AND DISCUSSIONS

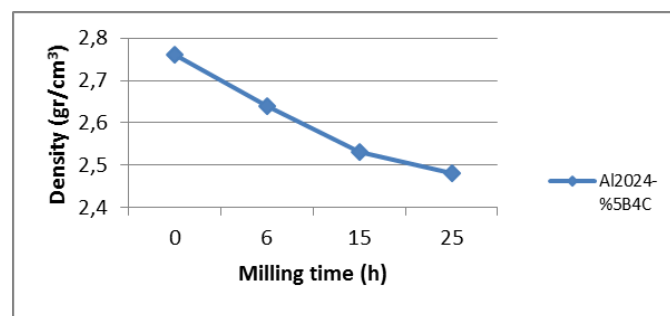
3.1. Density Measurements

First of all it should be noted that the properties of milled powders are very effective on corrosion behaviour and physical properties of mechanically alloyed and pressed samples. Table 1 shows the alteration in the particle size of the AlCuMg matrix B4C reinforced nanocomposite powders with increasing milling time. As shown in Table 1, the average particle sizes decreased with increasing milling time. When the powders reached to the steady state at 25h milling time the average powder size decreased to the nanometric sizes.

Table 1. Particle size and hardness of milled powders

Milling time	0h	6h	15h	25h
Particle Size (μm)	24,48	12,74	7,65	0,12
Particle Hardness (HV 0,25)	82	152	296	336

Figure 1 illustrates experimental density and porosity measurements of nanocomposite samples changing with milling time. Results showed that, increasing the milling time resulted as an increase in porosities of composites. The reason for increasing in porosity as a function of increasing milling time can be explain by the work hardening affect of milling proces. As a consequence of collisions between powder particles and milling balls the powder hardness increased which was investigated in another study.[] While the hardness of powders increase the compressibility of powder decreases as a result of increased compressibility resistance of particles. The lowest relative density was seen in after 25h milling which is about %89.



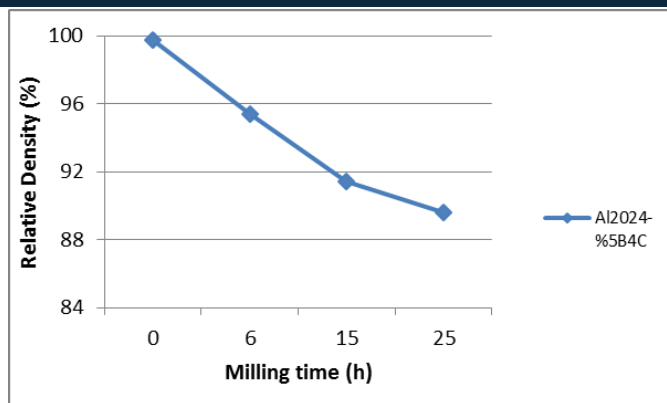


Figure 1. Density measurements of bulk AlCuMg-%5 B₄C samples

3.2. Hardness of bulk sample

Figure 2 shows the hardness of bulk AlCuMg-%5 B₄C composites. As the milling time increases from 0 to 25h, the hardness changes and increases significantly. This increase can be attributed to the increasing in powder hardness. Brinell hardness values are related to the powder properties which was used to fabricate bulk samples. As shown in Table 1, the micro hardness values of mechanically alloyed powders are increasing with increasing milling time. The highest Brinell hardness values were obtained for 25h composite which is about 7 times higher than unmilled composite.

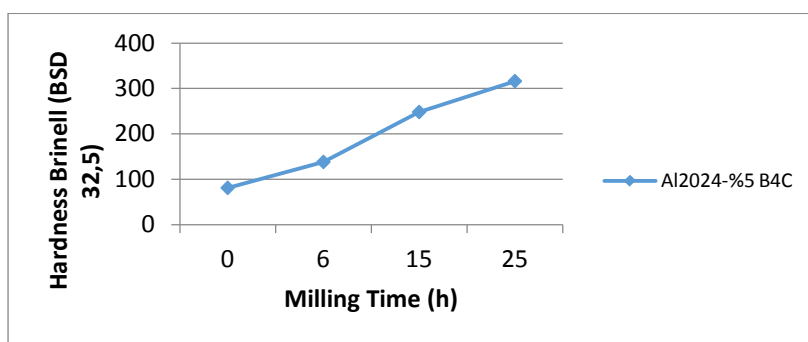


Figure 2. Hardness of bulk AlCuMg-%5 B₄C samples

3.3. Corrosion Behaviour

In this study, it is shown that the milling time has important affect on corrosion behavior of AlCuMg-%5B₄C composites. Table 2 shows the electrochemical parameters of composite samples related to the milling time. It can be seen that, corrosion rate of samples are increased with increasing milling time which means the corrosion resistant of samples are decreased. This decrease can be explained by the relative densities and porosities of samples. While the porosities increase the corrosion resistant increase because of relatively increased surface area of samples. The grain boundaries and porous areas supply the corrosion starting fields because of the lack of contunity in the surface due to the change in the structure.

Milling time	E _{corr} (mv)	I _{corr} (A/ cm ² x10 ⁻⁶)	Corrosion rate (mpy)
0h	-898	20,1	0,74
6 h	-714	13,8	2,27
15 h	-661	12,6	4,02
25h	-571	5,64	7,98

4. CONCLUSION

In summary, AlCuMg/ 5wt% B₄C composites with changing alloying time produced by hot pressing and consolidation method. The corrosion performances of composites were evaluated by potentiodynamic polarization scans in 3.5 % NaCl solution. The results showed that;

- The porosities of composite samples increased with increasing milling time.
- The hardness of composites increased with increasing milling time.
- The corrosion rate of samples increased with increasing milling time in other words the corrosion resistant of samples decreased with increasing milling time.

REFERENCES

- [1] K.R. Ravi, V.M. Sreekumar, R.M. Pillai, C. Mahato, K.R. Amaranathan, R.A. Kumar, B.C. Pai, *Mater. Des.* 28 (2007) 871–881.
- [2] L. Xiaowei, R. Jean-Charles, Y. Suyuan, *Nucl. Eng. Des.* 227 (2004) 273–280.
- [3] A. Daoud, *Mater. Lett.* 58 (2004) 3206–3213.
- [4] H. Wang, G. Li, Y. Zhao, G. Chen, *Mater. Sci. Eng. A* 527 (2010) 2881–2885.
- [5] C. Suryanarayana, *Prog. Mater. Sci.* 46 (2001) 1–184.
- [6] J.B. Fogagnolo, D. Amador, E.M. Ruiz-Navas, J.M. Torralba, *Mater. Sci. Eng. A* 433(2006) 45–49.
- [7] J.B. Fogagnolo, E.M. Ruiz-Navas, M.H. Robert, J.M. Torralba, *Scripta Mater.* 47(2002) 243–248.
- [8] X.H. Wei, L. Liu, J.X. Zhang, J.L. Shi, Q.G. Guo, *Mater. Lett.* 63 (2009) 1618–1620.

Study On Microstructure And Wear Properties Of B₄C Nanoparticle Reinforced ZA27 Nanocomposites

E.D.Yalcin¹, A.Canakci², S.Ozkaya², T.Varol²

Abstract

Among the group of zinc base alloys, the zinc–aluminum alloys have gotten a lot of attention in the last years like substitute materials of aluminum based alloys, irons and brasses. ZA-27 has the highest aluminum content, highest strength, highest melting point, and lowest density of the ZA group. ZA 27 alloy, in particular, has been used in bearings and bushing applications, as a replacement for bronze bearings because of its low cost and equivalent or superior bearing performance. However their mechanical and tribological properties are not enough to be used as unreinforced alloy. In early studies to provide their mechanical and tribological behaviours ceramic particles (Al₂O₃, B₄C, SiC) were used as reinforcing materials. Among the group of these ceramic particles, the B₄C particles are known as being harder and having less density. In this study to investigate the tribological behaviours of Za27 matrix B₄C nanoparticle reinforced nanocomposites the samples were fabricated by powder metallurgy technique. The abrasive wear behaviour of nanocomposites were investigated using ball on disc wear test at different loadings of 5 and 10 N. Results of the wear tests revealed that the wear rate and wear resistance of nanocomposites decreased with an increase in the B₄C content. The best wear resistance was obtained at 3 wt % B₄C nanoparticle reinforced nanocomposites.

Keywords: ZA27, B₄C, Nanocomposite, Wear, Tribology

1. INTRODUCTION

Particulate-reinforced metal matrix composites (MMCs) exhibit improved mechanical and physical properties that combine the advantages of both the matrix and the reinforcing materials. Although various metals have been studied as matrix materials, aluminum alloys have been used as the matrix materials in most of the particulate-reinforced MMCs in industry. Superior wear resistance is one of the attractive properties in MMCs. It has been found that particulate-reinforced MMCs show wear resistance on the order of 10 times higher than the unreinforced materials in some load ranges. B₄C is one of the reinforcing materials that has been used in particulate-reinforced MMCs [1-3]. Zinc–aluminum alloys containing small amount of copper have been observed to be cost- and energy-effective substitutes to a variety of ferrous and non-ferrous alloys owing to their higher strength, better wear resistance, low casting temperature and abundant resources [4-5].

Among the group of zinc base alloys (ZA 4, ZA 8, ZA 12, ZA 27), the zinc–aluminum alloys (ZA or ALZEN) have gotten a lot of attention in the last years like substitute materials of aluminum base alloys, irons and brasses [6]. The members of the ZA casting alloys are: ZA 8, ZA 12, and ZA 27. These alloys have many advantages over aluminum-based alloys, namely; high strength, good machining and tribological properties, and low casting temperature. ZA 27 alloy, in particular, has been used in bearings and bushing applications, as a replacement for bronze bearings because of its low cost and equivalent or superior bearing performance. Moreover, ZA 27 is classified as a high strength alloy with a tensile strength substantially higher than that of ordinary cast aluminum alloys. Zinc – aluminum alloys as general-purpose casting appeared more recently in industry for their good ambient temperature mechanical properties, damping capacities and wear resistance [7-8]. In the industrial production it is very important to increase the quantity of quality products and without defects, where the structural morphology can also play an important role in the corrosion behavior of the metallic alloys. Although it is well-known that, as much the quantity as the homogeneity in the distribution of second phases are important parameters that define the level of mechanical resistance of the alloy [9-10-11].

This study investigates the production, microstructural characterization, hardness, wear, and corrosion characteristics of B₄C particle reinforced Zn-Al alloy matrix composites, containing different rates of B₄C, produced using modified conventional casting method.

2. EXPERIMENTAL STUDY

A mixture of ZA27 and B₄C nano particle was used as the starting material. The chemical composition of ZA 27 is (in weight percent) of 27.2% Al, 2.01% Cu, 0.02% Mg and balance Zn. The mechanical milling (MM) process was

Corresponding author: Aykut Canakci, Karadeniz Technical University, Metallurgy and Materials Engineering, , Trabzon, Turkey.
aykut@ktu.edu.tr

¹Abdullah Kanca Vacational School, Metal Technologies, Trabzon, Turkey

²Karadeniz Technical University, Metallurgy and Materials Engineering, , Trabzon, Turkey

conducted in a planetary ball mill (Retsch PM 100) using tungsten carbide containers and balls at the room temperature. Mechanical milling was carried out at the durations of 15 min for mixing of composite powders. In order to avoid excessive temperature during milling, the process was stopped every 30 min then resumed when the temperature of the bowl had decreased to room temperature. Bowl temperature was measured between 35 and 55°C with an infrared thermometer. The mixtures of ZA 27/B₄C powders were loaded into a steel die, cold pressed at 200 MPa and then hot-pressed for 3h at 430°C at pressure of 500 MPa. Zinc stearate was coated on the inner wall of the mold and surface of the samples as a lubricant. For the microstructural characterization of the specimens they were prepared by grinding paper from 800 to 1200 grit and metallographically polished with 1 μm alumina. The microstructure of the composites was characterized by means of scanning electron microscopy (SEM). The experimental densities for the contact samples were determined using Archimedes method. The hardness values of the samples were measured by the Brinell hardness method, and the mean of at least six readings was recorded at a load of 31.25 kgf. Wear behavior of the composites was examined by using a ball on disk wear tester. For wear test, the each composite samples were ground with a 1200 SiC abrasive paper and further washed in acetone. The initial average surface roughness (Ra) of a polished sample was 0.4 μm. A H11 hot-work tool steel ball with diameter of 10 mm and mirror-like surface was contacted on the surface of disk at either 5 or 10 mm from the disk center under the loads of 5 and 10 N. The disk was concurrently rotated for 48 min with a rotation speed of 100 rpm at room temperature.

3.RESULTS AND DISCUSSIONS

3.1. Porosity and hardness

Figure 1 shows the porosities of ZA27 alloy and composites. A important increase of the porosity content of the composite from 0.16% to 5.1 % with reinforcements of B₄C content of 2% wt. was obtained. Moreover, 2wt% B₄C reinforced composites has lower density than ZA 27 alloy. The density decreases with increasing reinforcement. As compared to composites, ZA 27-B₄C sample has higher density due to its higher densification ability and the less agglomeration. The density of composites decreases with increase in the B₄C content. This can be attributed to the effect multiple pressing during the densification process. The increase in the B₄C content from 1wt. % to 3wt% result in few decreasing of density of composite, However a significant increase porosity content of 5wt% B₄C reinforced ZA 27 matrix was obtained. The results show that higher than 5wt% B₄C content adverse effect on the densification of composites during compaction.

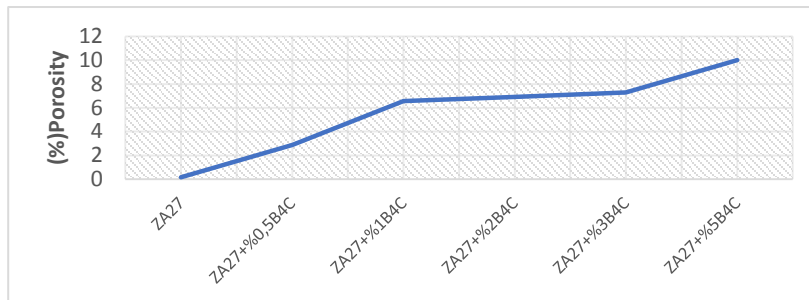


Figure 1. The porosities of ZA 27 alloy and composites

Figure 2 shows the Brinell hardness values of ZA 27 alloy and composites. As the content of B₄C increases from 0 to 2 wt.%, the hardness a decrease substantially. A decrease in the hardness value from 130 to 102.3 HB is observed with reinforcement of B₄C into the ZA 27 alloy matrix. The relatively lower hardness value for ZA 27-B₄C composite sample are due to agglomeration of reinforcing B₄C particles and the higher porosity content. Under the same applied load during pressing, B₄C particles in ZA 27- composites will collide few rapidly than ZA 27 alloy powders. A few extensive plastic deformation in the ZA 27-B₄C composites sample is occurred. So, the lower stresses are developed at the ZA 27-B₄C reinforcement interface.

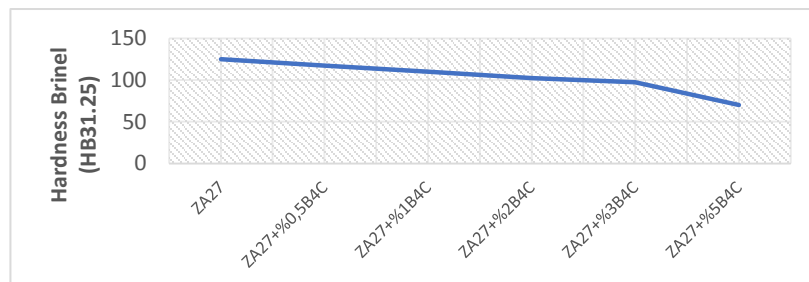


Figure 2. The hardness value of ZA 27 alloy and composites

3.2. Wear

The effect of the nano B_4C content on the wear of the composites are shown in Figs. 3 and 4, respectively. A decrease in the weight loss with increasing B_4C content up to 5 wt.% was obtained. This can be attributed to increasing load carrying capacity with increasing reinforcement content but the bonding strength between the ZA 27 alloy matrix and B_4C reinforcement materials decreases significantly. As the applied load change from 5 to 10 N, the wear regime of the ZA 27-5wt.% B_4C composite less changed. As can be seen in Fig. 5, the wear mechanism includes the abrasion and adhesion mechanisms.



Figure 3. The weight loss value of ZA27 alloy and composites(5N-300m)



Figure 4. The weight loss value of ZA 27 alloy and composites(10N-300m)

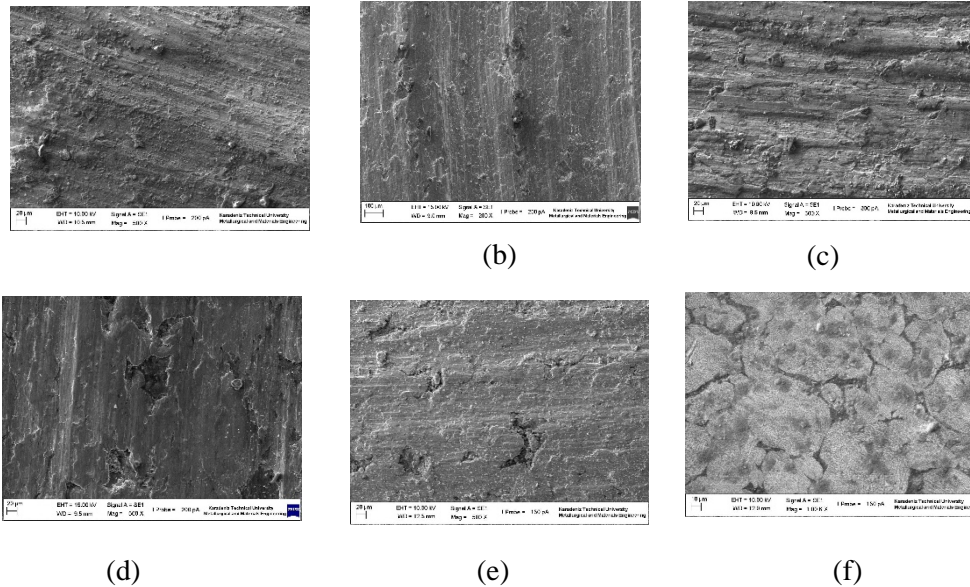


Figure 5. SEM micrographs of the worn surfaces of alloy and composites wear tested at 10N (a) ZA 27 alloy, (b) ZA 27–0.5wt.% B4C , (c) ZA 27–1wt.% B4C, (d) ZA 27–2wt.% B4C , (e) ZA 27–3wt.% B4C, (f) ZA 27–5wt.% B4C

4. CONCLUSIONS

In this work, nano B4C reinforced ZA-based 27 alloy matrix composites were synthesized by hot pressing method. Dry sliding wear tests were conducted on ball specimens of the composites with a ball-on-disk tribometer until a sliding distance of 300 m. The sliding speed ranged from 100 rpm and the load ranged from 5 to 10 N. The main conclusions of this study may be summarized as follows:

- 1- The hardness of the ZA-based 27 alloy reached 130 Hb in comparison to 117,2 Hb of the ZA27 /B₄C composite reinforced with 0,5 wt.% of B4C .
- 2- The effect of B4C content and applied load on the wear behavior of ZA 27 /B4C is analyzed in detail. The weight loss decreases with increasing B4C content while the ZA 27-5wt.%B4C composite has higher wear rate. The SEM images of the worn surfaces of the ZA 27 /B4C indicates wear mechanism has the adhesive and abrasive wear.
- 3-The weight loss of composite (5 wt.% b4c) was approximately 90% lower than that of composite(0,5wt.%b4c)under the same test condition. this experimental result indicates a significant effect of the b4c particles on enhancing the wear resistance of these composites.

REFERENCES

- [1] W.H. Hunt, Particulate reinforced MMCs, in: T.W. Clyne (Ed.), *Comprehensive Composite Materials, Metal Matrix Composites*, vol. 3, Elsevier Ltd., 2003, pp. 701–715.
- [2] J. Zhang, A.T. Alpas, Wear regimes and transitions in Al₂O₃particulate-reinforced aluminum alloys, *Mater. Sci. Eng. A* 161 (1993) 273–284.
- [3] A.R. Kennedy, B. Brampton, The reactive wetting and incorporation ofB4C particles into molten aluminium, *Scripta Mater.* 44 (2001) 1077–1082.
- [4] E. Gervias, R.J. Barnhurst, C.A. Loong, *J. Met.* 37 (1985) 43
- [5] T.S. Calayag, *Min. Eng.* 35 (1983) 727.
- [6] L.J. Yang, *J. Mater. Process. Technol.* 140 (2003) 391
- [7] Smith, W., *Structures and properties of engineering alloys*. McGraw Hill, New York, 1993, 2nd edition,pp. 561-566
- [8] W. Weaver, S.P. Timoshenko, D.H. Young, *Vibration Problems in Engineering*, Wiley, New York, 1990, p. 140.
- [9] U. Feurer, in: *The Symposium on Quality Control of Engineering Alloys*, Delft, 1977, p. 131.
- [10] R. Trivedi, W. Kurz, *Int. Mater. Rev.* 39 (1994) 49.
- [11] R.N. Grugel, *J. Mater. Sci.* 28 (1993) 677.

BlueScan: an Advanced Sensing Experimentation Platform

Cigdem Polat Dautov¹

Abstract

The Internet of Things (IoT) is a recently emerged concept which has a potential to revolutionize how technology is being used in modern world. IoT is comprised of objects of different types that are capable of collecting and exchanging information. Due to various natures of possible applications IoT has brought serious research challenges to many fields including wireless communication, signal processing and networking. Addressing these challenges requires existence of efficient and easy to use tools for gathering and collecting data from smart devices. This work proposes BlueScan, an advanced mobile platform which brings rich functionality to researchers. BlueScan allows for gathering Received Signal Strength Indicator (RSSI) estimates as well as hardware/software sensor data from multiple smart devices. The proposed platform provides real time data tracking and visualization. Gathered data can be also saved for post processing. Thus, the number of potential research problems where BlueScan can be applied is endless. The platform can be installed on Android OS 4.2 or higher and uses widely available Bluetooth technology at its core. BlueScan is the first platform of its kind available on Google Play at no cost. This study explains technologies behind BlueScan, the platform itself and gives examples of its most probable use cases.

Keywords: *Bluetooth; Experimental Platform; Internet of Things; Received Signal Strength Indicator*

1. INTRODUCTION

Wireless communication is the transfer of information between two or more devices that are not connected with a wire. Easiness of implementation, relatively cheap maintenance, and ability to establish a communication link when cabled technologies failed are the most important advantages of wireless technology compared to traditional wired communication. Wireless technology is the most efficient and scalable approach when deploying a corporate level network. This is of particular importance since current networks consist of millions of computers, smart phones, tablets, and other gadgets such as sensors, webcams, game consoles, picture frames, and even household electronics. Every day, the number of smart electronic devices with wireless capabilities increases which emerges the Internet of Things (IoT), a new concept of making these devices serve a common purpose. Internet of Thing allows us to access remote sensor data and remotely control the physical world [1] by establishing a networked interconnection of smart everyday objects. These kind of large-scale systems commonly encounter variety of challenges with a direct impact on the performance of the system. Collisions and interference among the devices, security, network infrastructures and limited network resources are among the most critical [1]. Information about the behavior of the wireless channel can be useful in overcoming the challenges mentioned above [2]. The Received Signal Strength Indication (RSSI) is one of the most popular and easily accessible metric for understanding the character of the wireless channel. RSSI provides a relative indication of the power level being received by the antenna in a wireless environment. RSSI gives important implications about the wireless transmission and thus is widely used in many applications. In particular, can be employed in localization and tracking of the devices where Global Positioning System (GPS) is not available [3]. Another major portion of RSSI applications is related to healthcare services. In [4] RSSI is utilized for acquisition of human kinematics such as tracking different body parts displacement, gain patterns of daily life activities to enhance medical diagnosis. It was shown in [5] that variation in the signal strength is helpful for extracting a patient's breathing rate.

Advance sensor technologies made it possible for smart devices in IoT to be equipped with different type of sensors. A sensor is an electronic component whose purpose is detecting some characteristics of the environment. It is possible to see sensors in everyday objects like automatic doors, toasters, phones, etc. Sensor data is not usually able to provide direct information about the communication channel. However, it can be used to gather essential information related to a participating device and then applied to solve aforementioned IoT challenges. For instance, accelerometer data can be used for authentication purposes.

In this paper we introduce an advanced, intuitive and easy to use mobile experimentation platform named BlueScan. The initial preliminary version of the platform is discussed in [6]. The new version presented in the current work is meant to be used as a supplementary or main tool for conducting profound research in the field of Internet of Things, wireless communications, signal processing and networking. The platform employs Bluetooth 4.0 wireless technology for communication purposes. The targeted devices are those that run Android Operating System. Unlike [6], within

¹ Corresponding author: Bitlis Eren University, Department of Electrical and Electronics Engineering, 13000, Merkez/Bitlis, Turkey. cpolat@beu.edu.tr

new BlueScan we provide truly unique functionality of gathering both RSSI values as well as various sensor data such as accelerometer, light sensor, GPS coordinates etc. Due to this fact research applications of the platform are practically infinite. The platform is also capable of visualizing, saving and transferring the collected data. The rest of the paper has the following format. In the second section we explained why we choose Bluetooth over WI-FI as a short range communication technology by comparing the advantages of Bluetooth and Wi-Fi. In the third section, we briefly describe the experimental platform software and its functionalities. In the fourth section, we explained the potential outcomes of the RSSI and sensor data and possible applications in different fields of research. Typical use cases are described in section five. Section six concludes the paper and discusses future work.

2. THE COMPARISON OF BLUETOOTH AND WI-FI

There are several protocols designed for short range wireless communications with low power consumption such as Bluetooth (IEEE 802.15.1), UWB (IEEE 802.15.3), ZigBee (IEEE 802.15.4) and Wi-Fi (IEEE 802.11 a/b/g/n). Among them Bluetooth and Wi-Fi are the most commonly used standards which are supported by majority of smart devices such as smart phones, tablets, computers and wearable electronics. For the early stage of design of the experimental platform, the question of which protocol to use emerged. In order to adequately address this question, we compared the main features and characteristics related to the applications of Bluetooth and Wi-Fi in terms of various metrics, complexity, connection requirements, topology, and power consumption.

By supporting 79 radio channels for frequency hopping (FHSS), Bluetooth provides a better communication with less collision and interference between the devices. On the other hand, Wi-Fi uses only 14 channels for FHSS which means there will be more collision and interference between the devices on a Wi-Fi network. This fact becomes more obvious in dense indoor environment with high data traffic [7].

Bluetooth standard allows user to get RSSI measurements from other devices without being logically connected. This fact better suits with the requirement of providing easy to configure and use experimental tool. In addition to the pre-connection requirements of Wi-Fi standard, a complex hardware and software configuration procedure is necessary in order to get any RSSI measurements from other devices. This fact makes Bluetooth a better option in accordance with the requirement of simplicity and low time consumption.

Another important point is that technologies like Bluetooth and Zigbee are intended for portable products, short range and limited battery power while Wi-Fi is designed for a longer range communication and assumes devices with substantial power supply. Therefore, using Bluetooth is beneficial if data collection from mobile devices is desired for extended period of time. By taking into consideration of all advantages of Bluetooth mentioned above and the experimental needs, it is safe to say that Bluetooth is a better choice for our purposes.

3. EXPERIMENTAL PLATFORM SOFTWARE

The BlueScan Experimentation Platform has been developed in order to help professionals, students and scholars who are interested in the field of wireless communications, networking, IoT. The platform allows user to get big scale raw RSSI measurements from other devices such as smart watches, tablets, phones which may or may not have same operating system. The platform also supports sensor technologies. The platform can be used for gathering, transferring, evaluating sensing data of in-built sensors and the signal strength of other devices within 2.4 GHz frequency band. The software platform requires a simple smart device with Android API 18 or higher versions and supports Bluetooth. The application requires Bluetooth Radio, internal memory space and Internet connection in order to execute several functions like visualizing the data and saving large data files on the phone and/or email them to the recipients. After installation on the device, BlueScan can be used immediately without any further configuration. The BlueScan's settings section enables setting Bluetooth ON/OFF and scanning for other smart devices. Related screenshots are shown in Figure 1 and Figure 2.

The scanning process allows user to find other smart devices such as laptops, desktops, smart phones, tablets and wearable devices which support Bluetooth technology. To discover and list available devices BlueScan will inquire the radio channel periodically every 2 seconds. Bluetooth enabled devices will appear under Available Devices as depicted in Figure 3.

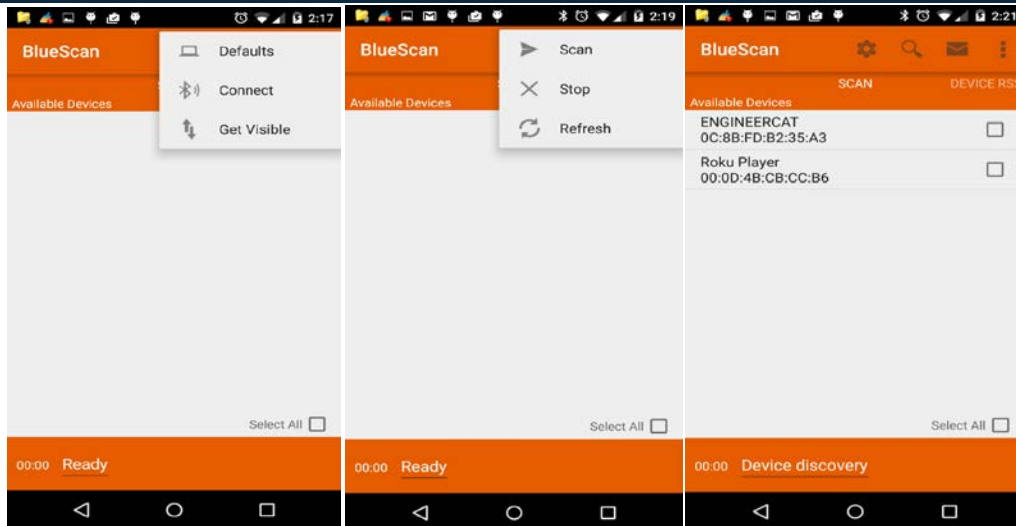


Figure 1: Settings Menu Figure 2: Experiment Menu Figure 3: Listed Available Device

In case of one or more discovered smart devices, experiment menu gets activated. By starting a new experiment, RSSI values can be collected for the selected devices. After starting the experiment, user can visualize the RSSI data coming from the selected devices in real time by clicking the Visualization. This helps user to gain a better control over the experiment along with deeper understanding. Example of Visualization Menu from 2 different devices is shown in Figure 4.

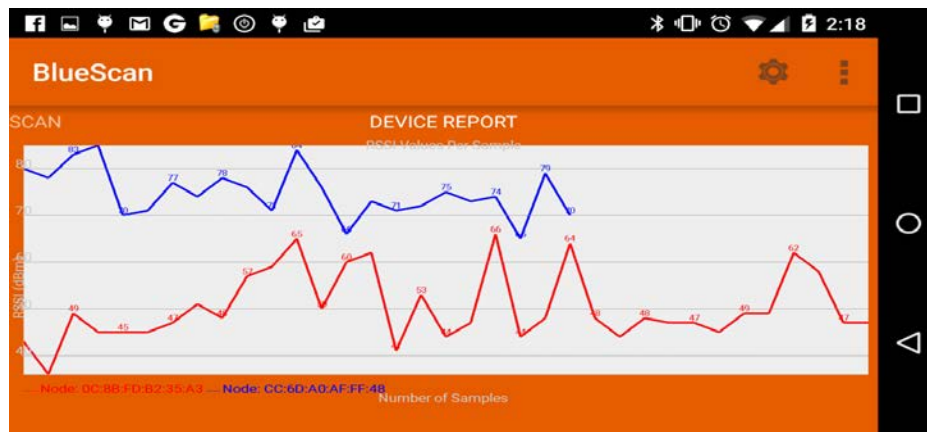


Figure 4: Visualization of RSSI data

The application also allows user to save and share the experimental data with other associates and also helps users back up their data on other computers, external hard drives or servers. User can continue his or her experiment while saving data or user can wait till the end of the experiment in order to save the full experimental data into a text file. User can choose any application on his/her device in order to send

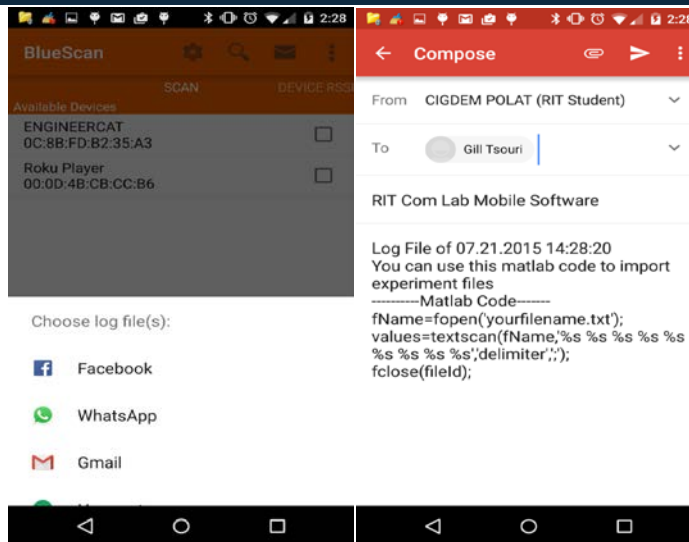


Figure 5: Choosing email application Figure 6: Sending email

an email (Figure 5). The email also includes the data file along with the Matlab script in order to import the data to Matlab (Figure 6).

The application has another function which allows user to control several built-in sensors on their devices. The user can activate one sensor at a time and collect sensing data such as accelerometer, ambient temperature, light, magnetic field, pressure and humidity (Figure 7). This screen has the exact same logical structure with the Scanning. In order to start data collection, user should choose one or more devices and a sensor. The data file saving, emailing and visualization functions are applied to the collected sensor data as well as RSSI data.

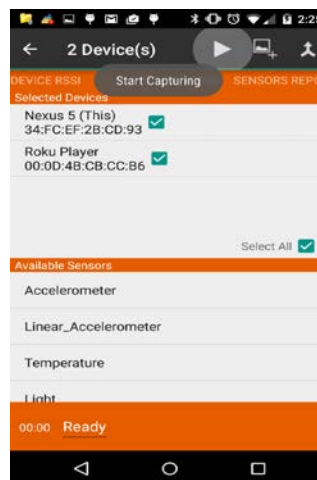


Figure 7: Device sensors

The important point is that user should check her or his device hardware to be sure these sensors exist otherwise this function of the application will not be able to collect any sensing data. For multiple device tests, it is important to synchronize the devices in terms of date and time in order to get accurate experiment results.

The newest installation version of the platform is currently available and can be downloaded from Google Play directly to your mobile device(s). The format of the application file is .apk which is a compatible Android application format for mobile devices. For specific instructions on how to install application on specific device refer to device's manual [8]. Further details about installation and other functionalities can be found in the full version of the study in the User Manuel section

4. APPLICATIONS OF THE PLATFORM

The BlueScan platform is a mobile and free alternative of experimental tools for researchers focused on wireless communications including Wireless Body Area Networks (BAN), Wireless Personal and Local Area Networks (WPANs/WLANs), IoT. Users can extract large scale RSSI and sensor data; process the large scale data, find possible outcomes of the data related to their research topics. We will be giving real life application areas such as

studies of radio signal propagation, indoor estimation of indoor location, social experiments and health care applications.

4.1. Radio Signal Propagation

BlueScan can be used to study radio signal propagation in indoor environments using smart devices leveraging the Bluetooth qualifications [10]. The user can conduct experiment with several robots equipped with smart devices and start the RSSI data capturing in an indoor hallway and laboratory environment in order to gather 40.000 or more samples of RSSI. Later, collected experimental RSSI data can be compared to simulated RSSI measurements using radio signal propagation models.

4.2. Indoor Localization

RSSI measurements can be also used for adaptive distance estimation, indoor localization and tracking where Global Positioning System (GPS) is not available [9]. Considering high pace technological development in the field of Internet of Things (IoT), there will be various kinds of smart devices including hearth monitoring implants, biochips, automobiles, house appliances and other embedded devices in our daily environment. This fact brings the need of tracking small smart devices such as smart watches, smart phones and even car keys. The platform can be used to find any missing smart device supporting Bluetooth technology by easy evaluation of RSSI values. Using device scanning feature of the software, user can understand if the device is close to her or his smart phone.

4.3. Social Analysis and Business Development

RSSI measurements can be applied to social fields such as examining the social connections, social relations and business development. For instance, the researcher can gain insights into social relations between people in a certain event where participants carry smart phones. By examining extracted RSSI values using the platform during the experiment, based on the correlation between participants RSSI measurements we can get information on which participants are socially related and which participants are not. Yet exciting idea is proposed by Libelium for gaining business intelligence [11]. In this work signal strength is used to measure the number of people in the stores for the sake of enhancing their user experience.

4.4. Healthcare Applications

Systems that recognize activities using sensors can be used in healthcare applications in various ways such as fitness monitoring, preventive and chronicle care, cognitive and eldercare assistance. The user can experiment where the smart phones used as healthcare application on human subjects. For instance, each test subject's accelerometer data can be sampled for certain amount of time. There are also various research using accelerometer-bases motion detectors in order to monitor and assess physical activities including posture and movement classification, estimation of energy expenditure, fall detection and balance control evaluation [12].

5. LOCALIZATION AND CHANNEL ESTIMATION USE CASES

In this chapter we will give a simple proof of concept applications of the proposed platform. We conduct an experiment with 3 participating devices named A, B and C and one host that gathers data. During the experiment A and B stick together with marginal movement. Whereas, device C is located at a different spot and closer distance to host. Figure 8 shows how RSSI values change during the experiment. It can be observed that while RSSI estimates for A and B vary around average of ≈ -82 dBm, C has average of ≈ -65 dBm. This result is to be expected. Since C's position is closer, received signal power from C is higher. Further work can be done on callibrating the RSSI estimates to get one to one correspondance with a distance. Implementing this approach and using several (at least 3) host devices can give very precise location of the device in consideration. Data from the same simple experiemnt can be used to get information about the communication channel. This task is of special importance in wireless transmission and helps to adequetly model the channel without performing real experiments. For example, in most cases, scattered electromagnetic waves propogation is described and modeled using Rician fading. Rician fading distribution is characterized by a Rician K factor which describes the relative power of a line of sight component. Figure 9 represents best Rician distribution fit to RSSI data from device B. From this fit, K factor can be estimated and later used to describe a particular channel.

Figure 8: RSSI values of different devices

Figure 9: Distribution of RSSI values

6. CONCLUSION

The increasing number of every day wireless smart objects gives a rise to many networking issues such as collision and interference between devices, security, infrastructures of the networks and many others. In this work we introduced an Android experimentation platform BlueScan which provides rich functionality for researchers in the field of Internet of Things, wireless communications, networking. The platform allows for gathering one of the most important characteristics of the wireless channel known as Received Signal Strength Indicator (RSSI). The RSSI is extracted from incoming Bluetooth advertisement packets of devices of interest. This allows for the software to be installed only on a single "server" mobile device leaving others platform independent. BlueScan is not limited to RSSI. It is also possible to extract raw data from hardware or software sensors available on the device. Along with RSSI or by itself this data may provide essential information related to the environment. Having sensors' data gives a lot of flexibility in the research experiment being conducted. Within the paper we gave multiple suggestions on how the platform can be used in the field. However, we hope that researches will find our tool useful for other applications as well. As part of the future work, we plan to provide an option of establishing Bluetooth connection between the server and other devices, and add relaying functionality. We also intent to conduct a set of experiments to show the rich capabilities of the proposed platform in various fields not limited to engineering.

REFERENCES

- [1] H.Kopetz, "Real Time Systems: Design Principles for Distributed Embedded Applications" Real-Time Systems Series, DOI 10.1007/978-1-4419-8237-7_13
- [2] Feng Xia, Laurence T. Y., Lizhe W. and Alex V., "Internet of Things", International Journal of Communication Systems, 2012, pp. 1101-1102, Int. J. Commun. Syst., 2012
- [3] Jung, Joonyoung, Dong-oh Kang, and Changseok Bae. "Peer to peer signal strength characteristic between IoT devices for distance estimation." In Internet of Things (WF-IoT), 2014 IEEE World Forum on, pp. 208-211. IEEE, 2014.
- [4] Blumrosen, Gaddi, and Ami Luttwak. "Human body parts tracking and kinematic features assessment based on RSSI and inertial sensor measurements." Sensors 13, no. 9 (2013): 11289-11313.
- [5] Tsouri, G. R., and O. Maimon. "Respiration rate estimation from channel state information in wireless body area networks." Electronics Letters 50, no. 10 (2014): 732-733.
- [6] Dautov P. Cigdem. and Tsouri, G. R. "A Mobile Experimental Platform", International Conference on Natural Science and Engineering, 2016. ICNASE 16' on, pp. 1770-1775, 2016.
- [7] Salazar, AE Salloum. "Positioning Bluetooth® and Wi-Fi™ Systems." Consumer Electronics, IEEE Transactions on 50, no. 1 (2004): 151-157.
- [8] Android API Guide, <http://developer.android.com/guide/index.html>
- [9] Awad, A., Frunzke, T and Dressler, F. "Adaptive Distance Estimation and Localization in WSN using RSSI Measures", Digital System Design Architectures, Methods and Tools, 2007. DSD 2007. 10th Euromicro Conference on, pp. 471-478. IEEE, 2007
- [10] Fink, J, Michael Nathan, Kushleyev A. and Kumar, V. "Experimental characterization of radio signal propagation in indoor environmental with application to estimation and control", Intelligent Robots and Systems, 2009. IROS 2009. IEEE/RSJ International Conference on, pp. 2834-2839, 2009
- [11] Libelium, <http://www.libelium.com/>
- [12] Lane N.D, Miluzzo E., Hong Lu and Peebles, D. "A survey of mobile phone sensing", Communications Magazine, IEEE (Volume: 48, Issue: 9), pp. 140-150. IEEE, 2010.